Turkey Flat, USA

Site Effects Test Area

REPORT 5

Weak-Motion Test: Statistical Analysis of Submitted Predictions and Comparisons to Observations

November 1990

TECHNICAL REPORT NO. 90-2

CALIFORNIA DEPARTMENT OF CONSERVATION

DIVISION OF MINES AND GEOLOGY

EARTHQUAKE SHAKING ASSESSMENT PROJECT

CALIFORNIA
DEPARTMENT
OF CONSERVATION
Division of Mines and Geology

The Turkey Flat site effects test area is one of a series of international test areas endorsed by the International Association of Physics of the Earth's Interior and the International Association of Earthquake Engineers.

Members of the Turkey Flat Site Effects Prediction Committee:

Dr. J. Carl Stepp (Chairman)
Electric Power Research Institute

Dr. C.Y. Chang
Geomatrix Consultants, USA

Dr. Neville C. Donovan
Dames & Moore, USA

Mr. James H. Gates
California Department of Transportation, USA

Dr. I.M. Idriss
University of California, Davis, USA

Dr. William B. Joyner
U.S. Geological Survey, USA

Dr. Marshall Lew
LeRoy Crandall and Associates, USA

Mr. Maurice S. Power
Geomatrix Consultants, USA

Mr. Charles R. Real
California Department of Conservation, USA

Mr. Bruce Redpath
Qest Consultants, USA

Dr. Wolfgang Roth
Dames & Moore, USA

Dr. Anthony F. Shakal
California Department of Conservation, USA

Dr. Jogeshwar P. Singh
Geospectra, USA

Dr. Brian E. Tucker
California Department of Conservation, USA

Mr. John Vrymoed
California Department of Transportation, USA

This report contains contributions in draft form and has not been edited to the standards of a formal publication. The views and conclusions contained in this document are those of the authors, and should not be interpreted as representing the official policies, either expressed or implied, of the State of California.

TURKEY FLAT, USA
SITE EFFECTS TEST AREA

Report 5

Weak-Motion Test: Statistical Analysis of Submitted Predictions and Comparisions to Observations

Prepared by

Chris H. Cramer and Charles R. Real

NOVEMBER 1990

TECHNICAL REPORT NO. 90-2
CALIFORNIA DEPARTMENT OF CONSERVATION
DIVISION OF MINES AND GEOLOGY
EARTHQUAKE SHAKING ASSESSMENT UNIT

Turkey Flat, USA
Site Effects Test Area

OVERVIEW

NEEDS The 1985 Mexico City and 1989 Loma Prieta earthquakes are our most recent reminders that local ground conditions can have a strong influence on where damage will occur in urbanized areas during an earthquake, and underscores the need to incorporate seismic shaking potential in land-use decisions. Although several different methods for making such assessments are currently in use, their accuracy and costs are not well known. Reliability and cost of methods must be known before they can be routinely used to provide a sound basis for safer land-use and construction practices.

GOALS The principal goals of the Turkey Flat Site Effects Test Area are to systematically compare and determine the reliability of contemporary methods used to estimate the effect of local geology on earthquake shaking, and to test the linearity of shallow stiff-soil site response.

OBJECTIVES Principal objectives are to collect high quality weak- and strong-motion data at several locations in the test area produced by local and regional earthquakes, quantify the site geology in terms of its geotechnical properties, and distribute the information to experts around the world.

APPROACH Using the acquired data, a series of "blind" predictions will be made by ground motion experts for test area locations where the response will be known, but not be available until all predictions have been received. Results of each prediction will be compared with one another and with actual observed ground motion.

PRODUCTS A series of reports describing each principal phase of the project will be available as the work progresses. An evaluation of all site response estimation methods will be prepared with recommendations as to suitability and cost of routine application for urban earthquake shaking hazard assessment.

Acknowledgments

Special recognition is due to the twenty-eight participants of the weak-motion blind prediction test, without which there would have been no test and no results to report. We also wish to thank the California Department of Conservation's Strong-Motion Instrumentation Program for assistance in processing the test data.

Most of all, we are grateful for the cooperation of Donald and Nila McCornack, owners of the land on which the Turkey Flat array is located.

TABLE OF CONTENTS

ILLUSTRATIONS

Figures

TABLES

Tables

FOREWORD

IASPEI/IAEE Joint Working Group

At the 1985 meeting of the International Association of Seismology and Physics of the Earth's Interior (IASPEI), held jointly with the International Association of Earthquake Engineering (IAEE) in Tokyo, Japan, a resolution was passed forming the IASPEI/IAEE Joint Working Group on The Effects of Surface Geology on Seismic Motion. The purpose of this group is to coordinate the establishment of an international series of test areas designed to provide a data base for comparing and testing contemporary methods, and developing new methods, to predict the effects of local geology on ground motion caused by earthquakes. The 1985 Michoacan and 1989 Loma Prieta earthquakes are only the most recent reminders that local ground conditions can have a major influence on where damage will occur in major earthquakes. Although methods for assessing site effects are being used to construct critical facilities around the world, the reliability of these methods has not been rigorously tested. It is the goal of this international program to fulfill this need. An international program provides a forum for experts around the world to exchange ideas, and significantly increases the prospects of acquiring the necessary data in a short time period.

Turkey Flat Experiment

The California Department of Conservation's Division of Mines and Geology (DMG) has, among other mandates, the responsibility to look after the interest of the State and its people with regard to seismic and geologic hazards and promote safe utilization of the State's terrain. Safety analyses of critical facilities such as nuclear power plants, liquid natural gas repositories, and hospitals, as well as provision of hazard information to local governments for planning and development, require application of state-of-the-art techniques in predicting ground motion expected from future earthquakes; however, contemporary methods have not been thoroughly validated. When asked why microzonation has not been implemented in the U.S., the answer is often: "If you ask ten different experts how the ground might shake at a specific site during an earthquake, you will get ten different answers." We see a strong need to identify those methods that are reliable and those that are not, and to establish guidelines and procedures that ensure repeatability, in order to effectively carry out DMG's mandates. As a consequence, we have established a test area at Turkey Flat, California, where a series of experiments will help answer this need.

Our general perceptions and experimental objectives echo

those of IASPEI/IAEE's Joint Working Group. In their first workshop, held during the XIX Assembly of the International Union of Geodesy and Geophysics in Vancouver, British Columbia, Canada in August of 1987, a resolution was passed incorporating the experiment at Turkey Flat into the international program.

The principal objectives of the Turkey Flat Experiment are to systematically test and compare all methods of estimating the influence of local geology on ground motion during earthquakes, in order to determine the reliability and cost effectiveness of each. Secondary objectives are to generate a database for the improvement of these methods, or the development of new methods, and to address the long-standing debate on the linearity of site response. The approach is to collect high quality weak and strong ground motion data, and geotechnical data, and carry out a series of "blind predictions." Experts from around the world are invited to use their preferred method and the acquired data to predict ground motion at locations where the actual response will be known but held in confidence until all predictions have been submitted.

The experiment is being conducted at a stiff-soil site and in a number of phases. This report constitutes a data report summarizing the results from phase IV, Weak-motion Blind

Prediction Test. A more detailed description of the overall experiment is provided in Report 1, Turkey Flat, USA, Site Effects Test Area: Needs, Goals and Objectives. A detailed description of the local site geology and geotechnical properties is provided in Report 2, Turkey Flat, USA, Site Effects Test Area: Site Characterization. A detailed description of the site effects blind prediction test phases at Turkey Flat is provided in Report 3, Turkey Flat, USA, Site Effects Test Area: Weak-Motion Test: Prediction Criteria and Input Rock Motions. Observations for the blind prediction test event are provided in Report 4, Turkey Flat, USA, Site Effects Test Area: Weak-Motion Test: Observed Seismic Response.

This report presents the results of a statistical analysis of the weak-motion predictions submitted during phase IV of the Turkey Flat experiment plus comparisons of those predictions to weak-motion observations. The report is composed of two principle sections: 1) a summary of results of the statistical analyses and comparisons with observations, and 2) a series of appendices containing all the plots of the analyses and comparisons performed. The emphasis is on presenting an overview of the submitted weak-motion predictions. The companion Report 6 presents all the weak-motion observations for Turkey Flat and the implications of the simple modeling of these observations done at DMG. Reports 5 and 6 will form a

basis for interpreting strong-motion results for Turkey Flat once strong-motion data are obtained.

Synopsis

A weak-motion site-effects blind prediction test for a stiff-soil site has been conducted at Turkey Flat, near Parkfield, California, in an effort to systematically compare contemporary methods used to estimate the effect of local geology on earthquake shaking, and to determine their reliability. The weak-motion test was conducted in two parts: the first using a surface bedrock record to predict response spectra, Fourier spectral ratios, and time histories across a shallow stiff-soil valley and the second using a valley-center downhole bedrock record to predict response spectra, Fourier spectral ratios, and time histories at the middle and surface of a 20m thick soil column. Predictors were required to submit predictions using the standard geotechnical model provided, but could also submit predictions based on their own preferred geotechnical model. Additionally, predictors were asked to provide uncertainty estimates for their predictions.

Twenty-eight individuals and groups from ten countries submitted predictions for the weak-motion blind prediction test. A statistical analysis of the submitted predictions and a comparison of predictions with observations provides the following results:

* Predictions submitted by participants tend to group together despite the variety of methods (8 classes of methods) and geotechnical models (1 standard, 6 preferred) used. The middle 50% of the submitted predictions tend to cluster within 10%, and occasionally within 50%, of the median of submitted predictions.

* Predictions tended to overestimate the actual observations, particularly at the valley center site. Overall shape and location of resonant peaks of predicted spectral ratios tend to reproduce observed spectral ratios, which suggests that velocities and layer thicknesses in the standard geotechnical model are reasonable for Turkey Flat. The overestimation of response amplitudes suggests that weak-motion damping values in the standard geotechnical model are too low.

* Uncertainties in peak value predictions provided by predictors tend to underestimate the average deviation of predicted values from the actual values, even for a given predictor's own results. The larger than expected deviations may be partly due to uncertainties in the Standard

Geotechnical Model.

In conclusion, comparison of observations with estimates of the weak-motion seismic response of a simple stiff-soil site suggests that, for this site class, accuracy of the geotechnical model used to characterize the site is more important than the particular method used to calculate the response.

Introduction

This part of the report provides a brief chronology of the weak-motion prediction test at Turkey Flat, describes the statistical methods used in the basic analysis of the submitted weak-motion predictions, and summarizes the results of the basic statistical analysis. The appendices provide the detailed plots for the comparisons summarized in this portion of the report.

Turkey Flat is located halfway between Los Angeles and San Francisco in the Central California Coast Range and near the San Andreas Fault just east of the town of Parkfield (Figure 1). The Turkey Flat, USA, Site Effects Test Area is located on a shallow, stiff-soil valley that is two kilometers in width. The four ground motion recording sites, two on rock and two in the valley, are shown in Figure 2. Figure 3 shows the seven surface and downhole sensor locations on cross-sections of the test site. Detailed geotechnical information is provided in Real (1988).

The weak-motion prediction test was conducted in two steps (Real and Cramer, 1989). First a weak-motion input time history recorded at the Rock South surface sensor R1 (Figures 2 and 3) was released to participants. Participants were asked to predict the time history for this event at Valley Center

Figure 1

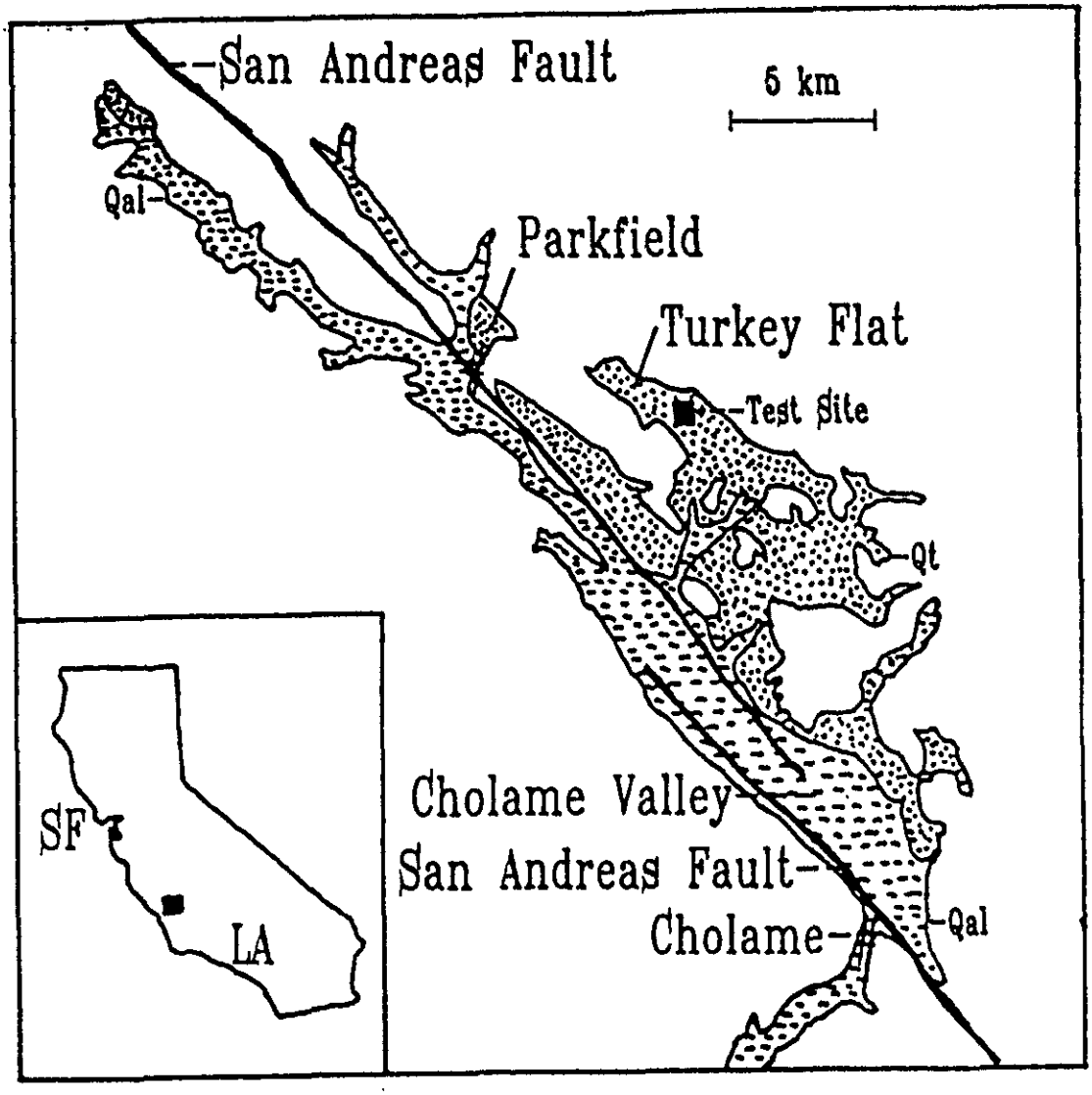

Location map for Turkey Flat Site Effects Test Area. Inset shows the location of the test area in Central California relative to San Francisco (SF) and Los Angeles (LA). The main map shows the location relative to Parkfield and the San Andreas Fault. Qal (dashed area) represents Quaternary alluvial deposits and Qt (dotted areas) represent Quaternary terrace deposits.

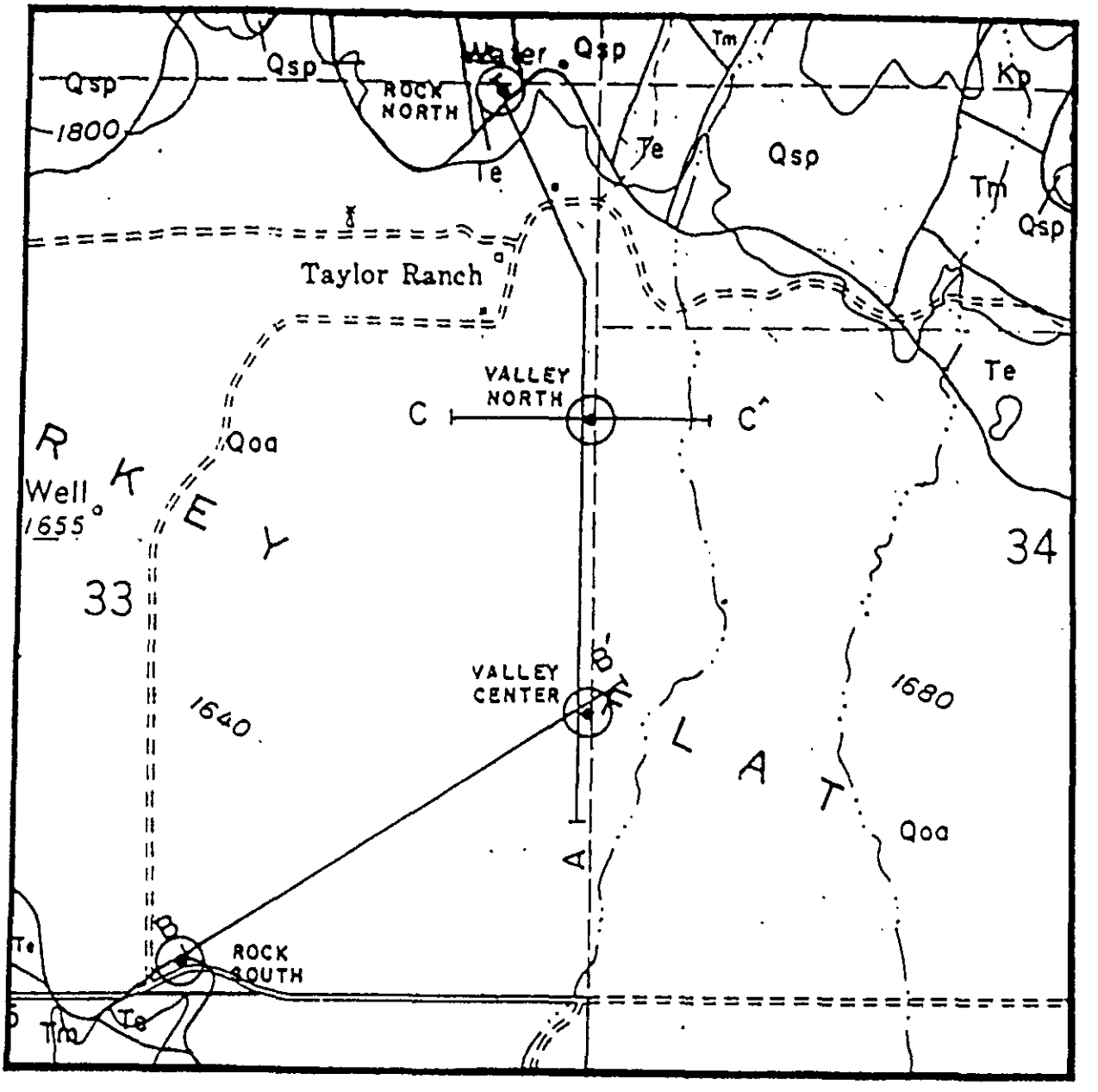

Figure 2. A map of the Turkey Flat Site Effects Test Area showing locations of the four ground motion recording sites, and three lines of profile that correspond to the cross sections shown in Figure 3. At these locations, numerous geophysical surveys and laboratory testing of rock and soil samples have been conducted for the purpose of characterizing the test area for analysis of ground response.

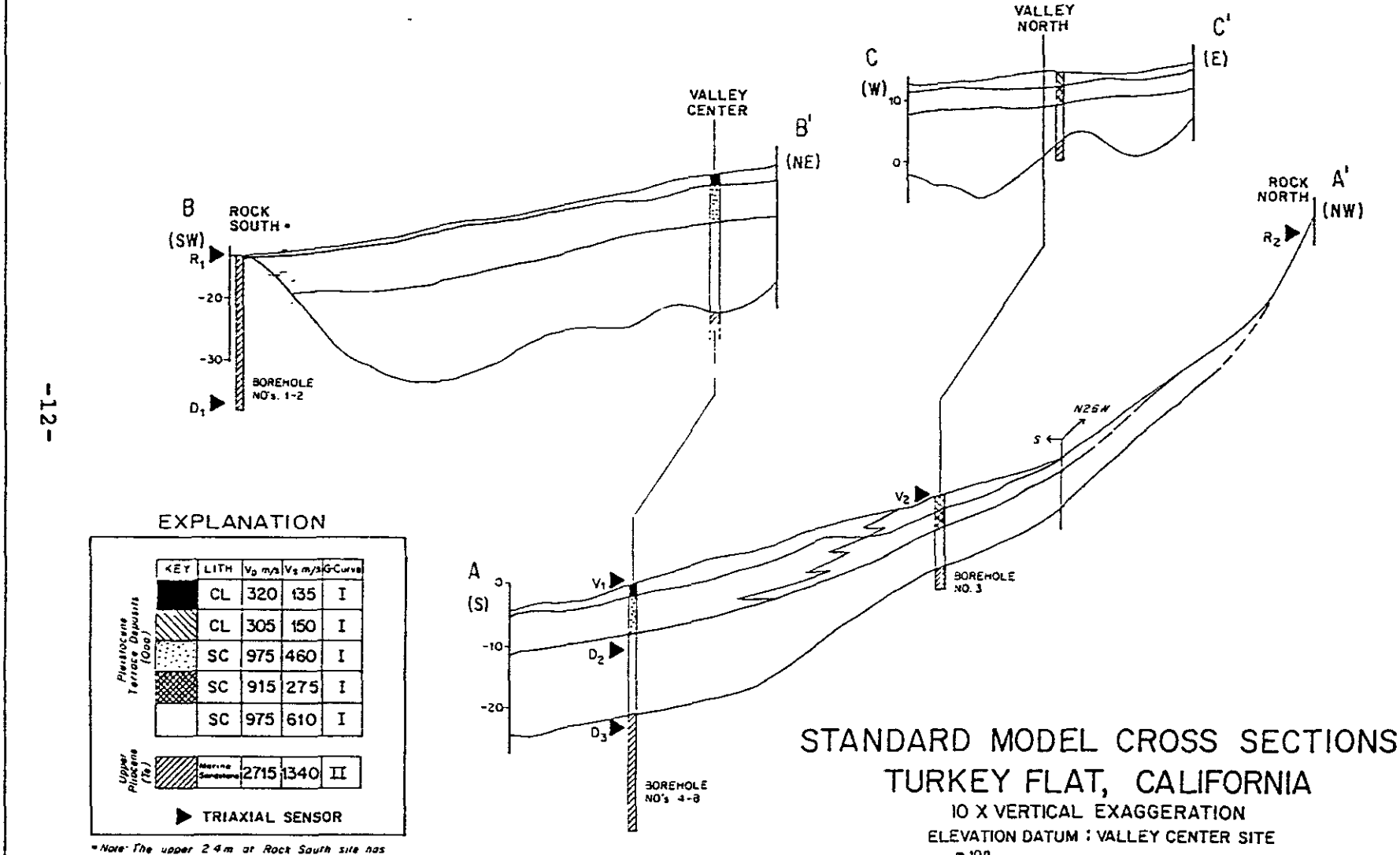
B
ROCK SOUTH *
(SW)
R1
-20
-30
D1
BOREHOLE NO's. 1-2
VALLEY CENTER
B'
(NE)
C
(W)
10
0
VALLEY NORTH
C'
(E)
ROCK NORTH
A'
(NW)
R2
N25W
S
V2
BOREHOLE NO. 3
A
(S)
0
-10
-20
V1
D2
D3
BOREHOLE NO's 4-8
EXPLANATION
KEY
LITH
Vp m/s
Vs m/s
G-Curve
CL 320 135 I
CL 305 150 I
SC 975 460 I
SC 915 275 I
SC 975 610 I
Pleistocene Terrace Deposits (Qog)
Upper Pliocene (Tp)
Marine Sandstone
2715 1340 II
TRIAXIAL SENSOR
* Note: The upper 2.4 m at Rock South site has Vp = 1980 m/s and Vs = 825 m/s.
STANDARD MODEL CROSS SECTIONS
TURKEY FLAT, CALIFORNIA
10 X VERTICAL EXAGGERATION
ELEVATION DATUM : VALLEY CENTER SITE
m 10
SCALE
100
200
300
400m

FIGURE 3

surface sensor V1 and to predict Fourier spectral ratios with respect to R1, response spectra, and peak values of acceleration, velocity, and displacement at the six remaining sensor locations D1, D2, D3, R2, V1, and V2. Additionally in the first step, an arbitrary strong-motion time history (Parkfield, 1966, Temblor 2, S25W record) was provided to participants, who could (at their option) provide predictions of the time history of Valley Center site V1 and all remaining (including V1) site response spectra, Fourier spectral ratios, and peak accelerations, velocities, and displacements assuming the arbitrary strong-motion record as the input ground motion at R1. The second step, conducted after the first step predictions were received, involved releasing to the participants the actual time history recorded at the Valley Center bottomhole (bedrock) sensor D3. In the second step participants were asked to predict only the time history at V1 plus Fourier spectral ratios with respect to D3, response spectra, and peak values of acceleration, velocity, and displacement at D2 and V1 (the other Valley Center sensor locations).

The chronology of the weak-motion prediction test went as follows: The R1 weak-motion record and arbitrary strong-motion record were mailed out in May 1989. R1 based predictions were originally due 1 September 1989, but the due date was extended first due to the slowness of

international mail delivery and then due to the occurrence of the 17 October 1989 M7.1 Loma Prieta earthquake in California. R1 based predictions were received in January and February 1990. The D3 weak-motion record was mailed out in late February 1990, and the D3 based predictions were received in June 1990.

Statistical Methods Used

Four statistical techniques and one data resampling technique were employed in the basic analysis and comparison of the submitted weak-motion predictions. Two statistical techniques, mean and standard deviations (submitted peak values only) and scatter plots, were used to depict the variability in predicted values and plots. Average deviations from actual peak values were compared to predictor's estimates of uncertainty to check the accuracy of peak value uncertainty estimates. Quartiles were used to demonstrate the consensus of the submitted predictions. Digital data files were not all submitted with the same sampling interval or with common sample values. Hence submitted prediction files were resampled using Wiggins' method (Wiggins, 1976) when statistical analyses were performed.

The mean and standard deviation (s.d.) of submitted peak values of acceleration, velocity, and displacement for each site were computed using standard formulas for samples from a population:

$$\text{mean} = \text{sum of values} / \text{number of values}$$

$$\text{s.d.} = [(\text{sumsqv} - \text{number} * \text{meansq}) / (\text{number} - 1)]^{1/2}$$

where sumsqv is the sum of the squared values and meansq is the mean squared.

The average deviation of submitted peak values from actual peak values of acceleration, velocity, and displacement were computed in the following manner (each horizontal component at a given station is treated as a separate station/component):

$$\%ad = \text{sum}[\text{abs}(pv_i - act_i) / act_i * 100.] / n$$

where %ad is the average deviation in percent, sum is a summation, abs is the absolute value, pv_i is the i'th station/component's predicted peak value, act_i is the i'th station/component's actual peak value, and n is the number of percent deviations in the summation. The observed standard deviation in the deviations of predicted peak values from actual peak values is given by

$$\%adsd = (\text{sum}([\text{abs}(pv_i - act_i) / act_i * 100.]^2) / n)^{1/2}$$

where %adsd is the observed standard deviation in percent.

Scatter plots of response spectra and Fourier spectral ratios were formed by plotting all received predictions for a given spectrum or ratio at a given site and for a given horizontal

component (east or north) on the same plot along with the corresponding observed spectrum or ratio. V1 time history predictions were compared with the V1 observations by placing them one below another, beneath the observed time histories and at a common fixed amplitude scale.

Quartiles (1st, median, and 3rd) were computed using the following formula for n discrete values v in ascending order:

$$Q_i = v_j + (r - j) * (v_{j+1} - v_j)$$

where i= 1,2, or 3 (the type of quartile being computed), the integer value j = i * (n+1) / 4, and the real value (with remainder) r = i * (n+1)/4. For response spectra and Fourier spectral ratios, quartile curves were generated by resampling predictions to a common set of sample points (response spectra) or a common sample interval (spectral ratios) and then computing quartile values for each common sample point. The series composed of a given quartile value at each common sample point becomes that quartile's spectra or ratio curve. Wiggins' (1976) resampling technique, as programed by Tull (1987), was employed in resampling response spectra and Fourier spectral ratios to common sample points for quartile analysis.

Summary of Results

This section of the report summarizes participation, types of predictions submitted, peak value statistics, comparisons among types of predictions, and conclusions reached. First a general review of participation and types of predictions submitted provides an overview for the analyses and comparisons presented. Next, a summary of analyses and comparisons is presented with supporting figures. Finally, this section closes with a summary of conclusions reached from the analyses performed for this report.

Predictions Submitted

Twenty-eight individuals and groups submitted one or more predictions based on input records at R1 and/or D3. Table 1 breaks out the participation by country. Participation is truly international in scale.

Tables 2 and 3 present a summary of numbers, types, and methods used for the R1 based predictions submitted. Twenty-six of the predictors in Table 1 submitted R1 based predictions (two submitted only D3 based predictions). Two predictors used more than one method and thus submitted more than one set of predictions based on the standard geotechnical model. Predictions based on the standard geotechnical model far

TABLE 1

Participation in Weak-Motion Prediction Test by Country

# of Participants	Country
1	Canada
3	China
2	Czechoslovakia
3	France
1	Germany
1	Italy
7	Japan
1	Mexico
1	New Zealand
8	United States
Total: 28	

TABLE 2

Number of Predictions by Type
for
R1 Test Record Based Predictions

Predictors Submitting R1 Predictions	26	
Types of Predictions Received	Required	Optional
Standard Geotechnical model	29	8
Preferred Geotechnical model	6	1

TABLE 3

Number of Predictions by Method
for
R1 Test Record Based Predictions

1D Methods:	Total #: 17
Equivalent linear methods: SIREN Linear viscoelastic EQLM SHAKE--LAYSOL, DESRA2, DYNA1D	8
Spectral methods: Boore (1983) stochastic Semi-analytic w/ plane & anti-plane wave calculations Stochastic w/ SH-wave propagators	3
Haskell-like methods: Haskell's method Discrete wavenumber boundary element method Sanchez-Sesma's hybrid ray theory/Haskell method	3
Wave propagation methods: Finite-difference Frequency-wavenumber Propagator matrix with source effect	3
2D Methods:	**Total #: 9**
Finite element methods Non-linear hysteretic model 2D elastic 2D viscoelastic 2D elastoplastic 2D F.E.M. (properties not given)	5
Wave propagation method Discrete wavenumber Haines' new technique	3
Boundary element method MISS2D	1
3D Methods:	**Total #: 2**
Wave propagation method: 3D viscoelastic	2
Not stated as 1D or 2D:	**Total #: 1**
Unknown method	1

outnumber predictions based on a predictor's preferred geotechnical model and consequently are the only group large enough for meaningful statistical comparisons. In Table 3 the required predictions based on the standard model are broken down into groups of one-dimensional (1D), two-dimensional (2D), and three-dimensional (3D) modeling methods with brief method descriptions provided for each group. Numbers of predictions were insufficient for statistical comparison of each method, but 1D methods can be compared with 2D/3D methods.

Tables 4 and 5 provide the same summary as Tables 2 and 3 only for submitted predictions based on the weak-motion record at D3. Eighteen of the predictors in Table 1 submitted D3 based predictions. Two predictors used two variations in method and thus submitted two sets of D3 based predictions (not the same two that submitted more than one set of R1 based predictions). Again, for predictions based on the D3

TABLE 4

Number of Predictions by Type
for
D3 Test Record Based Predictions

Predictors submitting D3 Predictions	18
Types of Predictions Received	Required
Standard Geotechnical Model	20
Preferrred Geotechnical Model	6

TABLE 5

Number of Predictions by Method
for
D3 Test Record Based Predictions

1D Methods:	Total #: 11
Equivalent linear methods: SIREN Linear viscoelastic EQLM SHAKE	5
Spectral method: Boore (1983) stochastic	2
Haskell-like methods: Discrete wavenumber boundary element method Sanchez-Sesma's hybrid ray theory/Haskell method	2
Wave propagation methods: Finite-difference Propagator matrix with source effect	2
2D Methods:	**Total #: 9**
Finite element methods: Non-linear hysteretic model 2D F.E.M. (properties not given)	2
Wave propagation methods: Discrete wavenumber Finite Difference Haines' New Technique	7

record, use of the standard geotechnical model far surpassed the use of preferred geotechnical models. Numbers of D3 based predictions in subgroups other than those using the standard model are too small for statistical comparisons.

Based on the summaries provided in Tables 2 through 5, the submitted predictions were grouped into the following sets for statistical comparisons: 1) R1 required standard model weak-motion predictions, 2) R1 preferred model weak-motion predictions (numbers insufficient for statistical comparisons), 3) R1 optional strong-motion predictions (arbitrary record as input and combining predictions using both the standard and a predictor's preferred model), 4) D3 weak-motion predictions (standard and preferred model predictions combined), 5) R1 standard model weak-motion predictions using 1D methods, and 6) R1 standard model weak-motion predictions using 2D or 3D methods. For each of the above listed six groups, response spectra and Fourier spectral ratio scatter plots and quartile vs observation plots have been made (see appendices). V1 time history comparison plots were also made for the first four groups listed above. Quartiles, means, standard deviations, and average deviations from actual values have been computed at each horizontal sensor for submitted peak values of acceleration, velocity, and displacement for both R1 and D3 predictions. Additionally, a descriptive comparison of a predictor's preferred model

prediction with their required standard model prediction has been carried out for each R1 and D3 preferred model prediction submitted.

Results

Peak Value Predictions

Figures 4 and 5 summarize the number, quartile, mean, and standard deviation statistics for peak accelerations, velocities, and displacements submitted for both steps of the weak-motion prediction test. For comparison, actual observed values are also plotted. Sample sizes vary from 16 to 23. Results are given for each horizontal component (east and north) at each requested sensor location (V1, V2, D1, D2, D3, and R2 for R1 based predictions in Figure 4 and V1 and D2 for D3 based predictions in Figure 5). In general, the submitted predictions tend to over-predict the peak values, particularly for R1 based predicted peak accelerations and for Valley Center (V1) predictions. Predictions generally match actual values at downhole (D1, D2, D3) and Rock North (R2) locations. Variability in predicted peak values, as indicated by standard deviations of 10 - 70 percent, is fairly large. But a majority of the predicted peak values tend to group together: Q_3 minus Q_1 variation (middle 50%) is usually <10% and occasionally up to 50%. **This indicates that predictors tend to get similar results regardless of method used.**

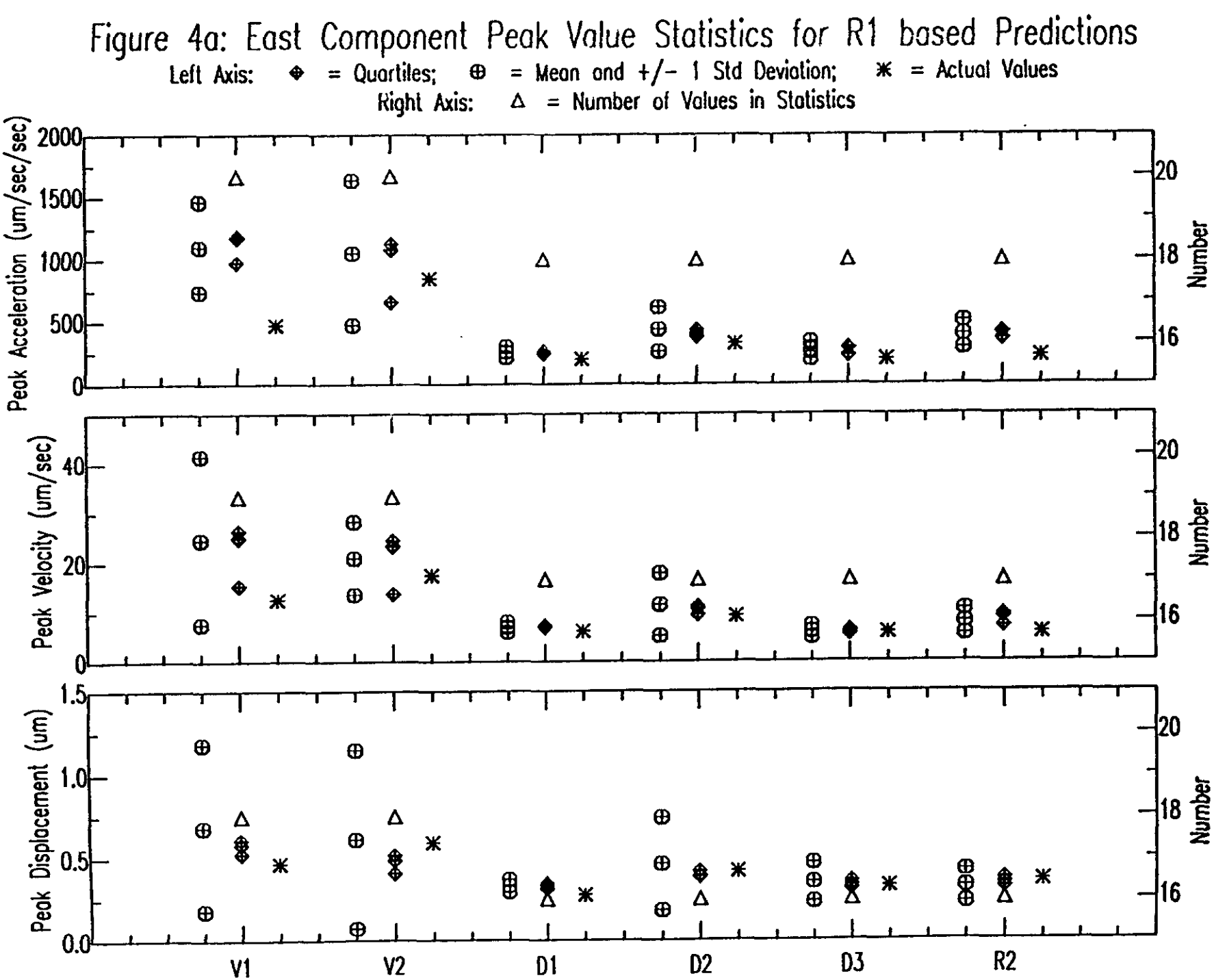
Figure 4a: East Component Peak Value Statistics for R1 based Predictions
Left Axis: ◆ = Quartiles; ⊕ = Mean and +/- 1 Std Deviation; ✱ = Actual Values
Right Axis: △ = Number of Values in Statistics
Peak Acceleration (um/sec/sec)
2000
1500
1000
500
0
Peak Velocity (um/sec)
40
20
0
Peak Displacement (um)
1.5
1.0
0.5
0.0
Number
20
18
16
V1
V2
D1
D2
D3
R2

Figure 4b: North Component Peak Value Statistics for R1 based Predictions

Left Axis: ◆ = Quartiles; ⊕ = Mean and +/- 1 Std Deviation; ✱ = Actual Values

Right Axis: △ = Number of Values in Statistics

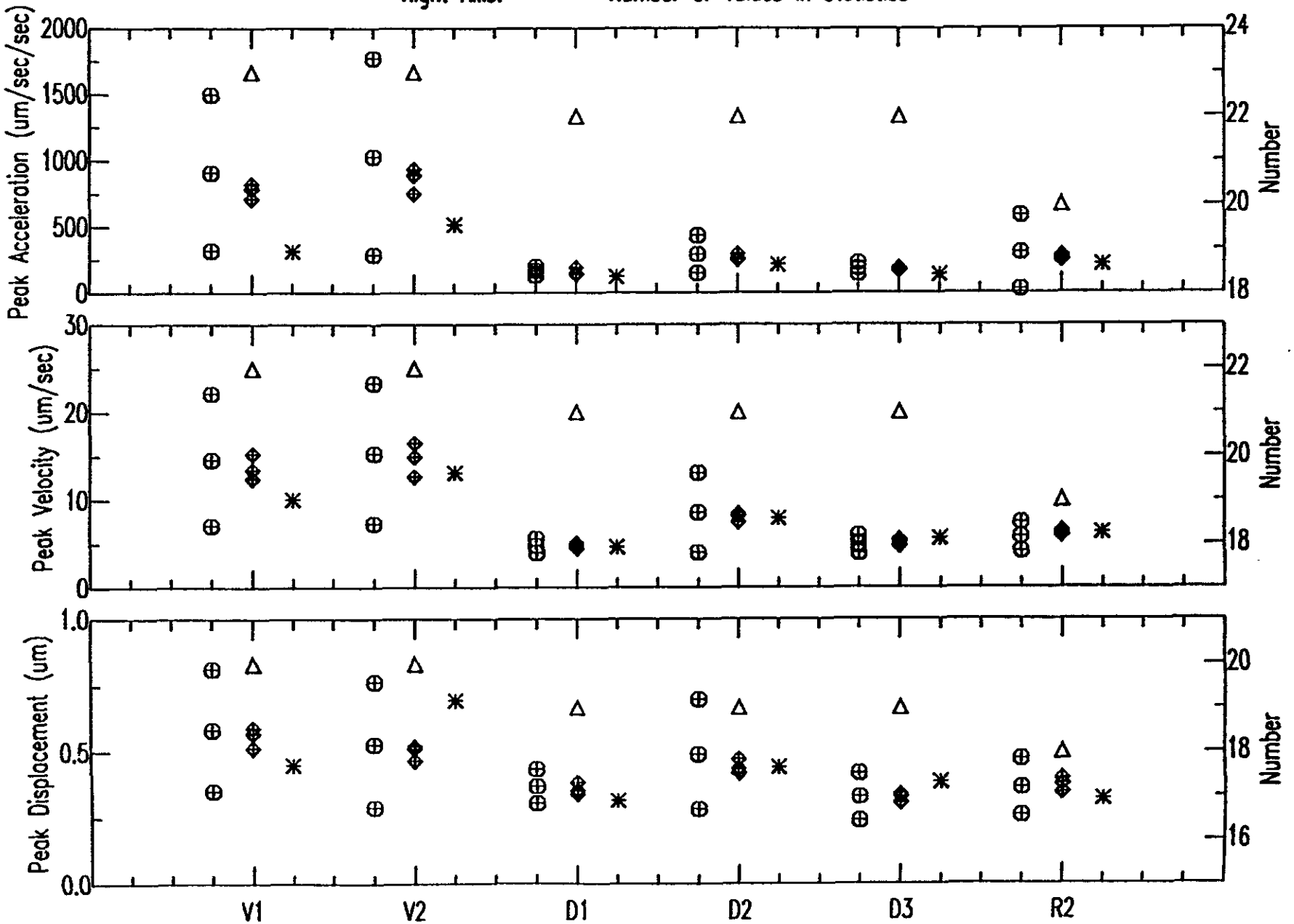

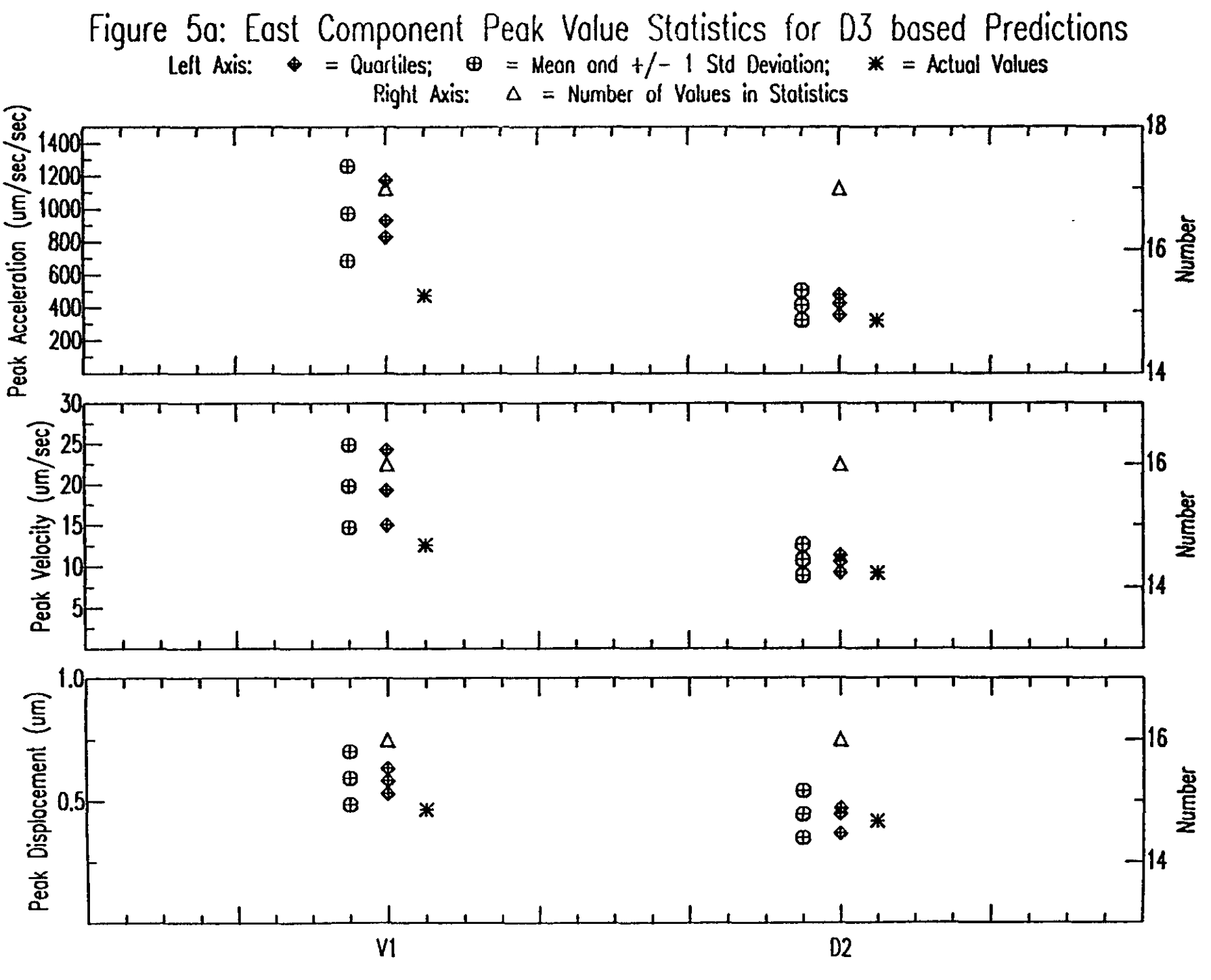
Figure 5a: East Component Peak Value Statistics for D3 based Predictions
Left Axis: ◆ = Quartiles; ⊕ = Mean and +/- 1 Std Deviation; ✱ = Actual Values
Right Axis: △ = Number of Values in Statistics
Peak Acceleration (um/sec/sec)
1400
1200
1000
800
600
400
200
18
16
14
Number
Peak Velocity (um/sec)
30
25
20
15
10
5
16
14
Number
Peak Displacement (um)
1.0
0.5
16
14
Number
V1
D2

Figure 5b: North Component Peak Value Statistics for D3 based Predictions

Left Axis: ◆ = Quartiles; ⊕ = Mean and +/- 1 Std Deviation; ✱ = Actual Values

Right Axis: △ = Number of Values in Statistics

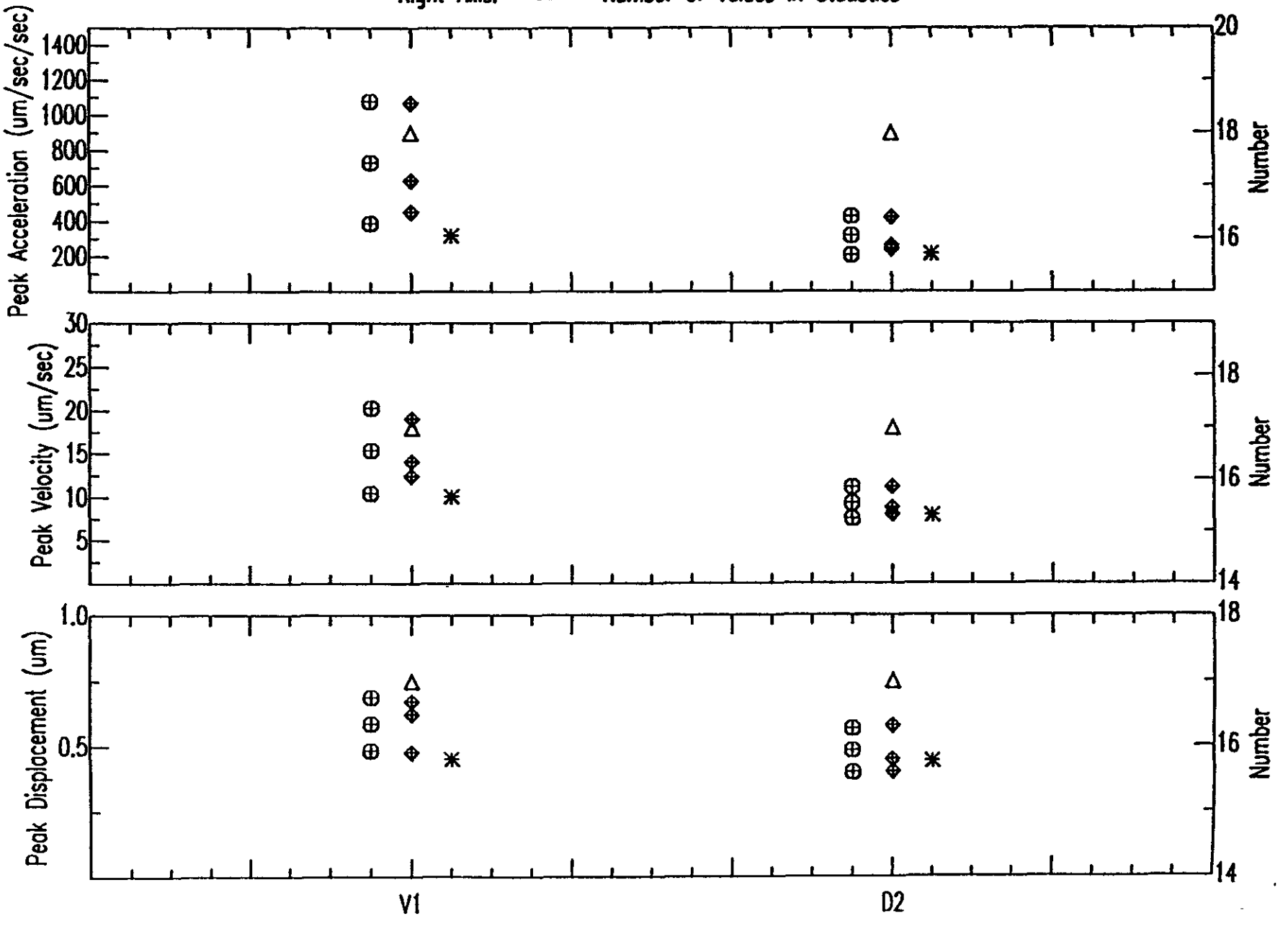

Uncertainty Predictions

Predictors were also asked to submit estimates of uncertainty in their acceleration, velocity, and displacement peak value predictions. Table 6 lists the six estimates of peak value uncertainties received for R1 predictions and the six estimates received for D3 predictions. For R1 predictions, predictors' estimates of peak value uncertainty range from 5 to 50%; for D3 predictions, predictors' estimates of peak value uncertainty range from 10 to 50%. Figures 6 and 7 compare individual predictor's estimates of uncertainty with the quartiles and mean and s.d. of the deviations of their predicted peak values from actual peak values for R1 and D3 predictions. Average deviations from actual peak values for predictors submitting uncertainty estimates range from 13 - 160% (Table 7). Figures 8 and 9 compare quartiles and mean and s.d. of submitted uncertainty estimates with quartiles and mean and s.d. of deviations from actual peak values by site for all R1 and D3 predictions. Average deviations from actual peak values for all predictors range from 3 - 185% (Table 8). **Although uncertainties in the Standard Geotechnical Model may contribute to the observed deviations, predictors' uncertainty estimates generally underestimate the actual deviations of their predictions from actual peak values, particularly for peak acceleration!**

Table 6

Submitted Uncertainty Estimates (in %)
for Peak Value Predictions

R1 Predictions:

Predictor	Acceleration	Velocity	Displacement
#86	50.	50.	50.
#95	10.	10.	10.
#105	10.	5.	5.
#123	10.	10.	10.
#135	20.	20.	20.
#145	5.	5.	5.
Mean(sd)*	17.5(16.7)	16.7(17.2)	16.7(17.2)

D3 Predictions:

Predictor	Acceleration	Velocity	Displacement
#86	50.	50.	50.
#93	15.	15.	15.
#95	10.	10.	10.
#105	10.	5.	5.
#123	10.	10.	10.
#135	20.	20.	20.
Mean(sd)*	19.2(15.6)	18.3(16.3)	18.3(16.3)

* Mean with standard deviation in parentheses

Figure 6: Predictors' Uncertainty Estimates for R1 based Predictions

Deviations from Actual Peak Values: ◆ = Quartiles; ⊕ = Mean and +/- 1 Std Deviation

Predictors' Estimates: ✳ = Individual Estimate; △ = Quartiles; ⊞ = Mean and +/- 1 Std Deviation

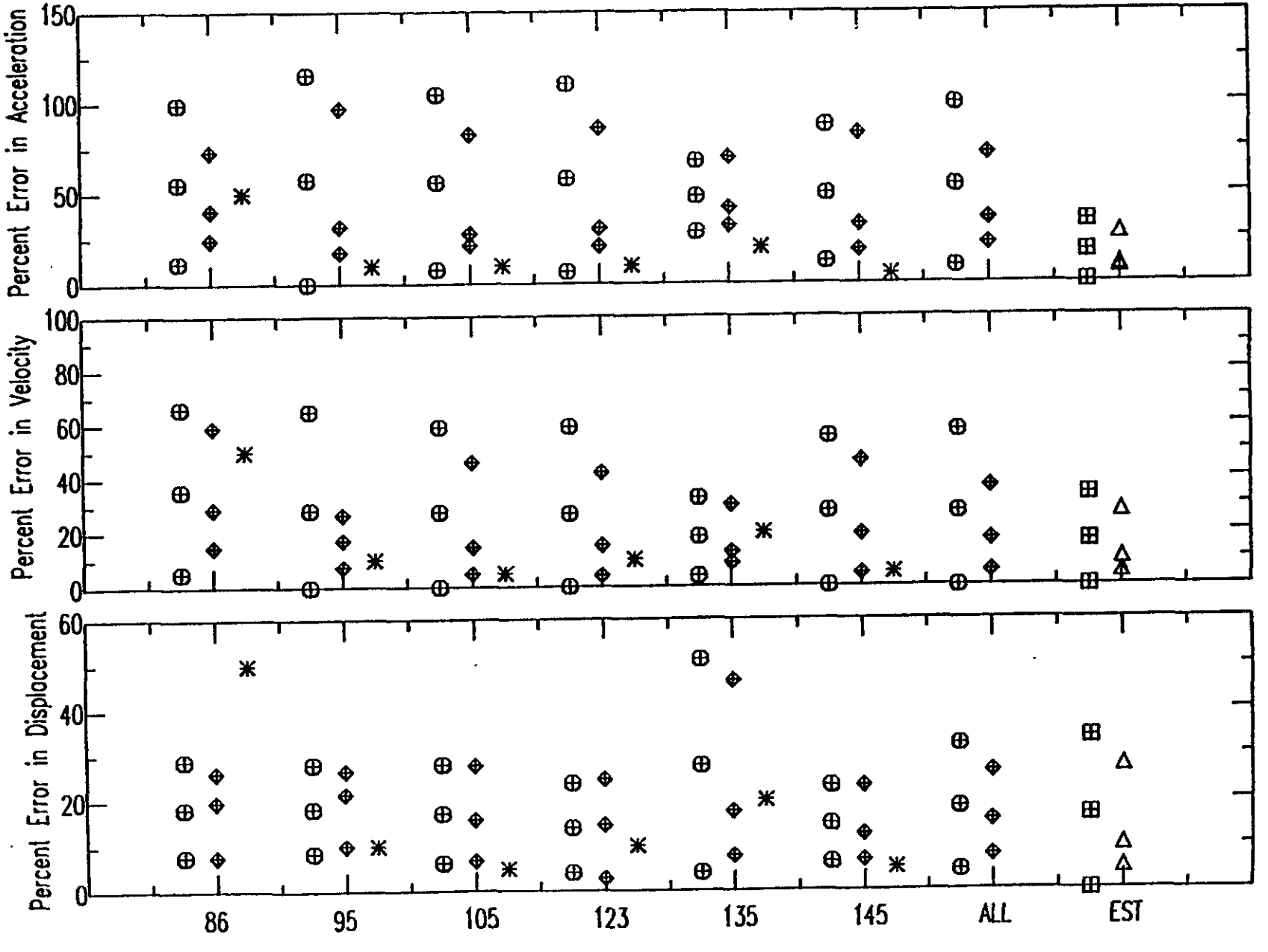

Figure 7: Predictors' Uncertainty Estimates for D3 based Predictions

Deviations from Actual Peak Values: ◆ = Quartiles; ⊕ = Mean and +/- 1 Std Deviation

Predictors' Estimates: ✳ = Individual Estimate; △ = Quartiles; ⊞ = Mean and +/- 1 Std Deviation

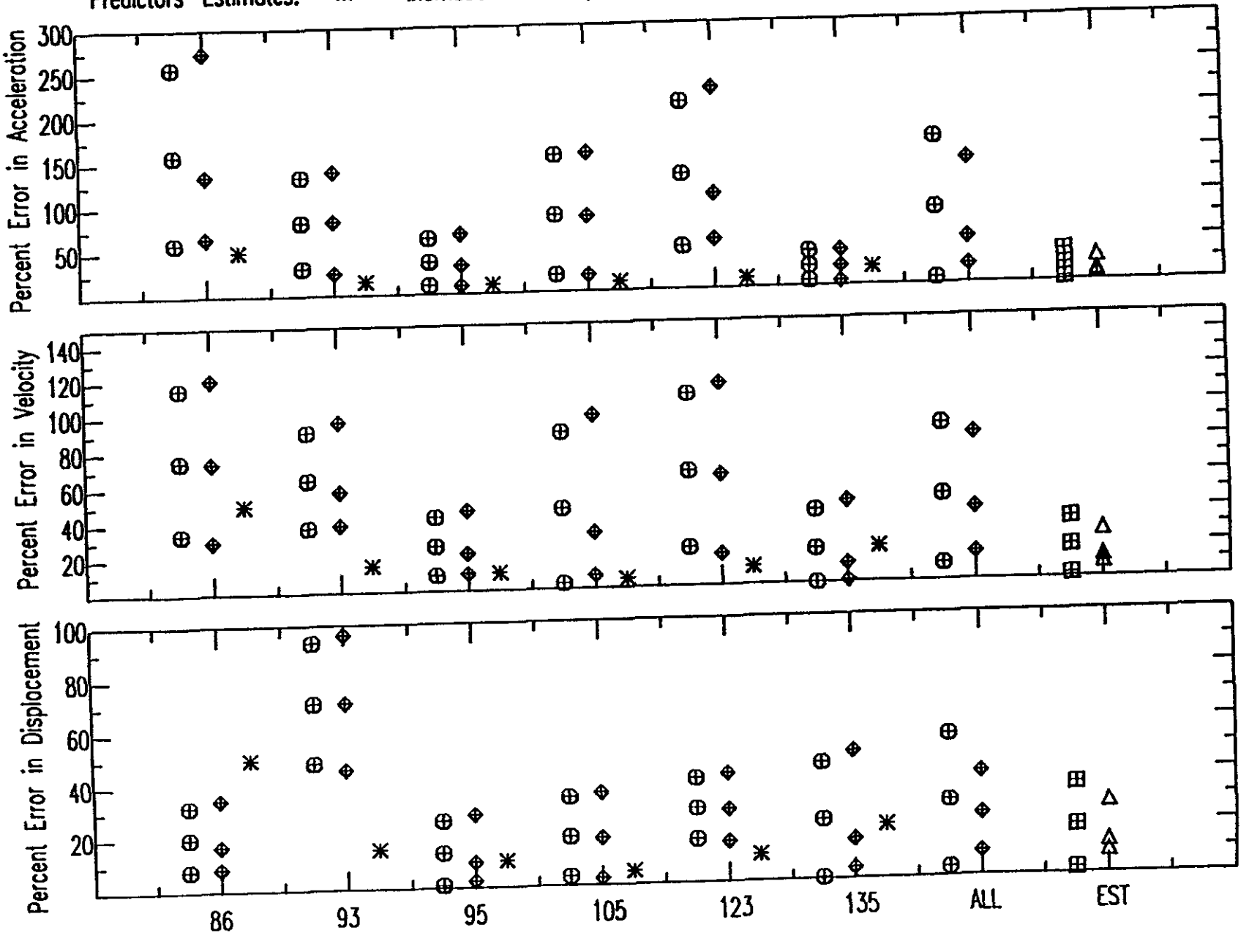

Table 7

Percent Average Deviation* from Actual Peak Values for Predictors Submitting Uncertainty Estimates

R1 Predictions:

Predictor	Acceleration	Velocity	Displacement
#86s	55.5 (12)	35.7 (12)	18.3 (12)
#95s	57.8 (12)	28.5 (12)	18.3 (12)
#105s	56.2 (12)	27.7 (12)	17.1 (12)
#123s	58.4 (12)	27.0 (12)	13.9 (12)
#135s	48.1 (12)	18.2 (12)	27.6 (12)
#145s	49.6 (12)	27.6 (12)	14.6 (12)
Whole Group	54.2 (72)	27.4 (72)	18.3 (72)

D3 Predictions:

Predictor	Acceleration	Velocity	Displacement
#86s	158.0 (4)	74.8 (4)	20.1 (4)
#93s	82.3 (4)	64.0 (4)	71.0 (4)
#95s	36.2 (4)	25.6 (4)	13.2 (4)
#105s	86.4 (4)	45.7 (4)	18.6 (4)
#123s	129.2 (4)	65.0 (4)	28.0 (4)
#135s	22.4 (4)	19.5 (4)	22.5 (4)
Whole Group	85.8 (24)	49.1 (24)	28.9 (24)

* Number in parentheses following % average deviation values is number of predicted peak values in that average.

Figure 8a: East Component Uncertainty Statistics for R1 based Predictions

Deviations from Actual Peak Values: ◆ = Quartiles; ⊕ = Mean and +/- 1 Std Deviation

Predictors' Estimates: ✱ = Quartiles; ⊞ = Mean and +/- 1 Std Deviation

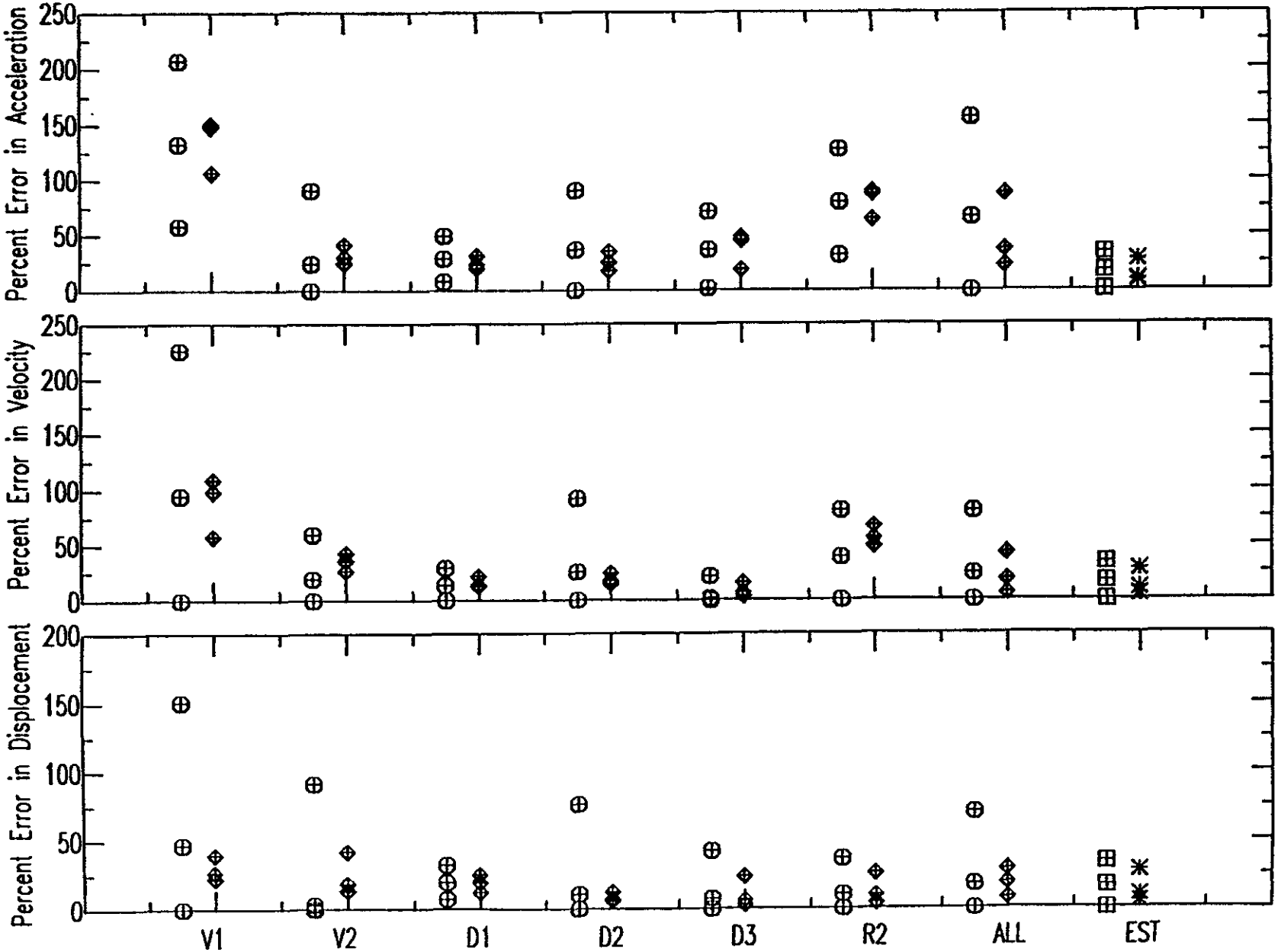

Figure 8b: North Component Uncertainty Statistics for R1 based Predictions

Deviations from Actual Peak Values: ◆ = Quartiles; ⊕ = Mean and +/- 1 Std Deviation

Predictors' Estimates: ✳ = Quartiles; ⊞ = Mean and +/- 1 Std Deviation

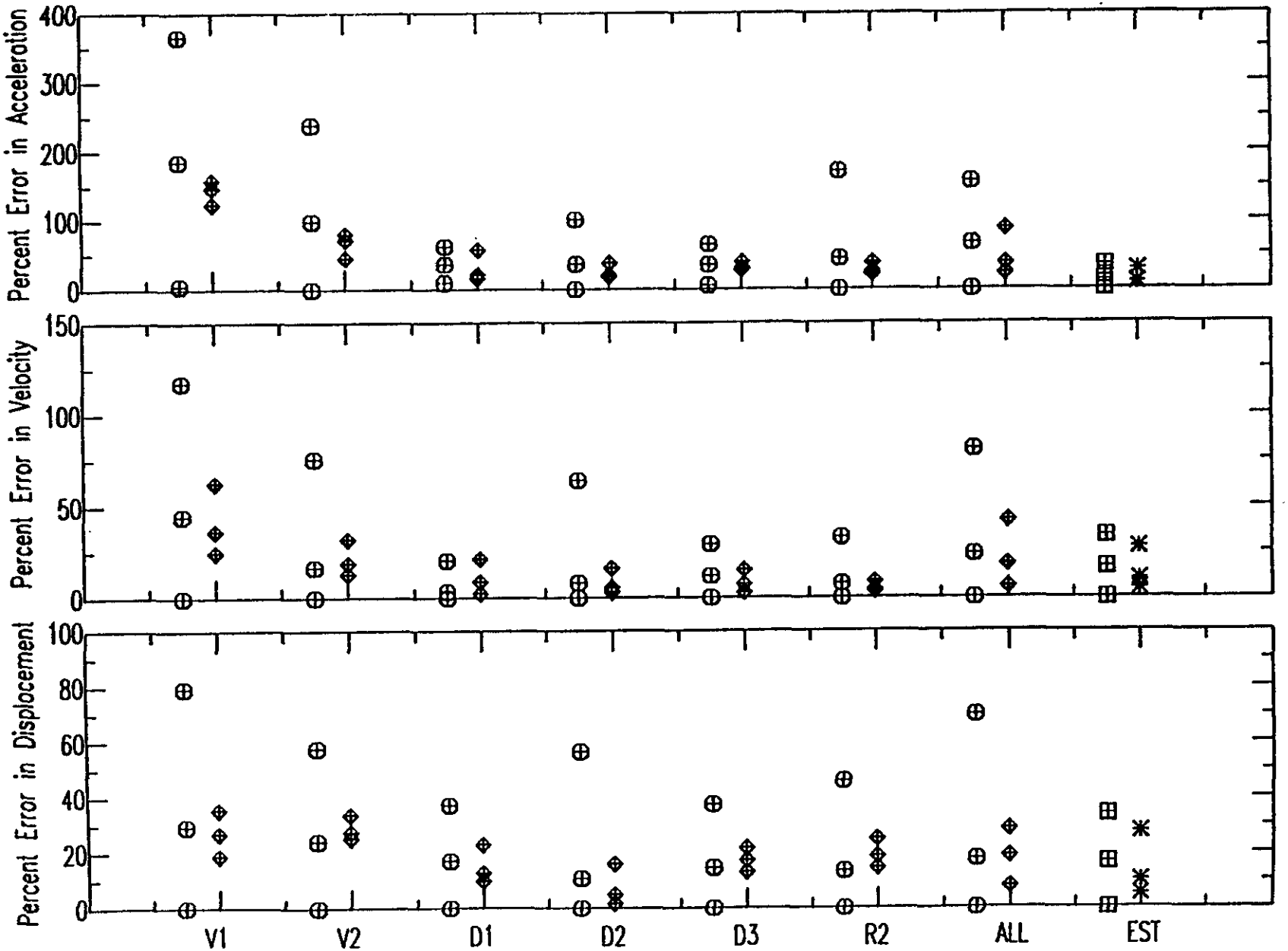

Figure 9a: East Component Uncertainty Statistics for D3 based Predictions

Deviations from Actual Peak Values: ◆ = Quartiles; ⊕ = Mean and +/- 1 Std Deviation

Predictors' Estimates: ✱ = Quartiles; ⊞ = Mean and +/- 1 Std Deviation

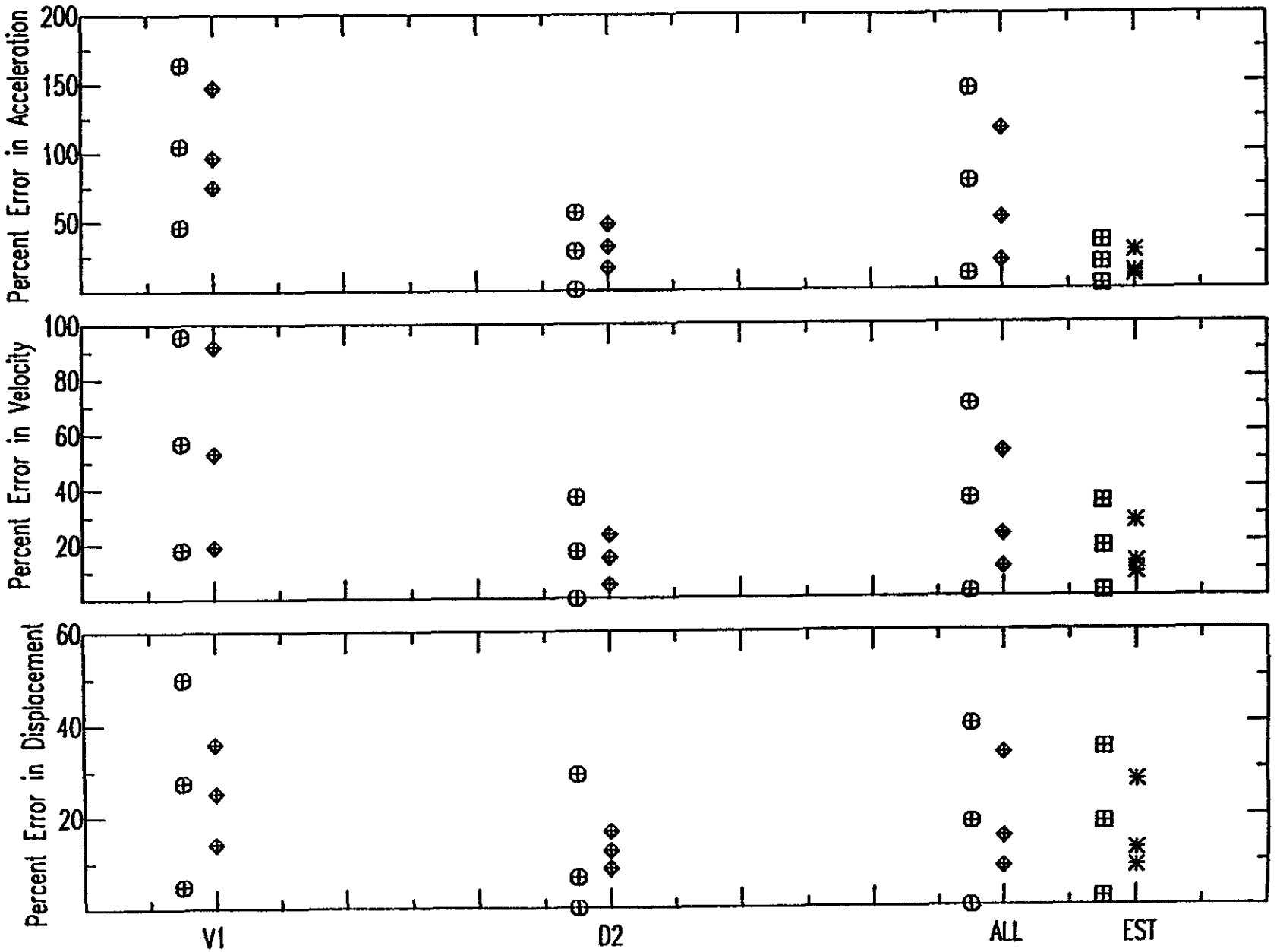

Figure 9b: North Component Uncertainty Statistics for D3 based Predictions

Deviations from Actual Peak Values: ⊕ = Quartiles; ⊕ = Mean and +/- 1 Std Deviation

Predictors' Estimates: ✳ = Quartiles; ⊞ = Mean and +/- 1 Std Deviation

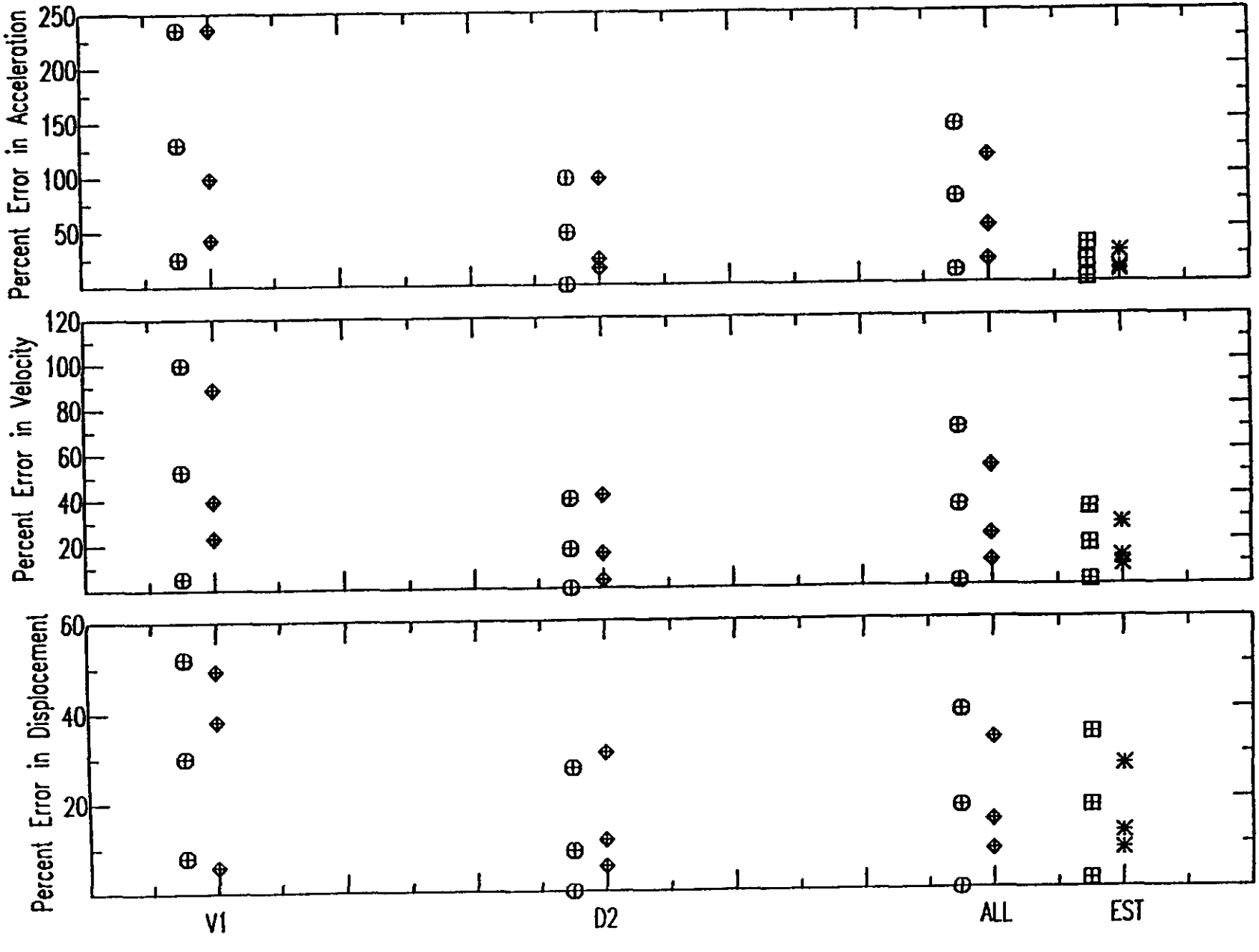

Table 8

Percent Average Deviation* from Actual Peak Values for All Predictors

R1 Predictions:

Sensor Location		Acceleration	Velocity	Displacement
V1	N	185.6 (23)	44.8 (22)	29.5 (20)
	E	132.6 (20)	94.9 (19)	46.8 (18)
V2	N	98.8 (23)	16.5 (22)	24.2 (20)
	E	24.2 (20)	19.4 (19)	3.3 (18)
D1	N	35.6 (22)	3.4 (21)	17.1 (19)
	E	28.7 (18)	13.6 (17)	19.8 (16)
D2	N	35.8 (22)	8.0 (21)	10.9 (19)
	E	36.1 (18)	25.4 (17)	10.9 (16)
D3	N	34.8 (22)	11.8 (21)	14.7 (19)
	E	36.6 (18)	2.2 (17)	7.8 (16)
R2	N	43.7 (20)	7.5 (19)	13.4 (18)
	E	79.5 (18)	38.7 (17)	10.6 (16)
Whole Group:		66.2 (244)	23.8 (232)	17.7 (215)

D3 Predictions:

Sensor Location		Acceleration	Velocity	Displacement
V1	N	130.4 (18)	52.5 (17)	30.0 (17)
	E	105.3 (17)	56.9 (16)	27.5 (16)
D2	N	48.0 (18)	17.5 (17)	9.1 (17)
	E	28.7 (17)	17.2 (16)	6.8 (16)
Whole Group:		78.4 (70)	36.0 (66)	18.4 (66)

* Number in parentheses following % average deviation values is number of predicted peak values in that average.

Spectral Predictions

Figures 10 - 13 compare observations with scatter plots and quartile plots of Fourier spectral ratios and response spectra predictions at V1 and V2, based on the weak-motion input record at R1 and the standard geotechnical model. Figure 11 shows the actual Fourier spectral ratio for the weak-motion test event, the mean and +/- one s.d. spectral ratios of all 33 weak-motion events (see Cramer, 1991), and the quartiles of the submitted R1 standard model predictions. The mean and +/- one s.d. spectral ratios give some indication of the stability of site response (this is discussed in greater detail in Cramer, 1991). The scatter plots (Figures 10 and 12) show the tendency of many predictions to group together as well as the great variability of some predictions within this grouping. The quartile plots (Figures 11 and 13) also show a tendency for V1 predictions to have larger than observed amplitudes and to have greater variance from the observed above 5 Hz (below .2 sec). V2 predictions seem to fit the observations fairly well. **Response spectra quartile plots (Figure 13) indicate that displacements tend to be predicted better than accelerations, particularly for V1.**

The effect of time domain window size on resulting spectral ratios has been pointed out by two participants in this experiment (Guo-Ming Xu, written communication, 1990; A.C. Heidebrecht, oral communication, 1990). Different time domain

Figure 10: R1 Fourier Spectral Ratio Predictions for Standard Geotechnical Model

Solid lines - Predictions; Dashed line - Observation

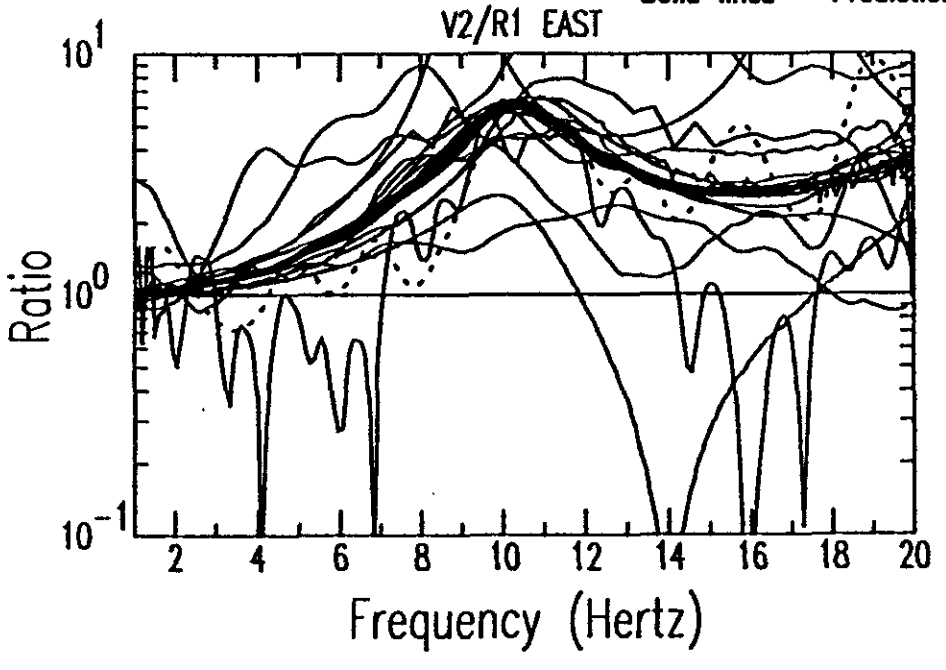

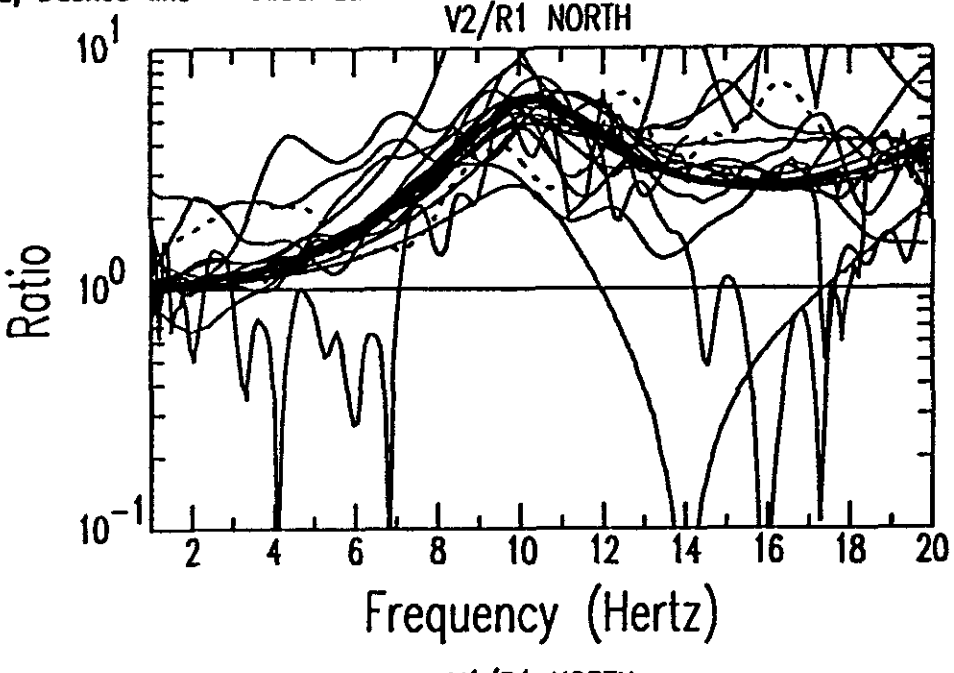

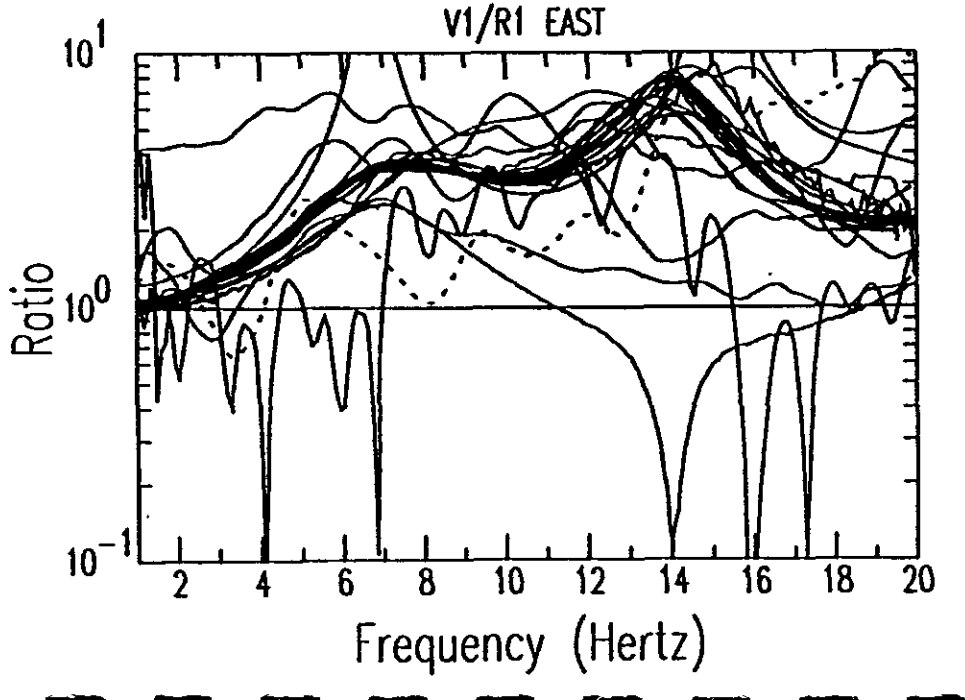

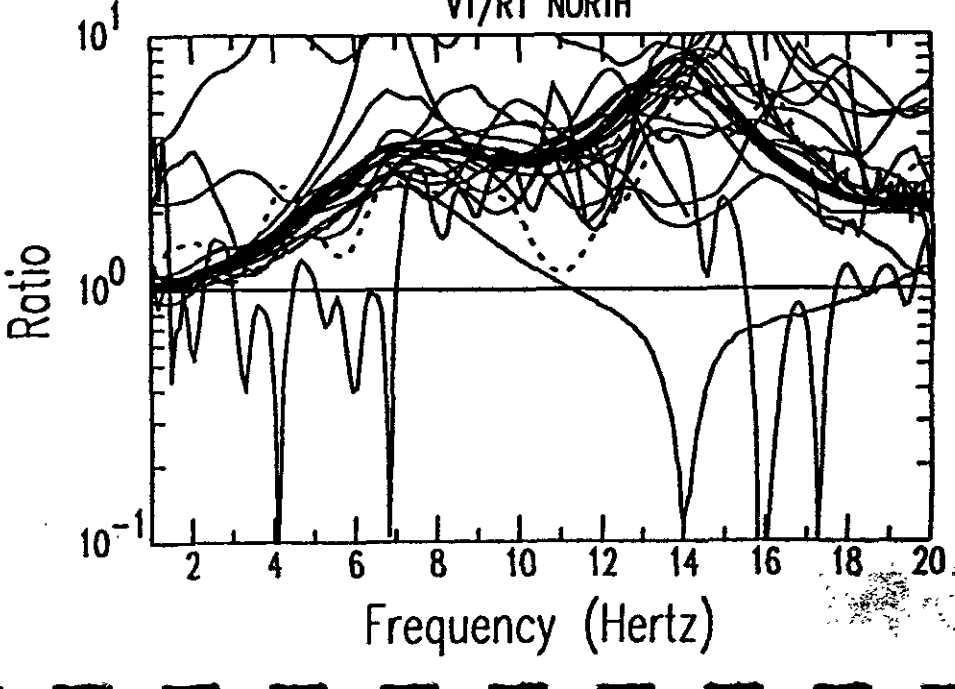

Figure 11: R1 Standard Model Spectral Ratio Prediction Quartiles vs Observations

Spectral Ratio Predictions: Dashed – quartiles

Observations: Solid – weak-motion test event; Dash-dotted – weak-motion mean; Dotted – 1 std deviation

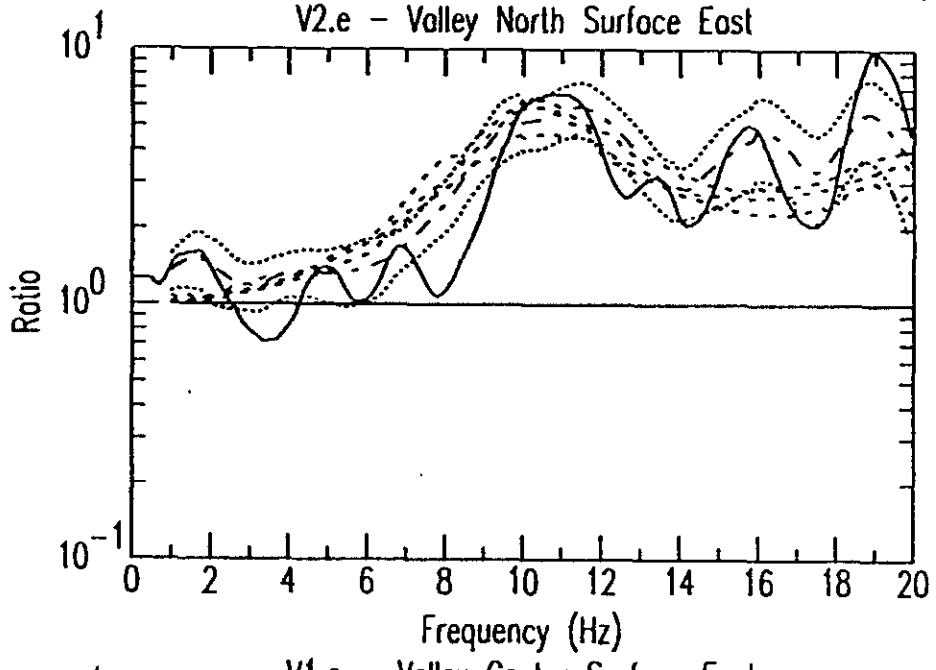

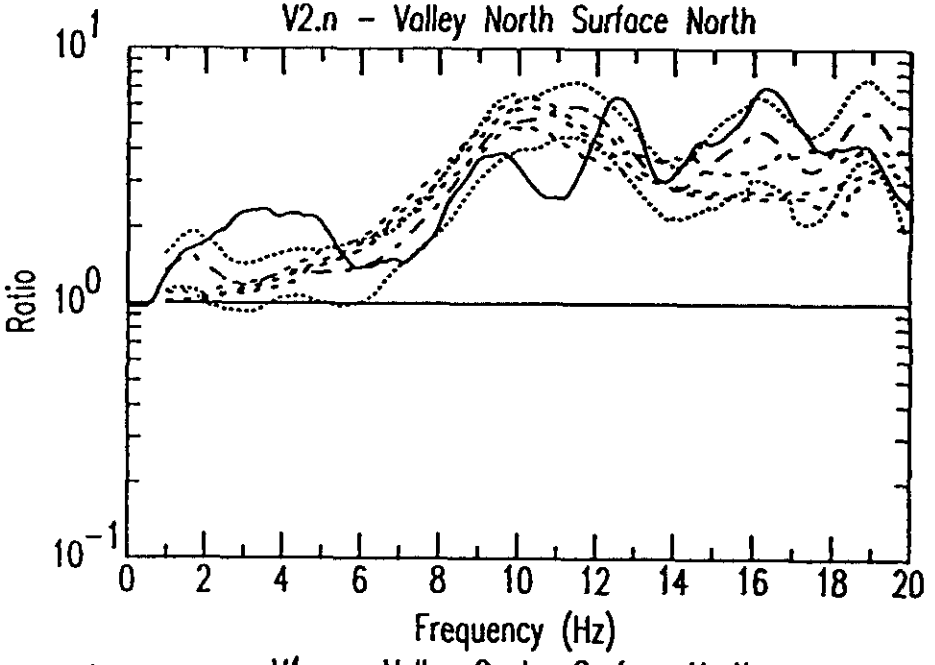

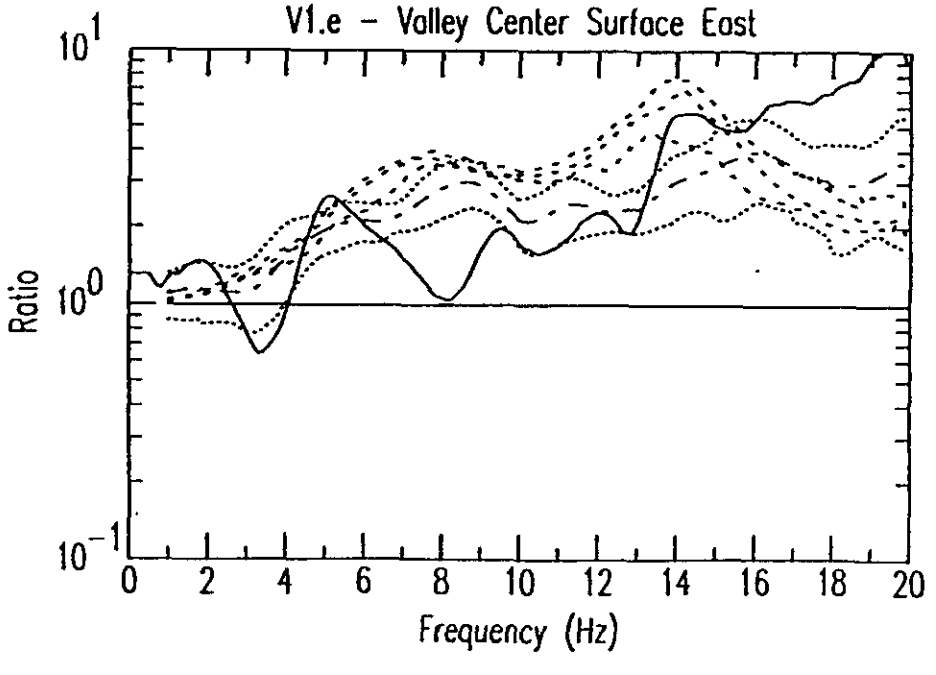

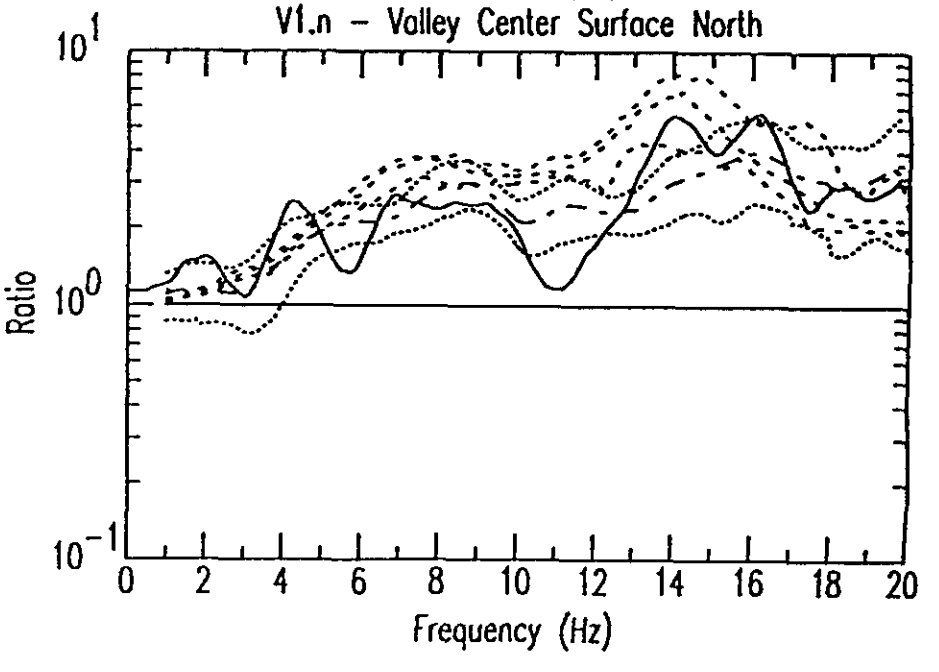

Figure 12: R1 Response Spectra Predictions for Standard Geotechnical Model

Solid lines – Predictions; Dashed line – Observed

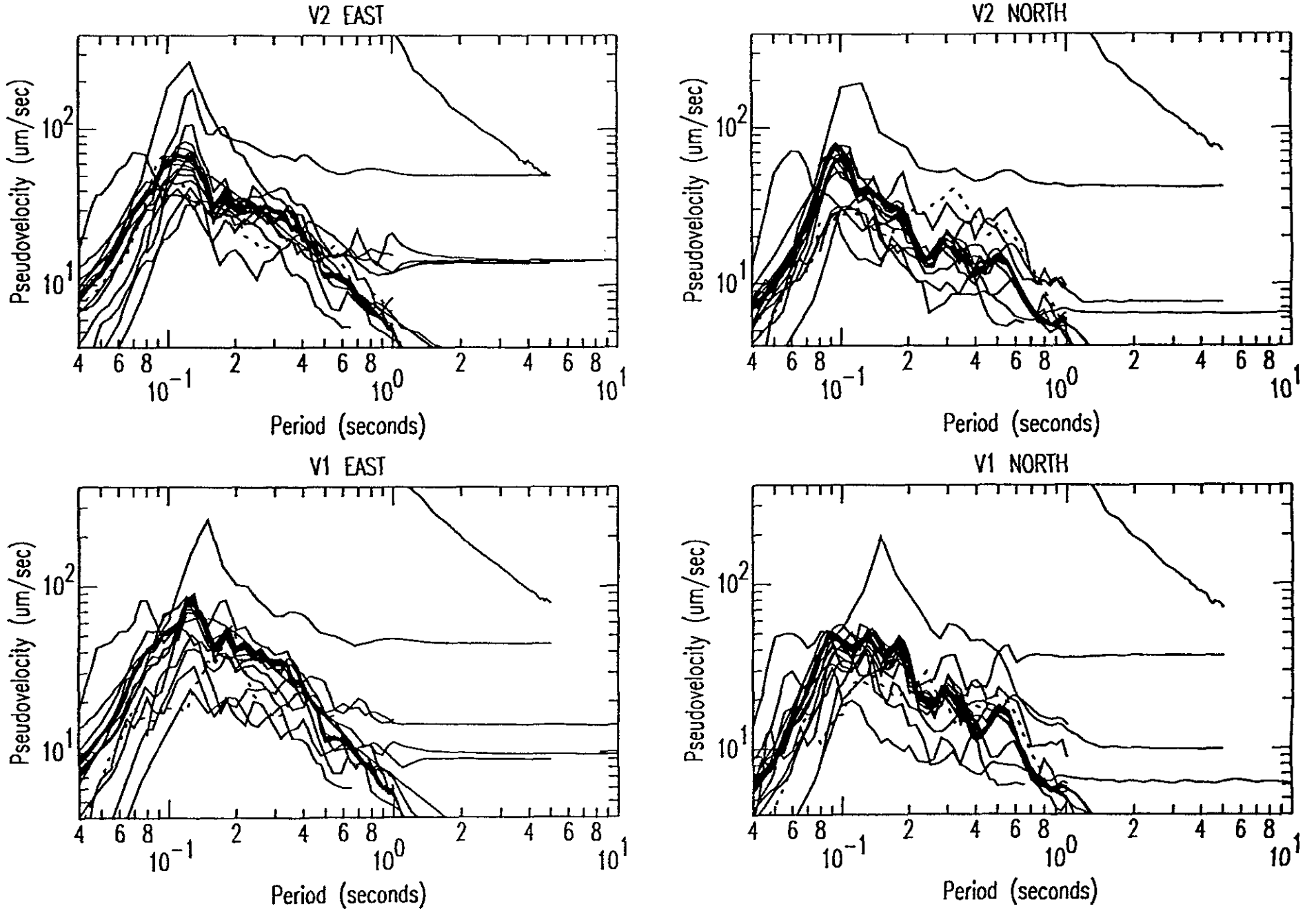

Figure 13: R1 Standard Model Response Spectra Prediction Quartiles vs Observations

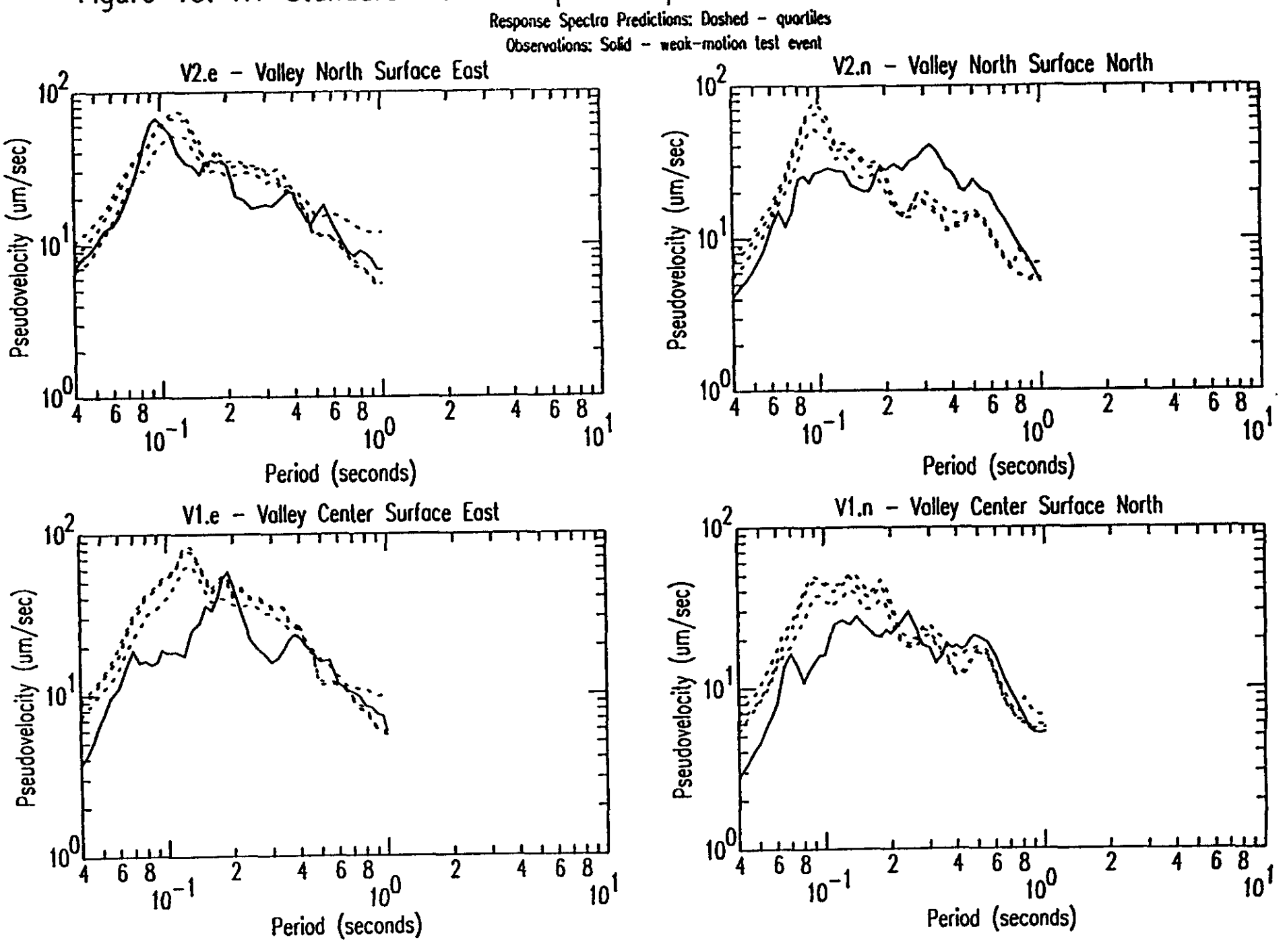

Figure 14: Standard Fourier Spectral Ratio Plot:
Spectral Ratio V1/R1 for Four Window Lengths

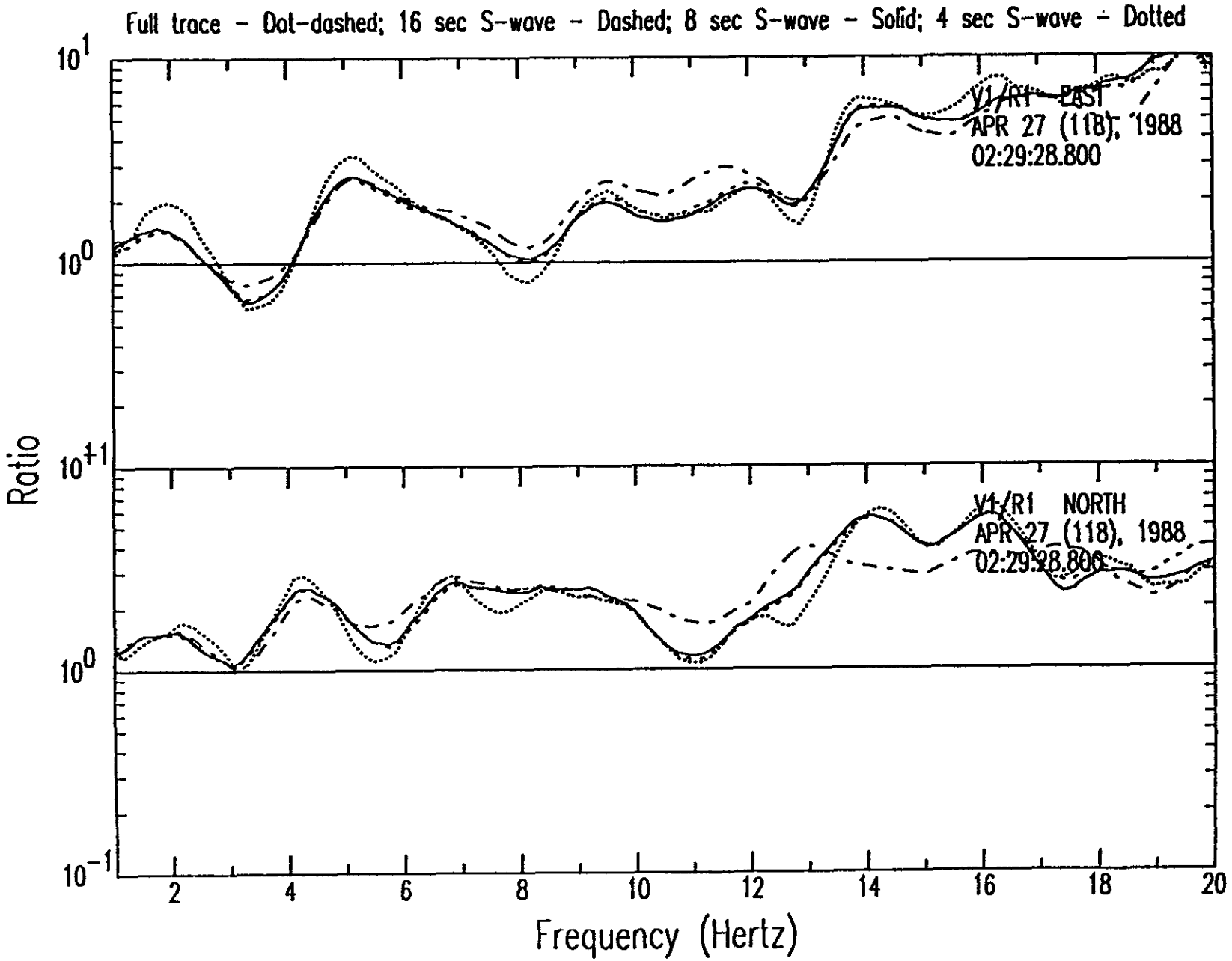

Figure 15: Standard Response Sprectra:
Station V1 Valley Center Surface for Four Window Lengths
Full trace - Dot-dashed; 16 sec S-wave - Dashed; 8 sec S-wave - Solid; 4 sec S-wave - Dotted

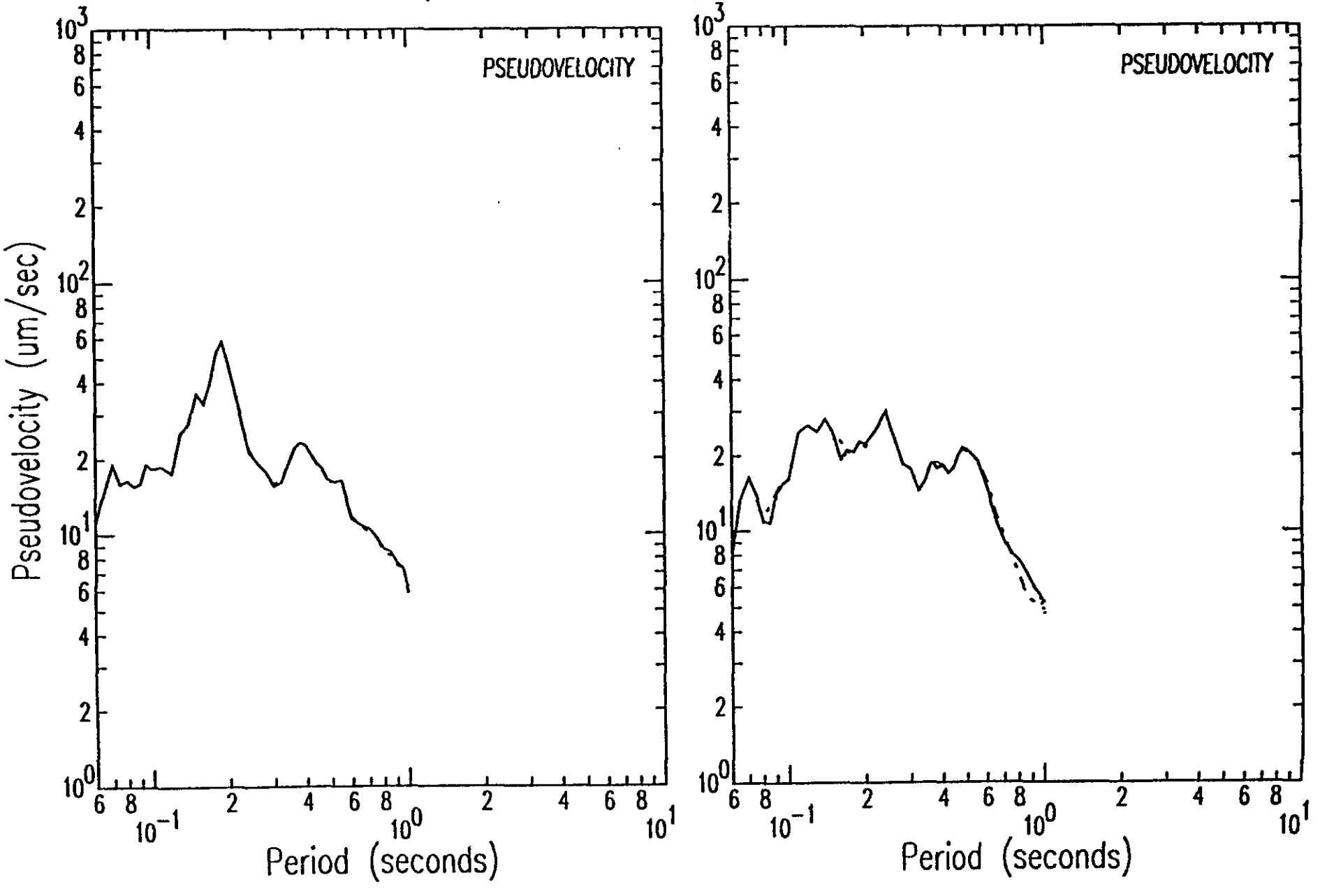

window sizes produce slightly different spectral ratios for the same time history and for the same spectral smoothing window (approximately 1 Hz) applied prior to calculating the spectral ratios (Figure 14). This variation could cause some of the observed scatter (less than a factor of 2) in the submitted Fourier spectral ratios (Figure 10) but not the major differences that appear in some submitted spectral ratios. The time domain window size, however, has no significant effect on response spectra (Figure 15).

Standard vs. Preferred Models

Figure 16 compares spectral ratio medians and Figure 17 compares response spectra medians for 1) R1 standard geotechnical model weak-motion predictions, 2) R1 preferred geotechnical model weak-motion predictions, 3) R1 1D standard geotechnical model weak-motion predictions, and 4) R1 2D/3D standard geotechnical model predictions. Generally, there appears to be little difference among these groups of predictions, especially for the response spectra. The medians for the preferred geotechnical model weak-motion predictions and the 2D/3D standard geotechnical model weak-motion predictions show the most variation from the median of all the standard geotechnical model predictions, but the variations are not significant, especially for the median of the preferred geotechnical model weak-motion predictions due to that group's small sample size (4-6).

Figure 16a: R1 Spectral Ratio Prediction Medians

Solid - standard model; Dash-dotted - preferred model;
Dashed - 1D standard model; Dotted - 2D/3D standard model

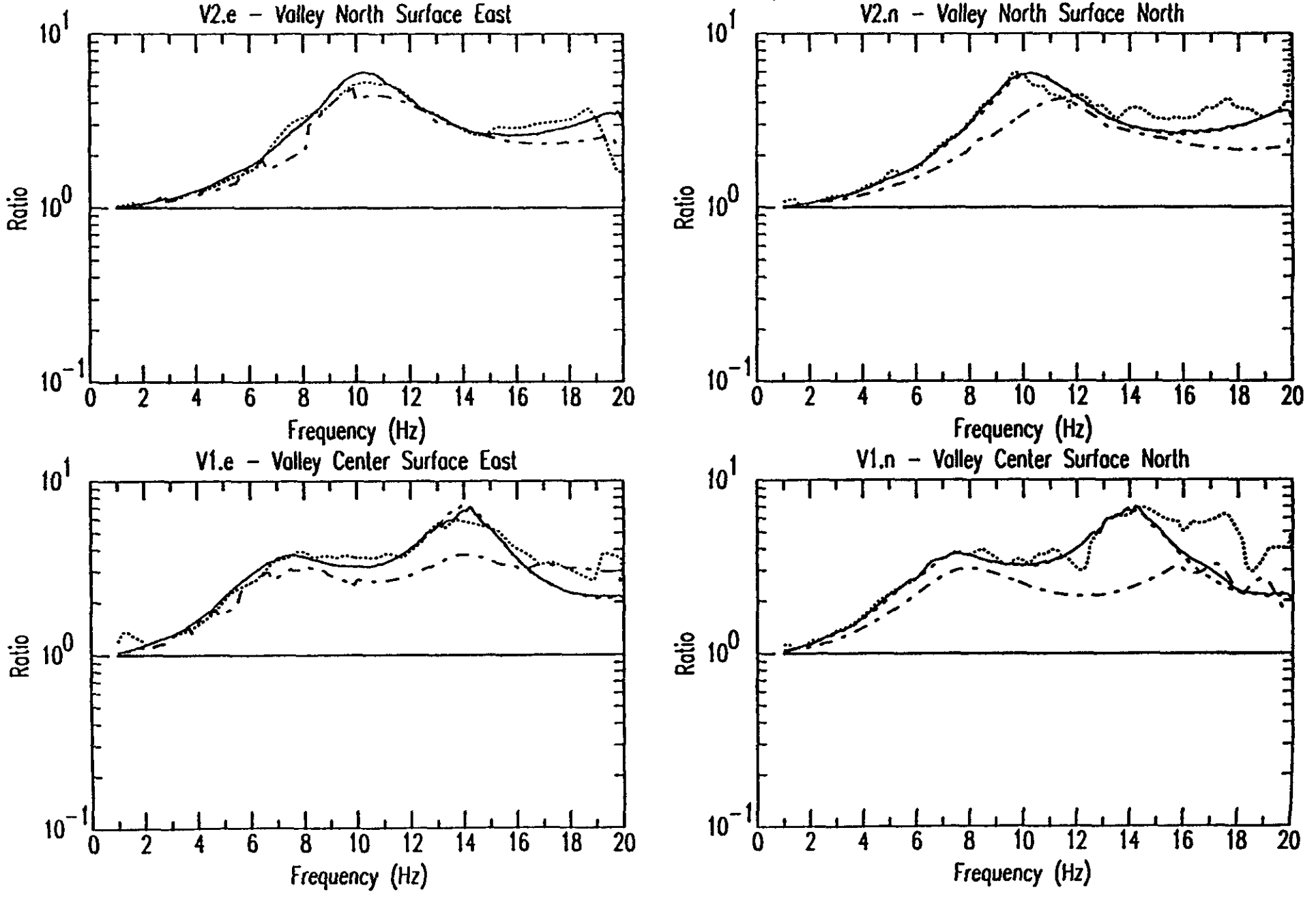

Figure 16b: R1 Spectral Ratio Prediction Medians

Solid - standard model; Dash-dotted - preferred model;
Dashed - 1D standard model; Dotted - 2D/3D standard model

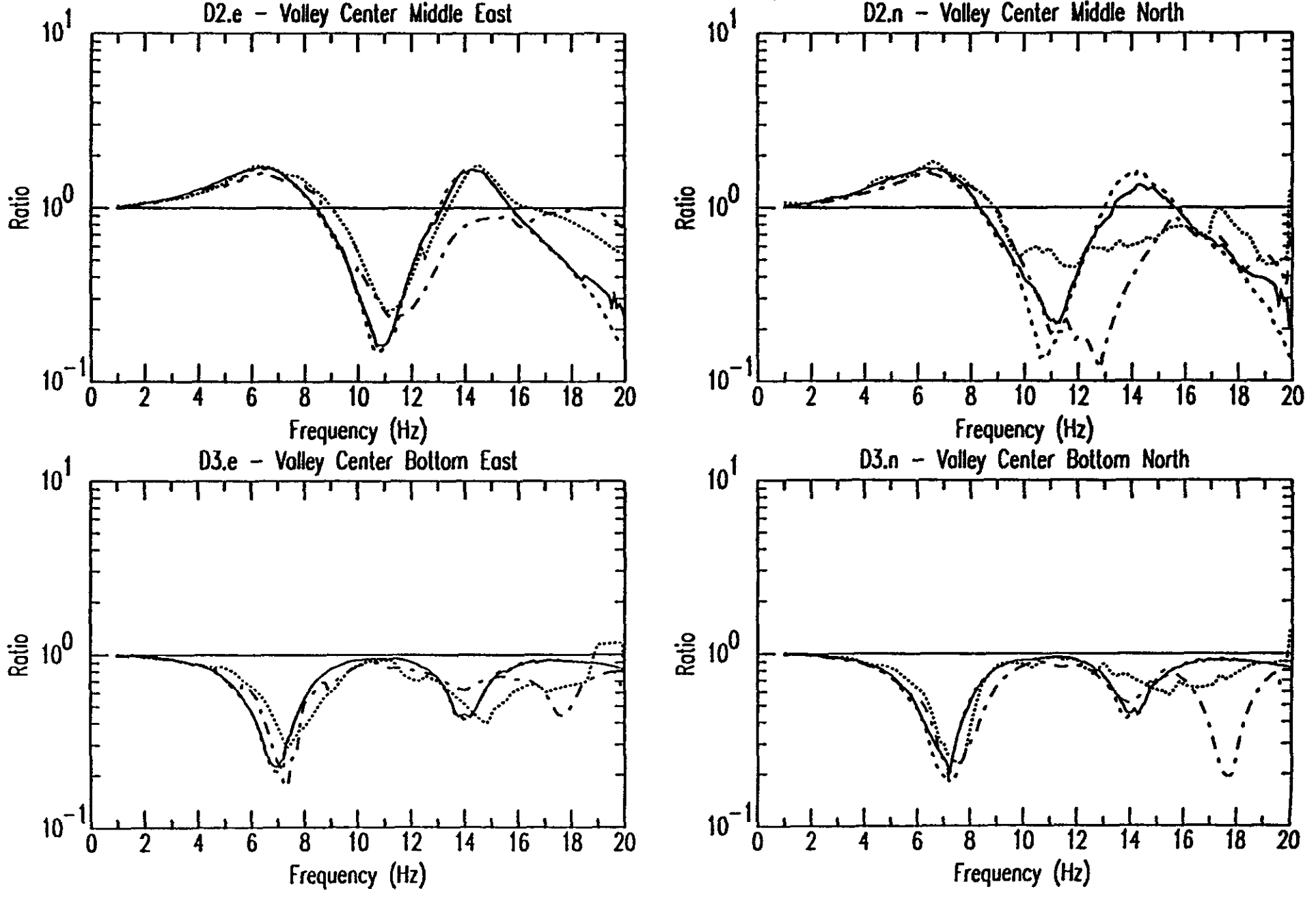

Figure 16c: R1 Spectral Ratio Prediction Medians

Solid - standard model; Dash-dotted - preferred model;
Dashed - 1D standard model; Dotted - 2D/3D standard model

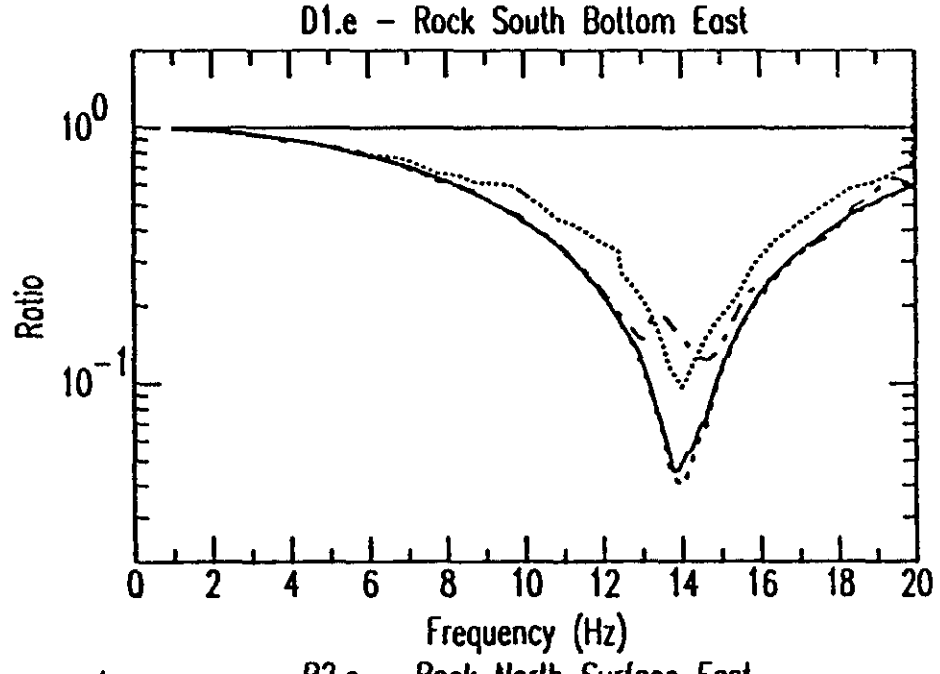

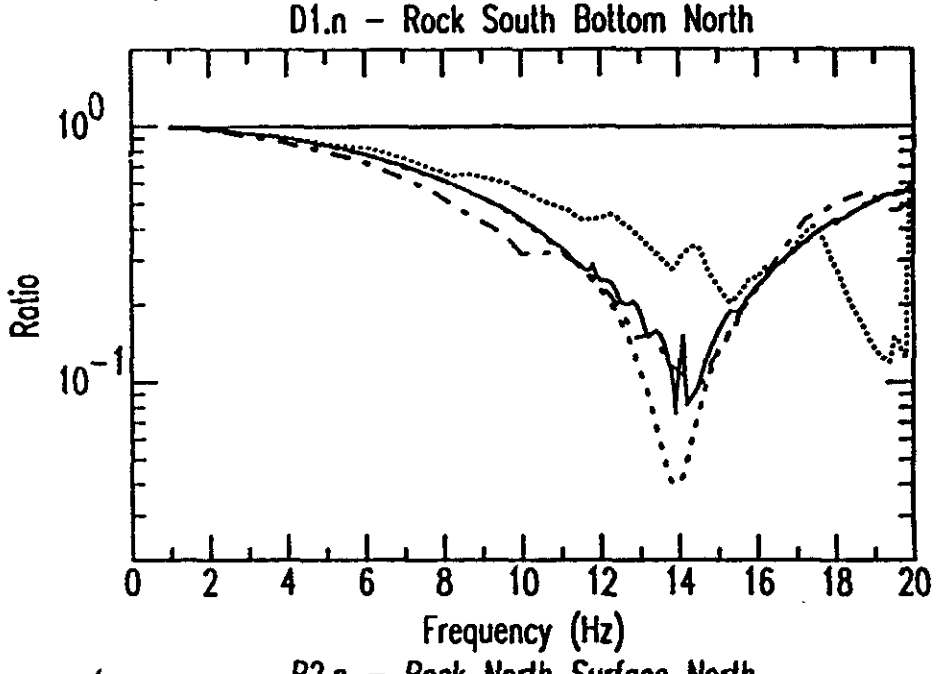

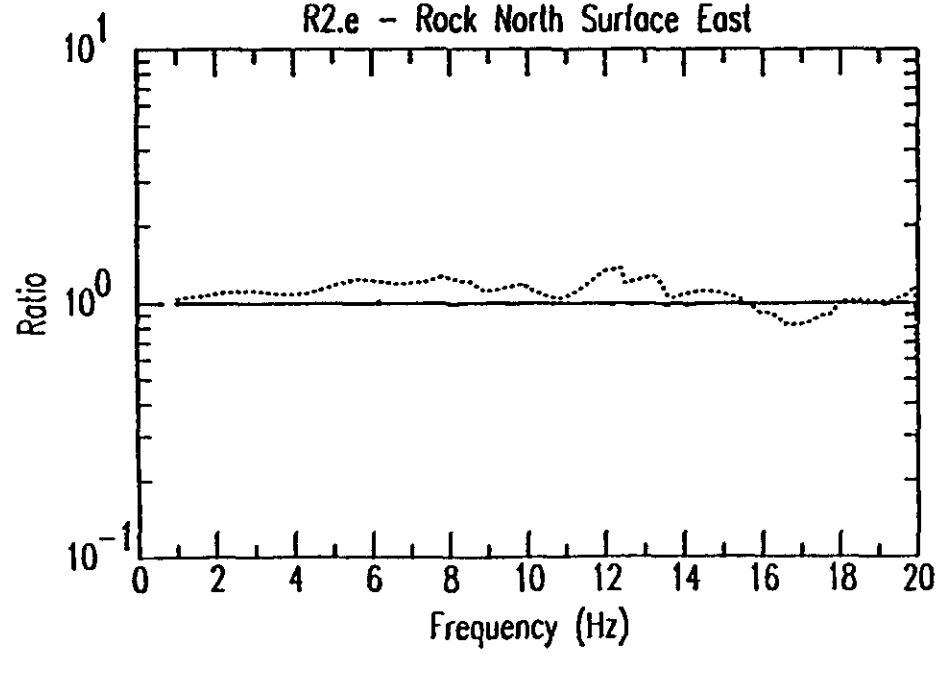

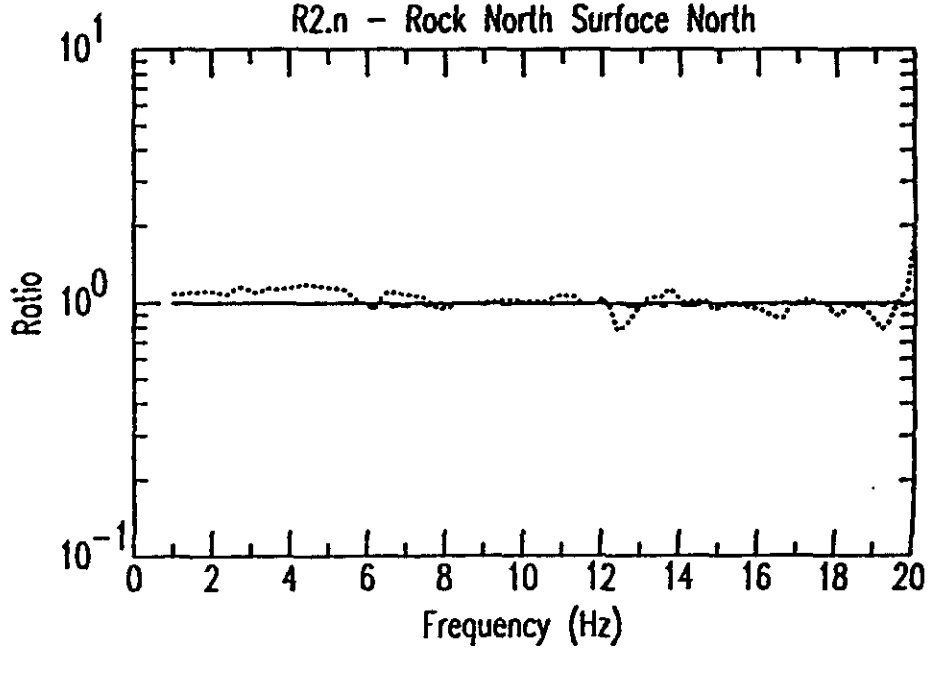

Figure 17a: R1 Response Spectra Prediction Medians

Solid - standard model; Dash-dotted - preferred model;
Dashed - 1D standard model; Dotted - 2D/3D standard model

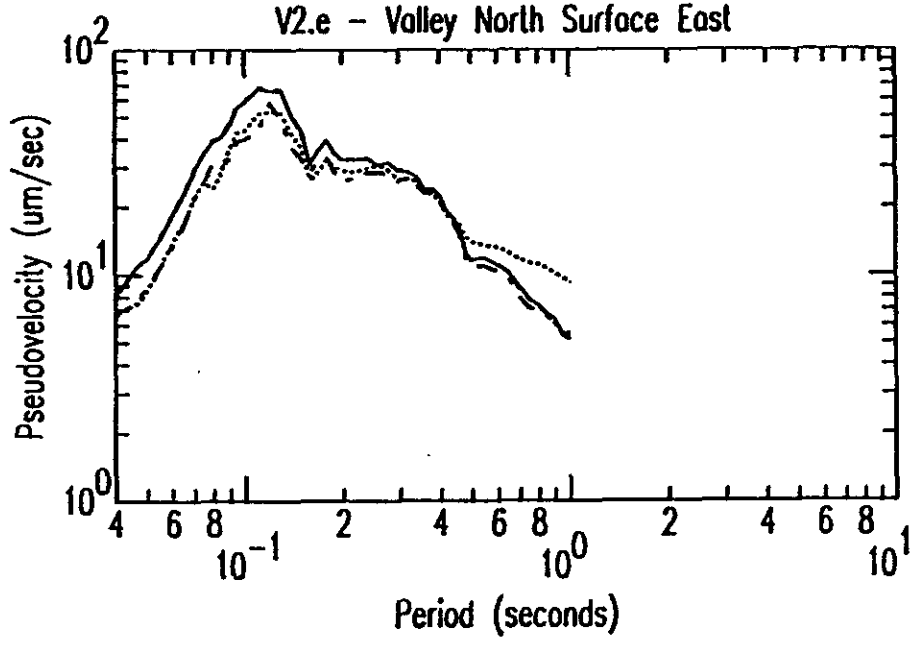

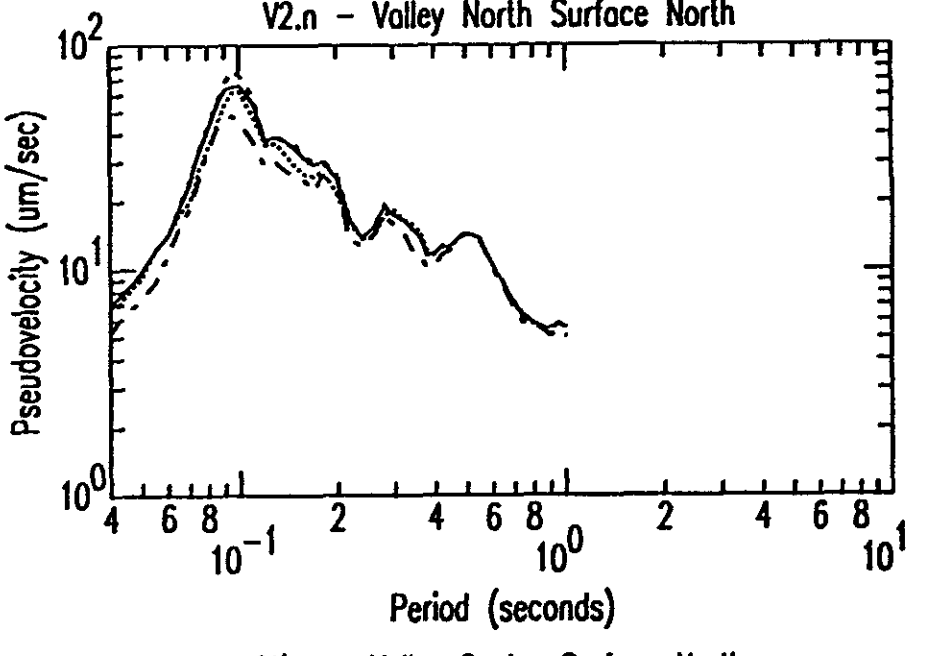

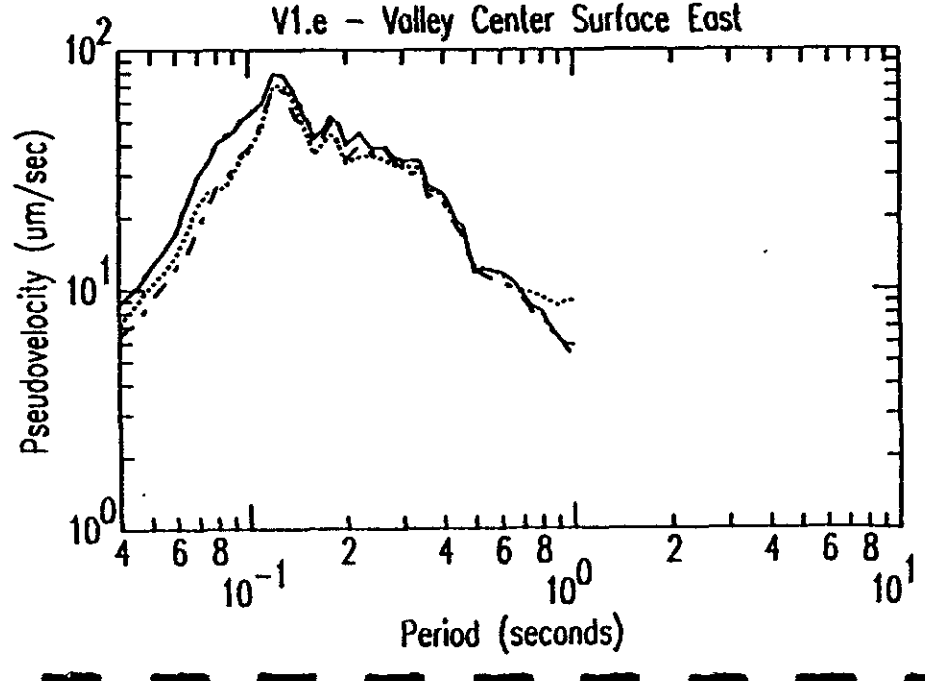

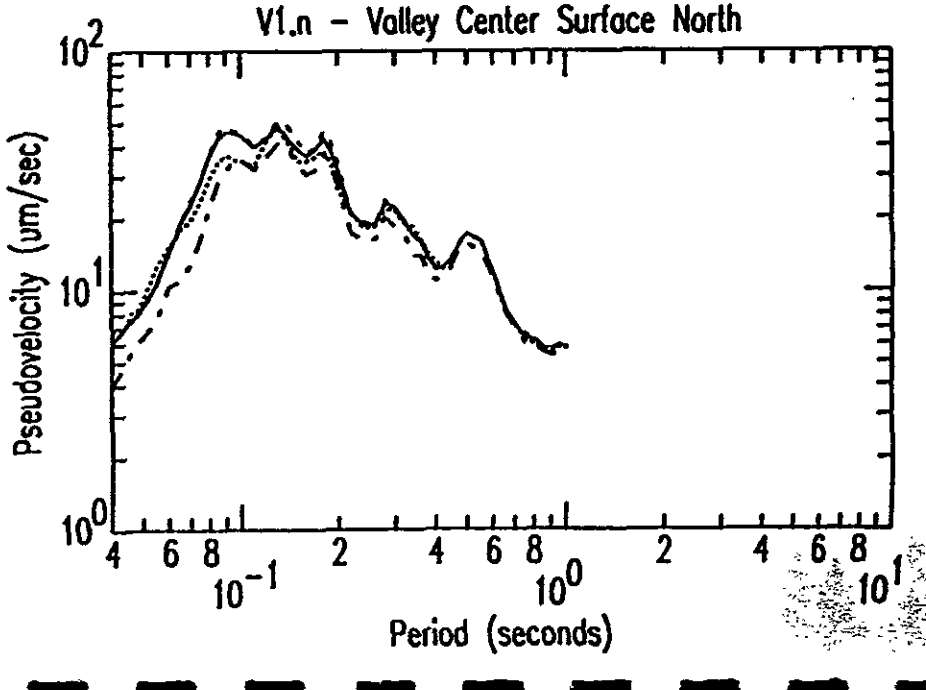

Figure 17b: R1 Response Spectra Prediction Medians

Solid - standard model; Dash-dotted - preferred model;
Dashed - 1D standard model; Dotted - 20/30 standard model

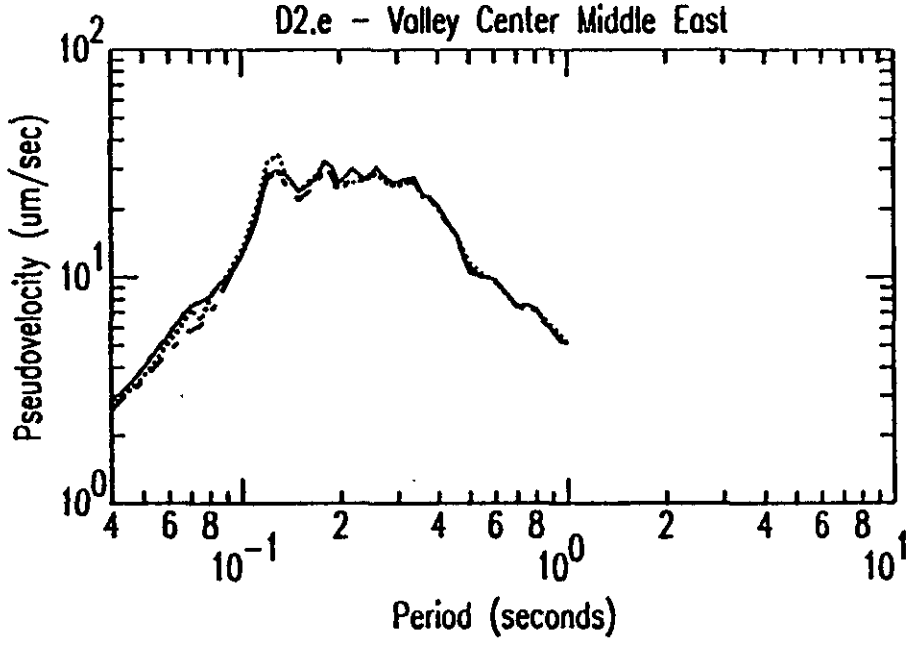

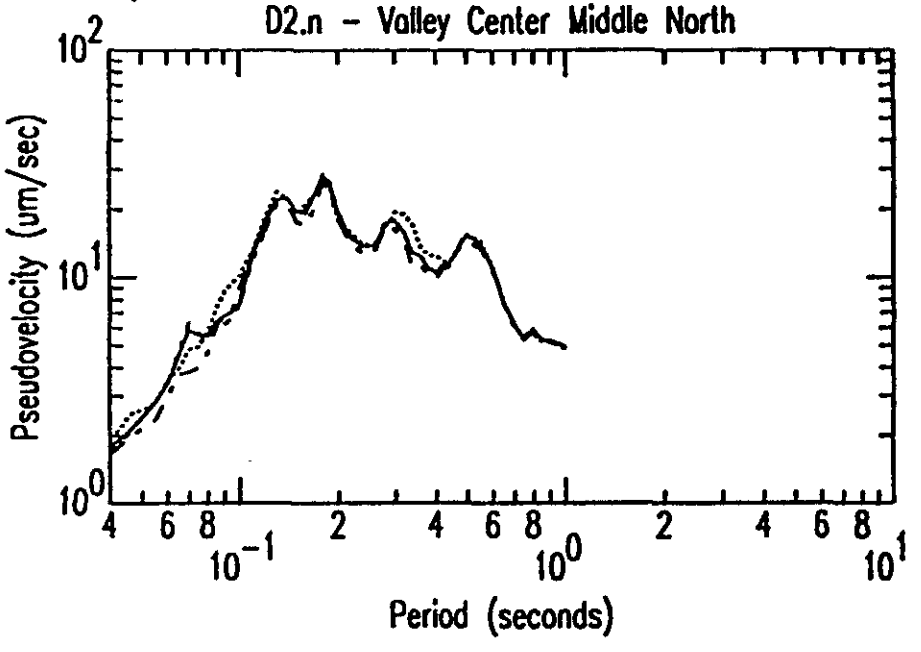

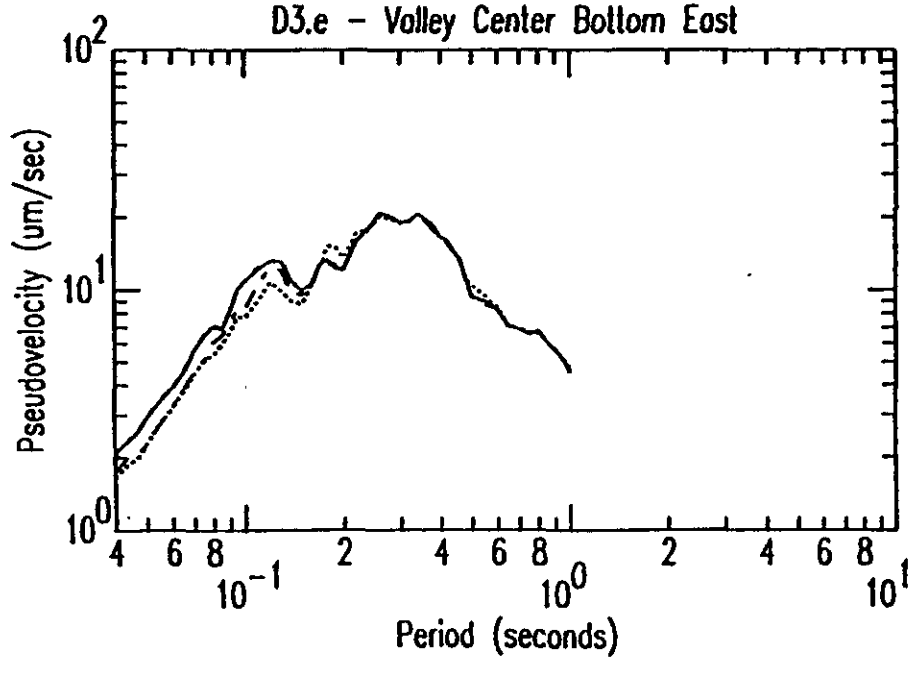

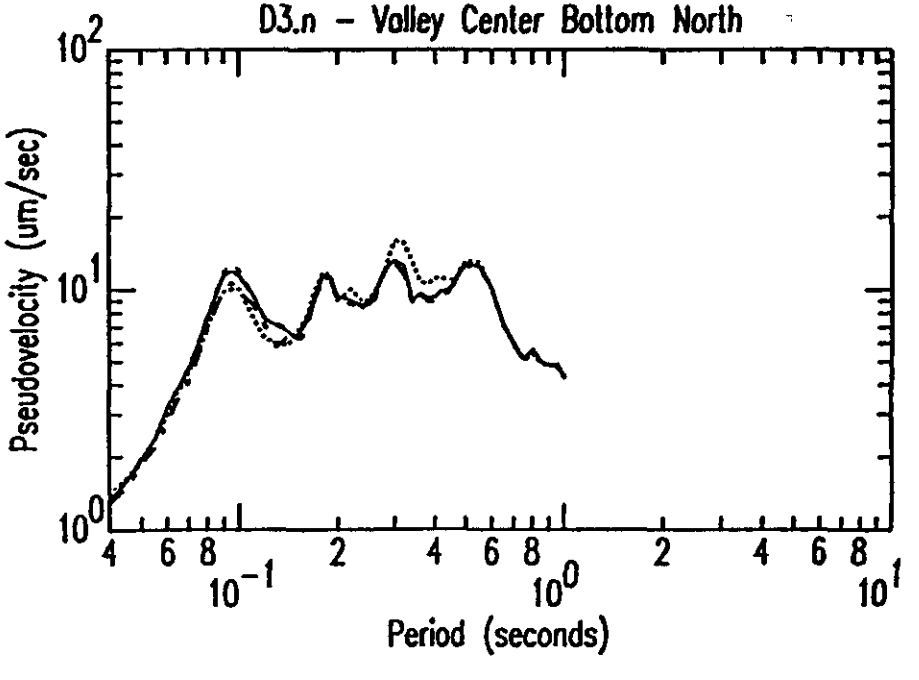

Figure 17c: R1 Response Spectra Prediction Medians

Solid - standard model; Dash-dotted - preferred model;
Dashed - 1D standard model; Dotted - 2D/3D standard model

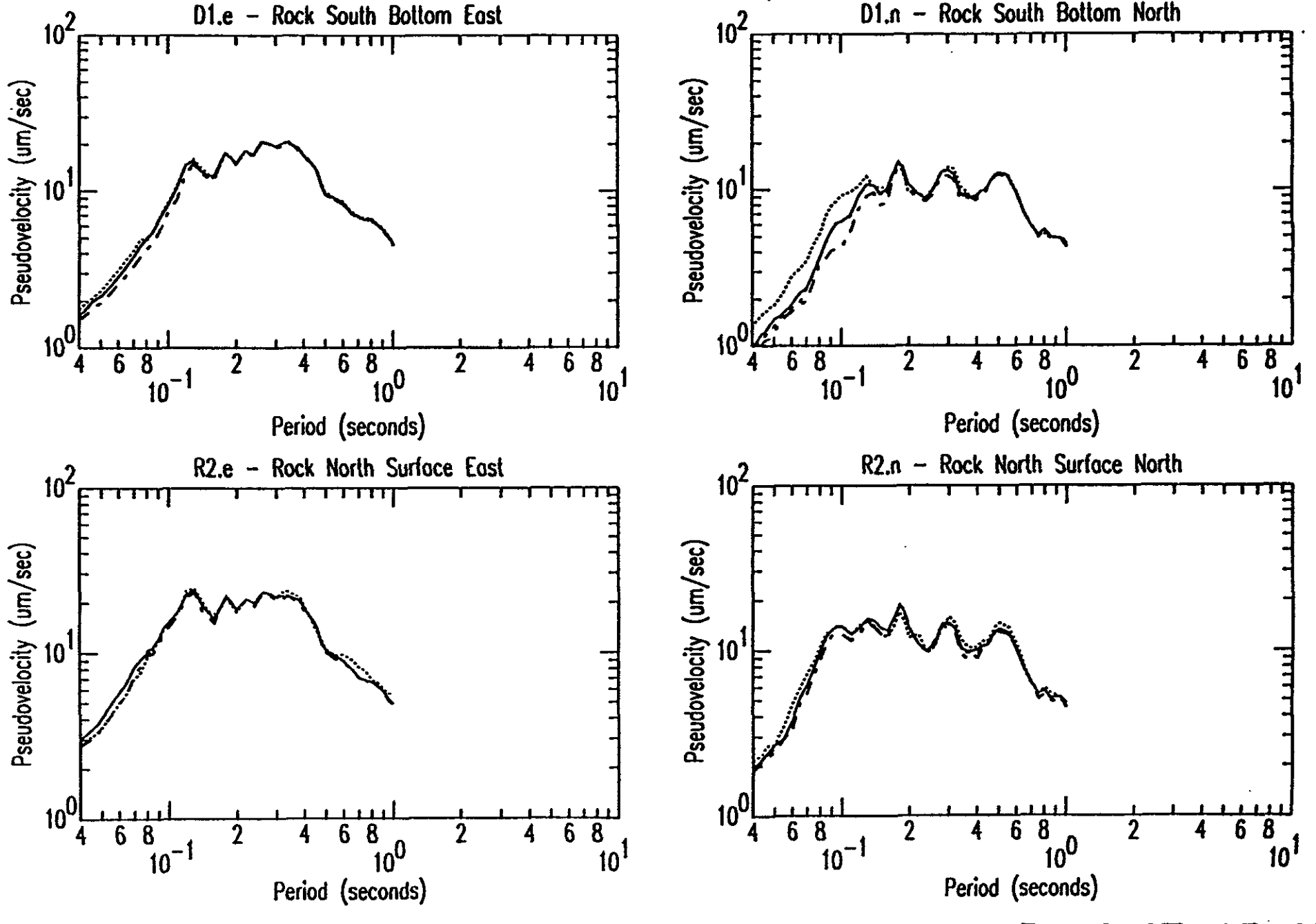

Table 9

Preferred vs Standard Model Predictions for same Predictor

R1 Predictions:

Predictor	Change from Standard Model	Effect
#8	Not stated - probably in velocity model.	Insignificant (very little) change except in D3 which had some improvement.
#9	Not stated - probably in velocity model.	Fsr's had mixed changes (both better and worse); rsp's had some improvement.
#40	Changes not stated; results only good below 10 Hz.	Preferred fit worse.
#86	Used Q = 10 (5% damping) - probably no change in velocity model.	Fsr's had decrease in amplitude; rsp's unchanged. Fit unchanged or slightly better.
#117	Not stated - probably in velocity model.	Fsr's had mixed changes (both better and worse); rsp's had some improvement.
#143	Preferred model used variation in technique.	Preferred results cut off at 10 Hz and changes in fit are mixed (both better & worse).

D3 Predictions:

Predictor	Change from Standard Model	Effect
#8	Not stated - probably in velocity model.	Fsr's has mixed changes (both better and worse); rsp's had some improvement.
#8sm	Not stated - probably in velocity model. High frequency response reduced.	Mixed changes (both better and worse).
#9	Not stated - probably in velocity model.	Fsr's had little change; rsp's had some improvement.
#40	Changes not stated; results only good below 10 Hz.	Little or no improvement.
#86	Velocity increased by 15% and damping increased (used 5% in R1 predictions).	Preferred fit much improved.
#117	Not stated - probably in velocity model.	Fsr's had slight improvement; rsp's generally improved.

Table 9 presents descriptive comparisons of preferred geotechnical model weak-motion predictions to required standard geotechnical model weak-motion predictions by the same predictors. There are six comparisons for R1 based predictions and six comparisons for D3 based predictions. **With the exception of predictor #86's D3 predictions, Table 9 suggests that preferred model predictions were no better in predicting the weak-motion observations than the standard model predictions made by the same predictor.**

Time History and Optional Predictions

Predicted V1 time histories (see Appendices 1 - 4) generally show similar durations to, and larger amplitudes than, the observed V1 time histories (east and north components). Apparent frequency content and waveform envelope shape vary among the predicted time histories.

There are no observations with which to compare the optional (arbitrary record) strong-motion predictions. Optional strong-motion predictions show similar patterns in their scatter and quartile plots as the weak-motion predictions, except that the Q_3 minus Q_1 scatter is larger than the weak-motion Q_3 minus Q_1 scatter for Fourier spectral ratios but not for the response spectra (Appendix 3). This increased scatter in Q_3 minus Q_1 is mainly due to the small number of optional predictions (6-8).

Conclusions

The consensus in the submitted predictions, as shown by the Q_3 minus Q_1 distribution (middle 50%) in the quartile plots and by a tight grouping of predictions on scatter plots, indicates a tendency to get similar results regardless of the method used to make ground motion predictions. Even predictors' preferred model results did not necessarily lead to improvements over standard model results nor provide a better fit to observations. Thus, for weak-motion response of simple stiff-soil sites, the accuracy of the geotechnical model used to characterize the site is more important than the particular method used to calculate the response.

Despite the tendency toward a consensus, there is significant scatter (factor of 2 and more) in the submitted predictions. While some of the scatter in Fourier spectral ratios might be explained by differences among predictor's time domain window lengths used in FFT's, this can only account for a small portion (less than a factor of 2) of the observed variance. The reason for this large scatter is either due to differences in the modeling techniques used or differences in how the standard geotechnical model was used.

The Q_3 minus Q_1 quartile distribution at Valley North, V2, coincides well with the observations, but at the Valley

Center surface site, V1, the Q_3 minus Q_1 quartile distribution is above the observations, particularly for peaks in the spectral ratios and for the peak acceleration end of the response spectra. This tendency may indicate that the Turkey Flat Standard Geotechnical Model for the Valley Center site has lower weak-motion damping than actually exists at the site. Companion report 6 on modeling of the weak-motion observations provides a clearer indication that damping in the Standard Geotechnical Model is, in general, too low except at the Valley North site.

Finally, those predictors that submitted estimates for uncertainty in their peak value predictions generally underestimated the magnitude of the deviations of predicted peak values from actual values for the weak-motion test event. For a given predictor's uncertainty estimates, this generally holds for the deviations of his predicted peak values from actual peak values and for deviations of all predicted peak values from actual peak values. Deviations in predicted acceleration peak values from actual peak accelerations are much greater than deviations in predicted displacement peak values from actual peak displacements.

REFERENCES

Cramer, C.H., 1991, Turkey Flat, USA, site effects test area, report 6, weak-motion test: observations and modeling: California Division of Mines and Geology, ESAU Technical Report No. 91-1.

Real, C.R., 1988, Turkey Flat, USA, site effects test area, report 2, site characterization: California Division of Mines and Geology, ESAU Technical Report No. 88-2.

Real, C.R., and Cramer, C.H., 1989, Turkey Flat, USA, site effects test area, report 3, weak-motion test: prediction criteria and input rock motions: California Division of Mines and Geology, ESAU Technical Report No. 89-1.

Tull, J.E., 1987, SAC - Seismic Analysis Code, command reference manual, version 10.2: Lawrence Livermore National Laboratory, informal report.

Wiggins, R.A., 1976, Interpolation of digital curves: Bull. Seism. Society of Am. v. 66, n. 6, p. 2077-2081.

Appendices

APPENDICES

These appendices present all the scatter plots and quartile plots for each grouping of submitted predictions analyzed in this report. The first six appendices cover the following subgroups, one to an appendix: 1) all submitted required R1 based weak-motion predictions using the standard geotechnical model; 2) all submitted R1 based weak-motion predictions using a predictor's preferred geotechnical model; 3) all submitted optional (arbitrary record) strong-motion predictions, regardless of geotechnical model used; 4) all submitted D3 based weak-motion predictions regardless of geotechnical model used; 5) all submitted 1D R1 based weak-motion predictions using the standard geotechnical model; and 6) all 2D and 3D R1 based weak-motion predictions using the standard geotechnical model. The seventh and last appendix presents all the comparison plots of a given predictor's preferred geotechnical model predictions with their corresponding standard geotechnical model predictions.

For the first six appendices, the plots are presented in the following order: Fourier spectral ratio scatter plots followed by quartile vs observation plots and response spectra scatter plots followed by quartile vs observation plots. The first four appendices have an additional set of time history plots after the response spectra plots.

Appendix A

Plots from Analysis of Submitted R1 based Weak-motion Predictions using the Standard Geotechnical Model

Figure A1a: Standard Fourier Spectral Ratio Plot:
Spectral Ratio V2/R1 for Standard Geotechnical Model

Solid lines – Predictions; Dashed line – Observed

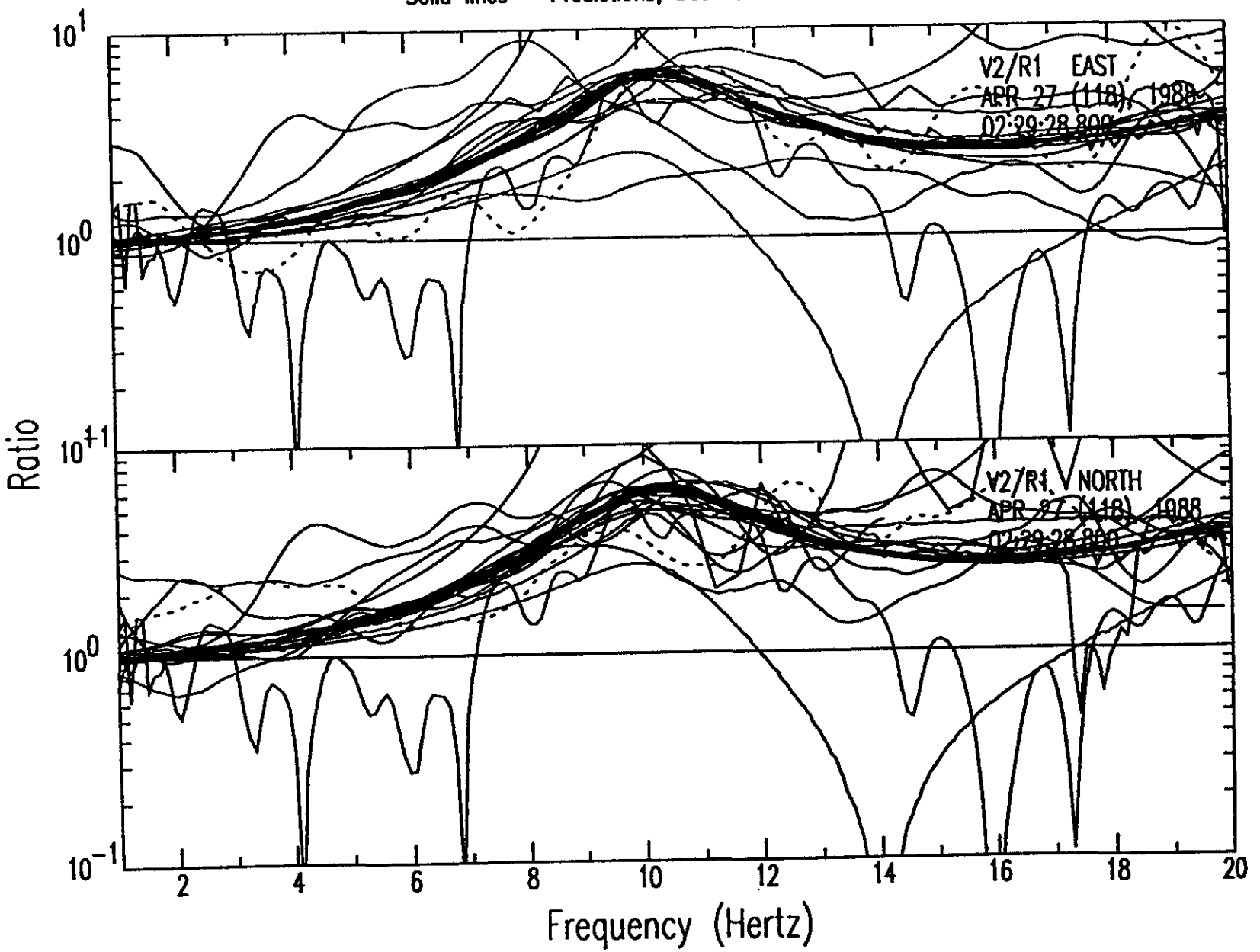

Figure A1b: Standard Fourier Spectral Ratio Plot:
Spectral Ratio V1/R1 for Standard Geotechnical Model

Solid lines – Predictions; Dashed line – Observed

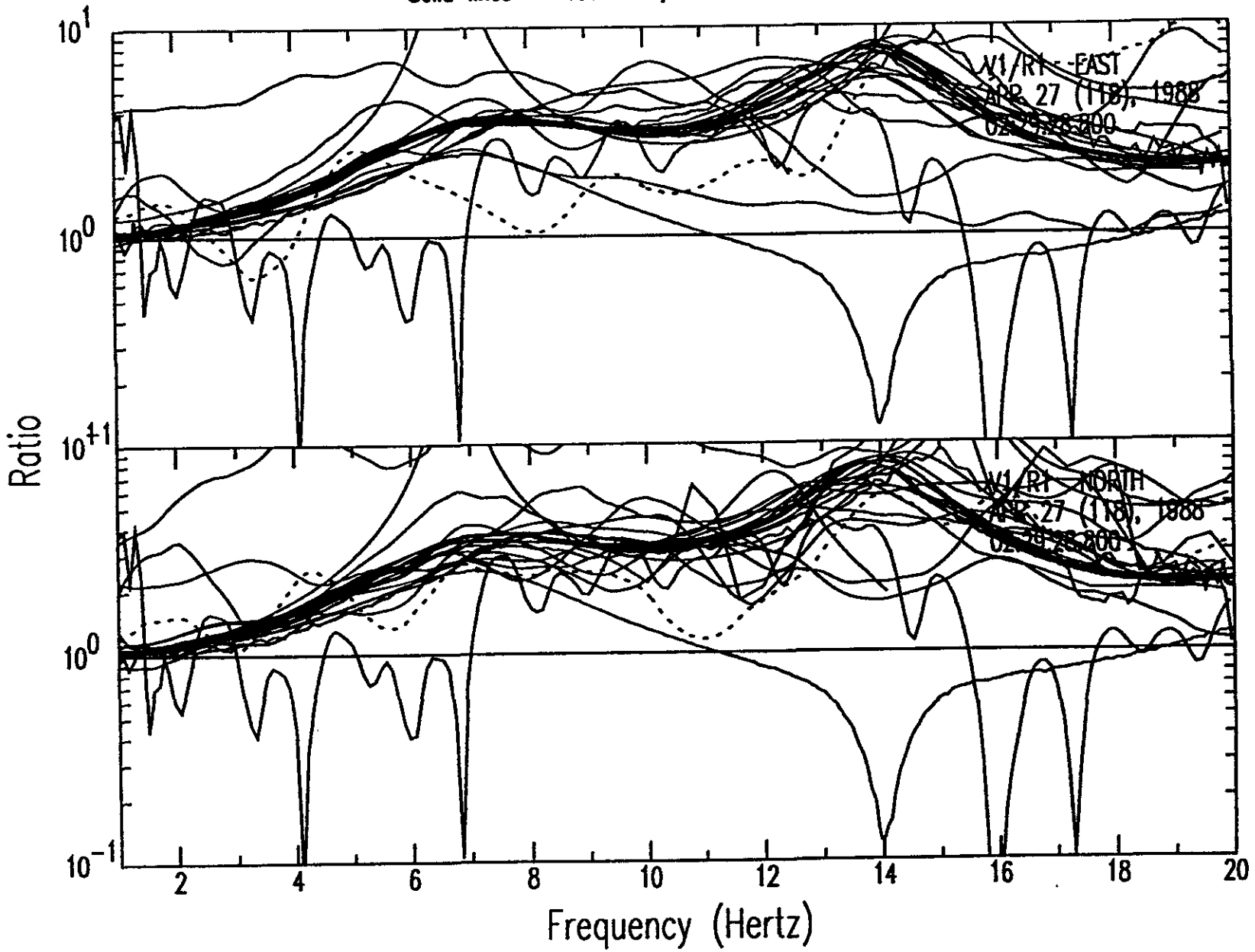

Figure A1c: Standard Fourier Spectral Ratio Plot:
Spectral Ratio D2/R1 for Standard Geotechnical Model

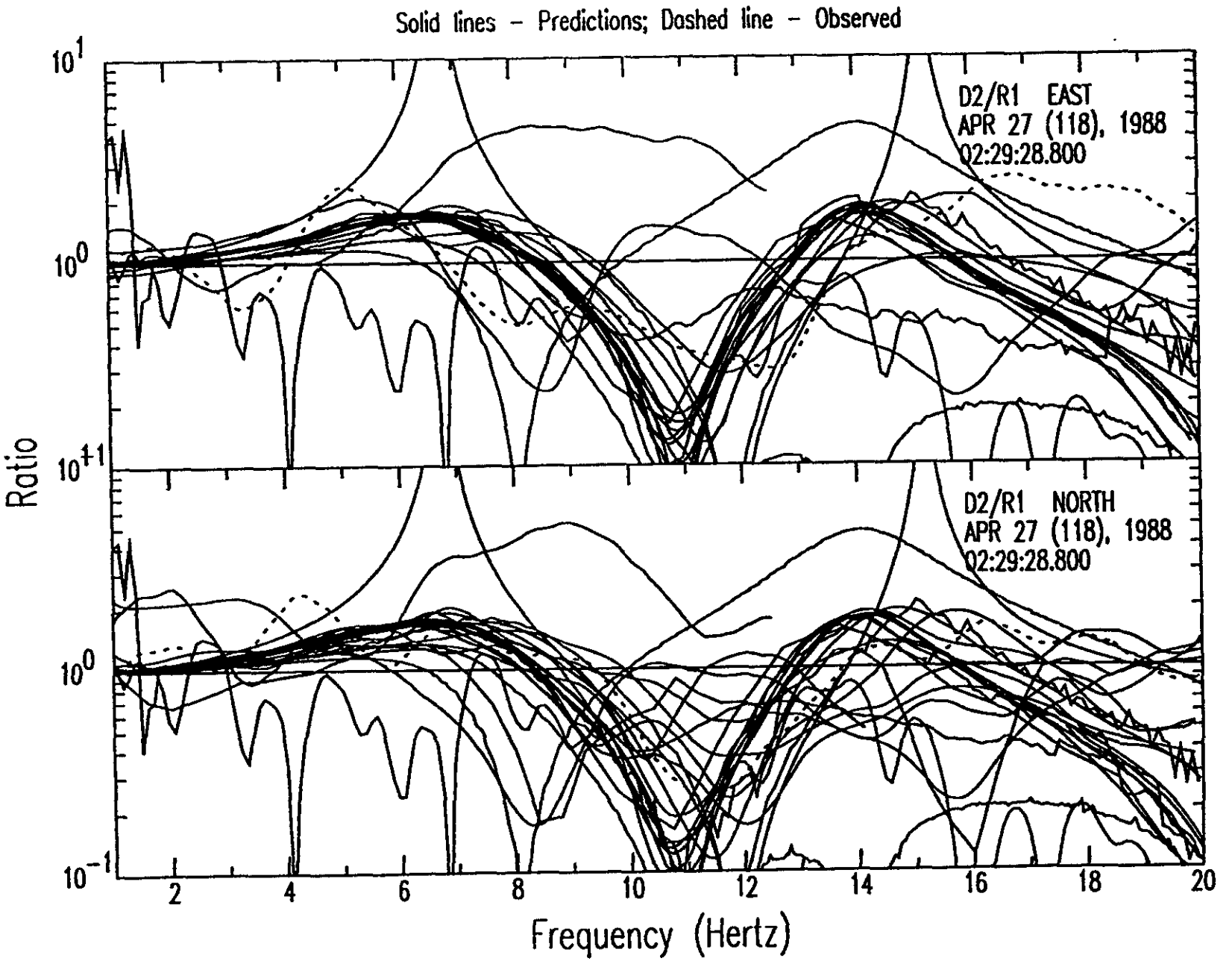

Figure A1d: Standard Fourier Spectral Ratio Plot:
Spectral Ratio D3/R1 for Standard Geotechnical Model

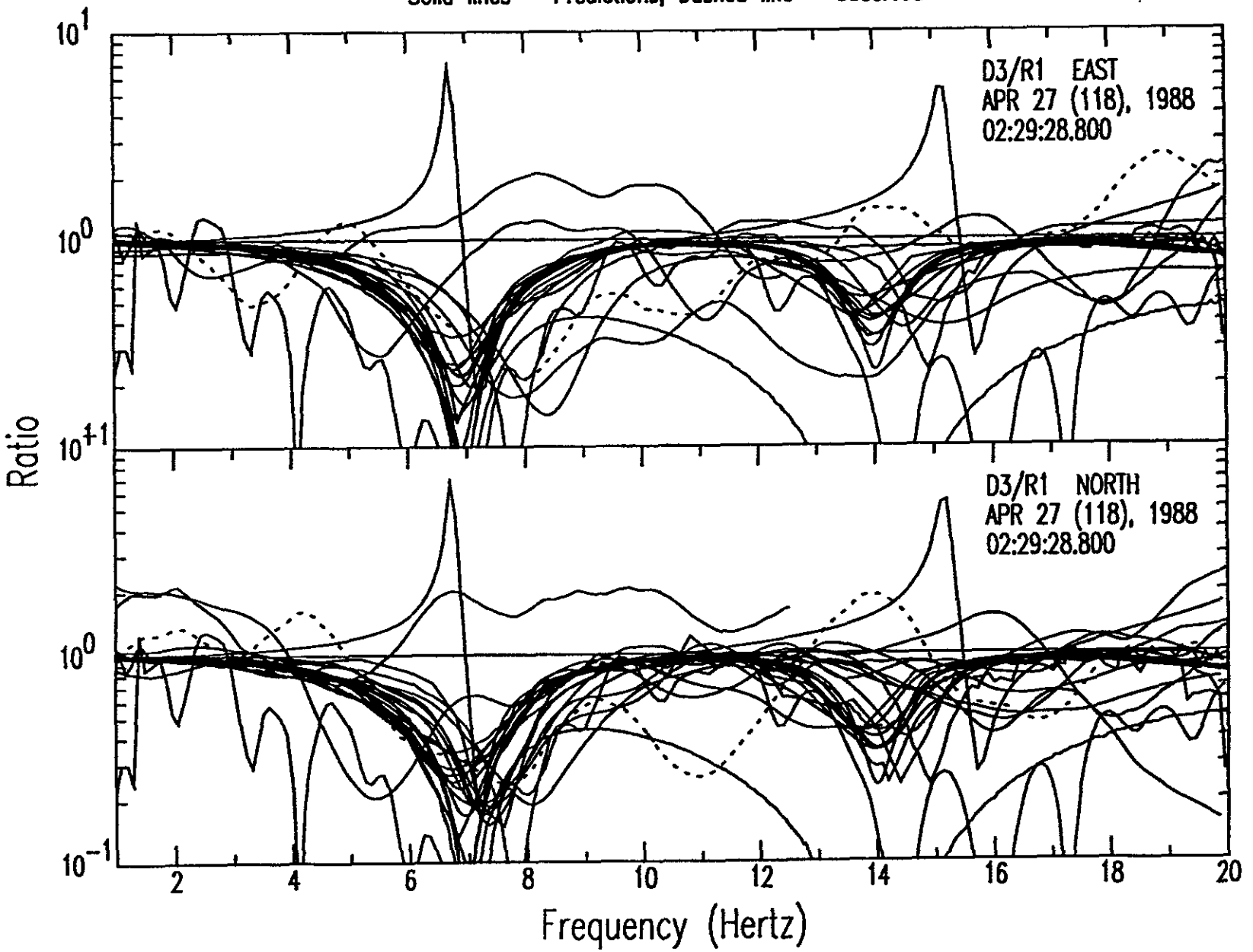

Figure A1e: Standard Fourier Spectral Ratio Plot:
Spectral Ratio D1/R1 for Standard Geotechnical Model

Solid lines – Predictions; Dashed line – Observed

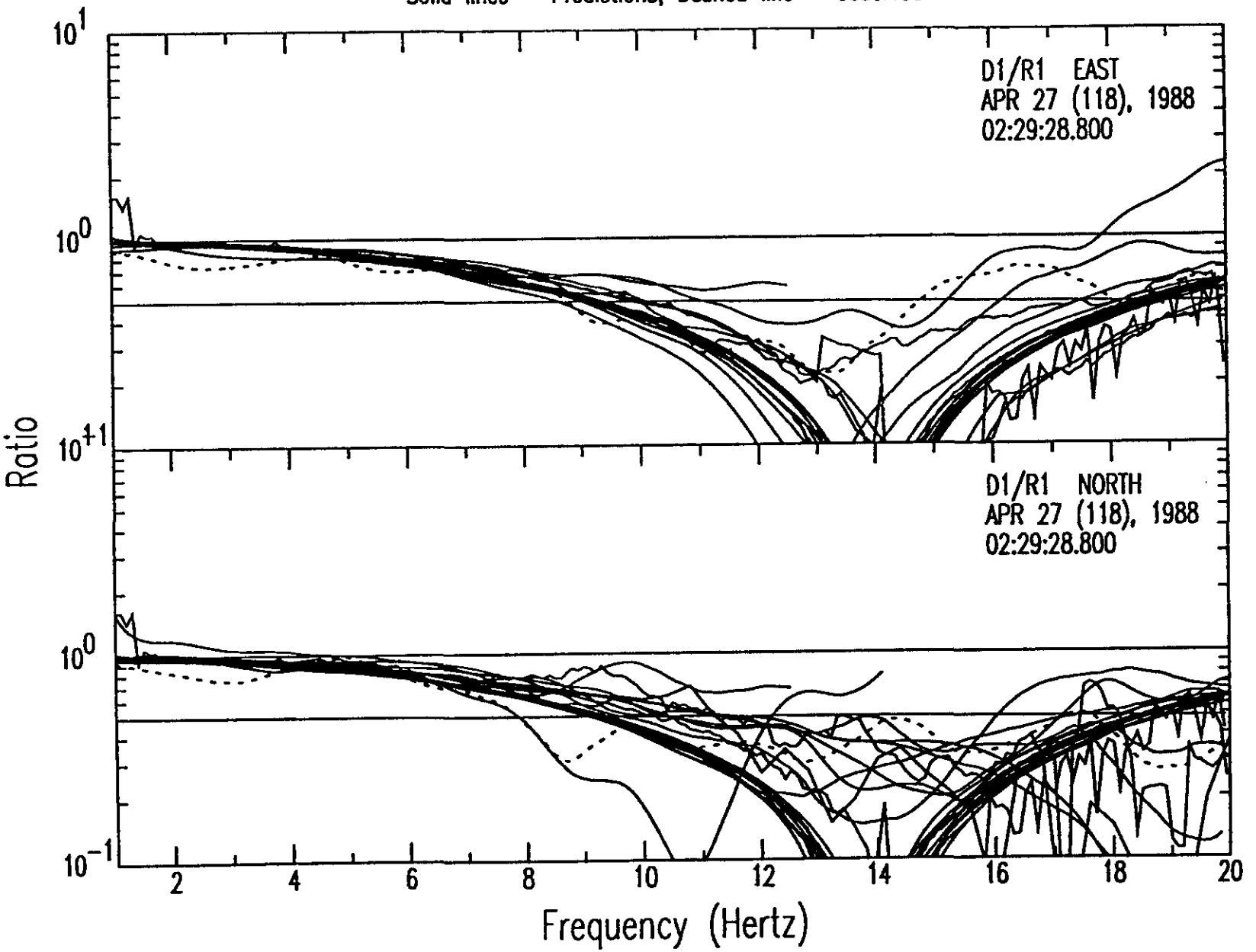

Figure A1f: Standard Fourier Spectral Ratio Plot:
Spectral Ratio R2/R1 for Standard Geotechnical Model

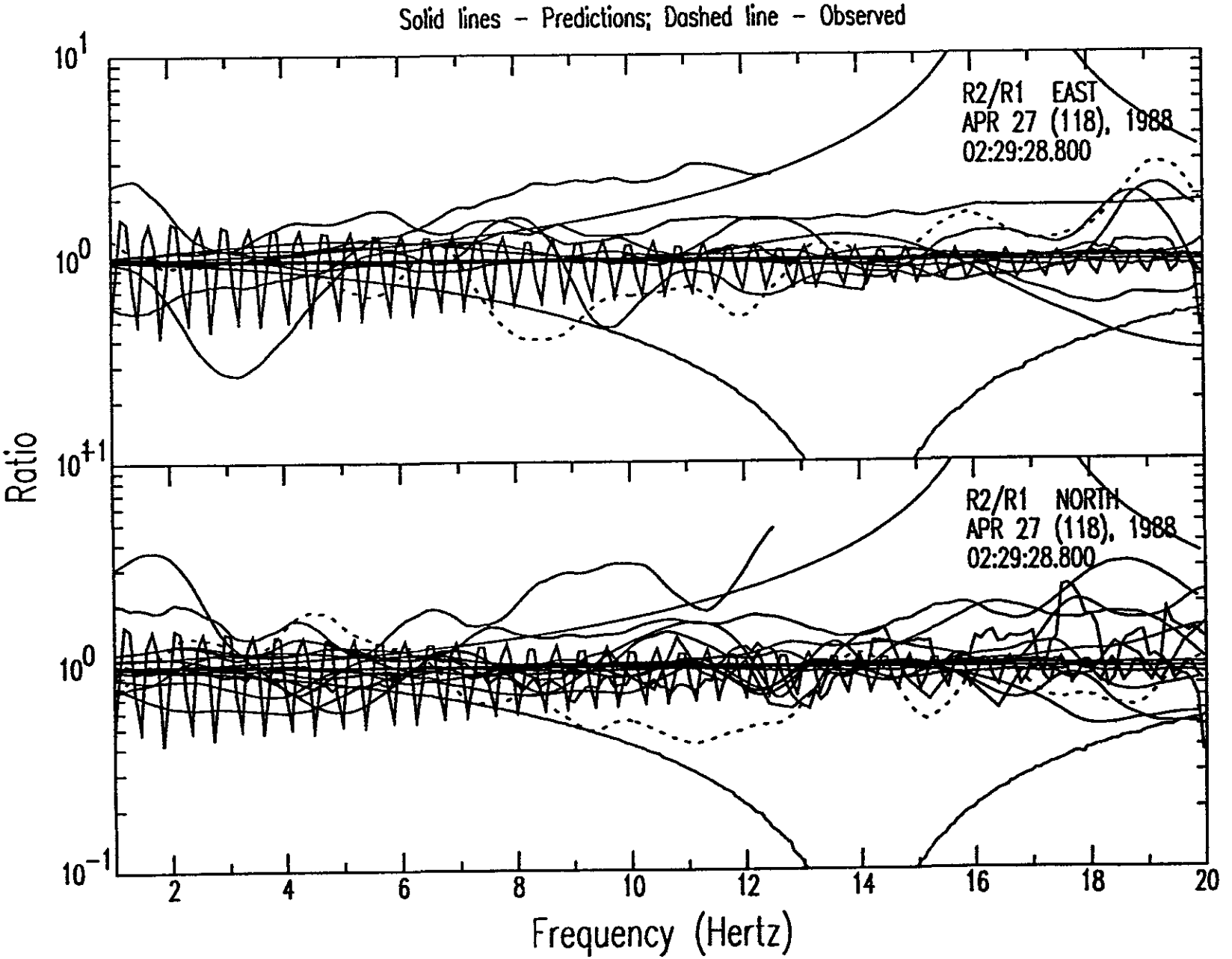

Figure A2a: Standard Model Spectral Ratio Prediction Quartiles vs Observations

Spectral Ratio Predictions: Dashed - quartiles

Observations: Solid - weak-motion test event; Dash-dotted - weak-motion mean; Dotted - 1 std deviation

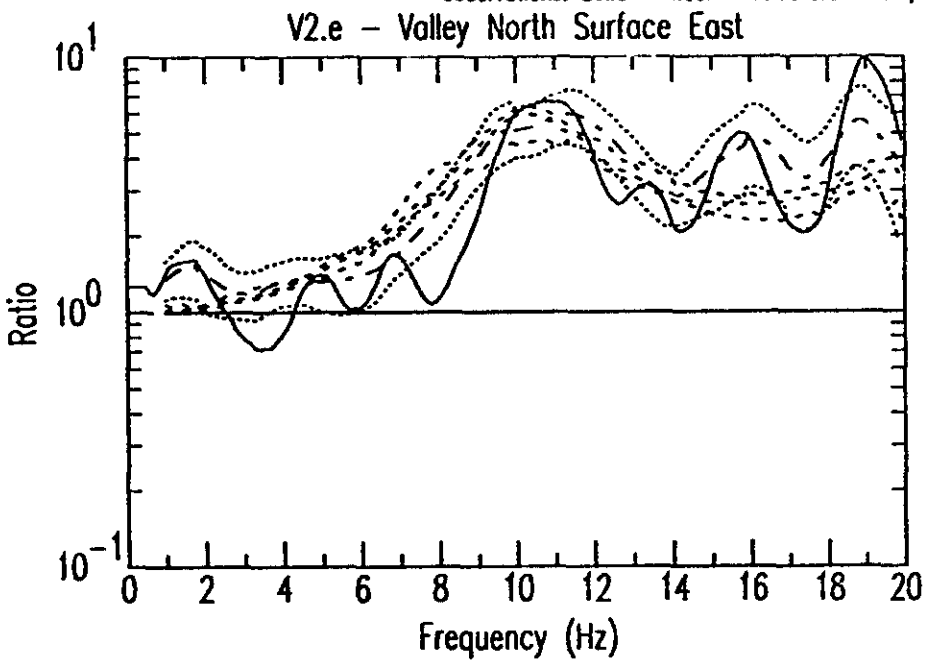

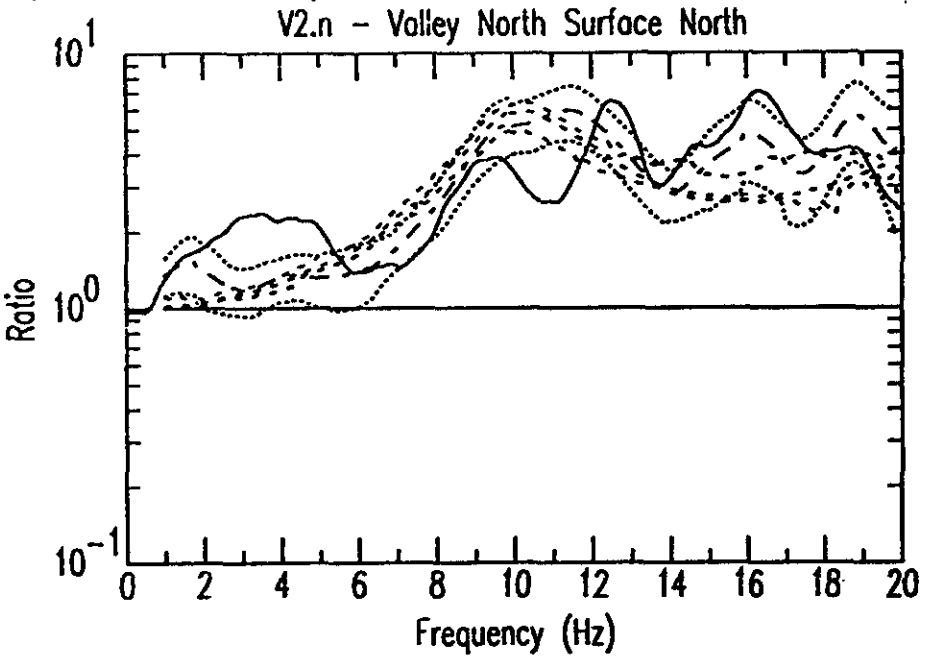

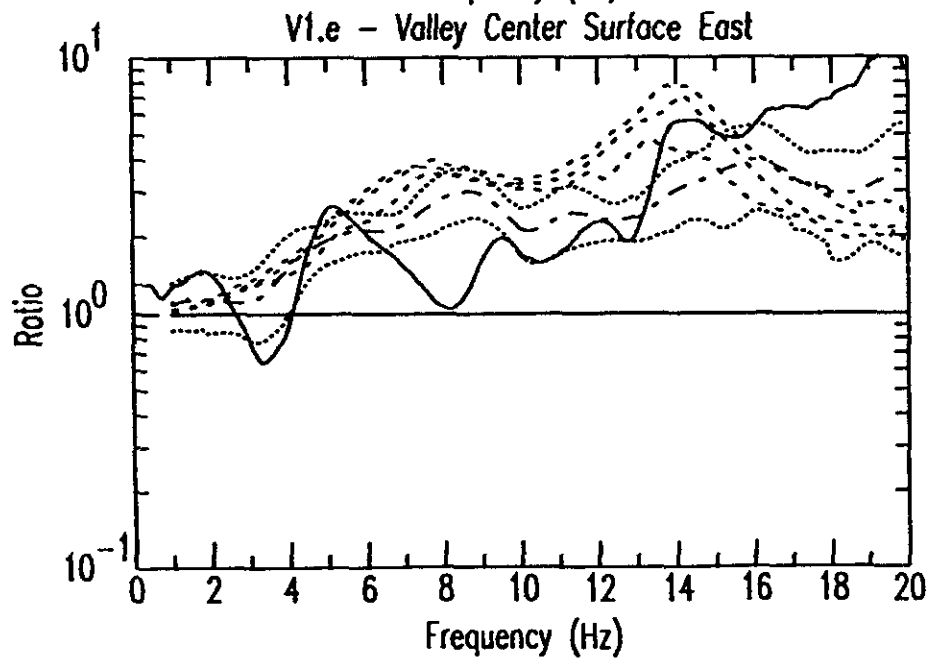

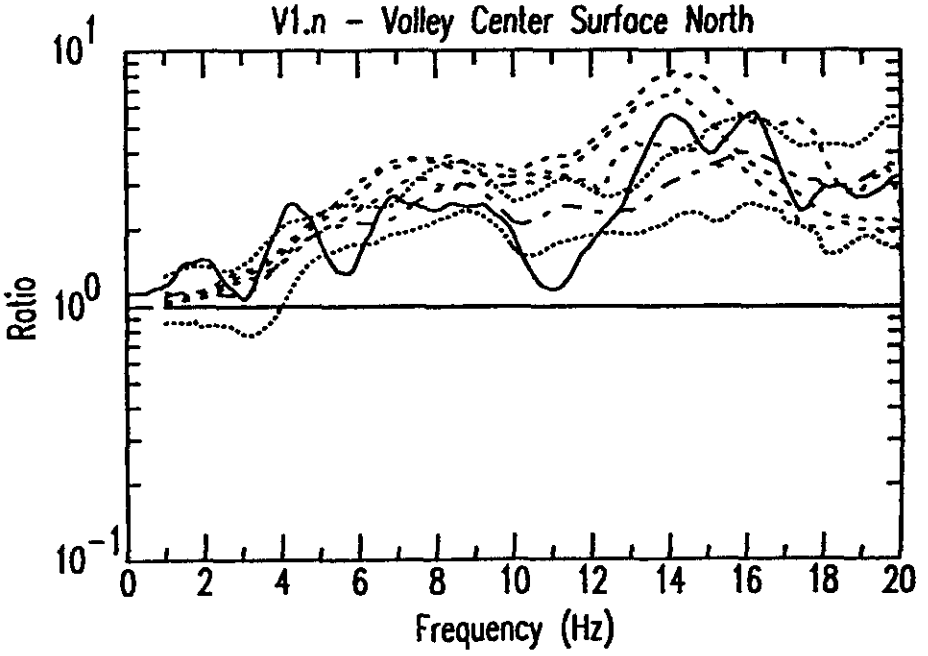

Figure A2b: Standard Model Spectral Ratio Prediction Quartiles vs Observations

Spectral Ratio Predictions: Dashed - quartiles

Observations: Solid - weak-motion test event; Dash-dotted - weak-motion mean; Dotted - 1 std deviation

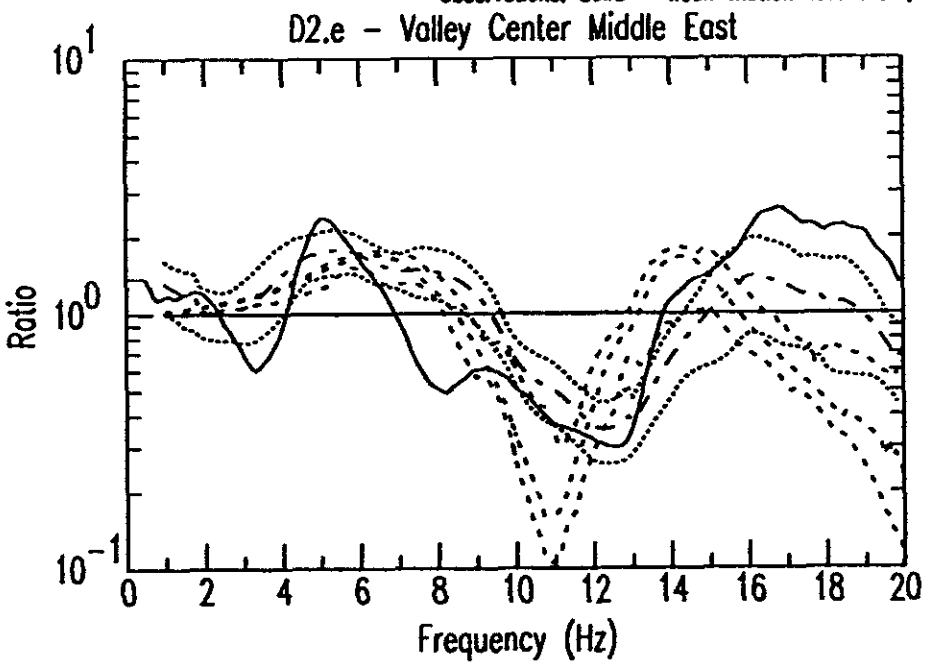

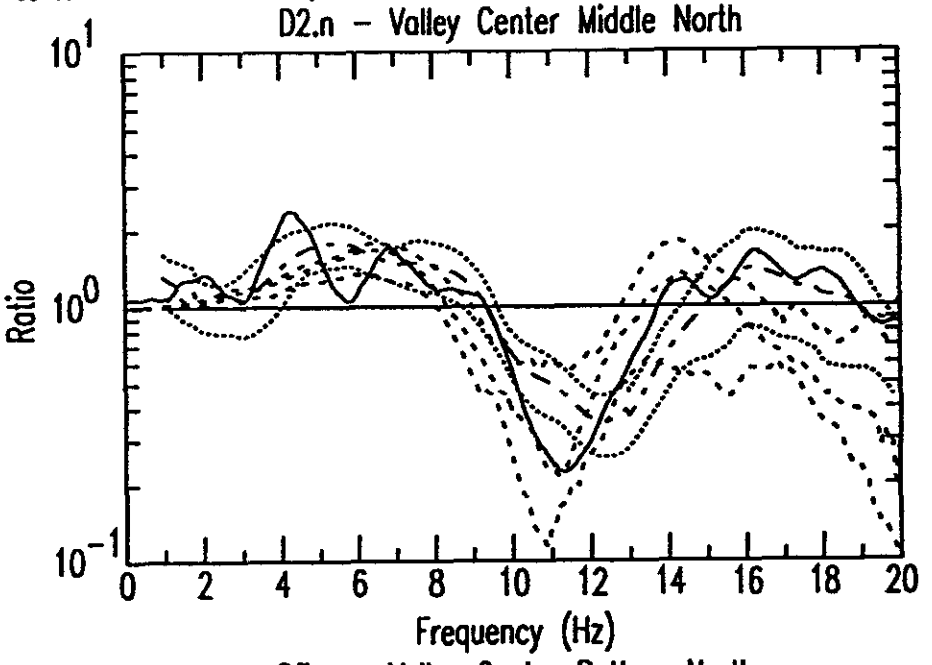

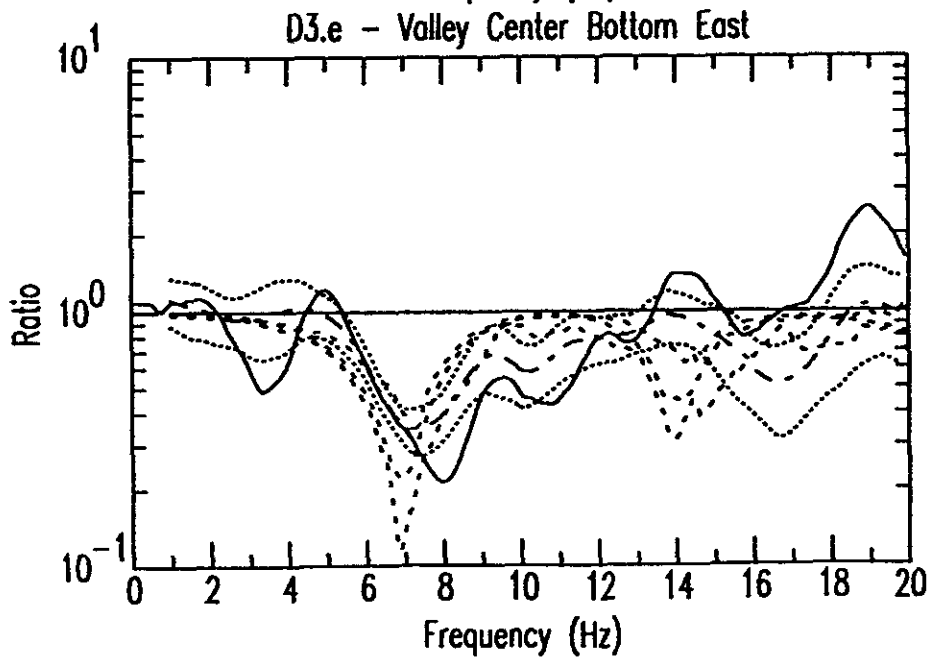

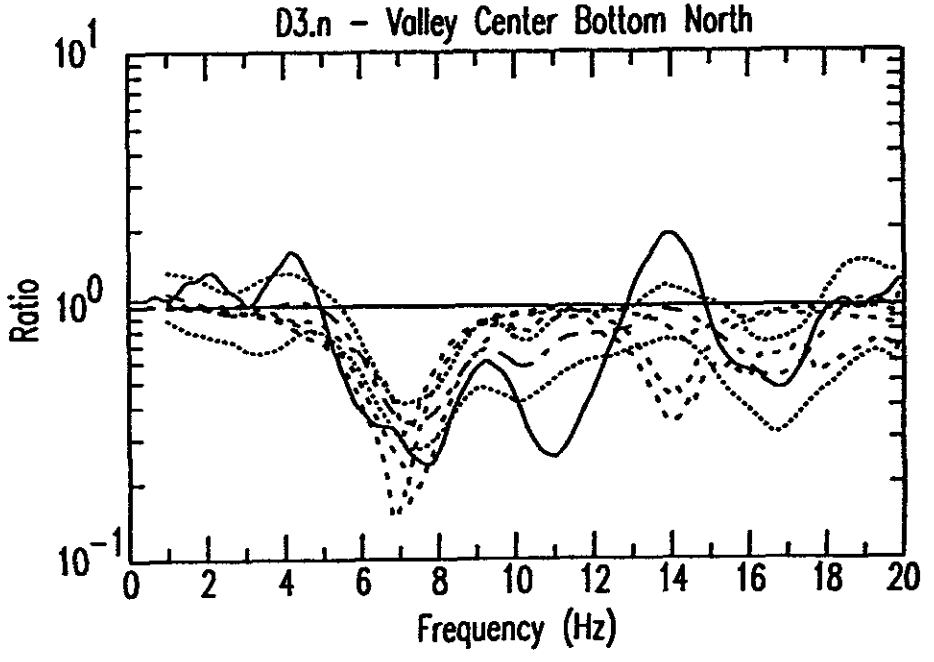

Figure A2c: Standard Model Spectral Ratio Prediction Quartiles vs Observations

Spectral Ratio Predictions: Dashed - quartiles

Observations: Solid - weak-motion test event; Dash-dotted - weak-motion mean; Dotted - 1 std deviation

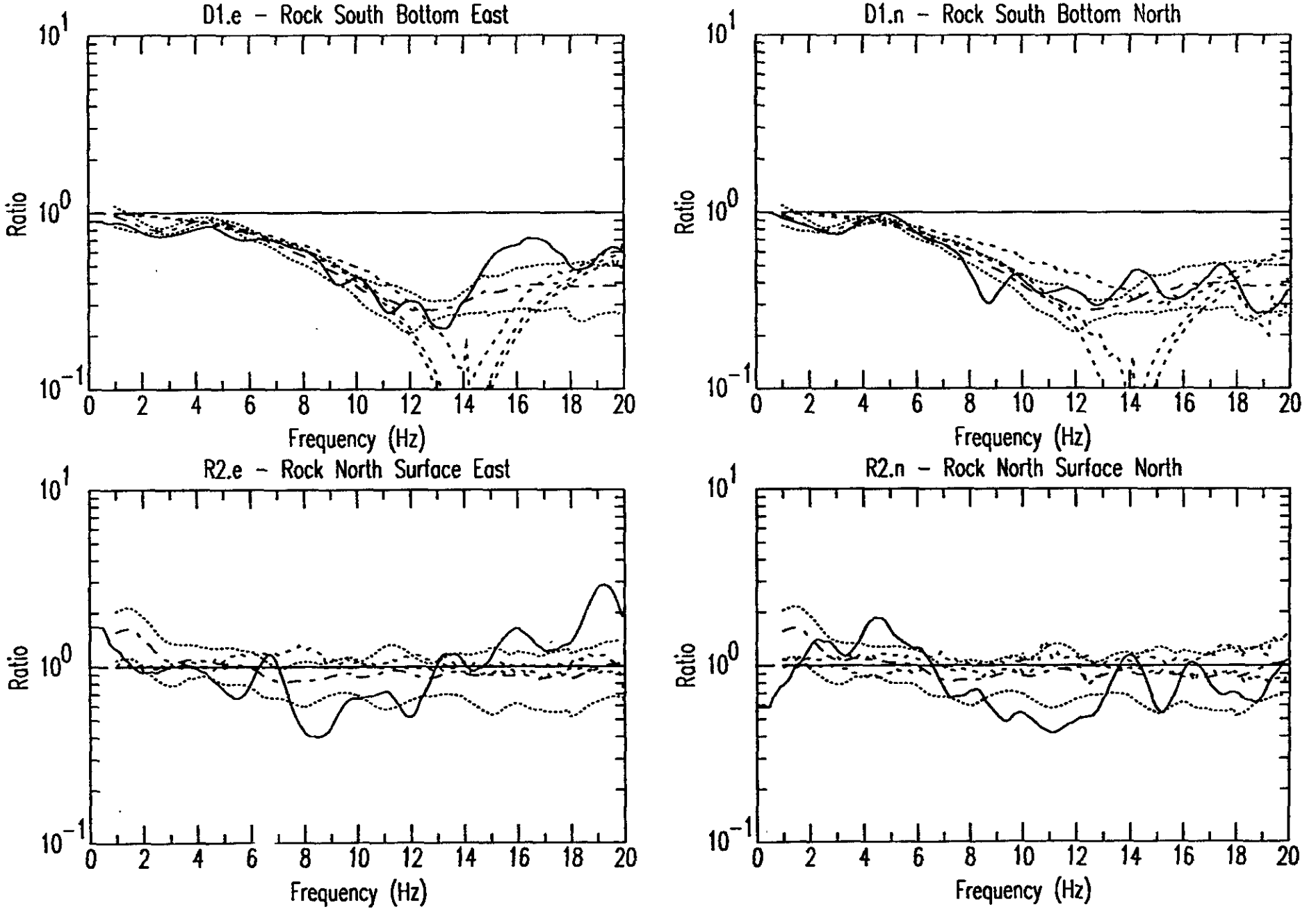

Figure A3a: Standard Response Spectra:
Station V2 Valley North Surface Standard Geotechnical Model
Solid lines - Predictions; Dashed line - Observed

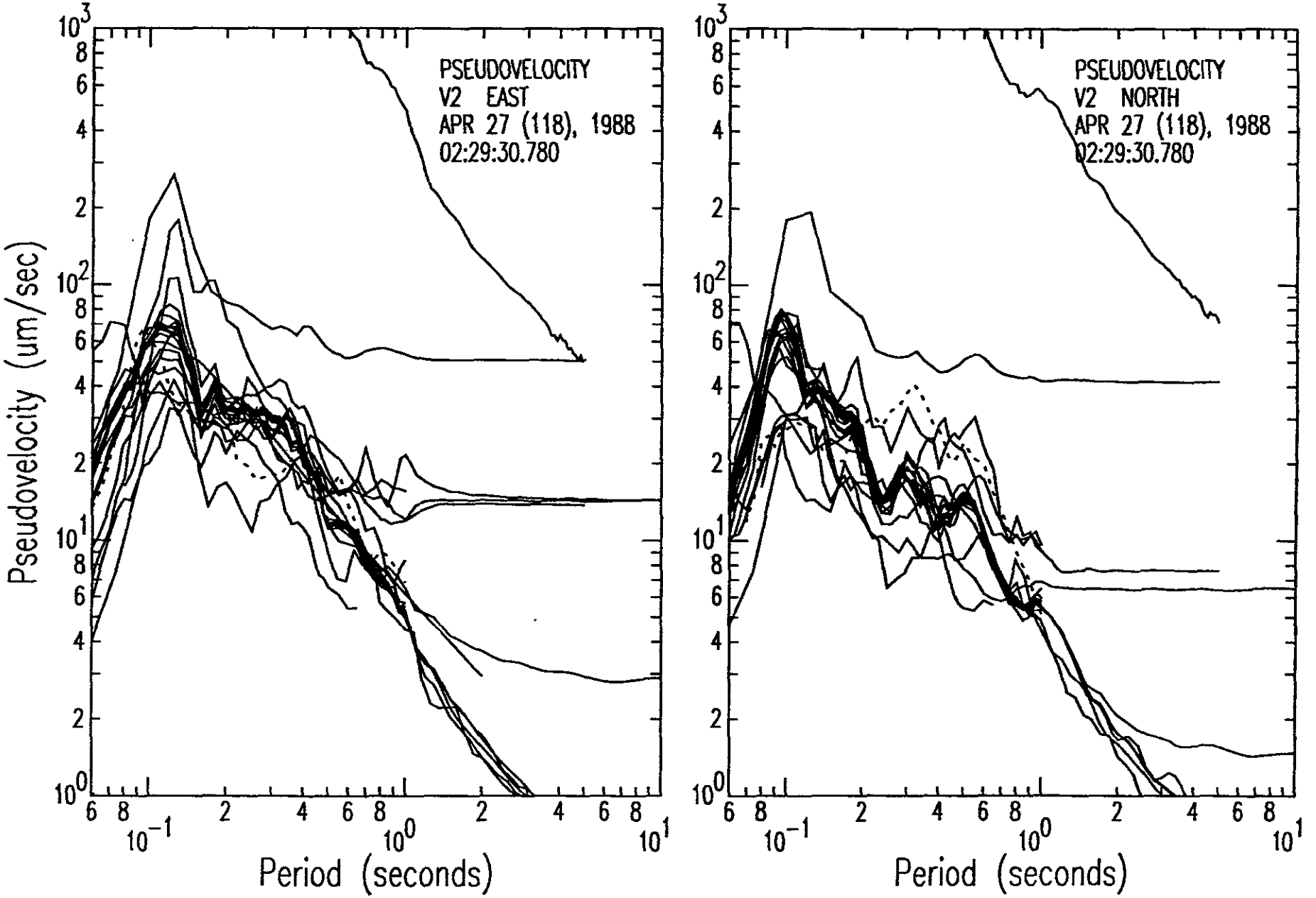

Figure A3b: Standard Response Spectra:
Station V1 Valley Center Surface Standard Geotechnical Model
Solid lines – Predictions; Dashed line – Observed

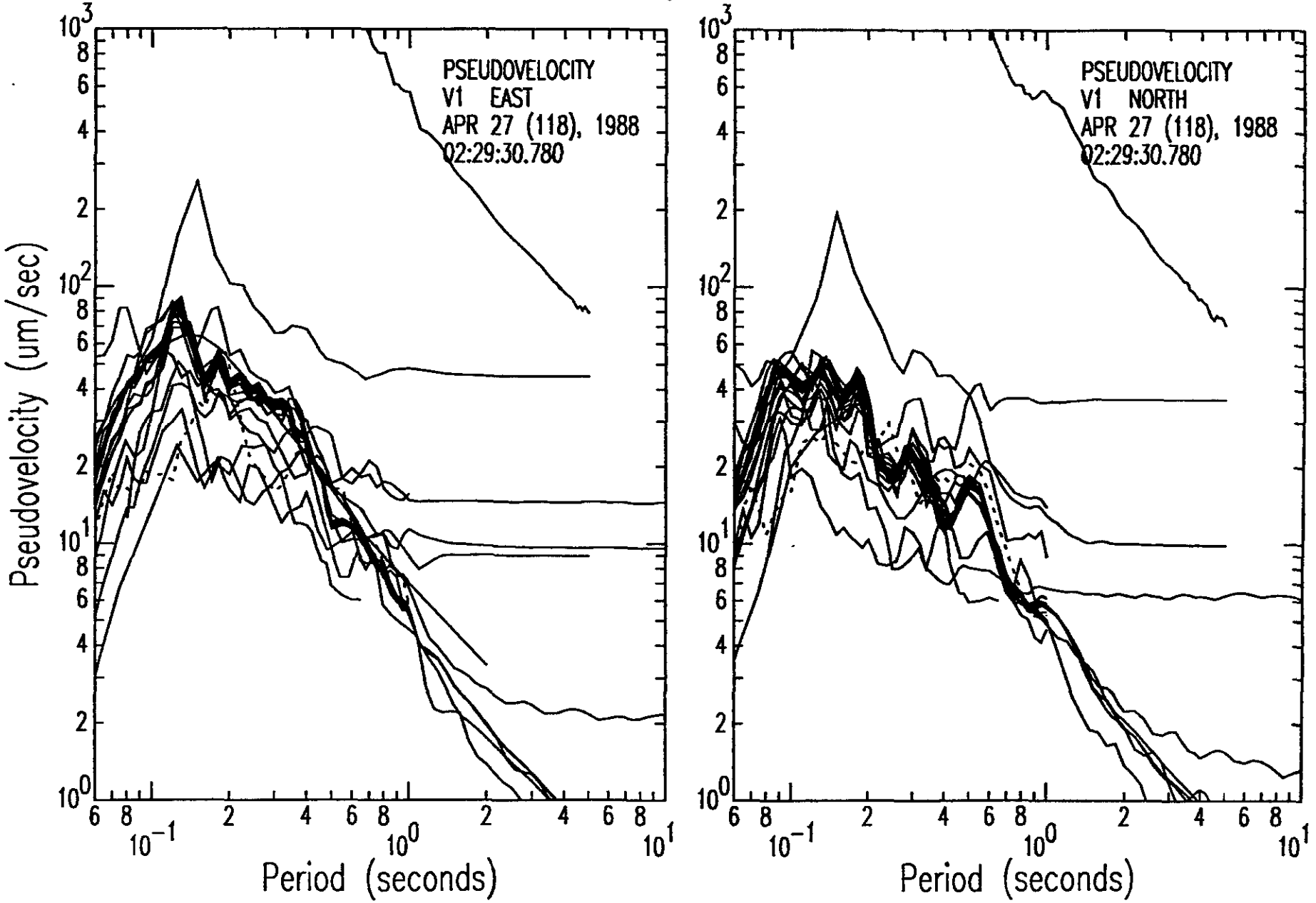

Figure A3c: Standard Response Spectra:
Station D2 Valley Center Middle Standard Geotechnical Model
Solid lines - Predictions; Dashed line - Observed

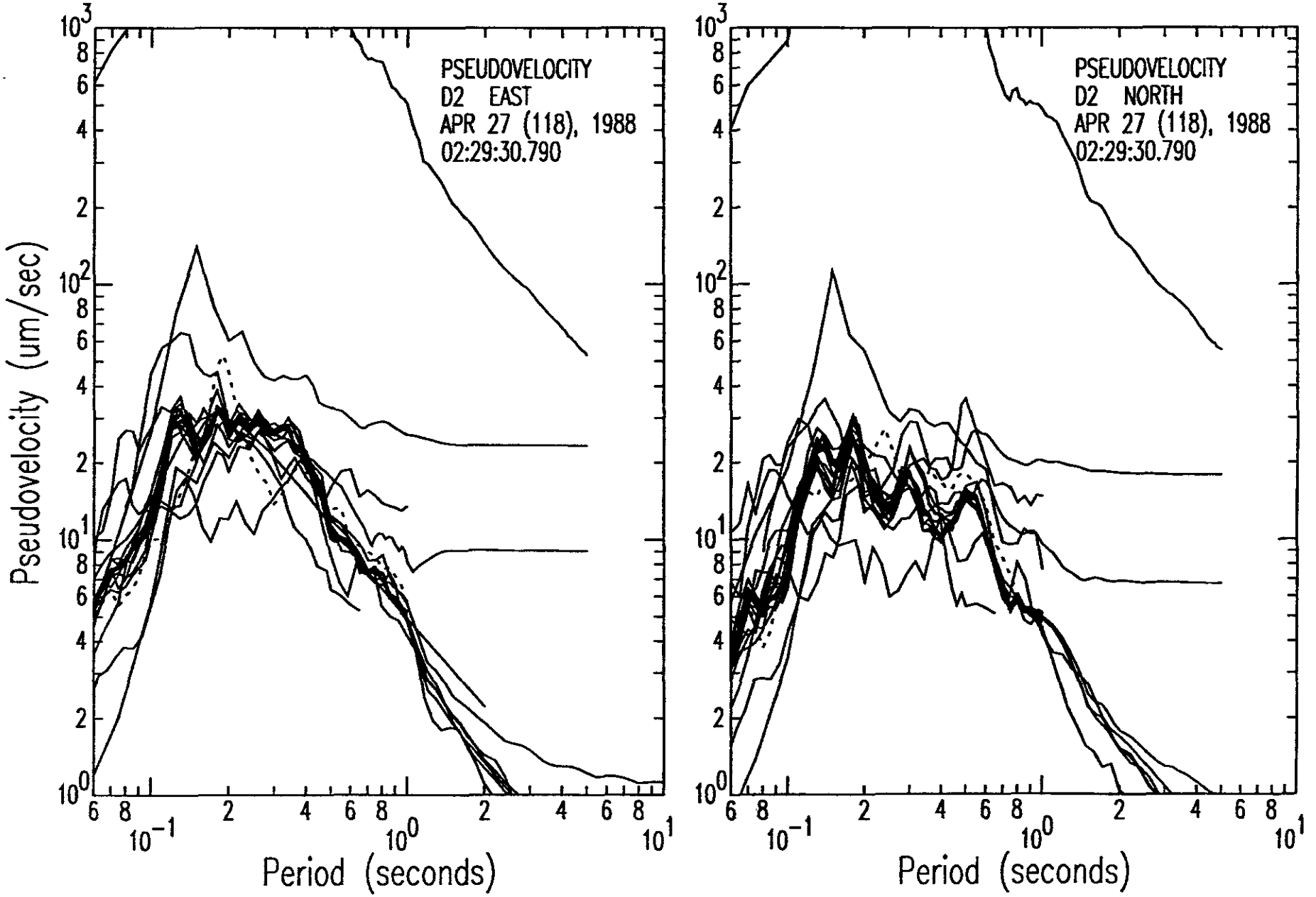

Figure A3d: Standard Response Spectra:

Station D3 Valley Center Bottom Standard Geotechnical Model

Solid lines – Predictions; Dashed line – Observed

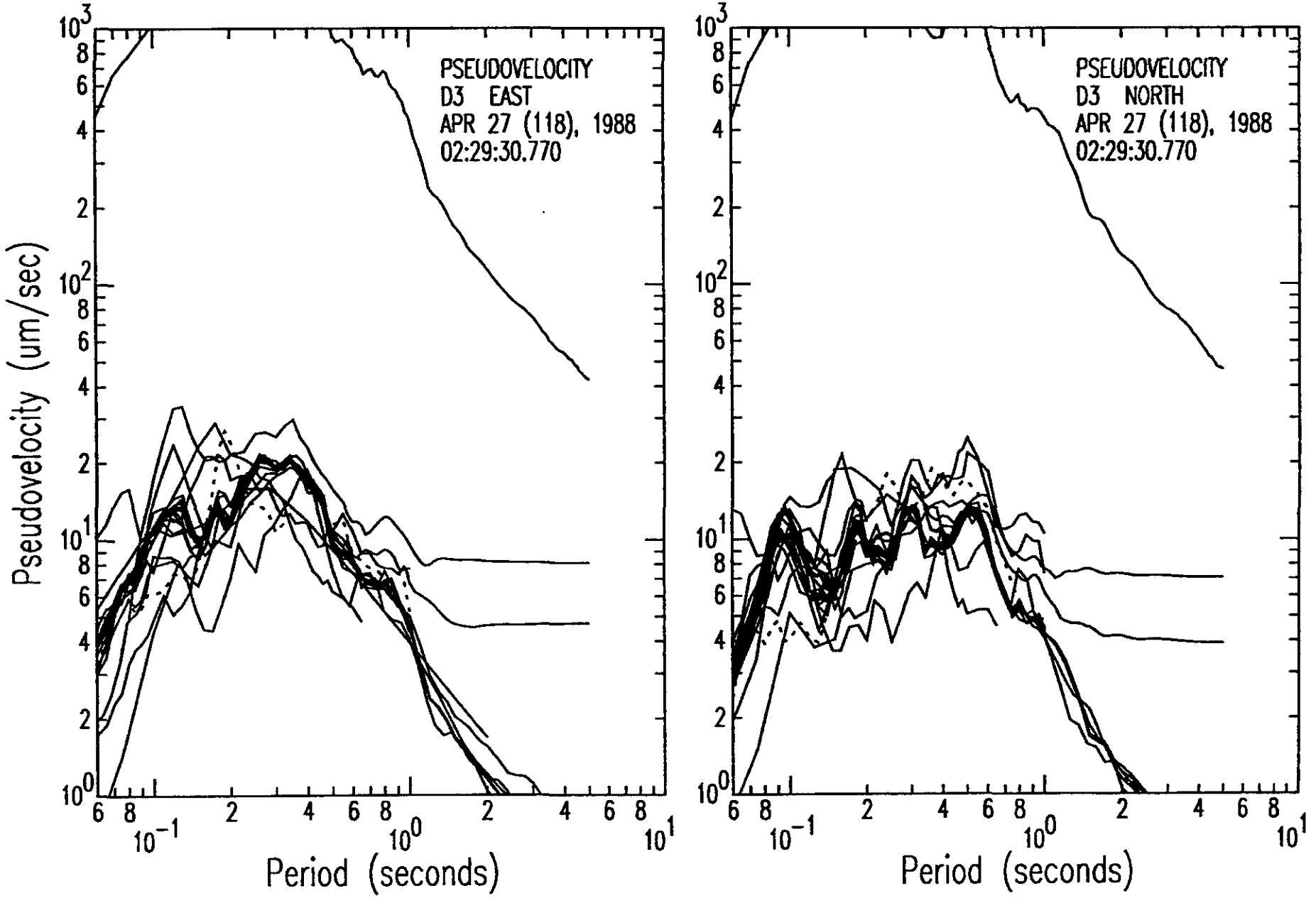

Figure A3e: Standard Response Spectra:
Station D1 Rock South Bottom Standard Geotechnical Model
Solid lines – Predictions; Dashed line – Observed

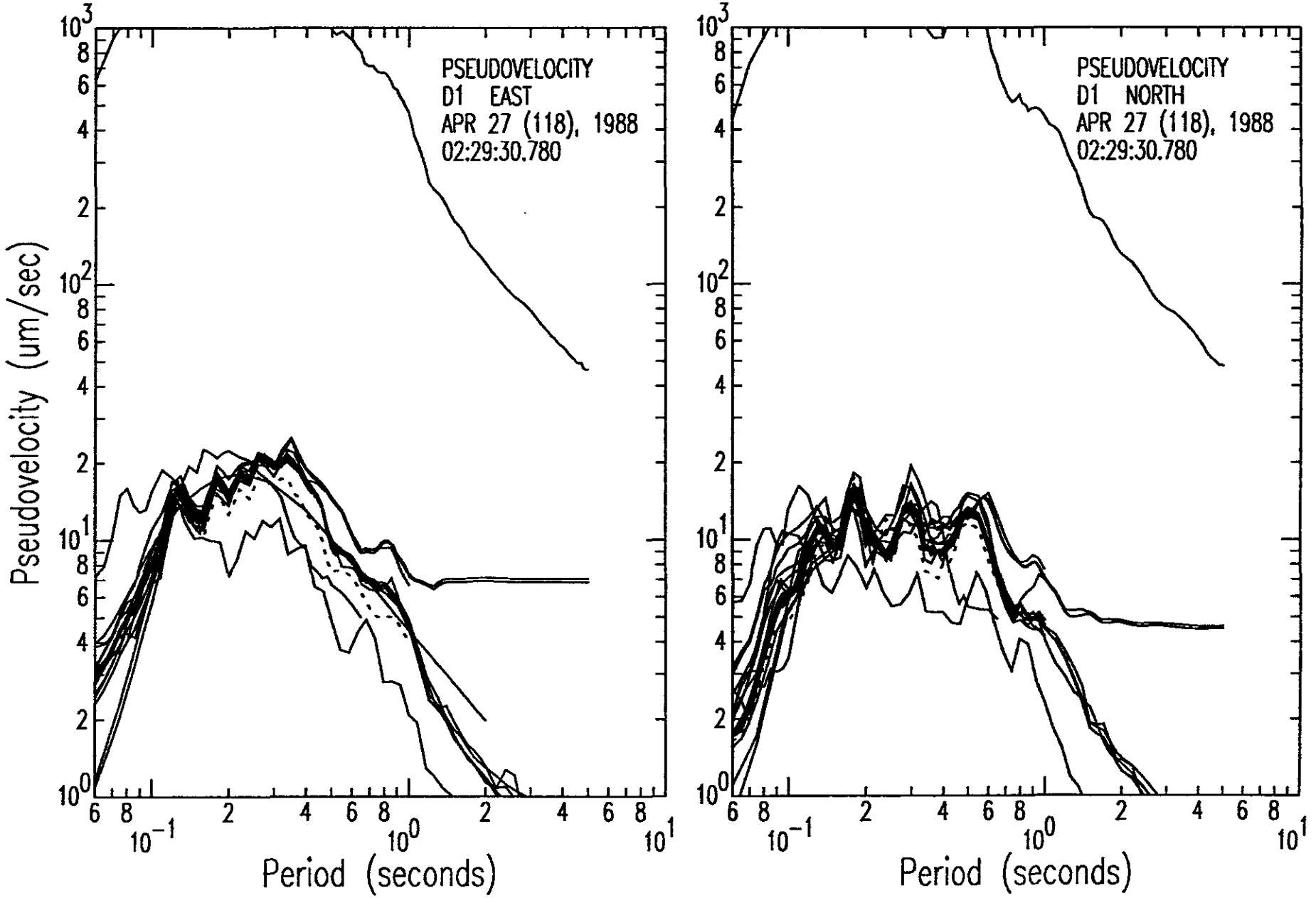

Figure A3f: Standard Response Spectra:
Station R2 Rock North Surface Standard Geotechnical Model

Solid lines – Predictions; Dashed line – Observed

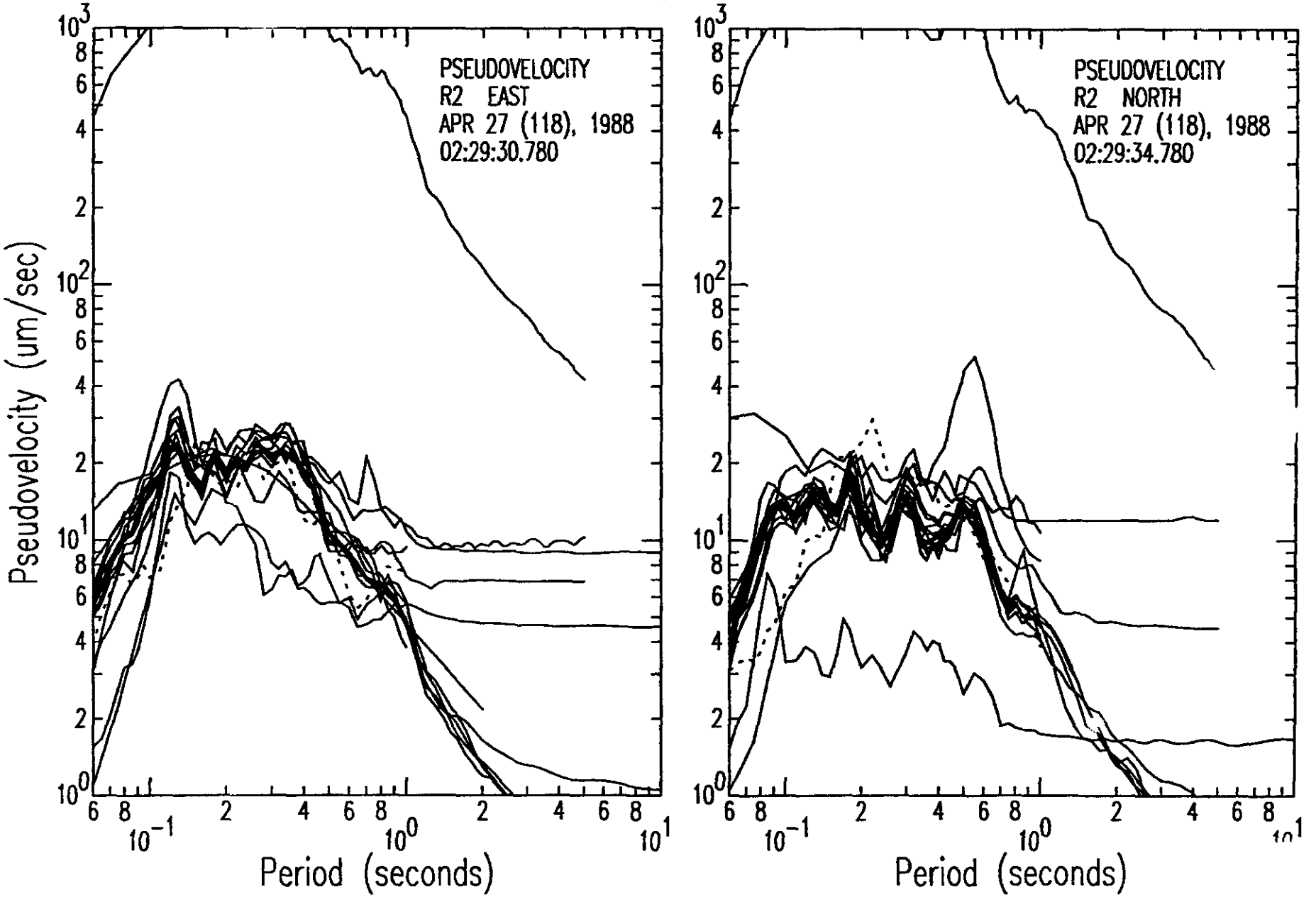

Figure A4a: Standard Model Response Spectra Prediction Quartiles vs Observations

Response Spectra Predictions: Dashed - quartiles

Observations: Solid - weak-motion test event

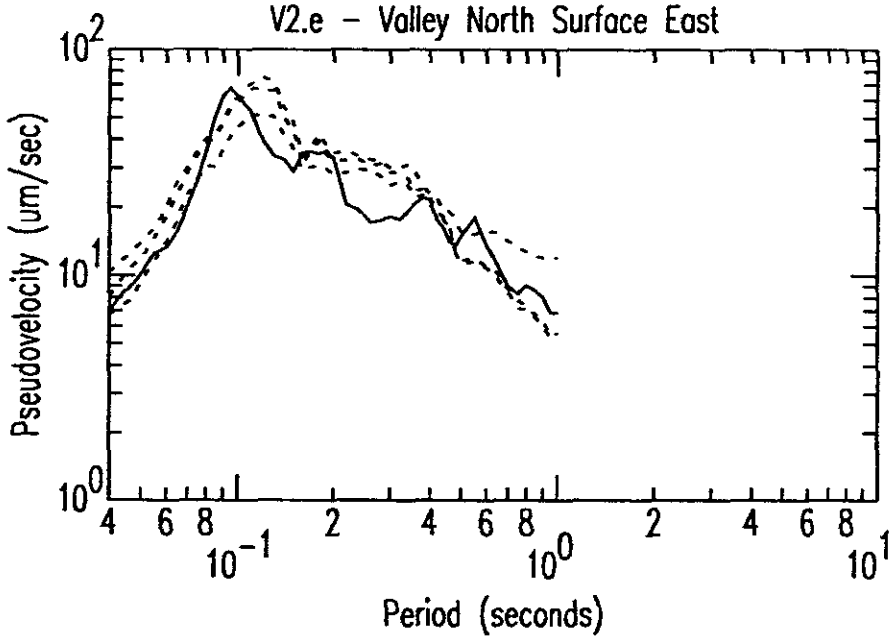

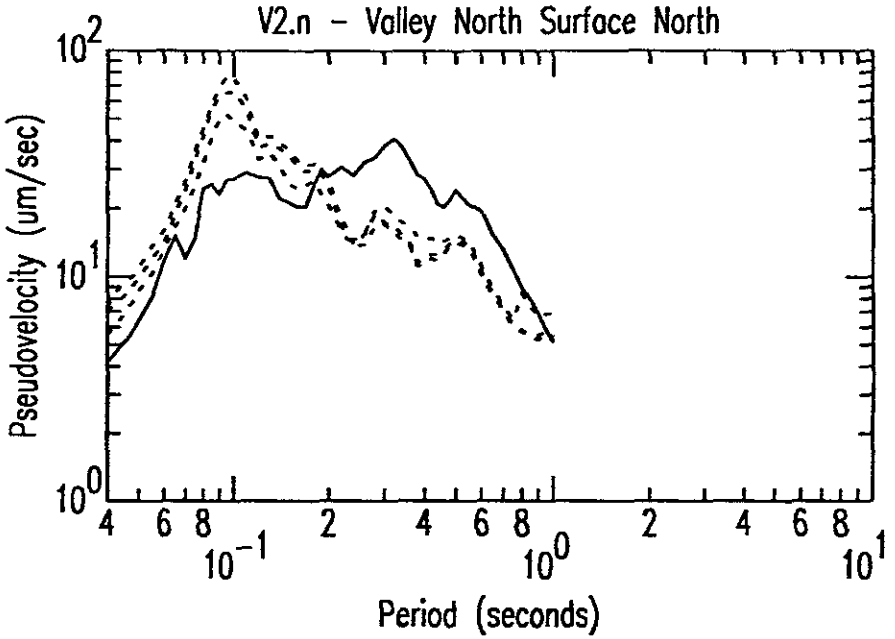

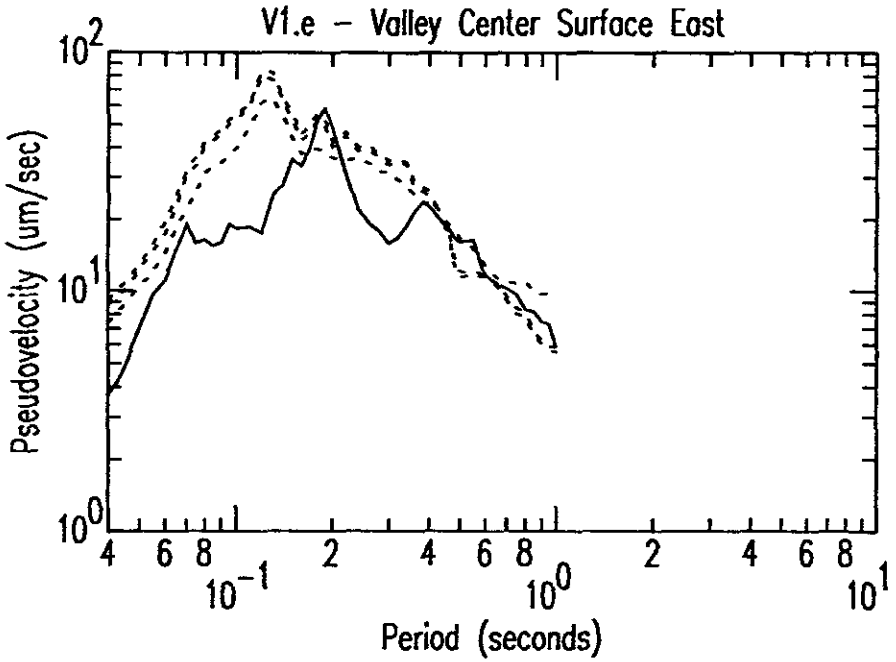

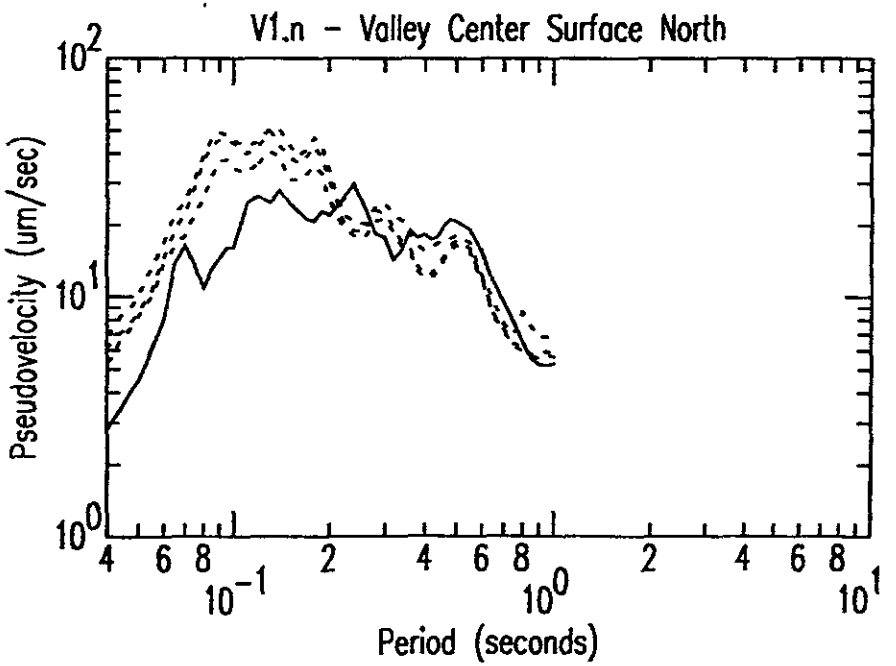

Figure A4b: Standard Model Response Spectra Prediction Quartiles vs Observations

Response Spectra Predictions: Dashed – quartiles
Observations: Solid – weak-motion test event

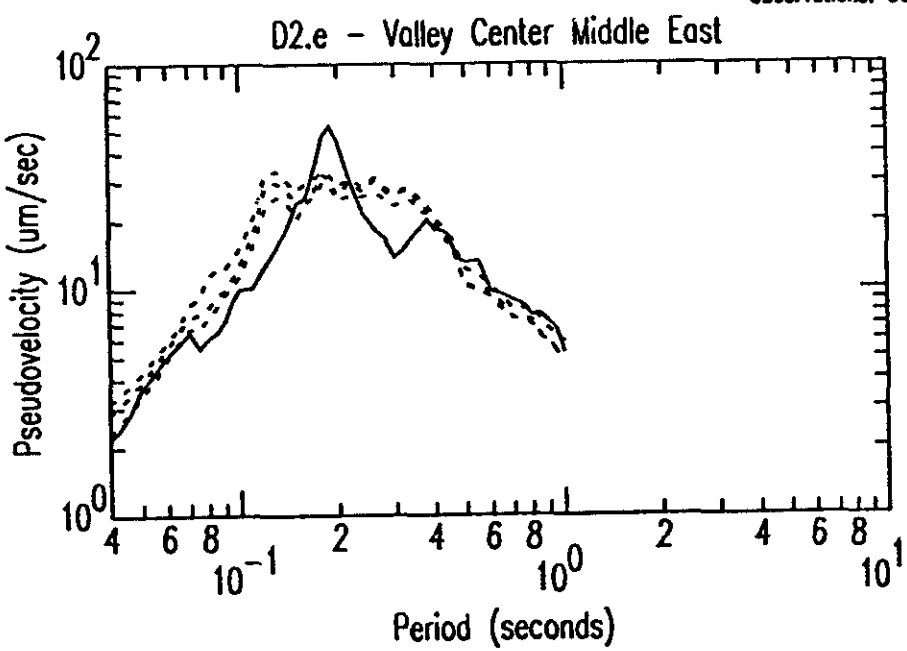

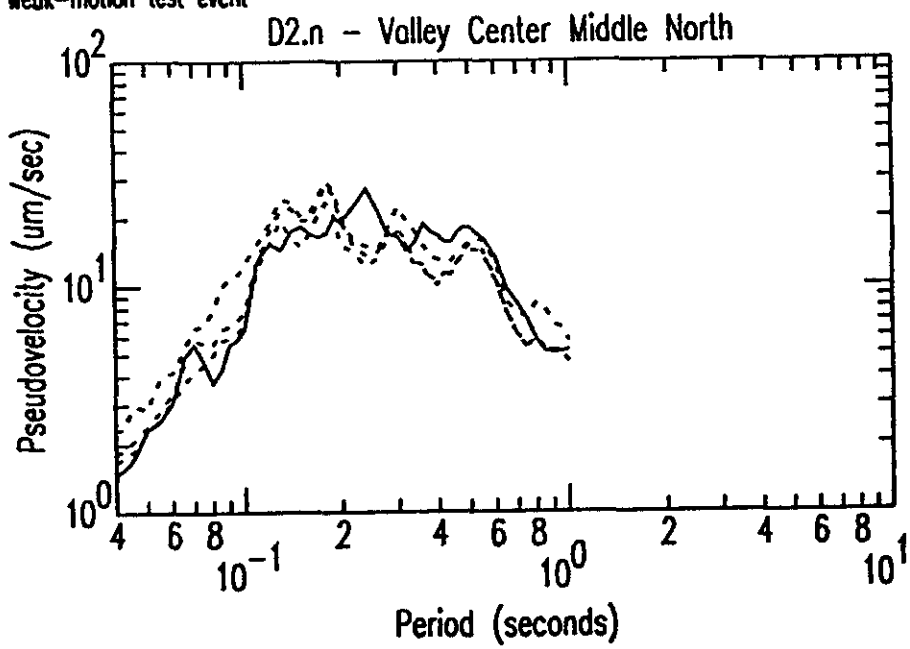

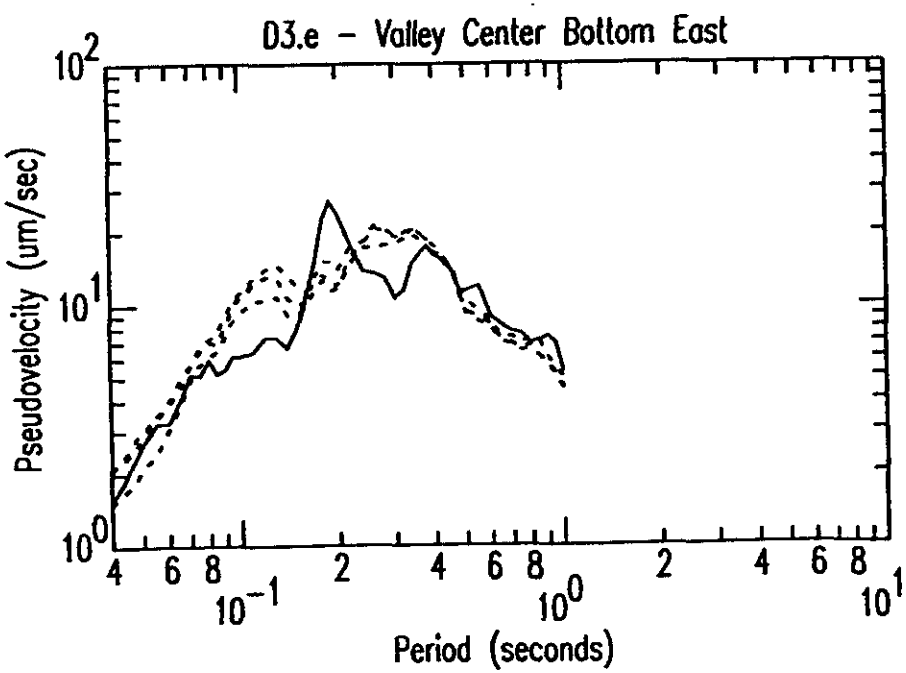

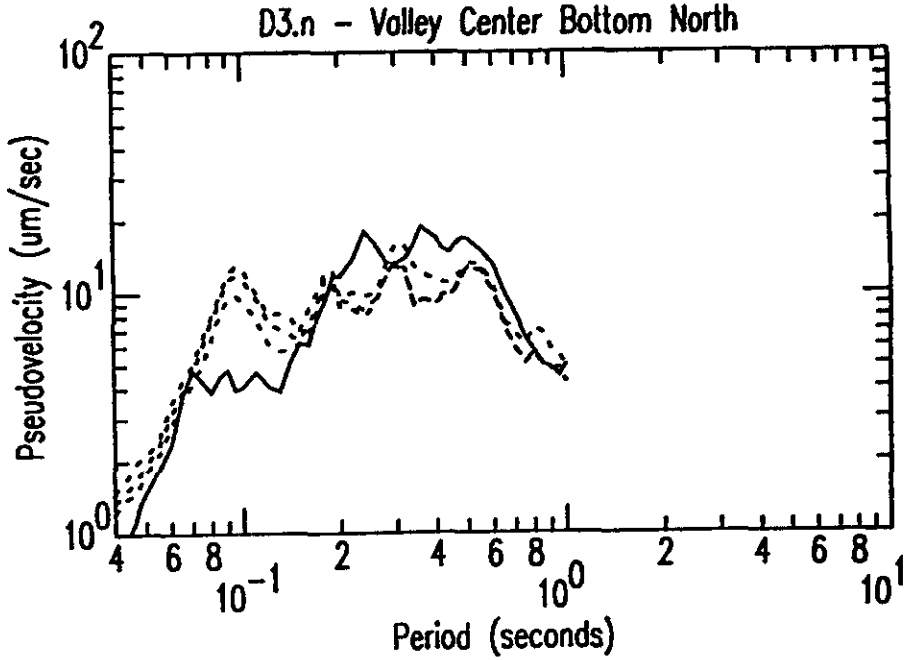

Figure A4c: Standard Model Response Spectra Prediction Quartiles vs Observations

Response Spectra Predictions: Dashed – quartiles
Observations: Solid – weak-motion test event

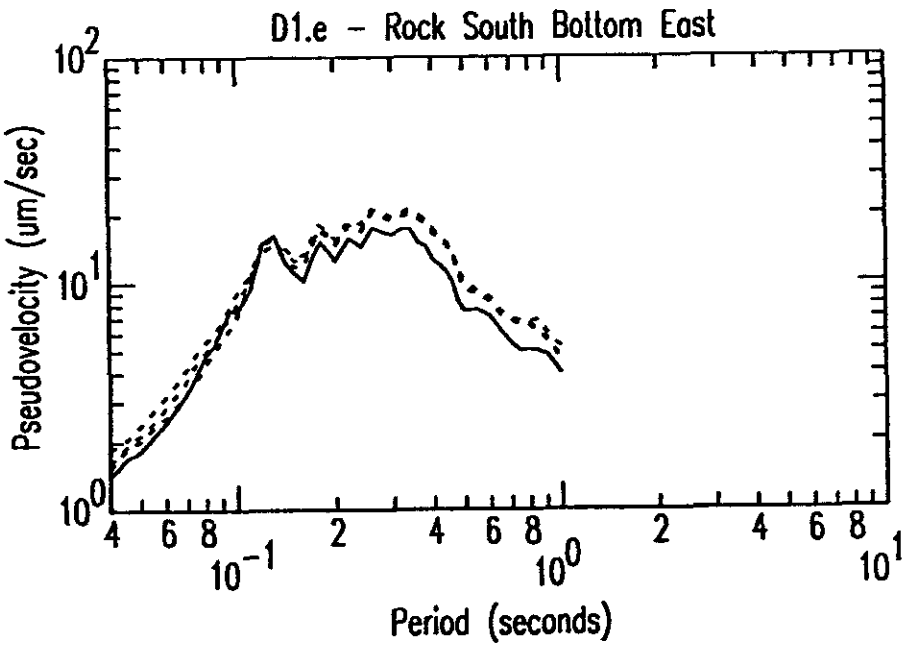

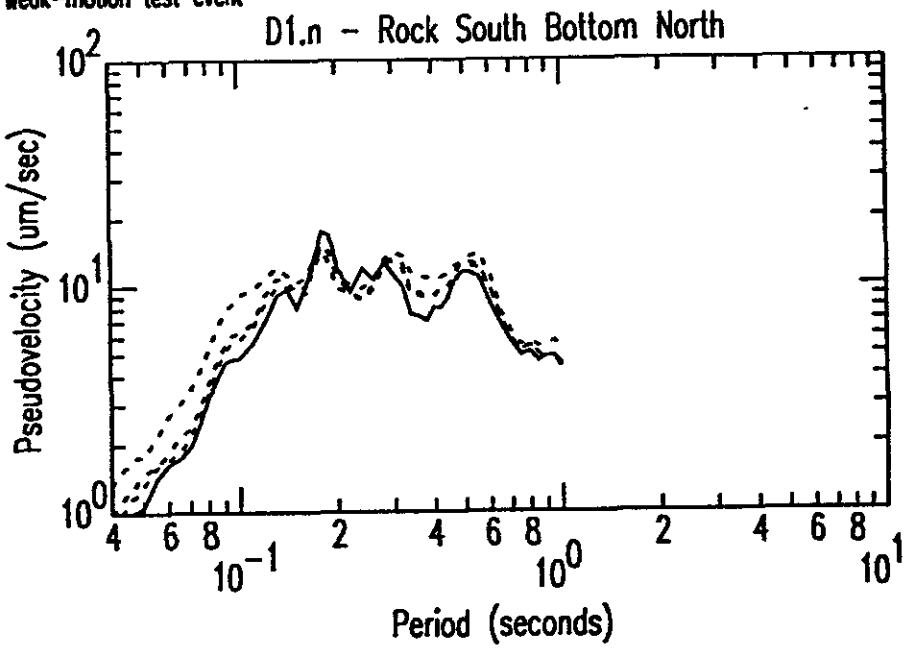

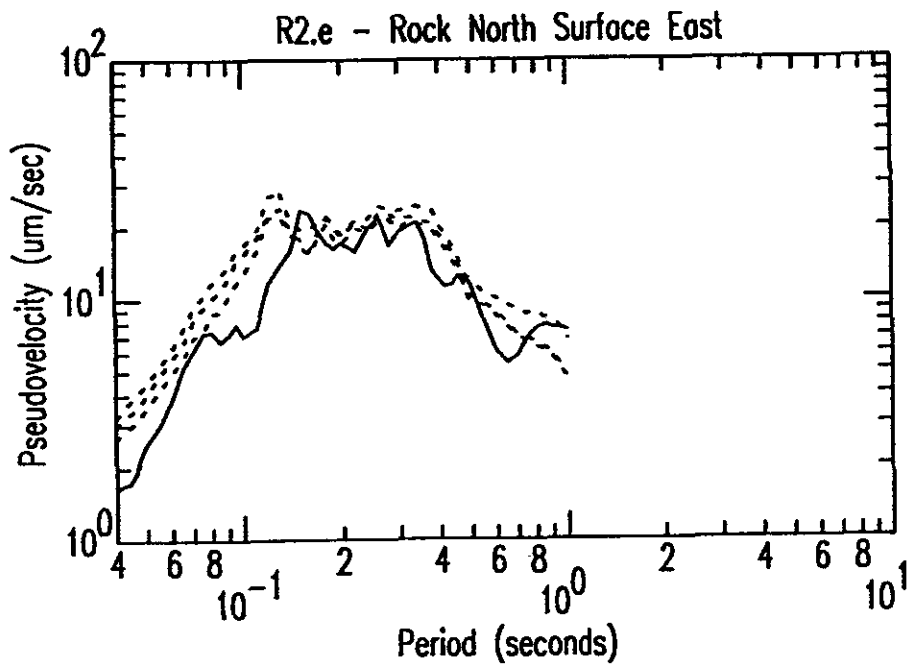

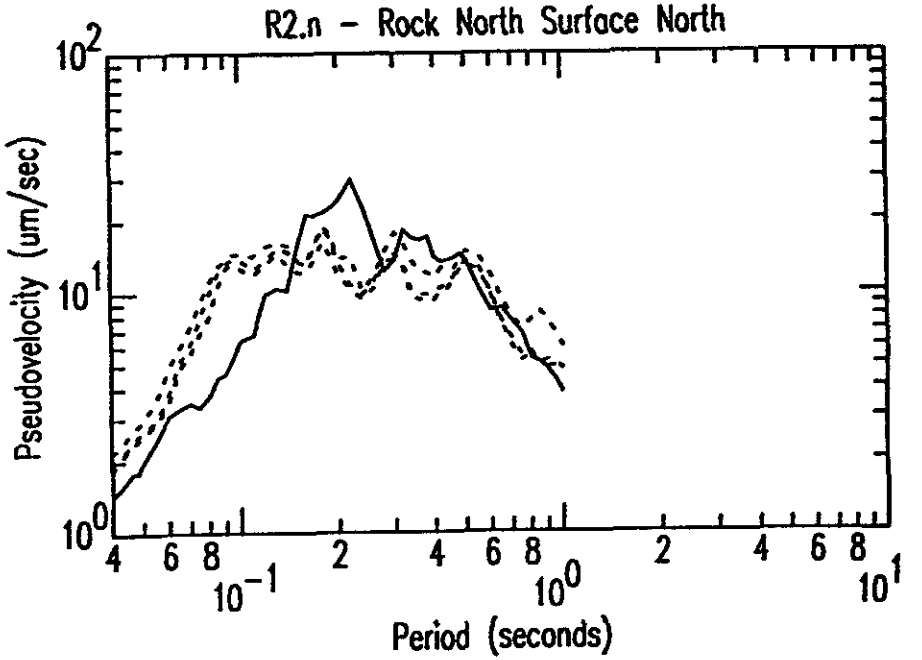

Figure A5a: Observed V1 vs Predicted V1 Standard Model Accelerograms (uM/sec/sec x 100)

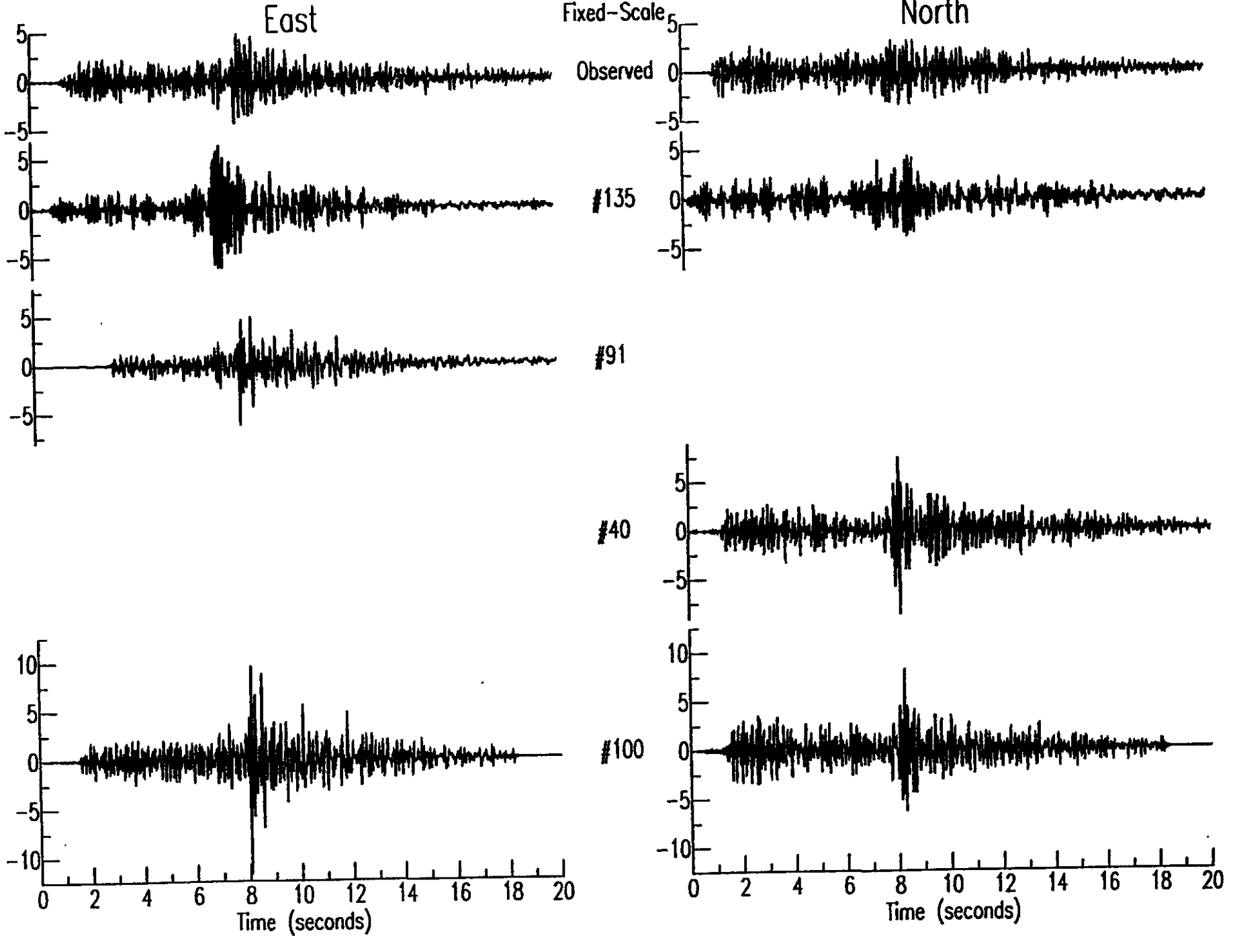

Figure A5b: Observed V1 vs Predicted V1 Standard Model Accelerograms (uM/sec/sec x 100)

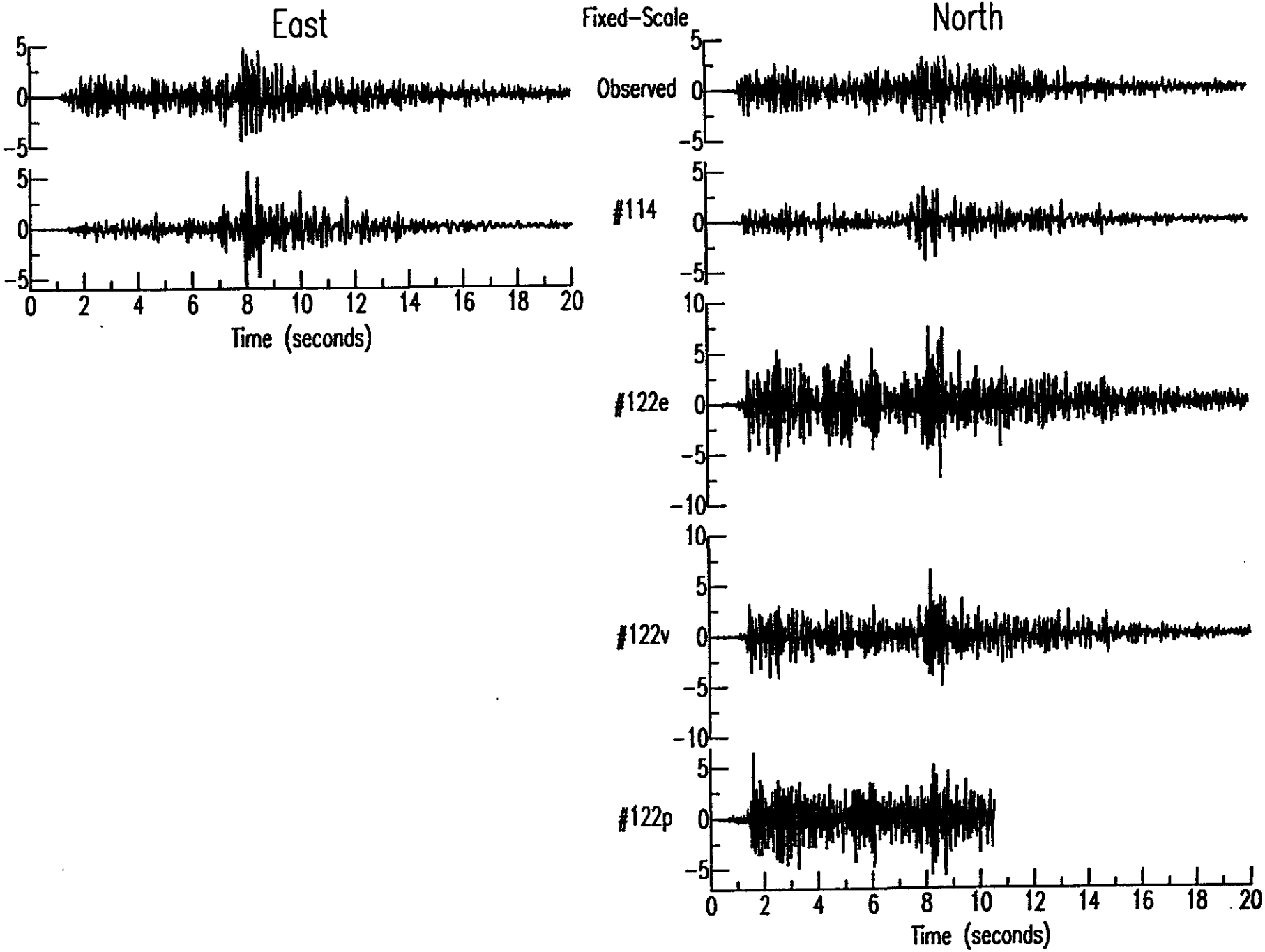

Figure A5c: Observed V1 vs Predicted V1 Standard Model Accelerograms (uM/sec/sec x 100)

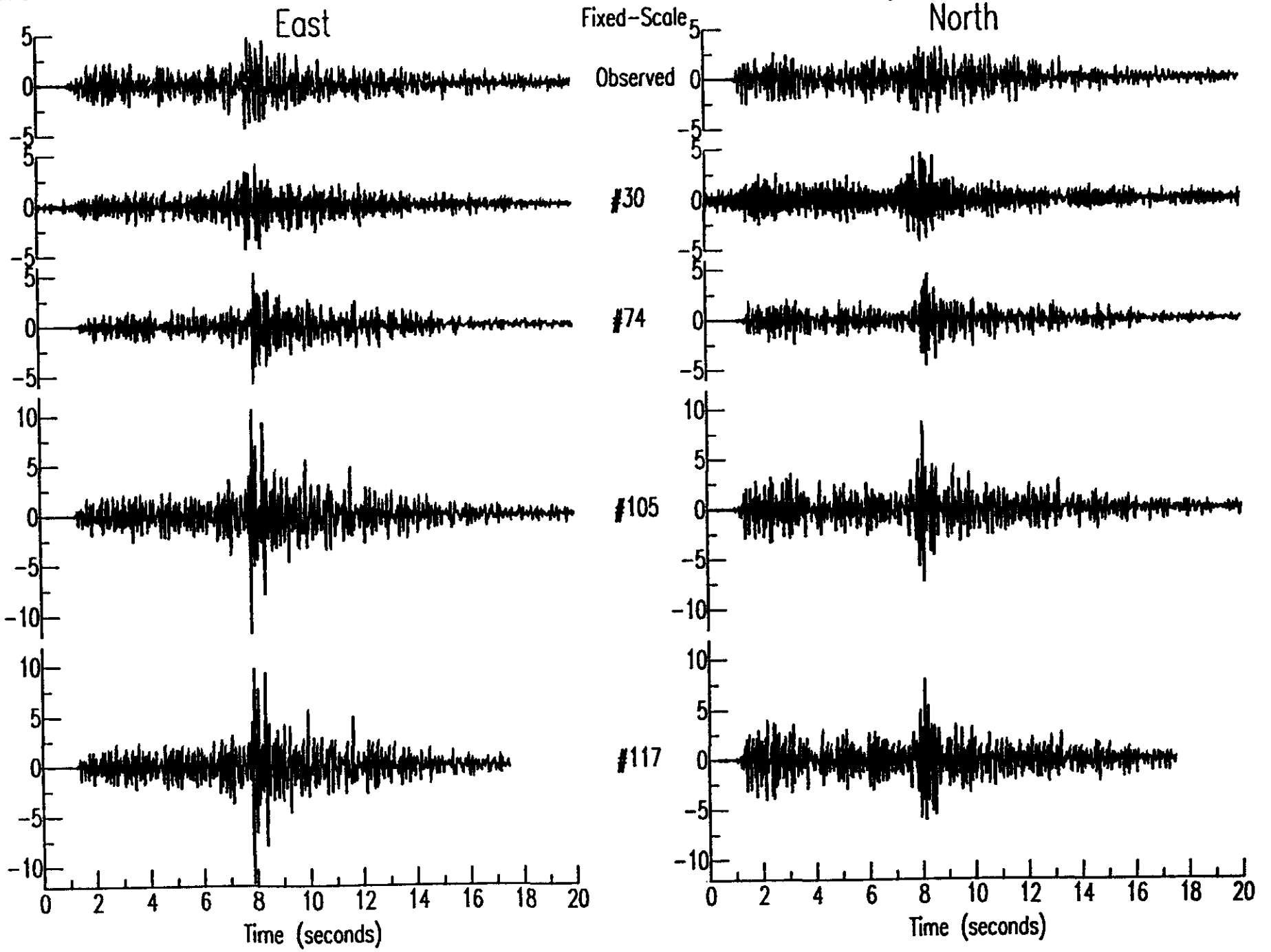

Figure A5d: Observed V1 vs Predicted V1 Standard Model Accelerograms (uM/sec/sec x 100)

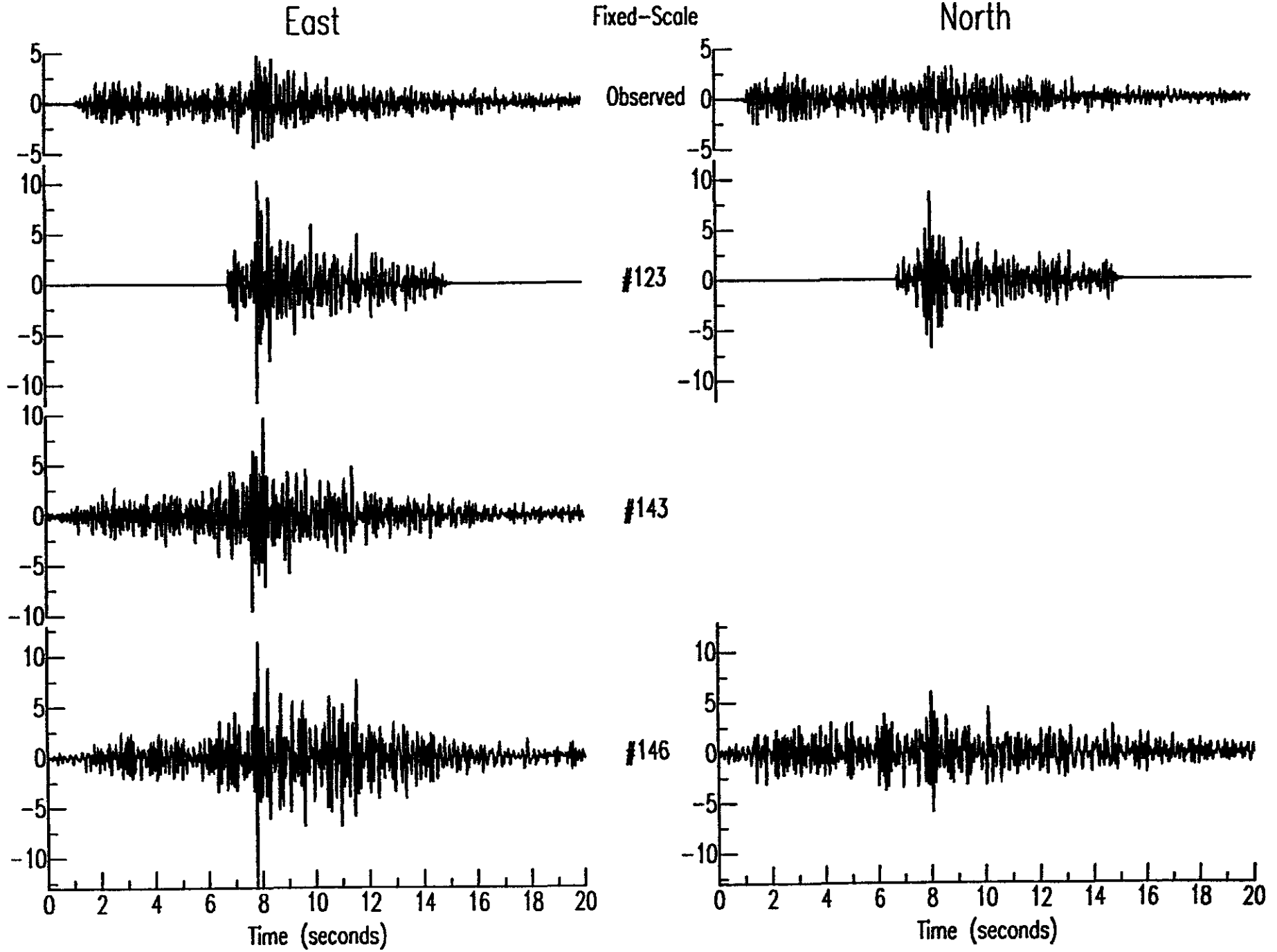

Figure A5e: Observed V1 vs Predicted V1 Standard Model Accelerograms (uM/sec/sec x 100)

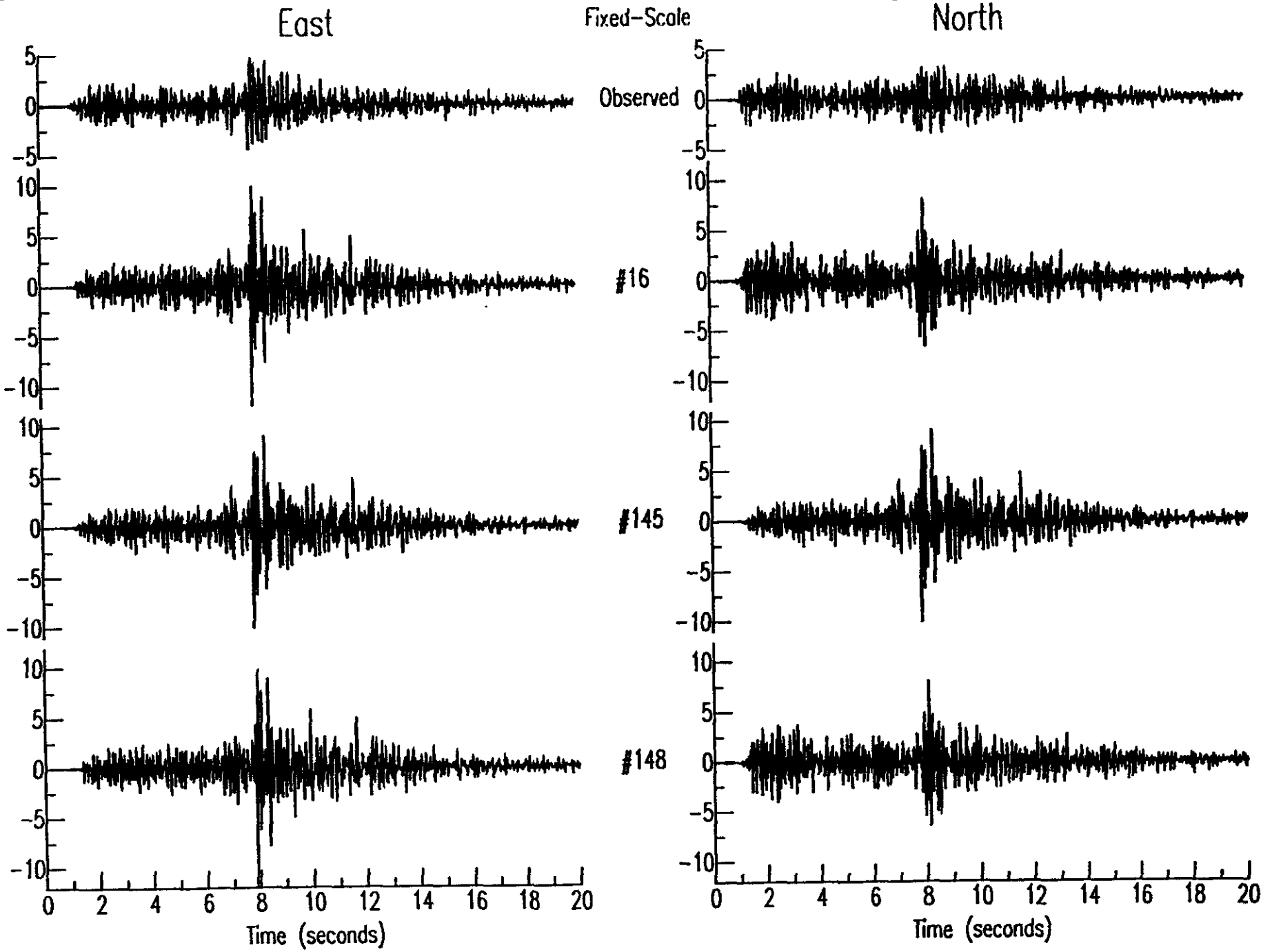

Figure A5f: Observed V1 vs Predicted V1 Standard Model Accelerograms (uM/sec/sec x 100)

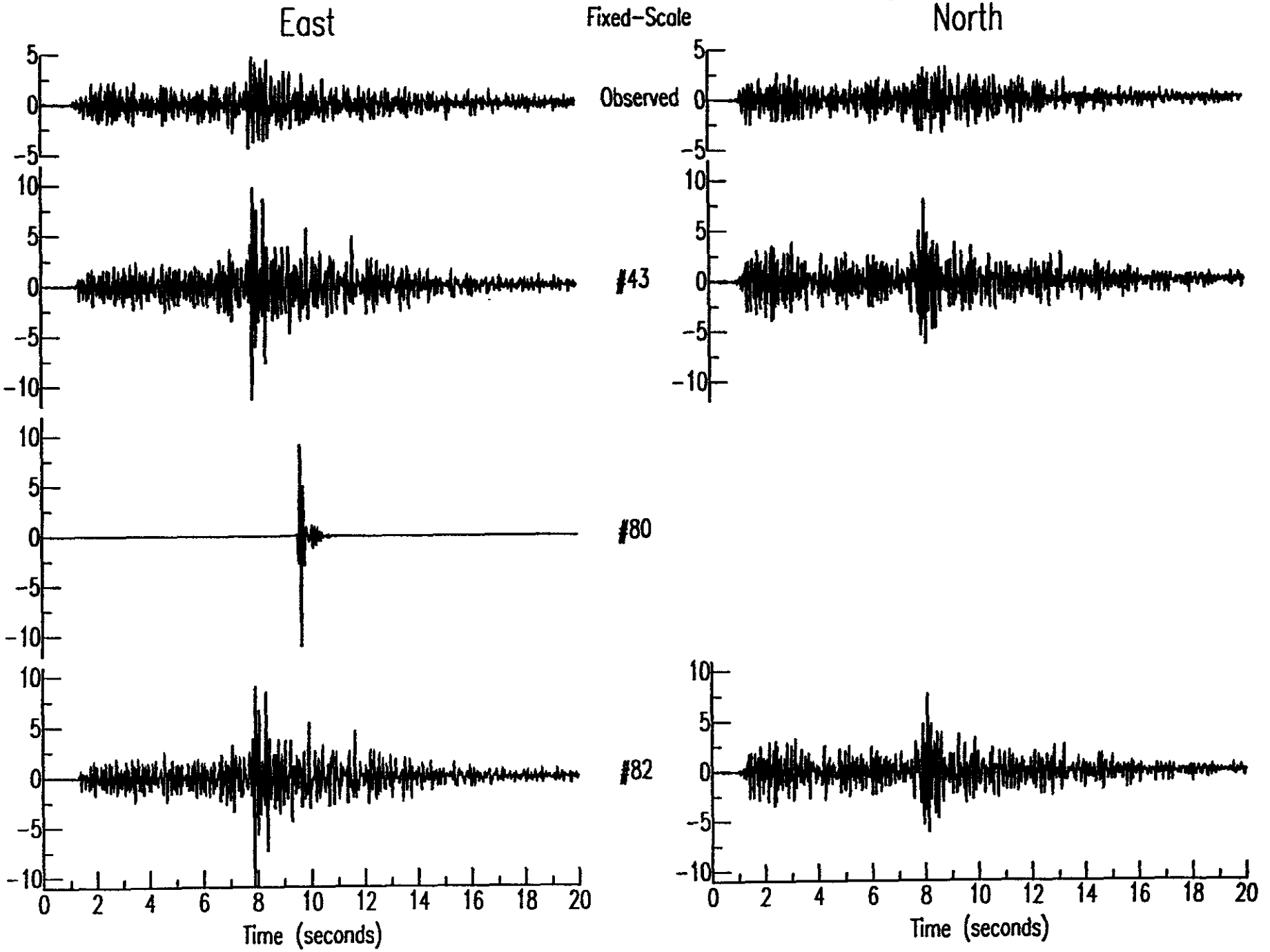

Figure A5g: Observed V1 vs Predicted V1 Standard Model Accelerograms (uM/sec/sec x 100)

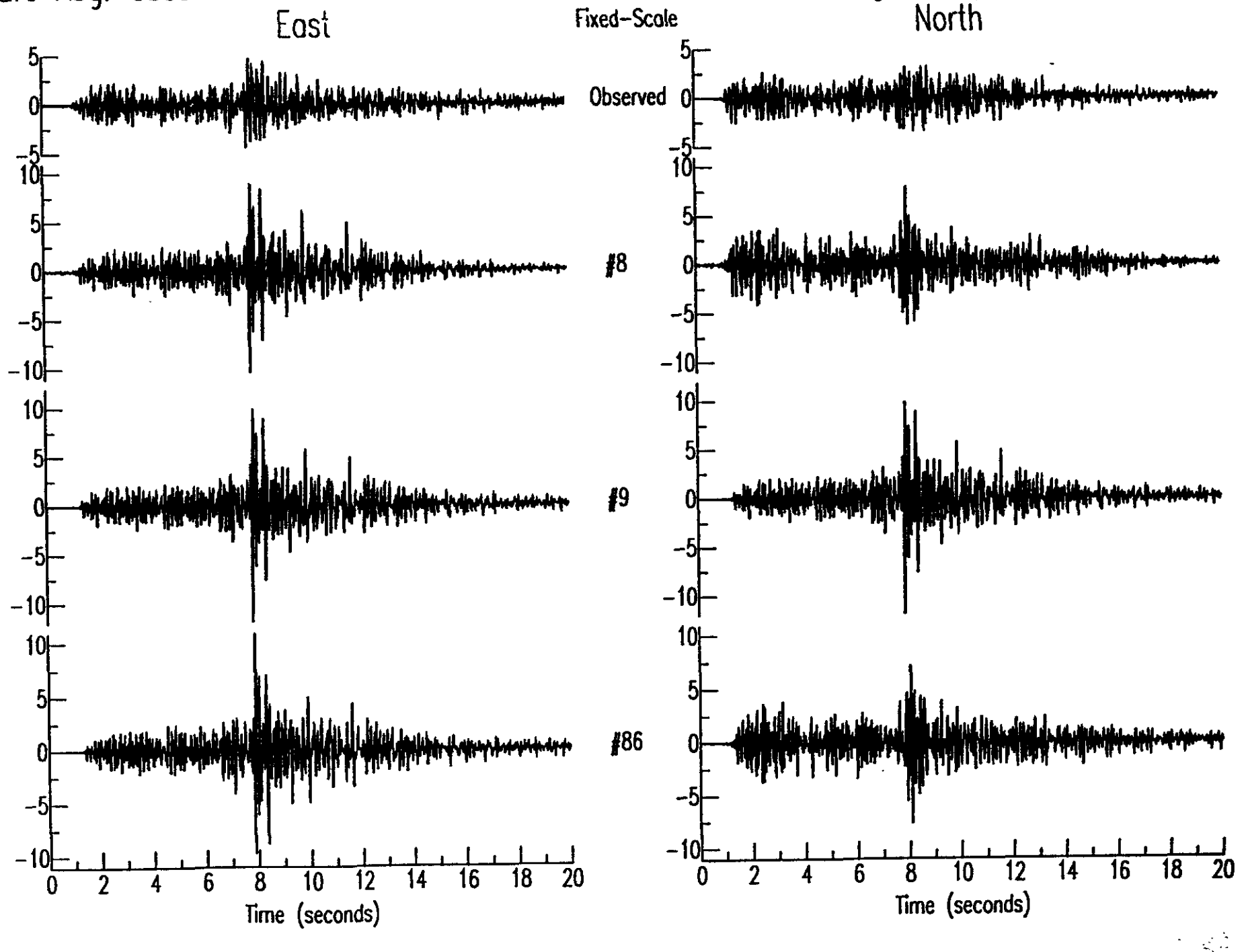

Figure A5h: Observed V1 vs Predicted V1 Standard Model Accelerograms (uM/sec/sec x 100)

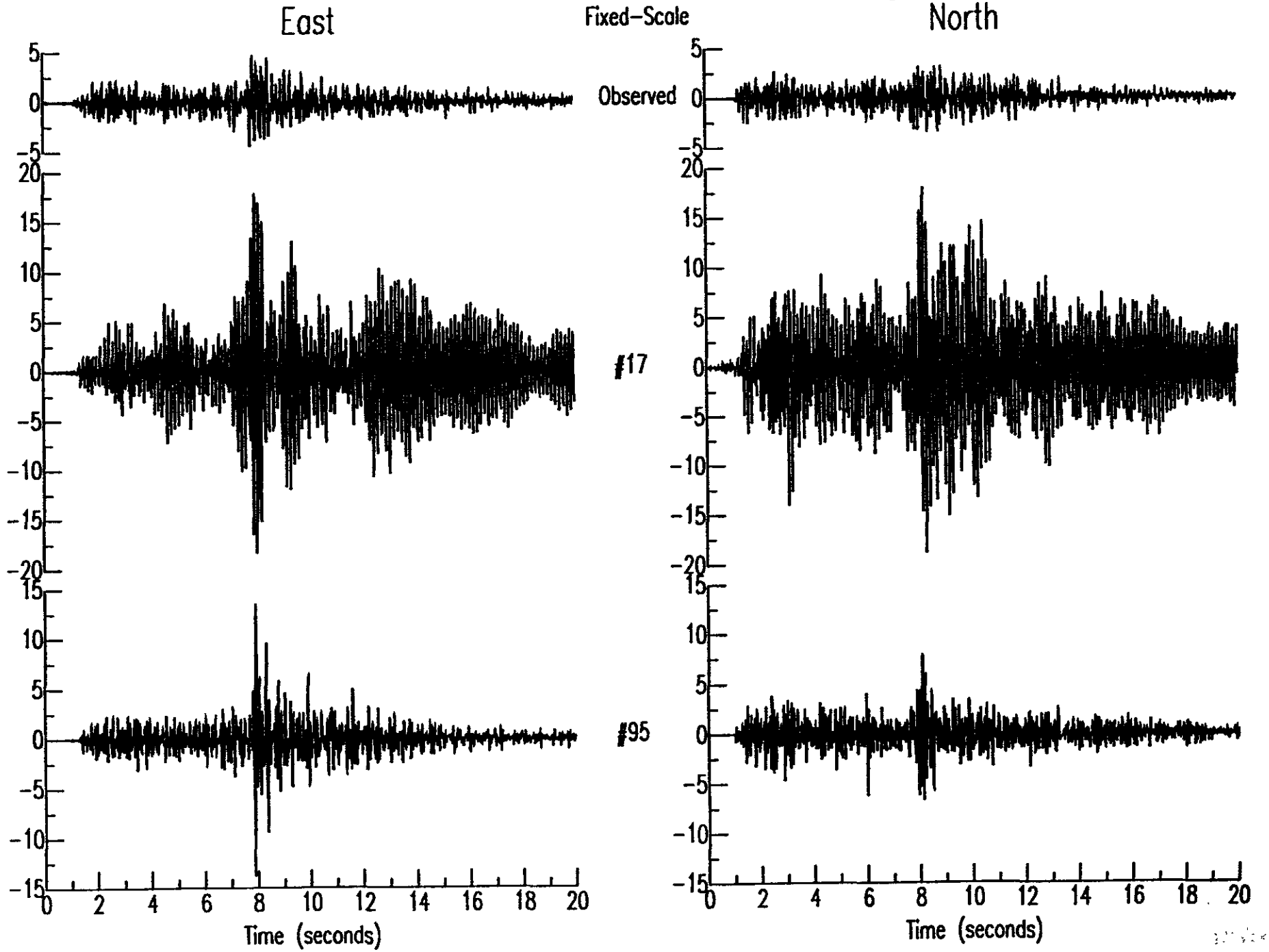

Figure A5i: Observed V1 vs Predicted V1 Standard Model Accelerograms (uM/sec/sec x 100)

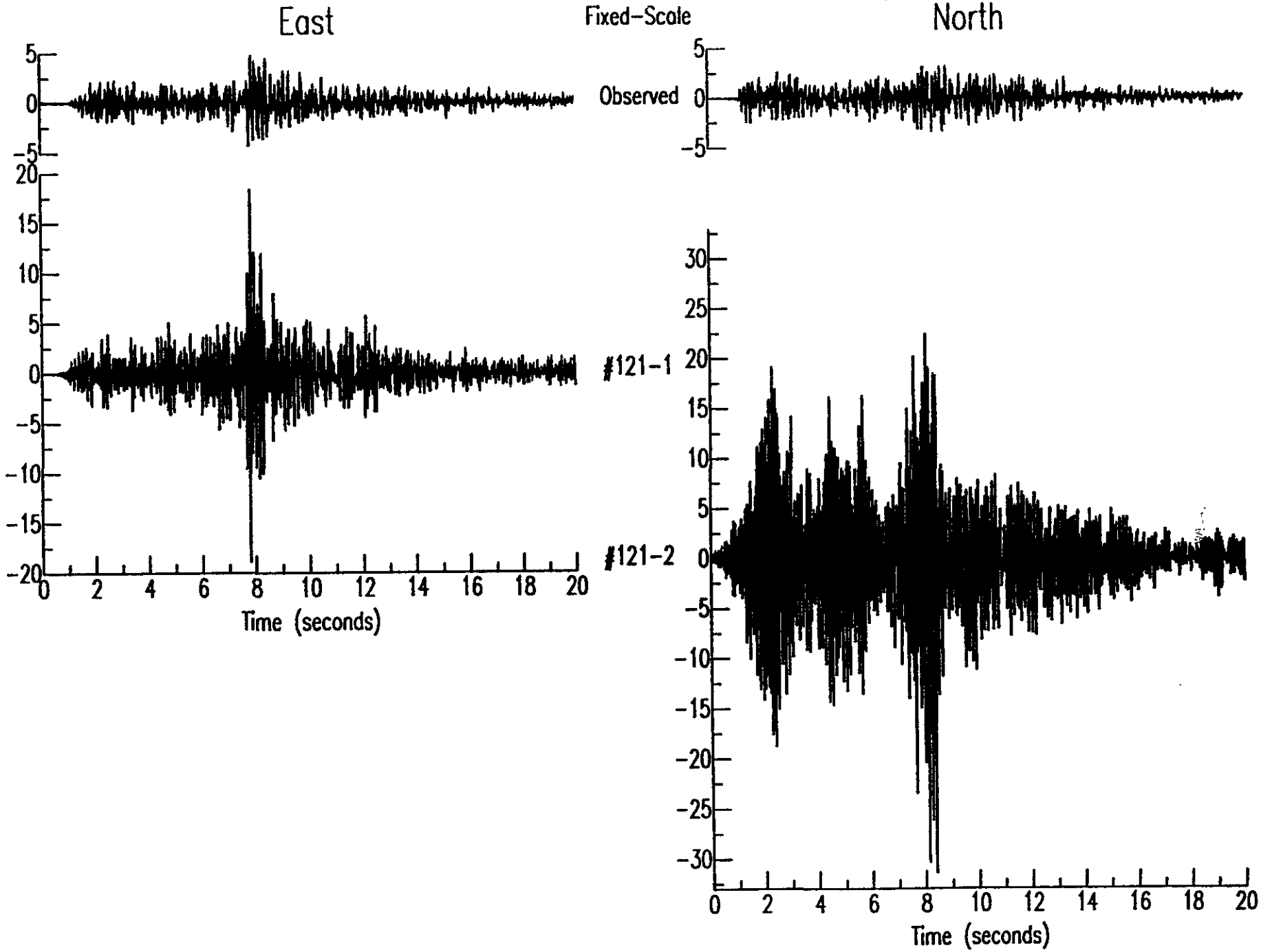

Figure A5j: Observed V1 vs Predicted V1 Standard Model Accelerograms (uM/sec/sec x 100)

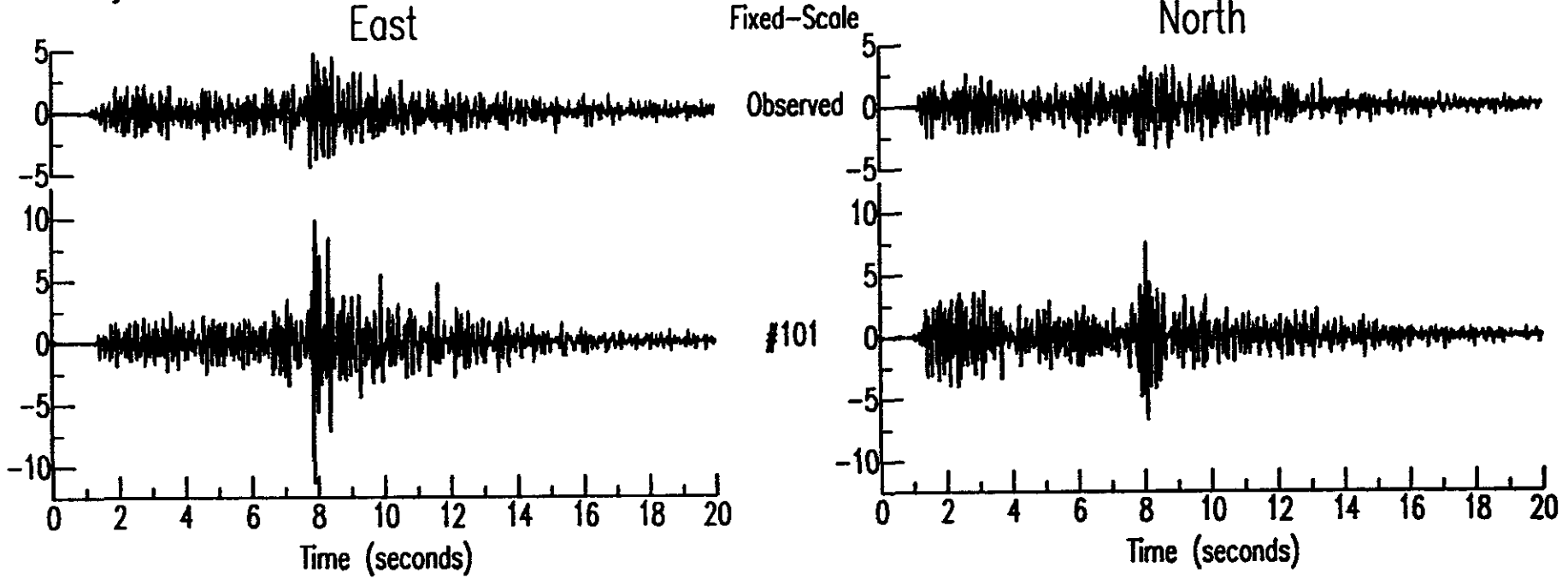

Appendix B

Plots from Analysis of Submitted R1 based Weak-motion Predictions using the Preferred Geotechnical Models

Figure B1a: Standard Fourier Spectral Ratio Plot:
Spectral Ratio V2/R1 for Preferred Geotechnical Model

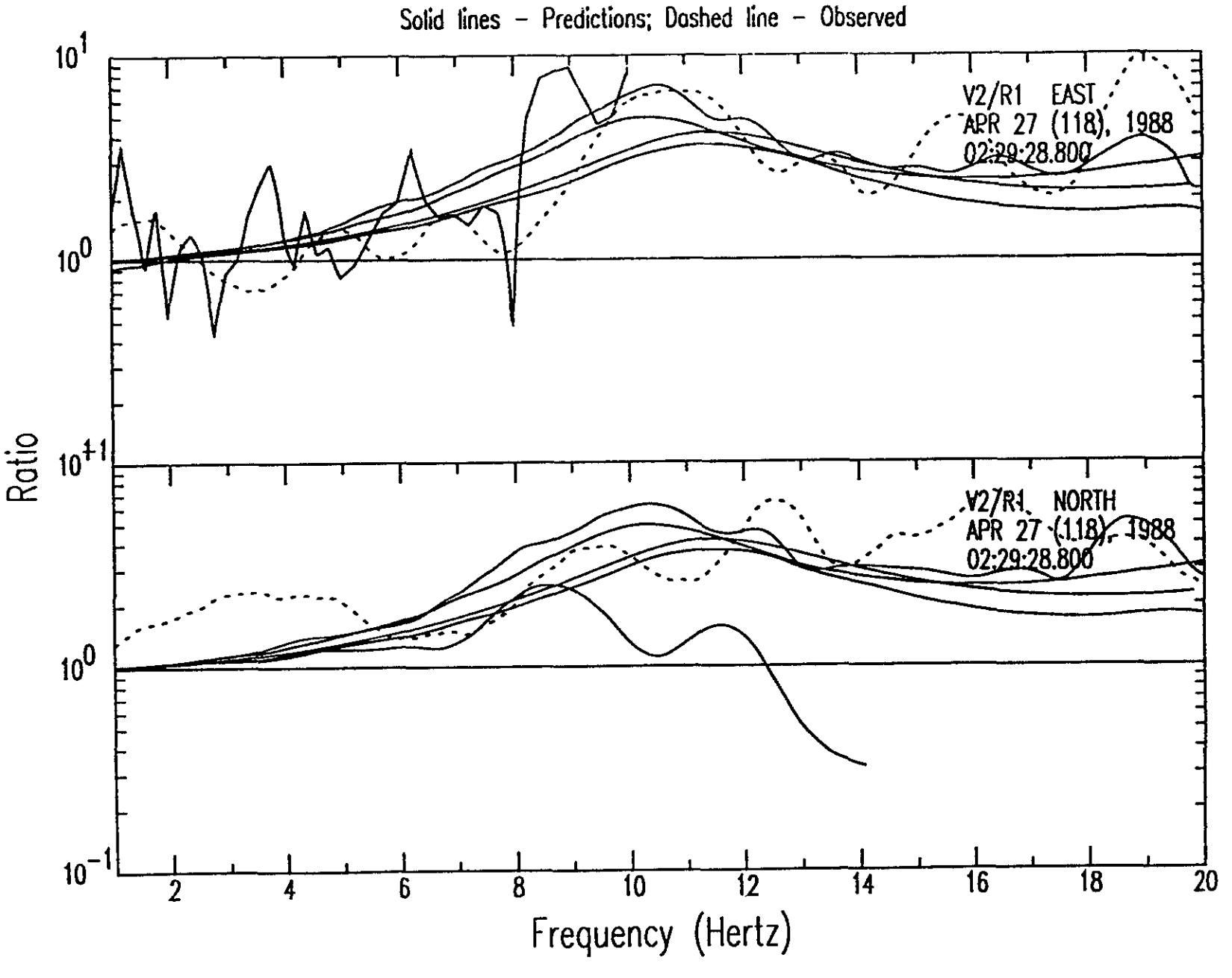

Figure B1b: Standard Fourier Spectral Ratio Plot:
Spectral Ratio V1/R1 for Preferred Geotechnical Model

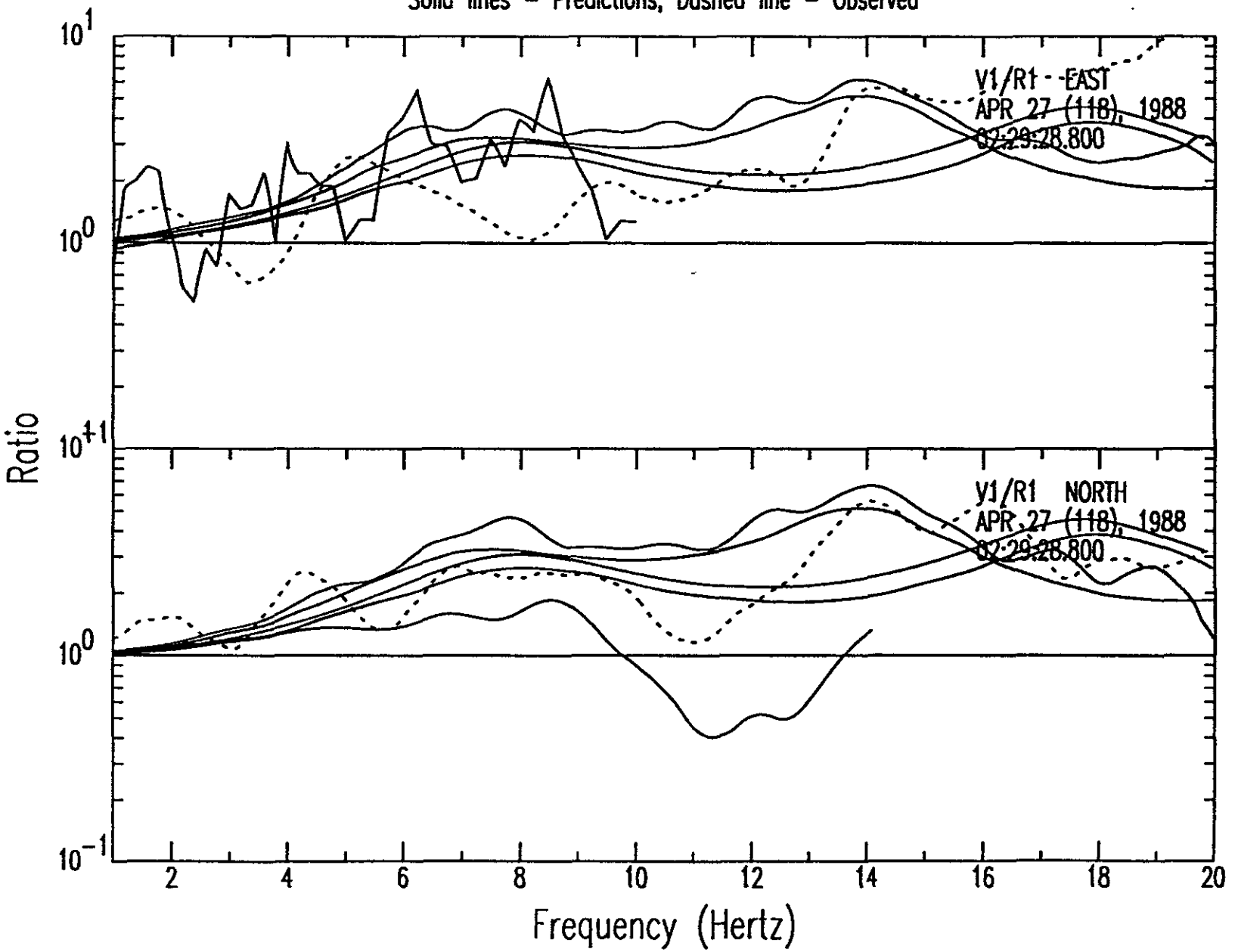

Figure B1c: Standard Fourier Spectral Ratio Plot:
Spectral Ratio D2/R1 for Preferred Geotechnical Model

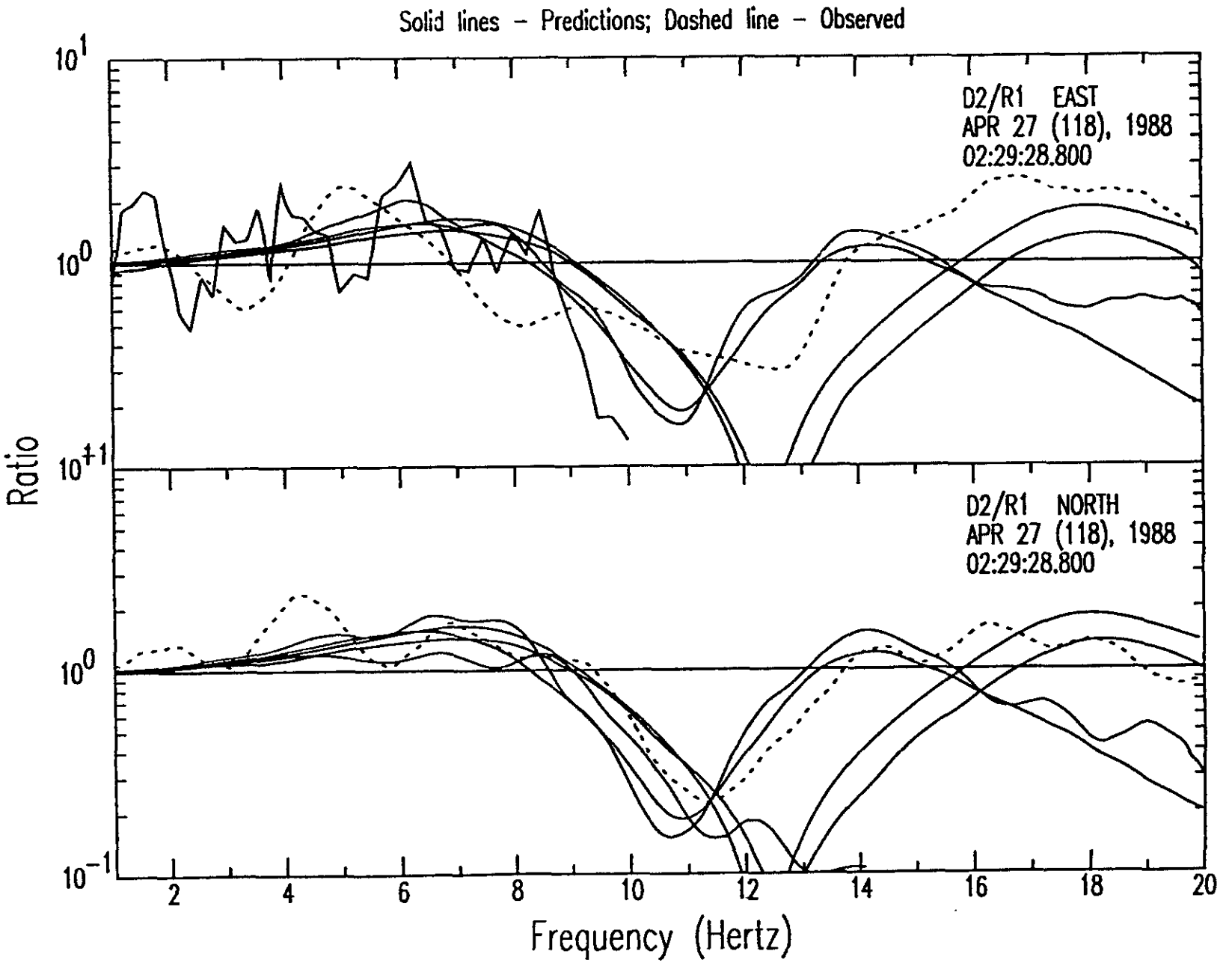

Figure B1d: Standard Fourier Spectral Ratio Plot:
Spectral Ratio D3/R1 for Preferred Geotechnical Model

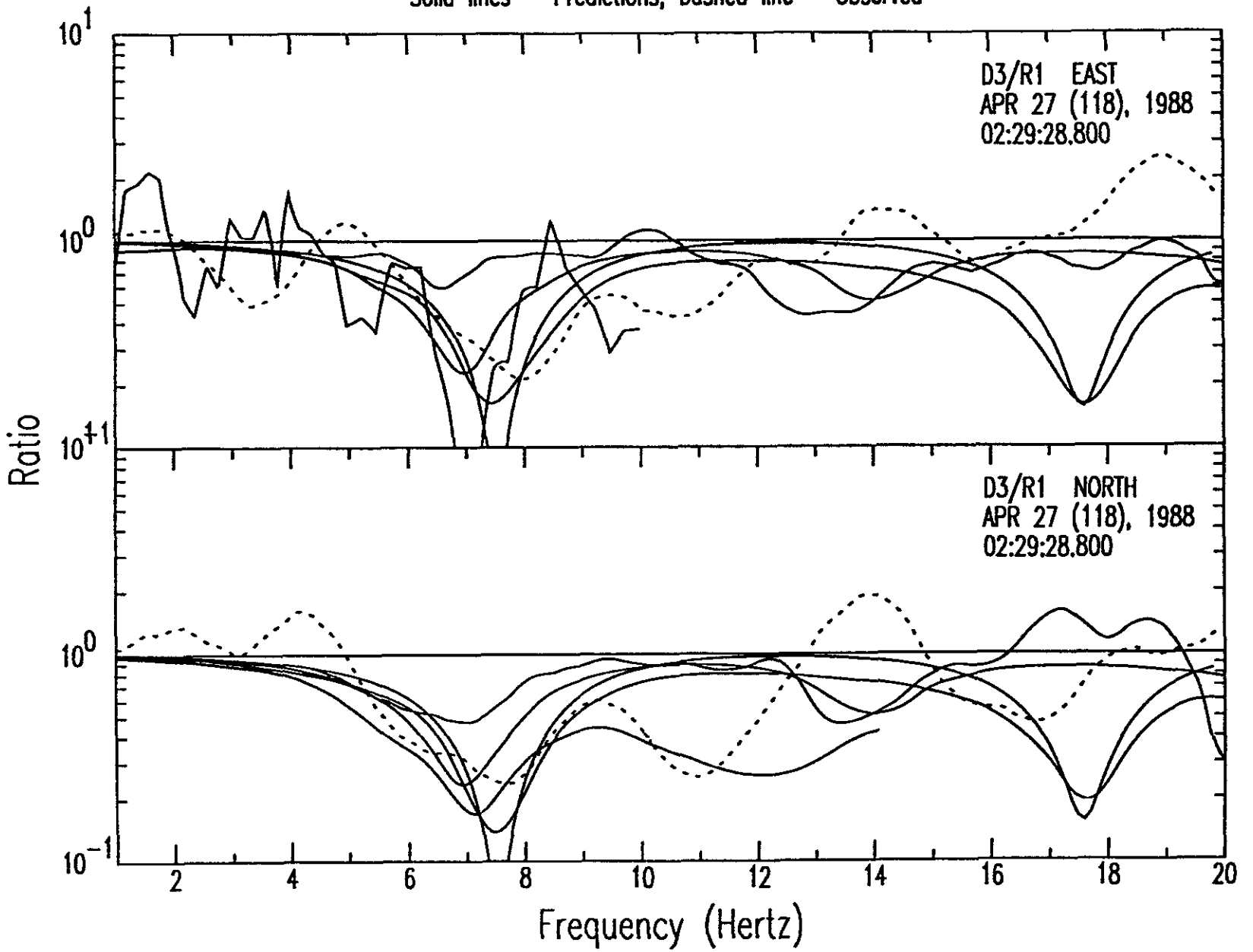

Figure B1e: Standard Fourier Spectral Ratio Plot:
Spectral Ratio D1/R1 for Preferred Geotechnical Model

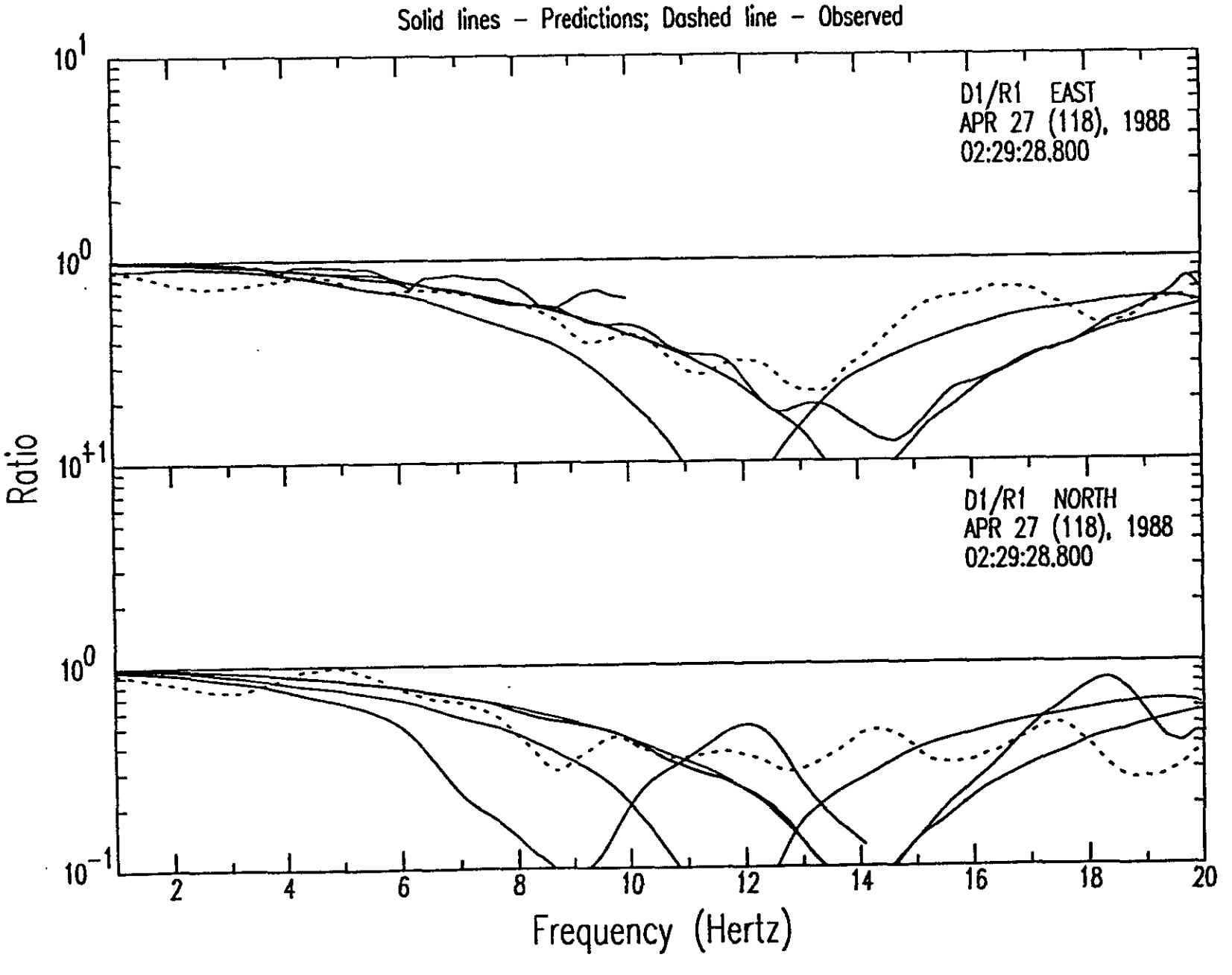

Figure B1f: Standard Fourier Spectral Ratio Plot:
Spectral Ratio R2/R1 for Preferred Geotechnical Model

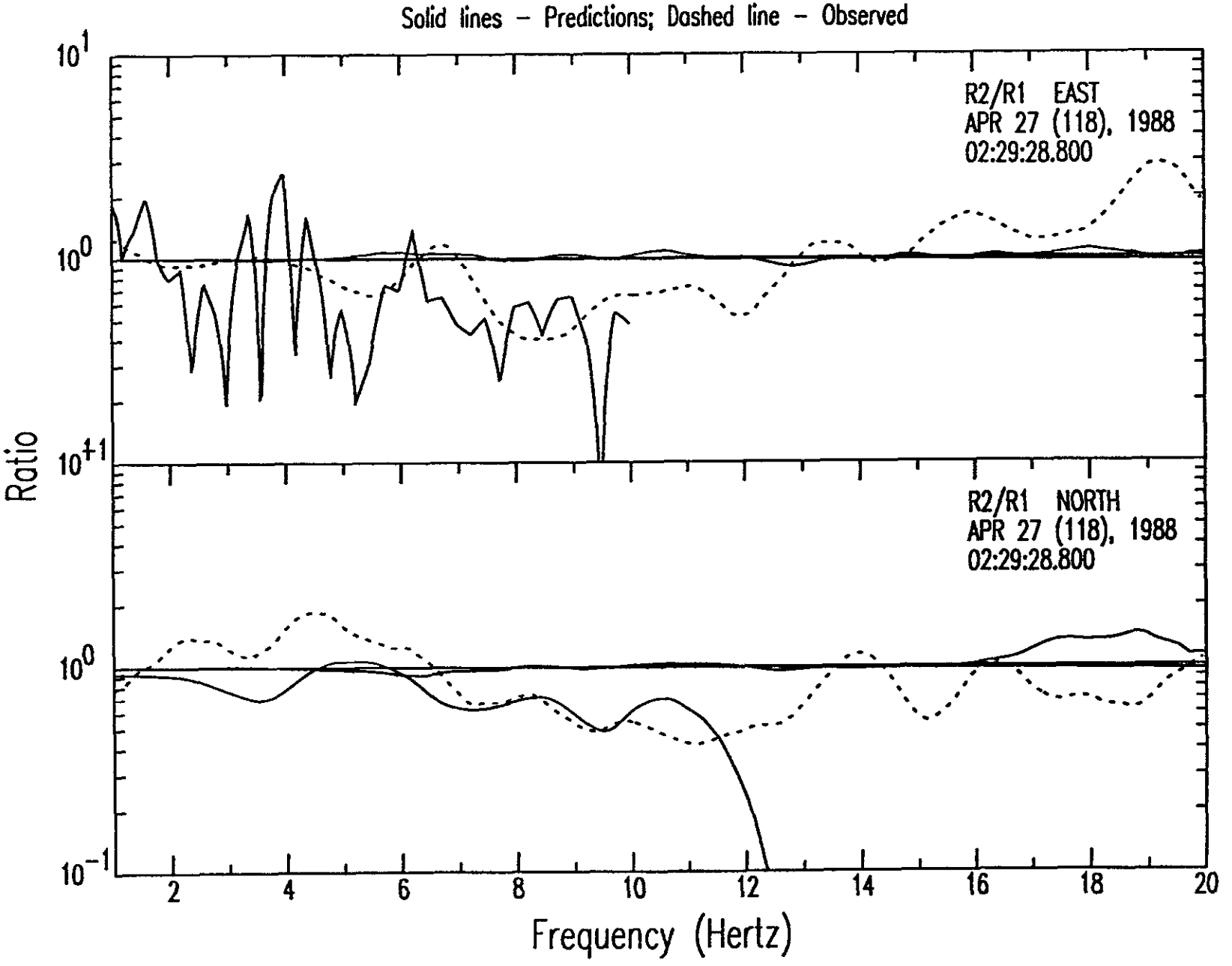

Figure B2a: Preferred Model Spectral Ratio Prediction Quartiles vs Observations

Spectral Ratio Predictions: Dashed - quartiles

Observations: Solid - weak-motion test event; Dash-dotted - weak-motion mean; Dotted - 1 std deviation

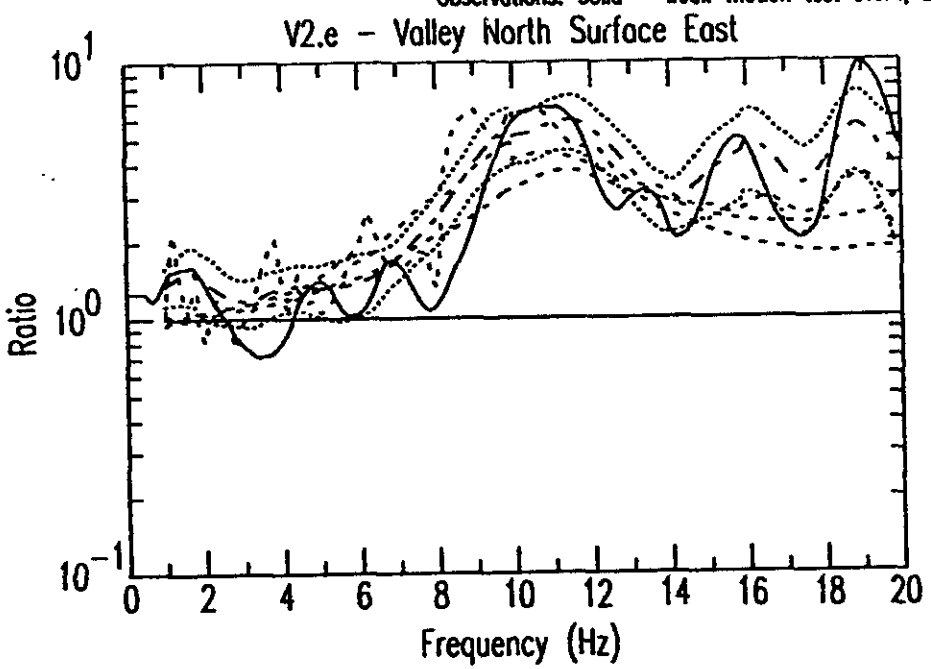

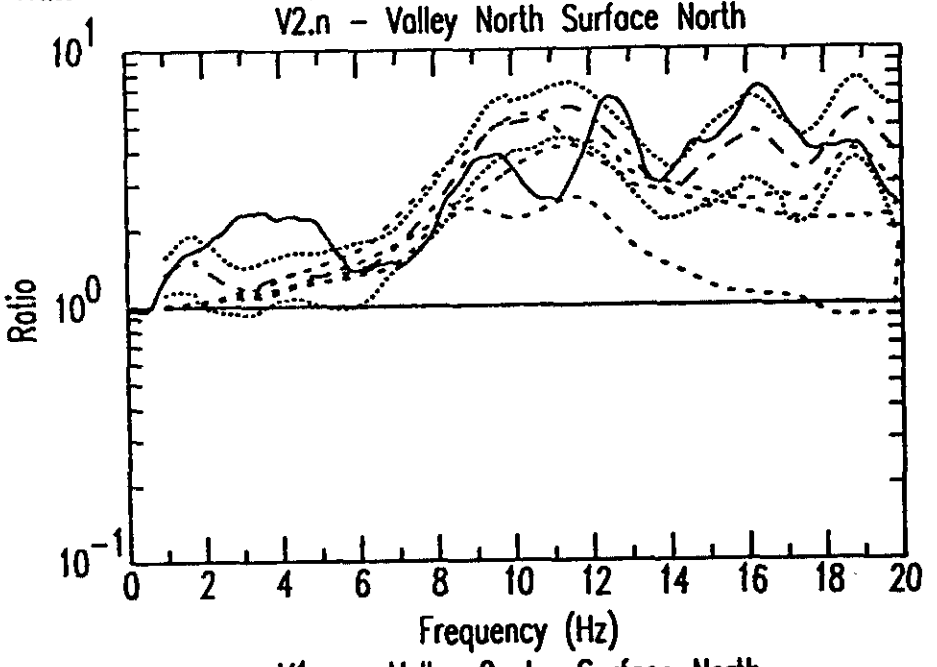

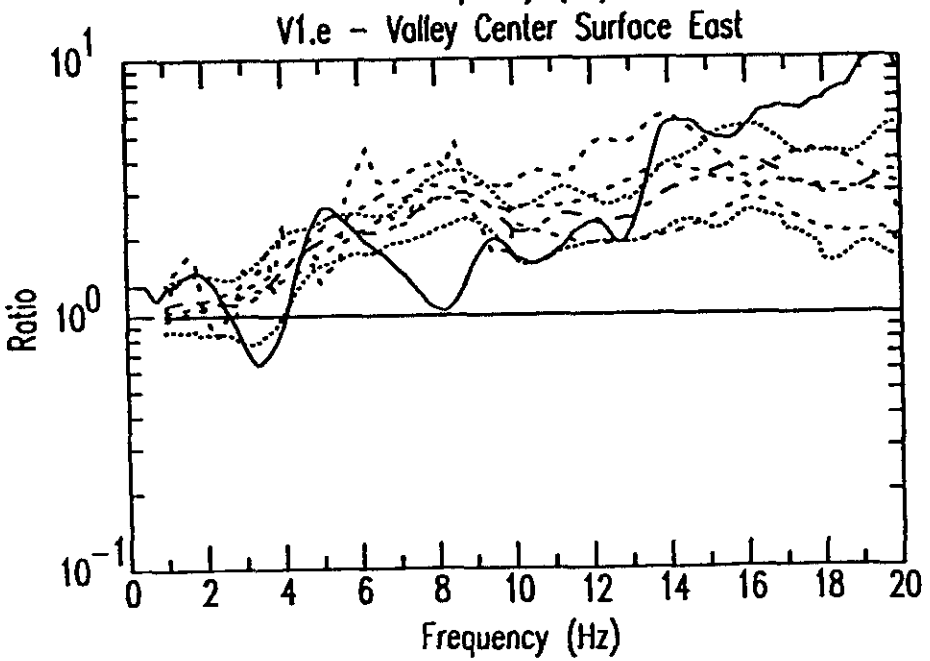

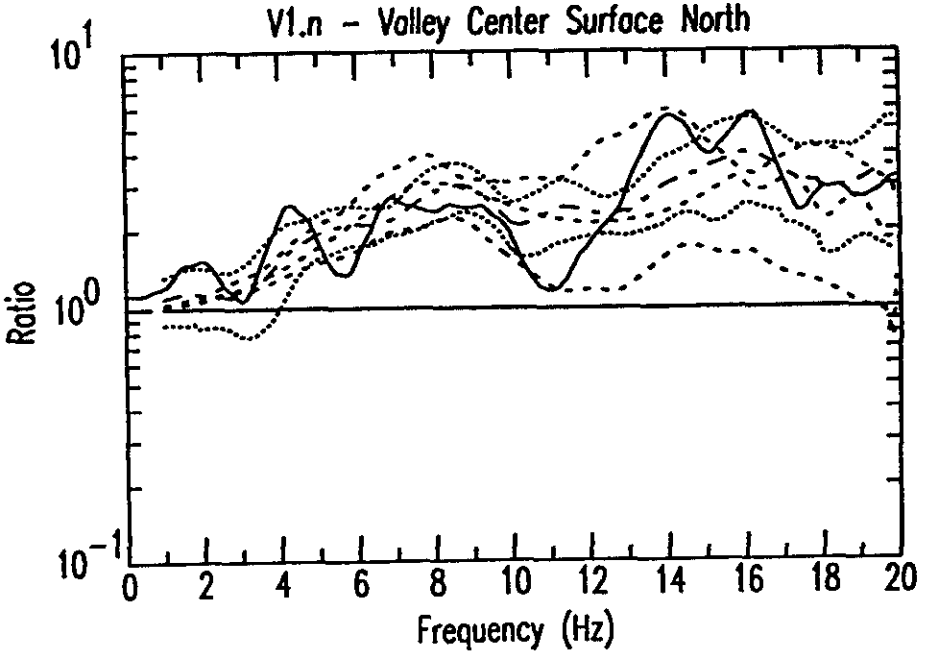

Figure B2b: Preferred Model Spectral Ratio Prediction Quartiles vs Observations

Spectral Ratio Predictions: Dashed – quartiles

Observations: Solid – weak-motion test event; Dash-dotted – weak-motion mean; Dotted – 1 std deviation

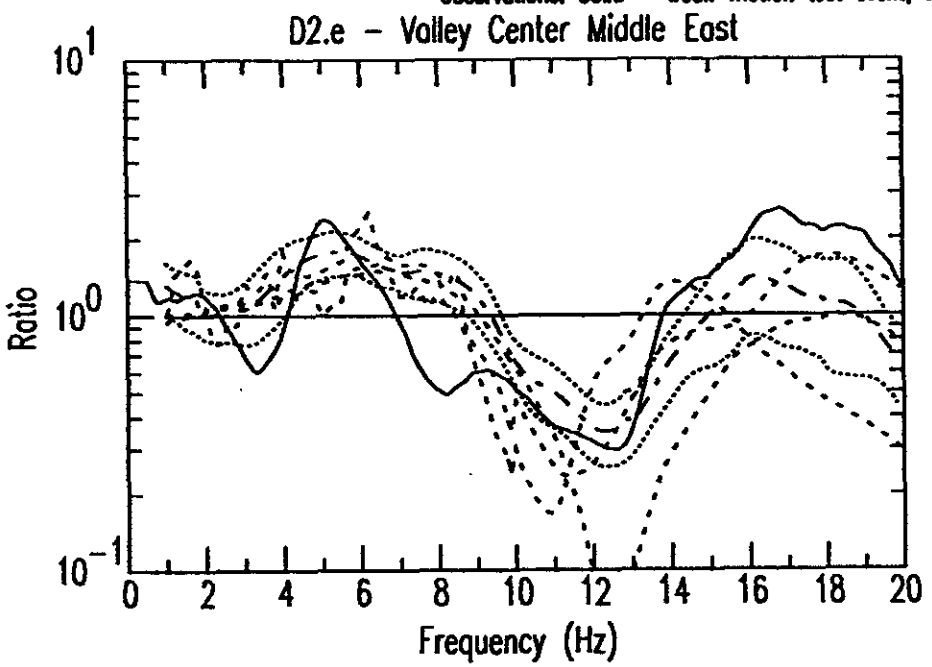

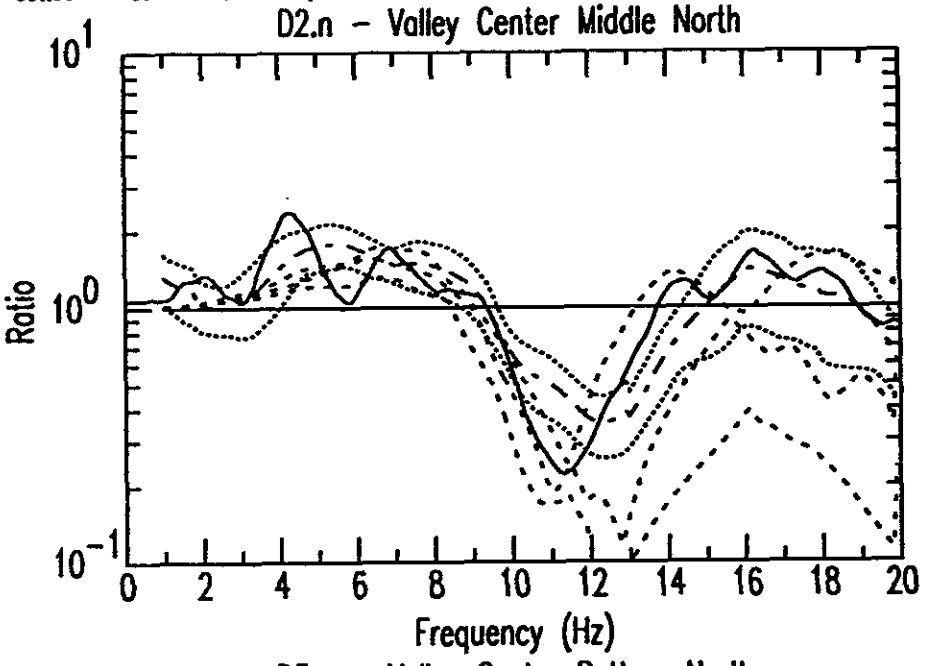

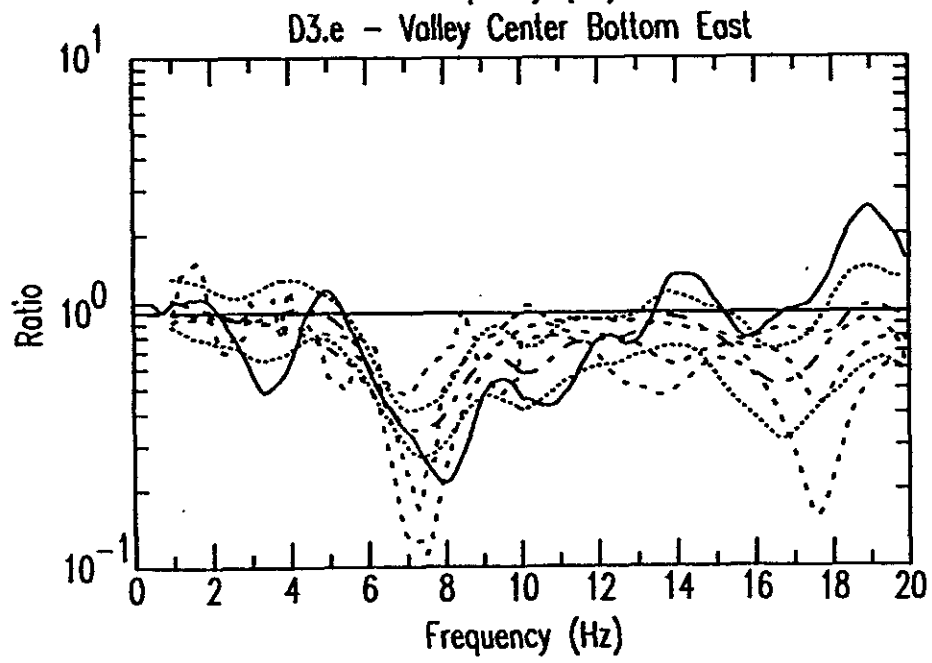

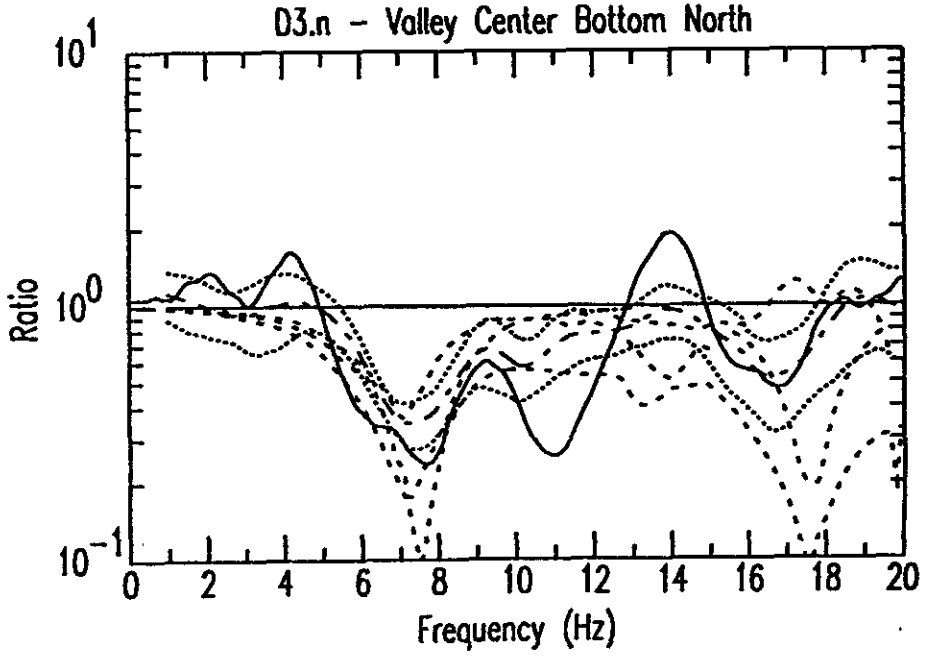

Figure B2c: Preferred Model Spectral Ratio Prediction Quartiles vs Observations

Spectral Ratio Predictions: Dashed - quartiles

Observations: Solid - weak-motion test event; Dash-dotted - weak-motion mean; Dotted - 1 std deviation

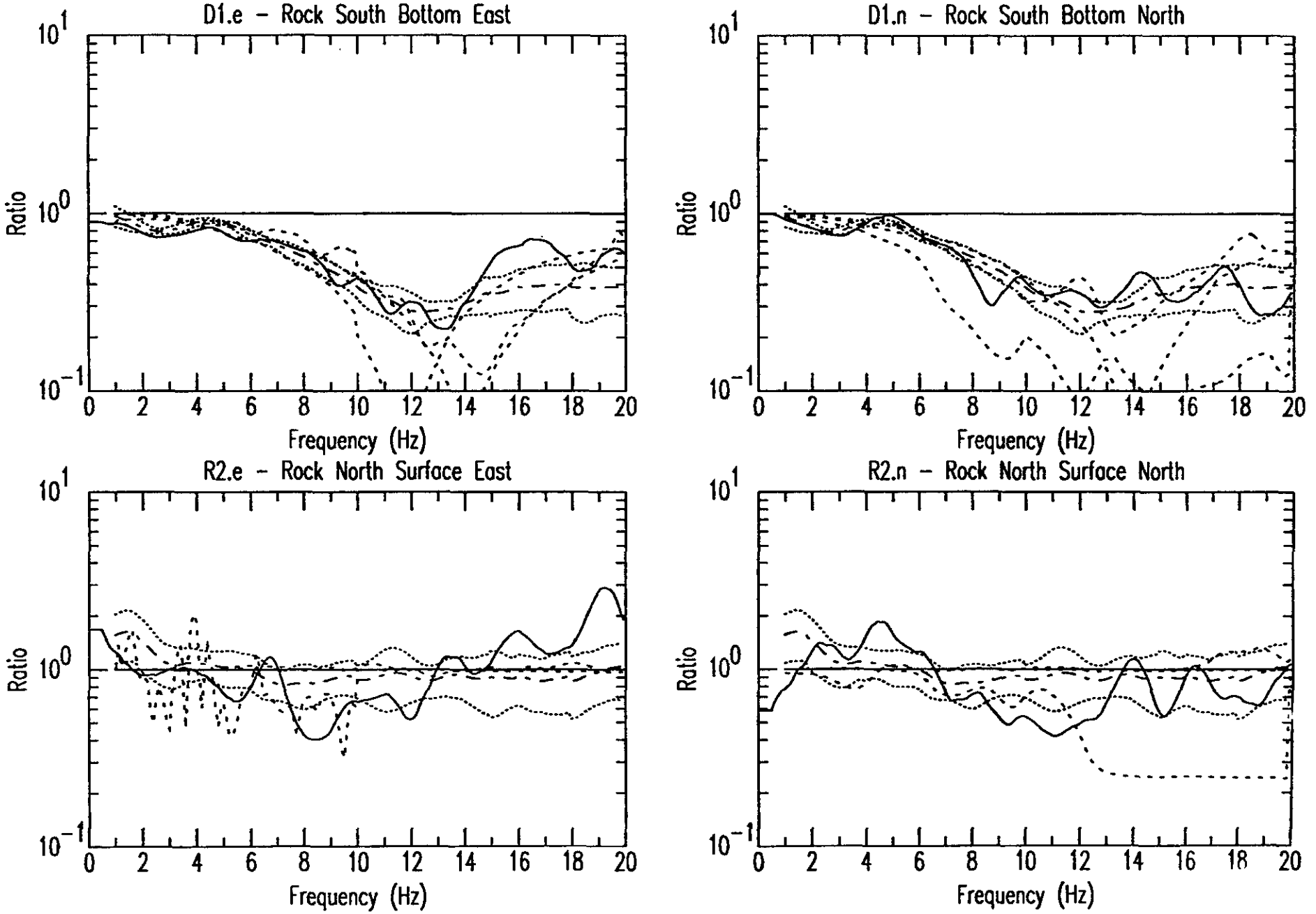

Figure B3a: Standard Response Spectra:
Station V2 Valley North Surface Preferred Geotechnical Model
Solid lines – Predictions; Dashed line – Observed

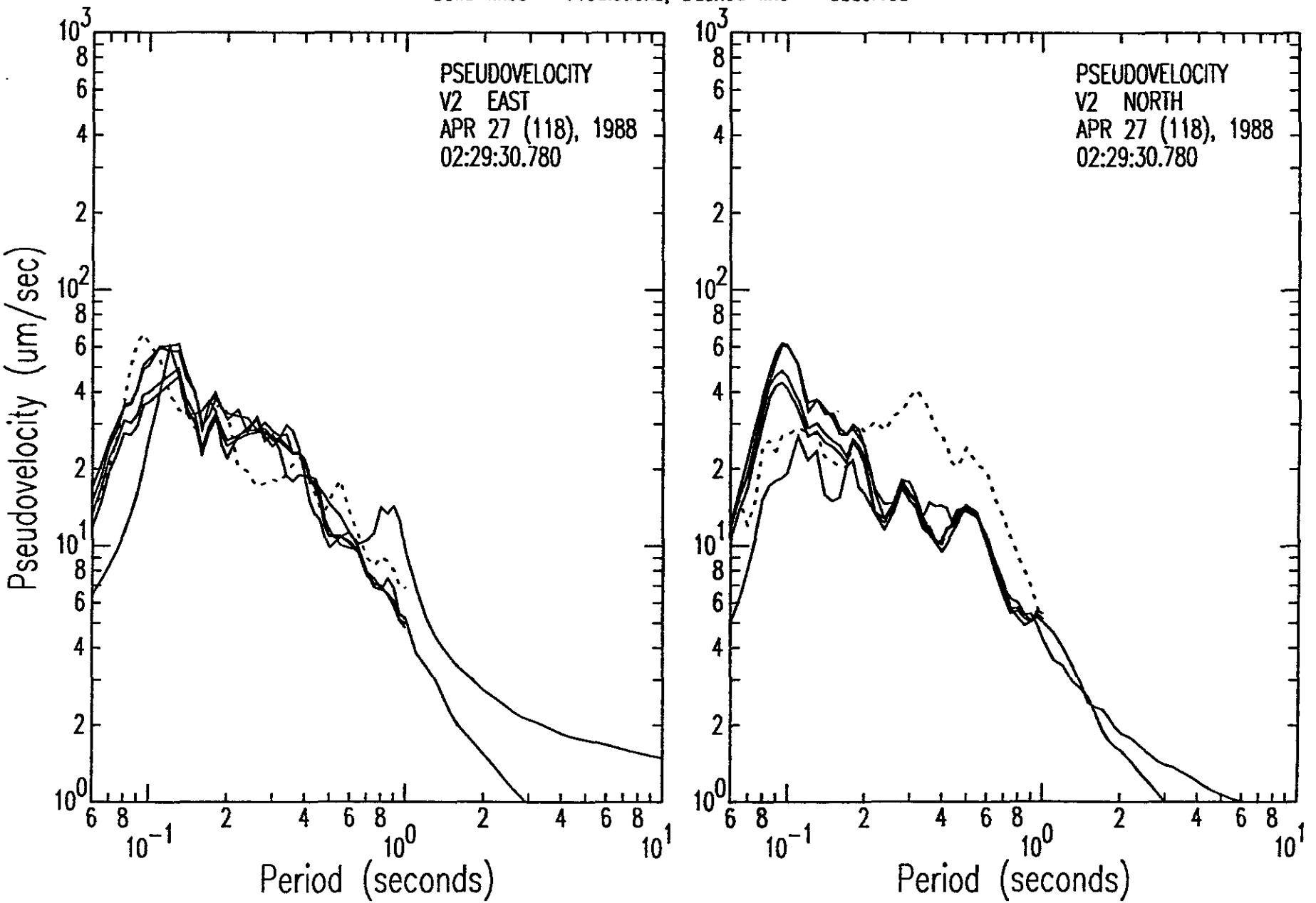

Figure B3b: Standard Response Spectra:
Station V1 Valley Center Surface Preferred Geotechnical Model
Solid lines – Predictions; Dashed line – Observed

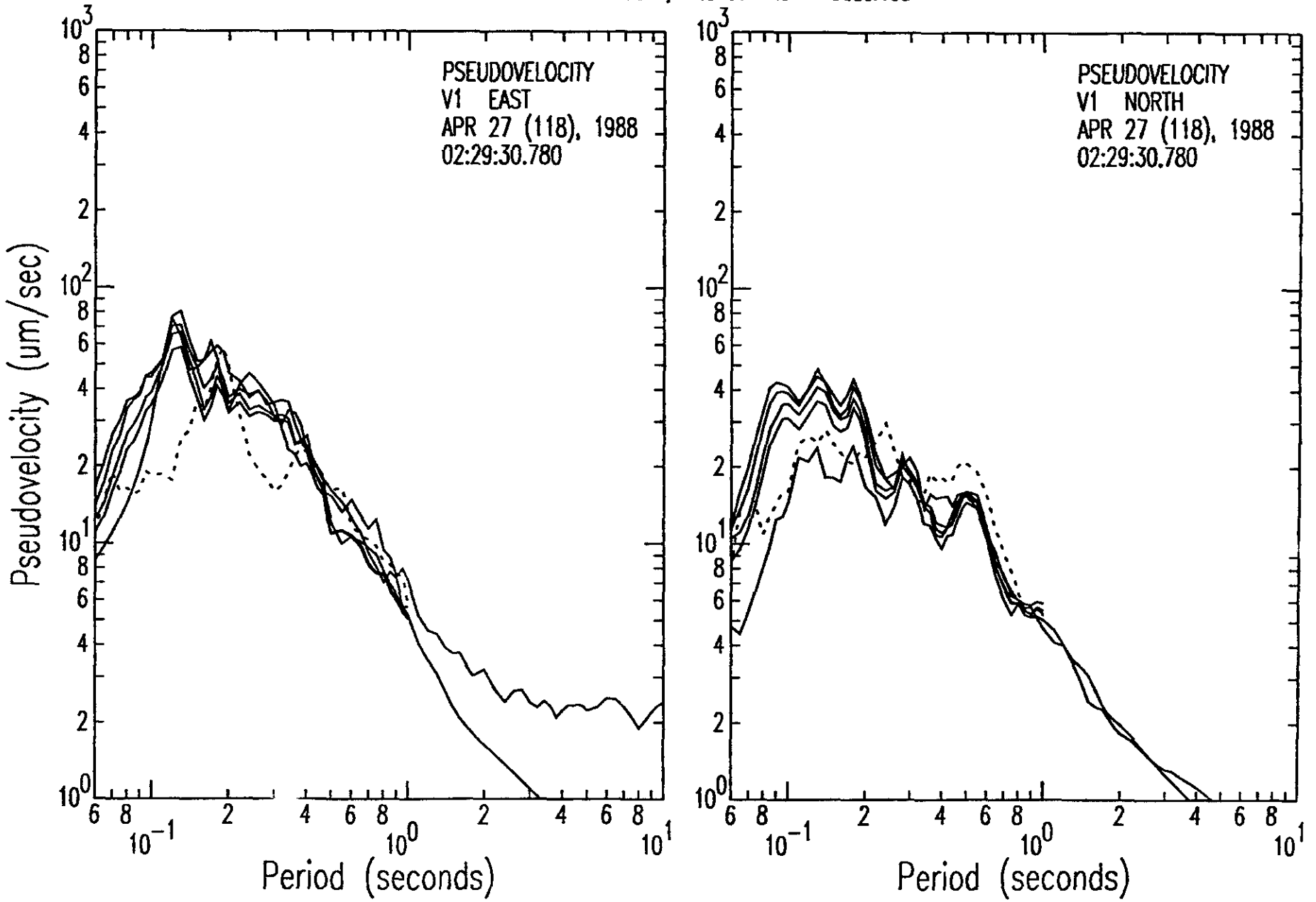

Figure B3c: Standard Response Spectra:
Station D2 Valley Center Middle Preferred Geotechnical Model
Solid lines – Predictions; Dashed line – Observed

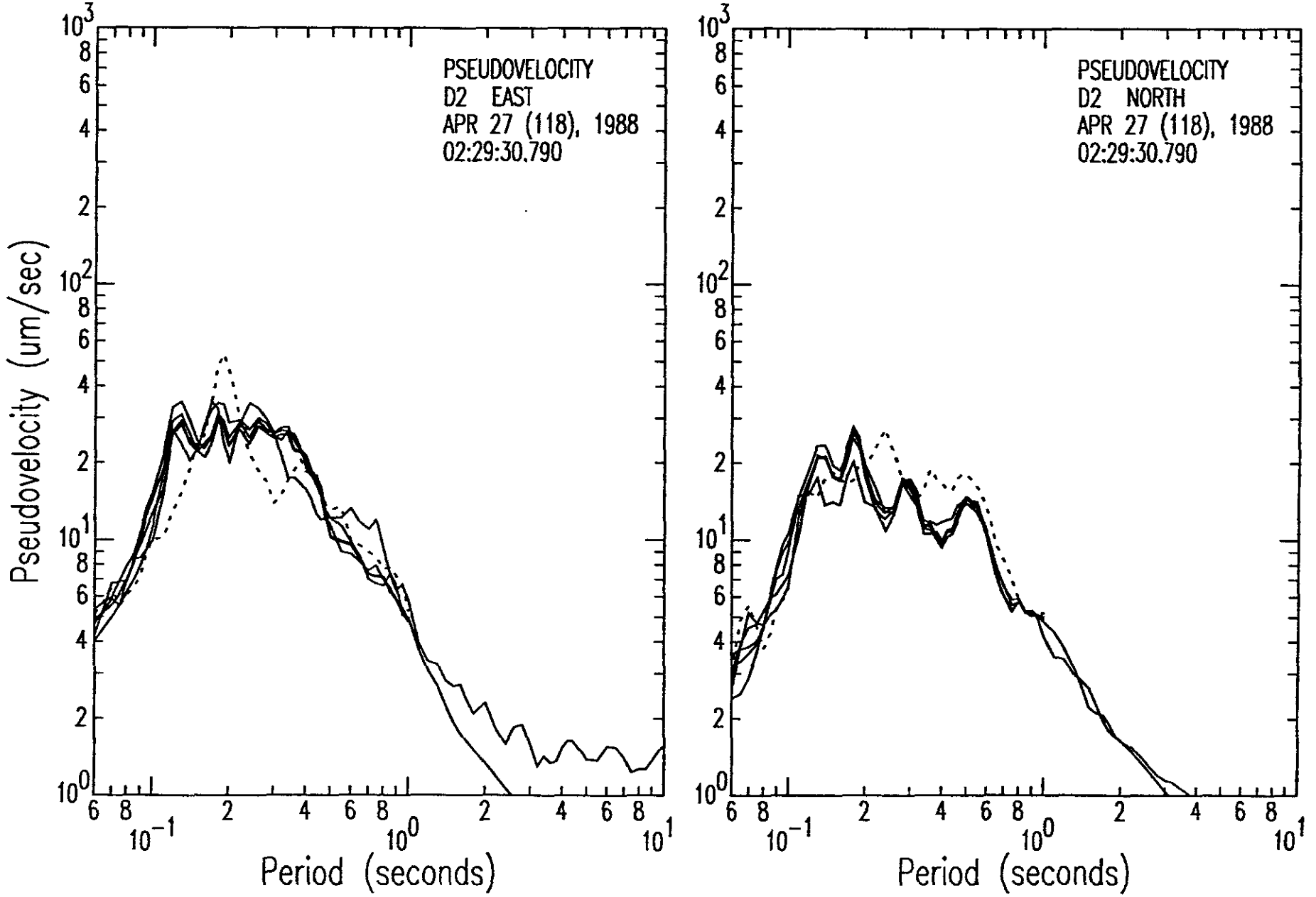

Figure B3d: Standard Response Spectra:
Station D3 Valley Center Bottom Preferred Geotechnical Model
Solid lines – Predictions; Dashed line – Observed

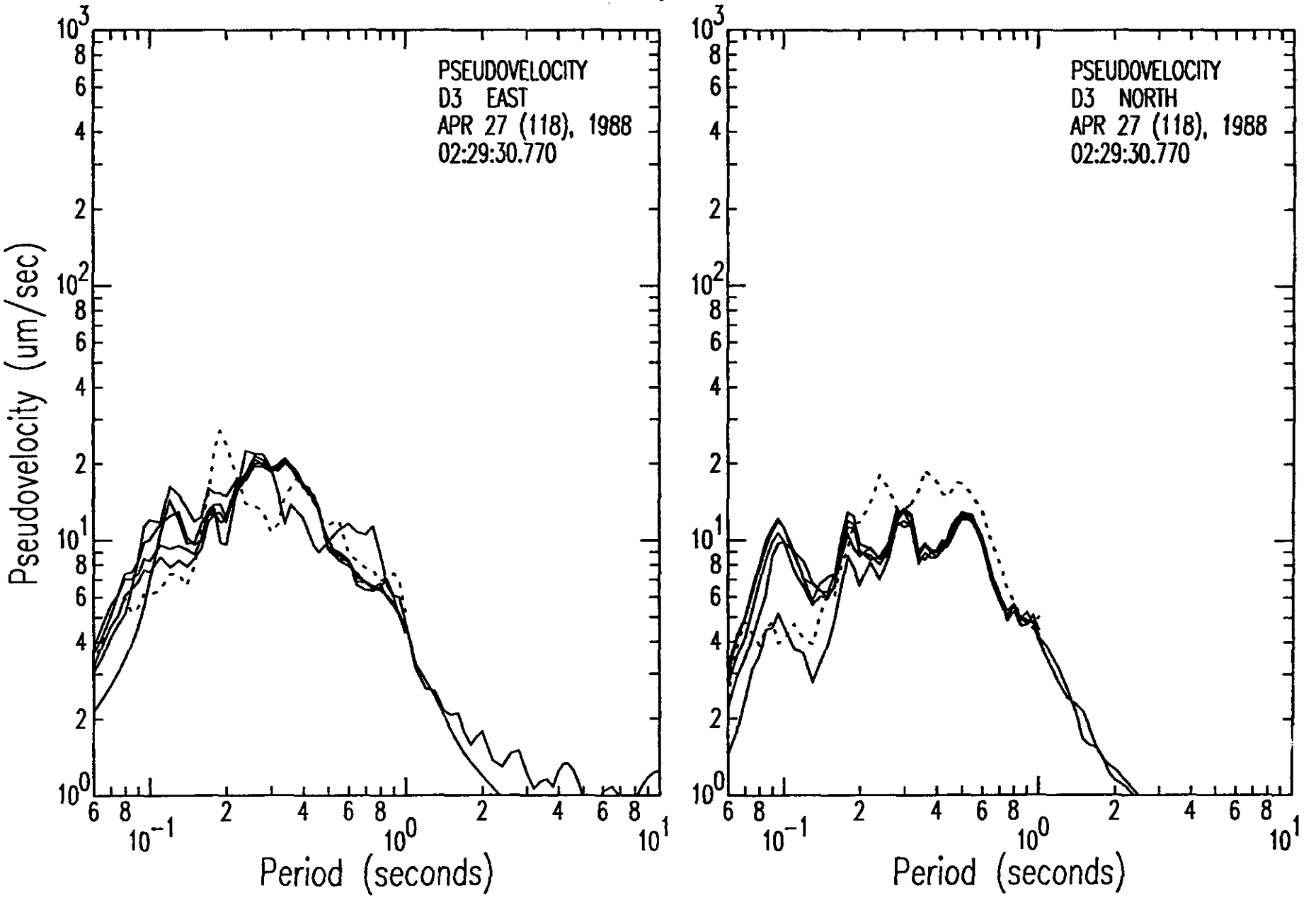

Figure B3e: Standard Response Spectra:
Station D1 Rock South Bottom Preferred Geotechnical Model
Solid lines - Predictions; Dashed line - Observed

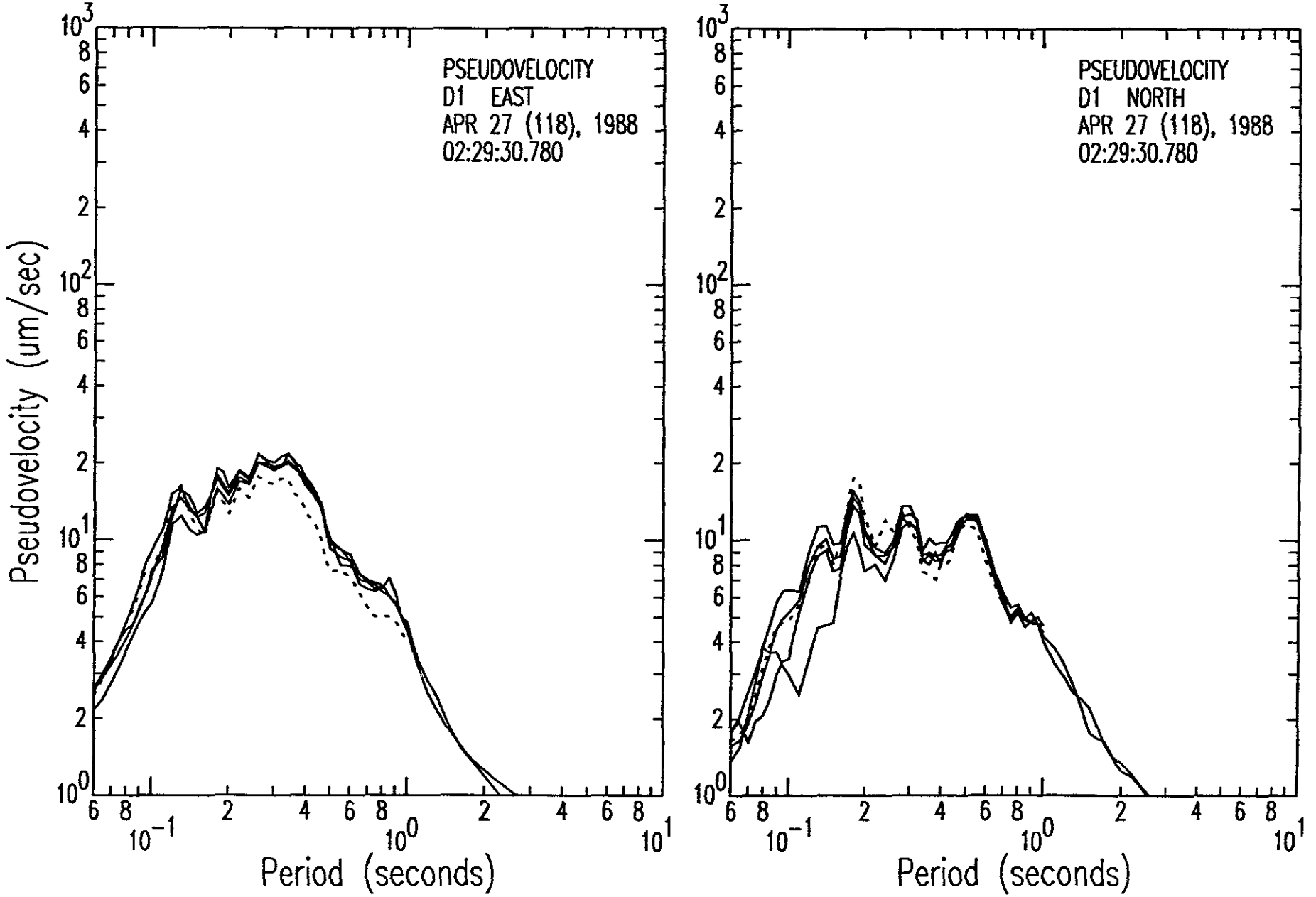

Figure B3f: Standard Response Spectra:
Station R2 Rock North Surface Preferred Geotechnical Model
Solid lines – Predictions; Dashed line – Observed

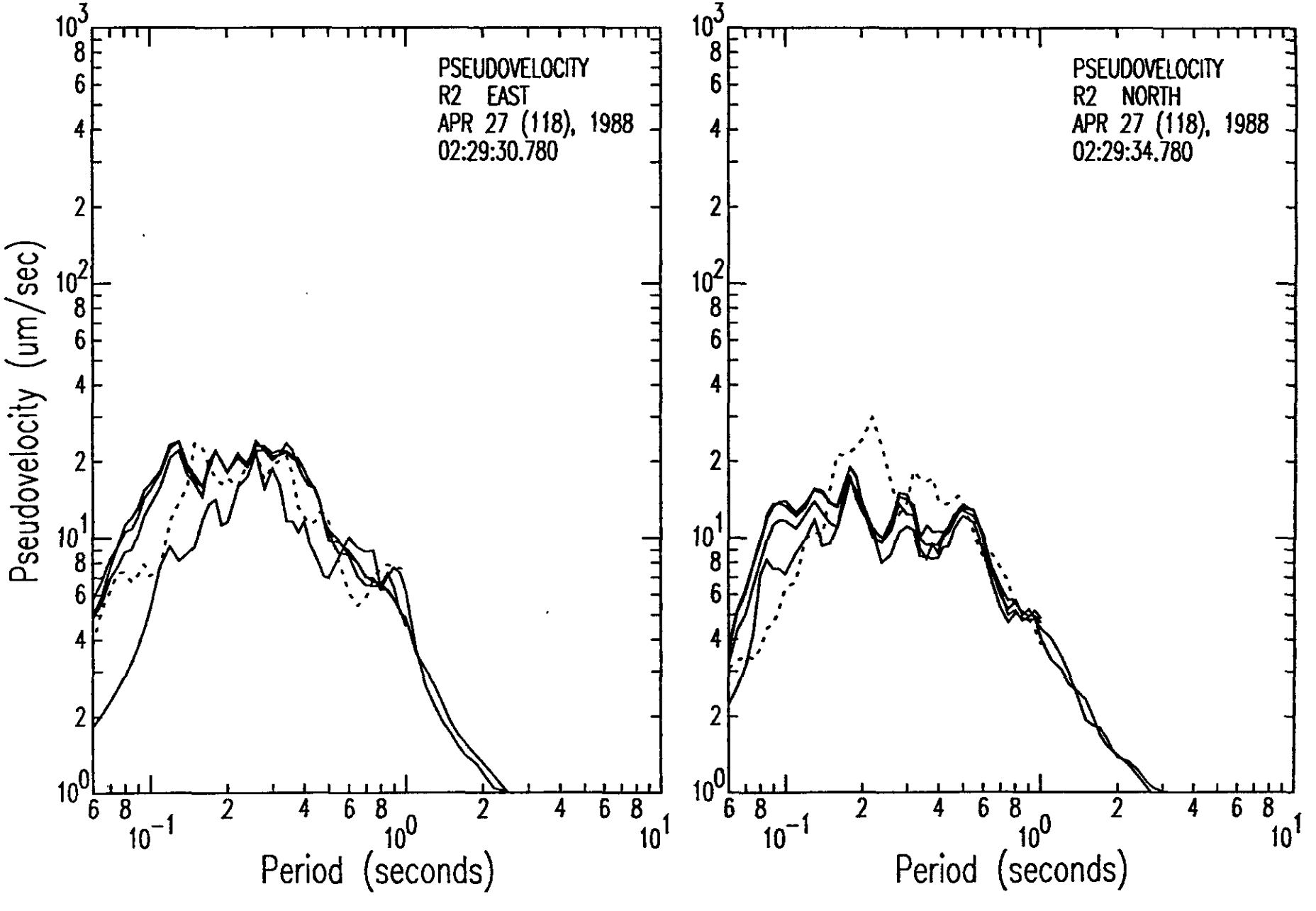

Figure B4a: Preferred Model Response Spectra Prediction Quartiles vs Observations

Response Spectra Predictions: Dashed – quartiles

Observations: Solid – weak-motion test event

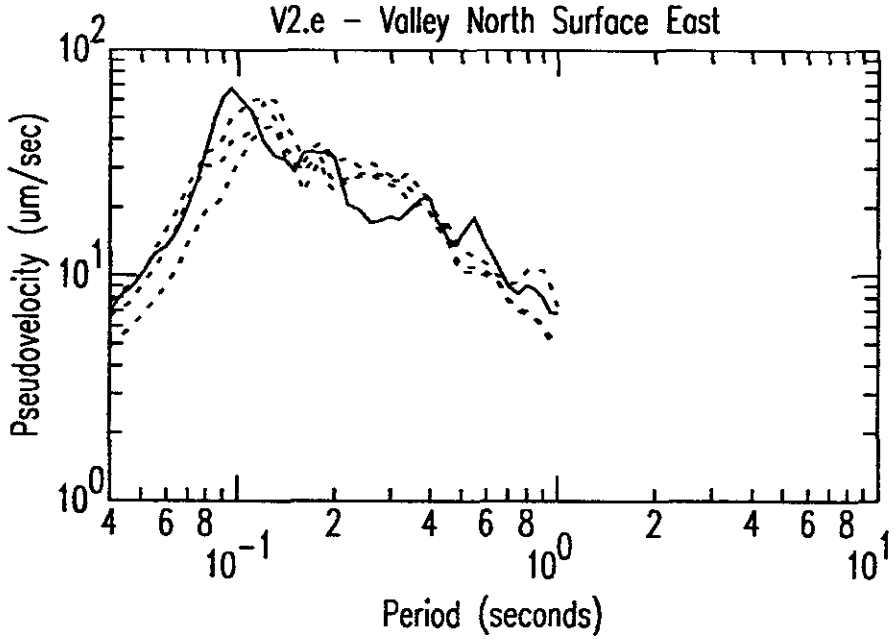

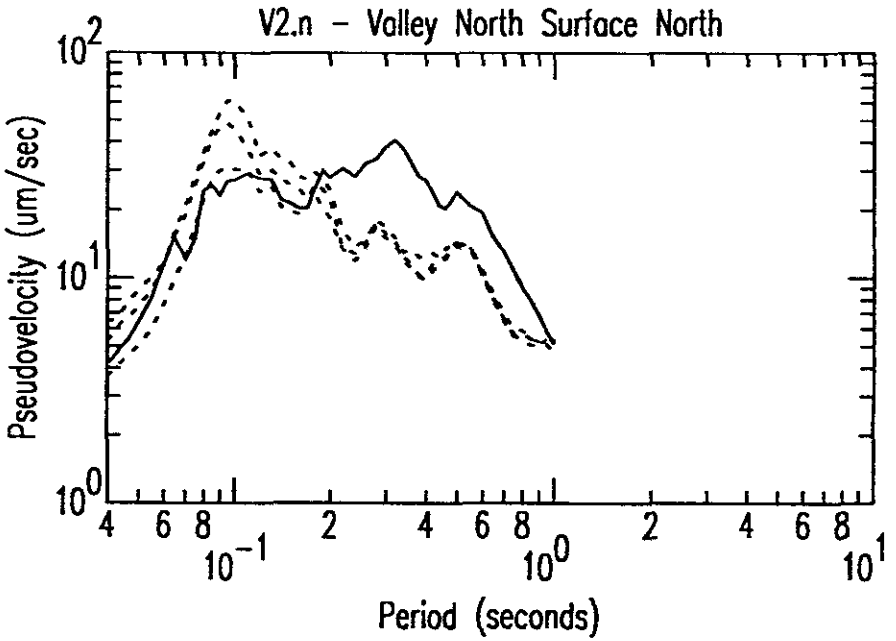

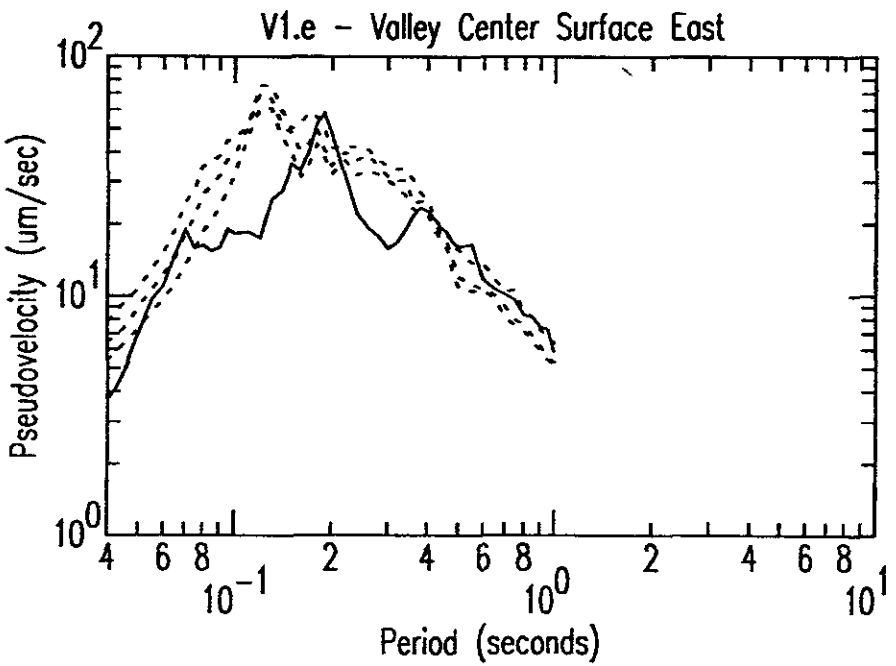

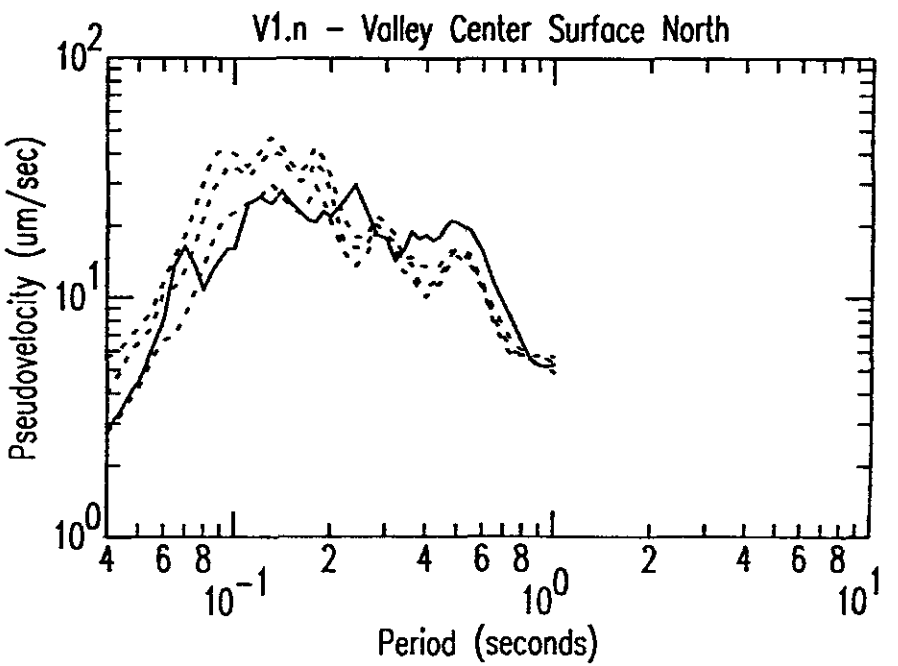

Figure B4b: Preferred Model Response Spectra Prediction Quartiles vs Observations

Response Spectra Predictions: Dashed - quartiles

Observations: Solid - weak-motion test event

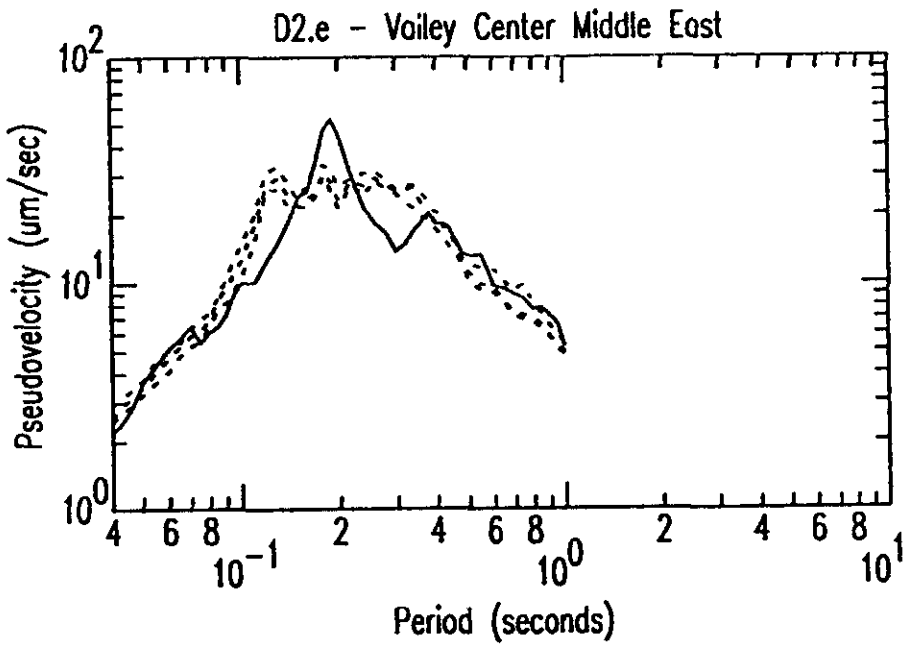

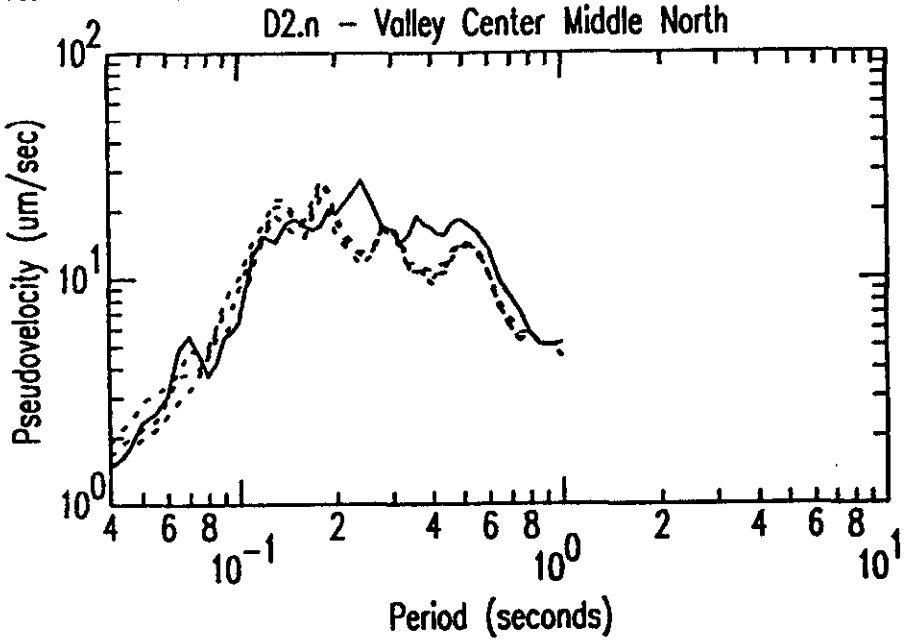

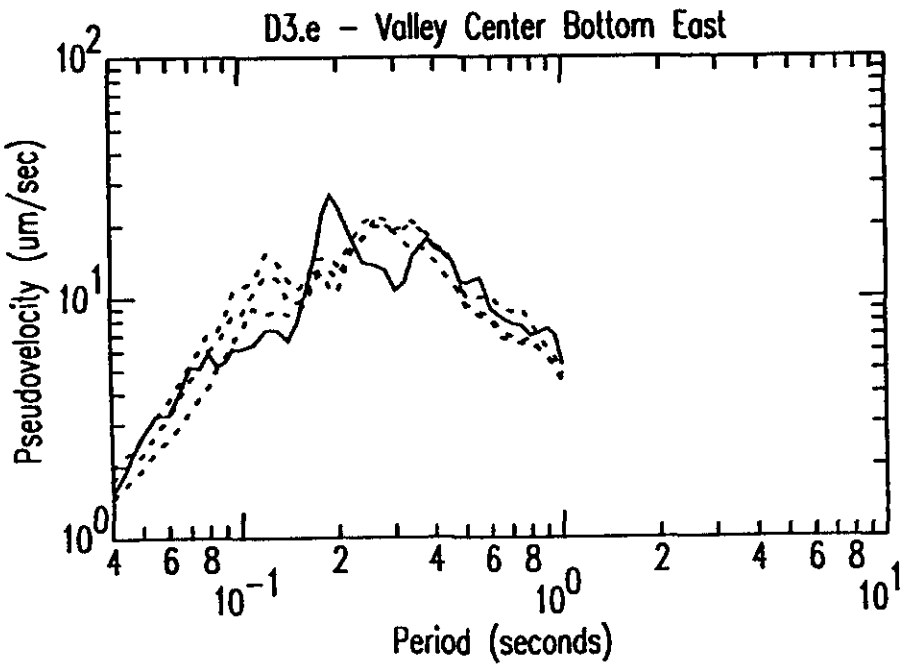

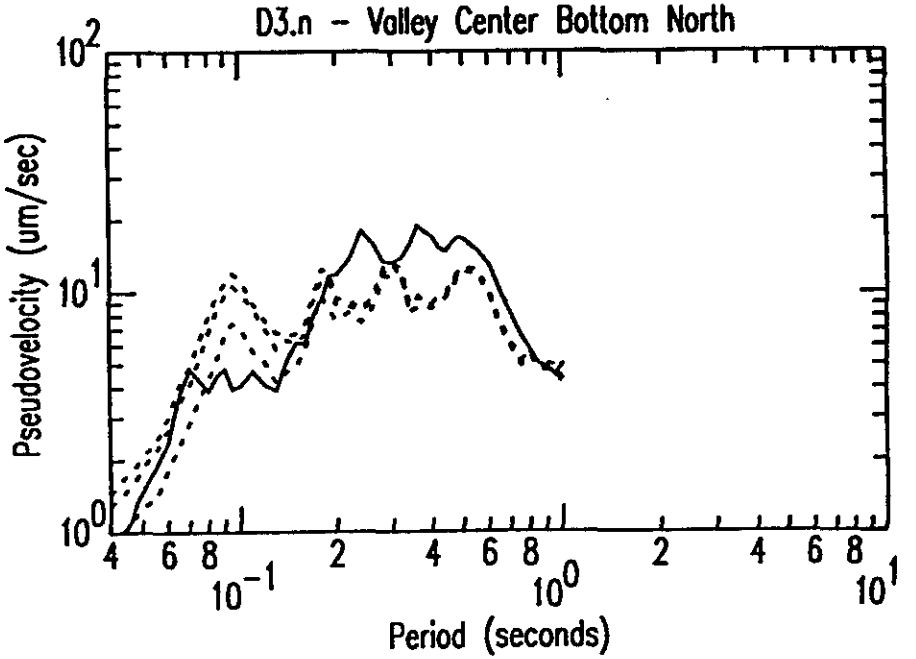

Figure B4c: Preferred Model Response Spectra Prediction Quartiles vs Observations

Response Spectra Predictions: Dashed - quartiles
Observations: Solid - weak-motion test event

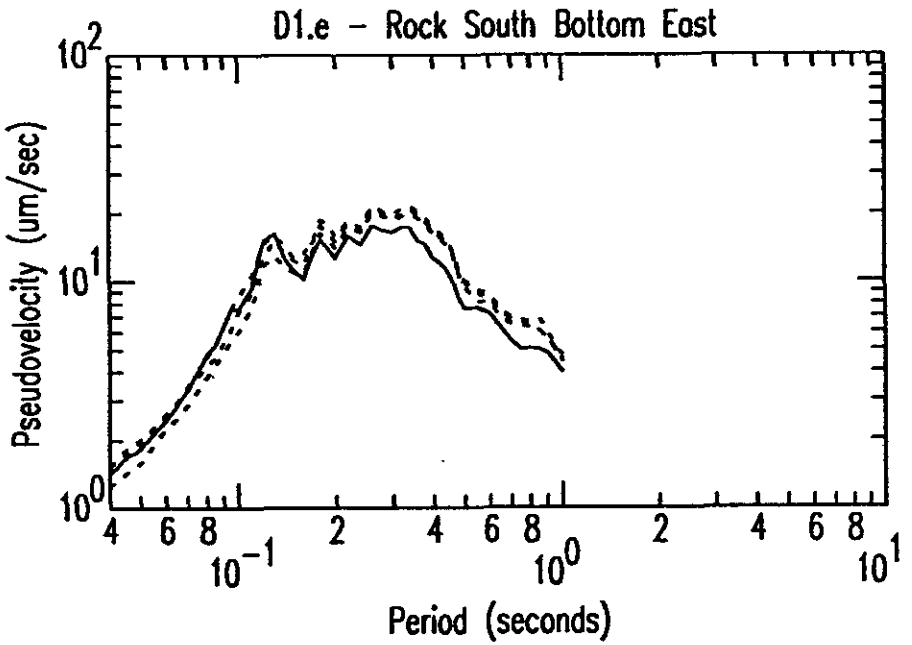

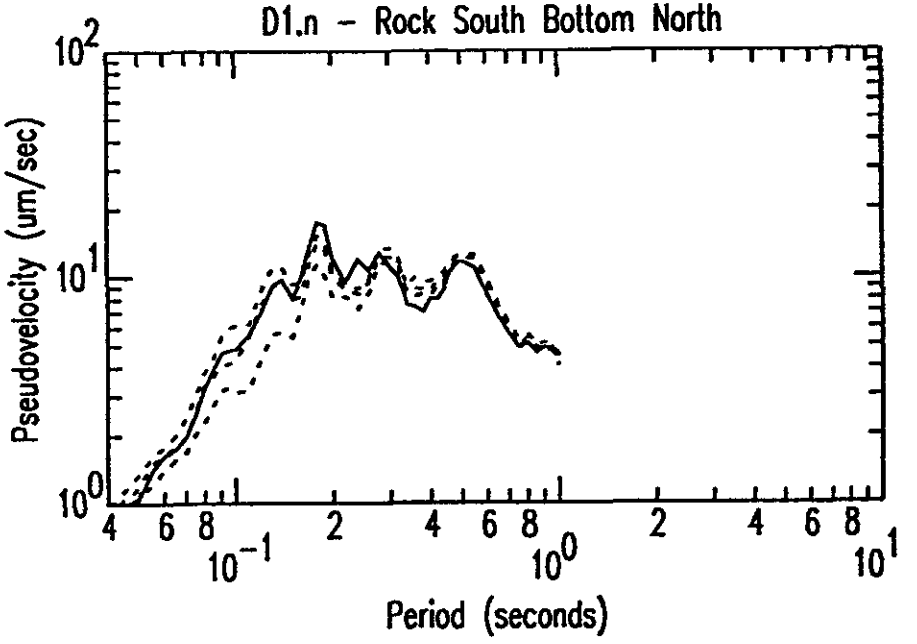

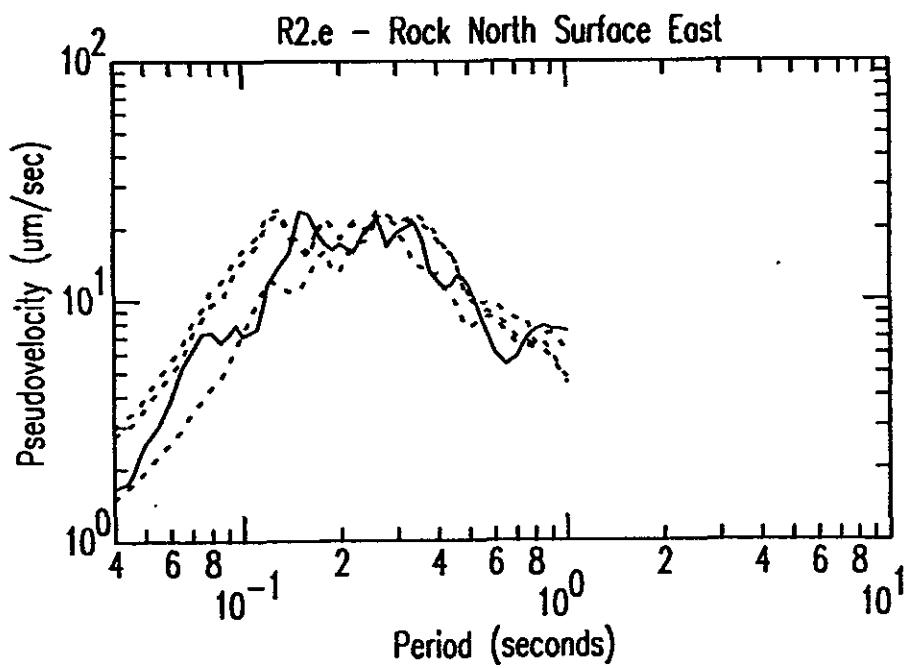

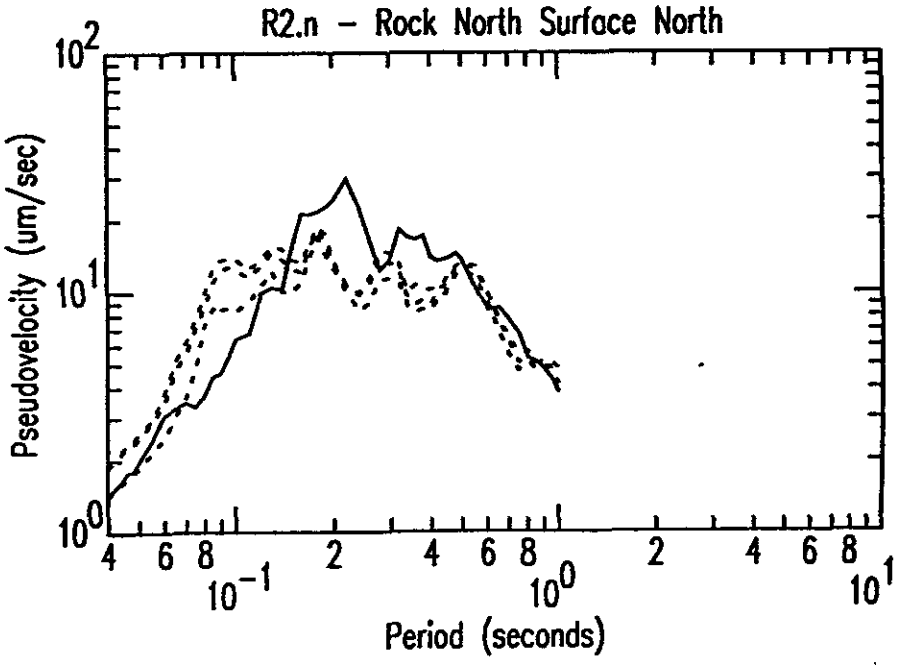

Figure B5a: Observed V1 vs Predicted V1 Preferred Model Accelerograms (uM/sec/sec x 100)

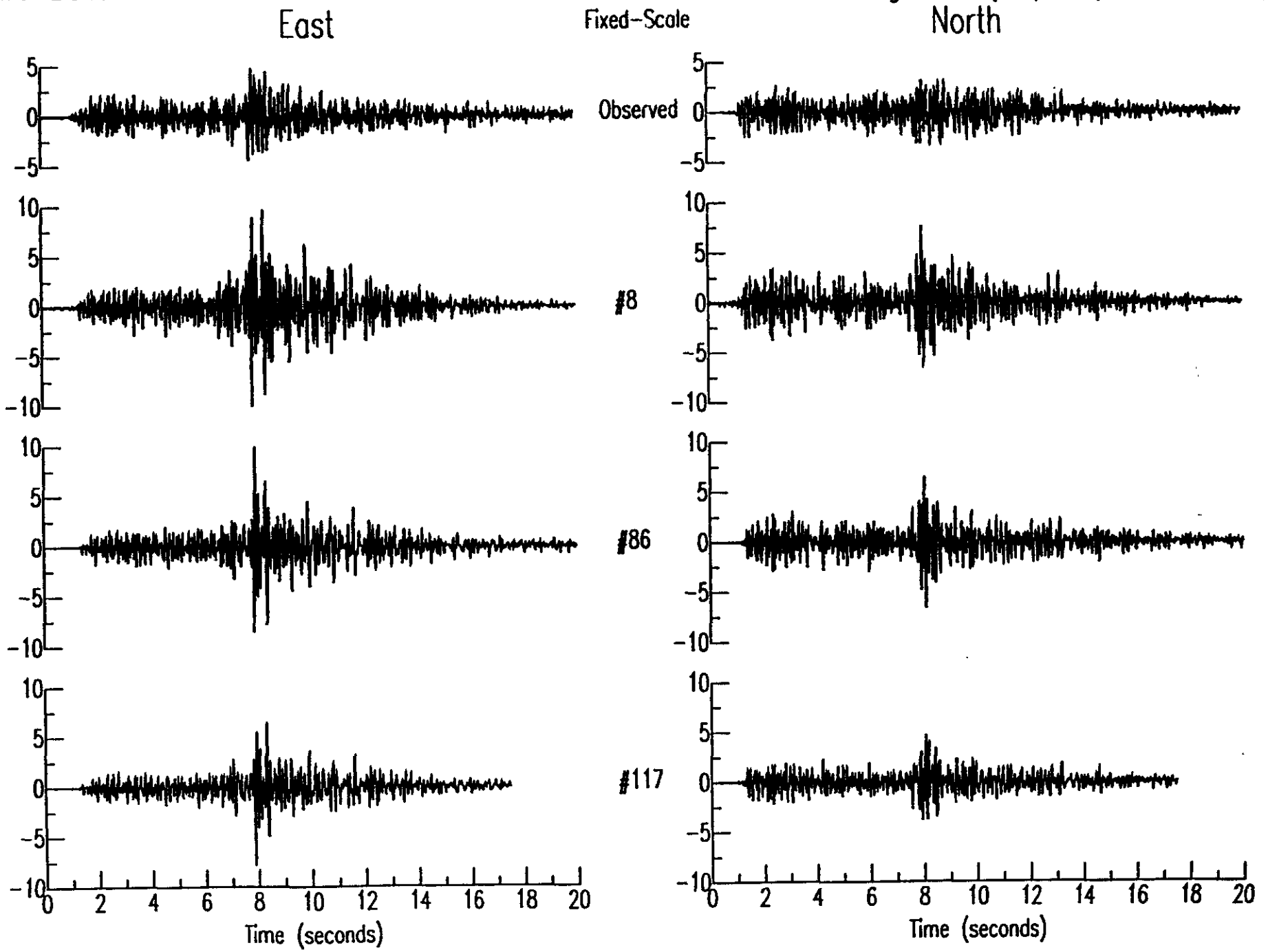

Figure B5b: Observed V1 vs Predicted V1 Preferred Model Accelerograms (uM/sec/sec x 100)

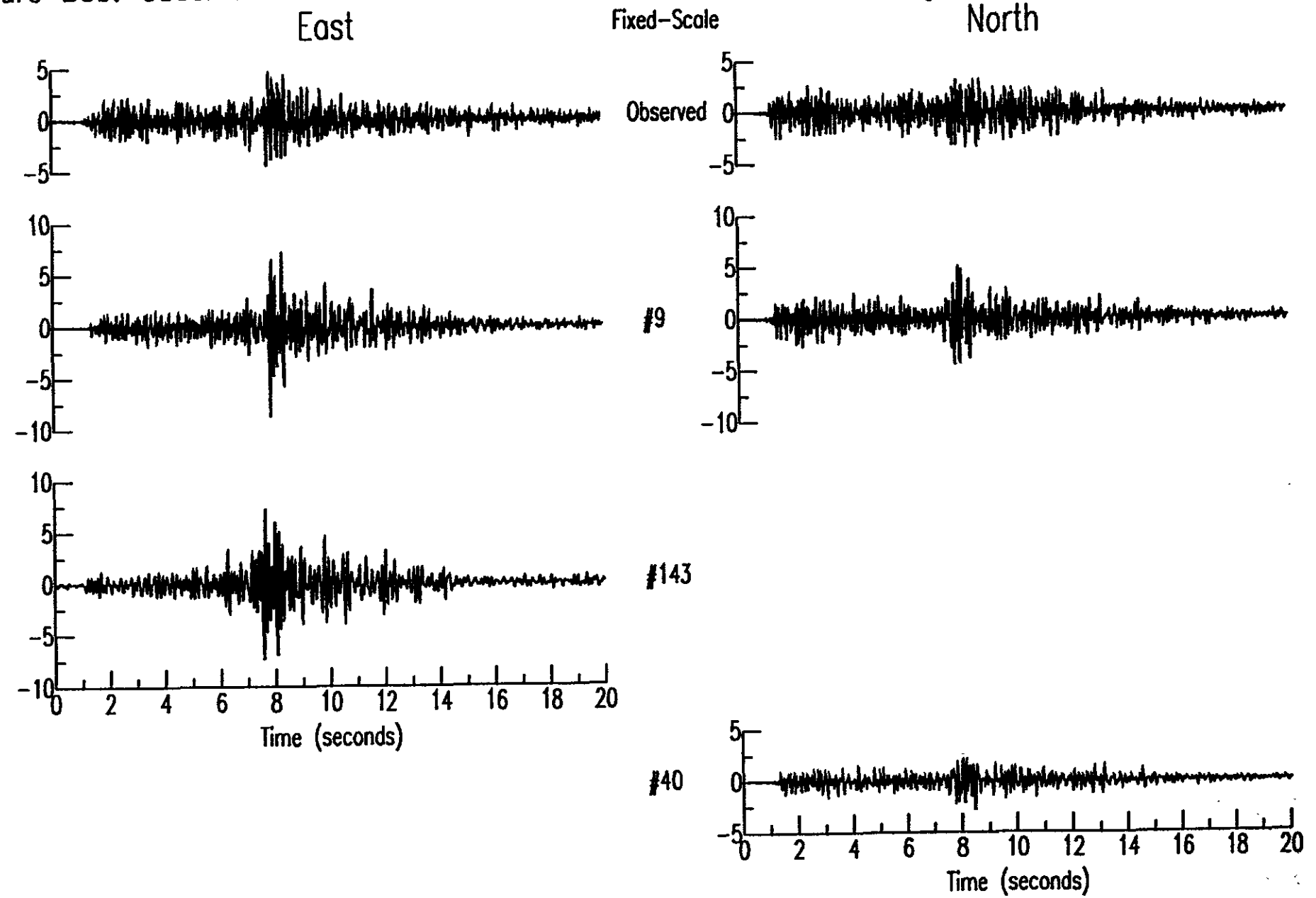

Appendix C

Plots from Analysis of Submitted Optional Strong-motion Predictions

Figure C1a: Standard Fourier Spectral Ratio Plot:
Spectral Ratio V2/R1 for Optional Predictions

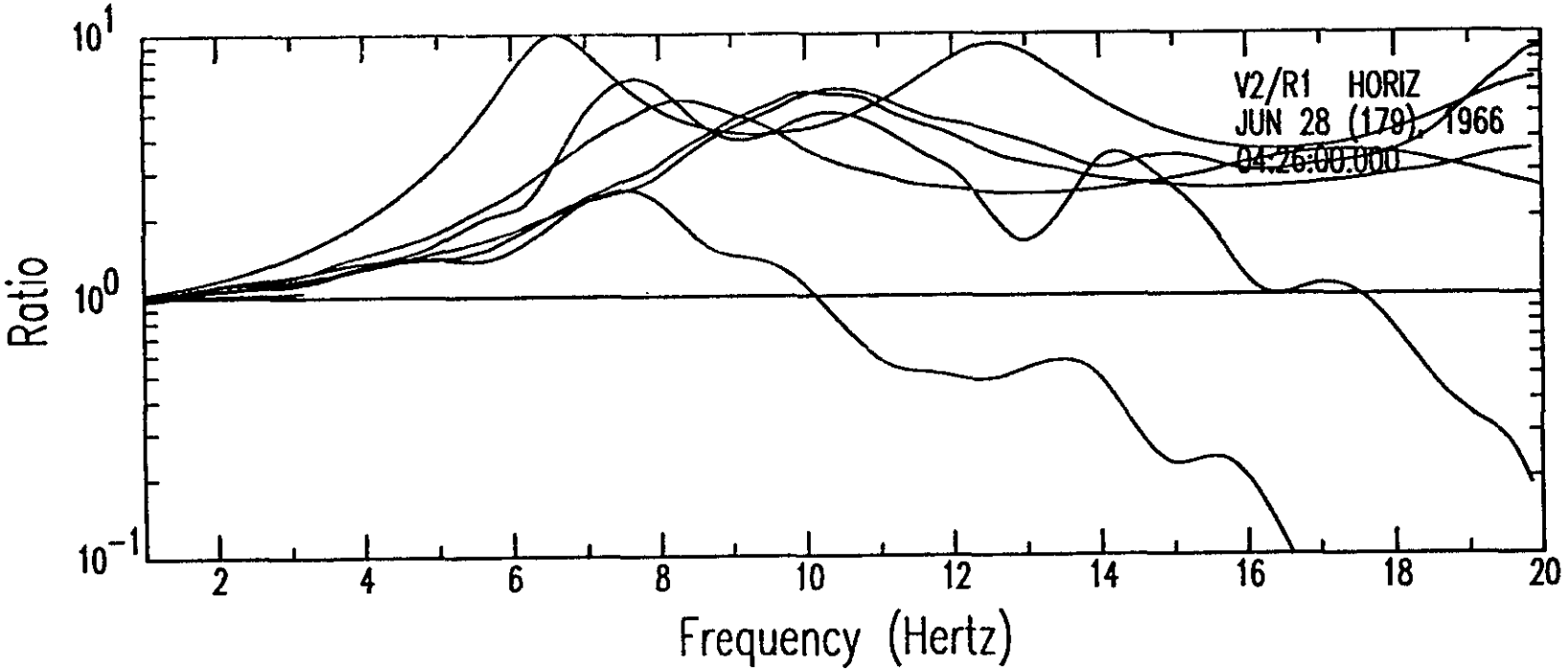

Figure C1b: Standard Fourier Spectral Ratio Plot:
Spectral Ratio V1/R1 for Optional Predictions

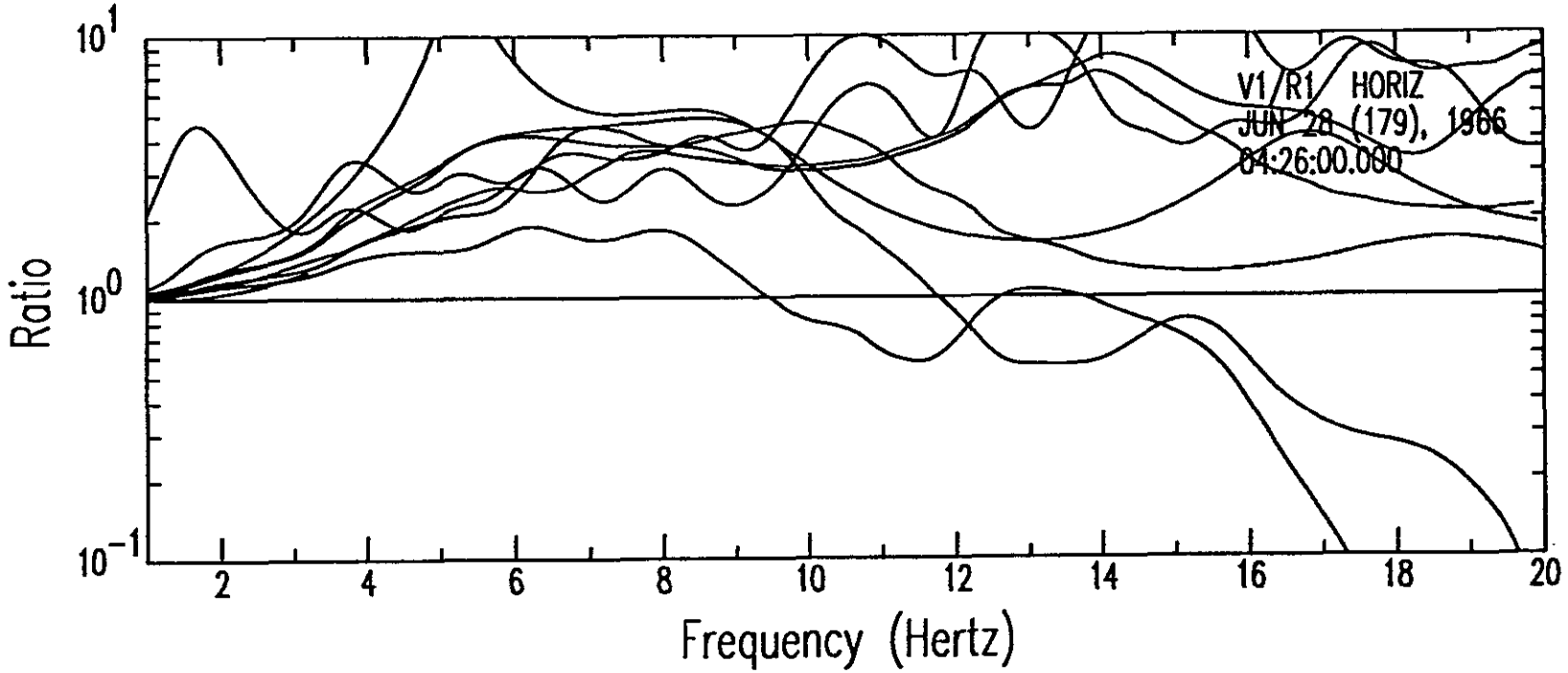

Figure C1c: Standard Fourier Spectral Ratio Plot:
Spectral Ratio D2/R1 for Optional Predictions

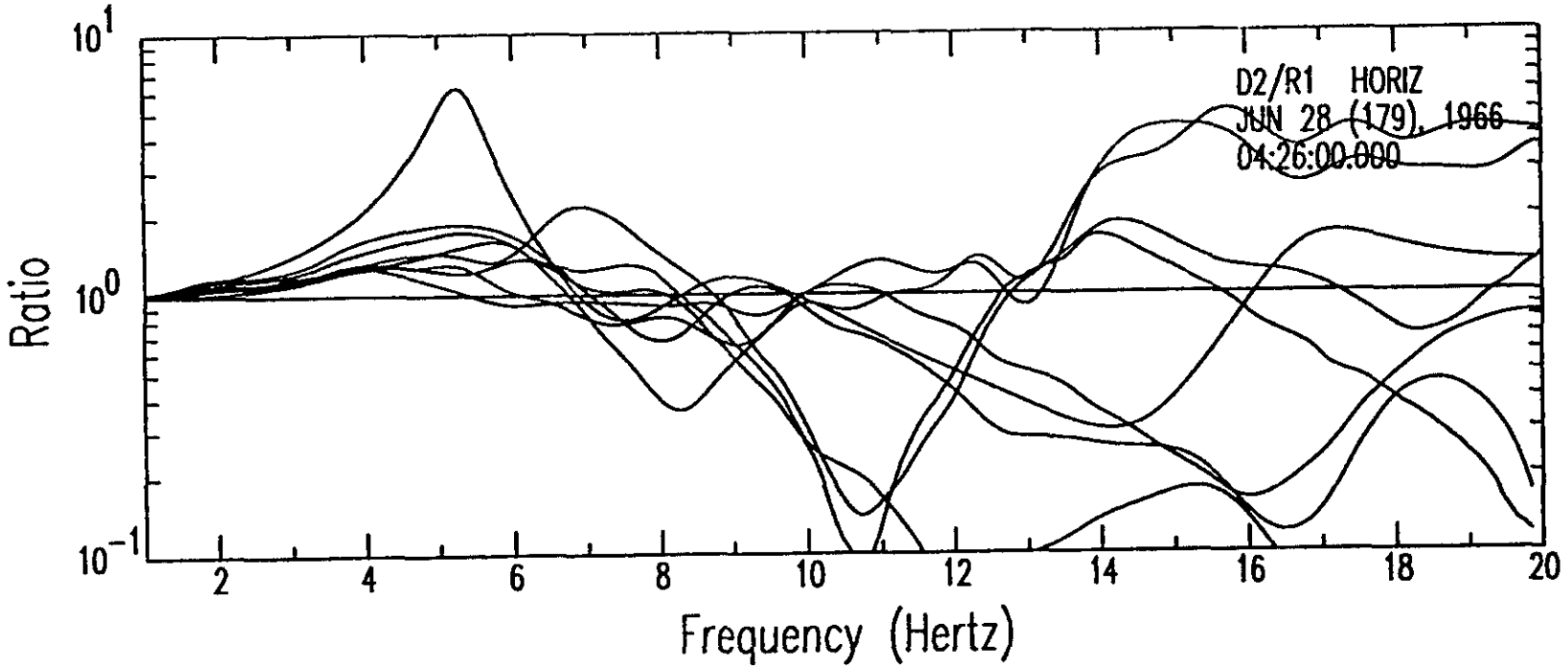

Figure C1d: Standard Fourier Spectral Ratio Plot:
Spectral Ratio D3/R1 for Optional Predictions

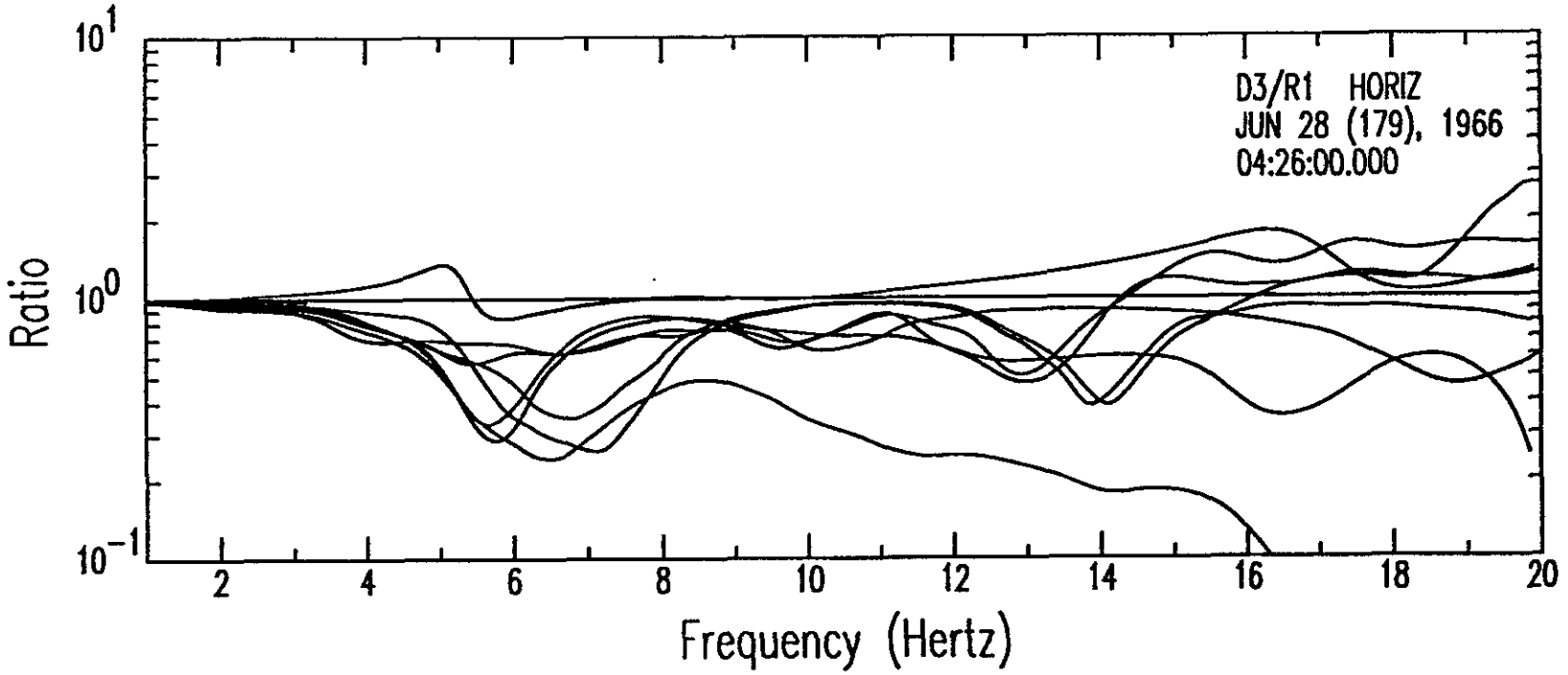

Figure C1e: Standard Fourier Spectral Ratio Plot:
Spectral Ratio D1/R1 for Optional Predictions

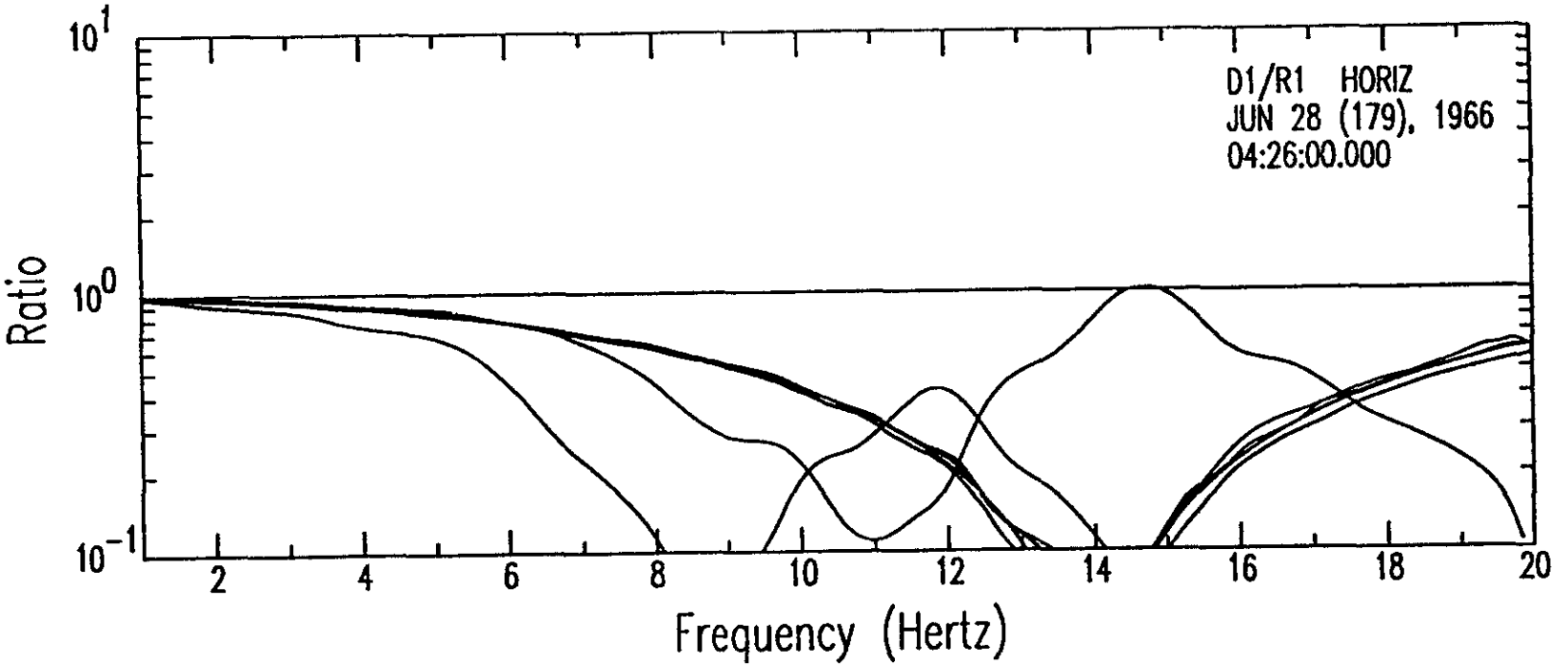

Figure C1f: Standard Fourier Spectral Ratio Plot:
Spectral Ratio R2/R1 for Optional Predictions

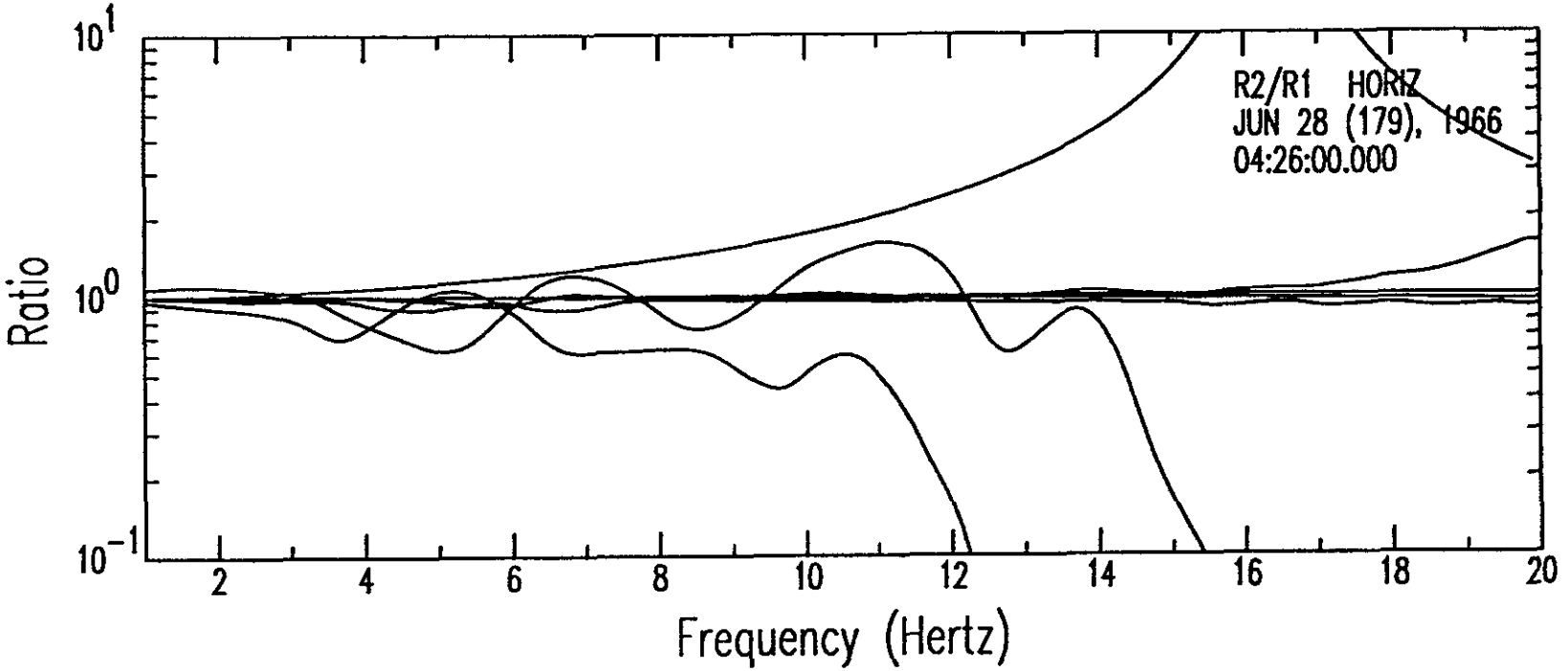

Figure C2a: Spectral Ratio Quartiles for Optional Predictions

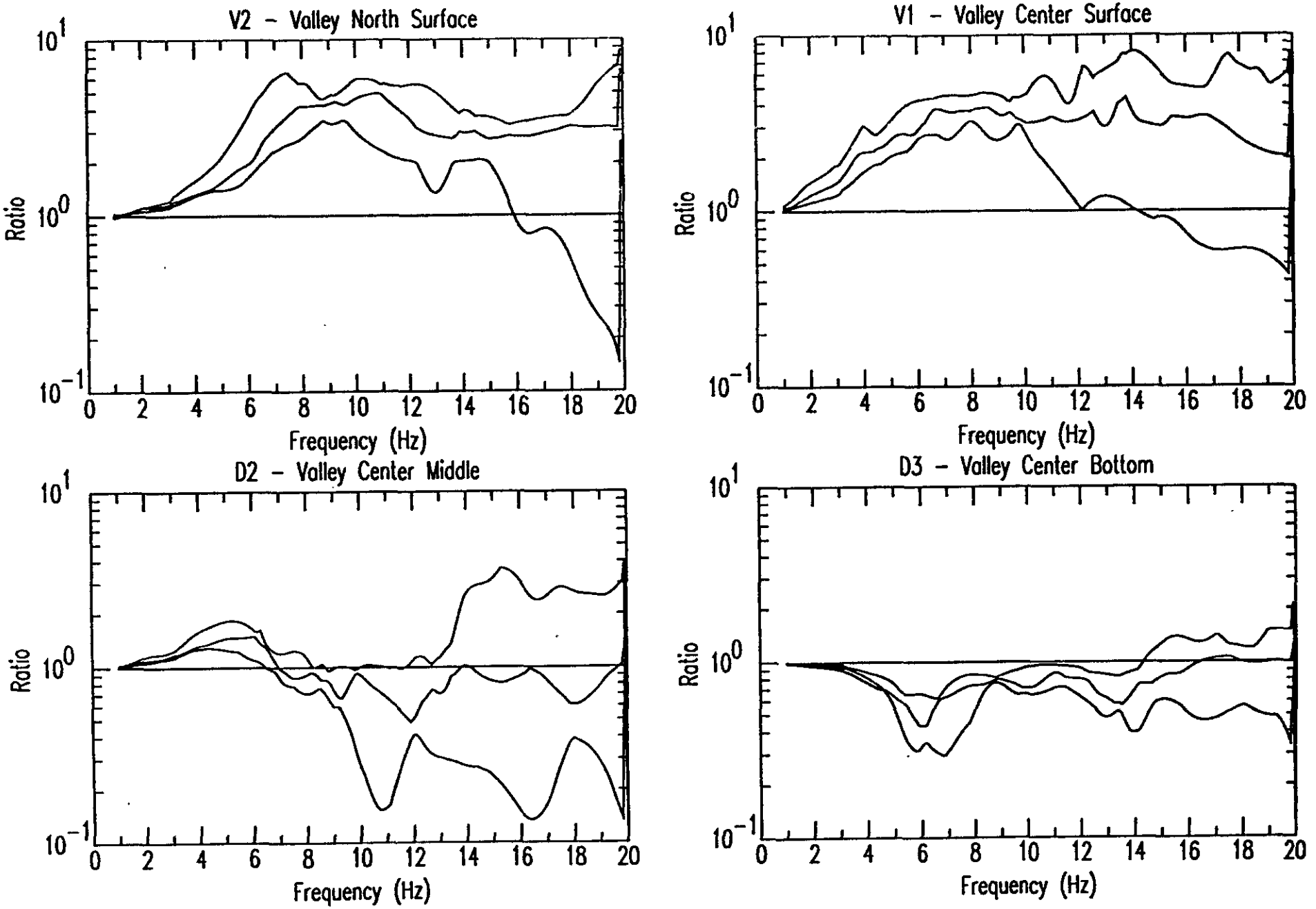

Figure C2b: Spectral Ratio Quartiles for Optional Predictions

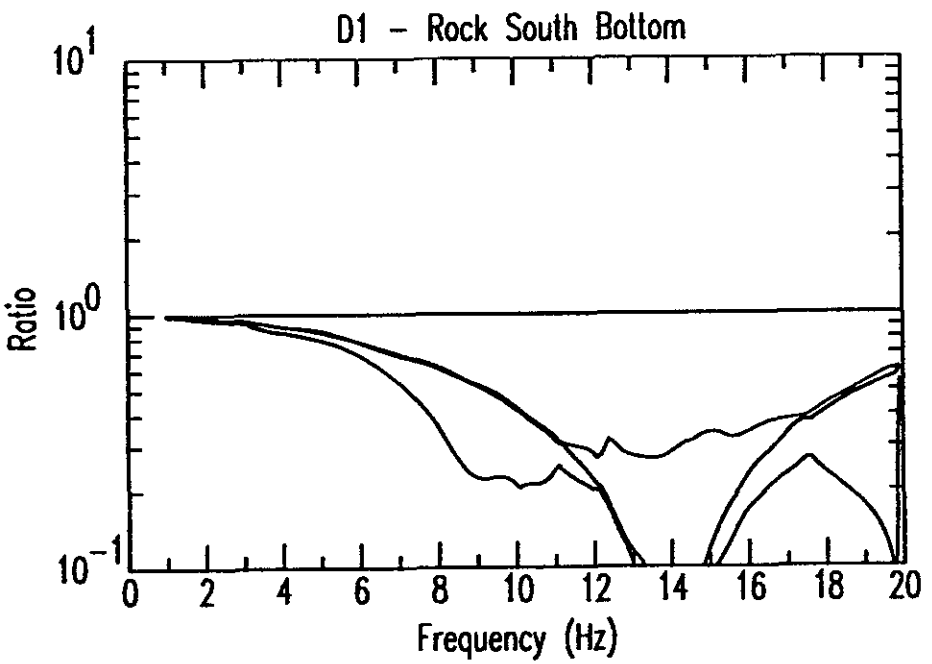

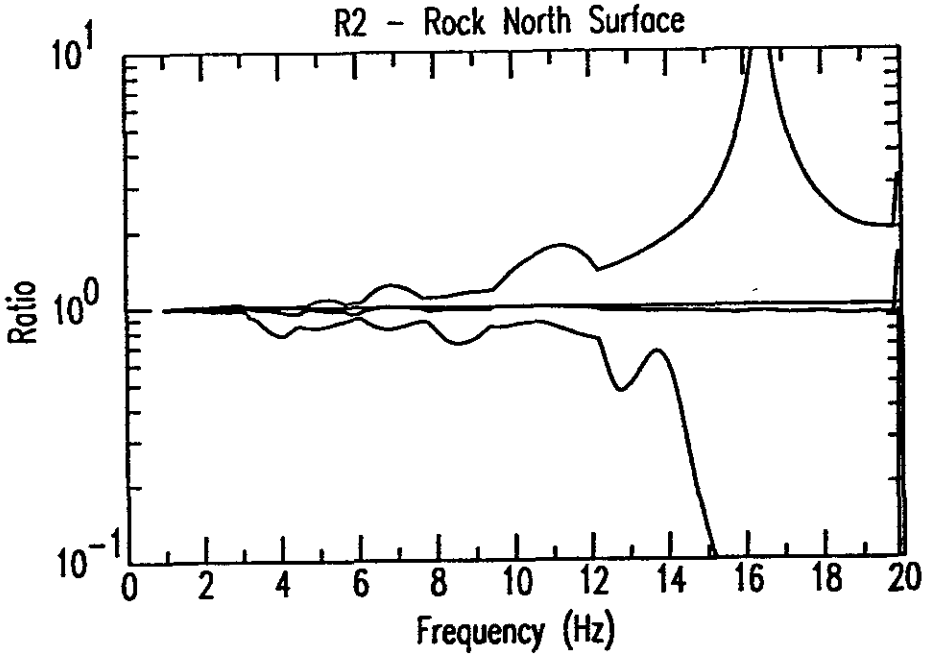

Figure C3a: Standard Response Spectra:
Station V1 Valley Center Surface Optional Predictions

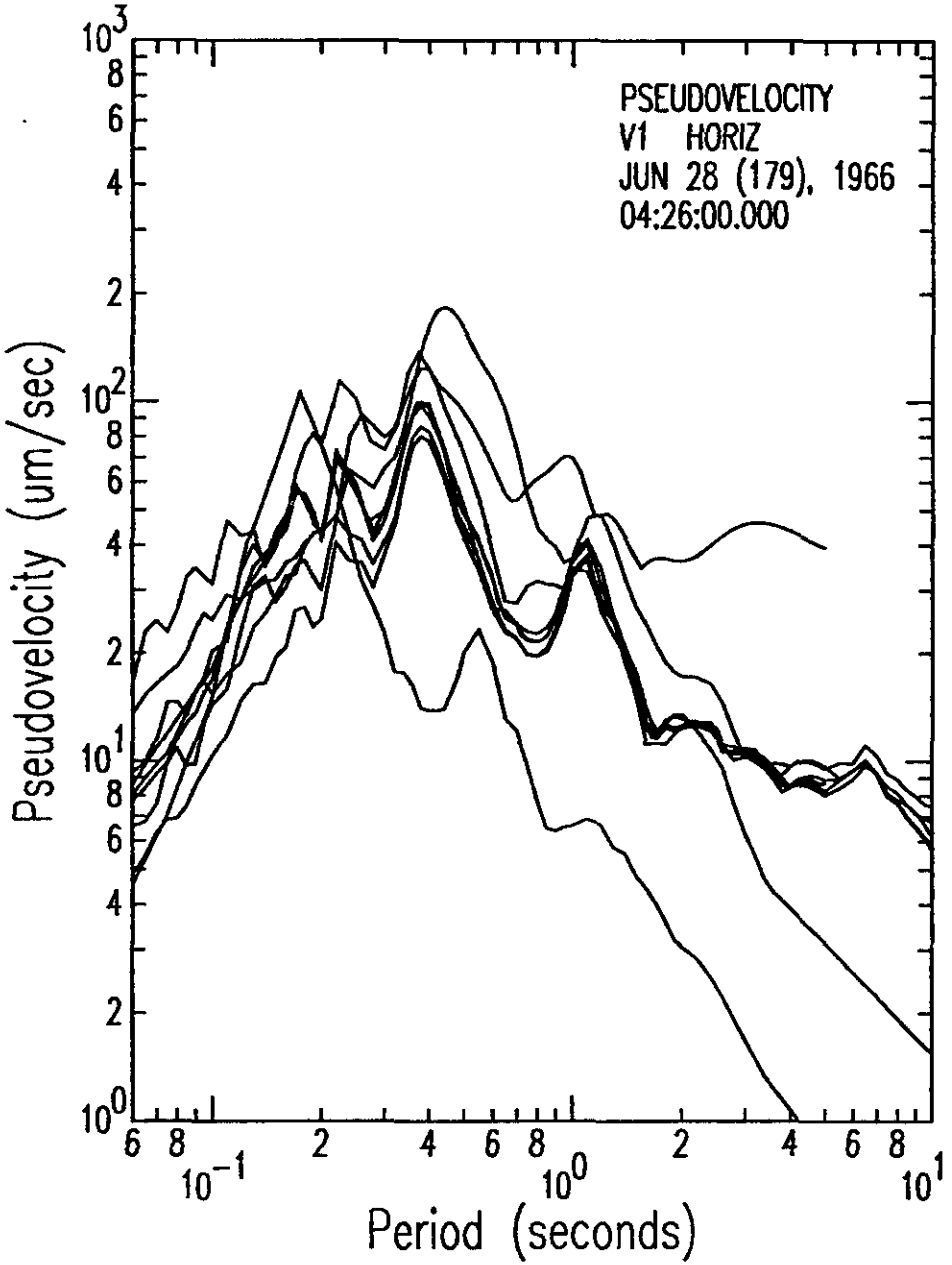

Figure C3b: Standard Response Spectra:
Station D2 Valley Center Middle Optional Predictions

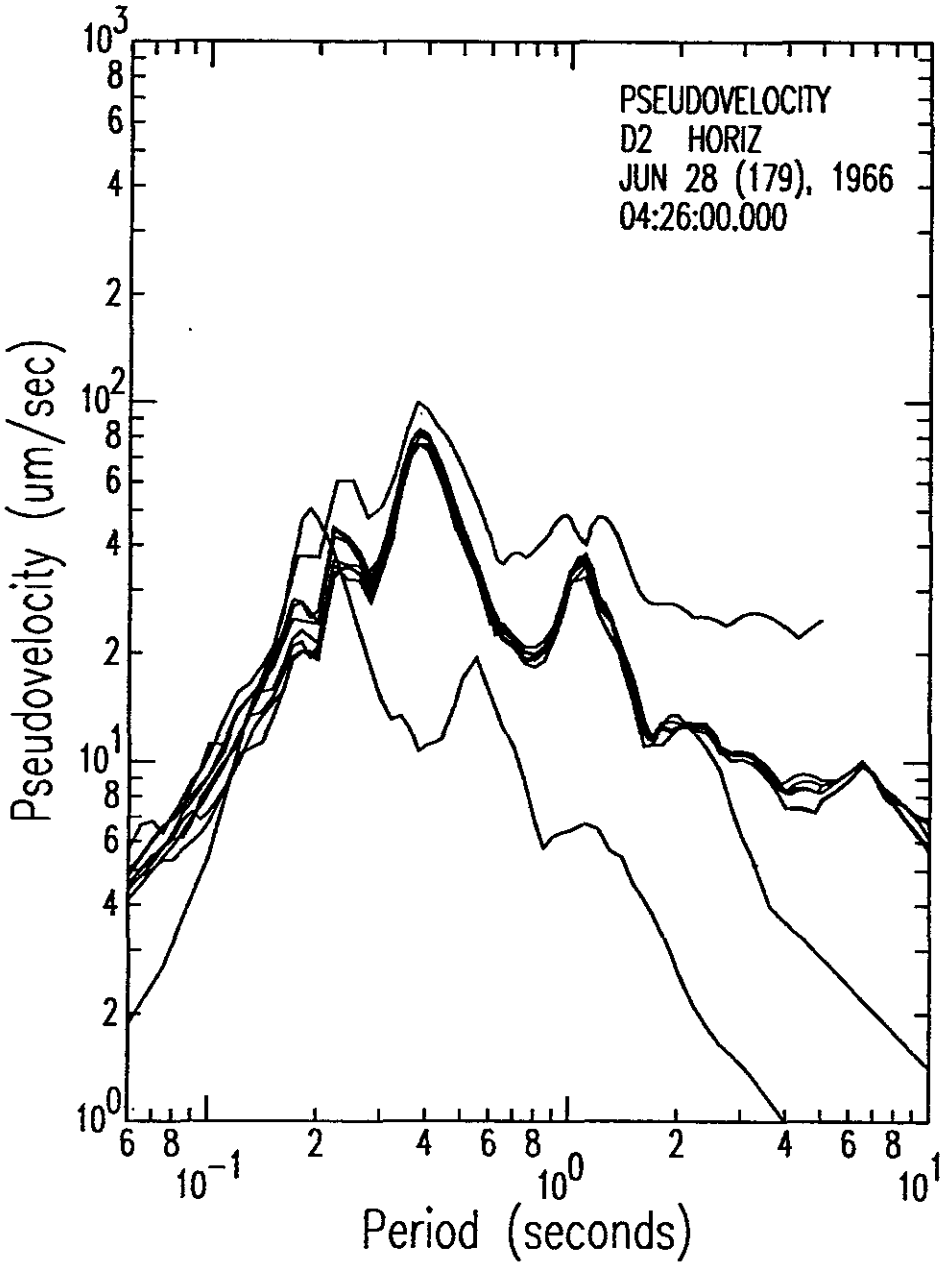

Figure C3c: Standard Response Spectra:
Station D3 Valley Center Bottom Optional Predictions

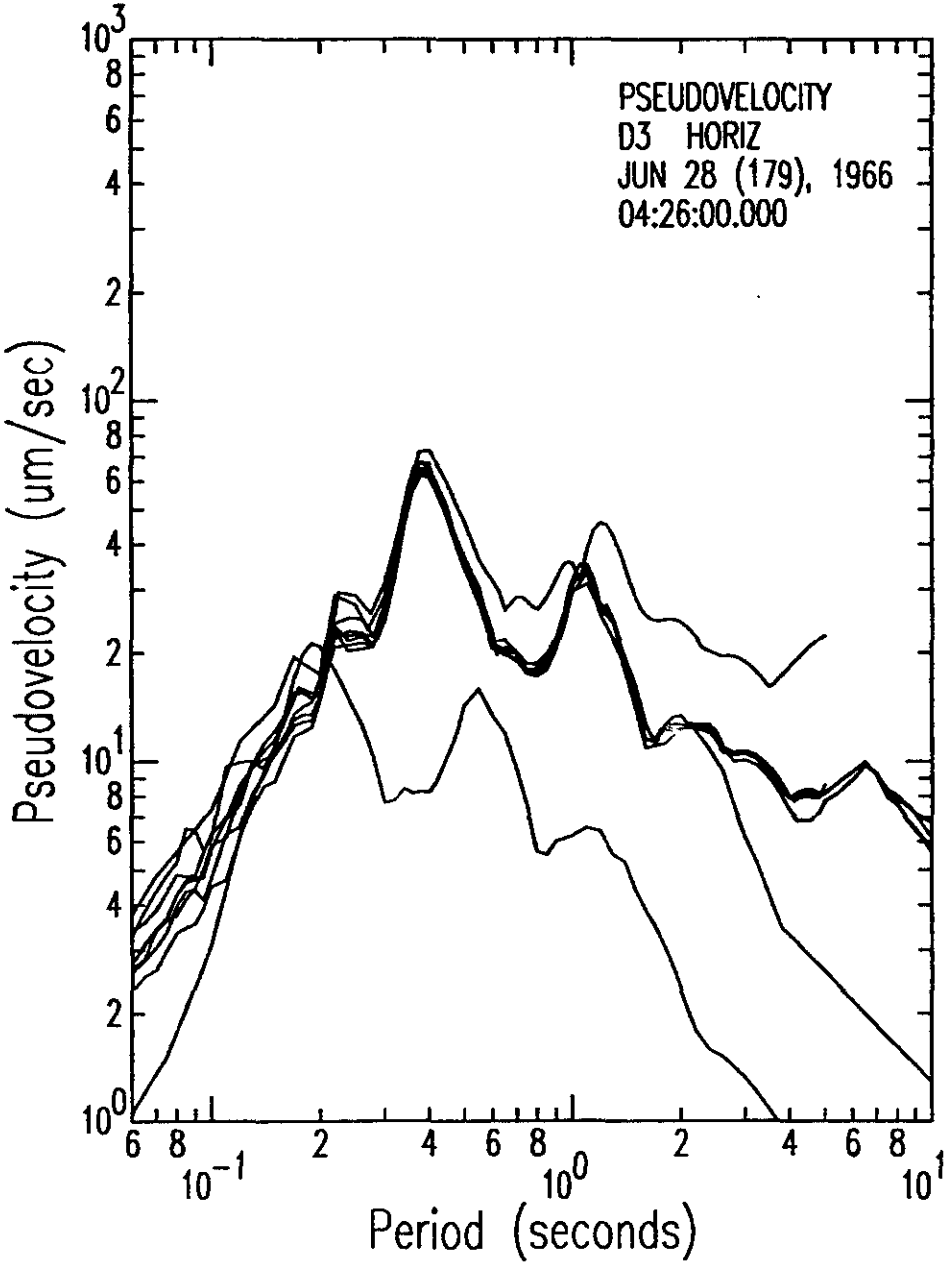

Figure C4: Response Spectra Quartiles for Optional Predictions

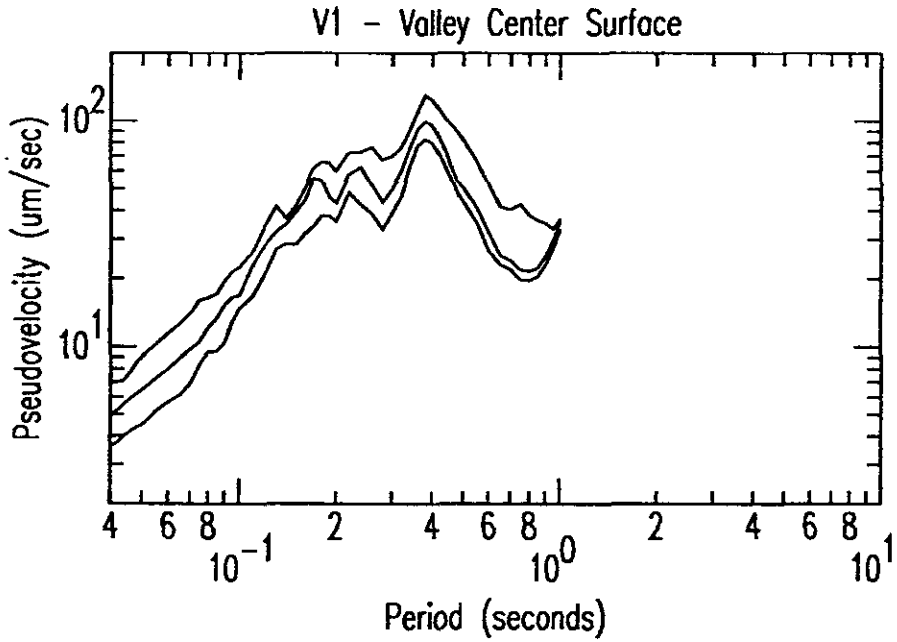

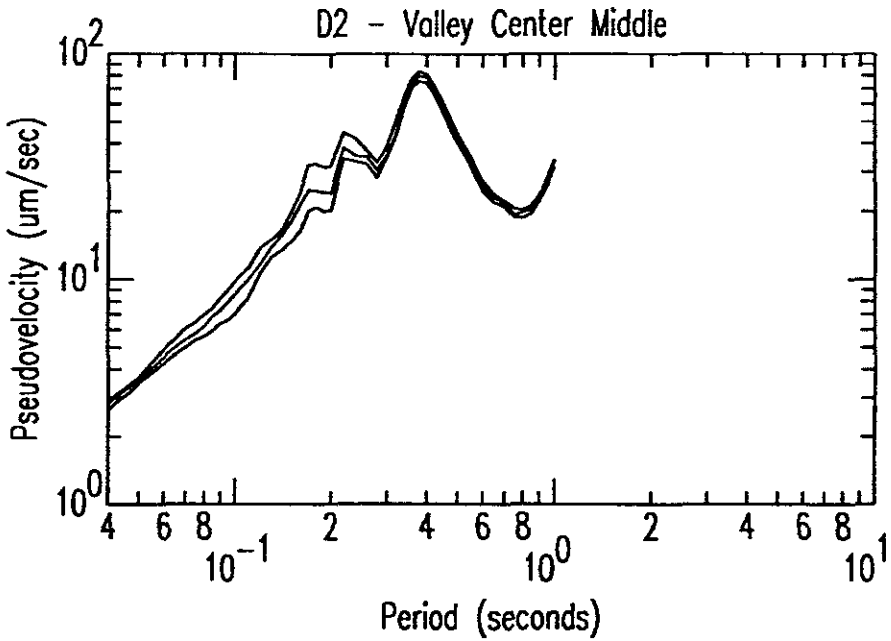

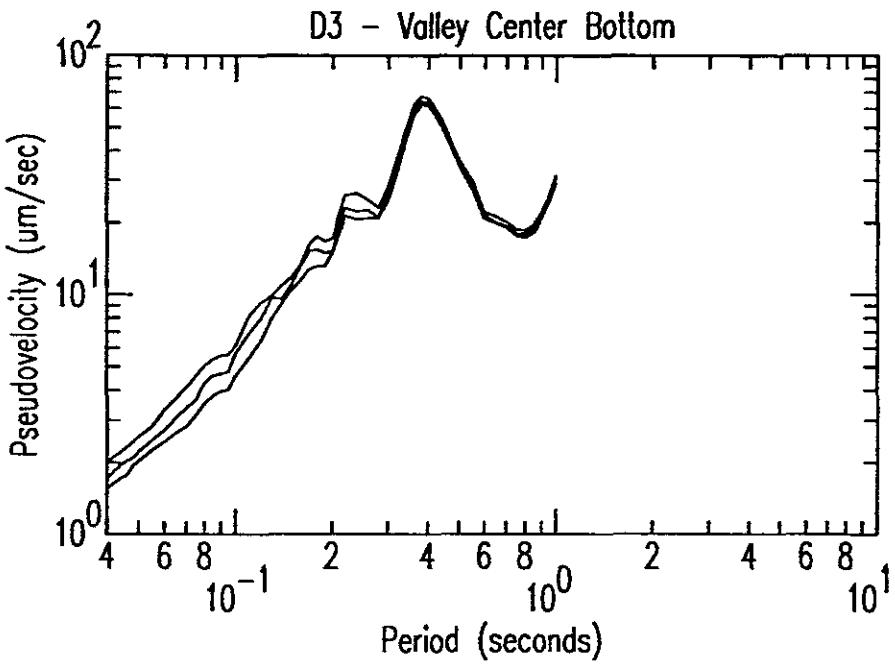

Figure C5a: Predicted V1 Optional Accelerograms (uM/sec/sec x 100)

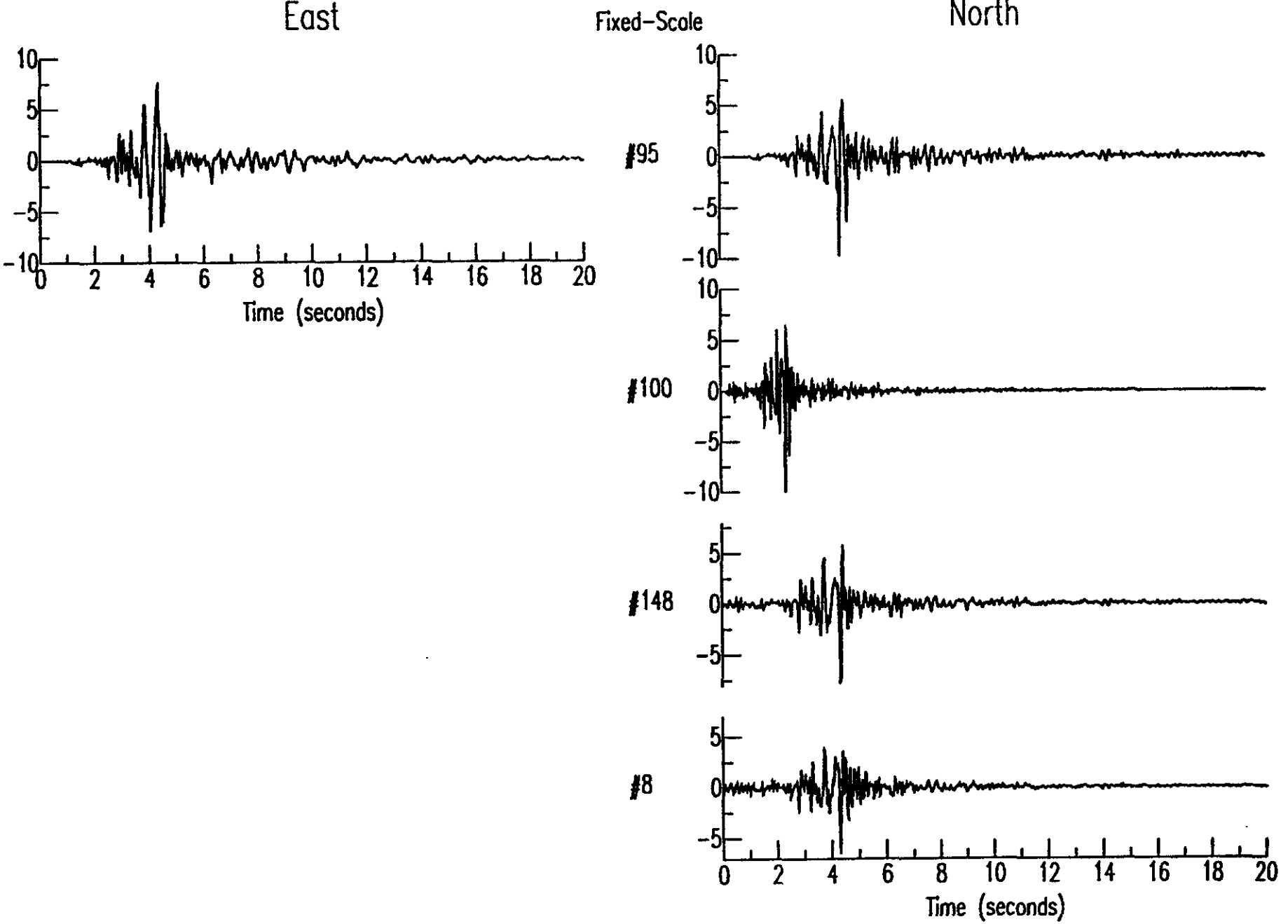

Figure C5b: Predicted V1 Optional Accelerograms (uM/sec/sec x 100)

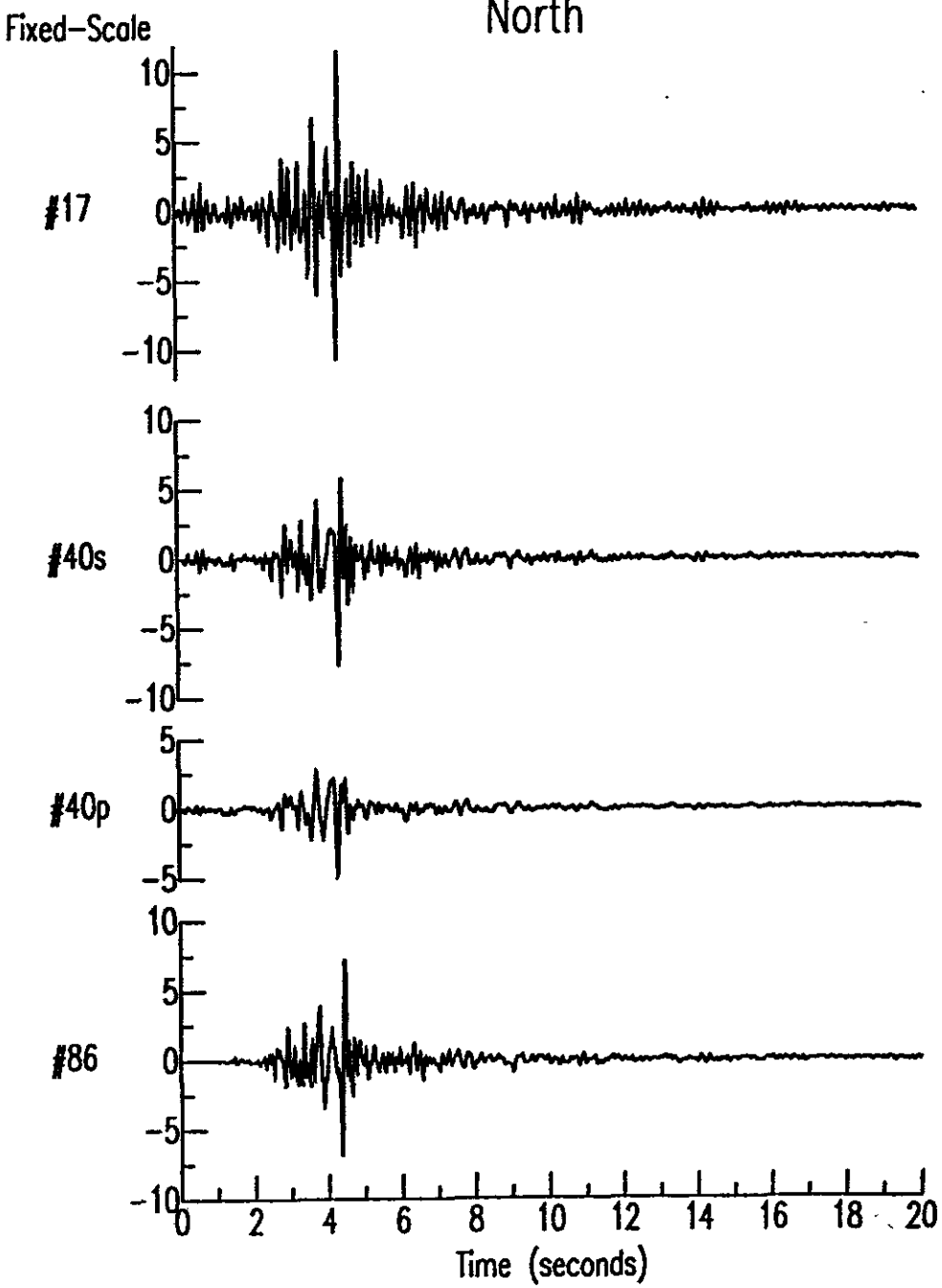

Appendix D

Plots from Analysis of Submitted

D3 based Weak-motion Predictions

Figure D1a: Standard Fourier Spectral Ratio Plot:
Spectral Ratio V1/D3 for D3 based Predictions

Solid lines – Predictions; Dashed line – Observed

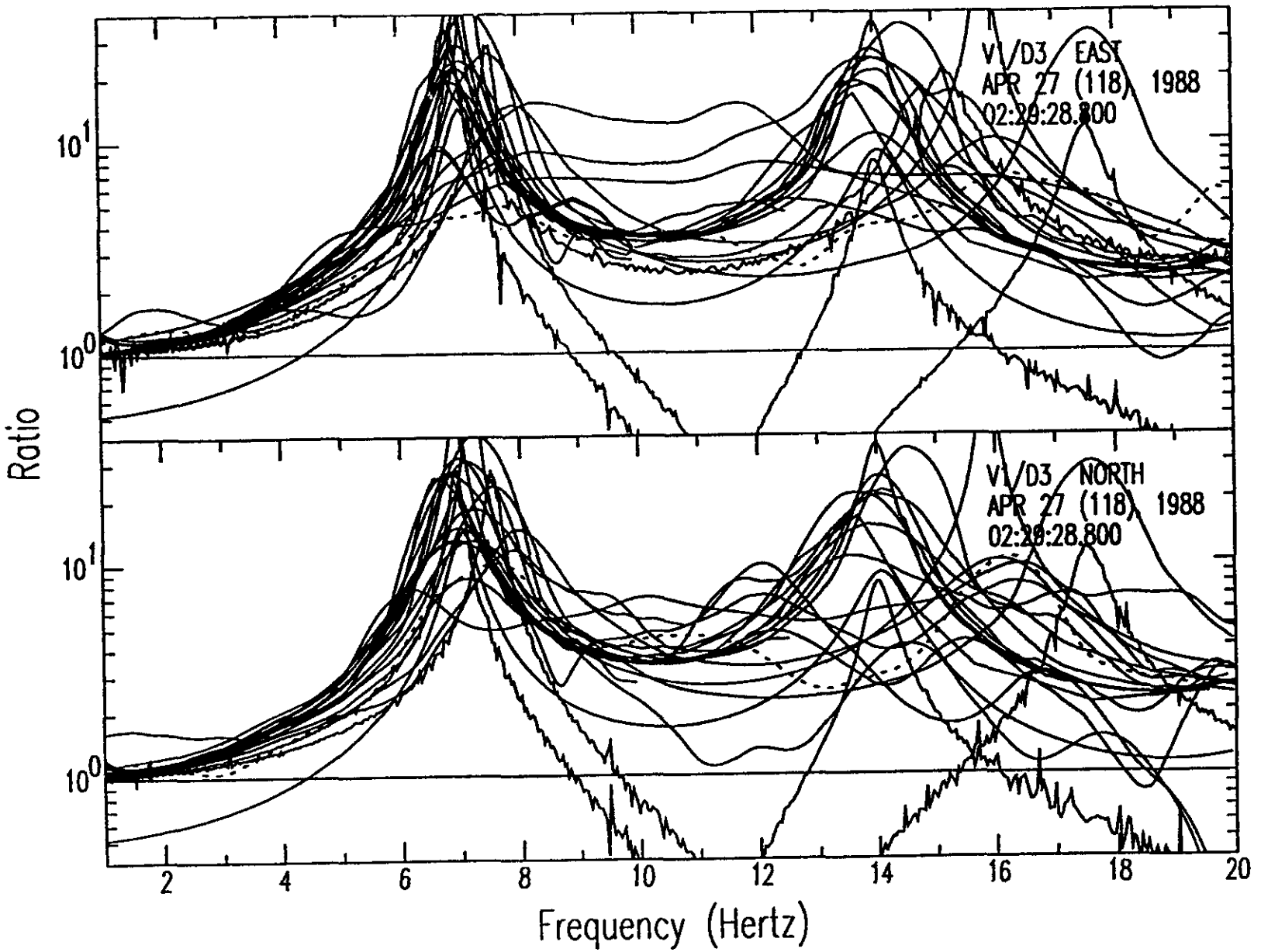

Figure D1b: Standard Fourier Spectral Ratio Plot:
Spectral Ratio D2/D3 for D3 based Predictions

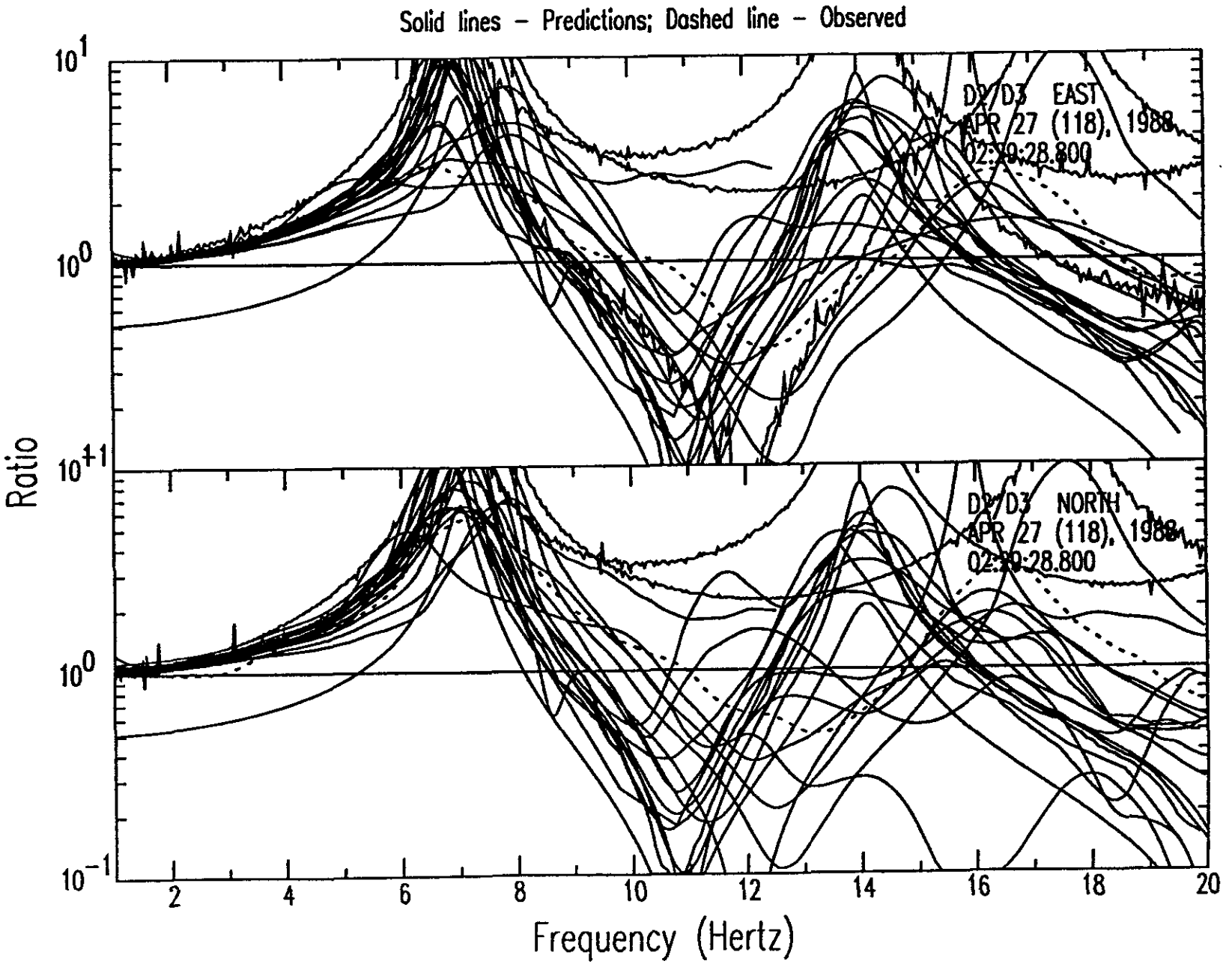

Figure D2: D3 Spectral Ratio Prediction Quartiles vs Observations

Spectral Ratio Predictions: Dashed – quartiles

Observations: Solid – weak-motion test event; Dash-dotted – weak-motion mean; Dotted – 1 std deviation

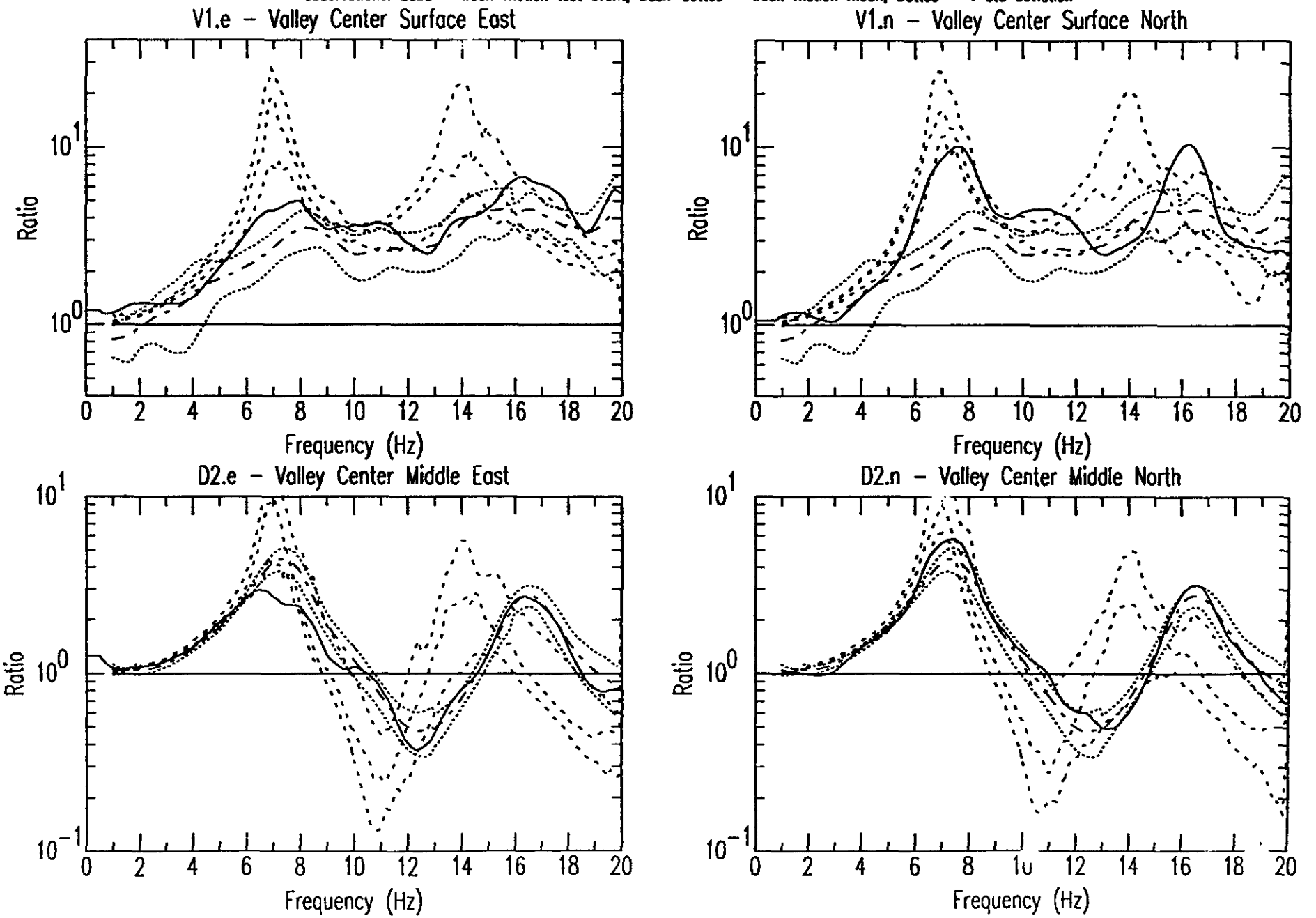

Figure D3a: Standard Response Spectra:
Station V1 Valley Center Surface D3 based Predictions
Solid lines - Predictions; Dashed line - Observed

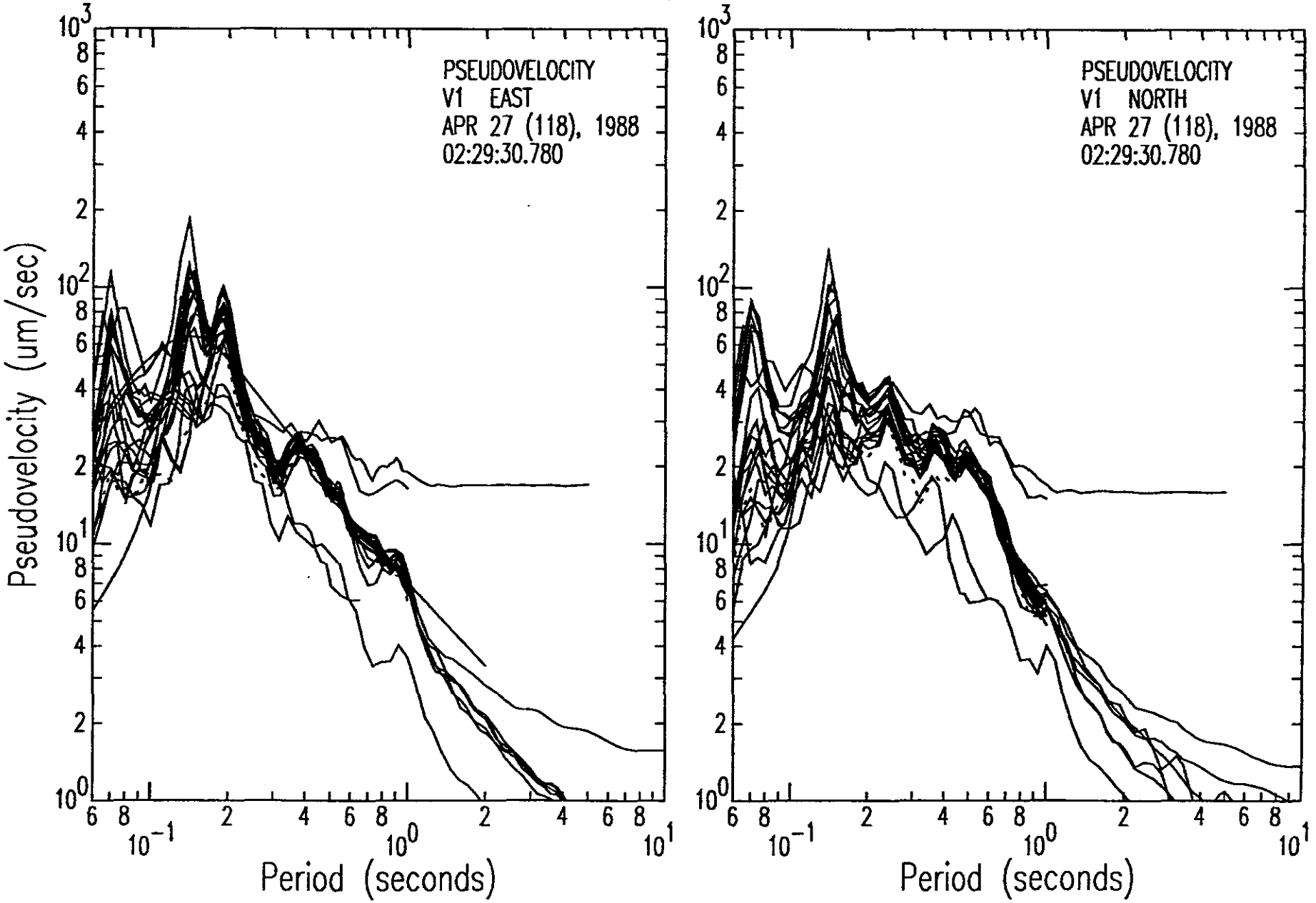

Figure D3b: Standard Response Spectra:
Station D2 Valley Center Middle D3 based Predictions
Solid lines - Predictions; Dashed line - Observed

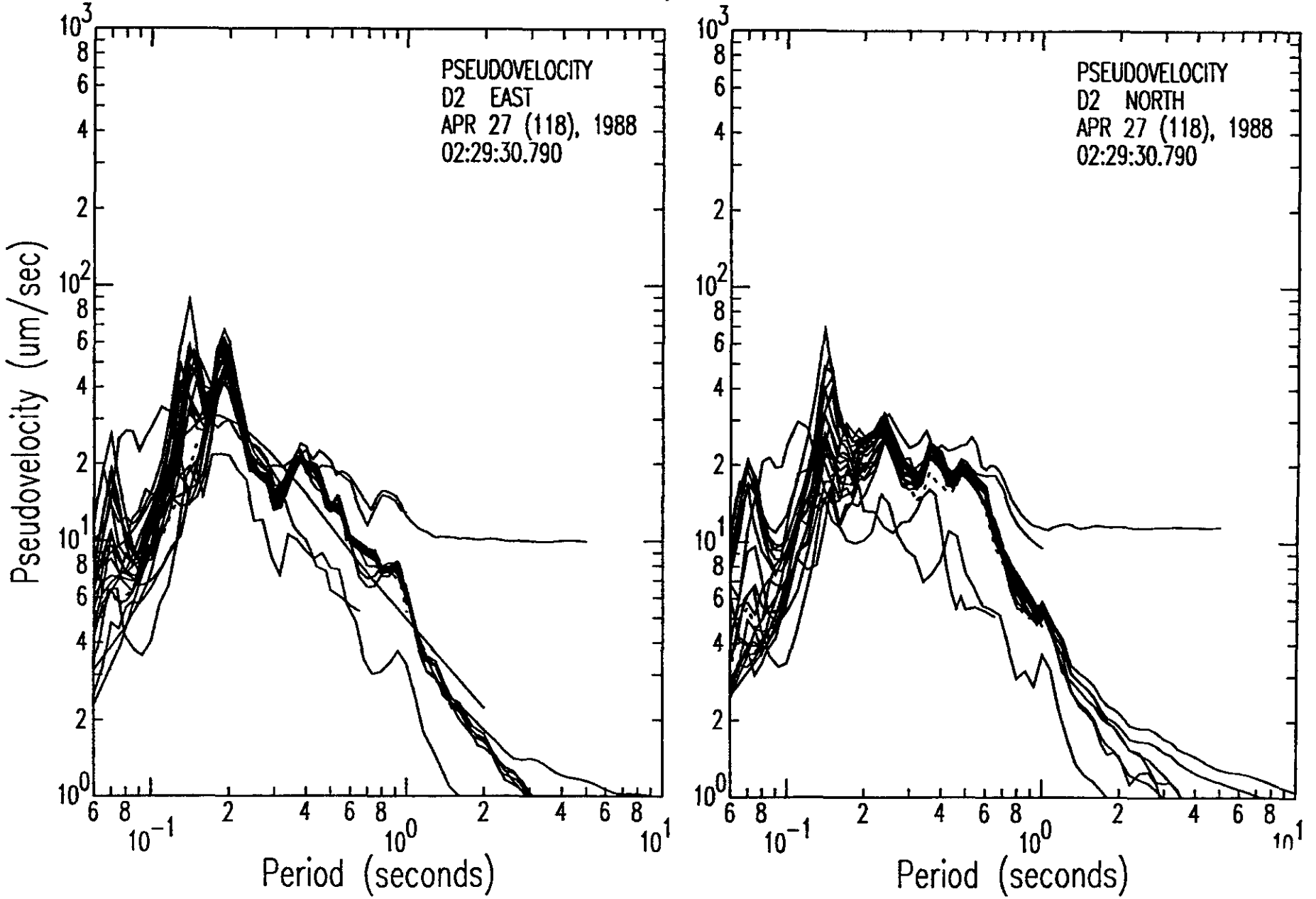

Figure D4: D3 Response Spectra Prediction Quartiles vs Observations

Response Spectra Predictions: Dashed – quartiles

Observations: Solid – weak-motion test event

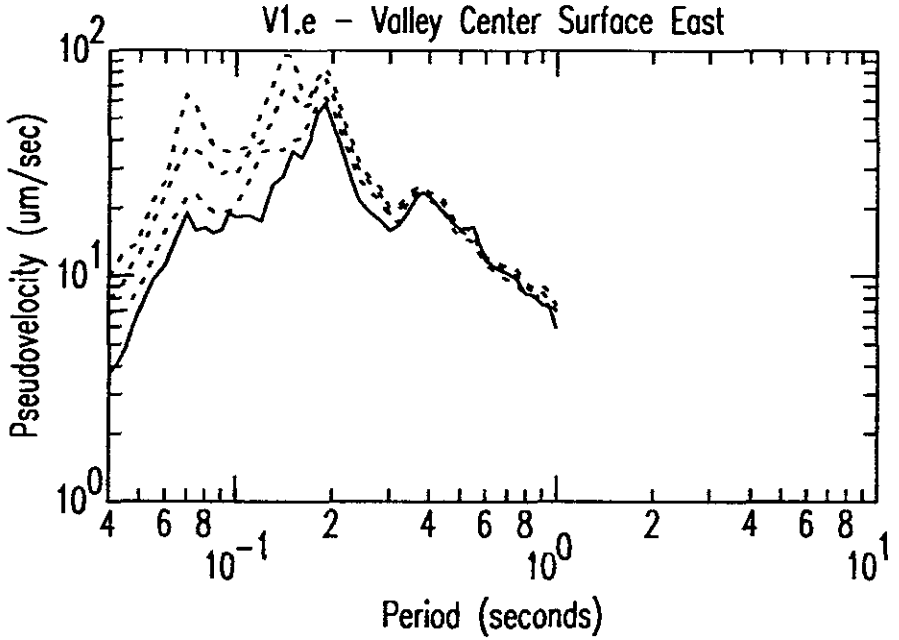

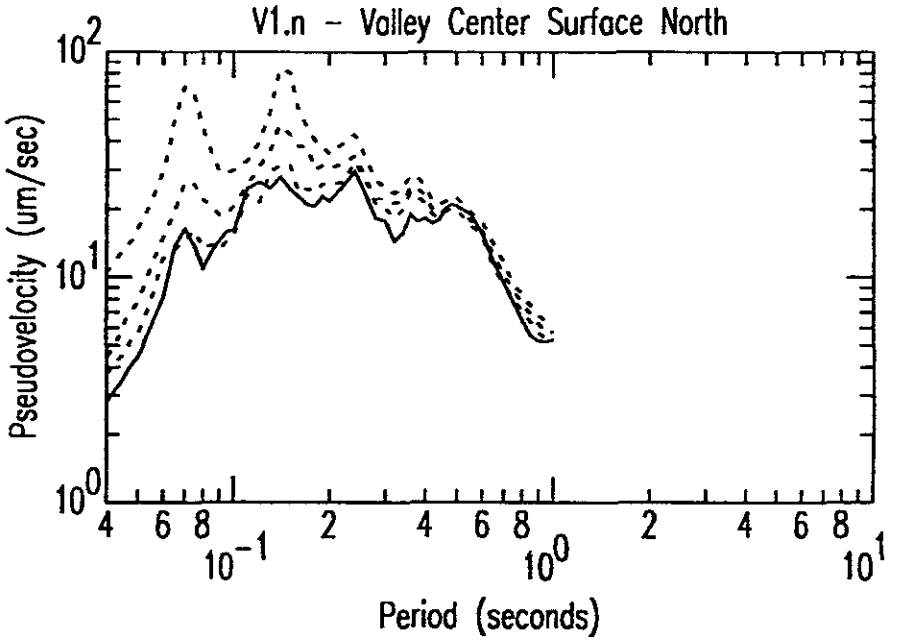

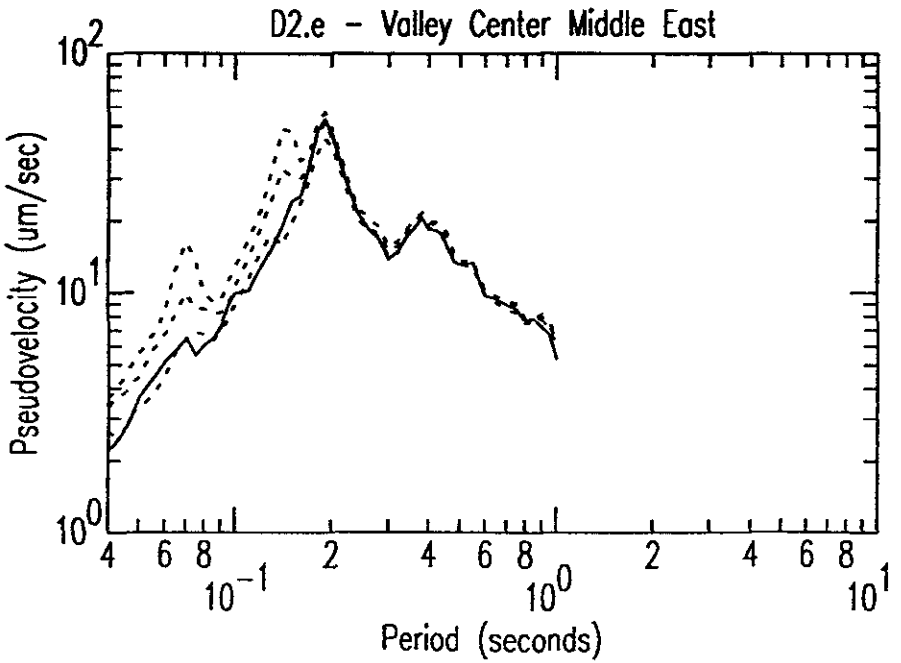

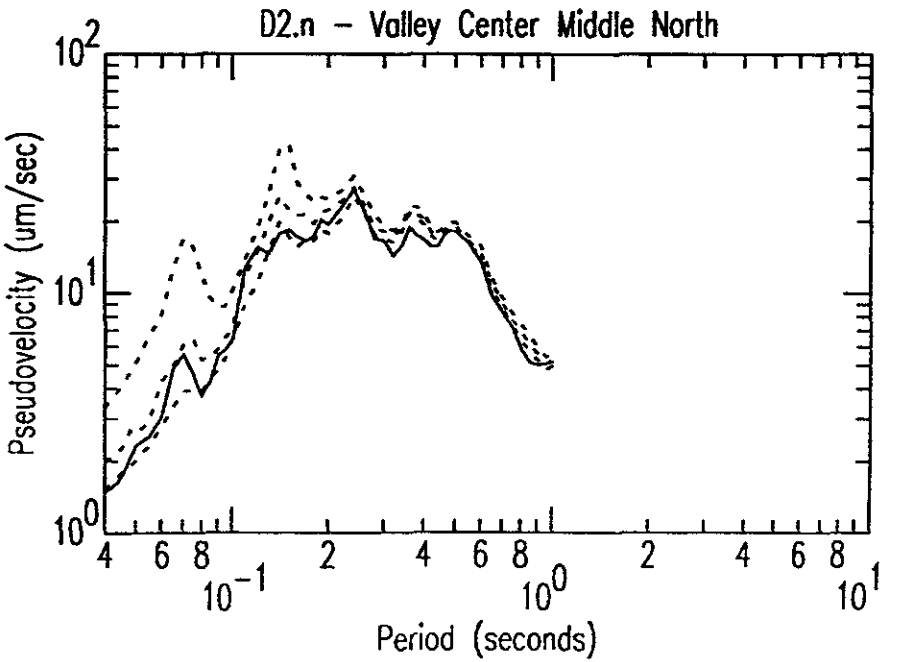

Figure D5a: Observed V1 vs Predicted V1 Accelerograms (uM/sec/sec x 100) based on D3

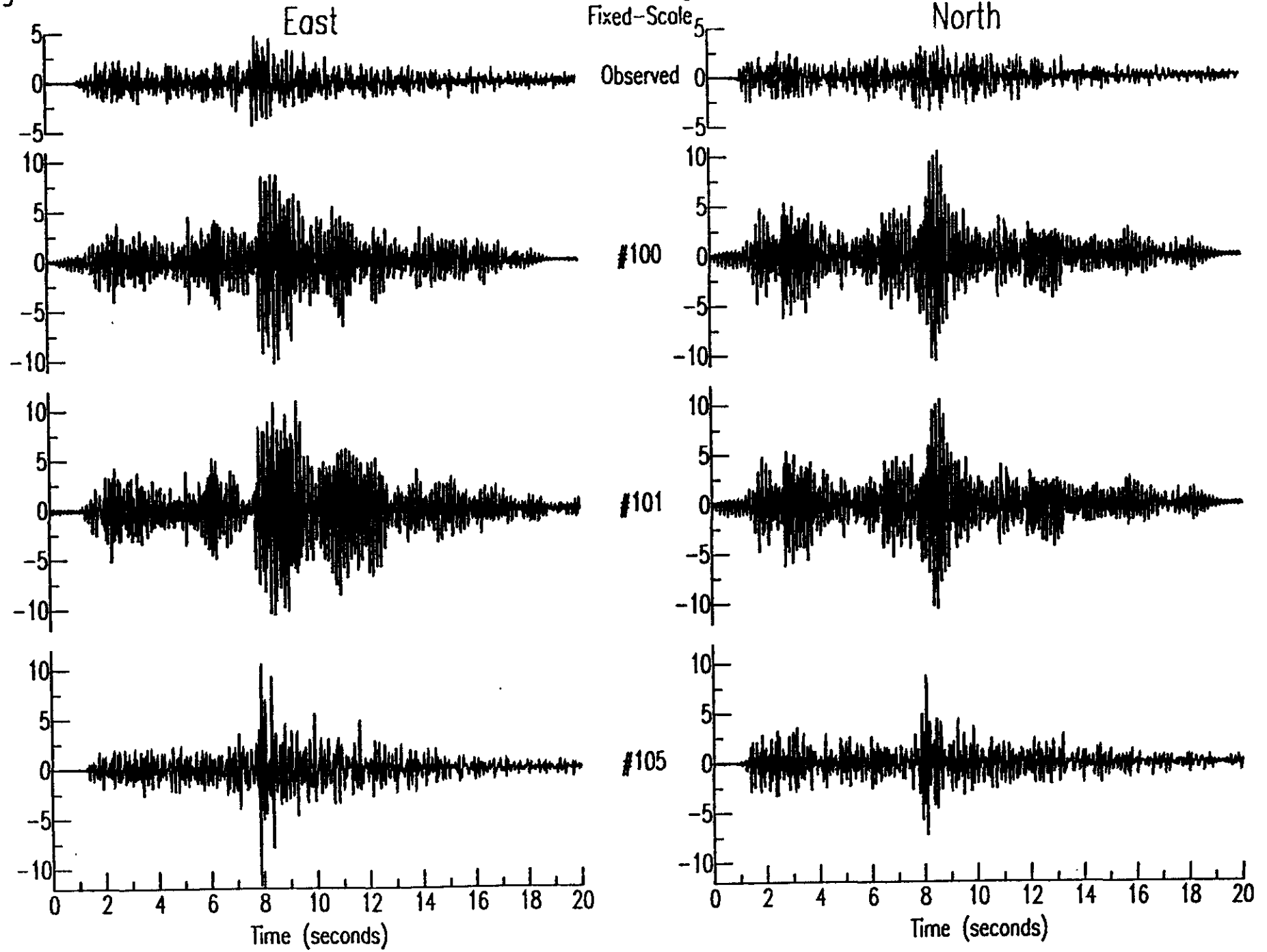

Figure D5b: Observed V1 vs Predicted V1 Accelerograms (uM/sec/sec x 100) based on D3

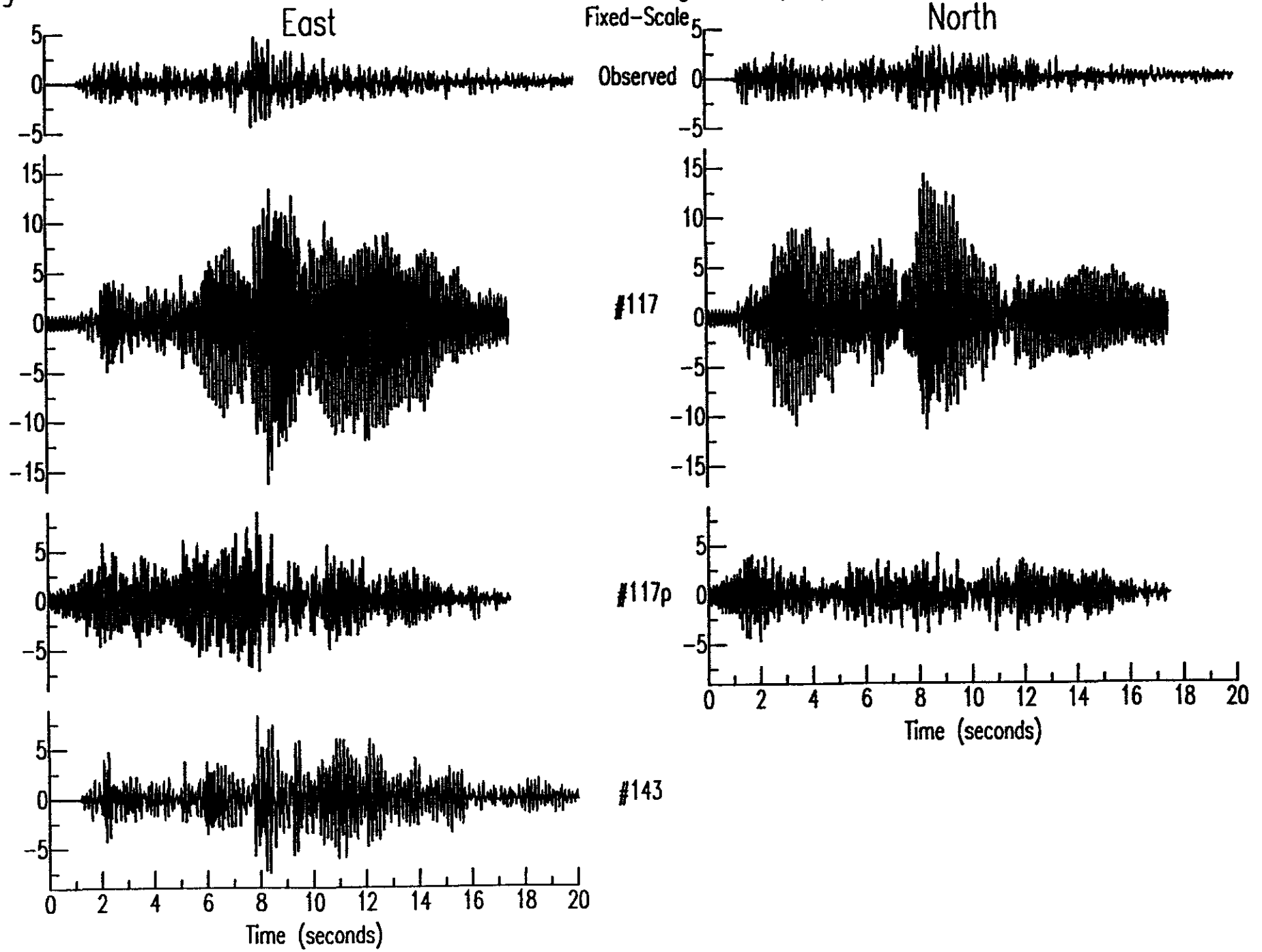

Figure D5c: Observed V1 vs Predicted V1 Accelerograms (uM/sec/sec x 100) based on D3

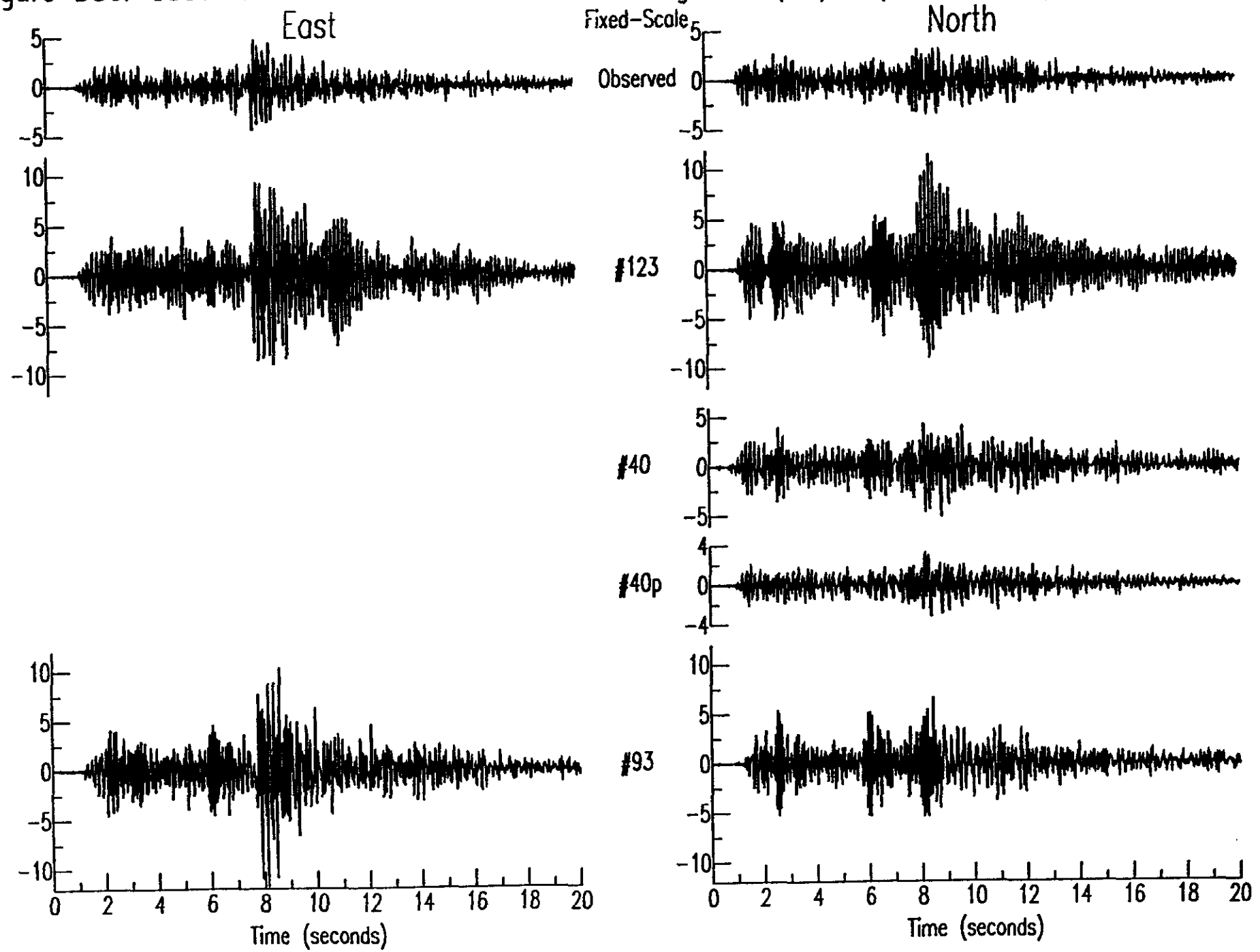

Figure D5d: Observed V1 vs Predicted V1 Accelerograms (uM/sec/sec x 100) based on D3

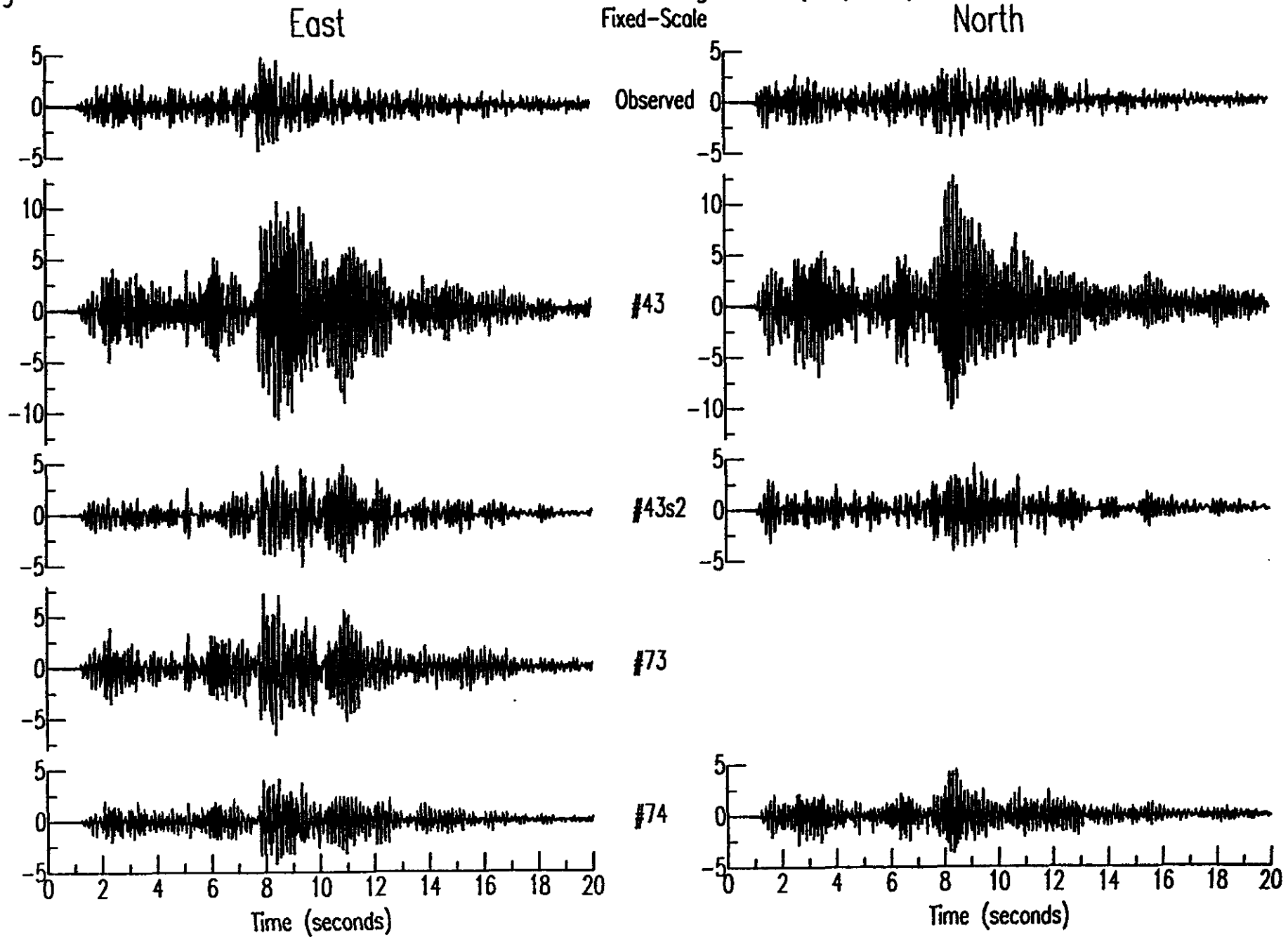

Figure D5e: Observed V1 vs Predicted V1 Accelerograms (uM/sec/sec x 100) based on D3

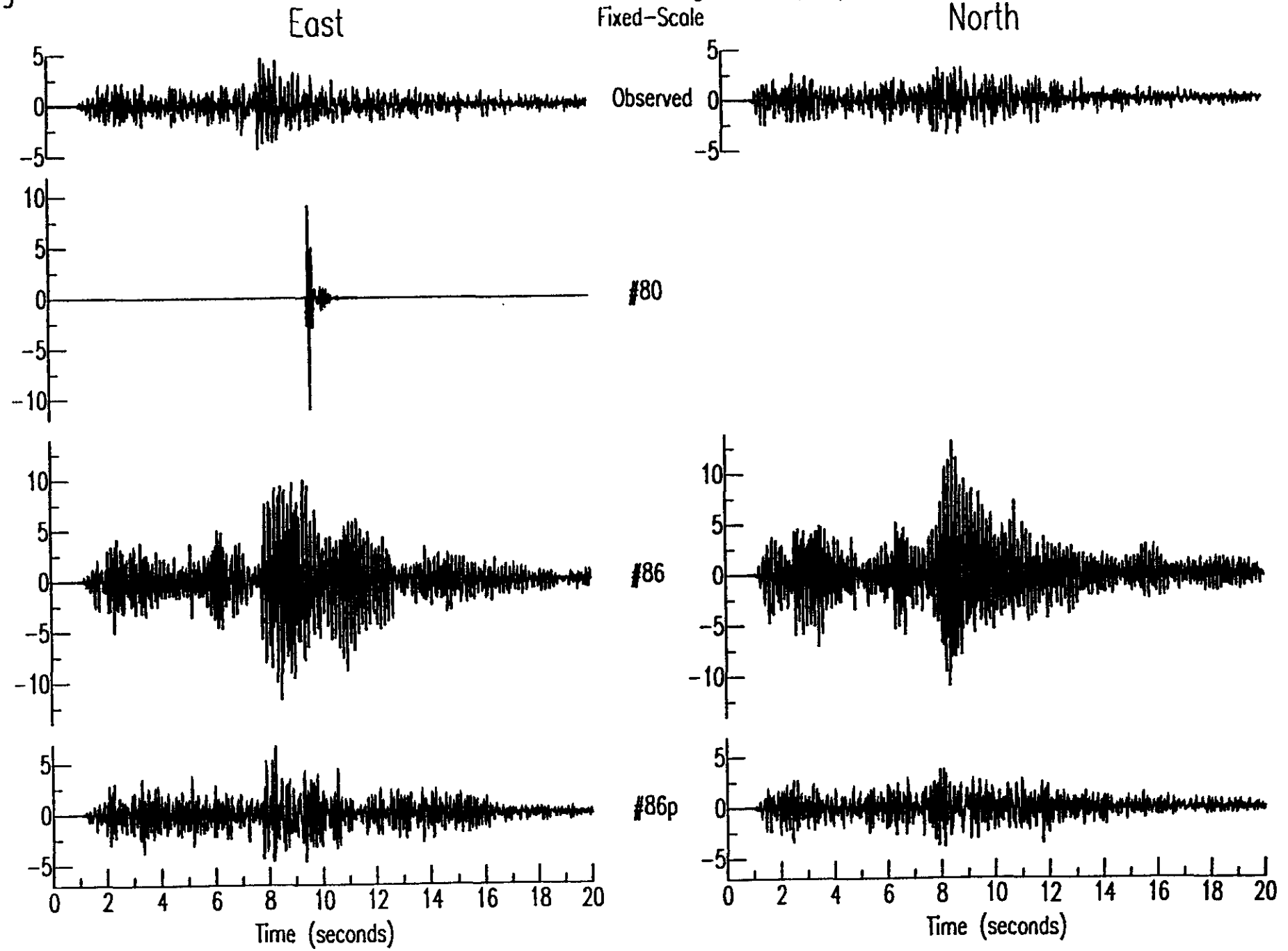

Figure D5f: Observed V1 vs Predicted V1 Accelerograms (uM/sec/sec x 100) based on D3

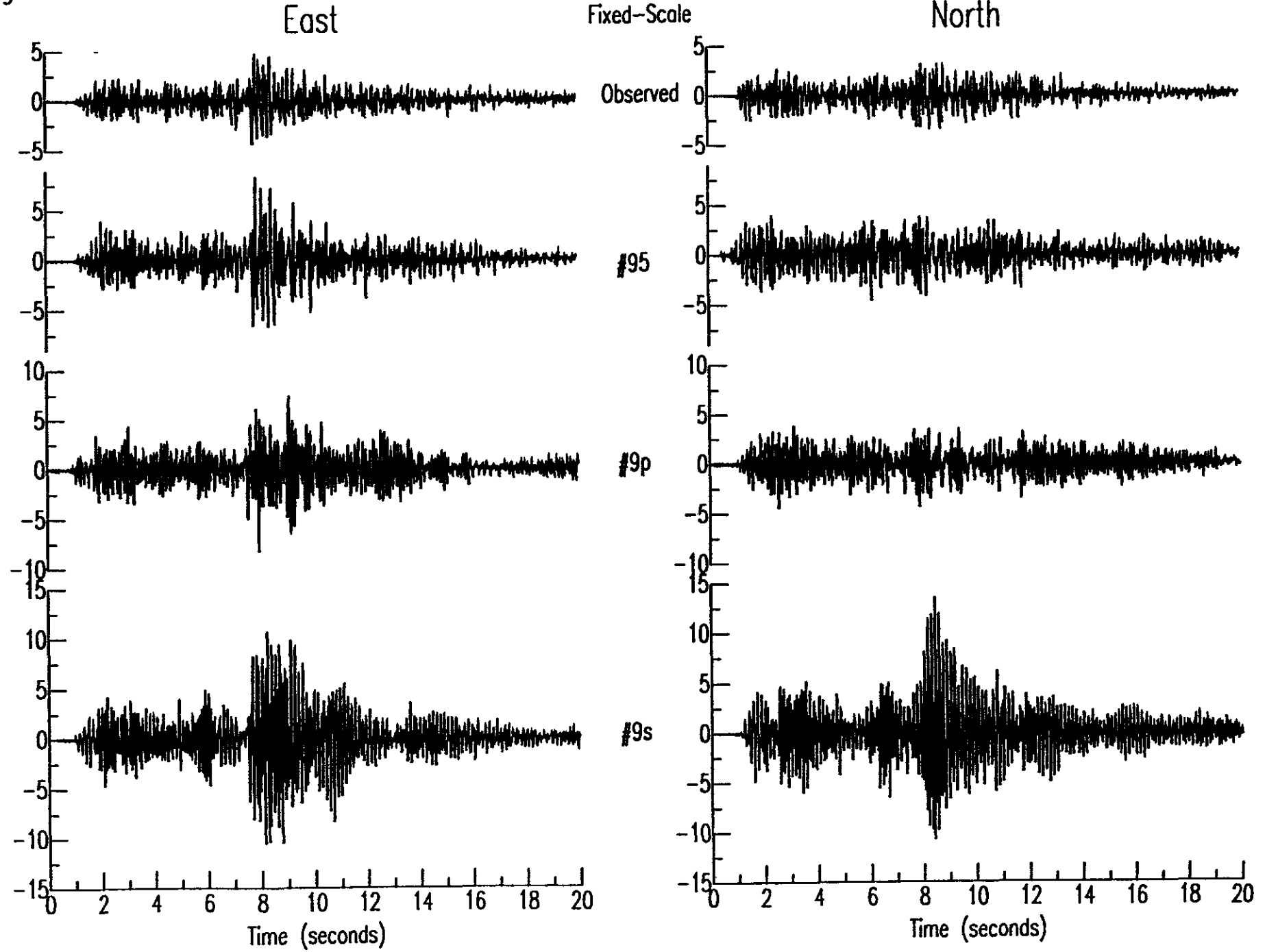

Figure D5g: Observed V1 vs Predicted V1 Accelerograms (uM/sec/sec x 100) based on D3

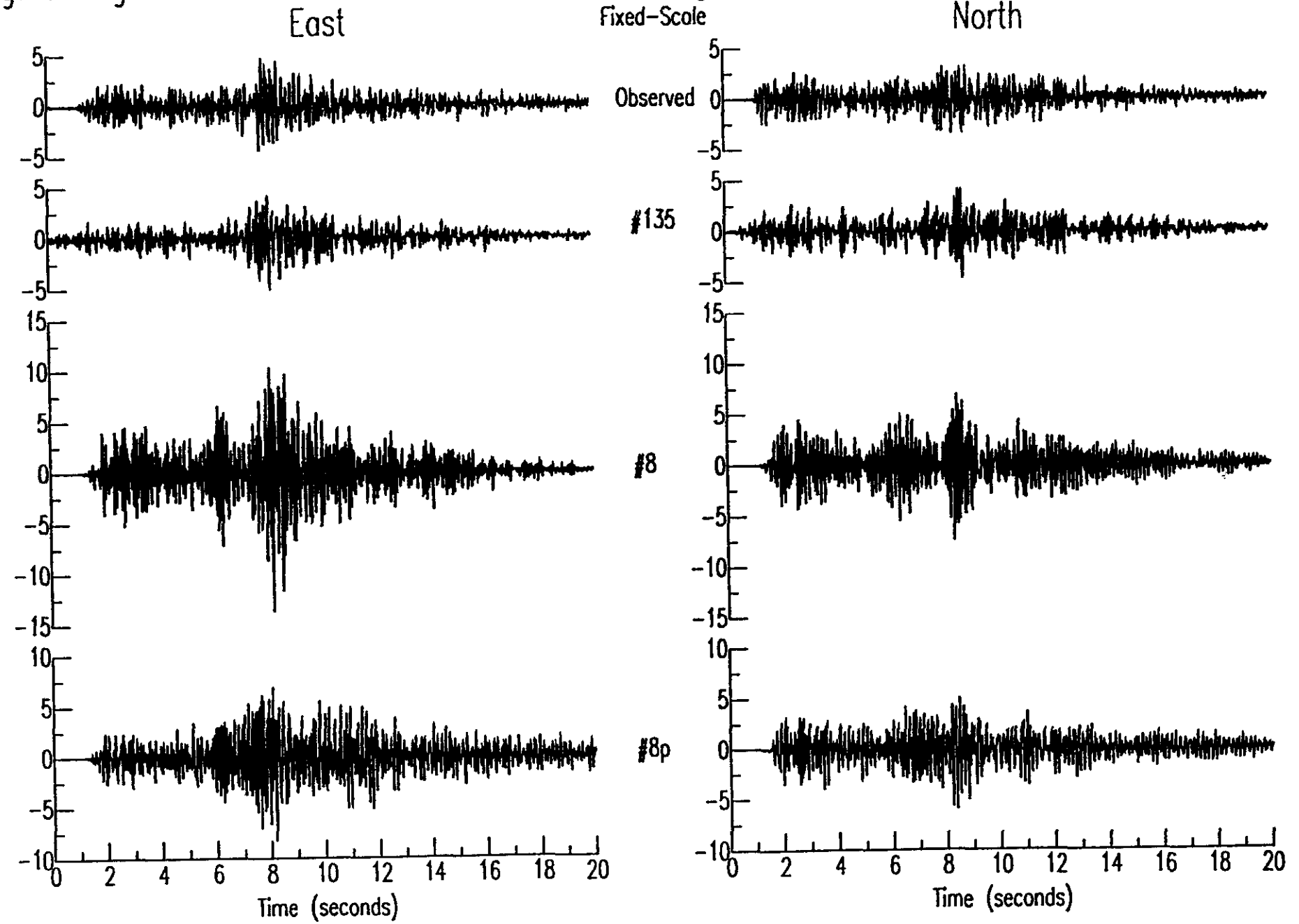

Figure D5h: Observed V1 vs Predicted V1 Accelerograms (uM/sec/sec x 100) based on D3

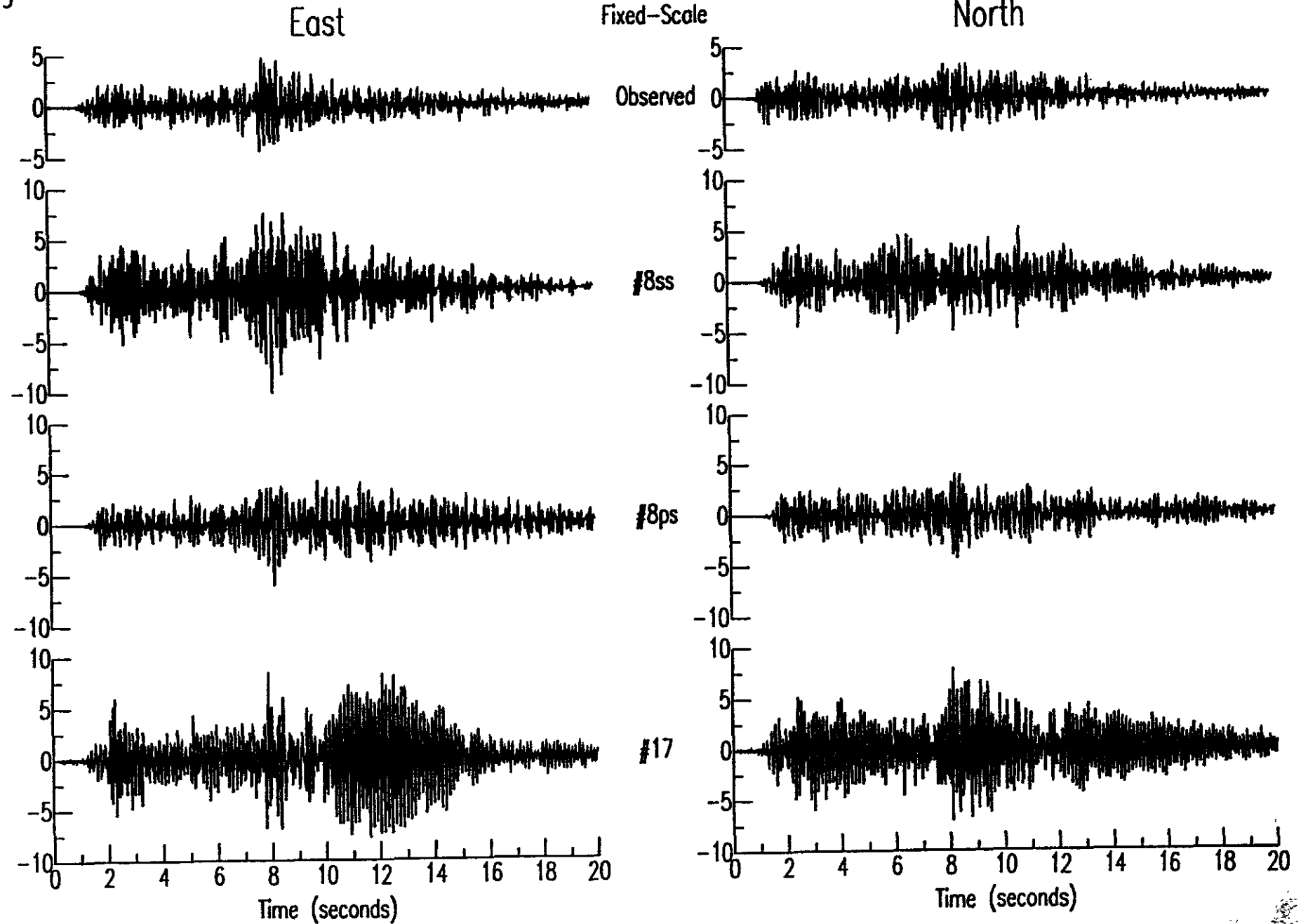

Appendix E

Plots from Analysis of Submitted R1 based Weak-motion Predictions using 1D techniques and the Standard Geotechnical Model

Figure E1a: Standard Fourier Spectral Ratio Plot:
Spectral Ratio V2/R1 for 1D Standard Geotechnical Models

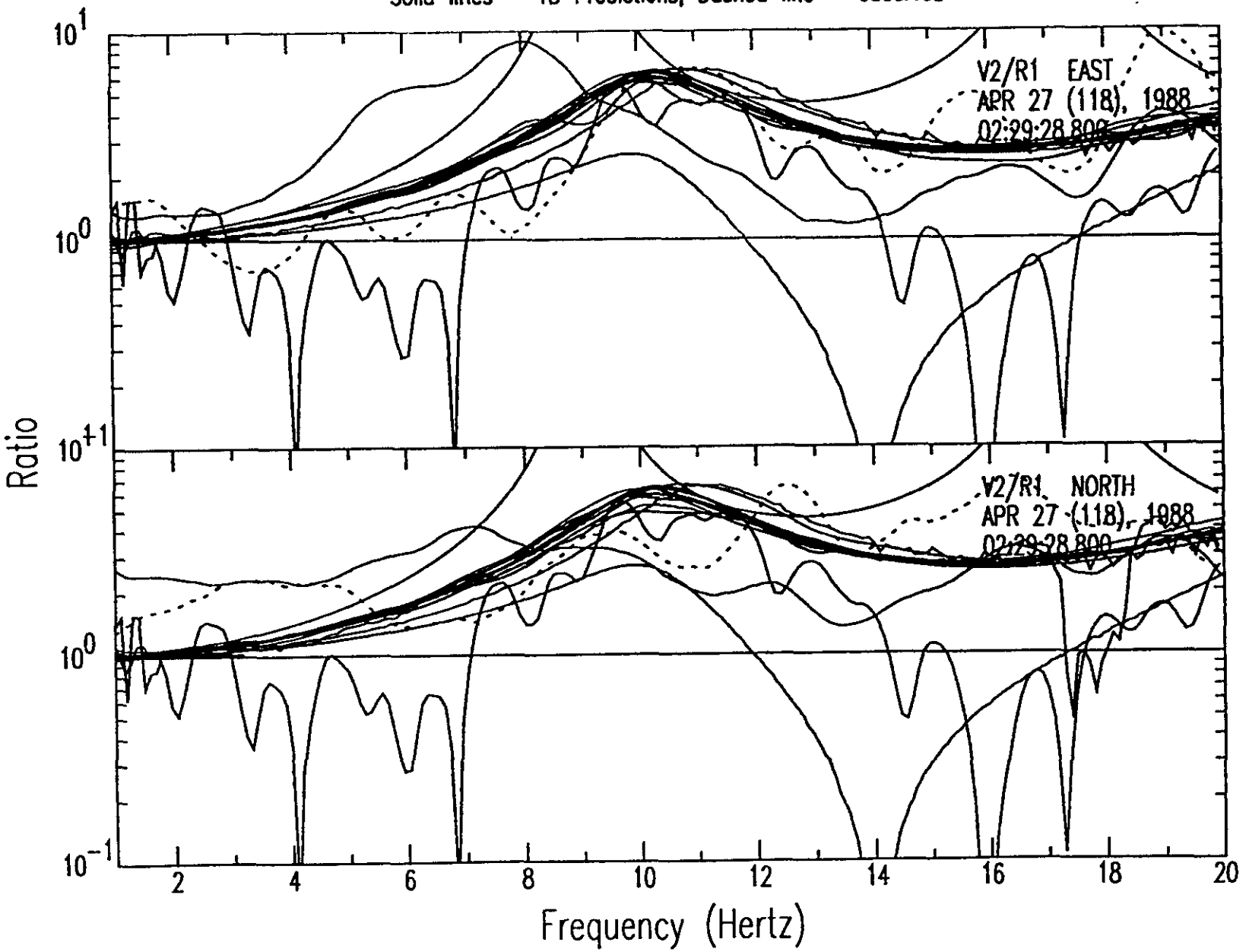

Figure E1b: Standard Fourier Spectral Ratio Plot:
Spectral Ratio V1/R1 for 1D Standard Geotechnical Models

Solid lines – 1D Predictions; Dashed line – Observed

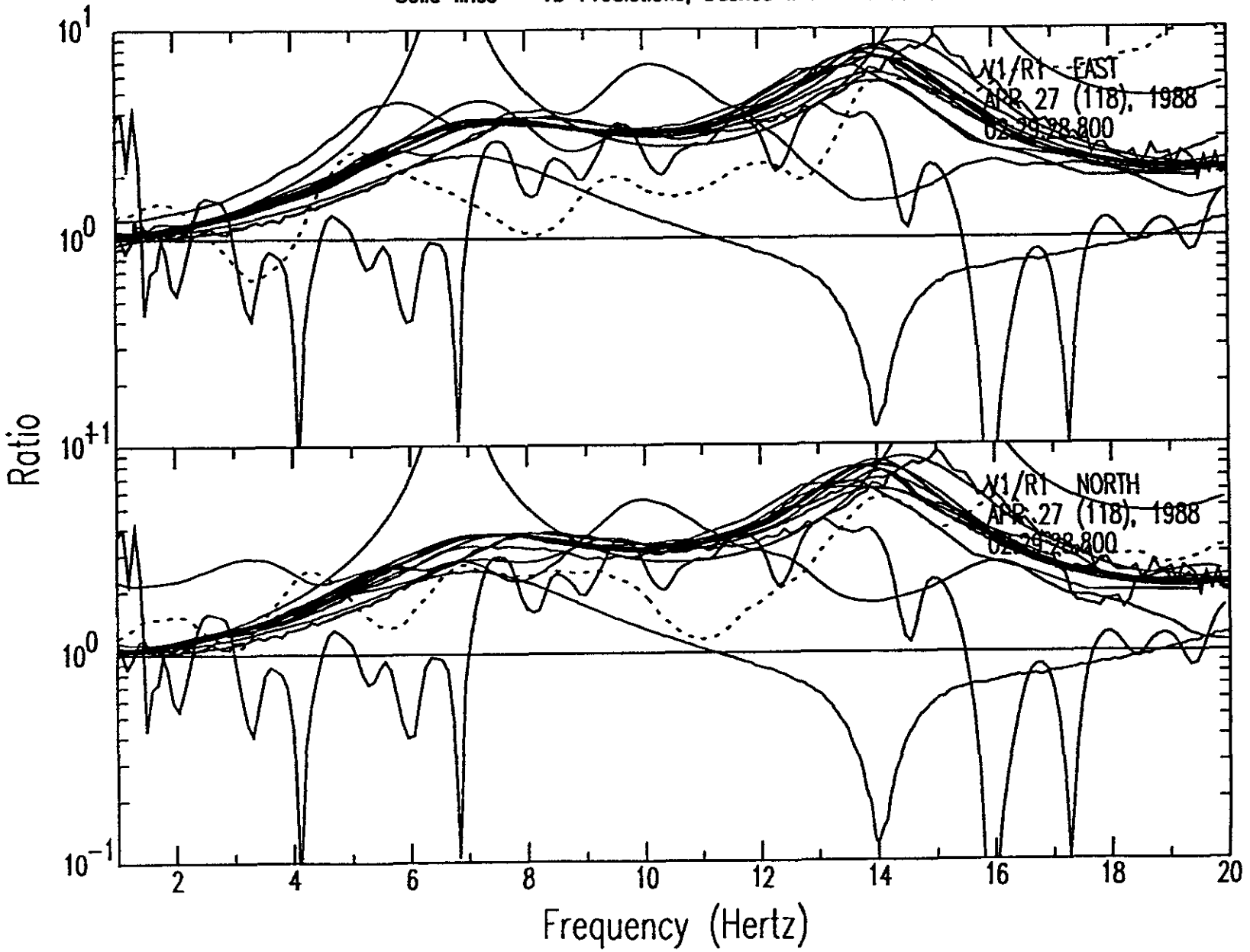

Figure E1c: Standard Fourier Spectral Ratio Plot:
Spectral Ratio D2/R1 for 1D Standard Geotechnical Models

Solid lines – 1D Predictions; Dashed line – Observed

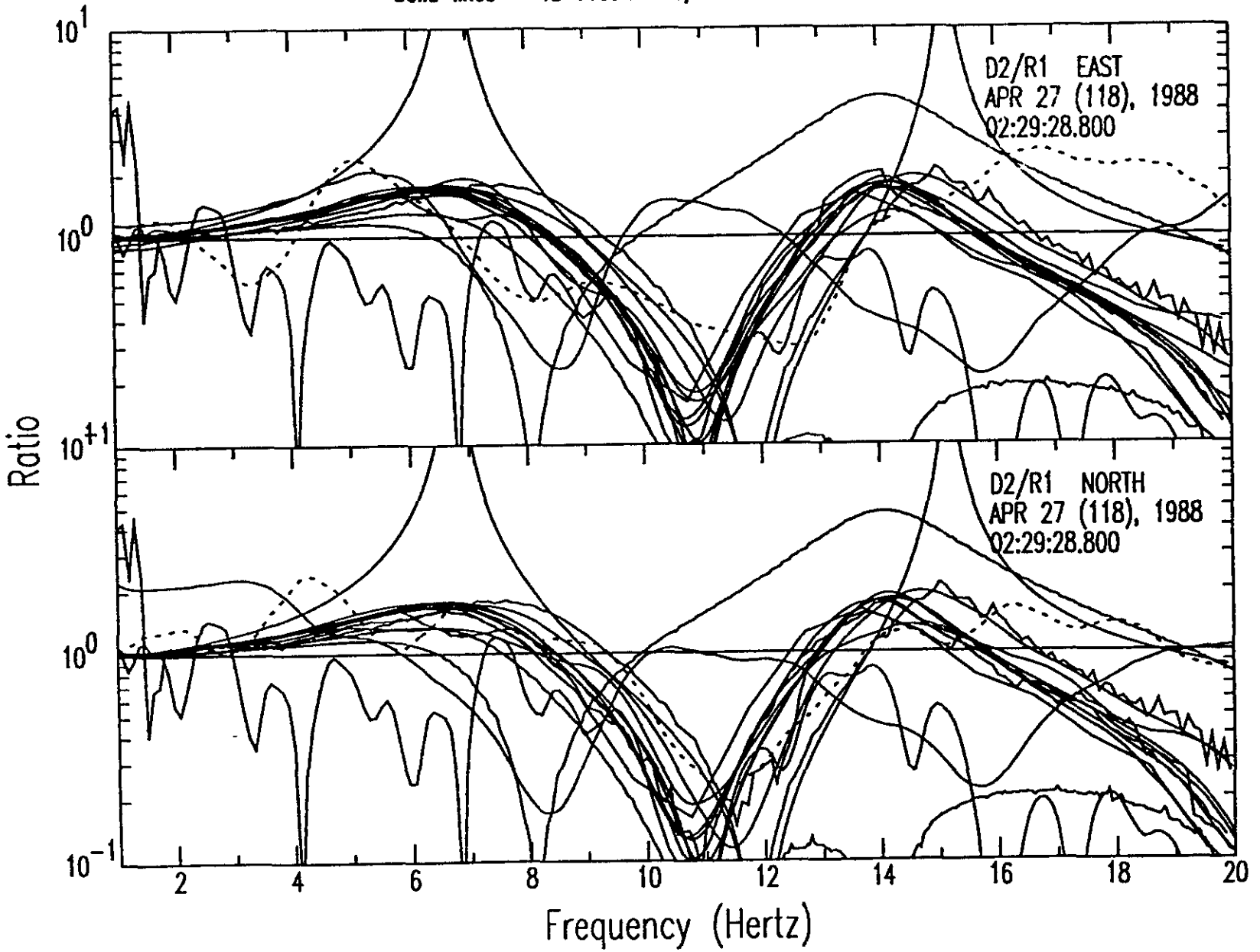

Figure E1d: Standard Fourier Spectral Ratio Plot:
Spectral Ratio D3/R1 for 1D Standard Geotechnical Models

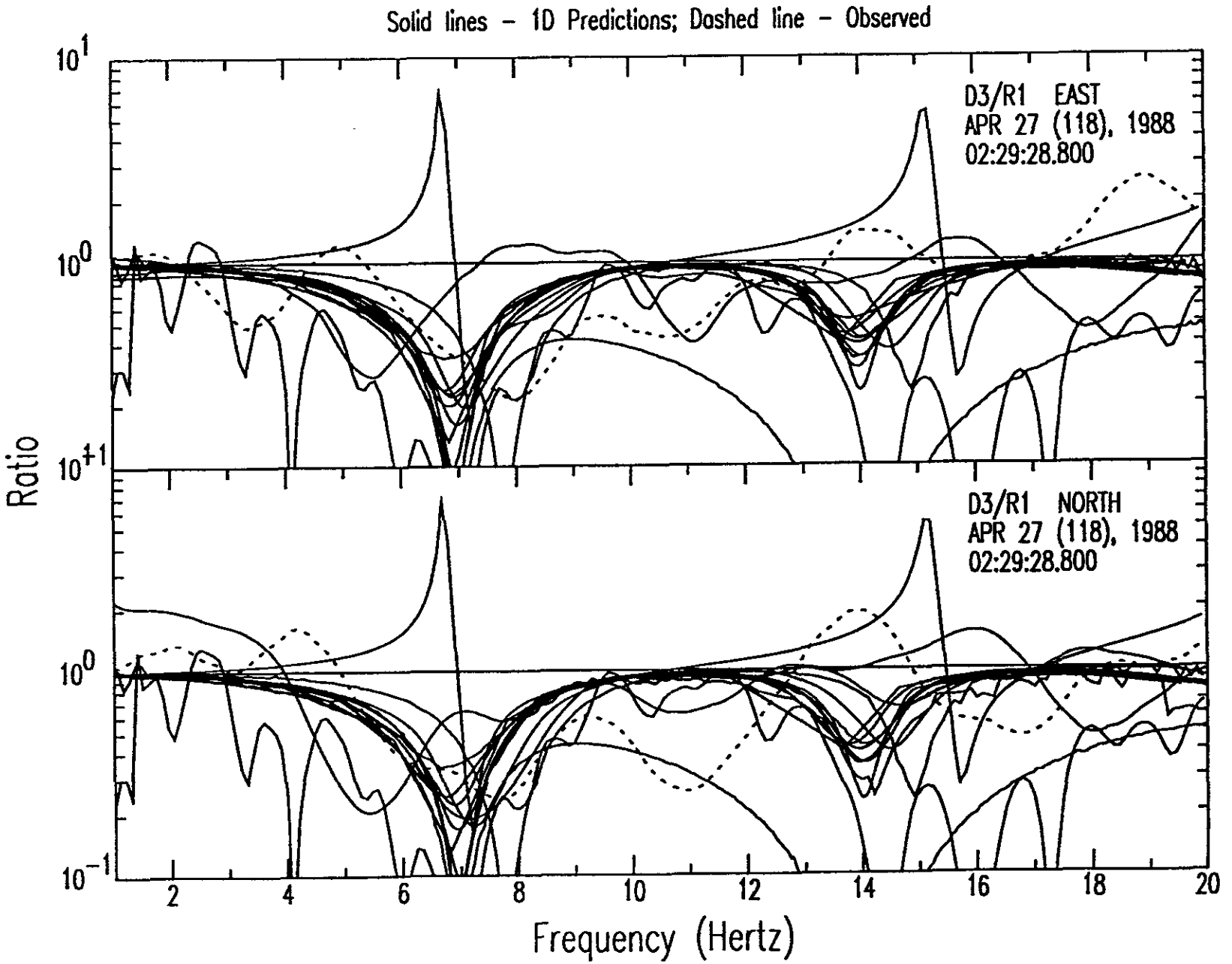

Figure E1e: Standard Fourier Spectral Ratio Plot:
Spectral Ratio D1/R1 for 1D Standard Geotechnical Models

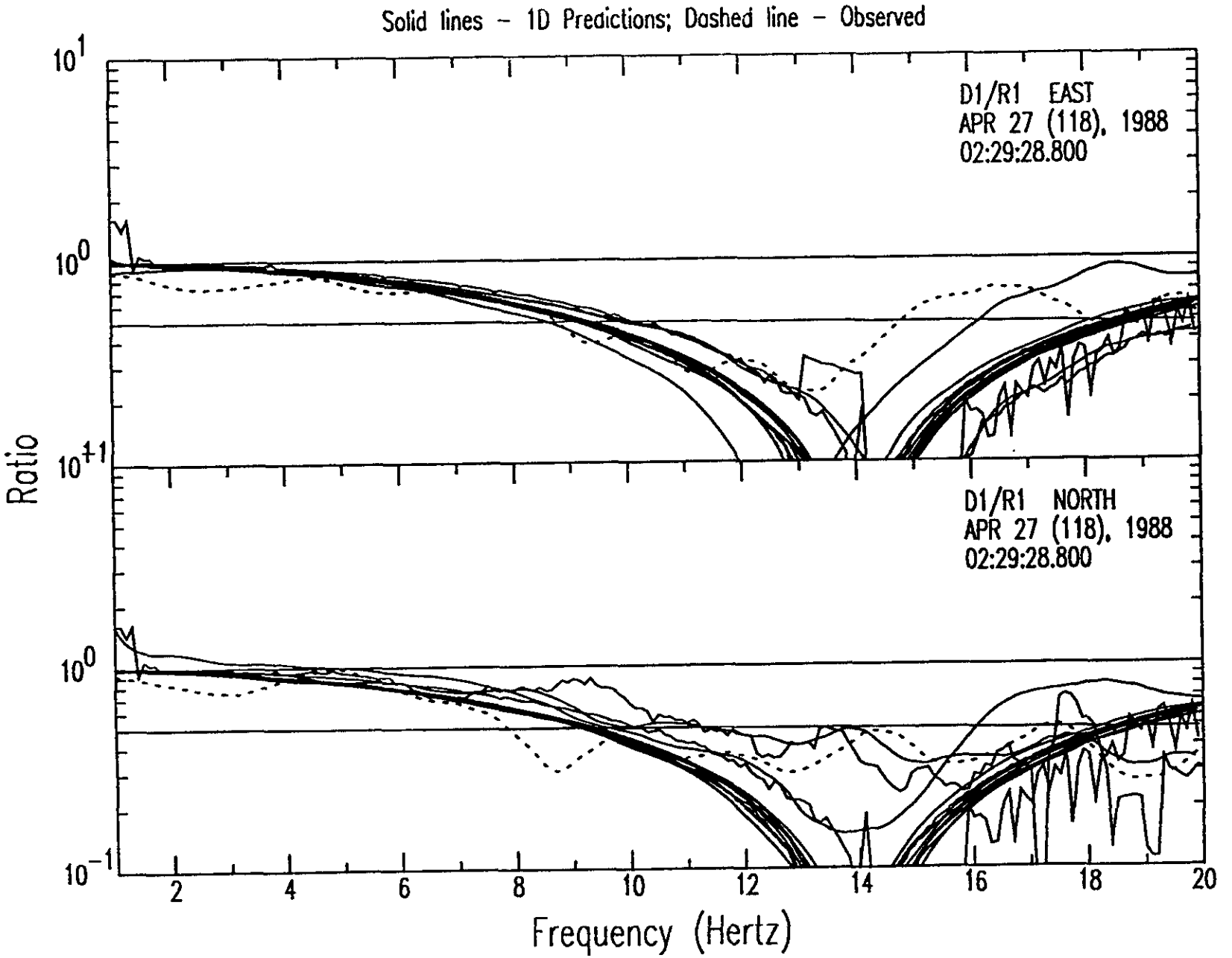

Figure E1f: Standard Fourier Spectral Ratio Plot:
Spectral Ratio R2/R1 for 1D Standard Geotechnical Models

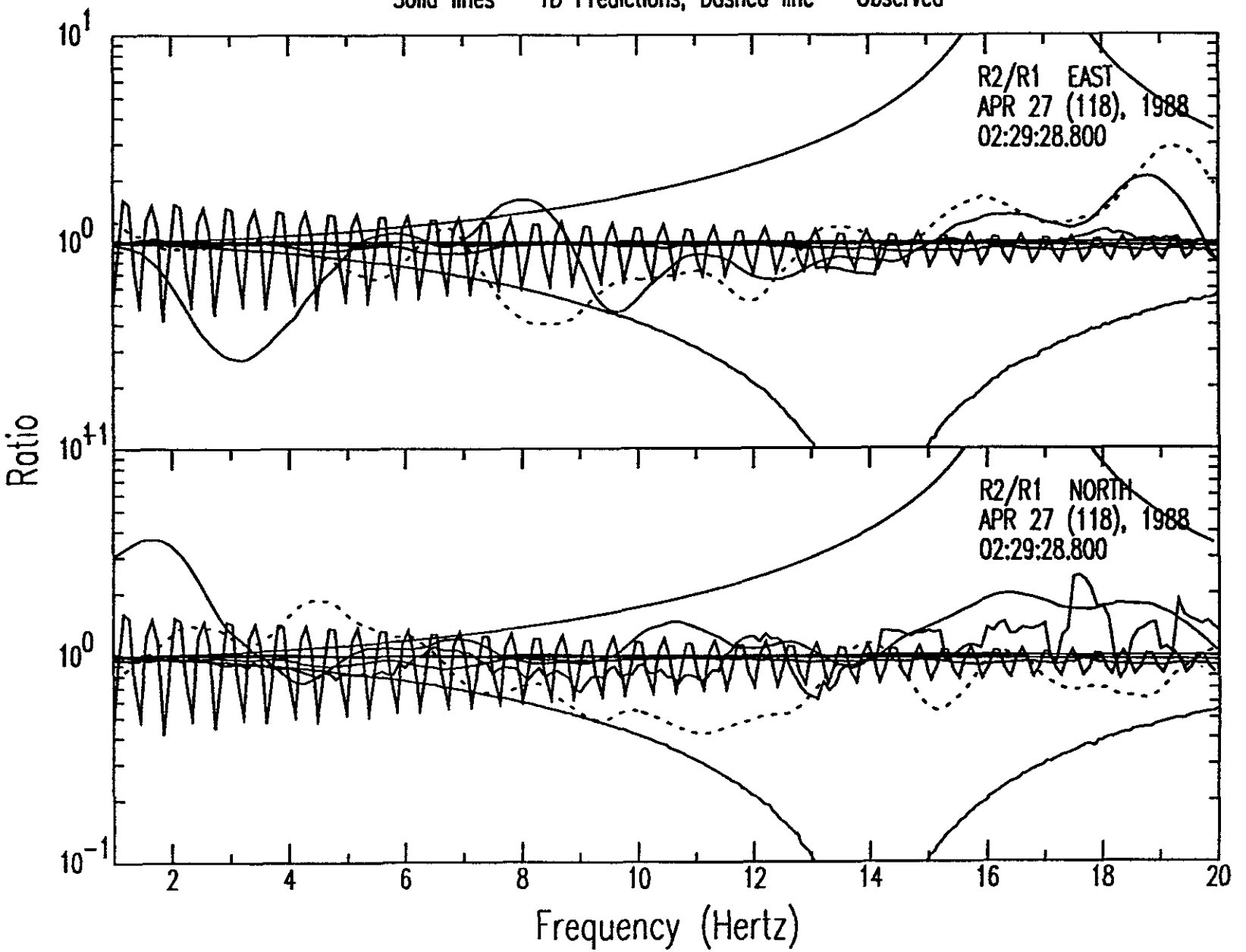

Figure E2a: 1D Standard Model Spectral Ratio Prediction Quartiles vs Observations

Spectral Ratio Predictions: Dashed – quartiles

Observations: Solid – weak-motion test event; Dash-dotted – weak-motion mean; Dotted – 1 std deviation

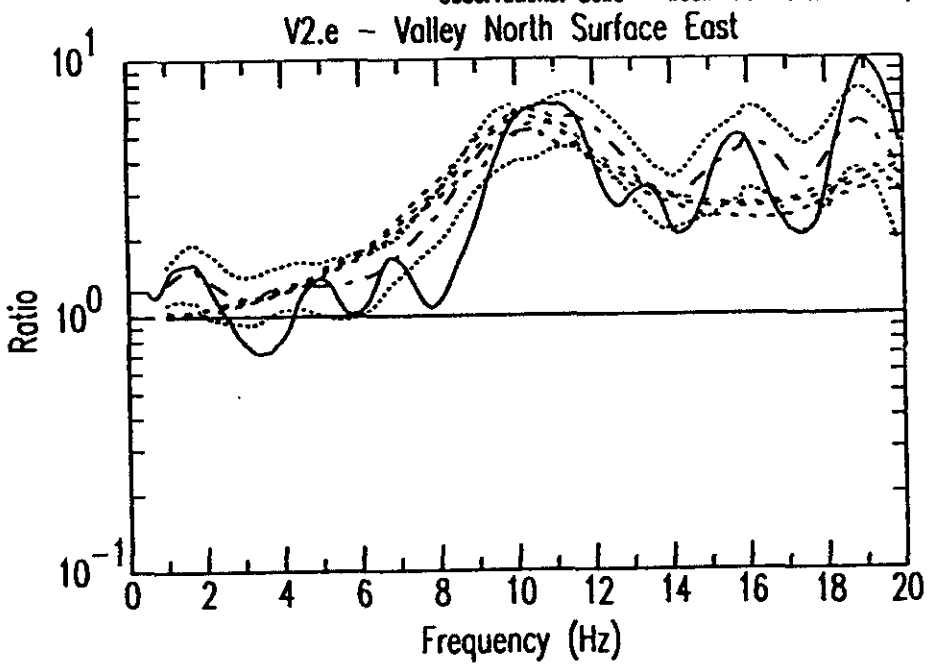

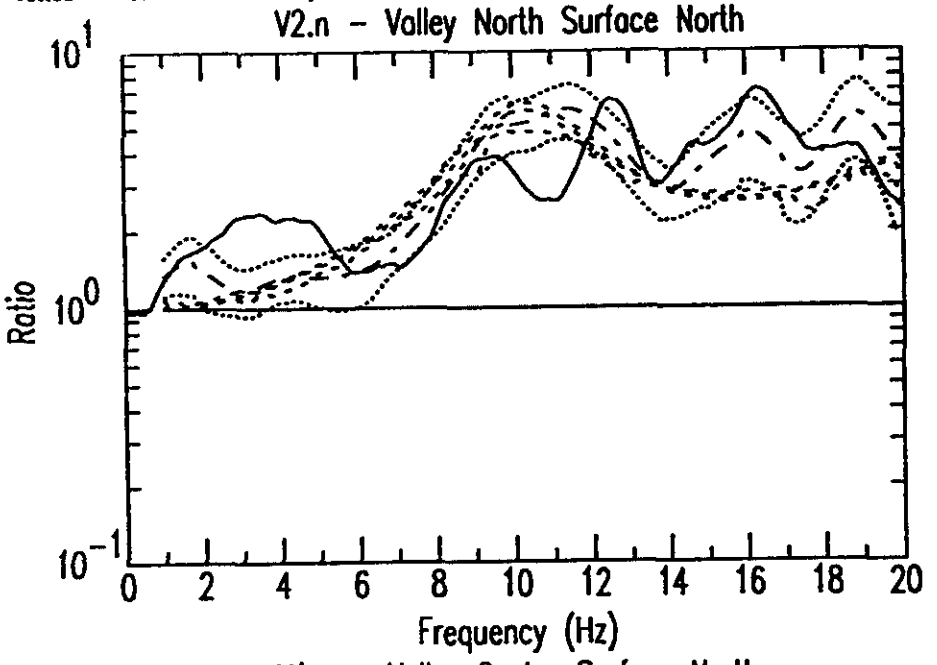

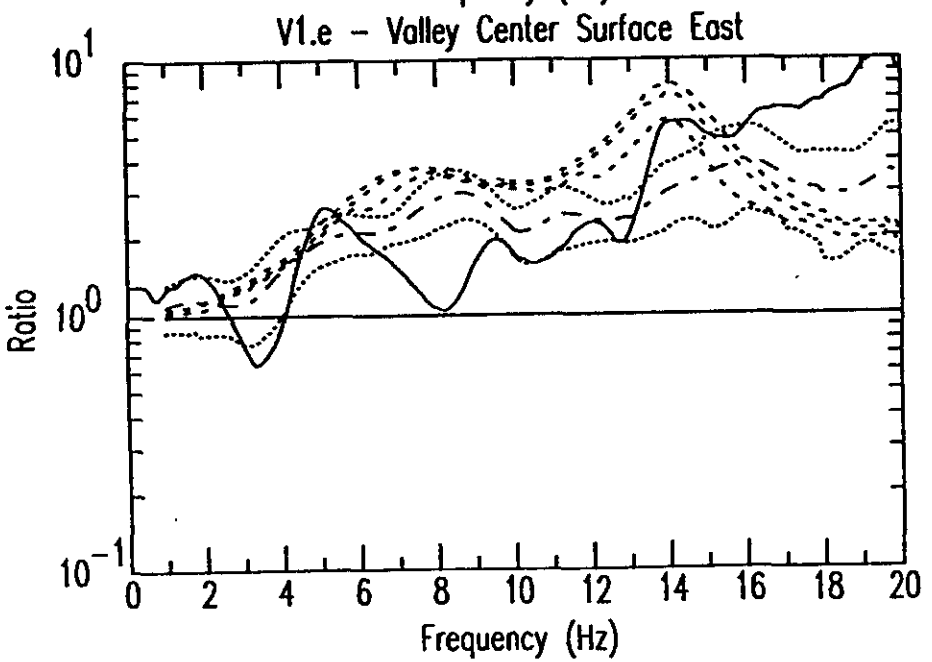

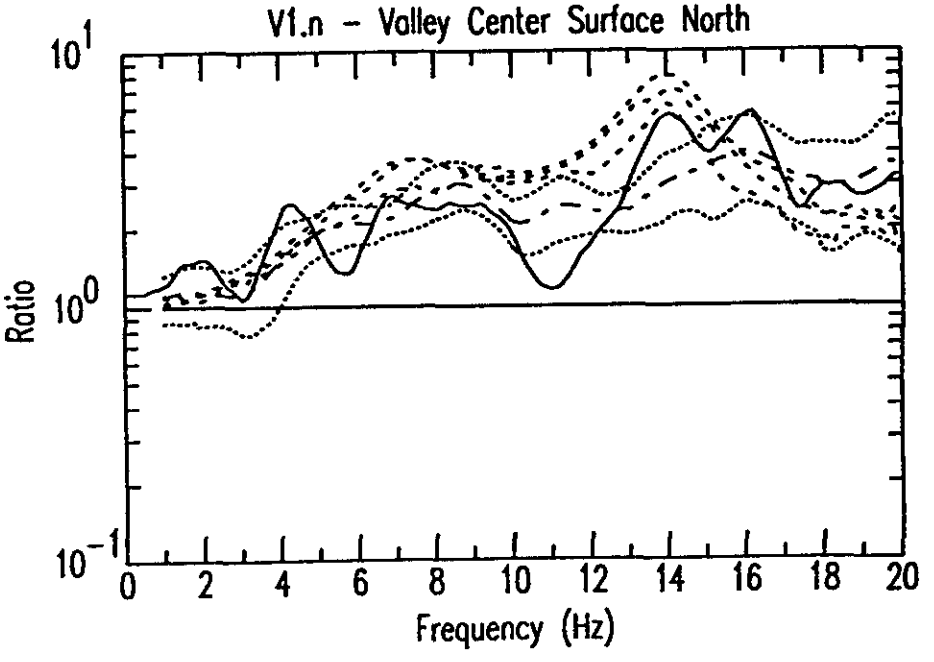

Figure E2b: 1D Standard Model Spectral Ratio Prediction Quartiles vs Observations

Spectral Ratio Predictions: Dashed – quartiles

Observations: Solid – weak-motion test event; Dash-dotted – weak-motion mean; Dotted – 1 std deviation

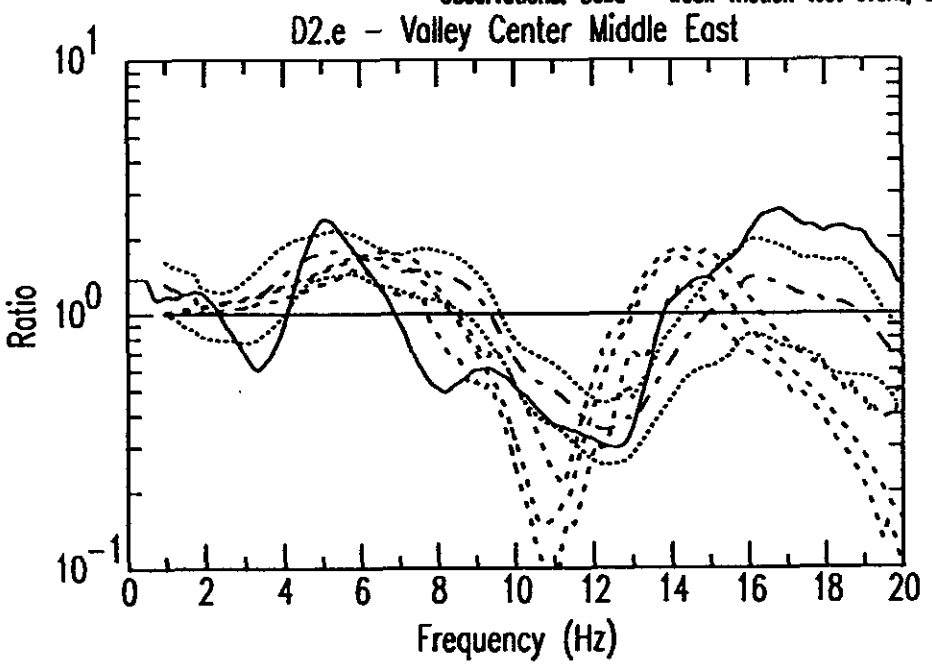

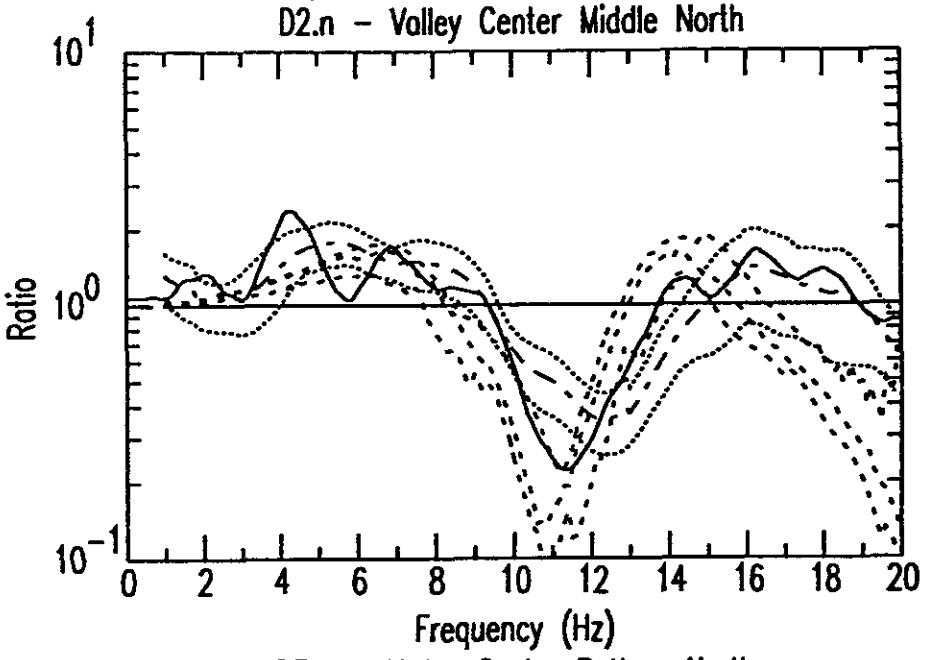

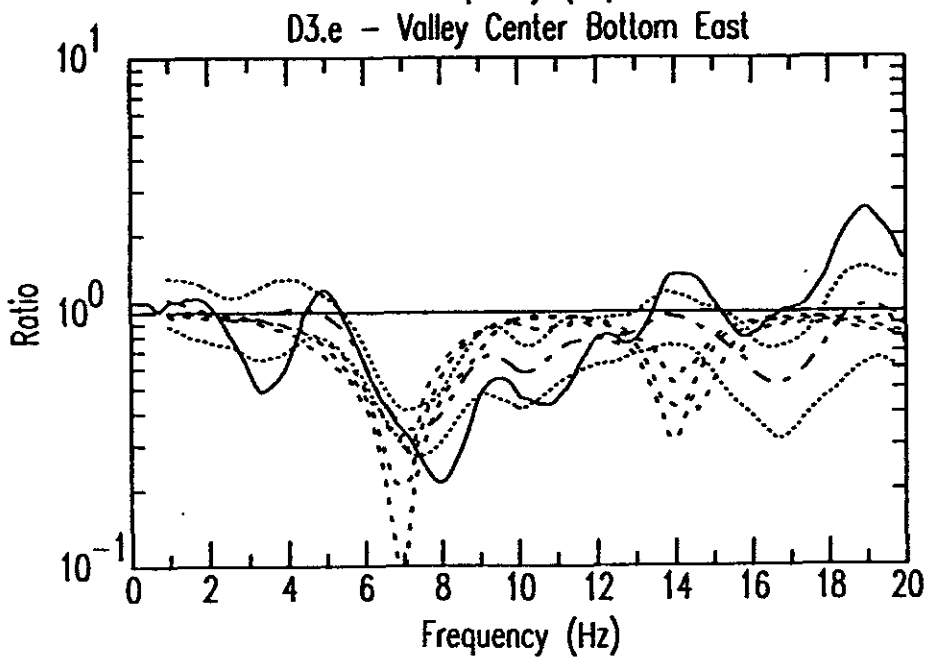

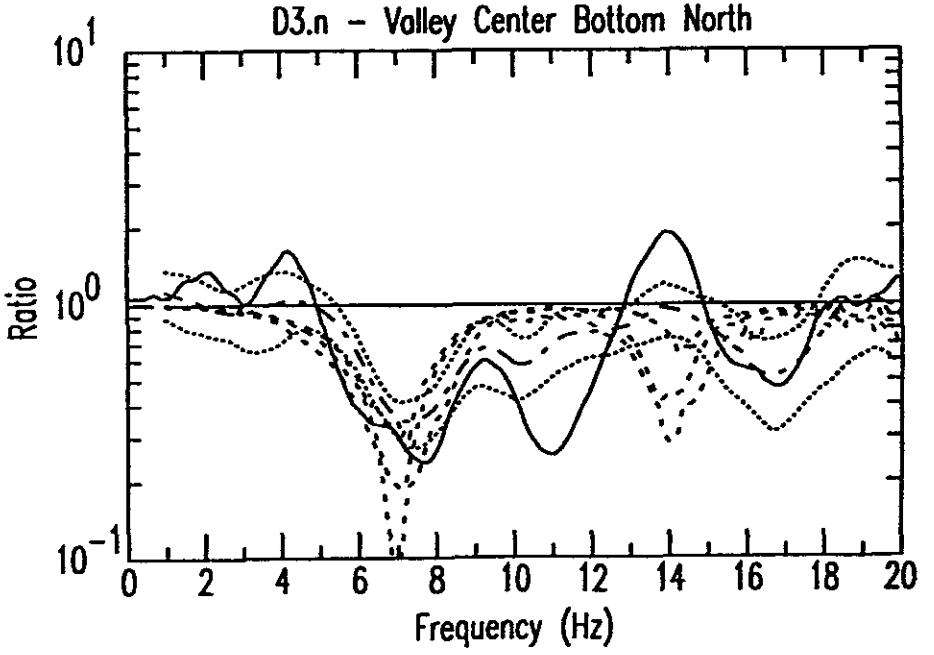

Figure E2c: 1D Standard Model Spectral Ratio Prediction Quartiles vs Observations

Spectral Ratio Predictions: Dashed – quartiles

Observations: Solid – weak-motion test event; Dash-dotted – weak-motion mean; Dotted – 1 std deviation

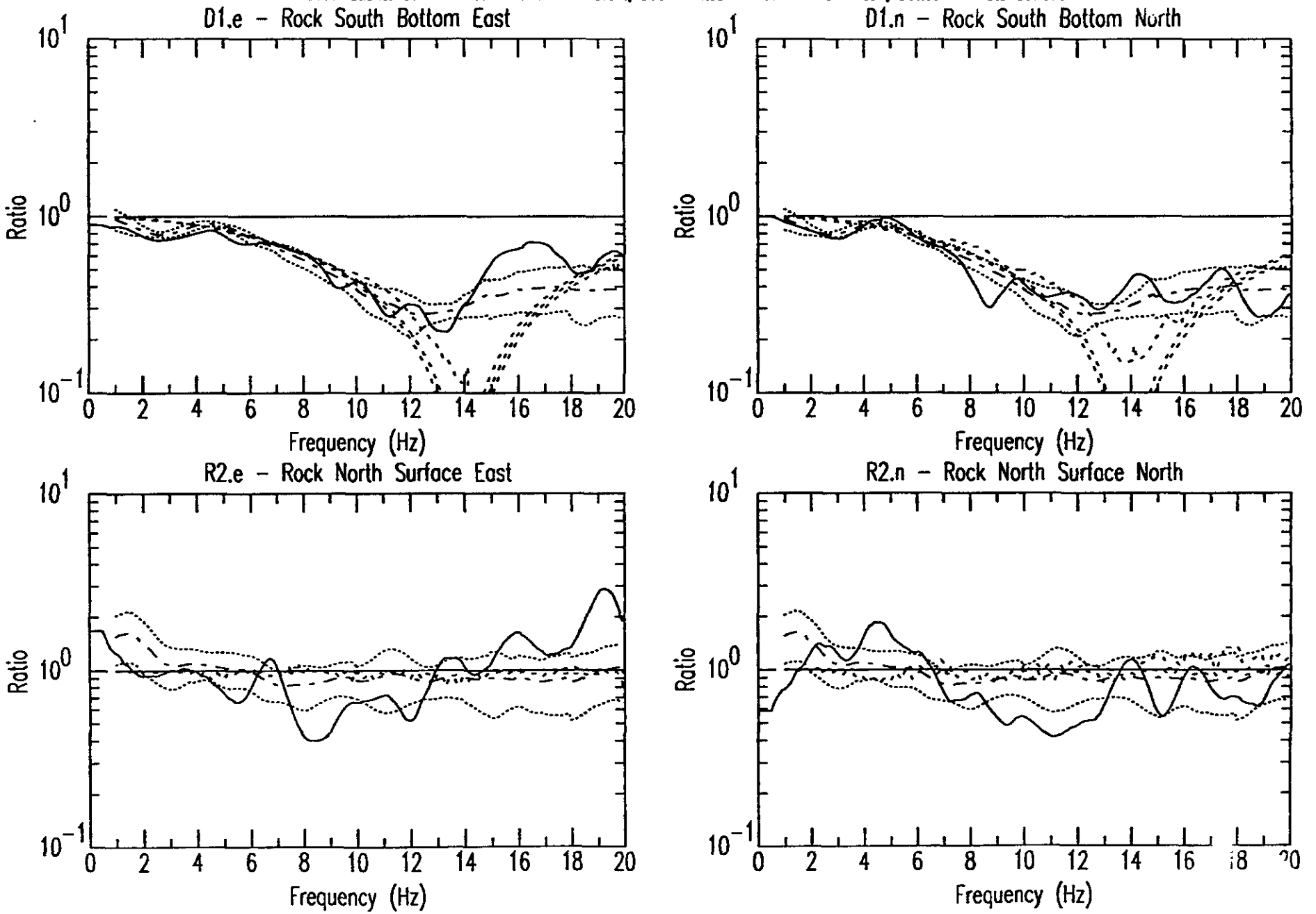

Figure E3a: Standard Response Spectra:

Station V2 Valley North Surface 1D Standard Geotechnical Models

Solid lines - 1D Predictions; Dashed line - Observed

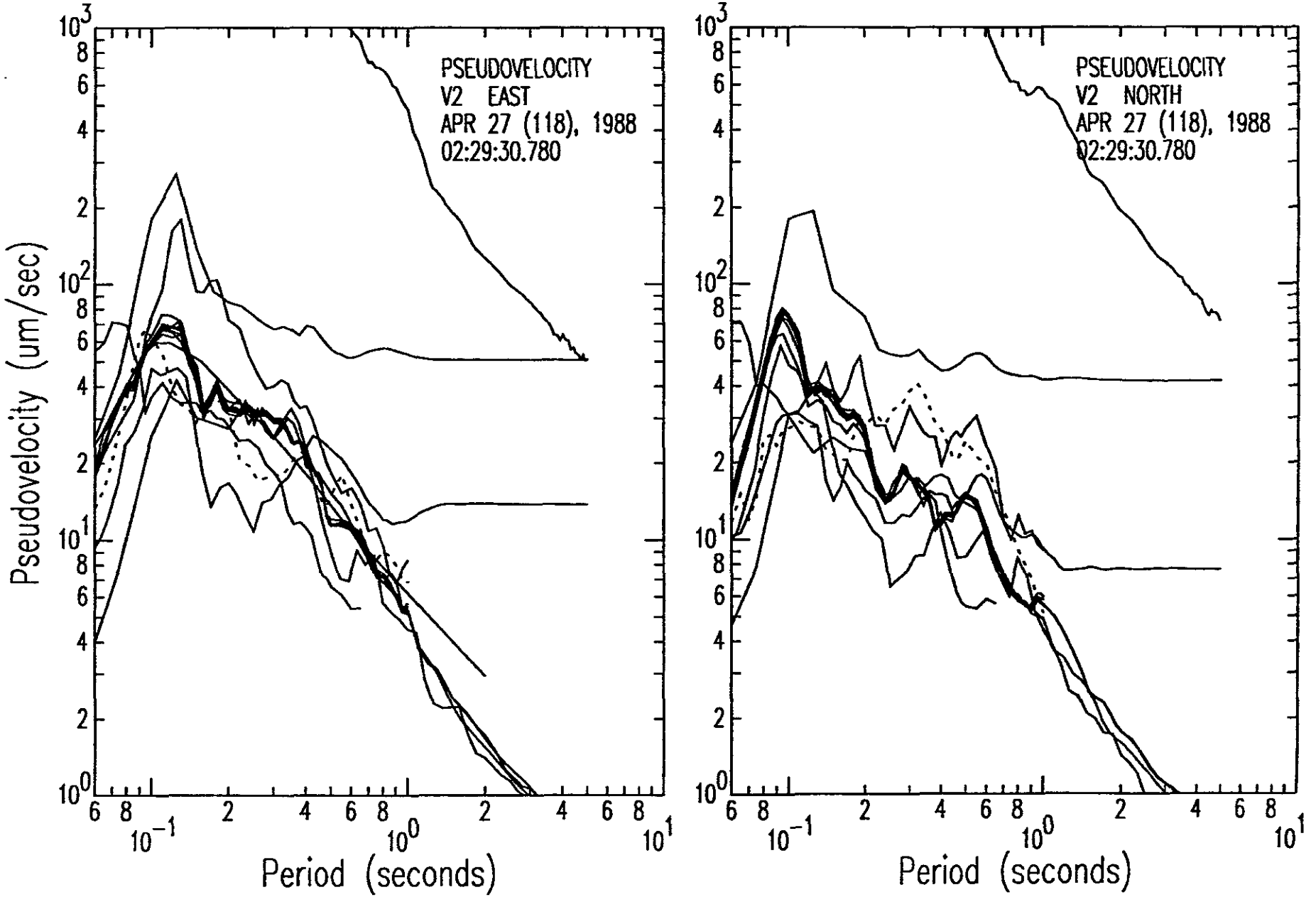

Figure E3b: Standard Response Spectra:
Station V1 Valley Center Surface 1D Standard Geotechnical Models
Solid lines - 1D Predictions; Dashed line - Observed

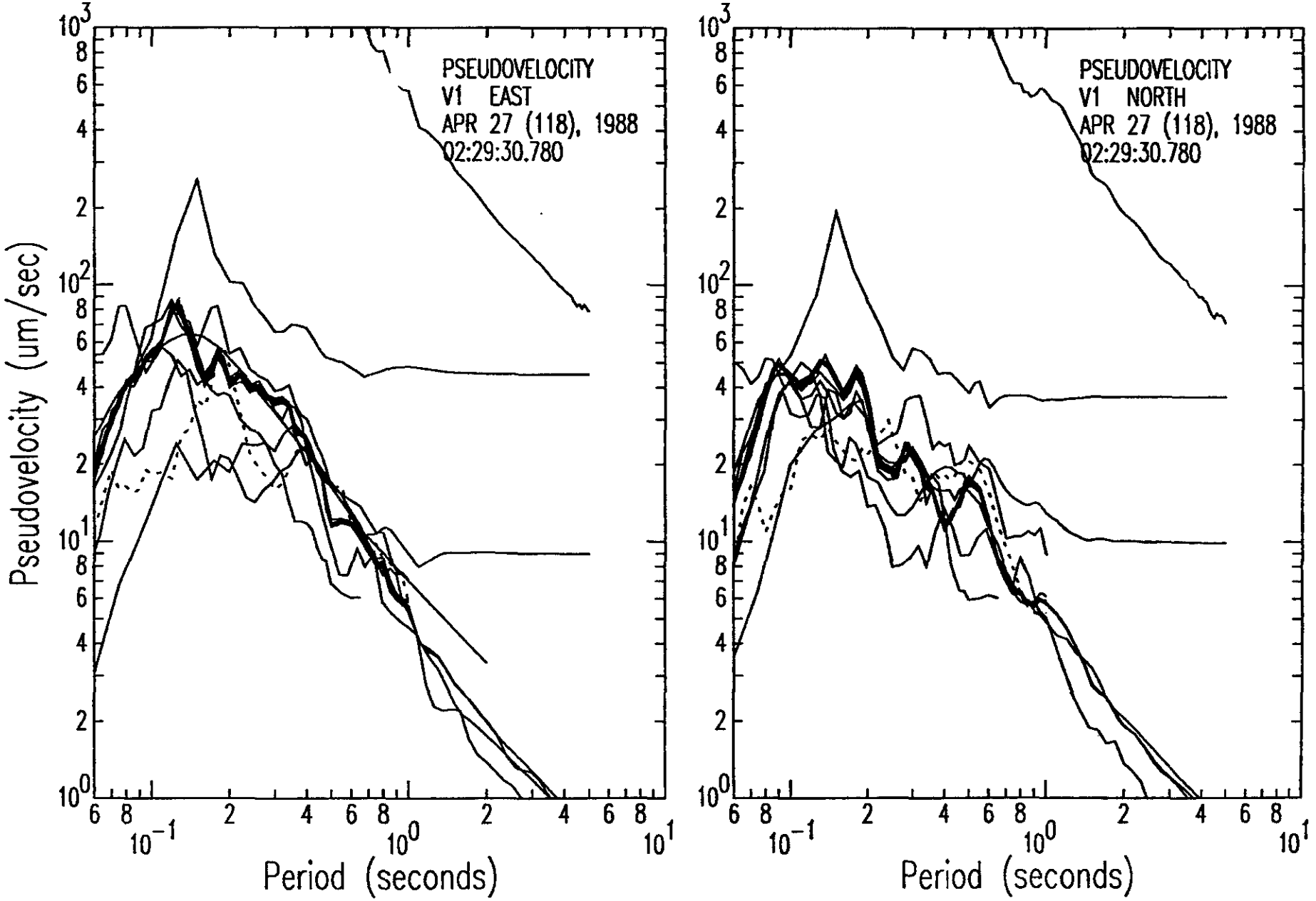

Figure E3c: Standard Response Spectra:
Station D2 Valley Center Middle 1D Standard Geotechnical Models
Solid lines - 1D Predictions; Dashed line - Observed

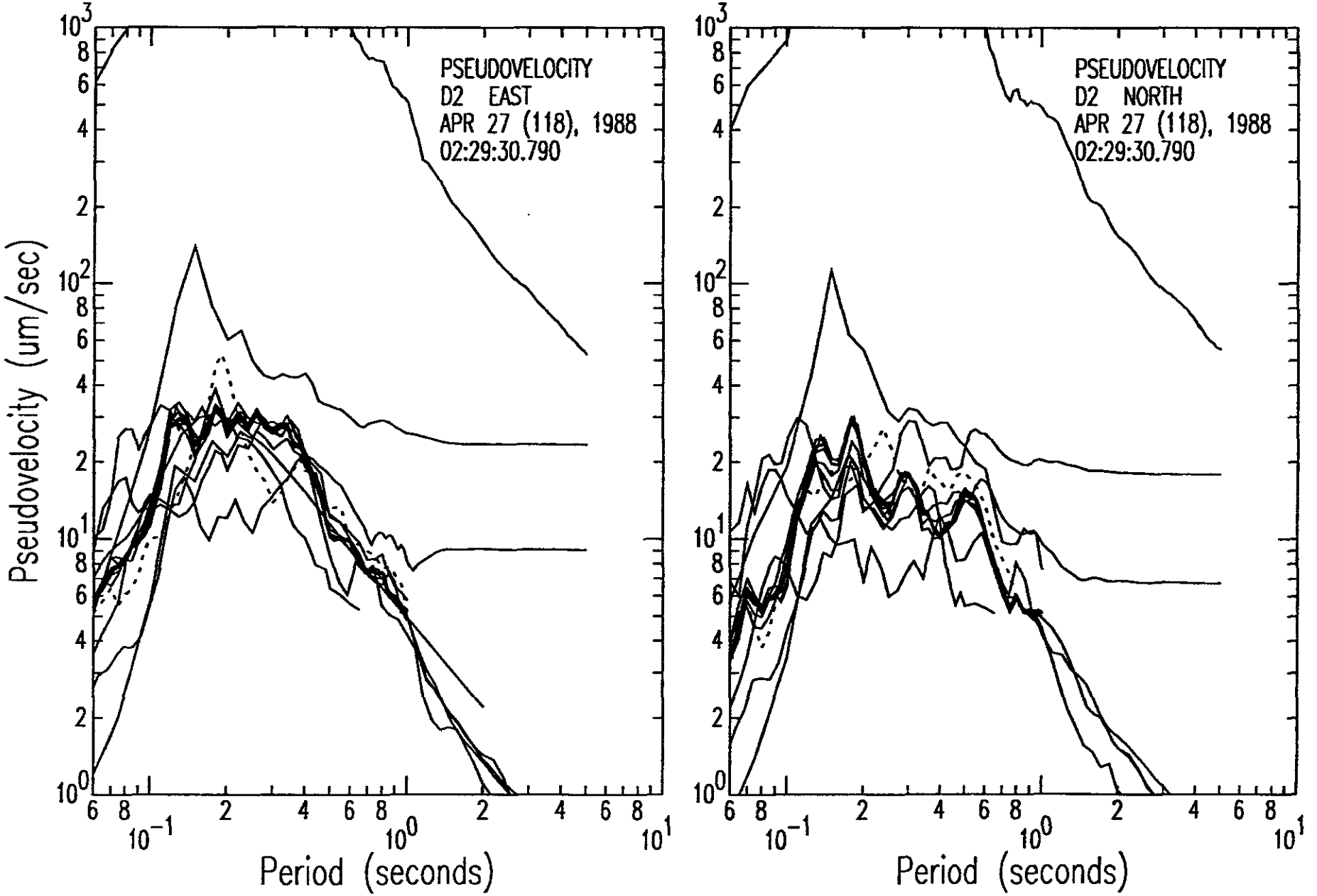

Figure E3d: Standard Response Spectra:
Station D3 Valley Center Bottom 1D Standard Geotechnical Models
Solid lines - 1D Predictions; Dashed line - Observed

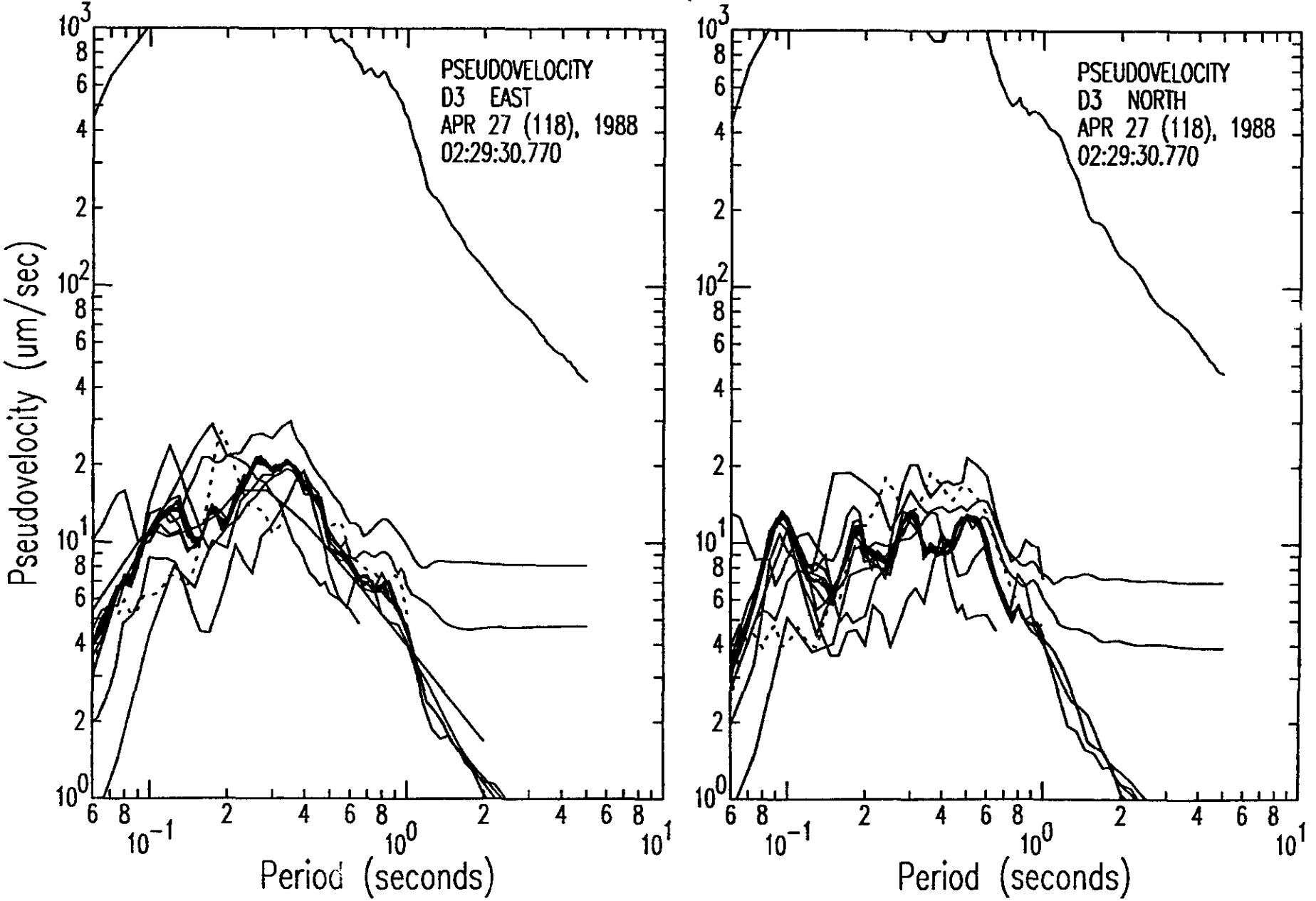

Figure E3e: Standard Response Spectra:
Station D1 Rock South Bottom 1D Standard Geotechnical Models
Solid lines – 1D Predictions; Dashed line – Observed

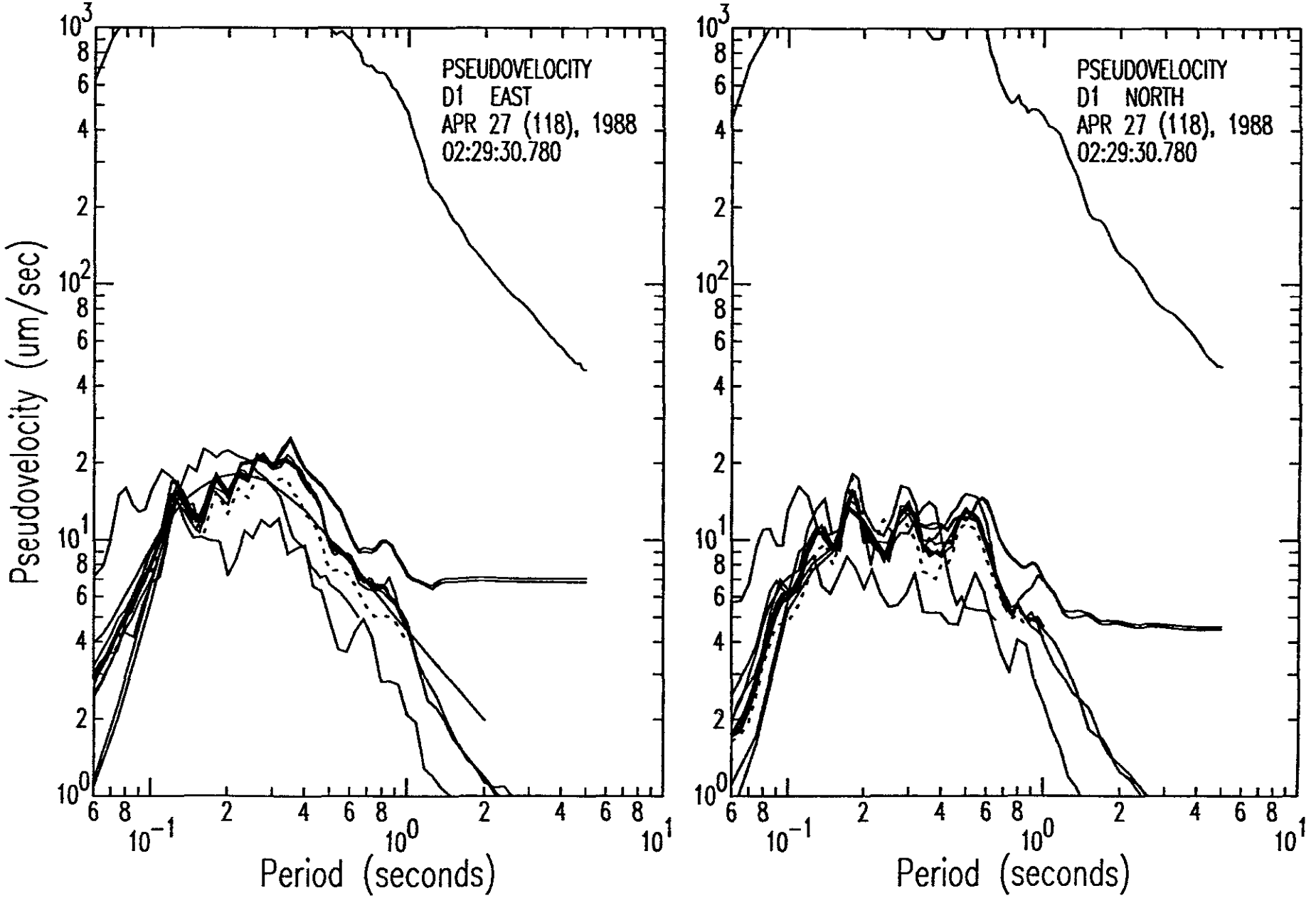

Figure E3f: Standard Response Spectra:
Station R2 Rock North Surface 1D Standard Geotechnical Models
Solid lines – 1D Predictions; Dashed line – Observed

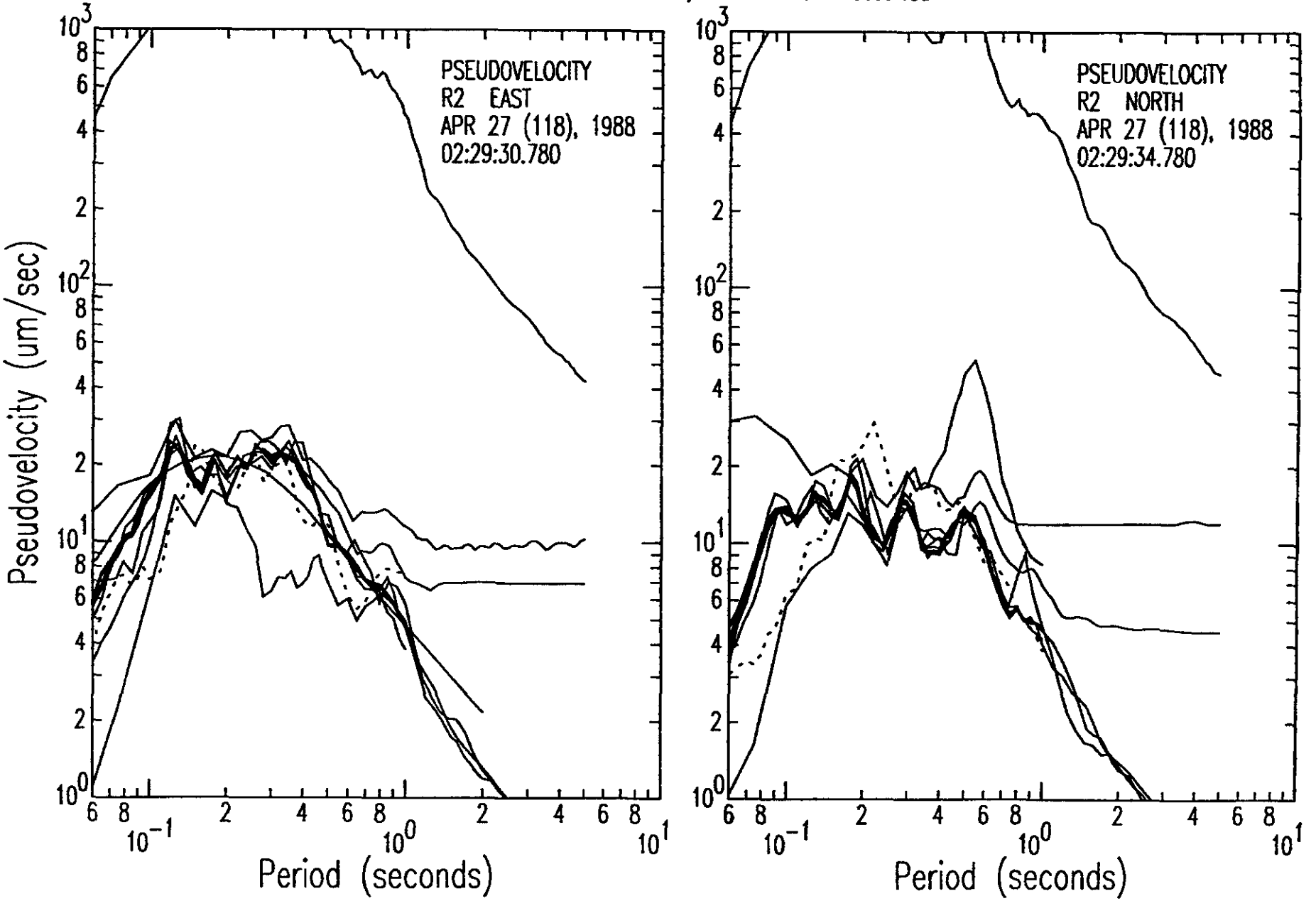

Figure E4a: 1D Standard Model Response Spectra Prediction Quartiles vs Observations

Response Spectra Predictions: Dashed – quartiles

Observations: Solid – weak-motion test event

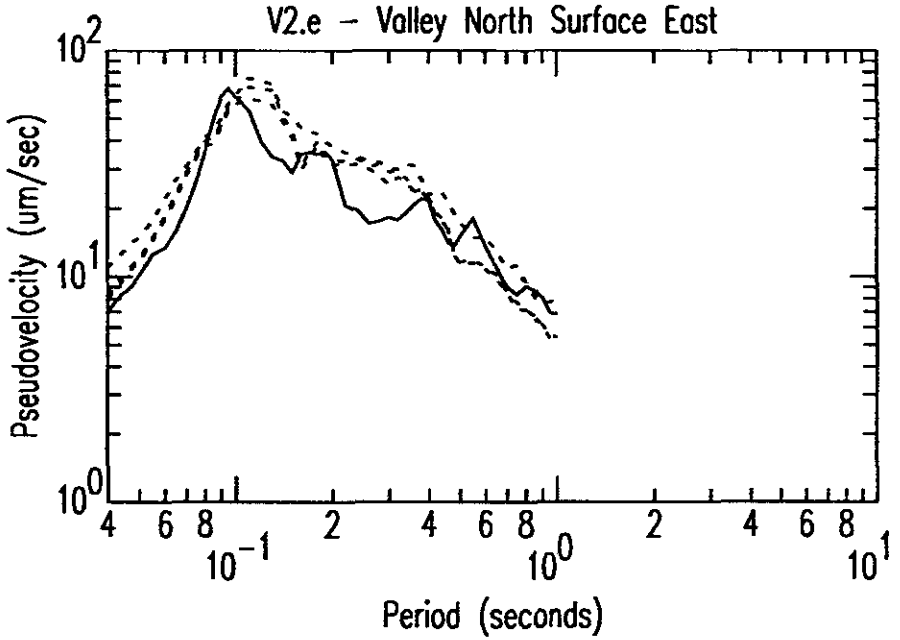

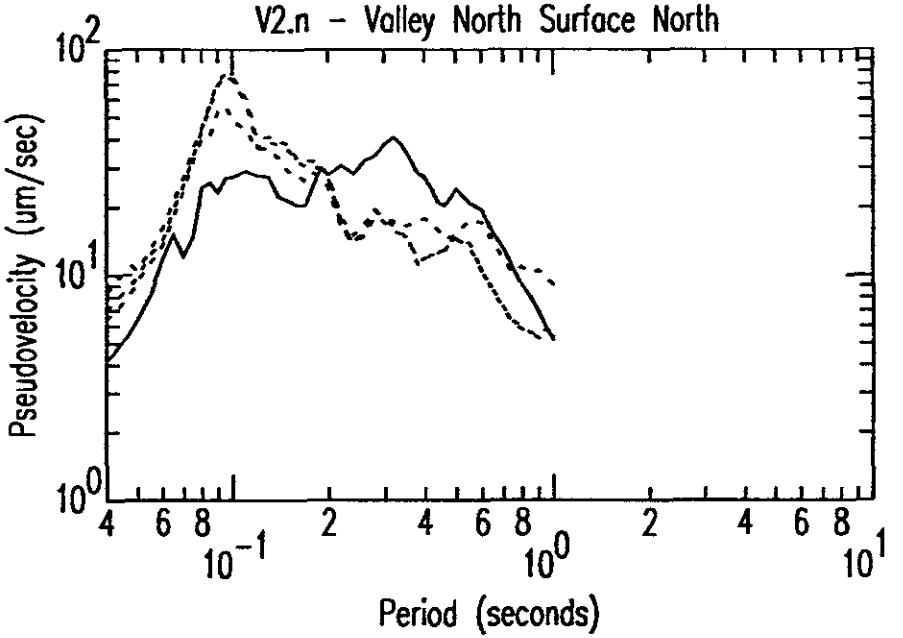

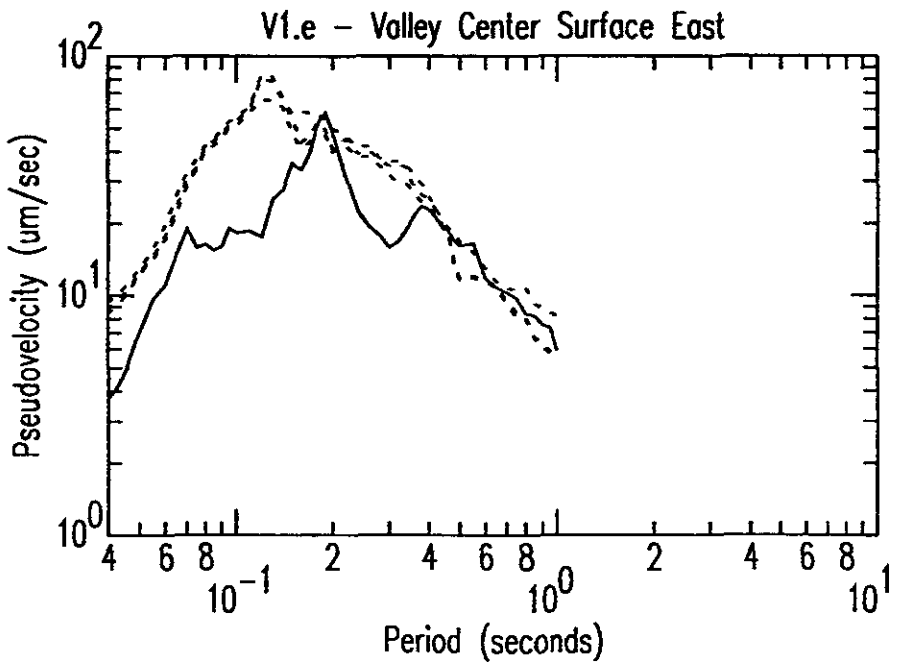

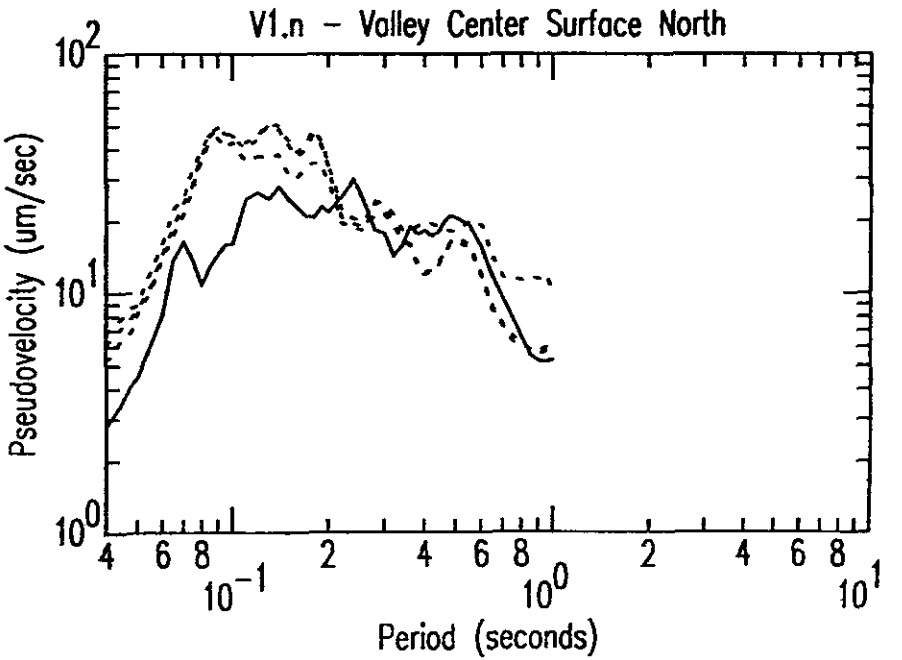

Figure E4b: 1D Standard Model Response Spectra Prediction Quartiles vs Observations

Response Spectra Predictions: Dashed - quartiles
Observations: Solid - weak-motion test event

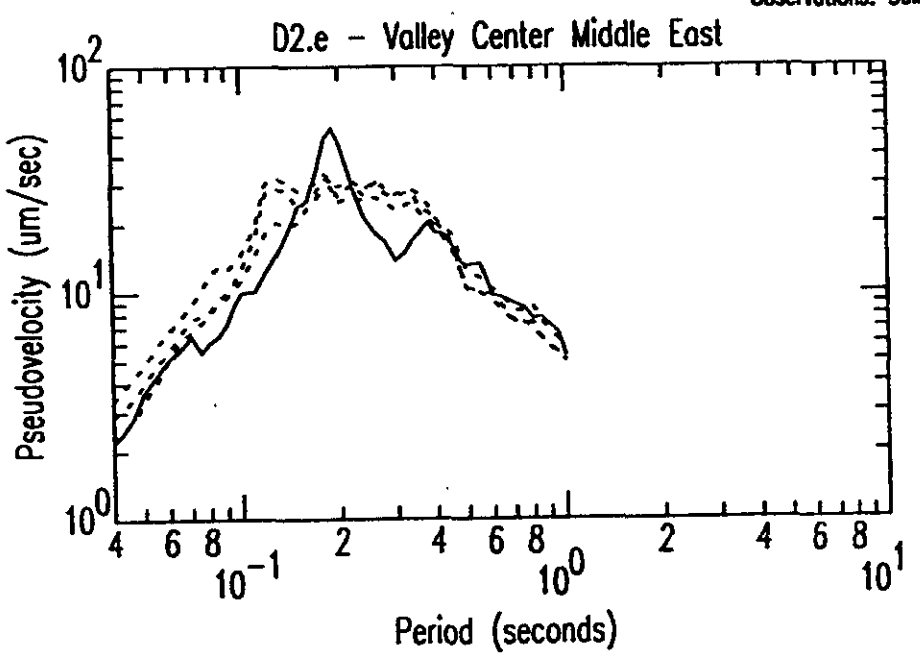

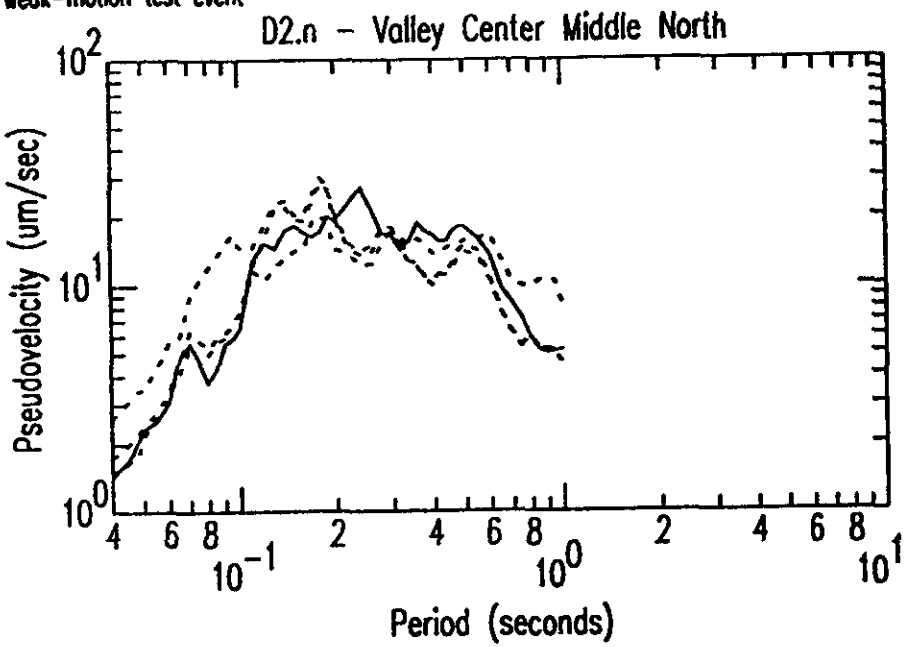

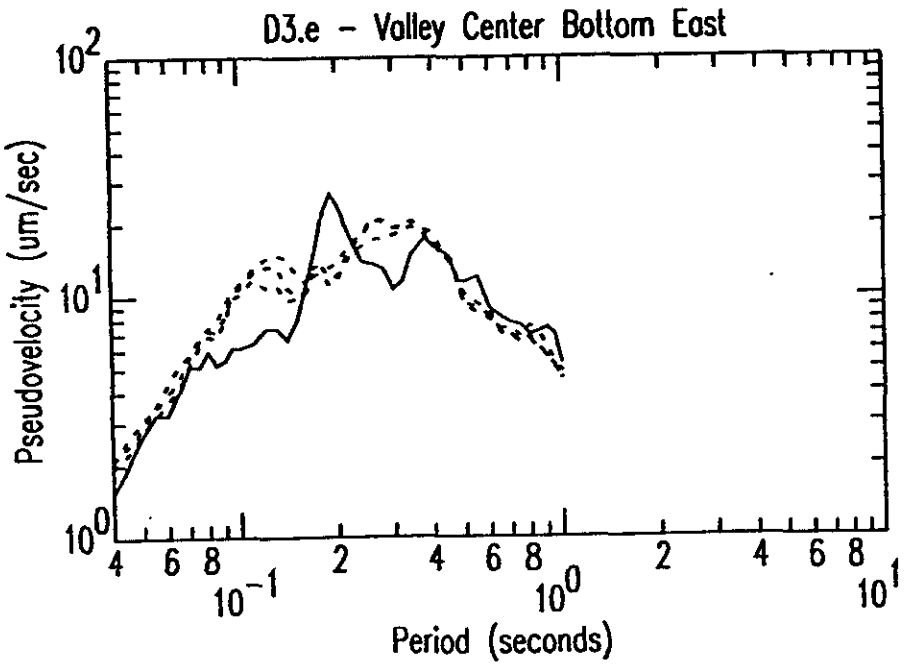

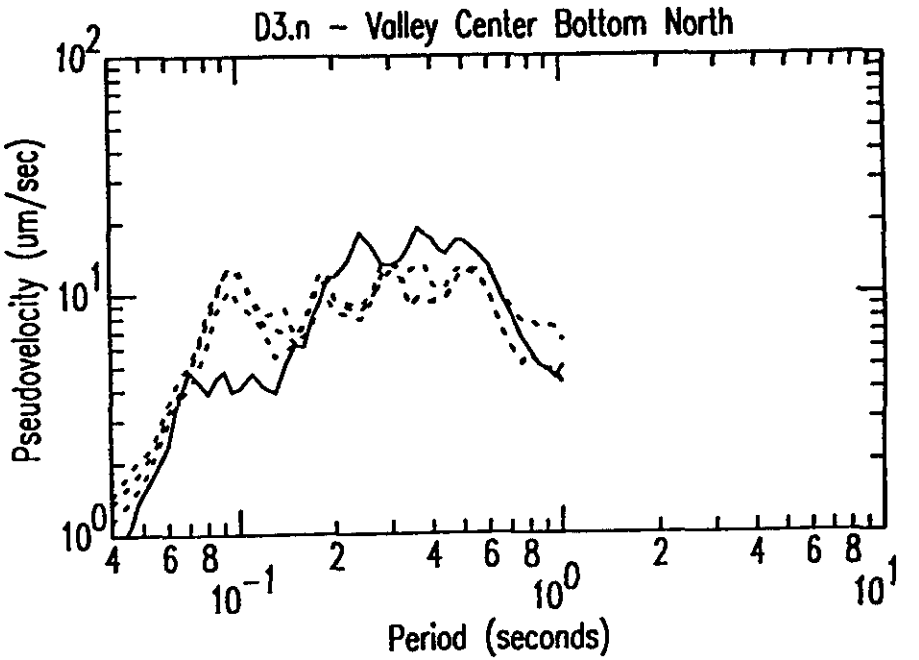

Figure E4c: 1D Standard Model Response Spectra Prediction Quartiles vs Observations

Response Spectra Predictions: Dashed – quartiles
Observations: Solid – weak-motion test event

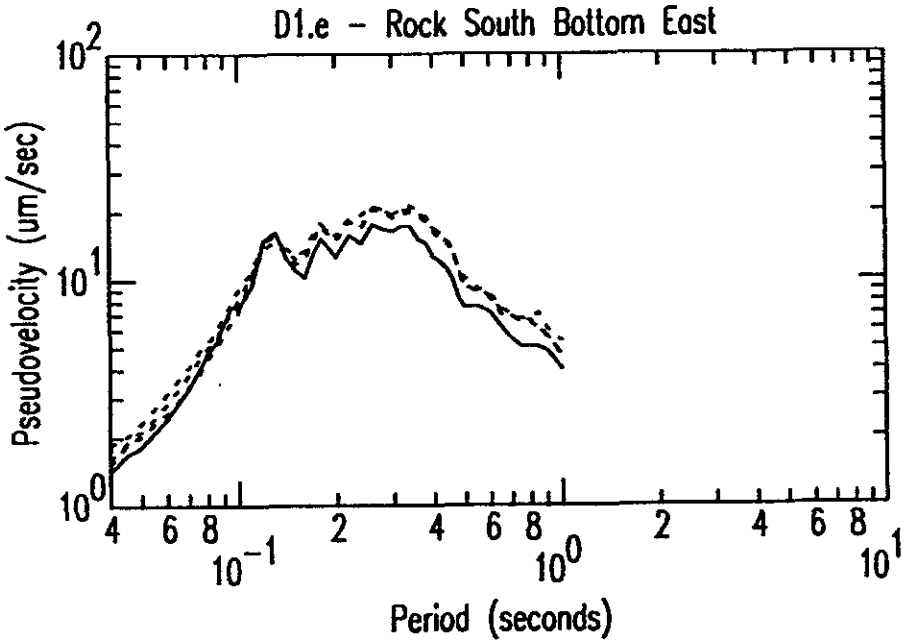

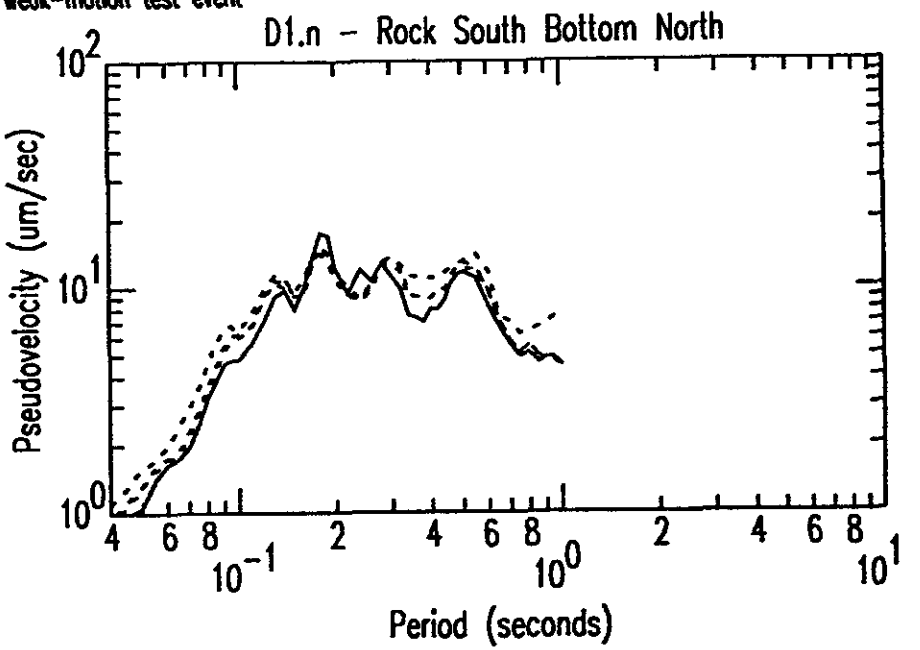

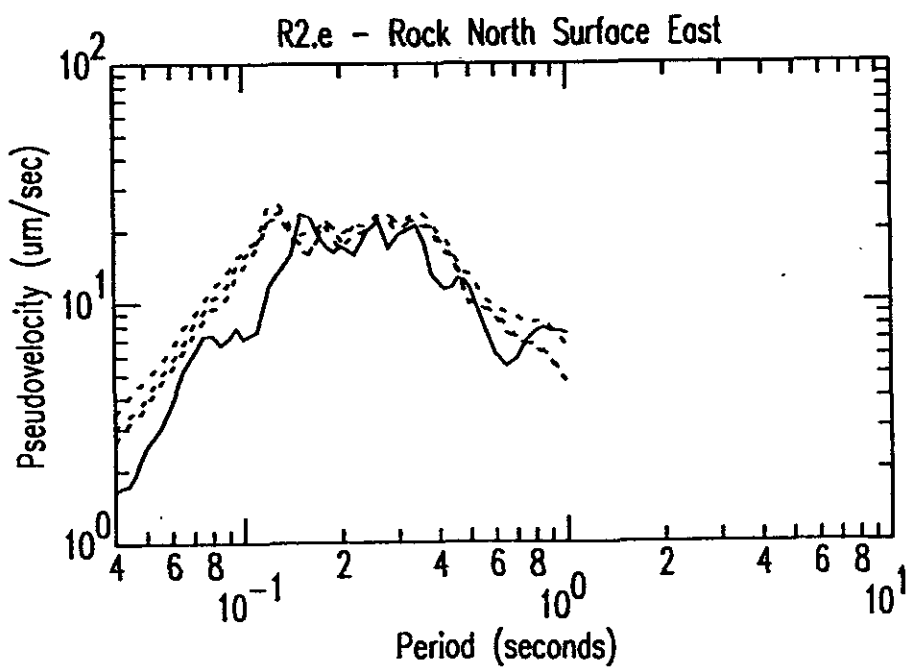

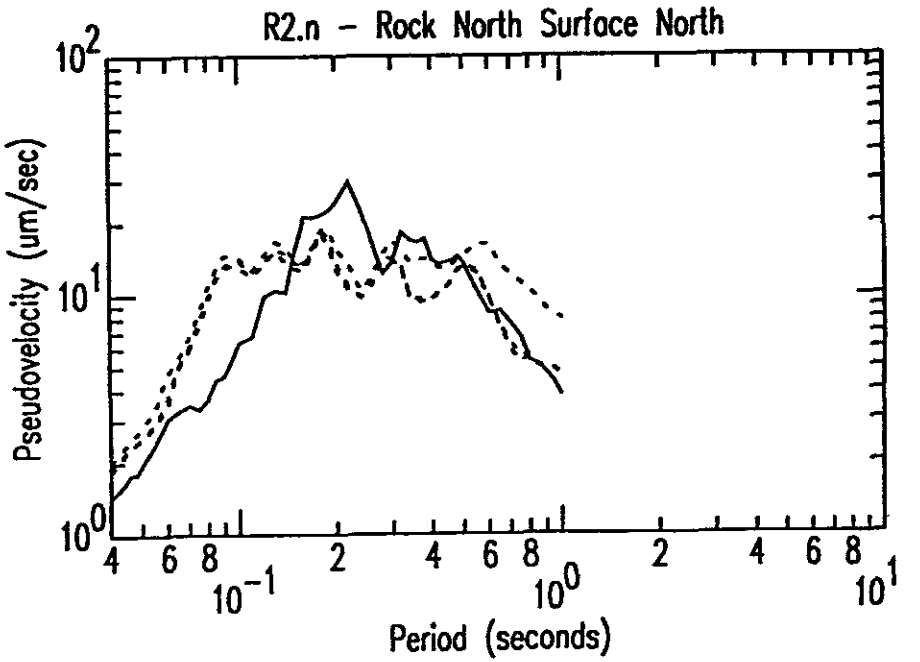

Appendix F

Plots from Analysis of Submitted R1 based Weak-motion Predictions using 2D/3D techniques and the Standard Geotechnical Model

Figure F1a: Standard Fourier Spectral Ratio Plot:
Spectral Ratio V2/R1 for 2D/3D Standard Geotechnical Models

Solid lines – 2D/3D Predictions; Dashed line – Observed

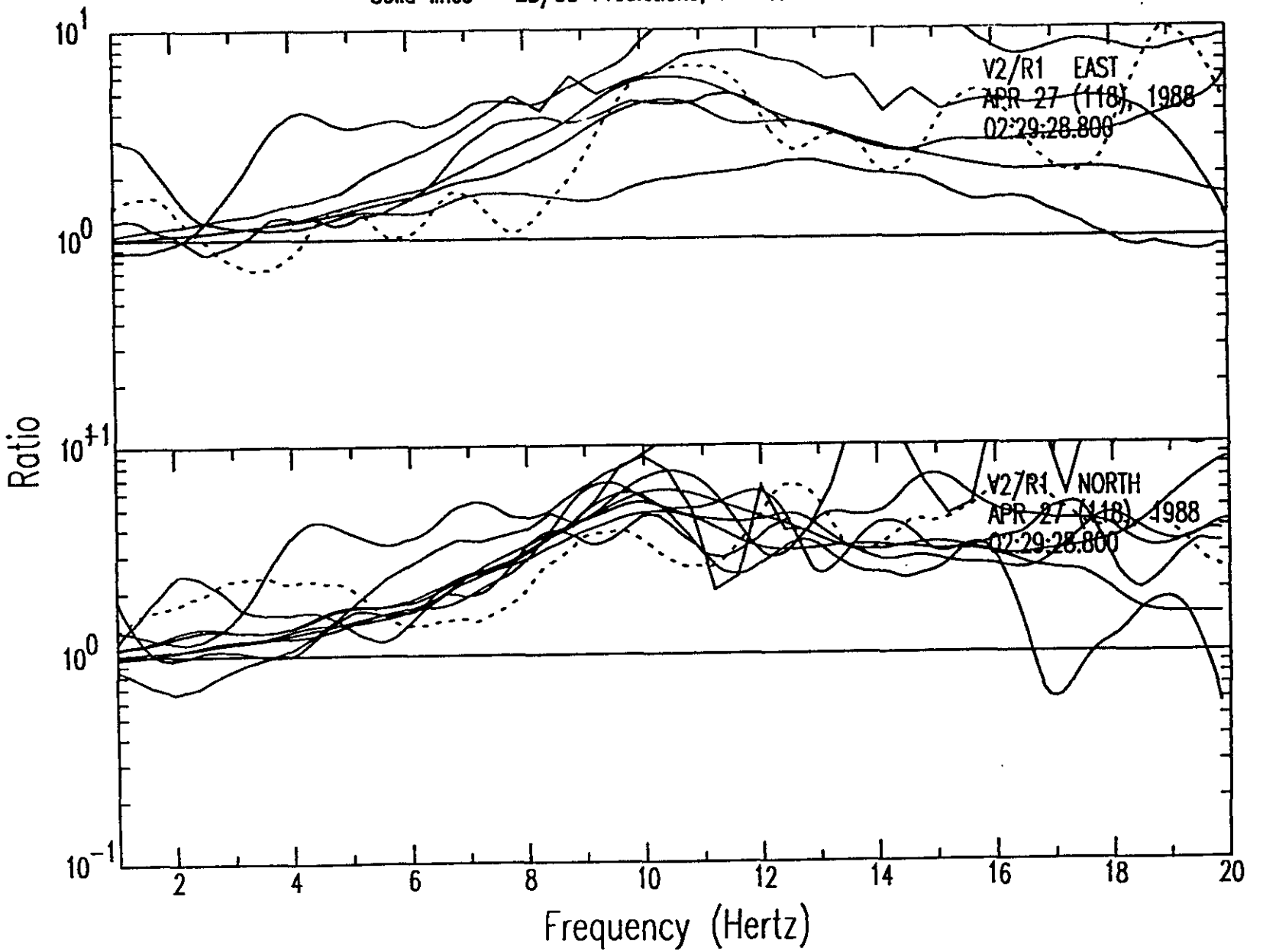

Figure F1b: Standard Fourier Spectral Ratio Plot:
Spectral Ratio V1/R1 for 2D/3D Standard Geotechnical Models

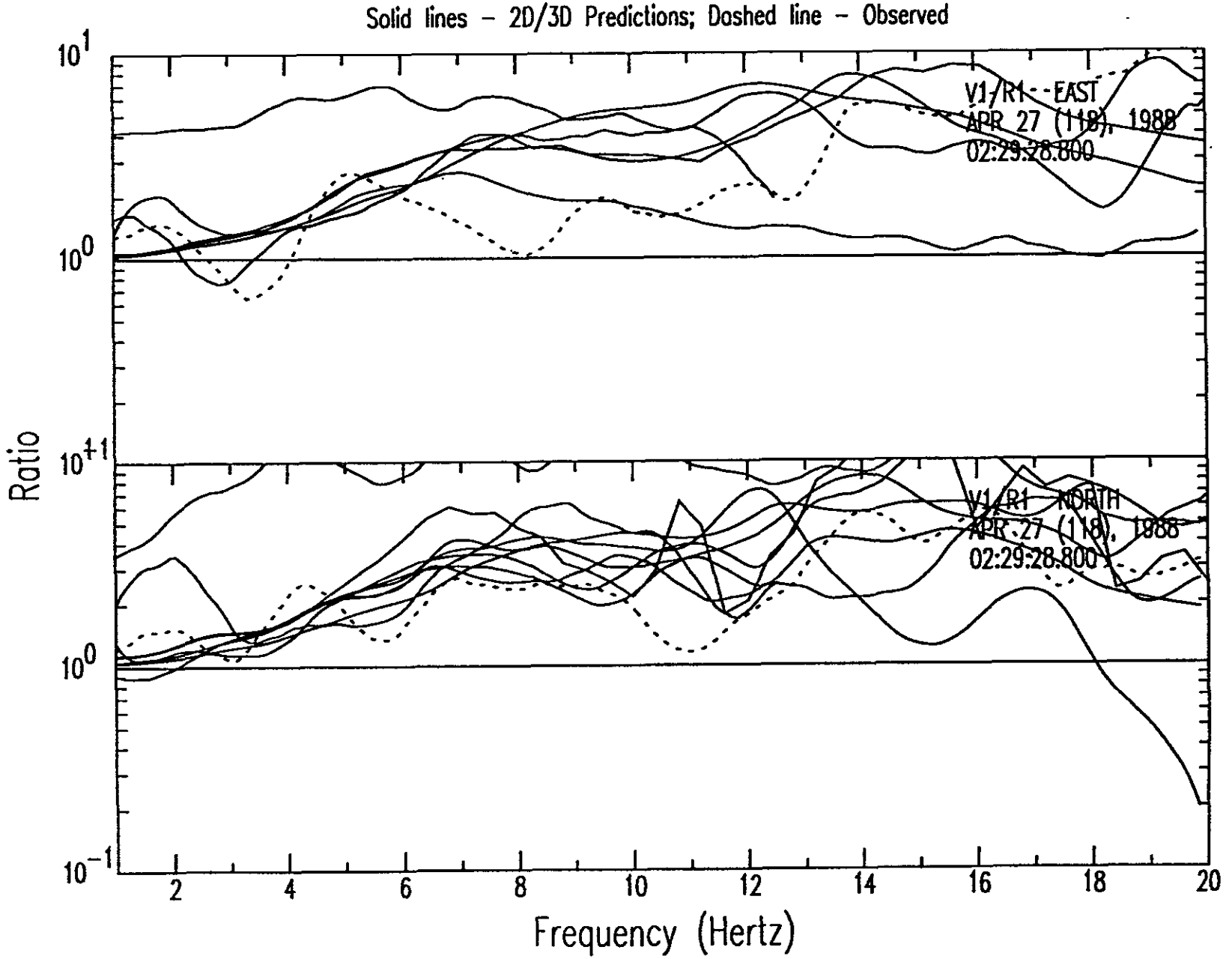

Figure F1c: Standard Fourier Spectral Ratio Plot:
Spectral Ratio D2/R1 for 2D/3D Standard Geotechnical Models

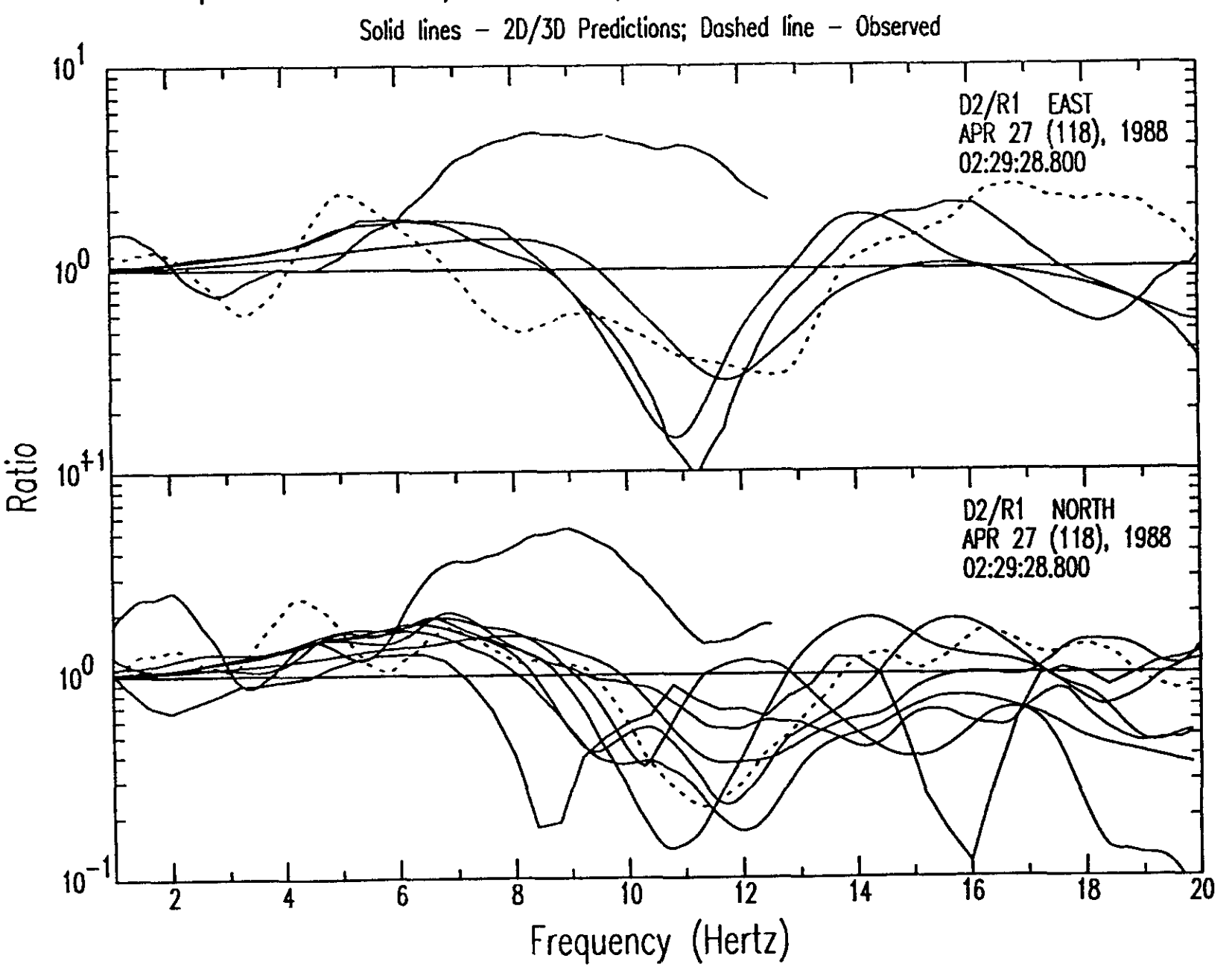

Figure F1d: Standard Fourier Spectral Ratio Plot:
Spectral Ratio D3/R1 for 2D/3D Standard Geotechnical Models

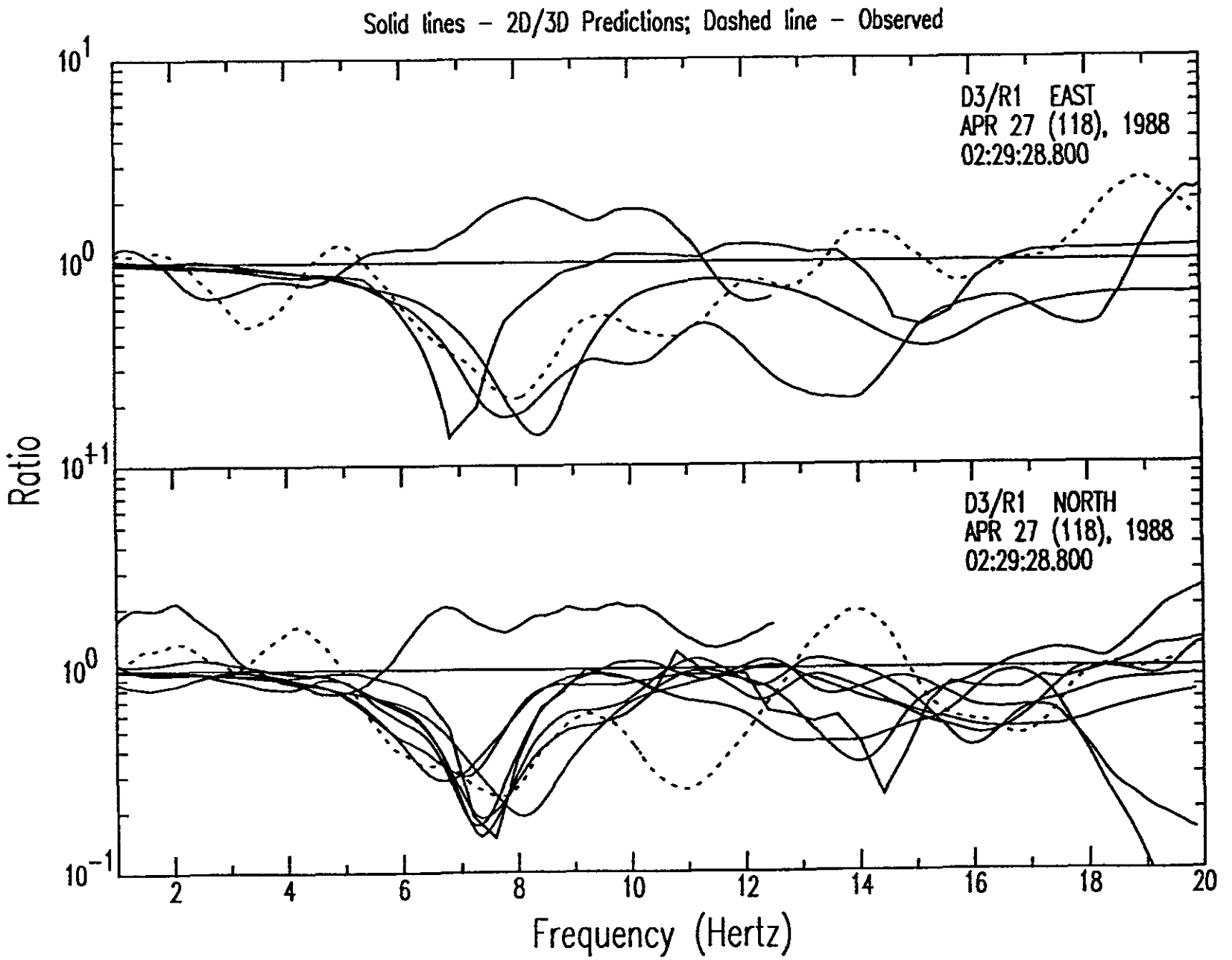

Figure F1e: Standard Fourier Spectral Ratio Plot:
Spectral Ratio D1/R1 for 2D/3D Standard Geotechnical Models

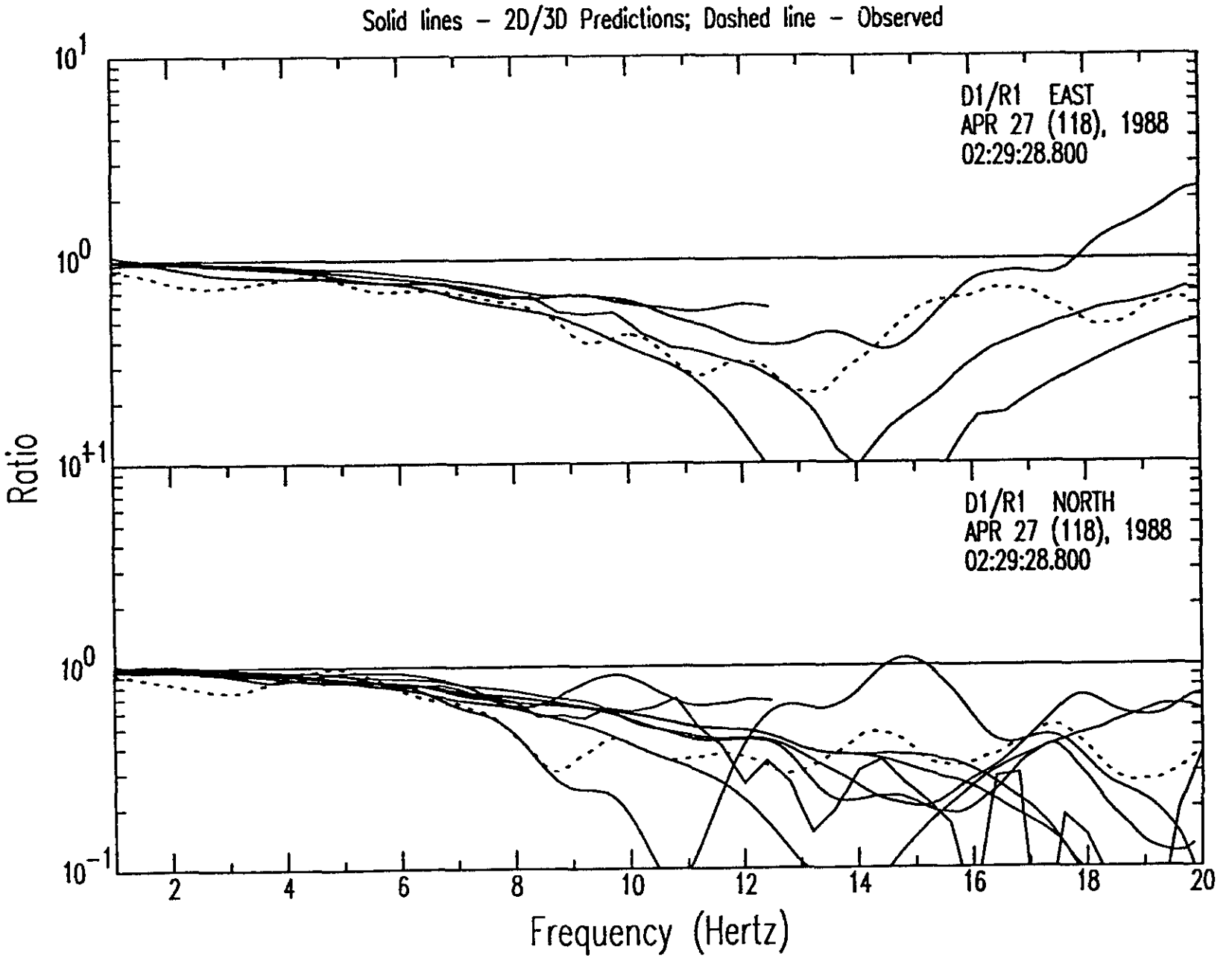

Figure F1f: Standard Fourier Spectral Ratio Plot:
Spectral Ratio R2/R1 for 2D/3D Standard Geotechnical Models

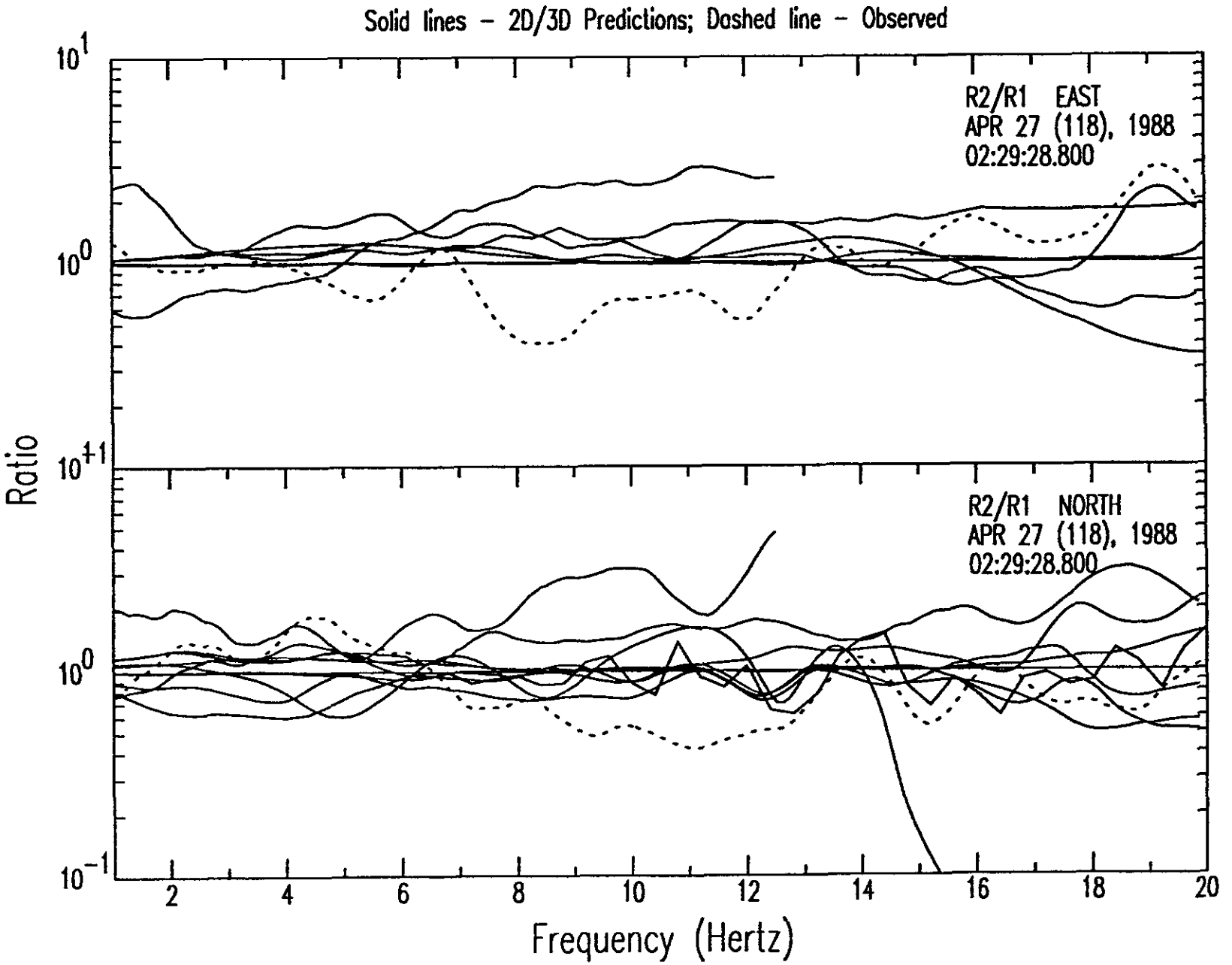

Figure F2a: 2D/3D Standard Model Spectral Ratio Prediction Quartiles vs Observations

Spectral Ratio Predictions: Dashed - quartiles

Observations: Solid - weak-motion test event; Dash-dotted - weak-motion mean; Dotted - 1 std deviation

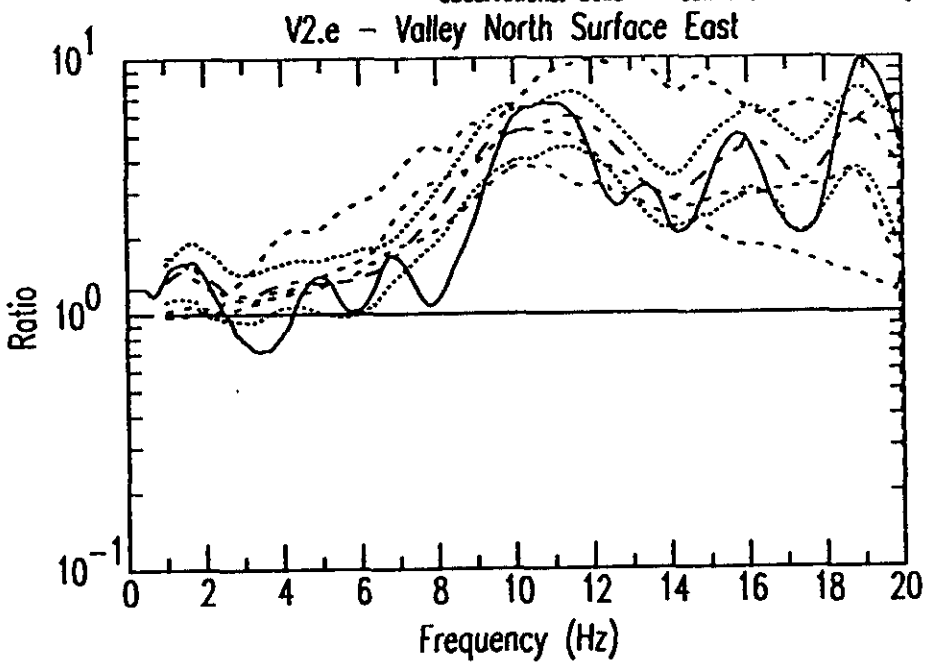

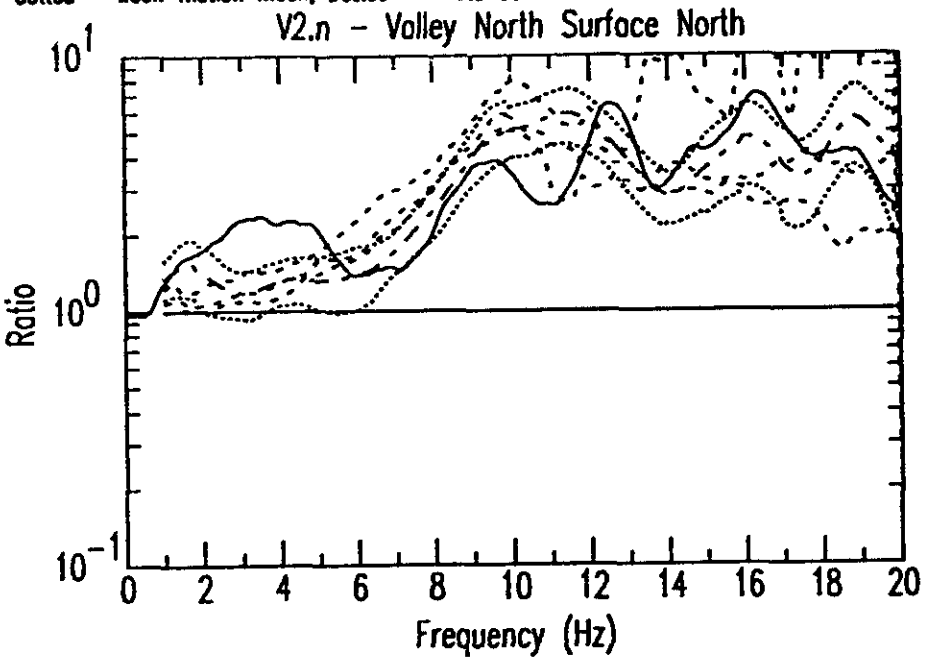

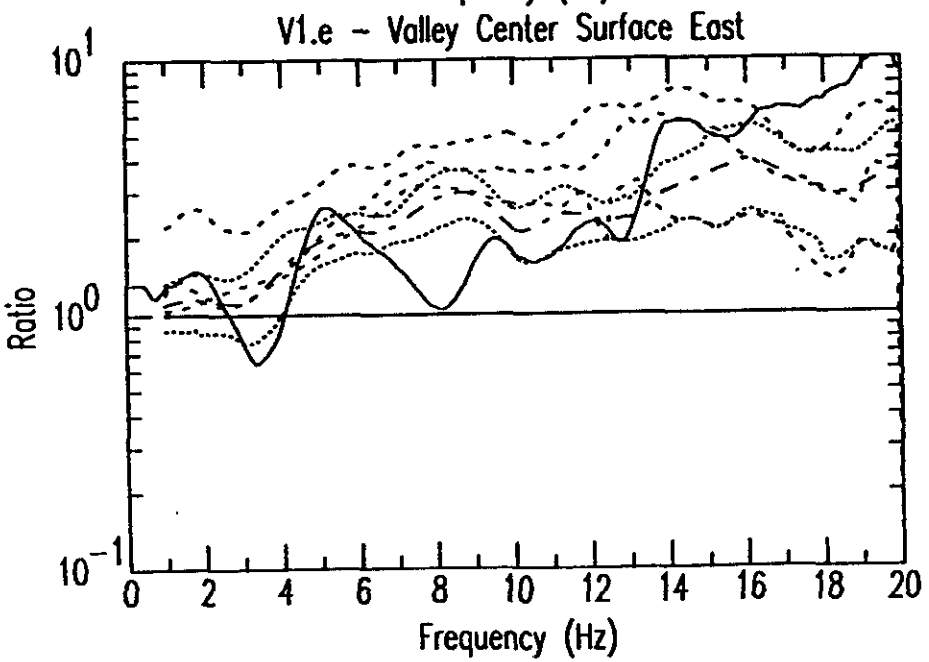

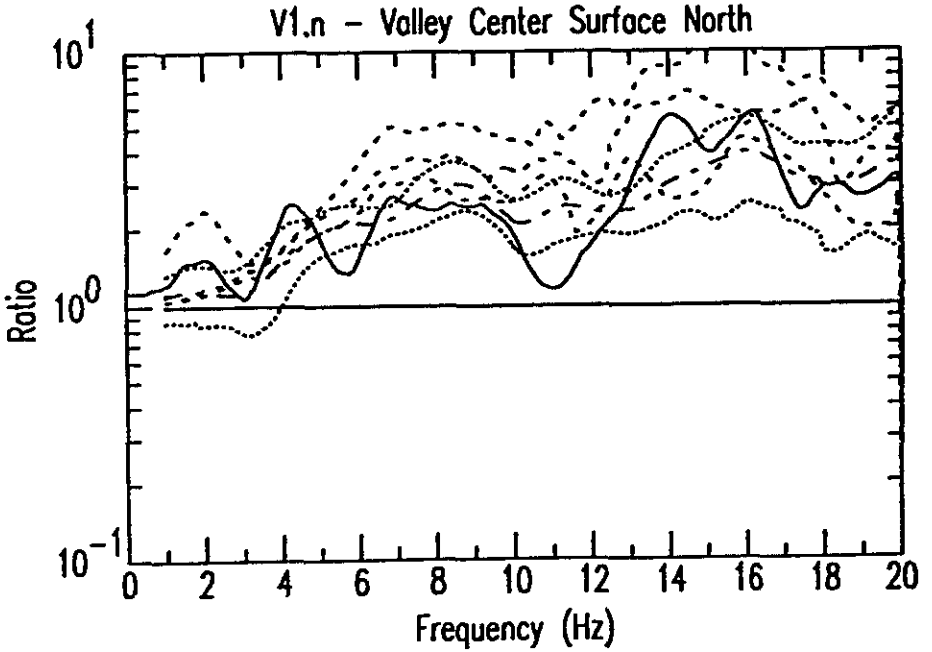

Figure F2b: 2D/3D Standard Model Spectral Ratio Prediction Quartiles vs Observations

Spectral Ratio Predictions: Dashed – quartiles

Observations: Solid – weak-motion test event; Dash-dotted – weak-motion mean; Dotted – 1 std deviation

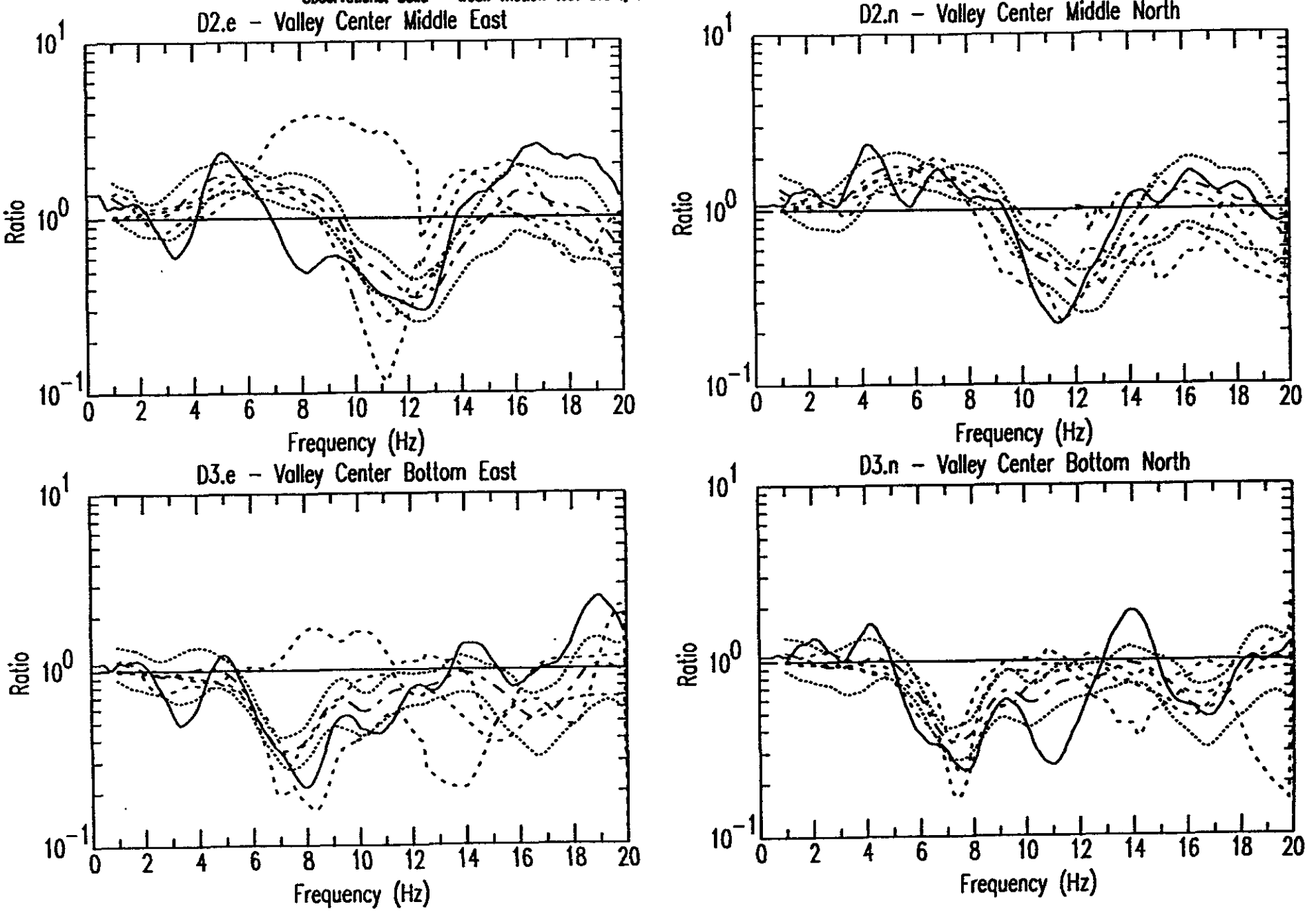

Figure F2c: 2D/3D Standard Model Spectral Ratio Prediction Quartiles vs Observations

Spectral Ratio Predictions: Dashed - quartiles

Observations: Solid - weak-motion test event; Dash-dotted - weak-motion mean; Dotted - 1 std deviation

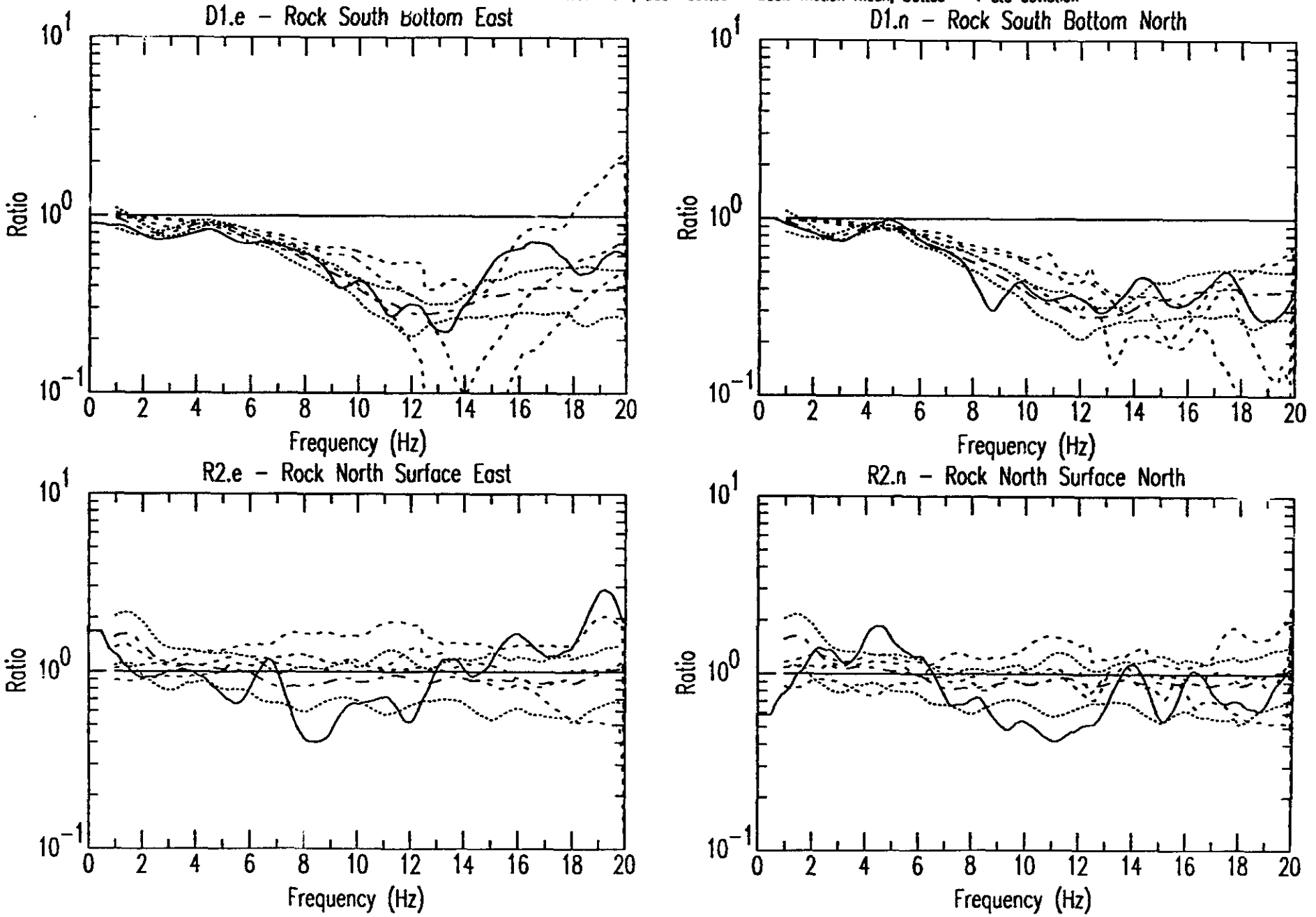

Figure F3a: Standard Response Spectra:
Station V2 Rock North Surface 2D/3D Standard Geotechnical Models
Solid lines - 2D/3D Predictions; Dashed line - Observed

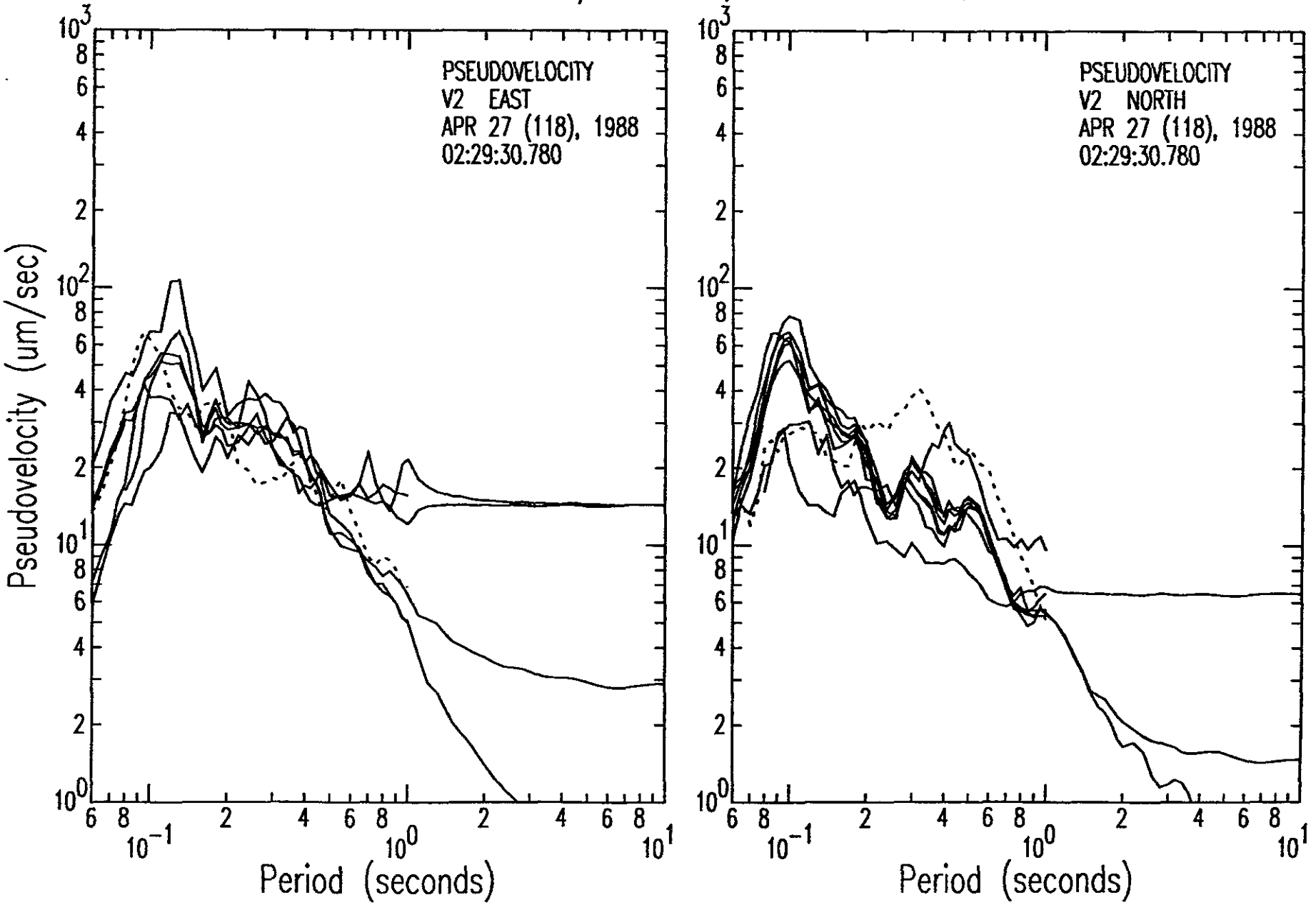

Figure F3b: Standard Response Spectra:

Station V1 Rock North Surface 2D/3D Standard Geotechnical Models

Solid lines - 2D/3D Predictions; Dashed line - Observed

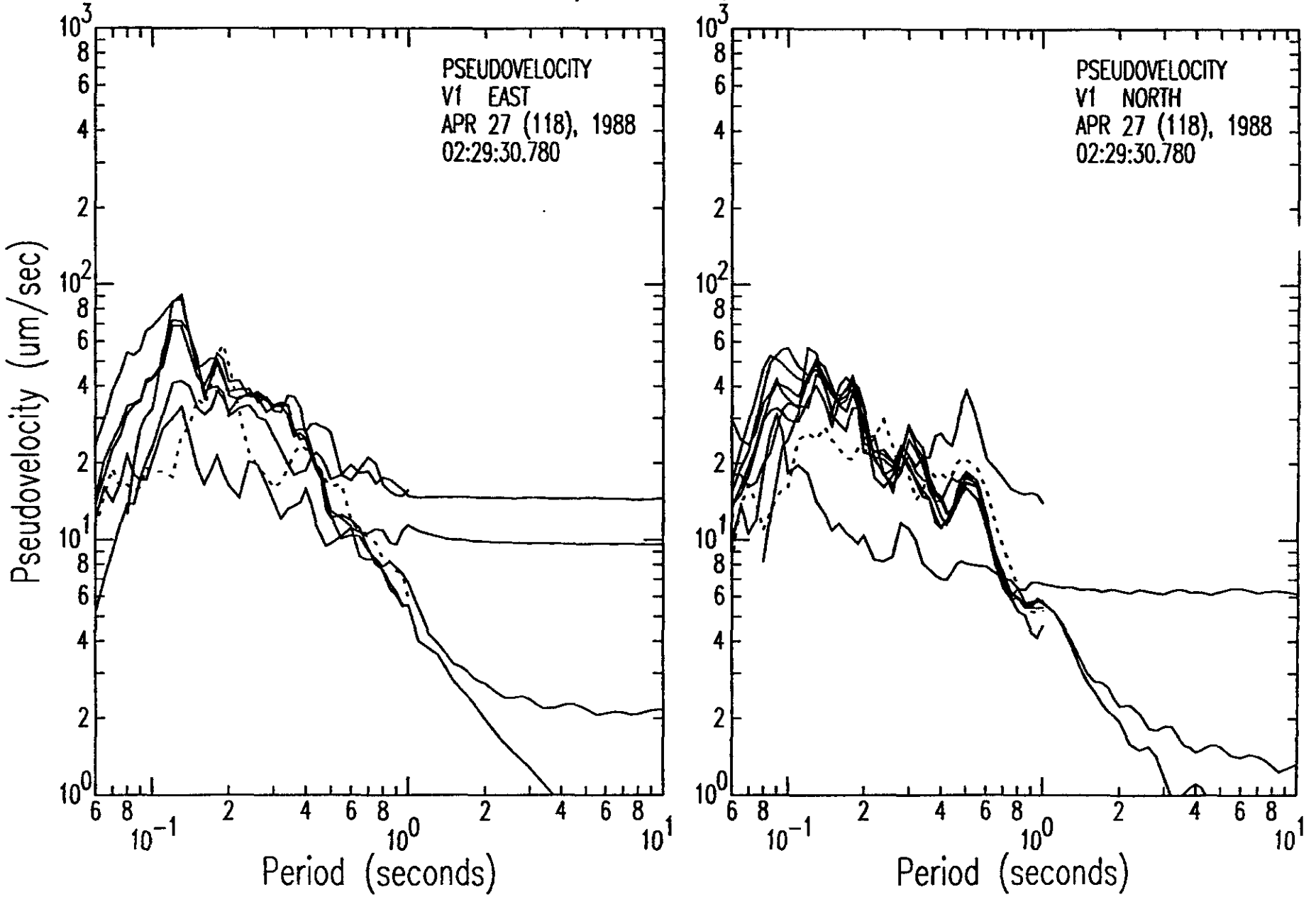

Figure F3c: Standard Response Spectra:
Station D2 Rock North Surface 2D/3D Standard Geotechnical Models
Solid lines – 2D/3D Predictions; Dashed line – Observed

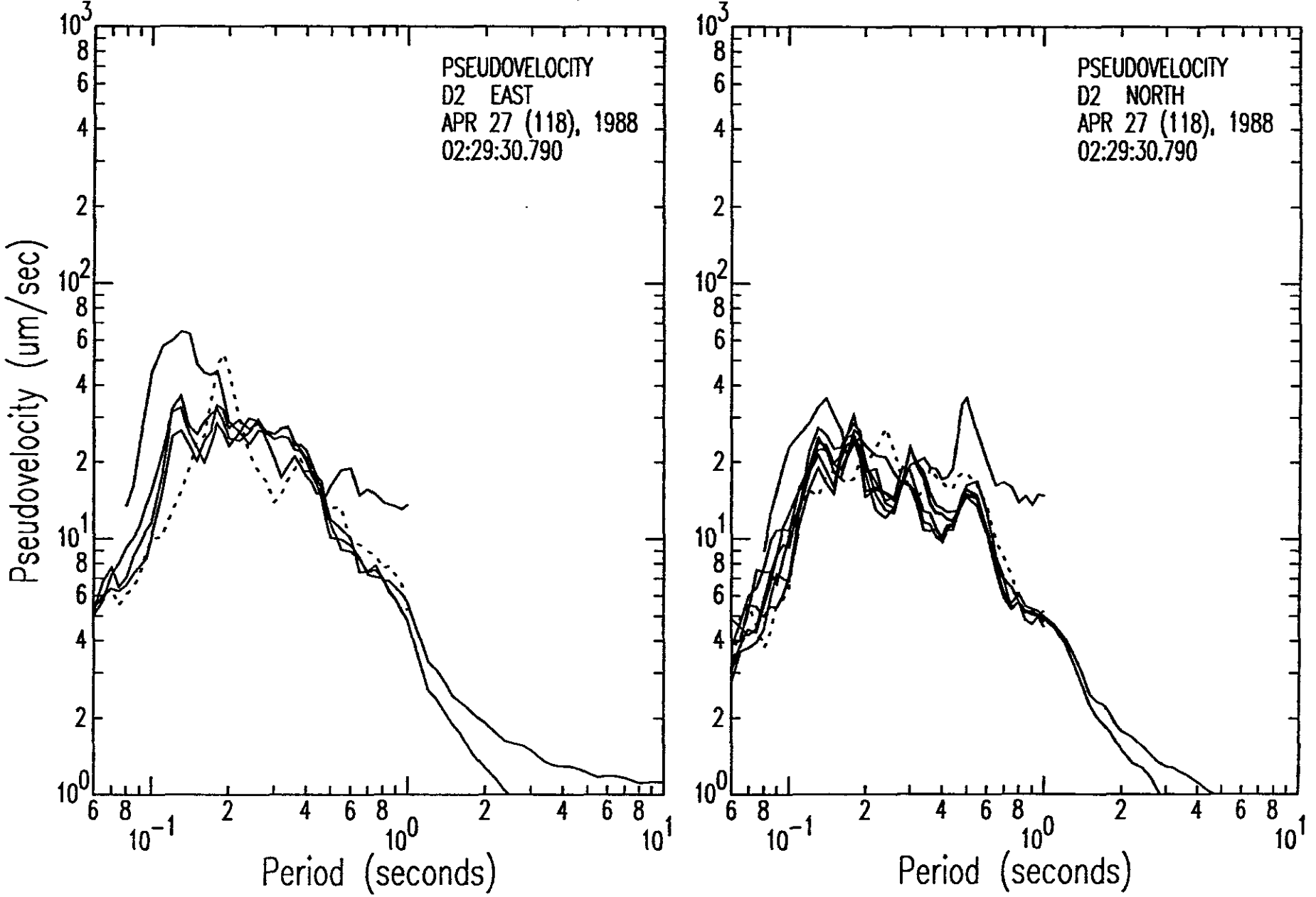

Figure F3d: Standard Response Spectra:
Station D3 Rock North Surface 2D/3D Standard Geotechnical Models
Solid lines - 2D/3D Predictions; Dashed line - Observed

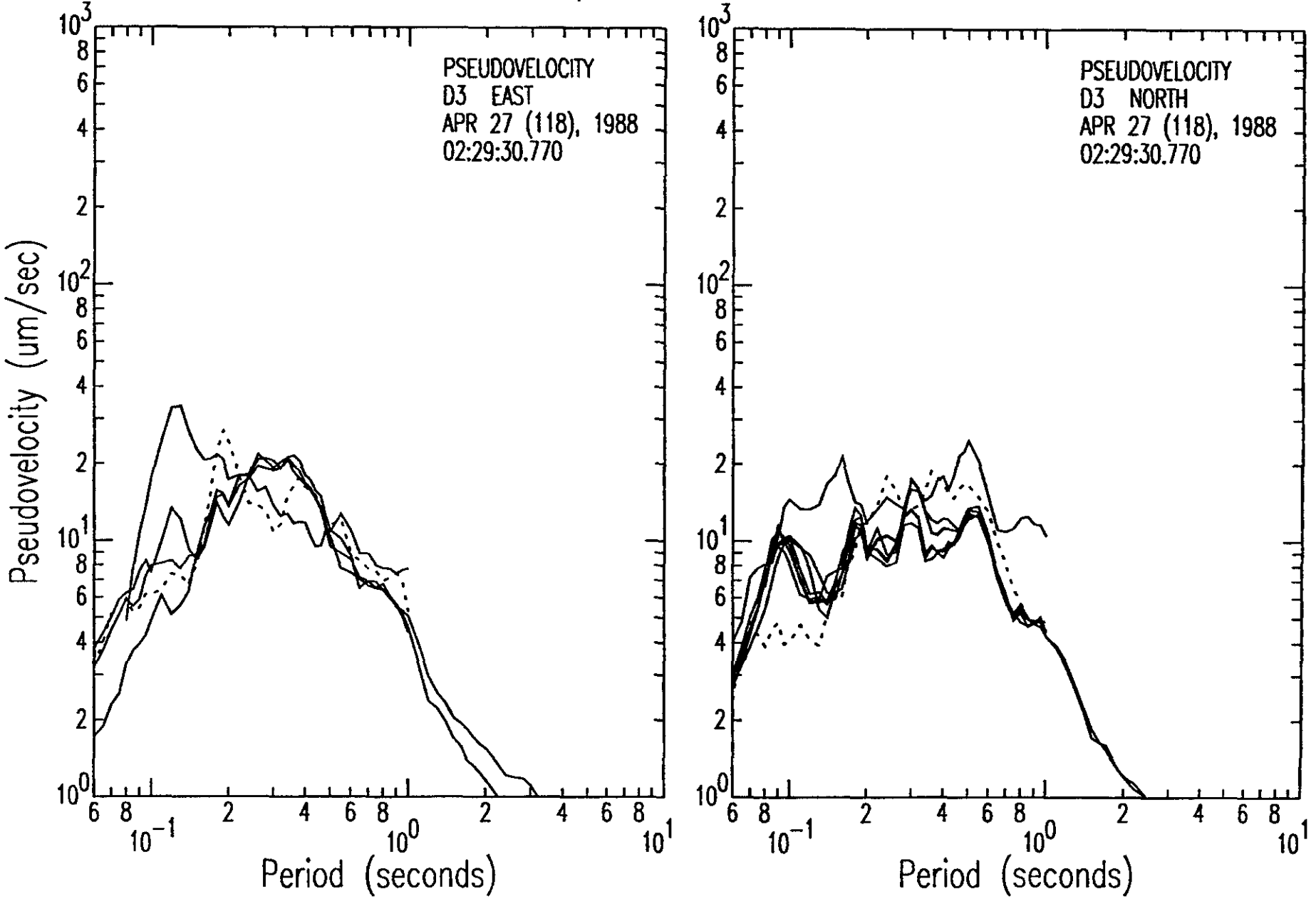

Figure F3e: Standard Response Spectra:
Station D1 Rock North Surface 2D/3D Standard Geotechnical Models
Solid lines - 2D/3D Predictions; Dashed line - Observed

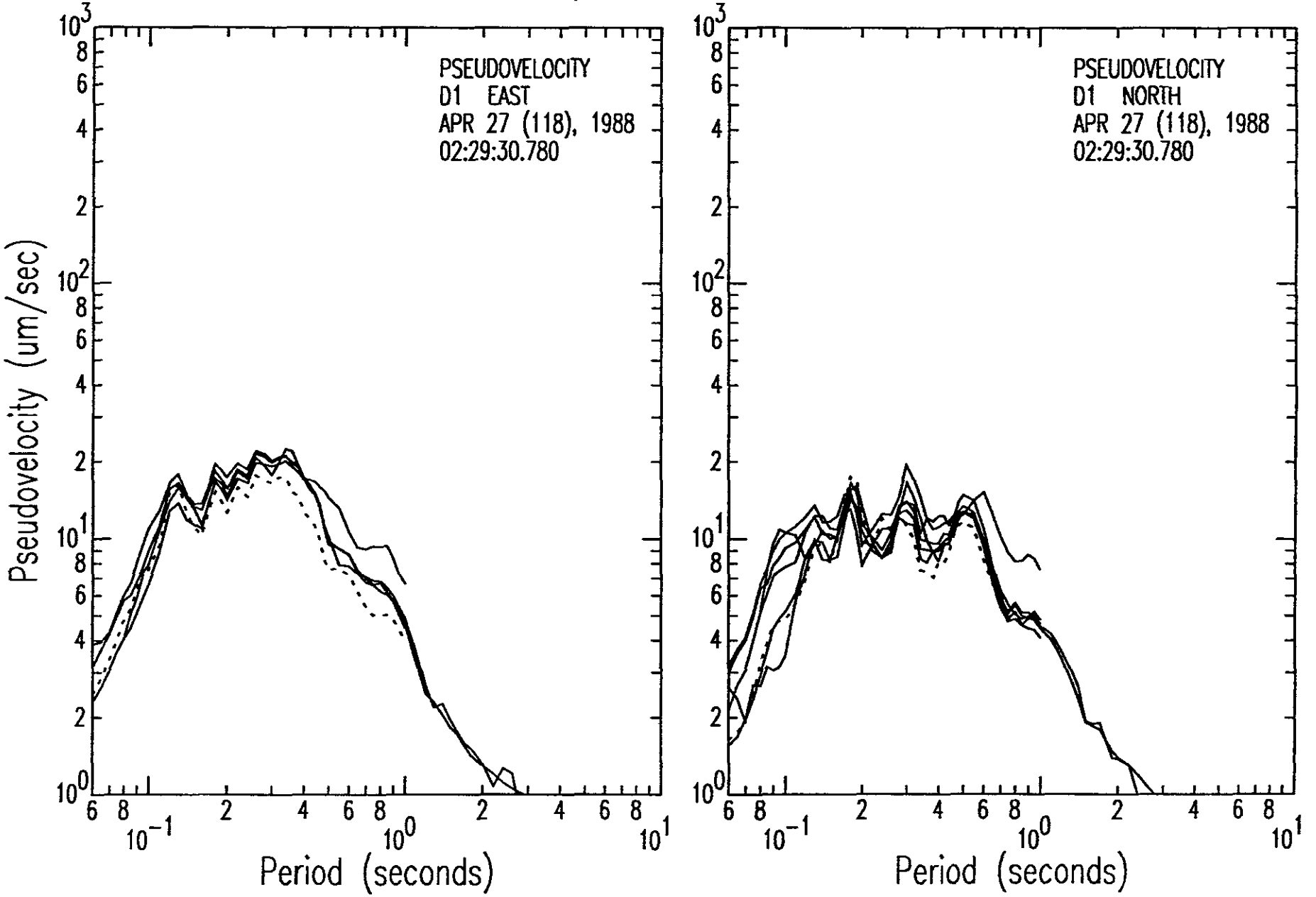

Figure F3f: Standard Response Spectra:
Station R2 Rock North Surface 2D/3D Standard Geotechnical Models
Solid lines – 2D/3D Predictions; Dashed line – Observed

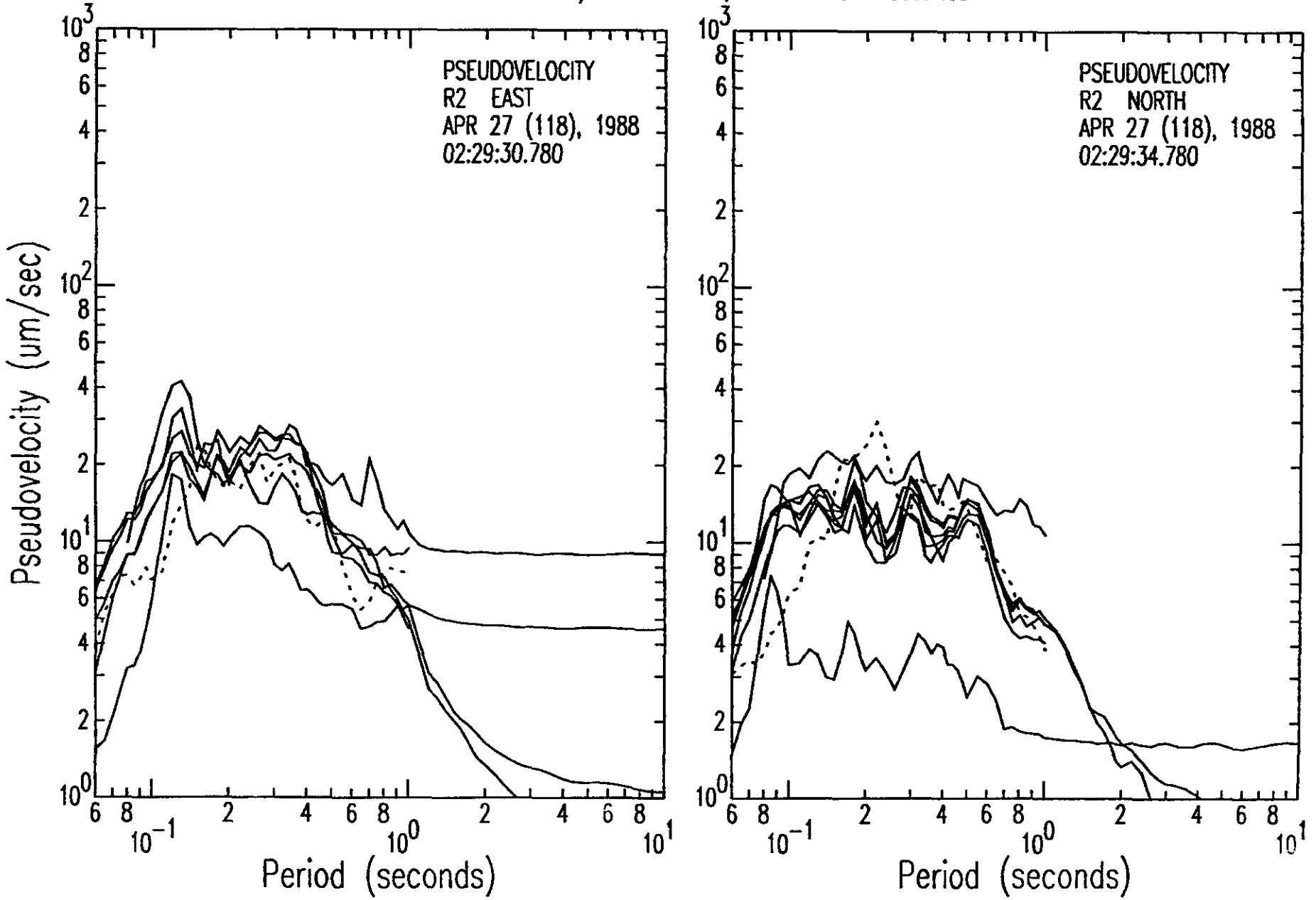

Figure F4a: 2D/3D Standard Model Response Spectra Prediction Quartiles vs Observations

Response Spectra Predictions: Dashed - quartiles
Observations: Solid - weak-motion test event

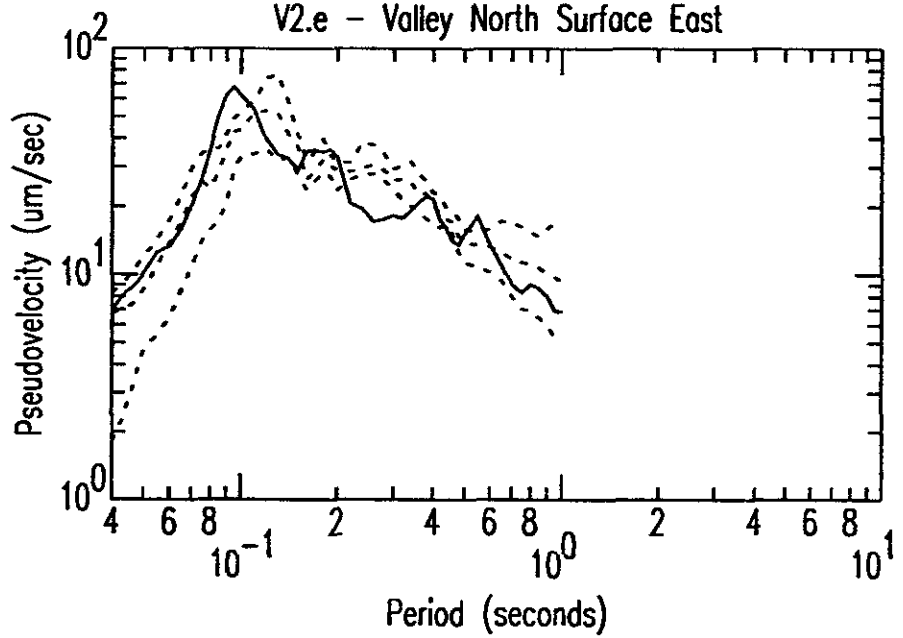

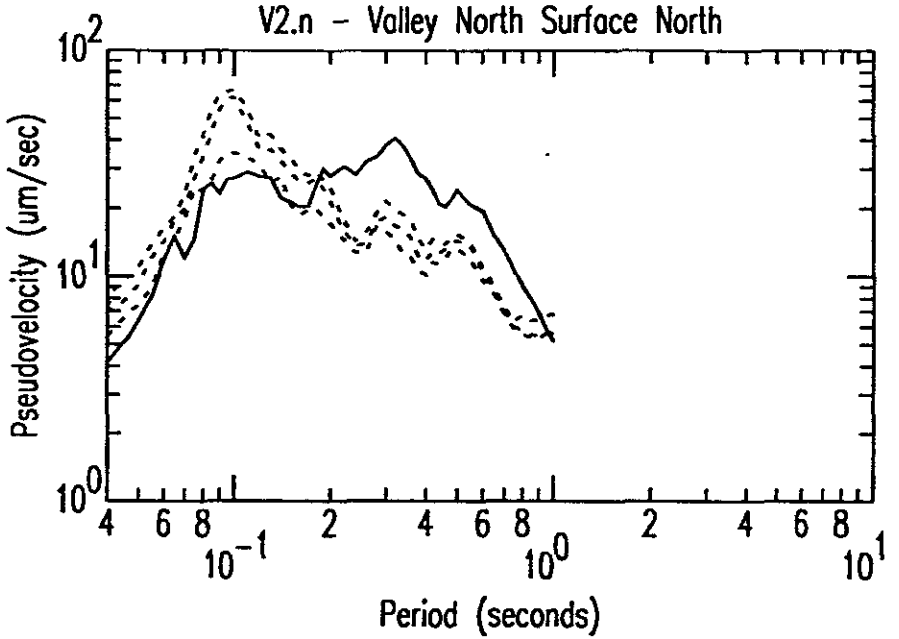

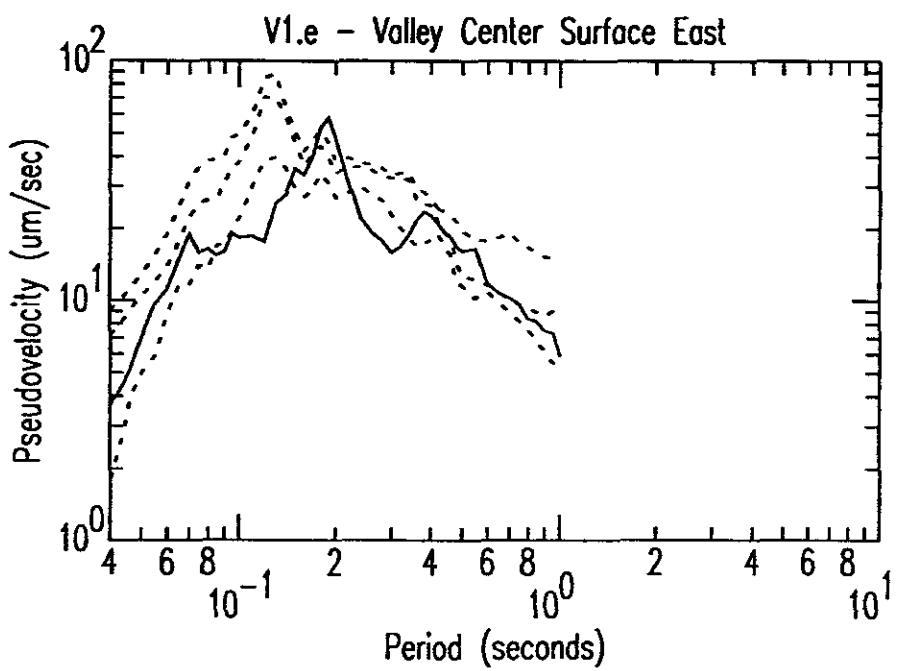

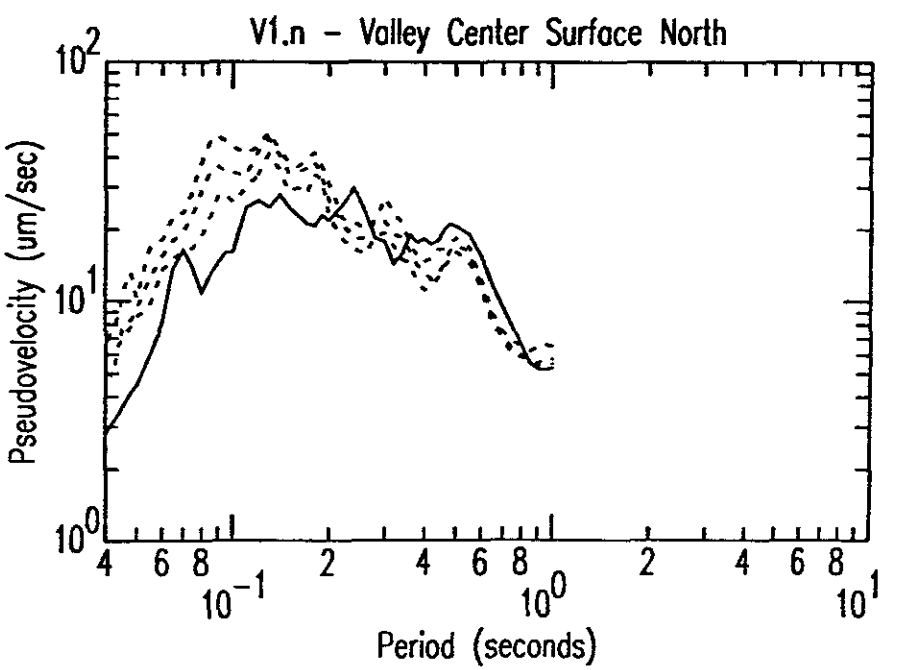

Figure F4b: 2D/3D Standard Model Response Spectra Prediction Quartiles vs Observations

Response Spectra Predictions: Dashed - quartiles
Observations: Solid - weak-motion test event

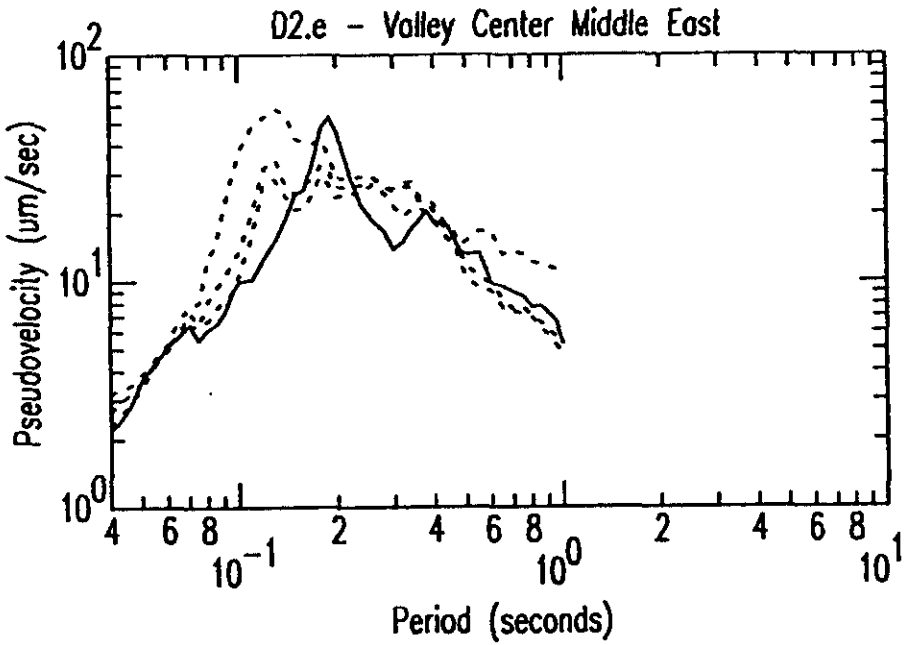

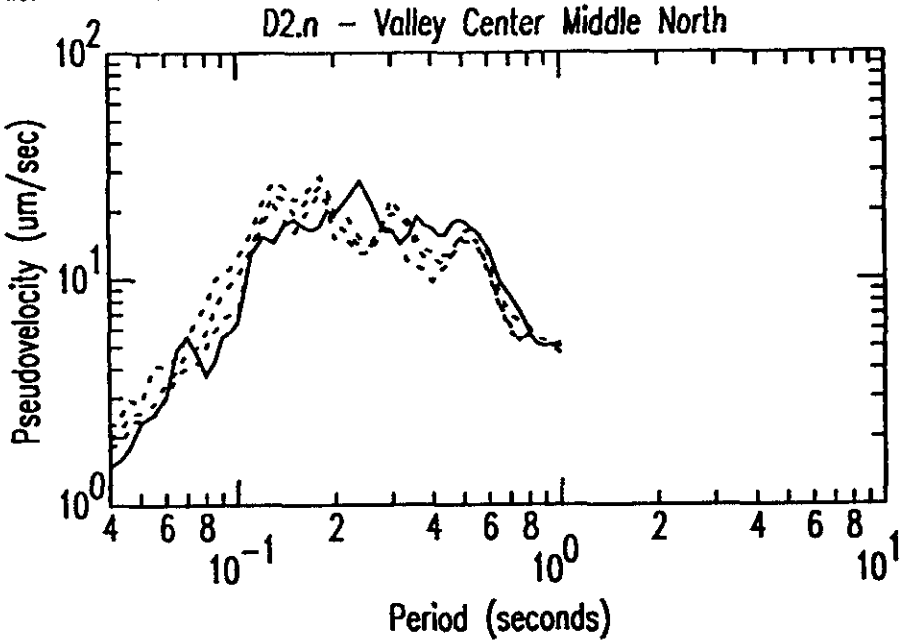

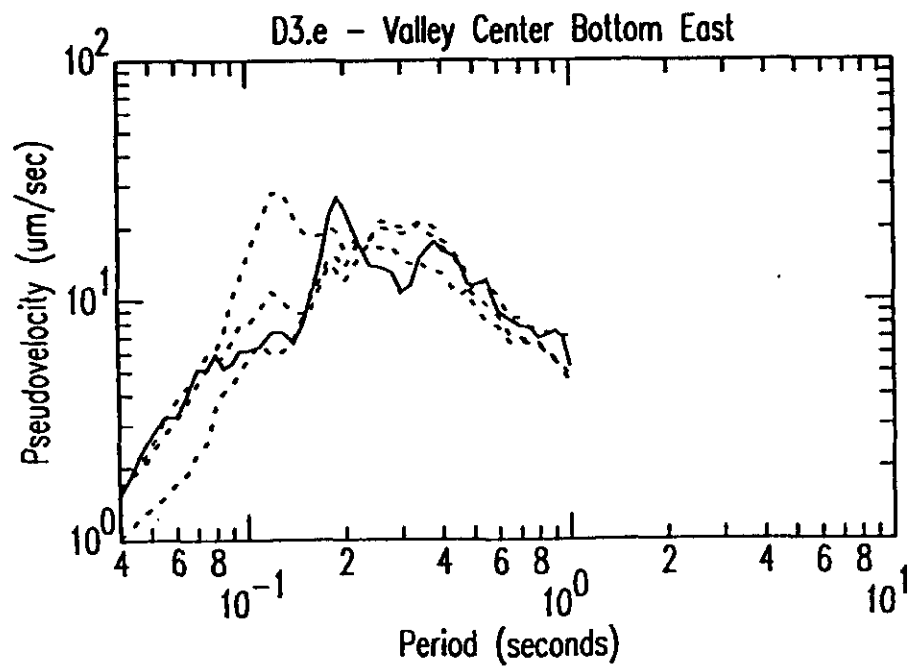

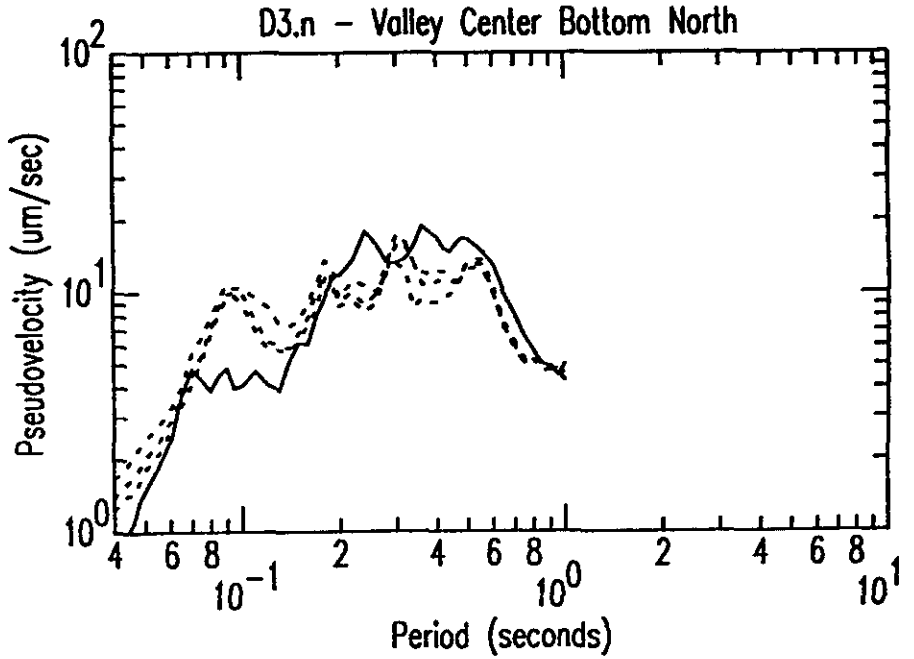

Figure F4c: 2D/3D Standard Model Response Spectra Prediction Quartiles vs Observations

Response Spectra Predictions: Dashed - quartiles
Observations: Solid - weak-motion test event

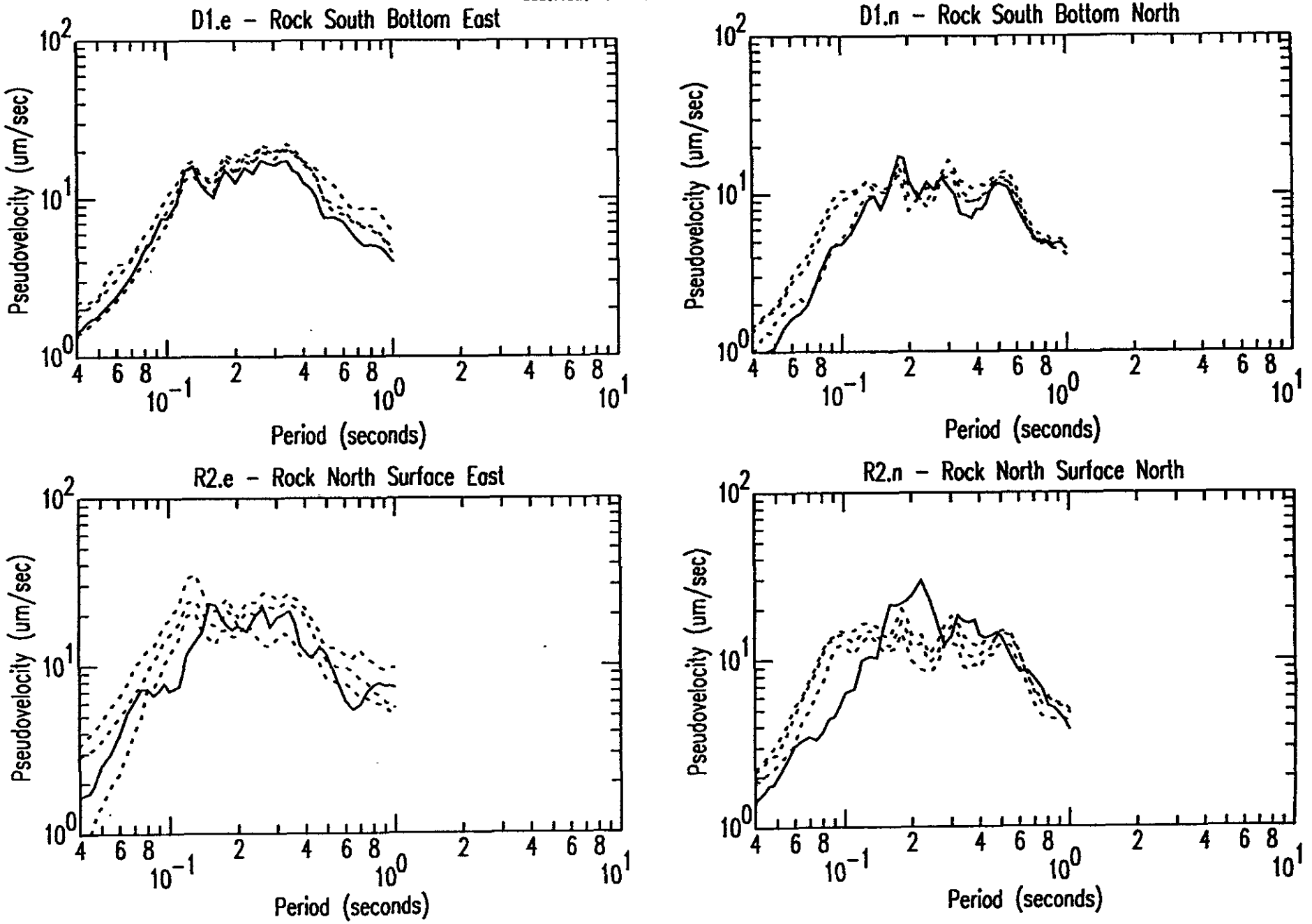

Appendix G

Plots from the Comparison of Submitted Weak-motion Predictions using a Preferred Geotechnical Model with the Corresponding Prediction using the Standard Geotechnical Model

Figure G1a: R1 Preferred and Standard Spectral Ratio Predictions by #8 vs Observations

Spectral Ratio Predictions: Dashed – Standard Model; Dotted – Preferred Model

Observations: Solid – weak-motion test event; Dash-dotted – weak-motion mean and 1 std deviation

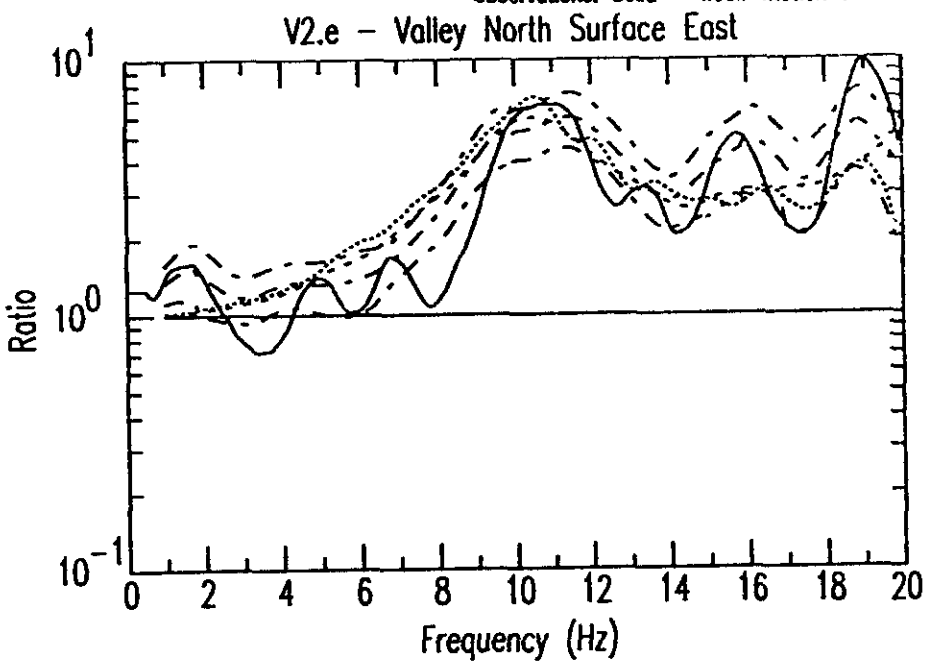

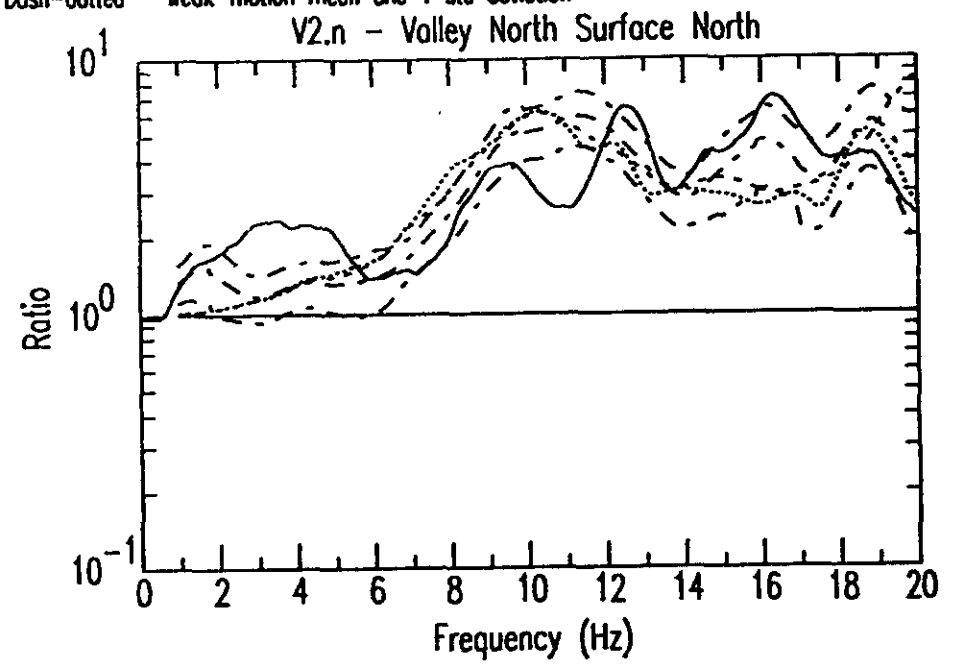

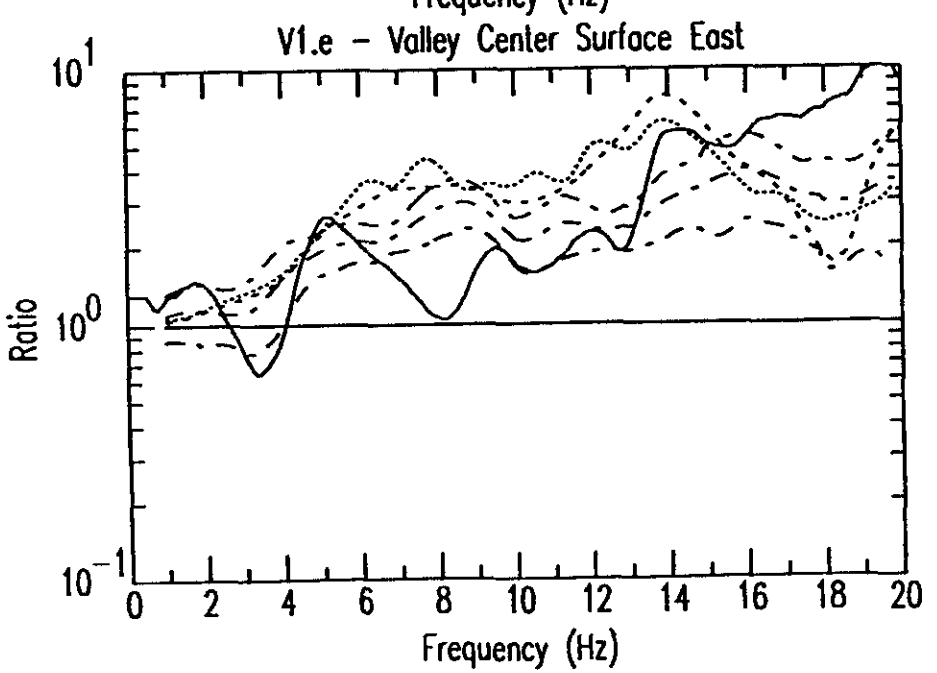

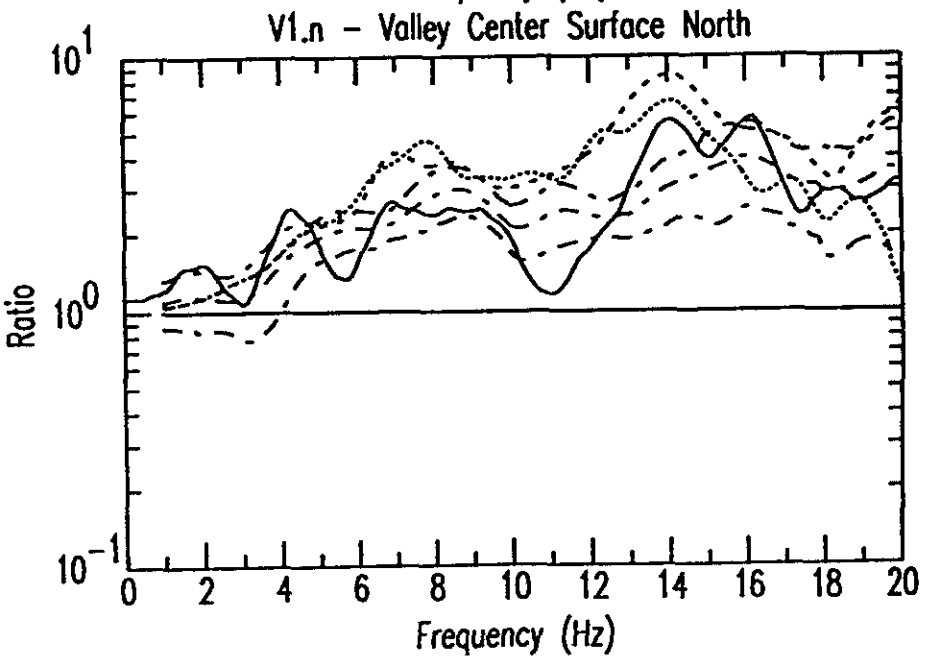

Figure G1b: R1 Preferred and Standard Spectral Ratio Predictions by #8 vs Observations

Spectral Ratio Predictions: Dashed – Standard Model; Dotted – Preferred Model

Observations: Solid – weak-motion test event; Dash-dotted – weak-motion mean and 1 std deviation

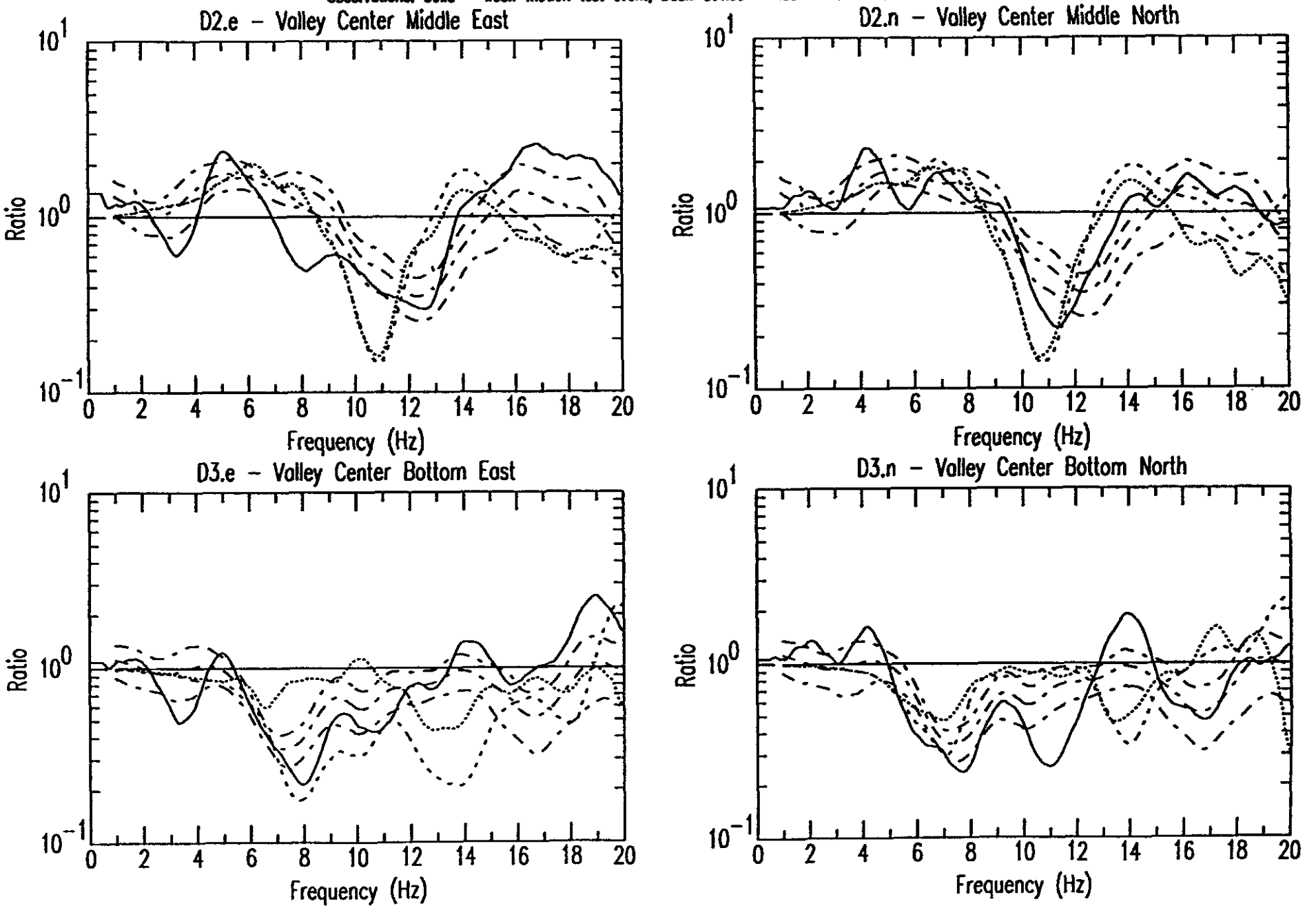

Figure G1c: R1 Preferred and Standard Spectral Ratio Predictions by #8 vs Observations

Spectral Ratio Predictions: Dashed - Standard Model; Dotted - Preferred Model

Observations: Solid - weak-motion test event; Dash-dotted - weak-motion mean and 1 std deviation

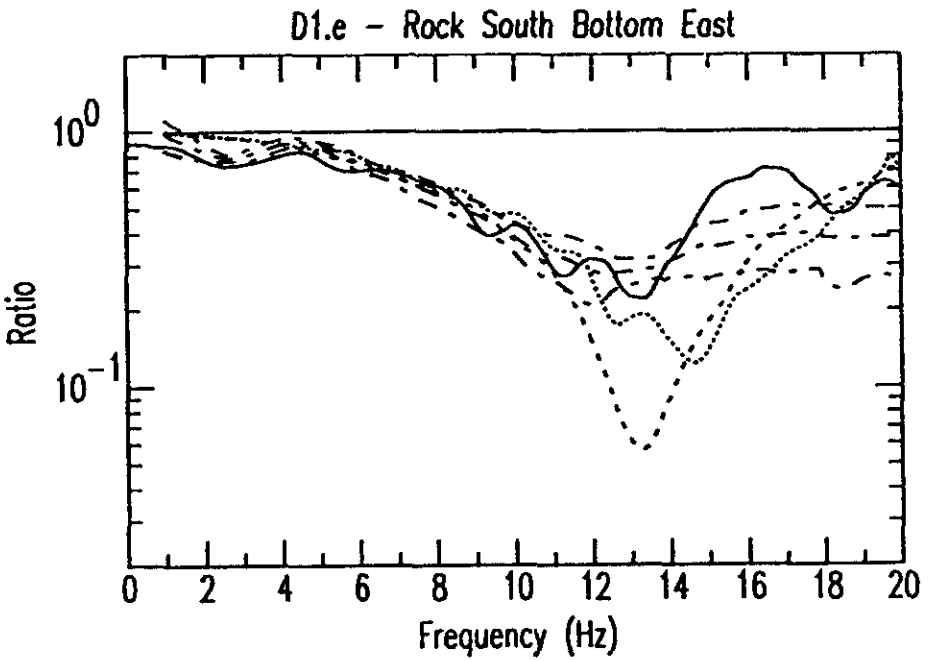

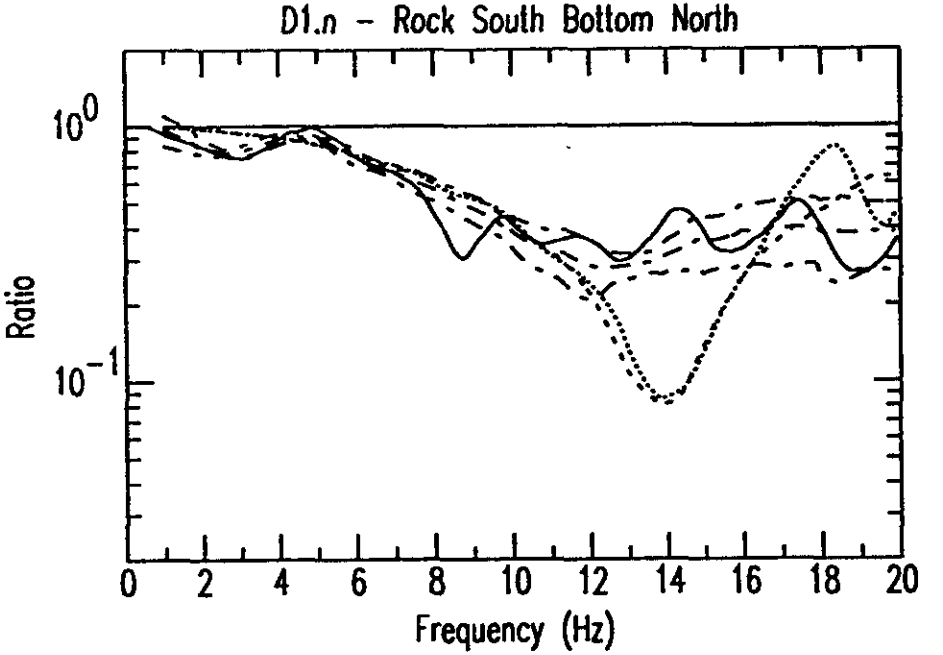

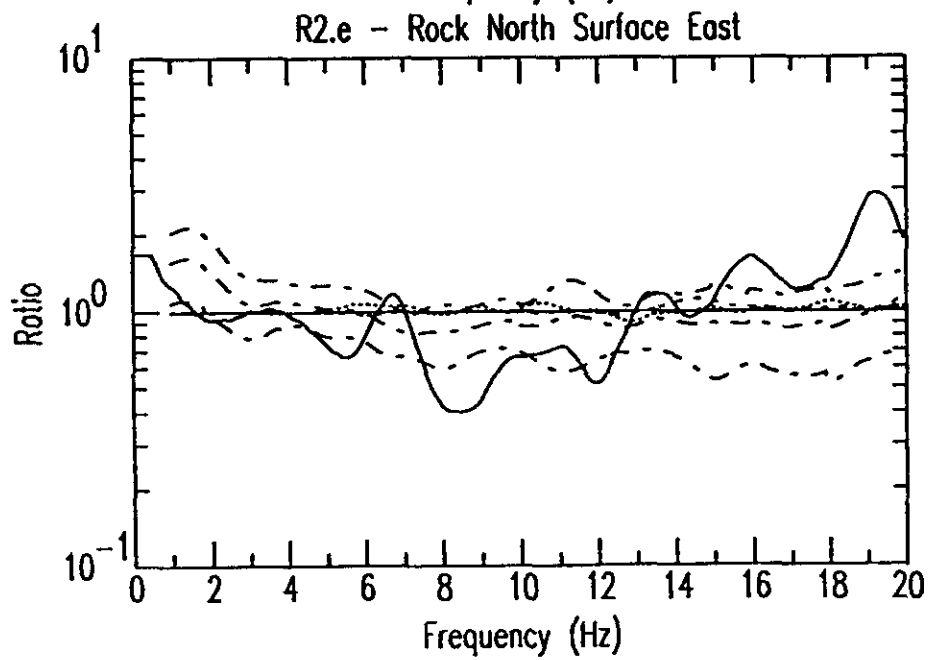

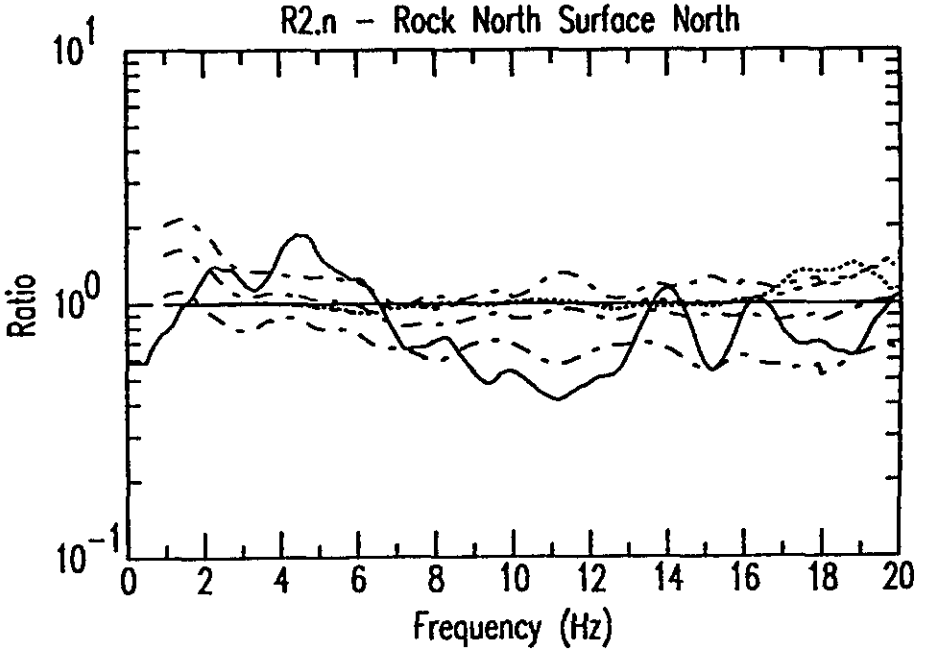

Figure G1d: R1 Preferred and Standard Response Spectra Predictions by #8 vs Observations

Response Spectra Predictions: Dashed – Standard Model; Dotted – Preferred Model

Observations: Solid – weak-motion test event

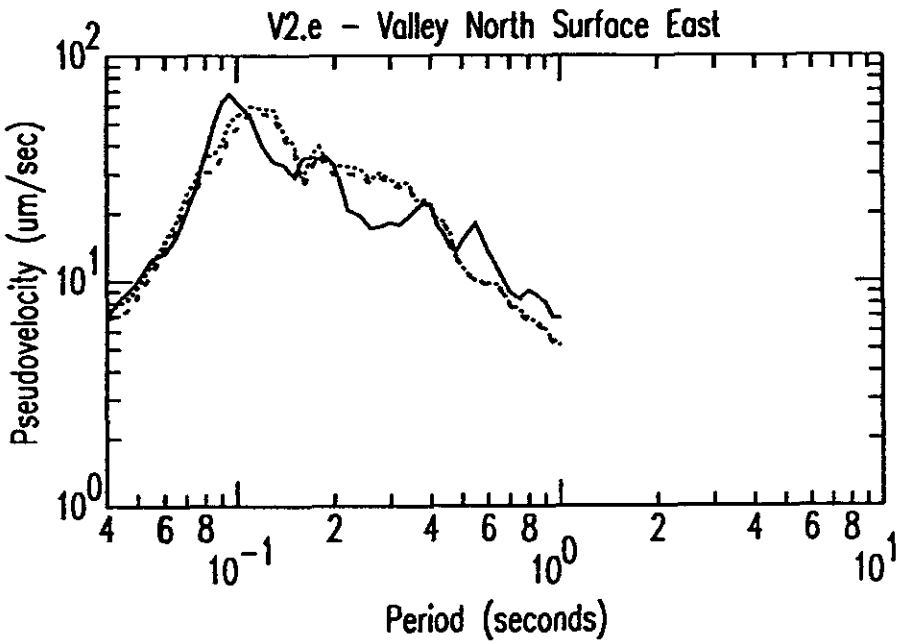

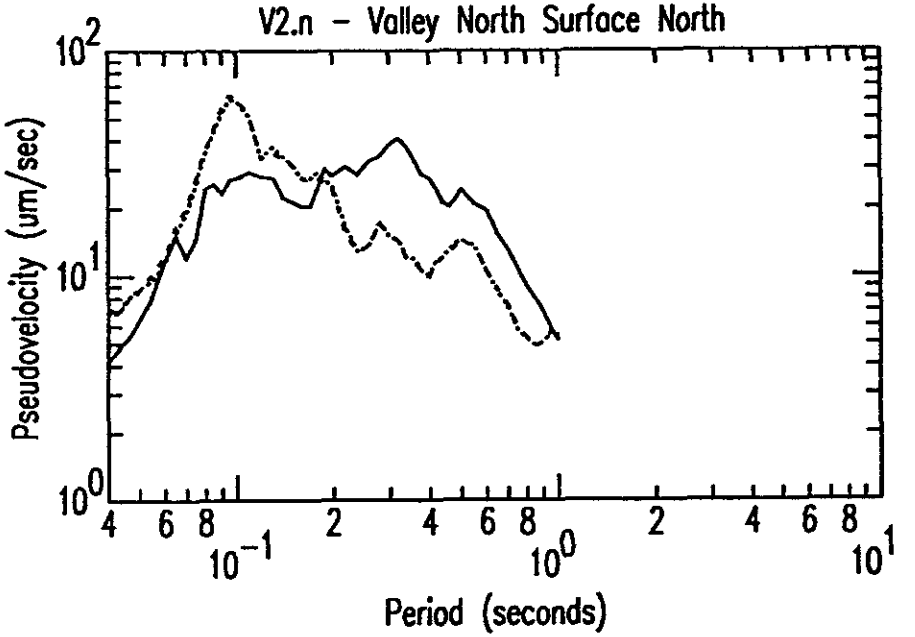

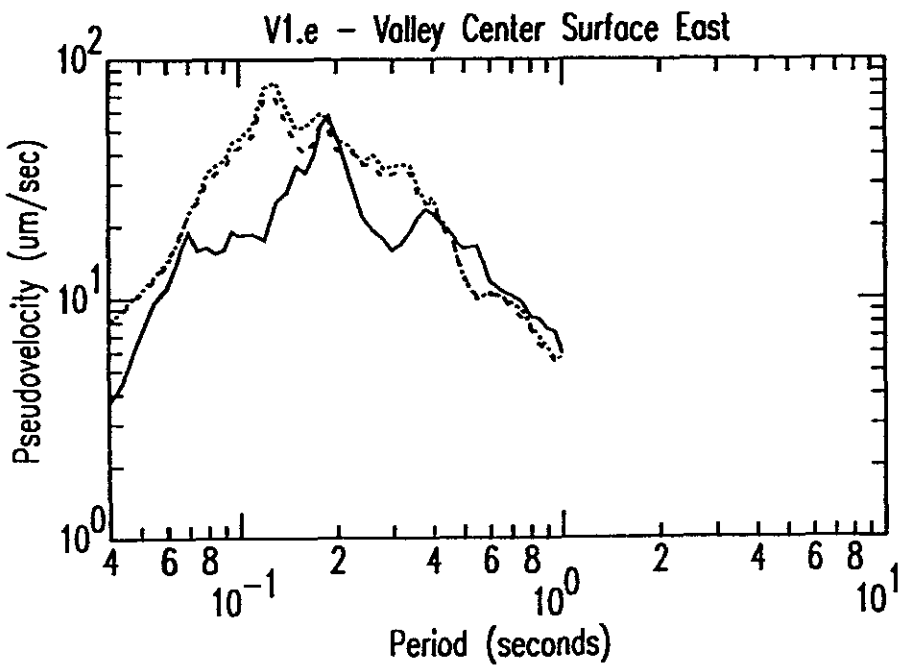

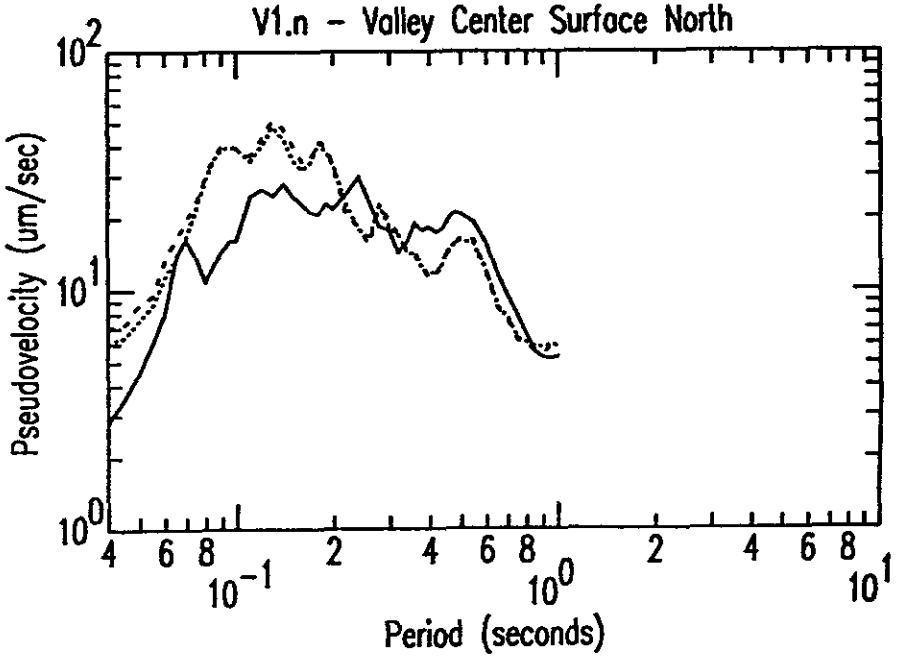

Figure G1e: R1 Preferred and Standard Response Spectra Predictions by #8 vs Observations

Response Spectra Predictions: Dashed – Standard Model; Dotted – Preferred Model

Observations: Solid – weak-motion test event

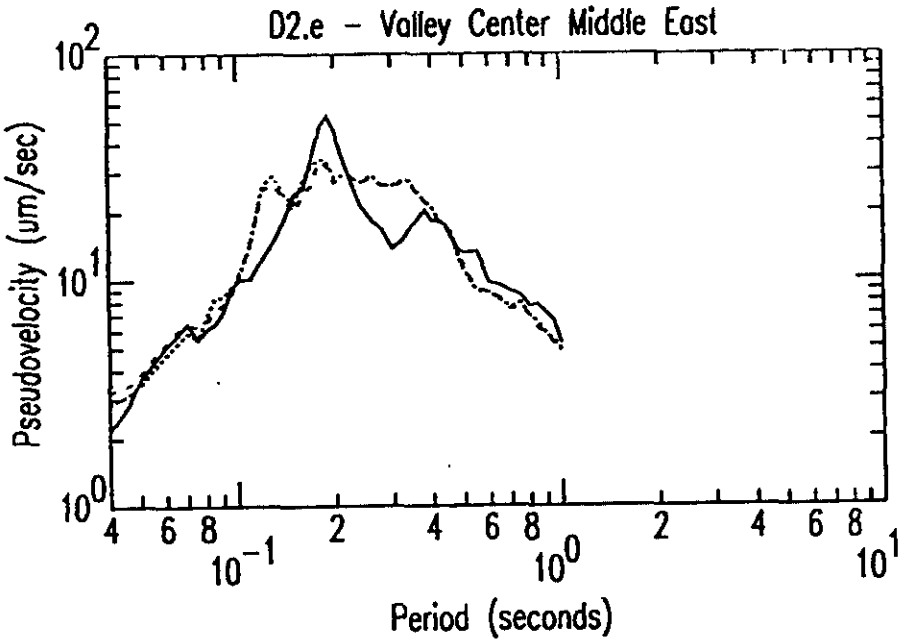

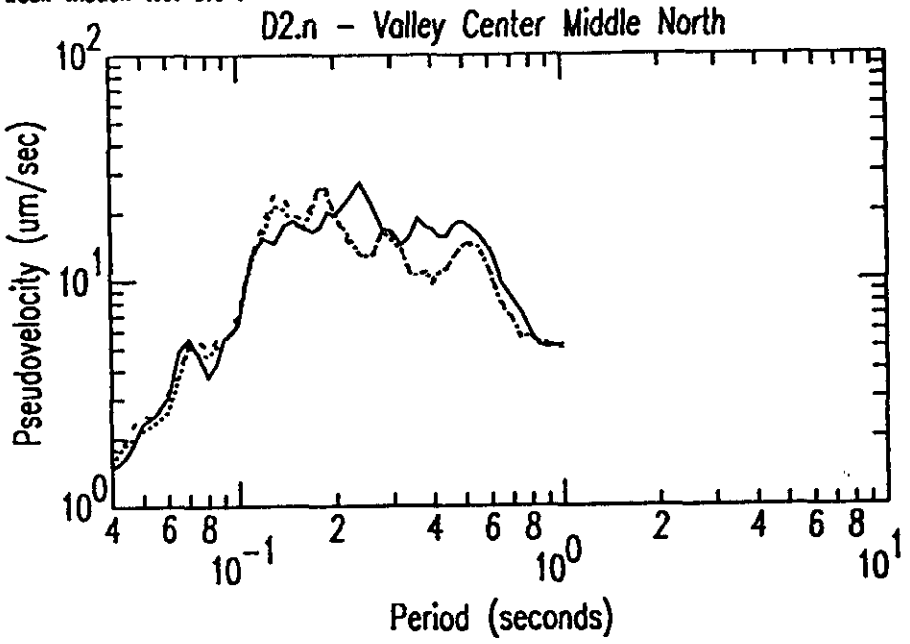

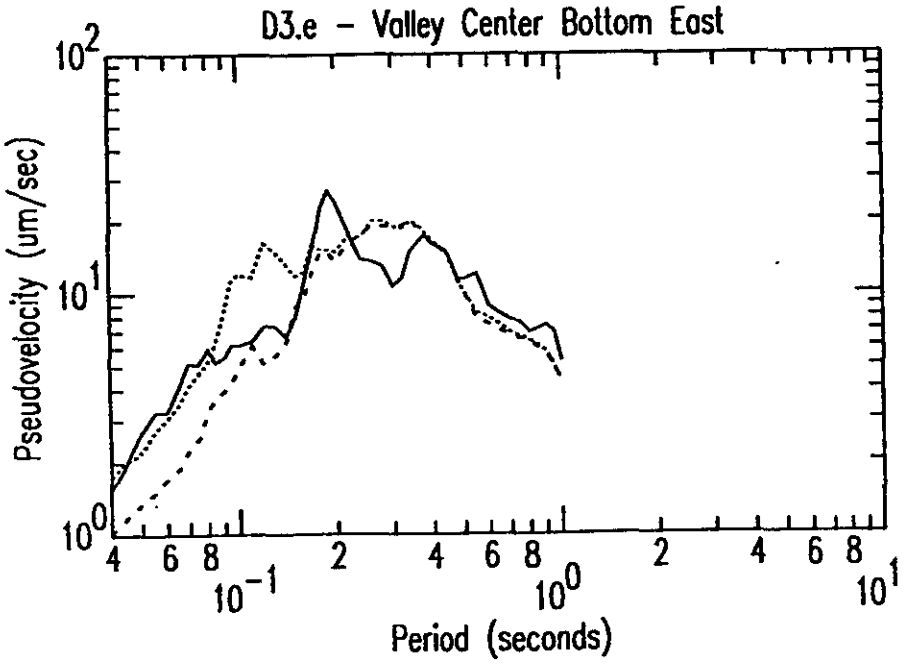

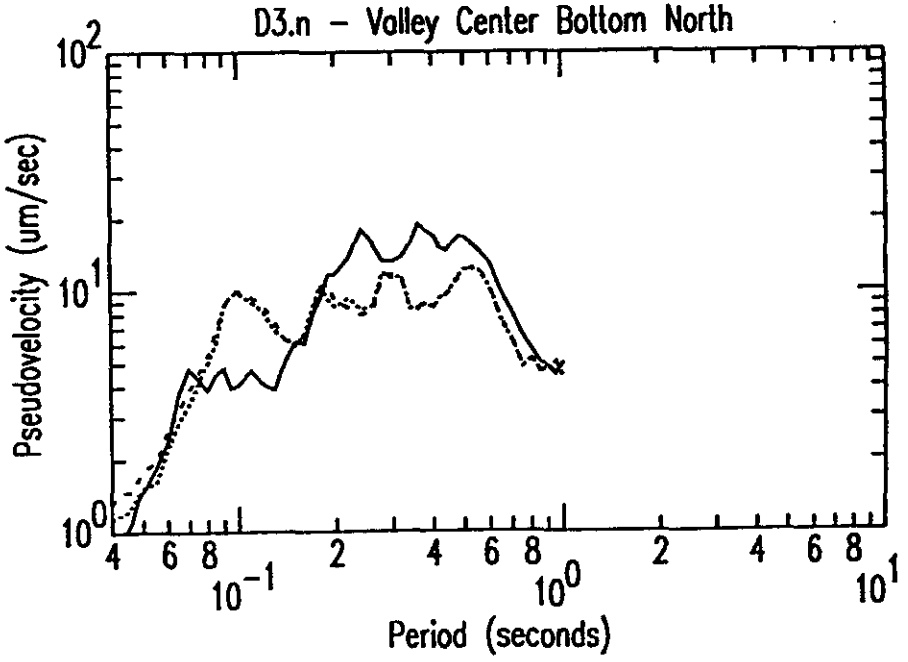

Figure G1f: R1 Preferred and Standard Response Spectra Predictions by #8 vs Observations

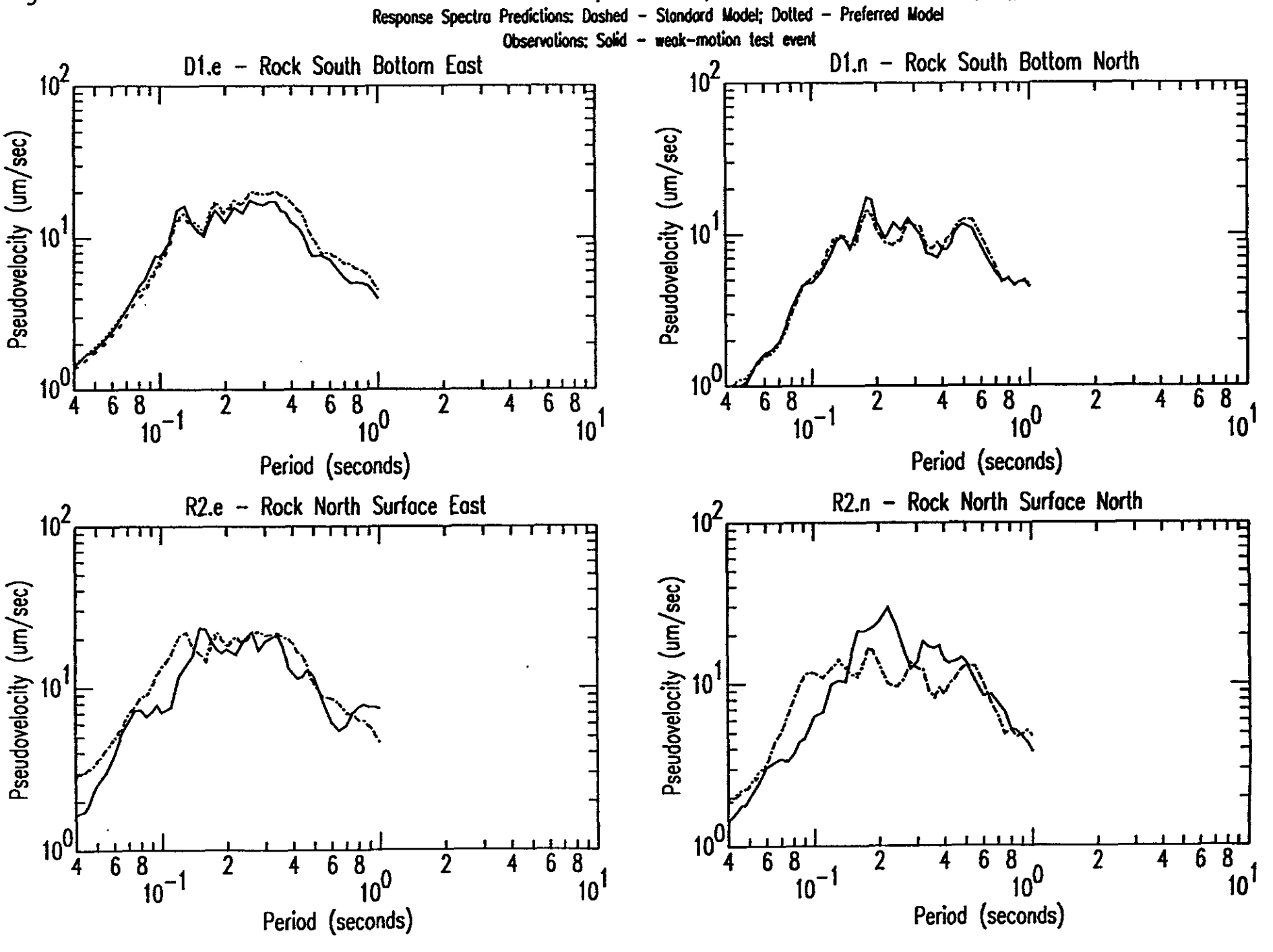

Figure G2a: R1 Preferred and Standard Spectral Ratio Predictions by #9 vs Observations

Spectral Ratio Predictions: Dashed – Standard Model; Dotted – Preferred Model

Observations: Solid – weak-motion test event; Dash-dotted – weak-motion mean and 1 std deviation

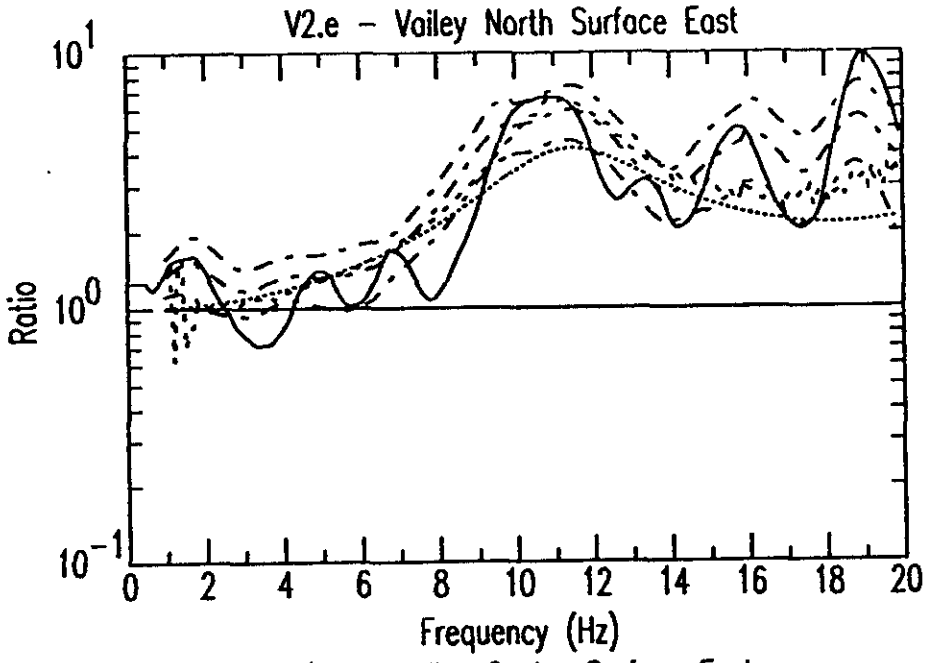

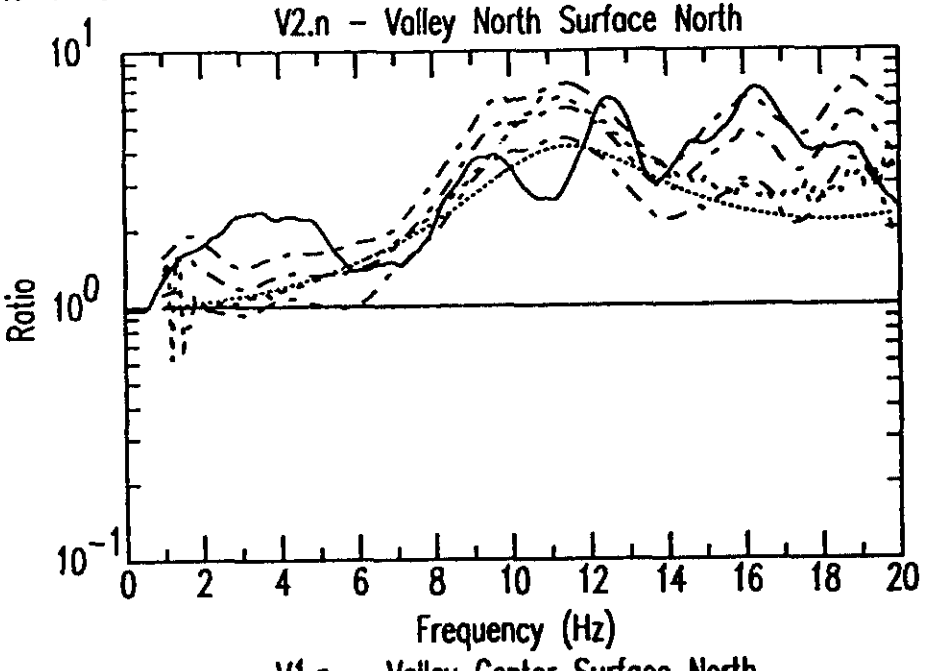

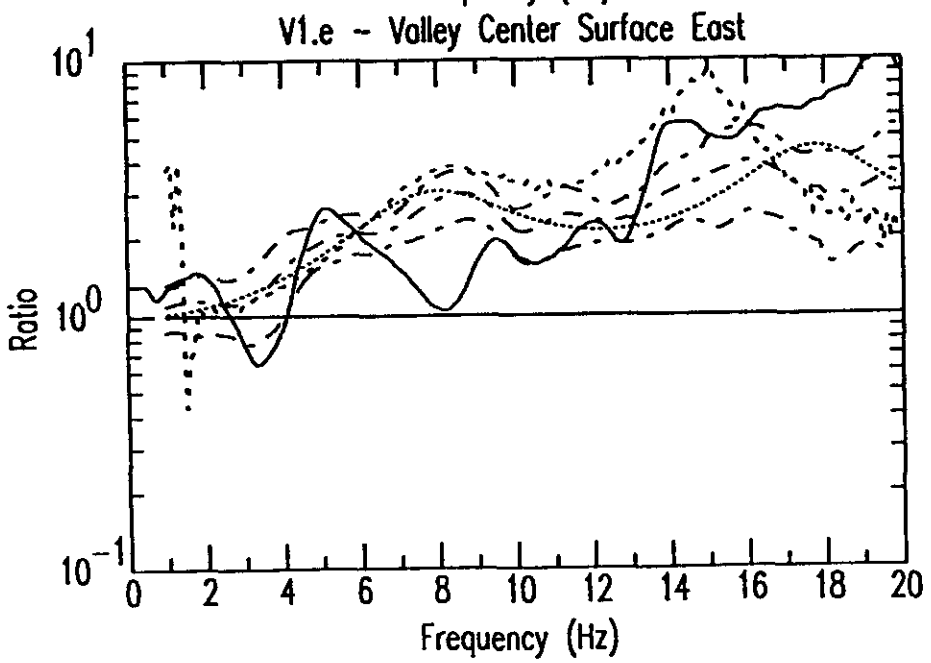

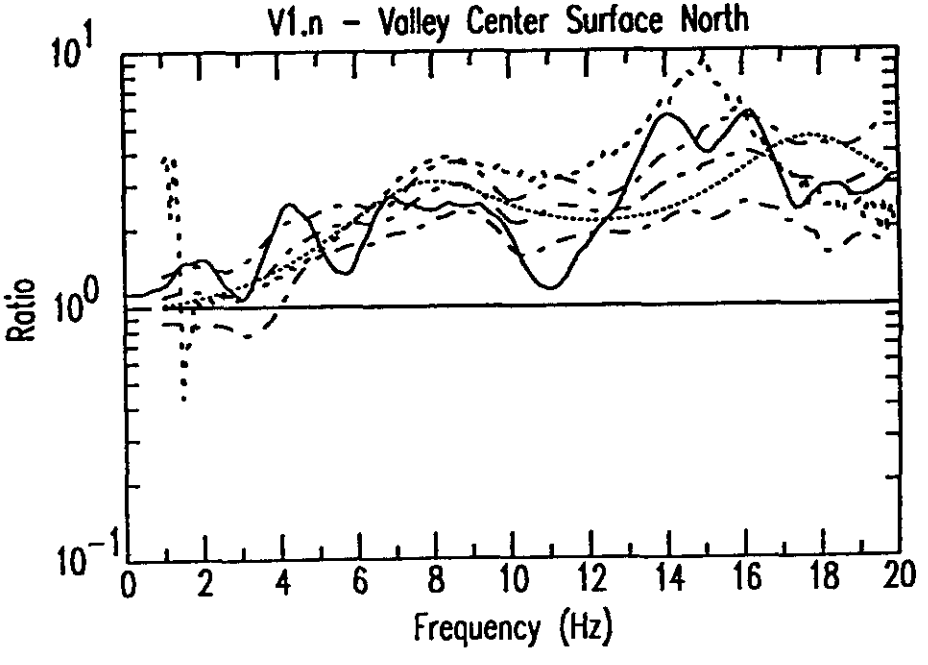

Figure G2b: R1 Preferred and Standard Spectral Ratio Predictions by #9 vs Observations

Spectral Ratio Predictions: Dashed – Standard Model; Dotted – Preferred Model

Observations: Solid – weak-motion test event; Dash-dotted – weak-motion mean and 1 std deviation

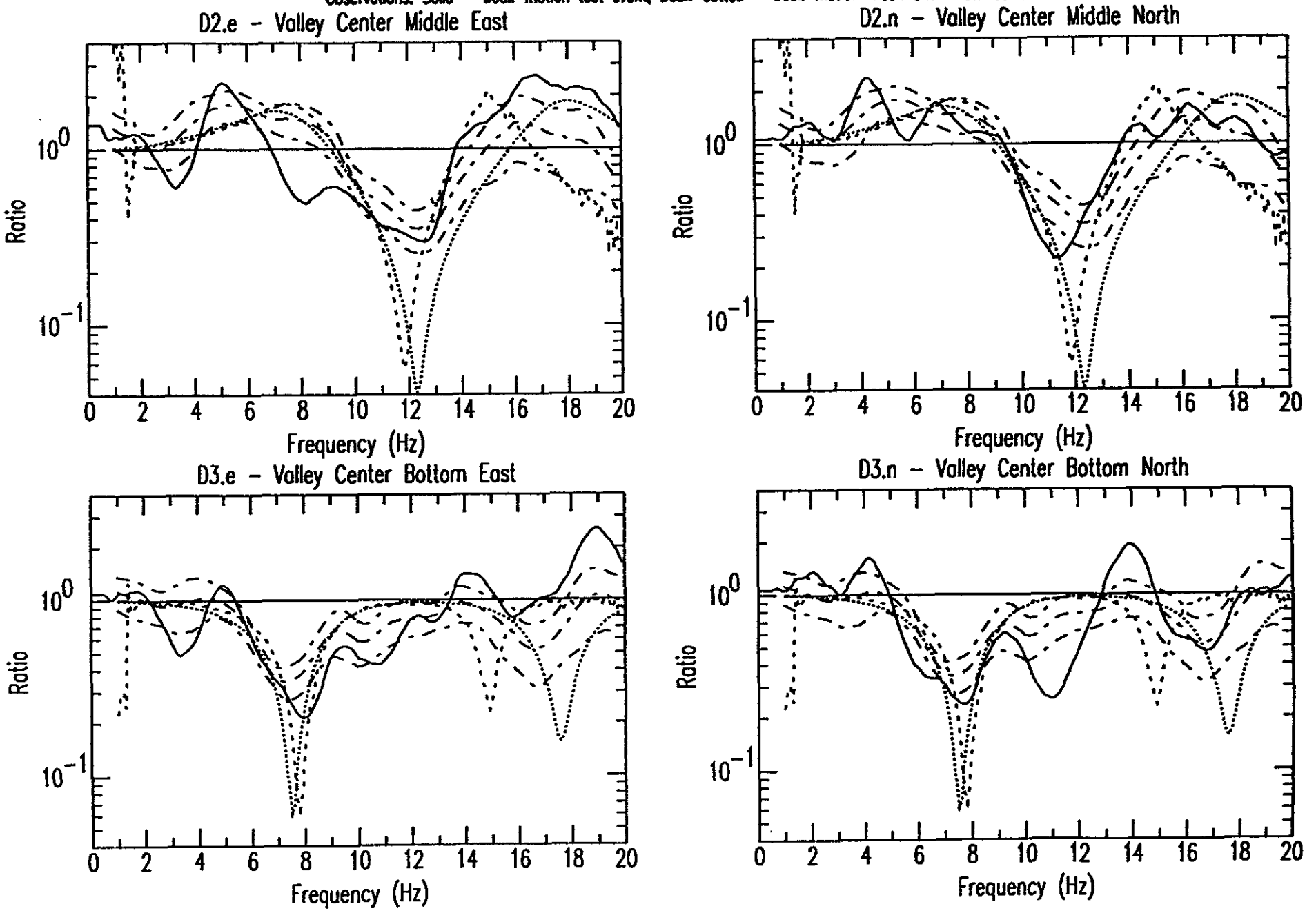

Figure G2c: R1 Preferred and Standard Spectral Ratio Predictions by #9 vs Observations

Spectral Ratio Predictions: Dashed – Standard Model; Dotted – Preferred Model

Observations: Solid – weak-motion test event; Dash-dotted – weak-motion mean and 1 std deviation

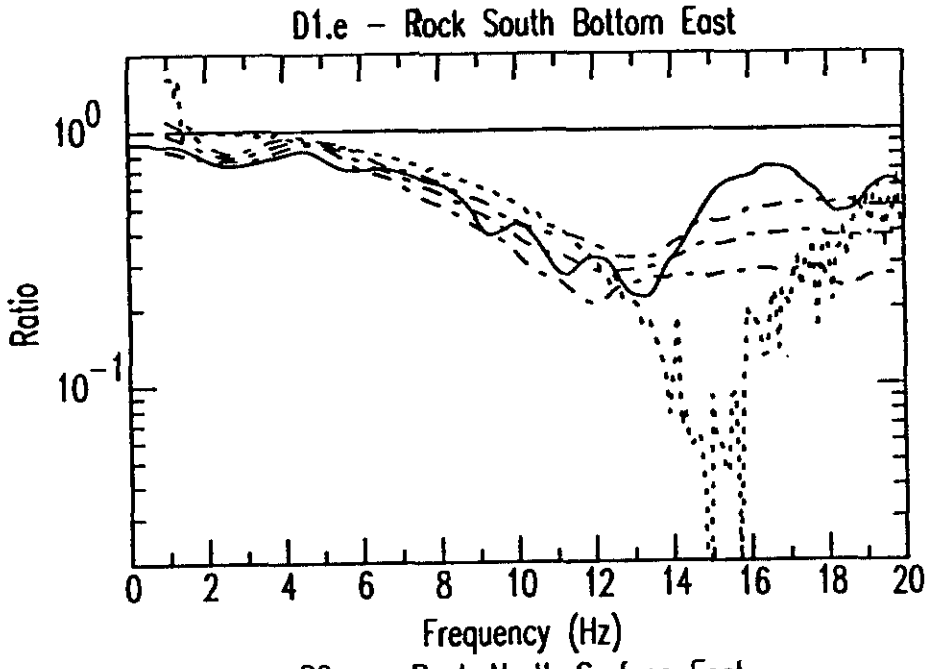

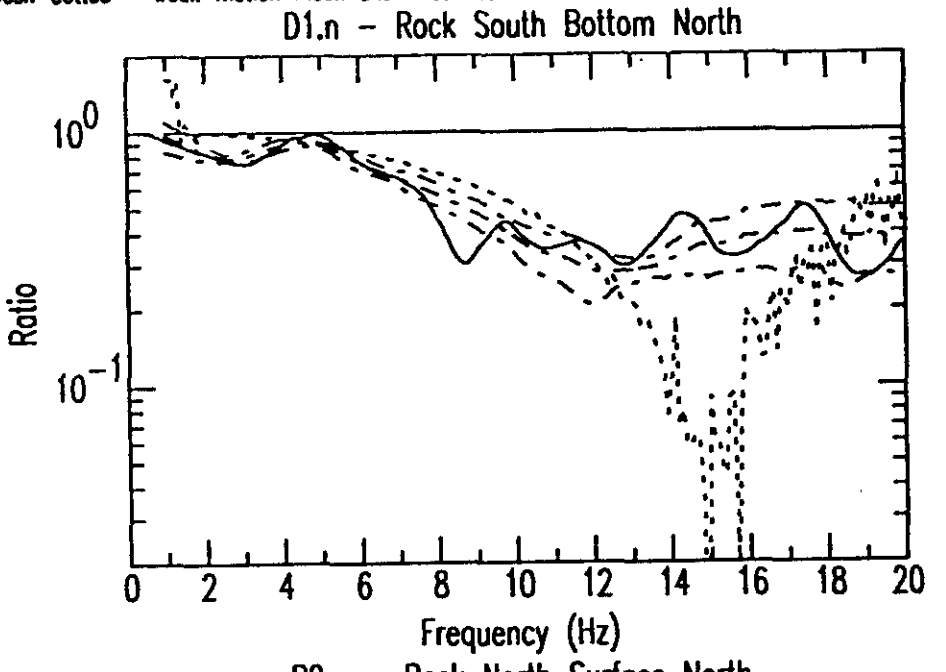

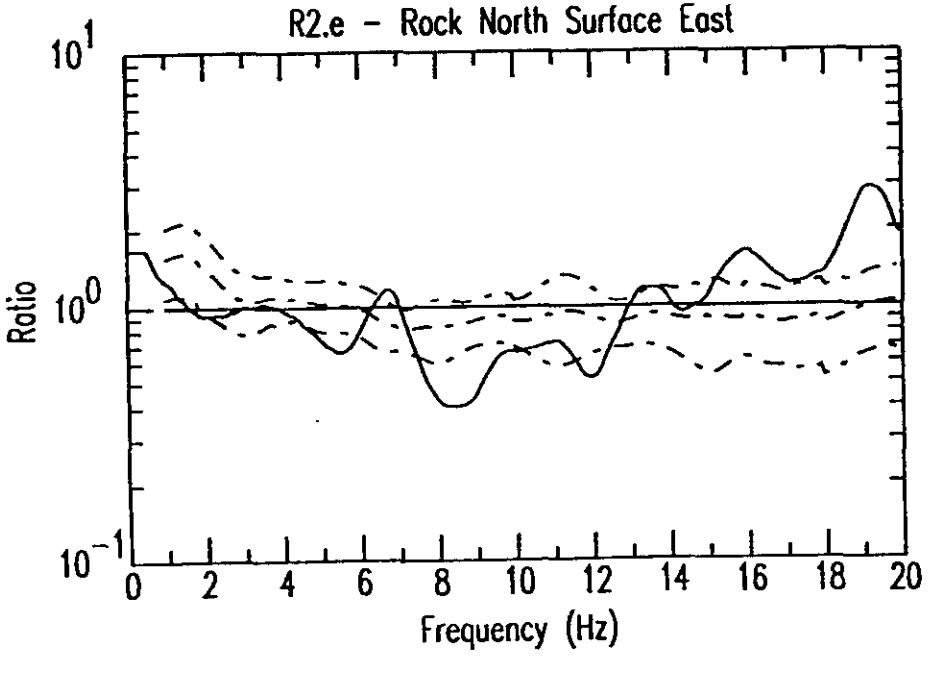

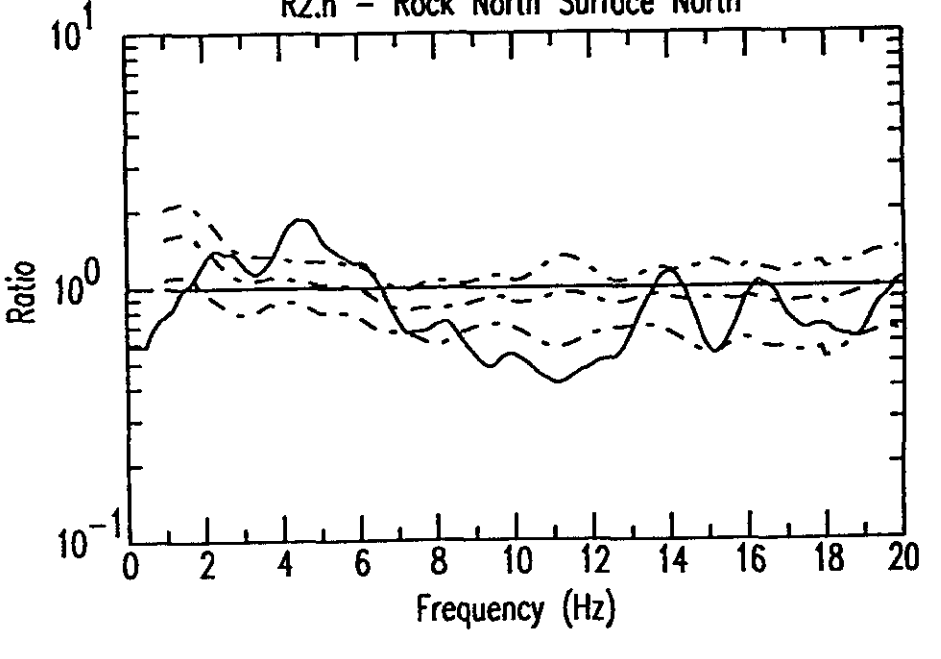

Figure G2d: R1 Preferred and Standard Response Spectra Predictions by #9 vs Observations

Response Spectra Predictions: Dashed - Standard Model; Dotted - Preferred Model

Observations: Solid - weak-motion test event

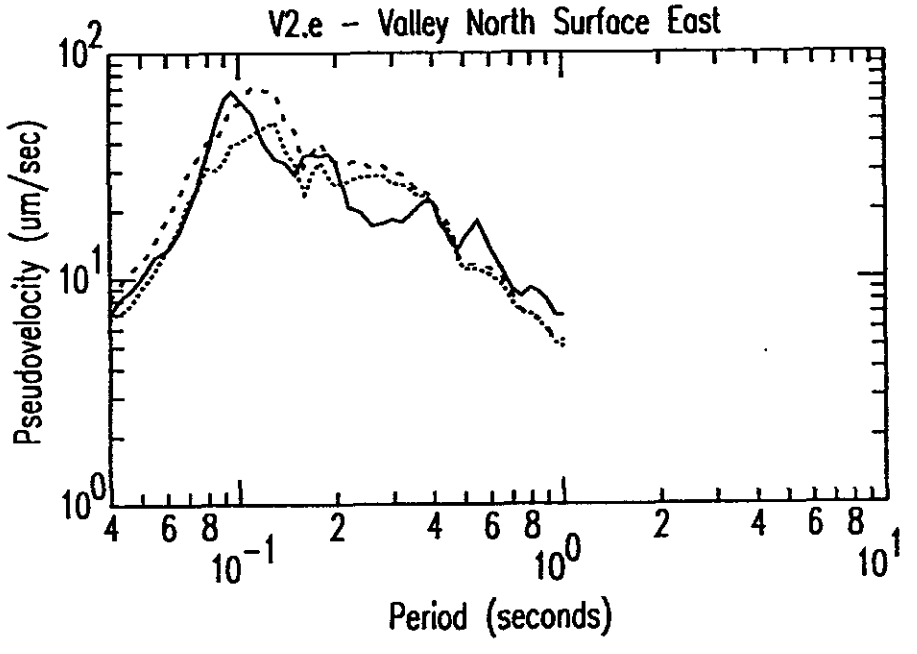

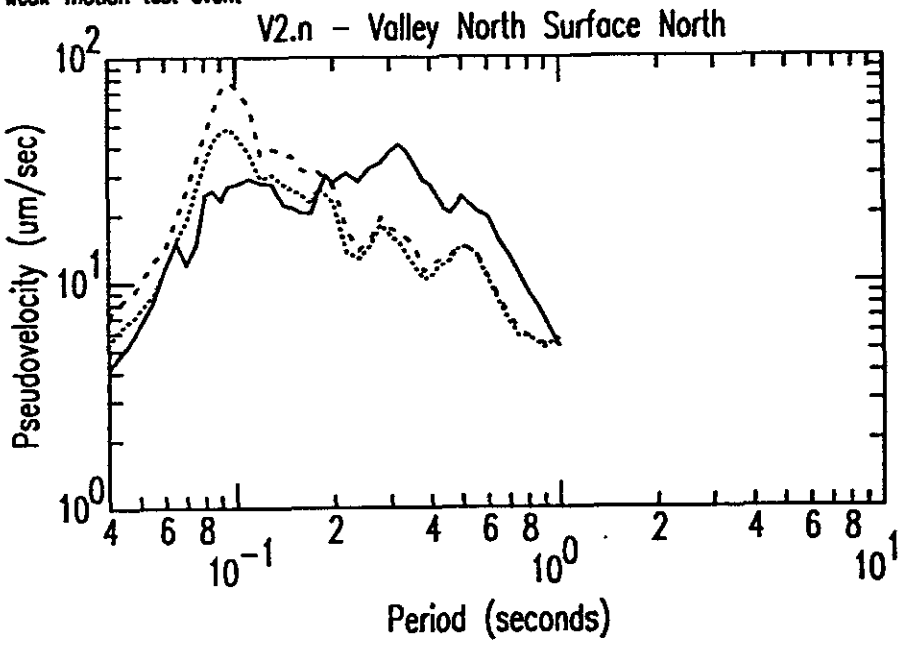

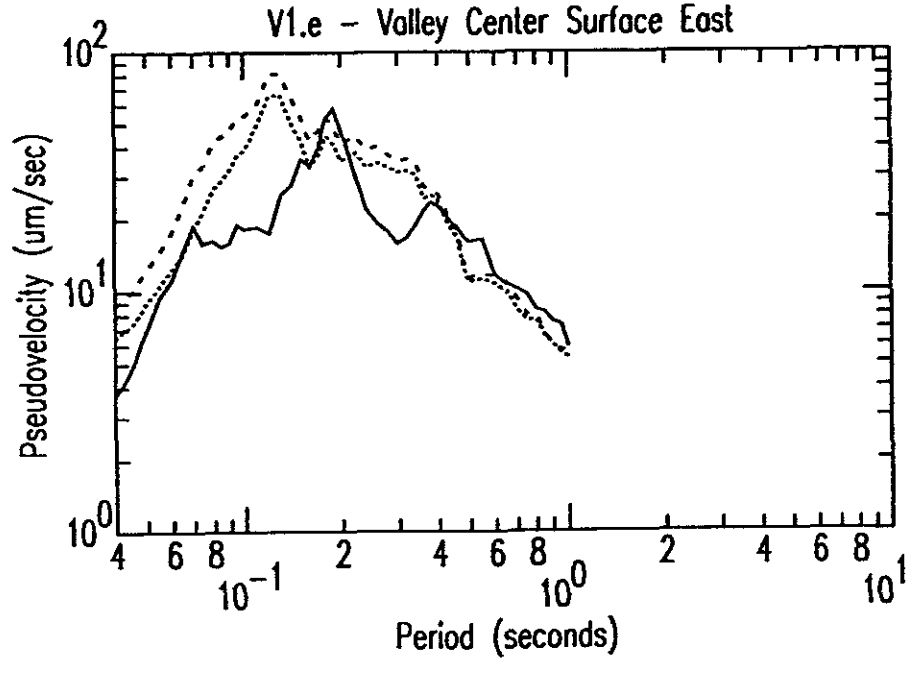

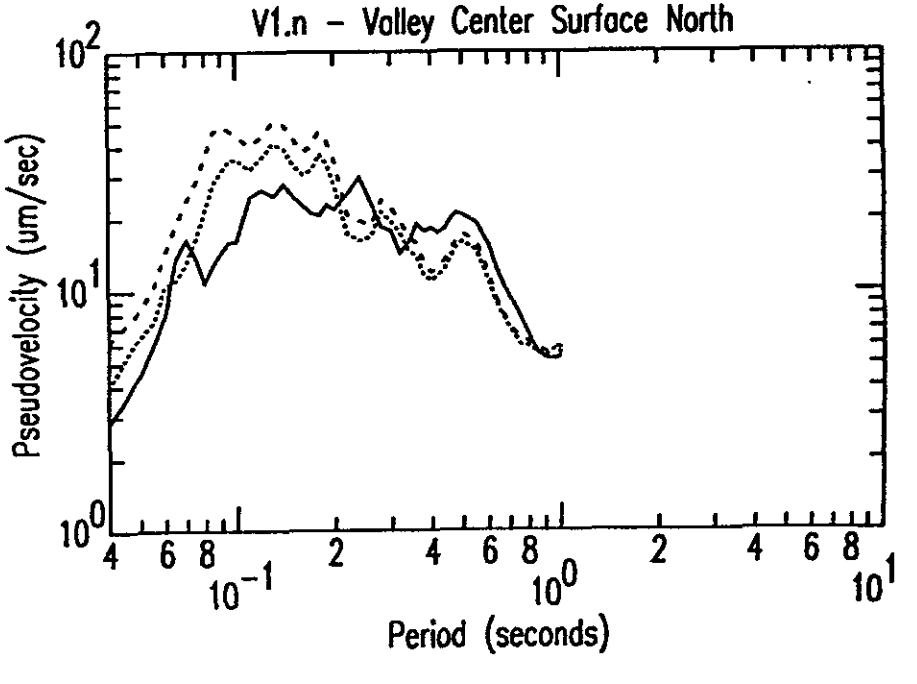

Figure G2e: R1 Preferred and Standard Response Spectra Predictions by #9 vs Observations

Response Spectra Predictions: Dashed - Standard Model; Dotted - Preferred Model

Observations: Solid - weak-motion test event

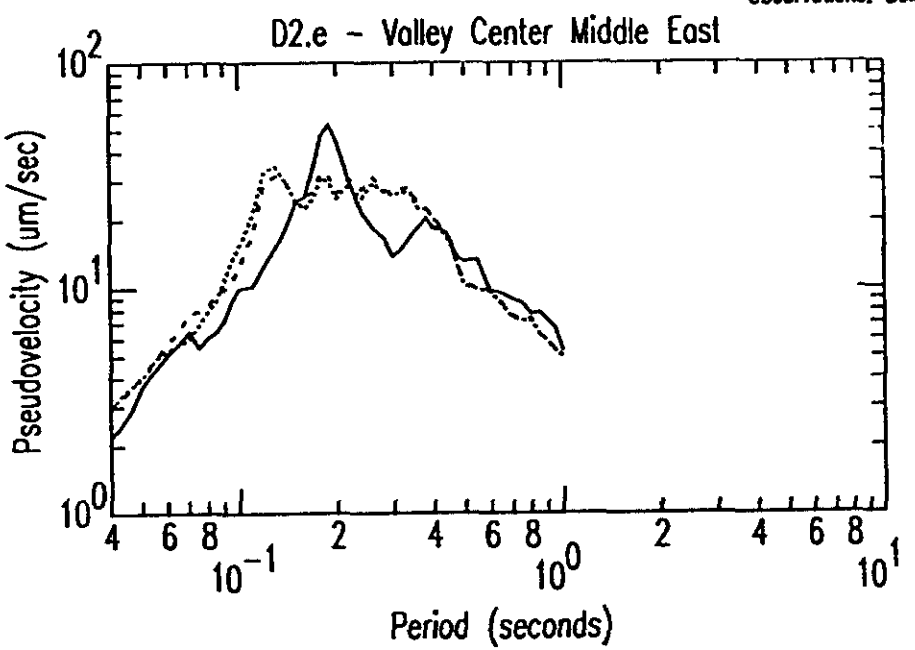

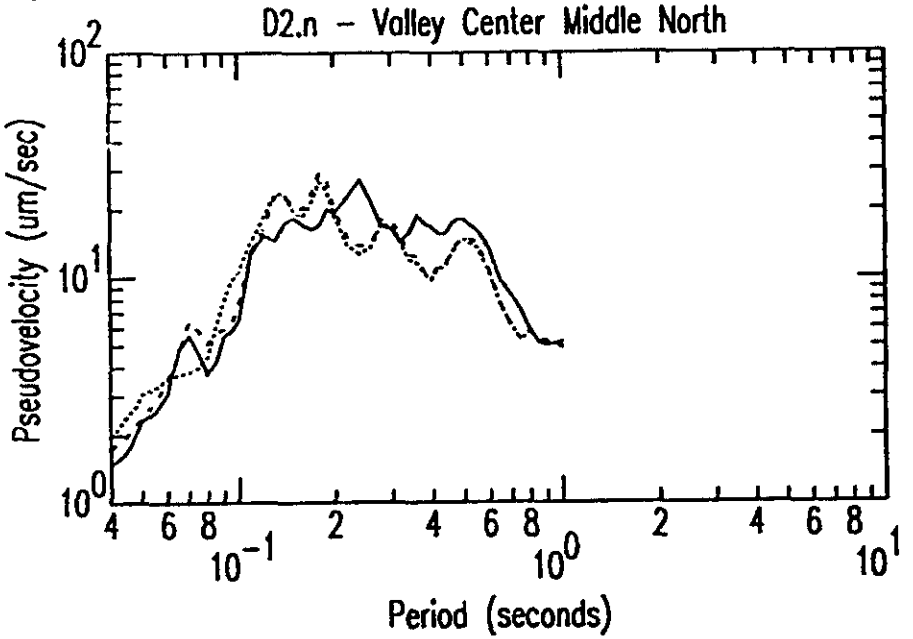

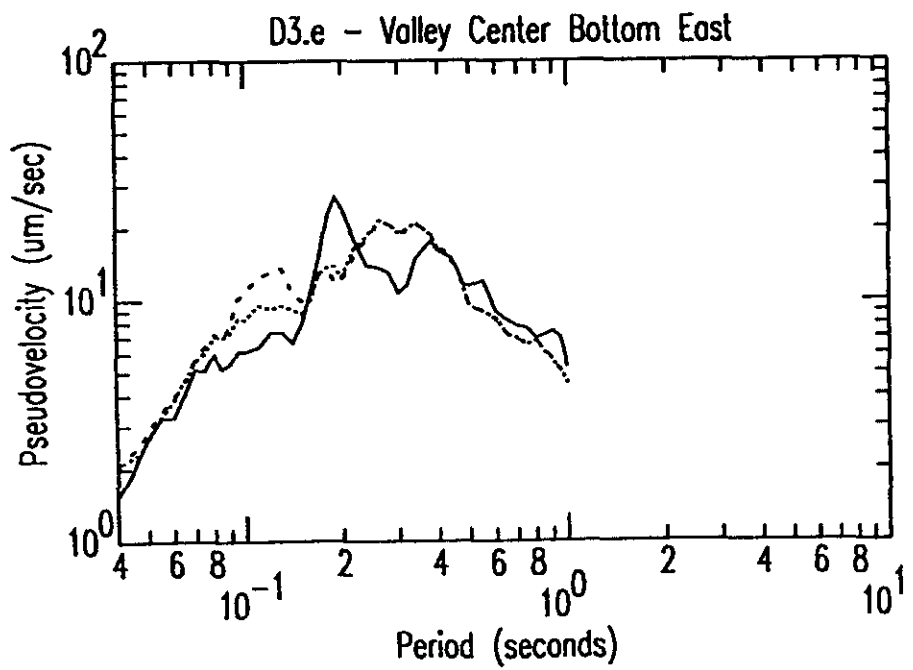

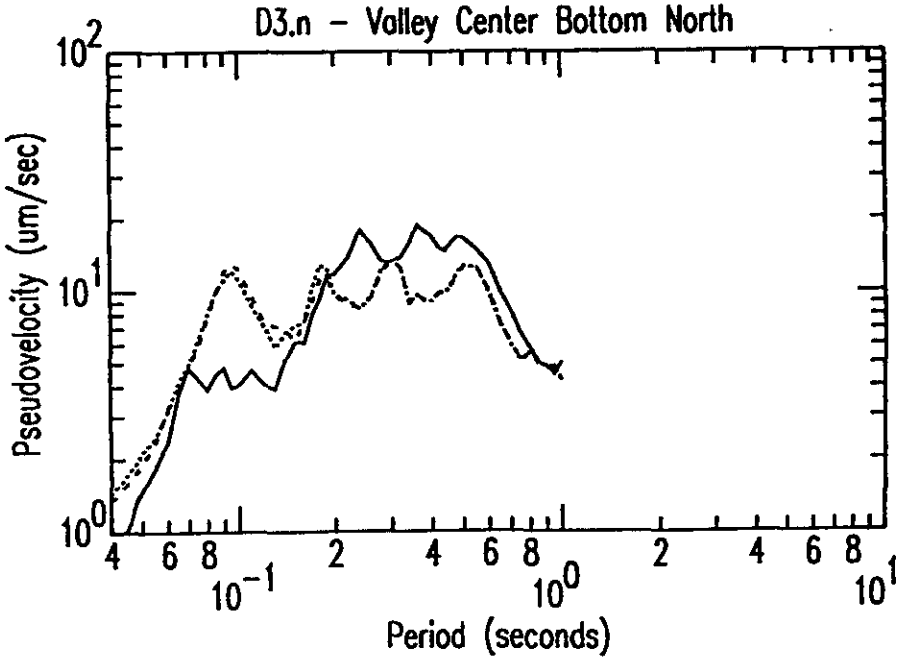

Figure G2f: R1 Preferred and Standard Response Spectra Predictions by #9 vs Observations

Response Spectra Predictions: Dashed - Standard Model; Dotted - Preferred Model

Observations: Solid - weak-motion test event

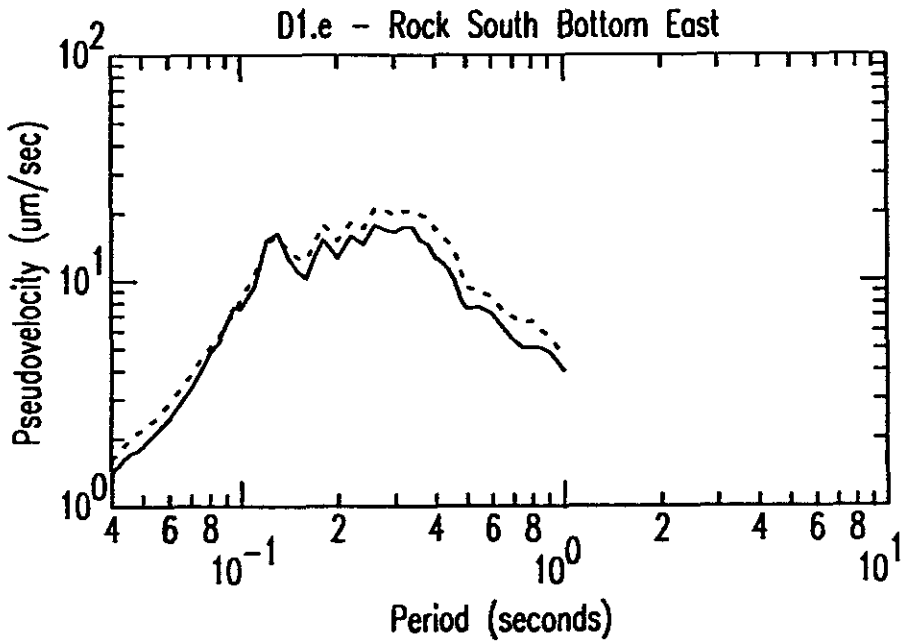

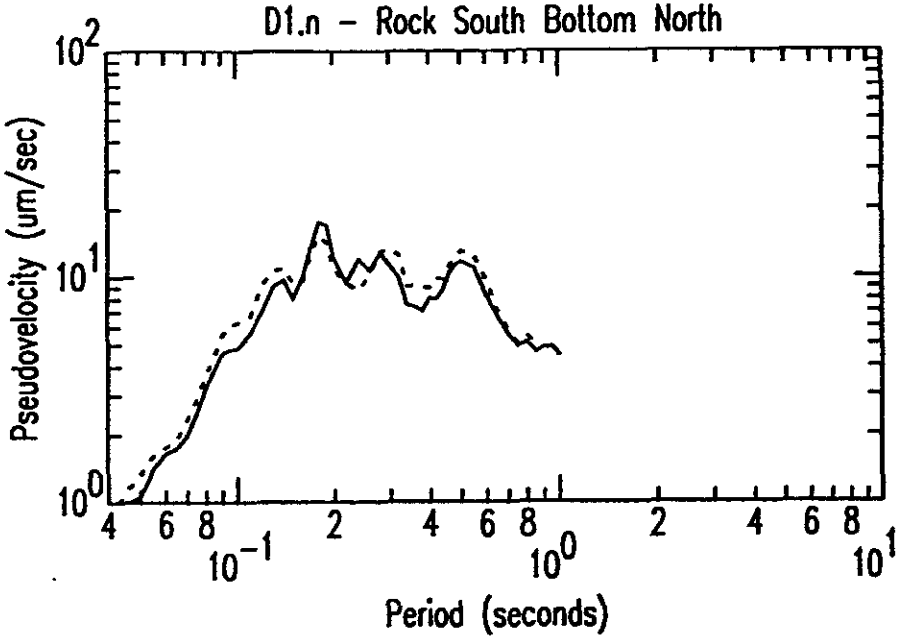

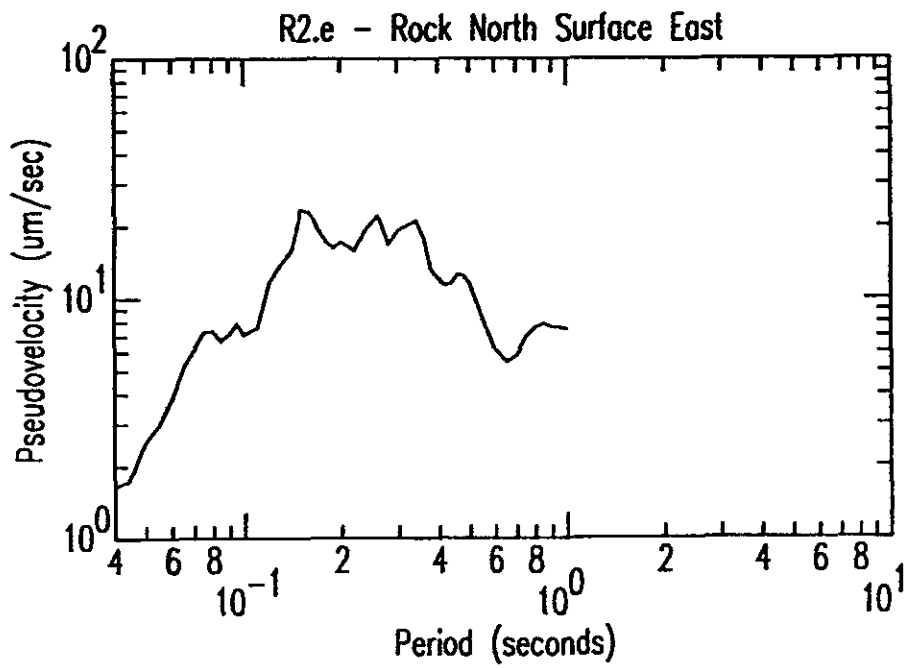

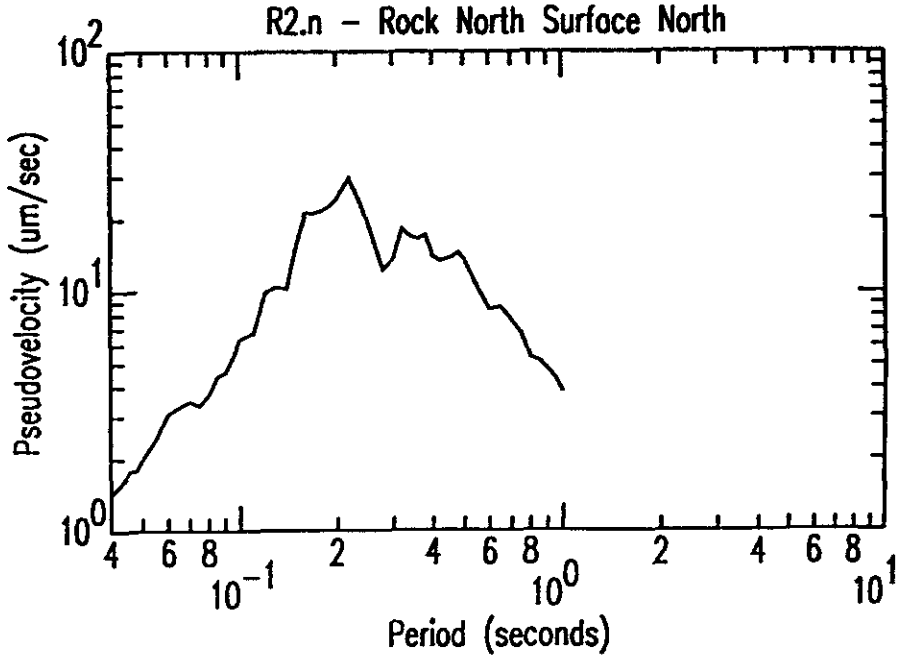

Figure G3a: R1 Preferred and Standard Spectral Ratio Predictions by #40 vs Observations

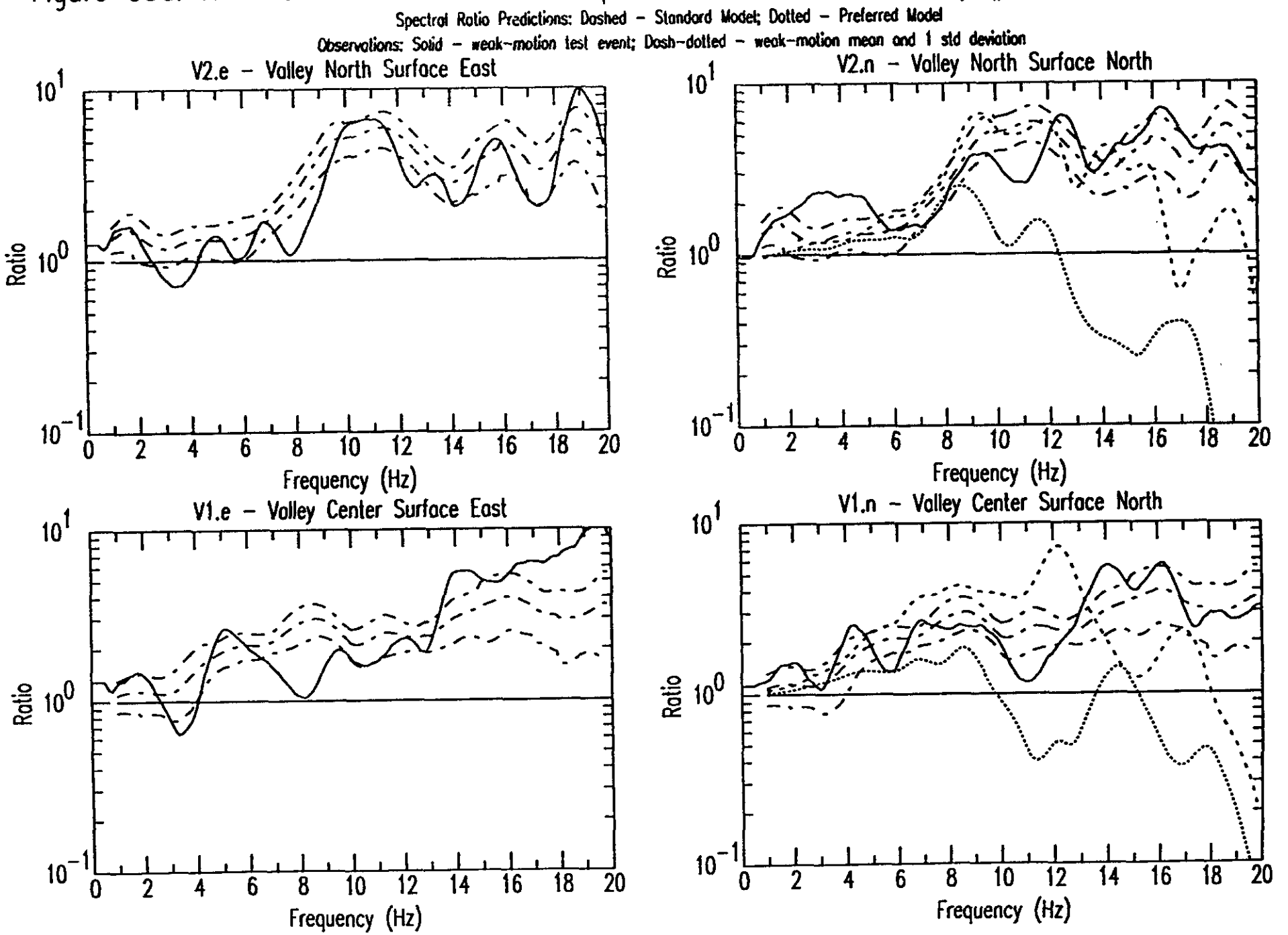

Figure G3b: R1 Preferred and Standard Spectral Ratio Predictions by #40 vs Observations

Spectral Ratio Predictions: Dashed – Standard Model; Dotted – Preferred Model

Observations: Solid – weak-motion test event; Dash-dotted – weak-motion mean and 1 std deviation

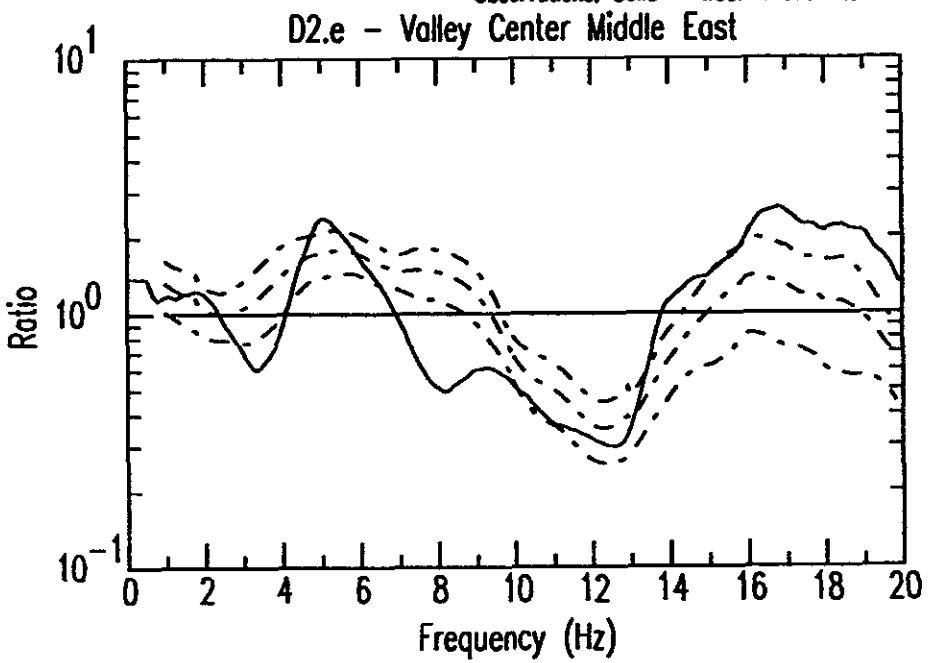

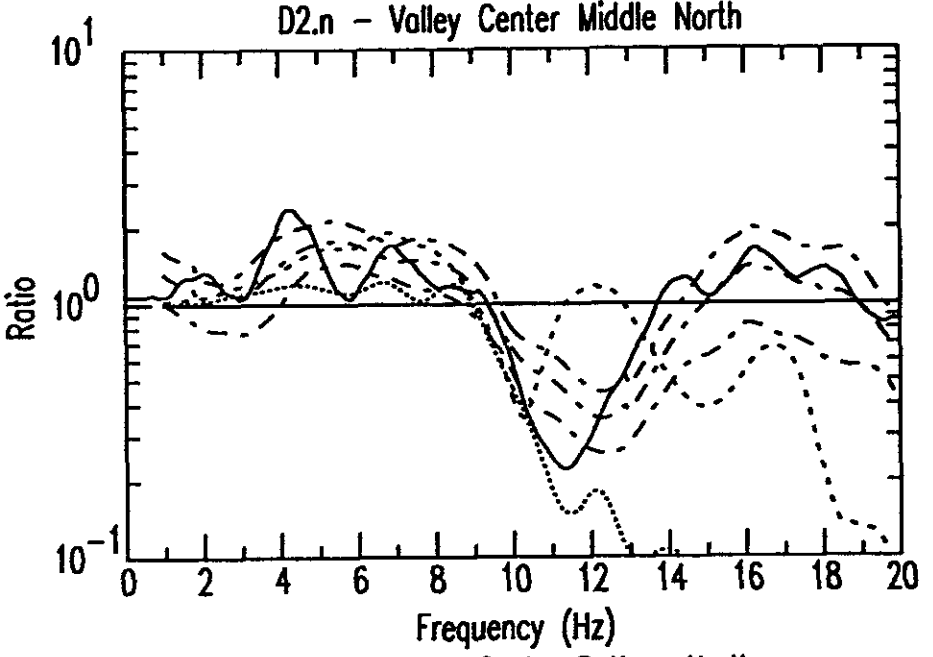

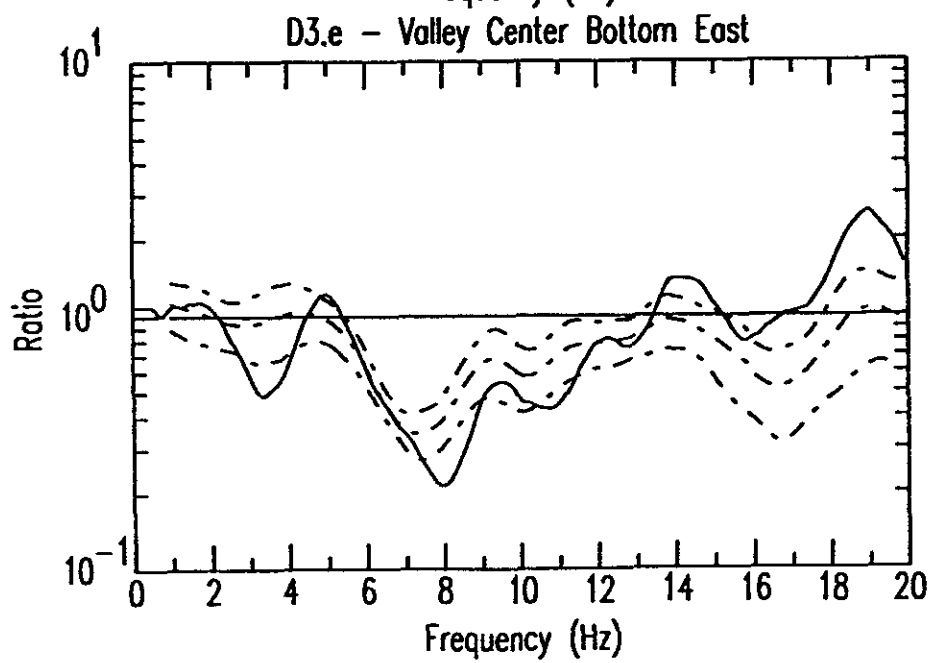

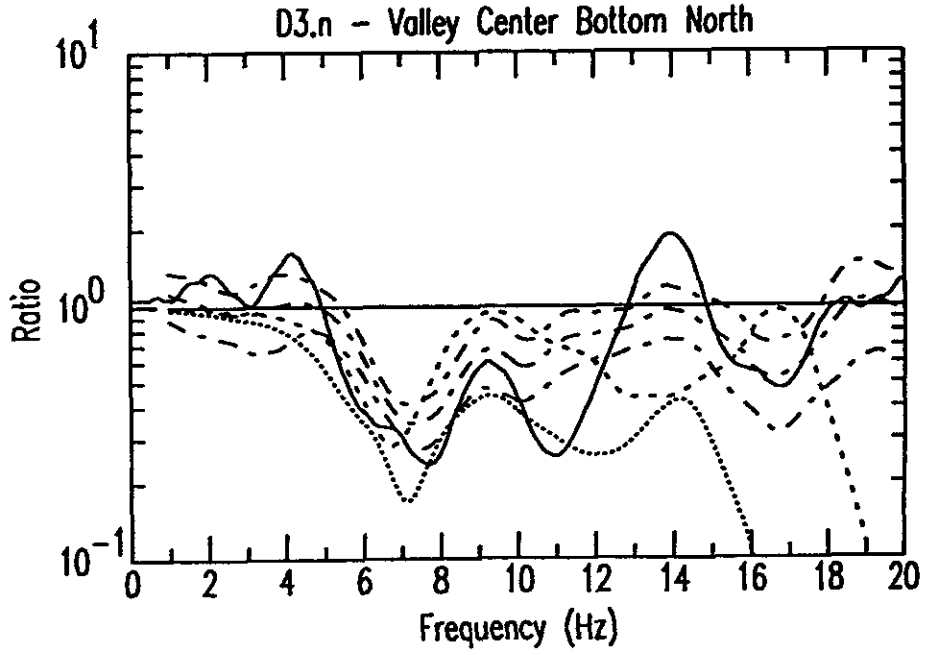

Figure G3c: R1 Preferred and Standard Spectral Ratio Predictions by #40 vs Observations

Spectral Ratio Predictions: Dashed - Standard Model; Dotted - Preferred Model

Observations: Solid - weak-motion test event; Dash-dotted - weak-motion mean and 1 std deviation

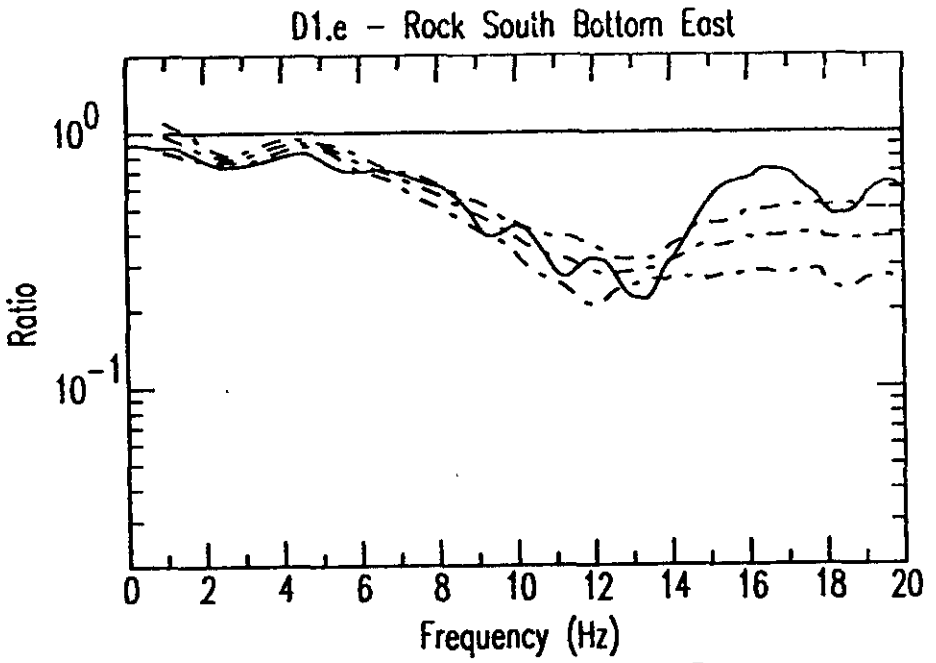

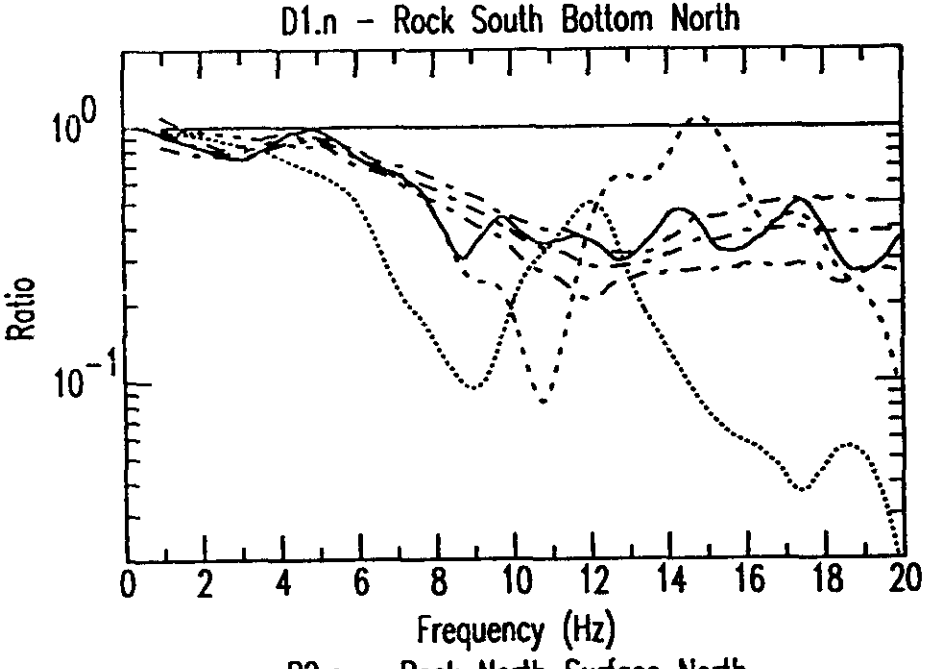

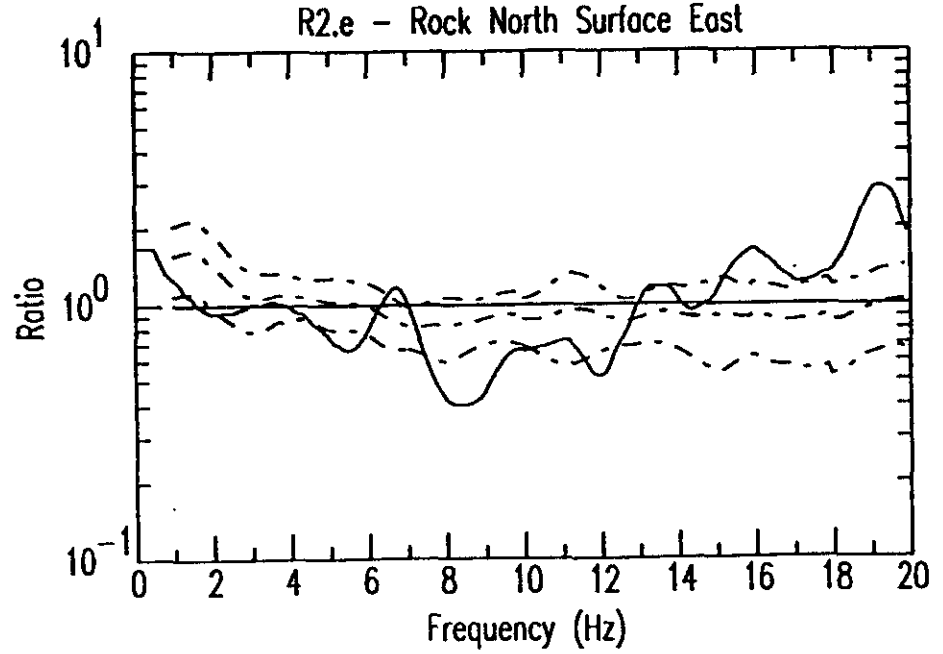

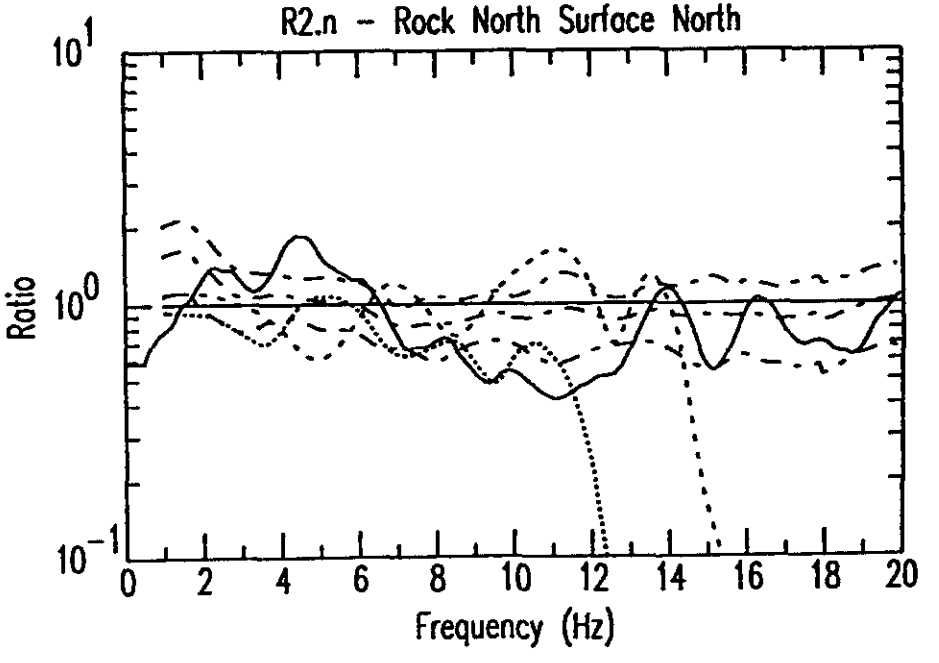

Figure G3d: R1 Preferred and Standard Response Spectra Predictions by #40 vs Observations

Response Spectra Predictions: Dashed - Standard Model; Dotted - Preferred Model

Observations: Solid - weak-motion test event

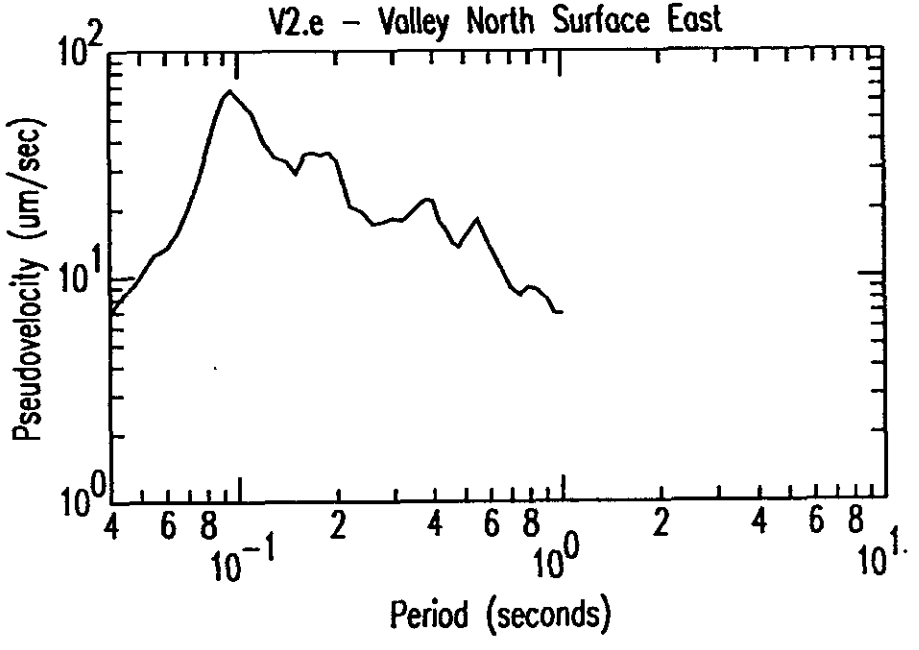

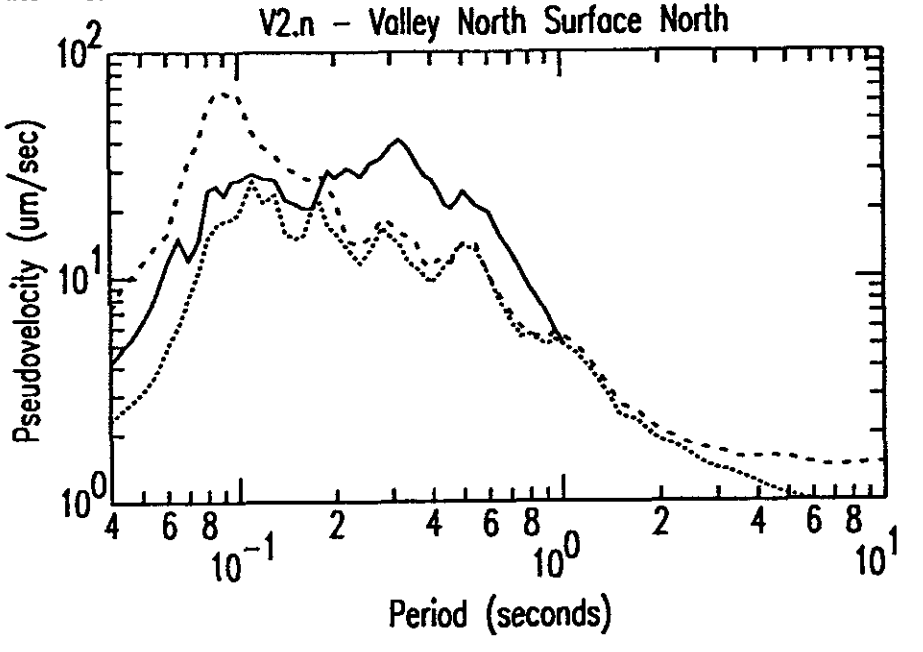

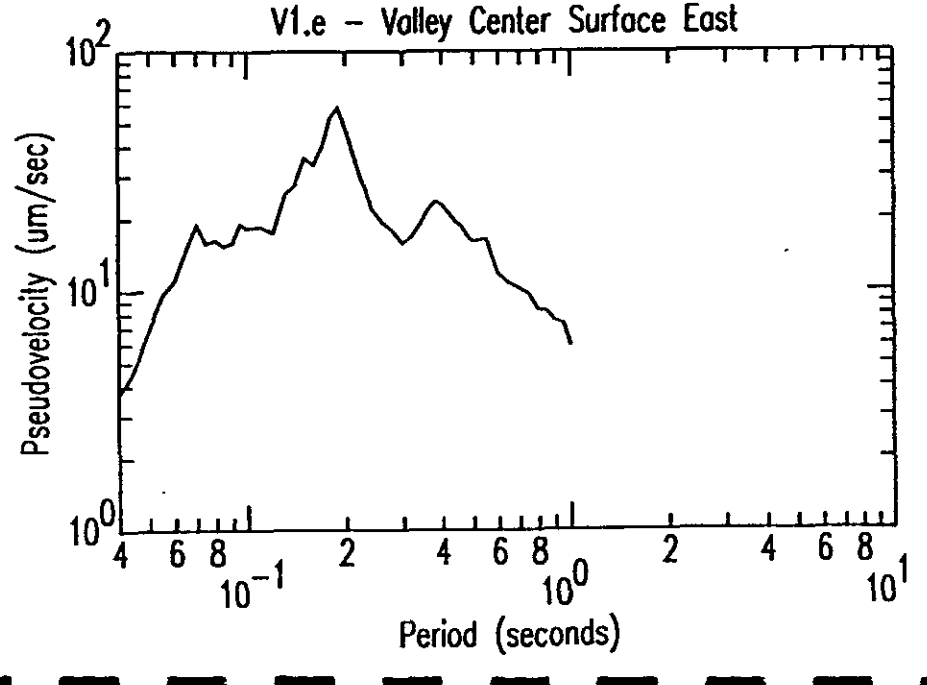

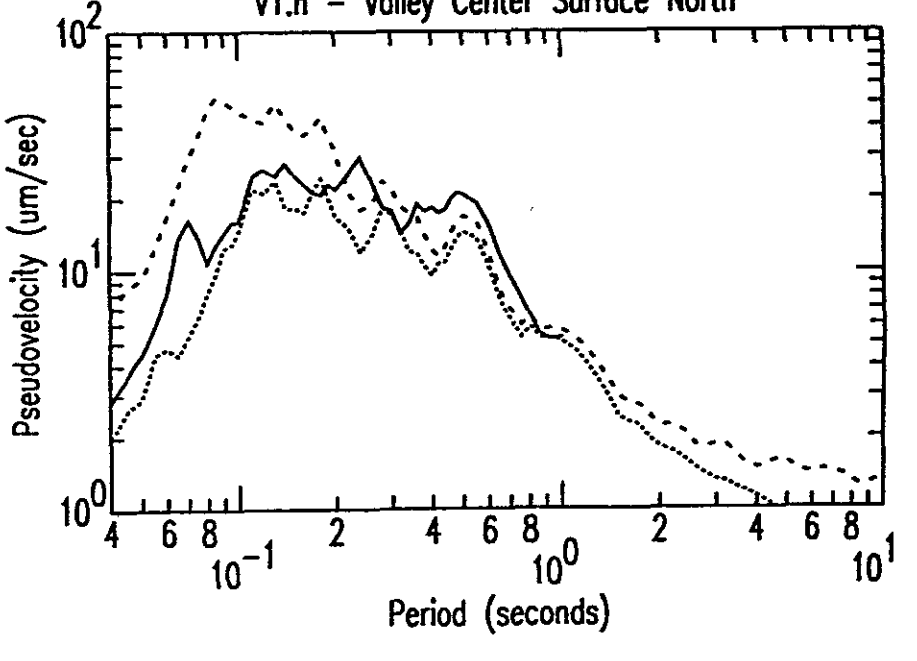

Figure G3e: R1 Preferred and Standard Response Spectra Predictions by #40 vs Observations

Response Spectra Predictions: Dashed - Standard Model; Dotted - Preferred Model
Observations: Solid - weak-motion test event

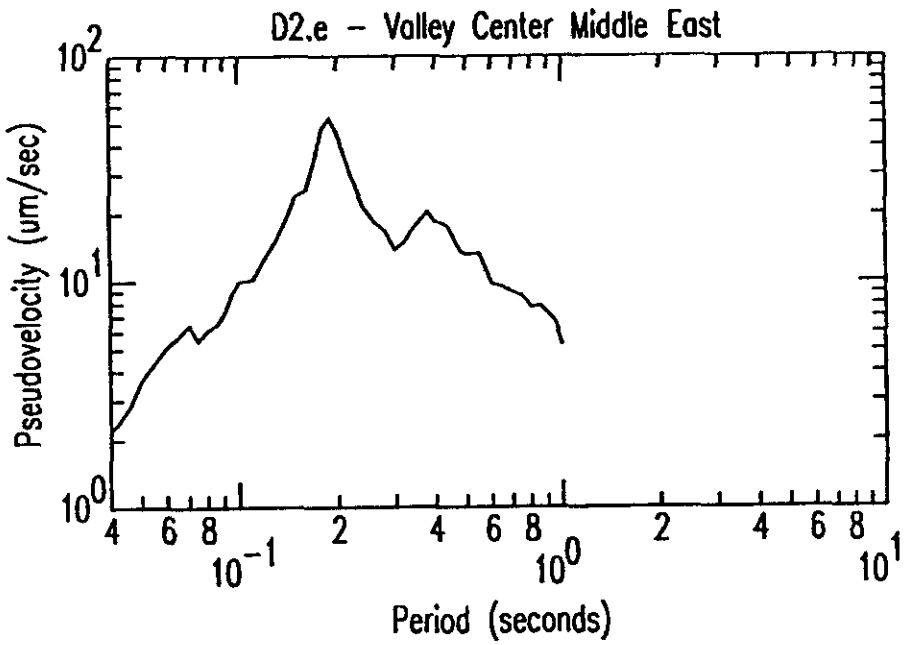

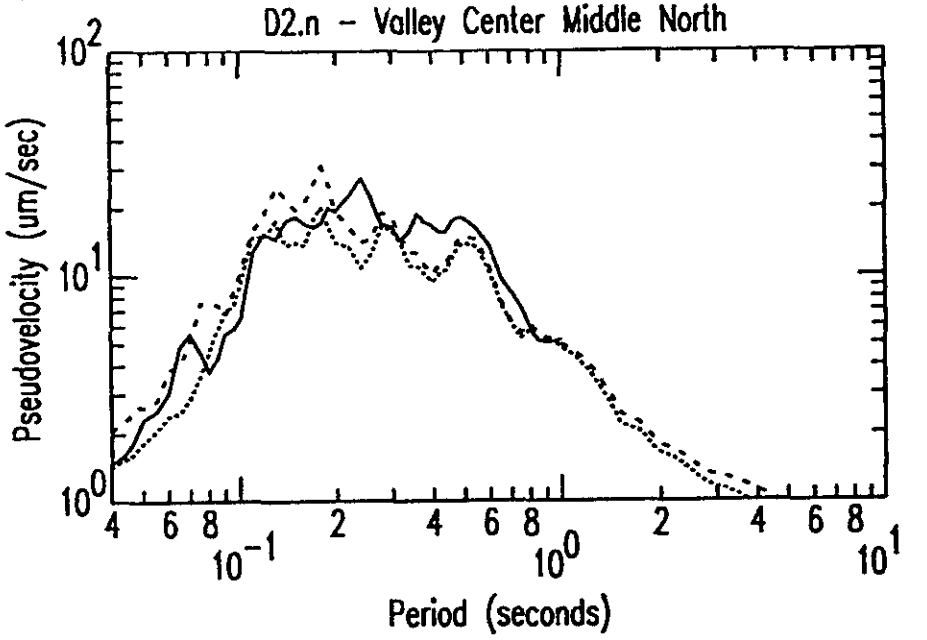

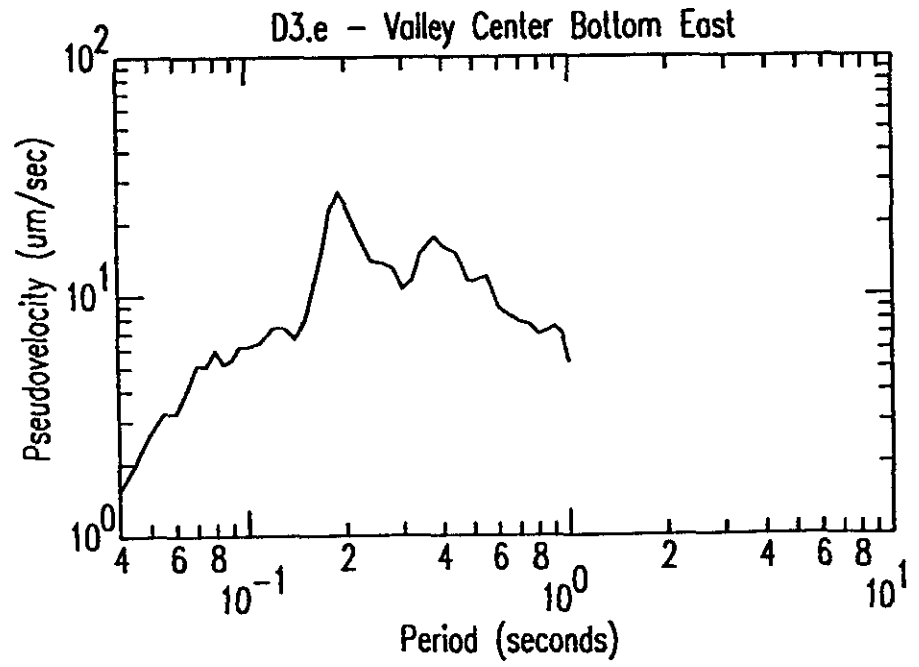

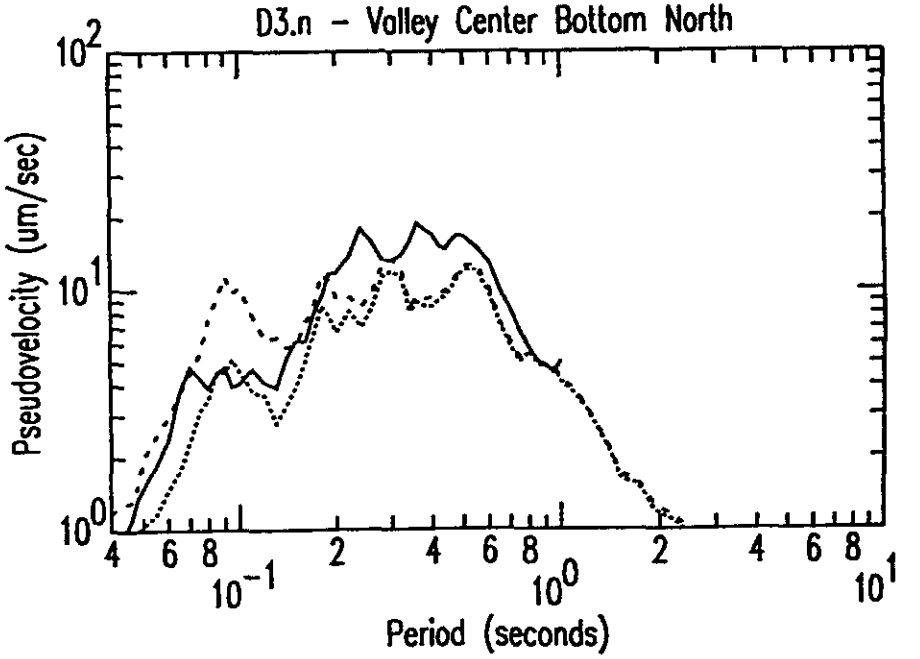

Figure G3f: R1 Preferred and Standard Response Spectra Predictions by #40 vs Observations

Response Spectra Predictions: Dashed - Standard Model; Dotted - Preferred Model

Observations: Solid - weak-motion test event

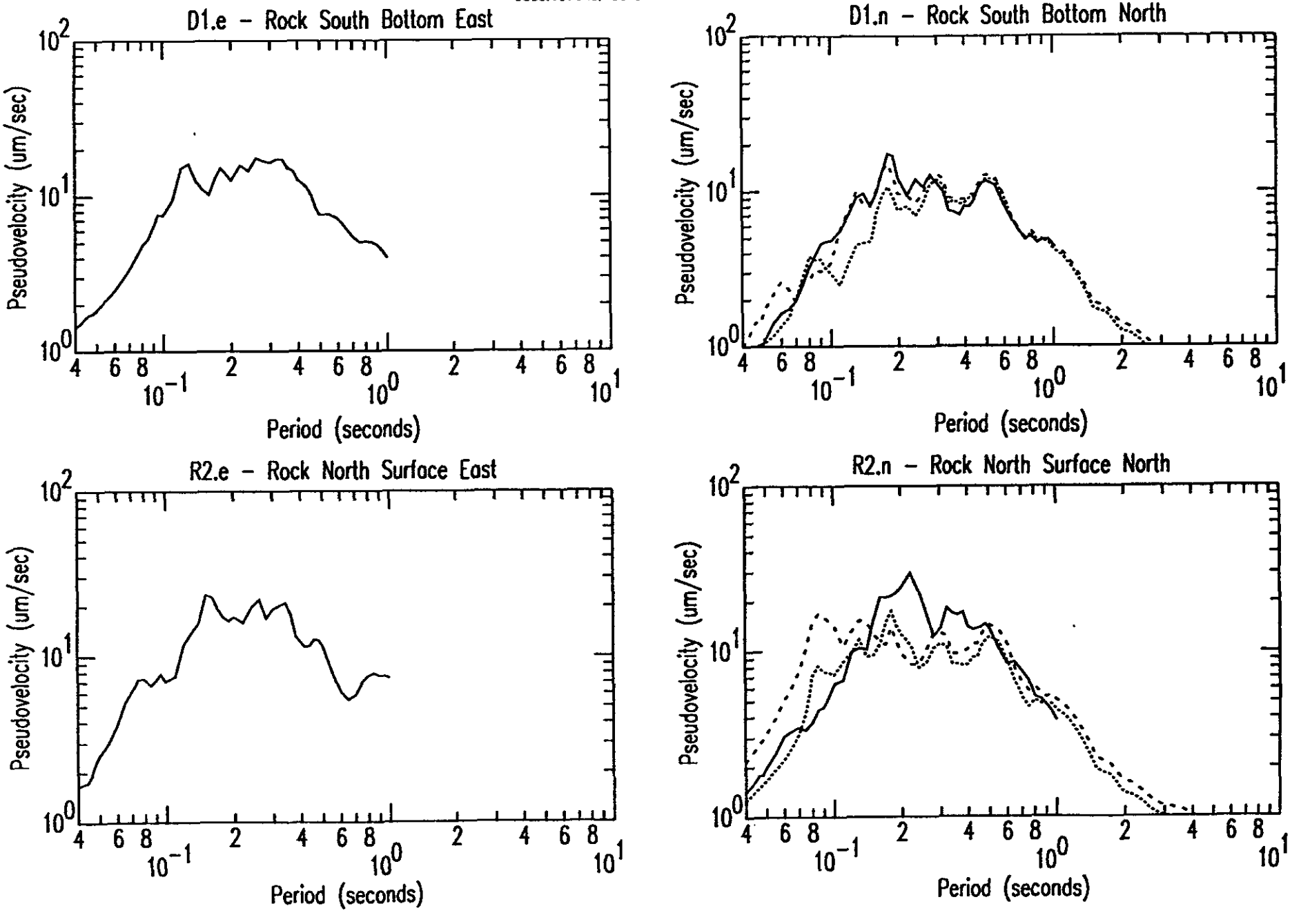

Figure G4a: R1 Preferred and Standard Spectral Ratio Predictions by #86 vs Observations

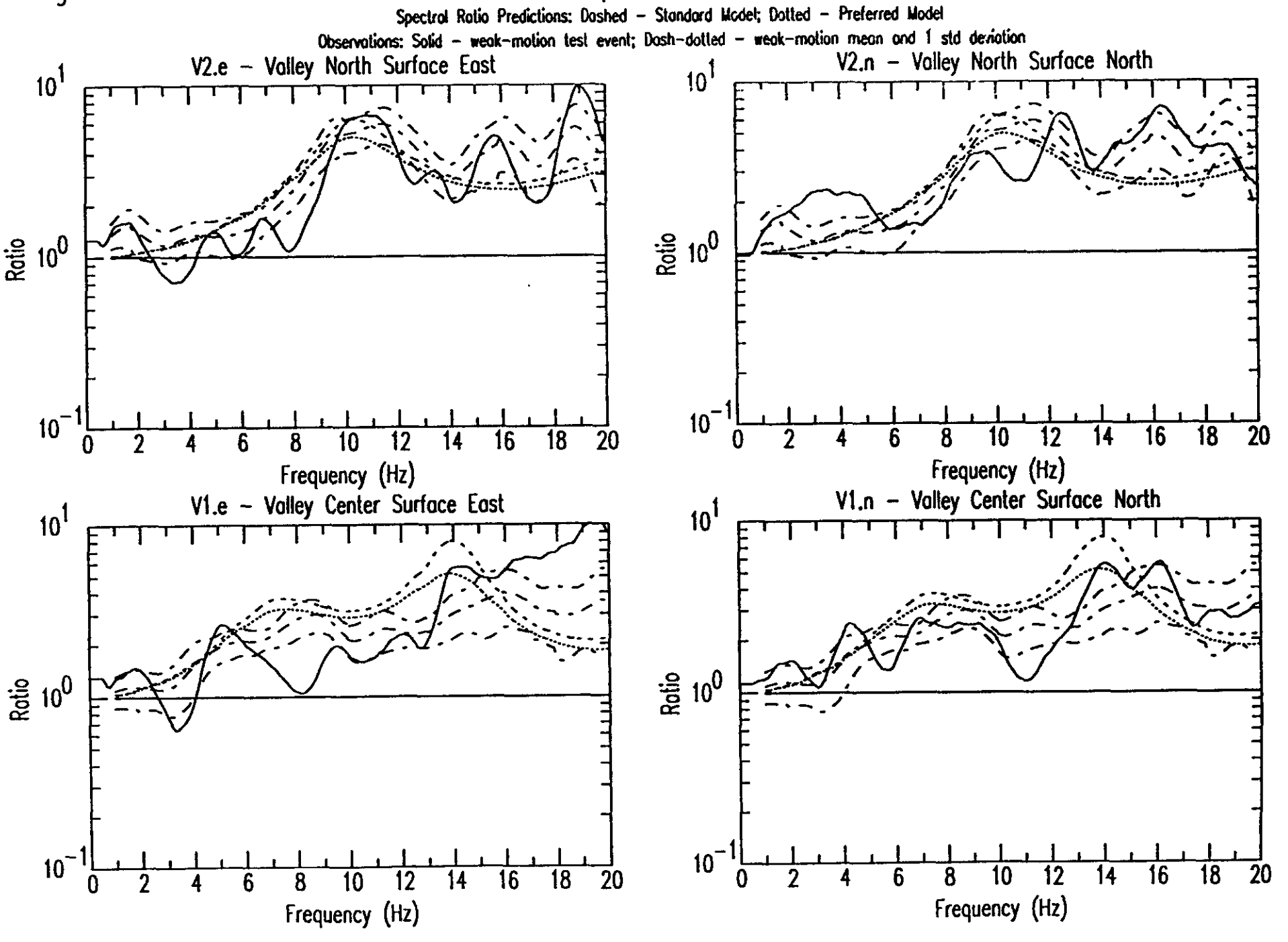

Figure G4b: R1 Preferred and Standard Spectral Ratio Predictions by #86 vs Observations

Spectral Ratio Predictions: Dashed - Standard Model; Dotted - Preferred Model

Observations: Solid - weak-motion test event; Dash-dotted - weak-motion mean and 1 std deviation

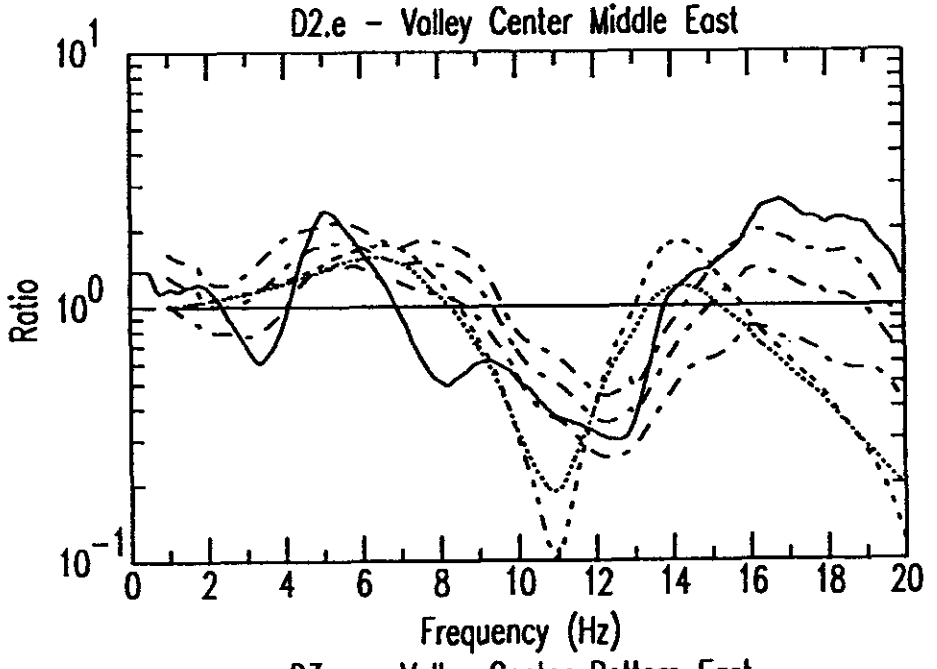

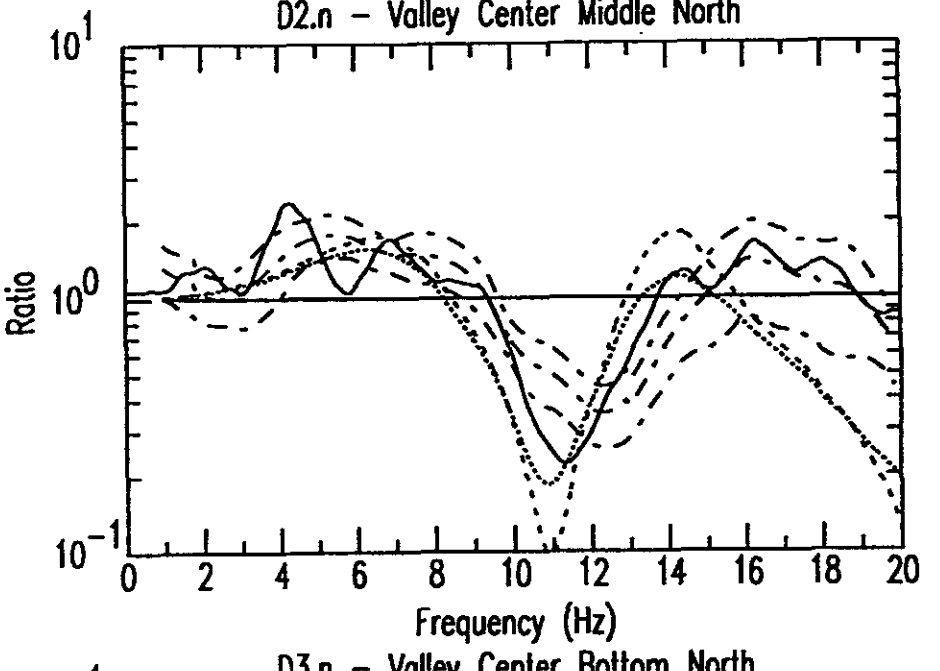

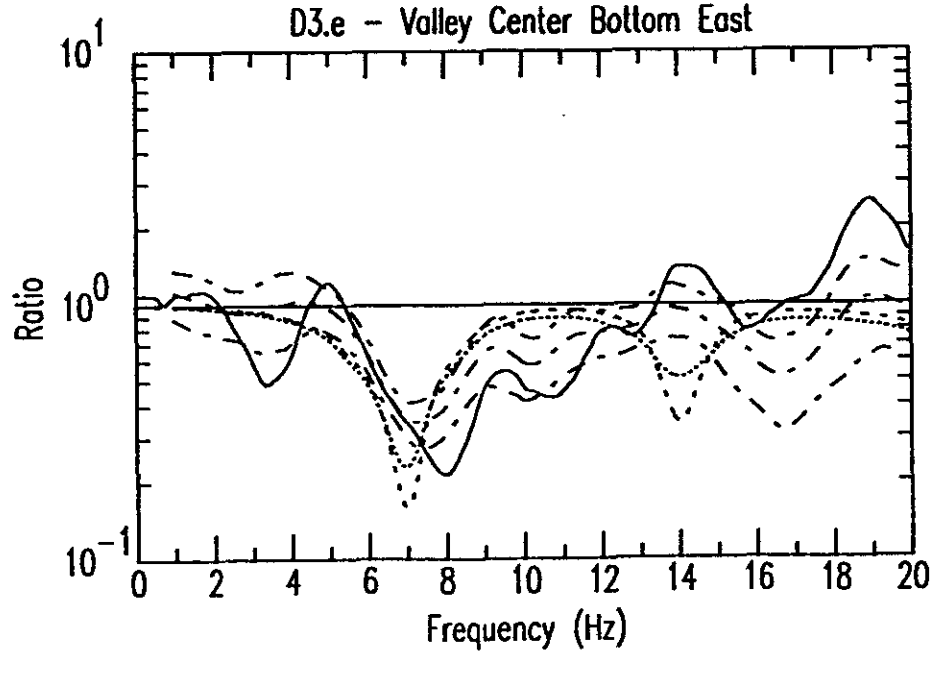

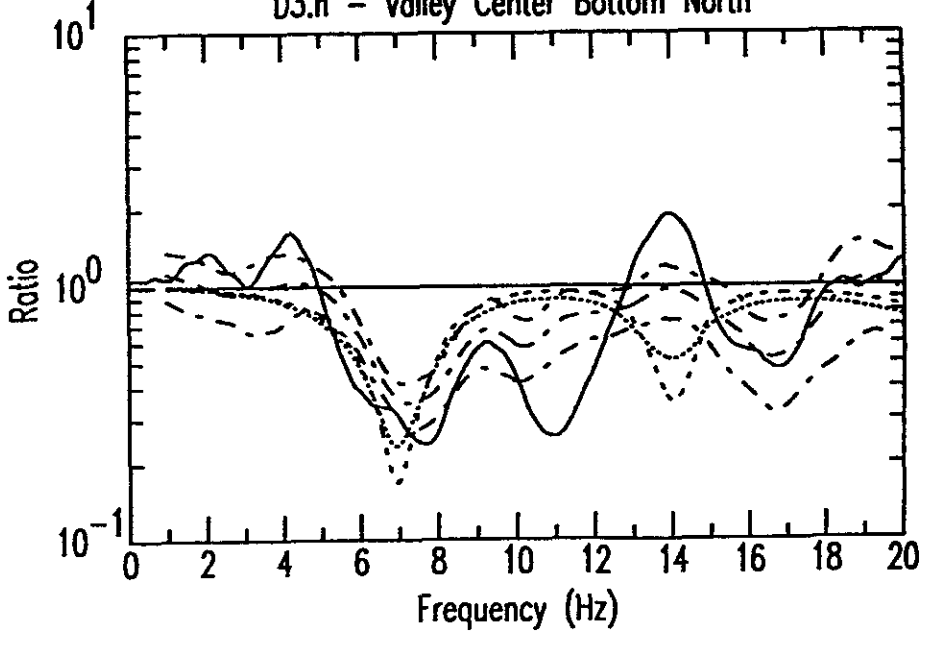

Figure G4c: R1 Preferred and Standard Spectral Ratio Predictions by #86 vs Observations

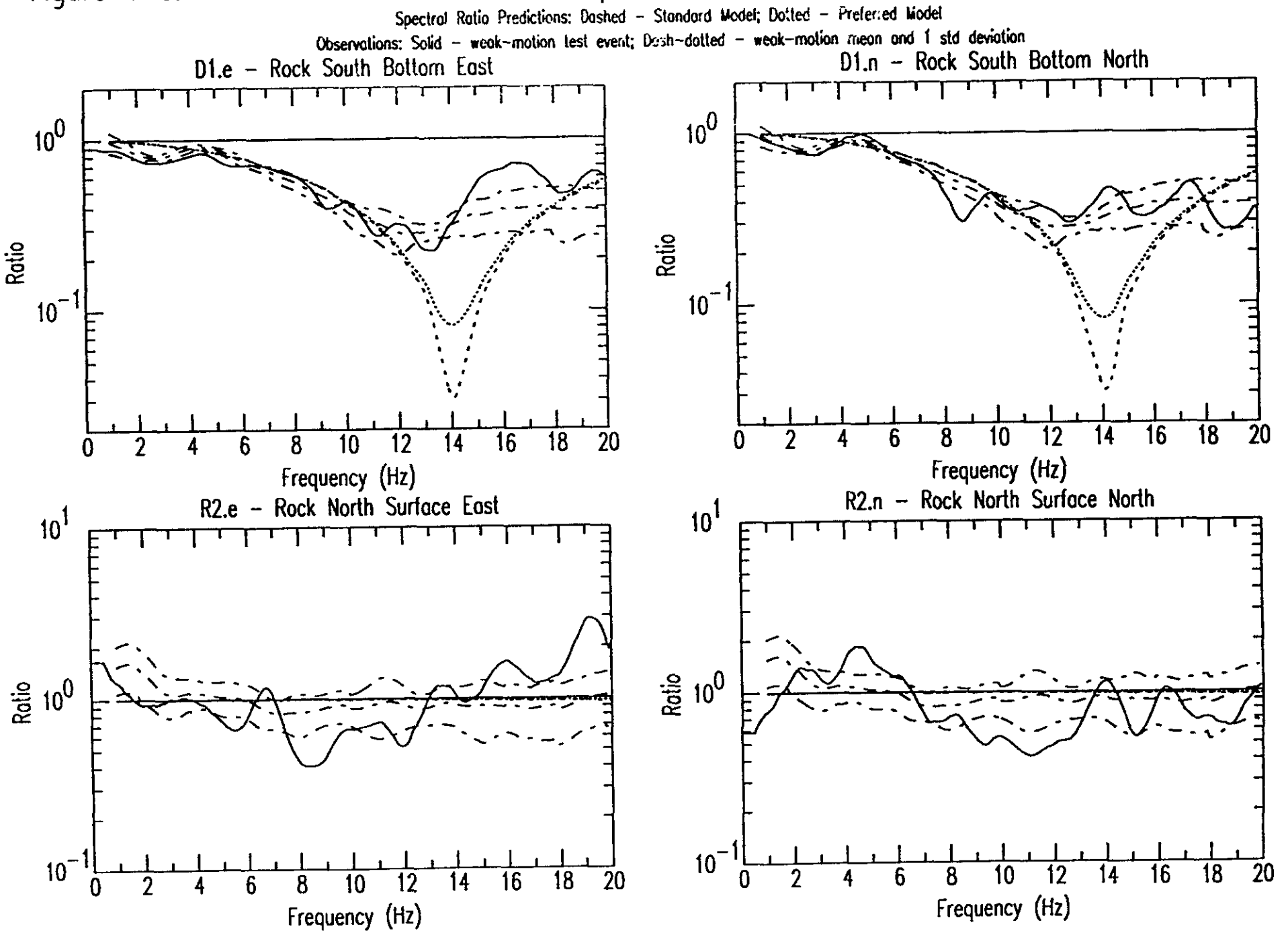

Figure G4d: R1 Preferred and Standard Response Spectra Predictions by #86 vs Observations

Response Spectra Predictions: Dashed - Standard Model; Dotted - Preferred Model

Observations: Solid - weak-motion test event

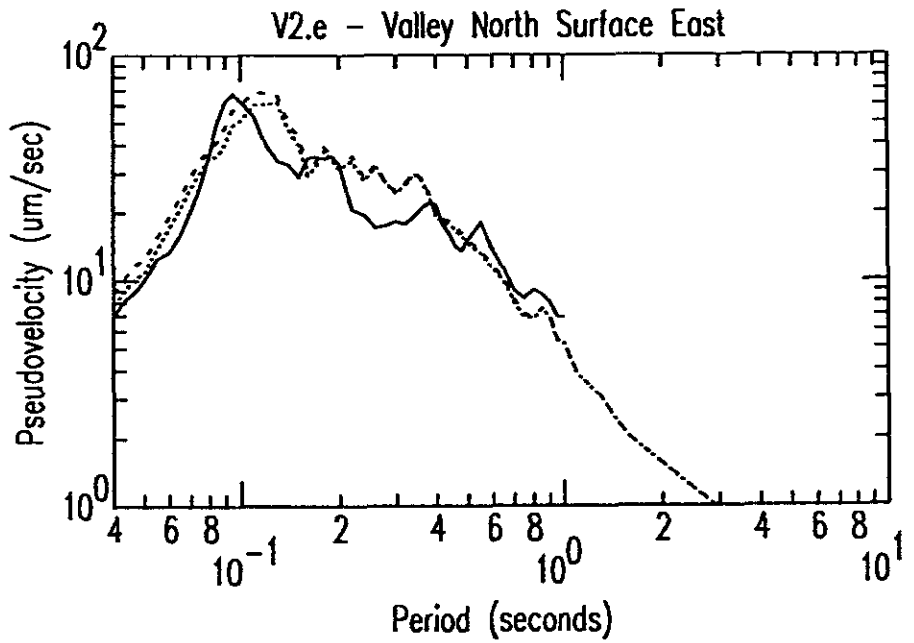

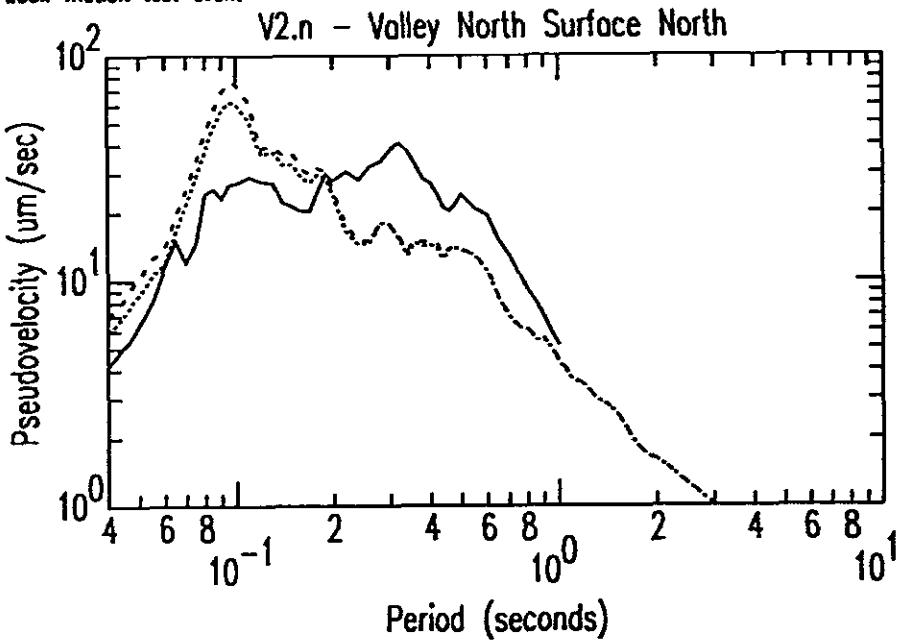

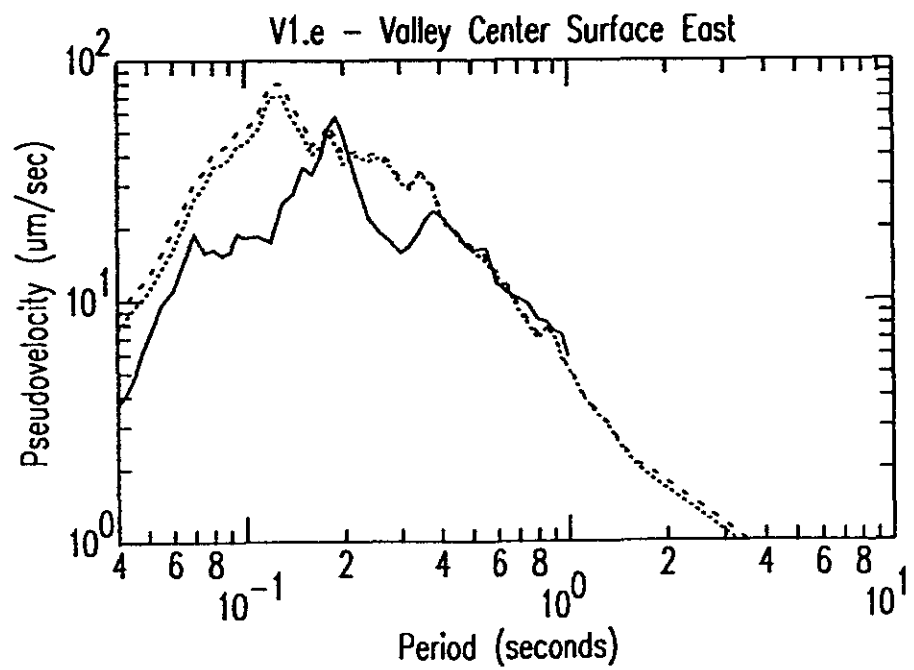

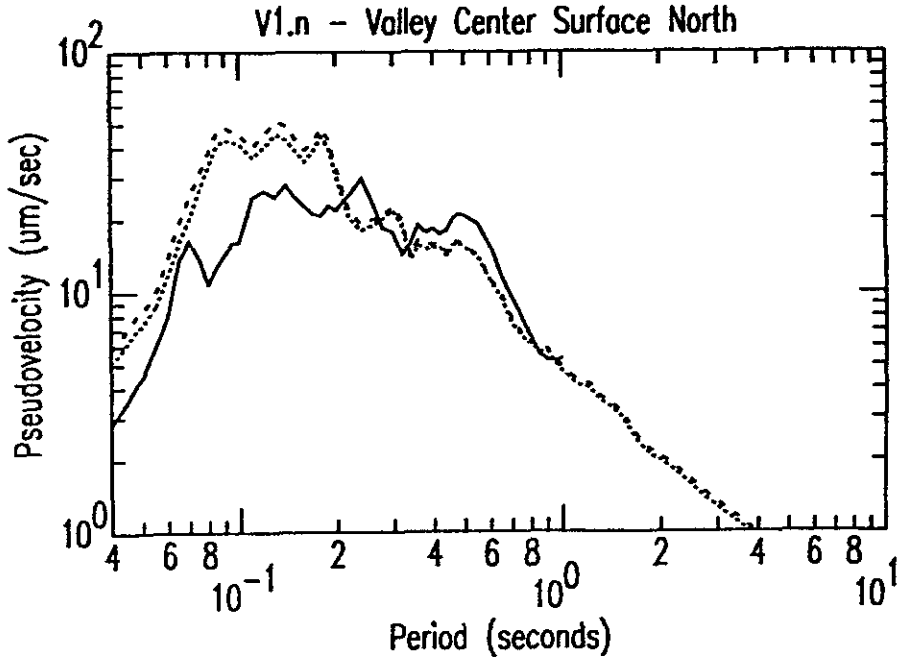

Figure G4e: R1 Preferred and Standard Response Spectra Predictions by #86 vs Observations

Response Spectra Predictions: Dashed - Standard Model; Dotted - Preferred Model

Observations: Solid - weak-motion test event

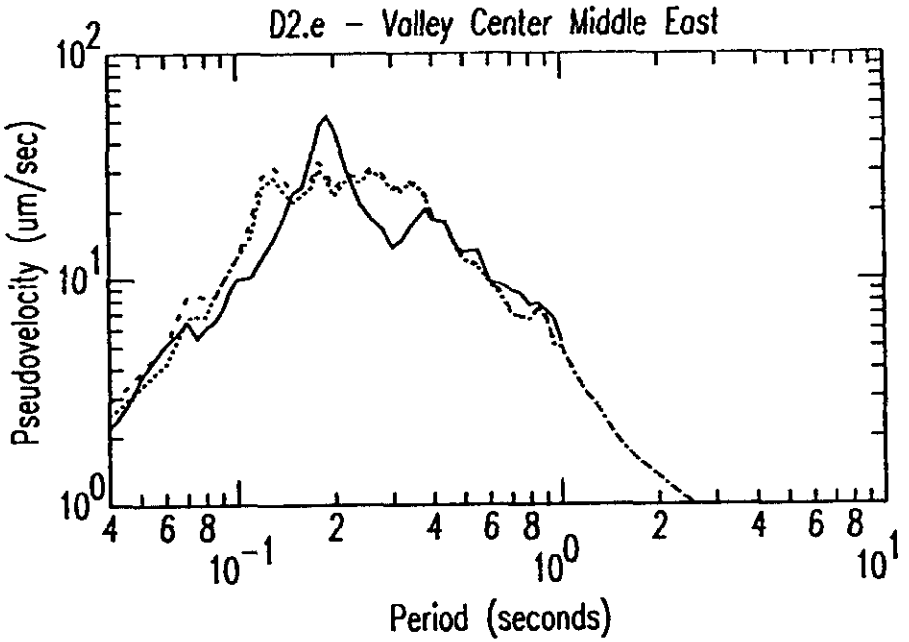

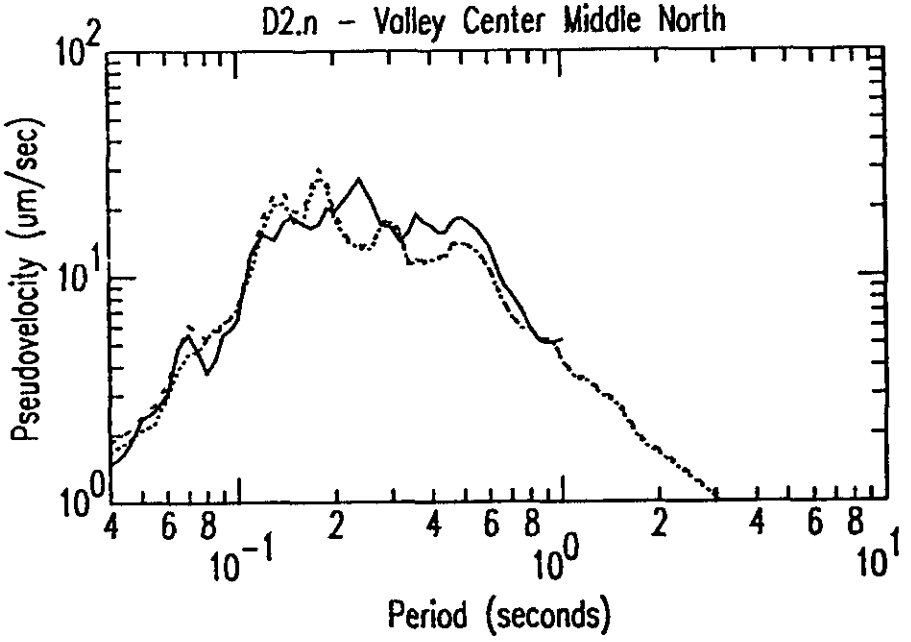

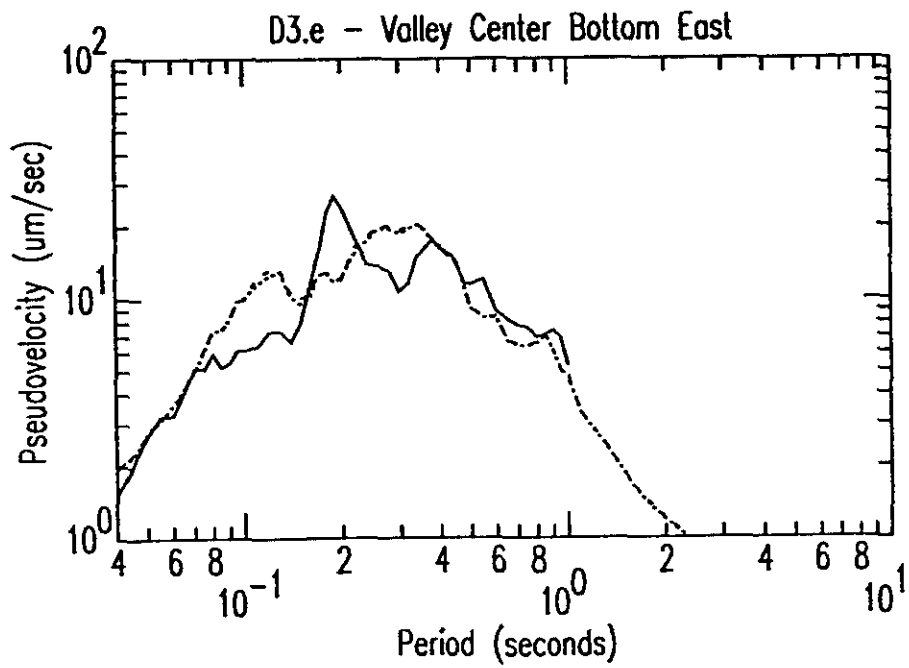

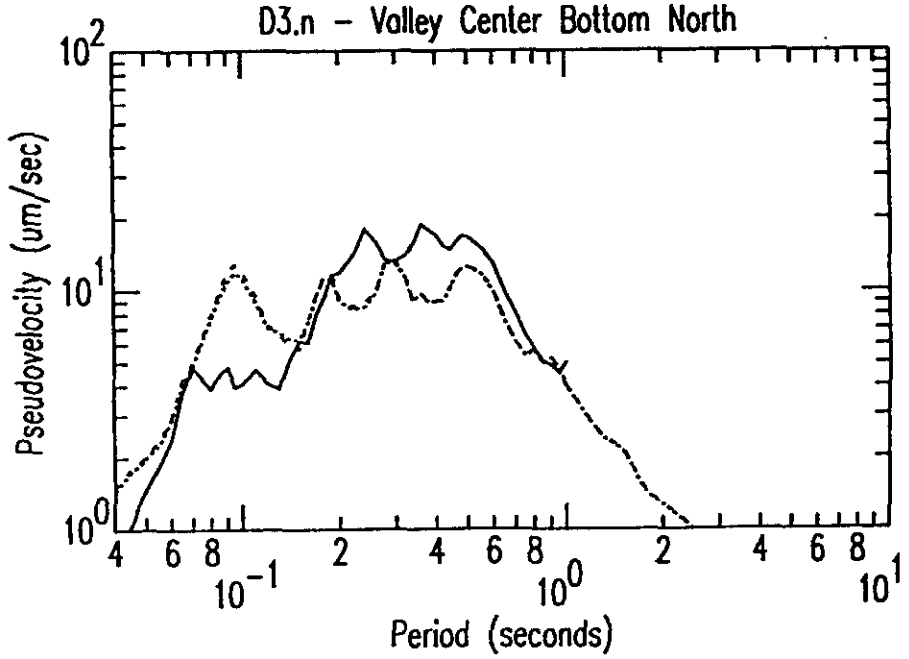

Figure G4f: R1 Preferred and Standard Response Spectra Predictions by #86 vs Observations

Response Spectra Predictions: Dashed - Standard Model; Dotted - Preferred Model

Observations: Solid - weak-motion test event

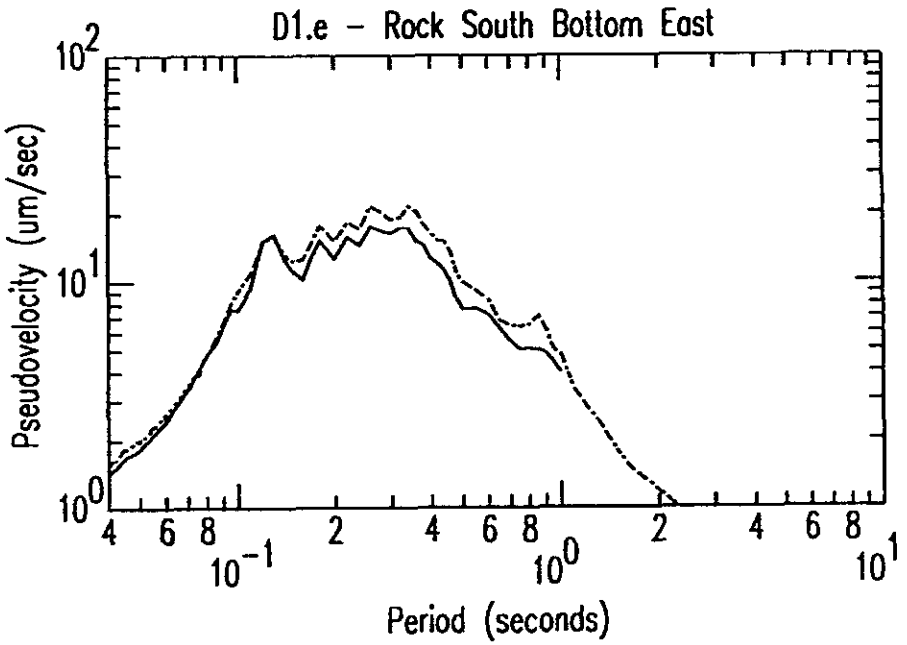

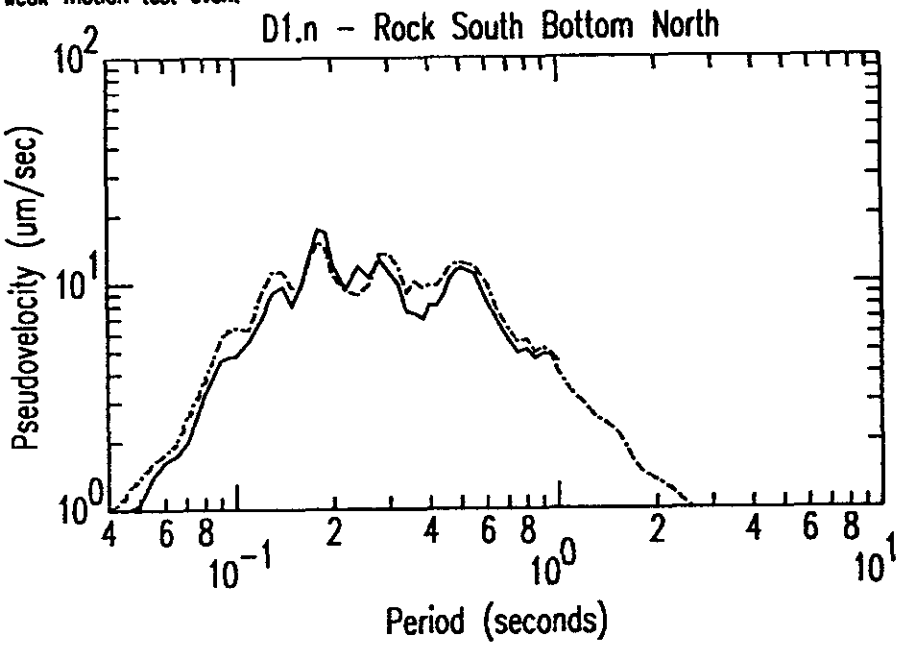

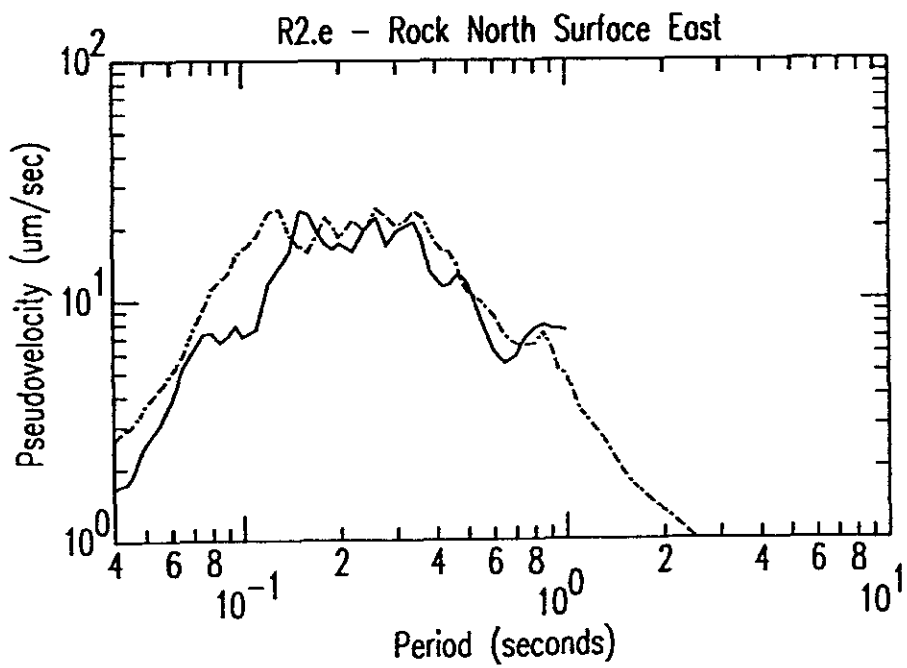

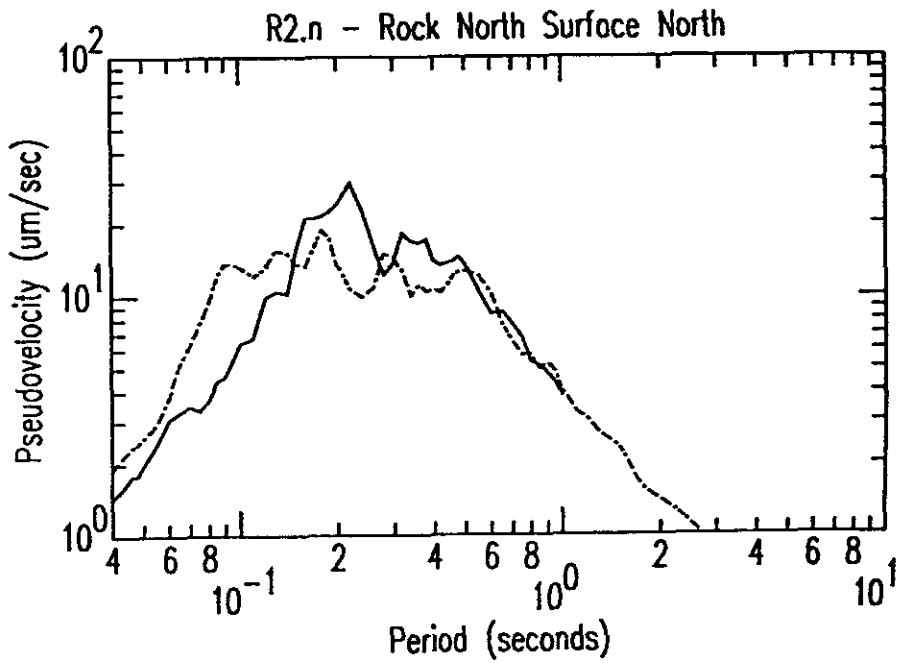

Figure G5a: R1 Preferred and Standard Spectral Ratio Predictions by #117 vs Observations

Spectral Ratio Predictions: Dashed - Standard Model; Dotted - Preferred Model

Observations: Solid - weak-motion test event; Dash-dotted - weak-motion mean and 1 std deviation

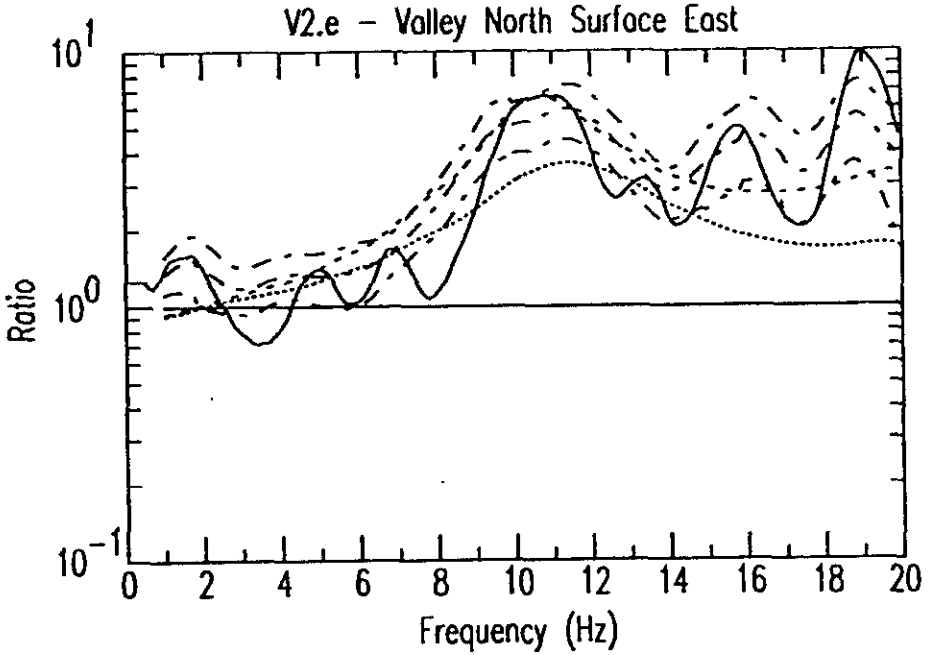

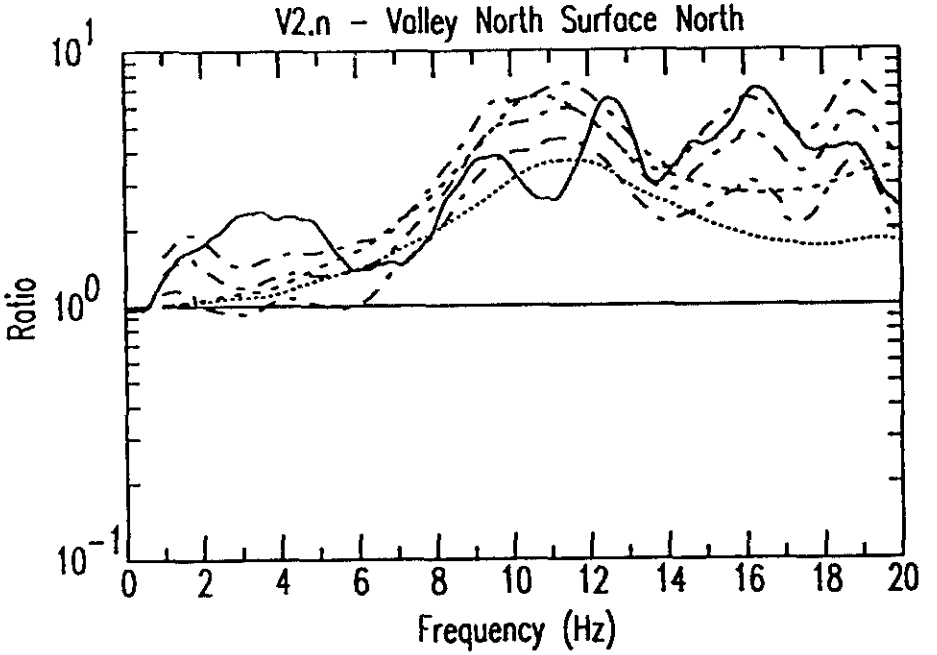

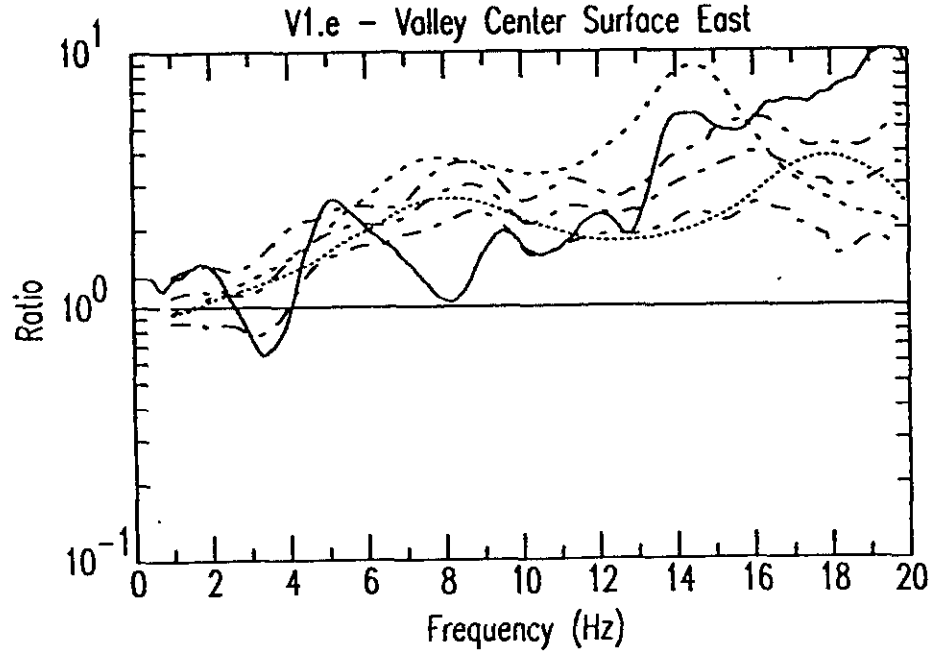

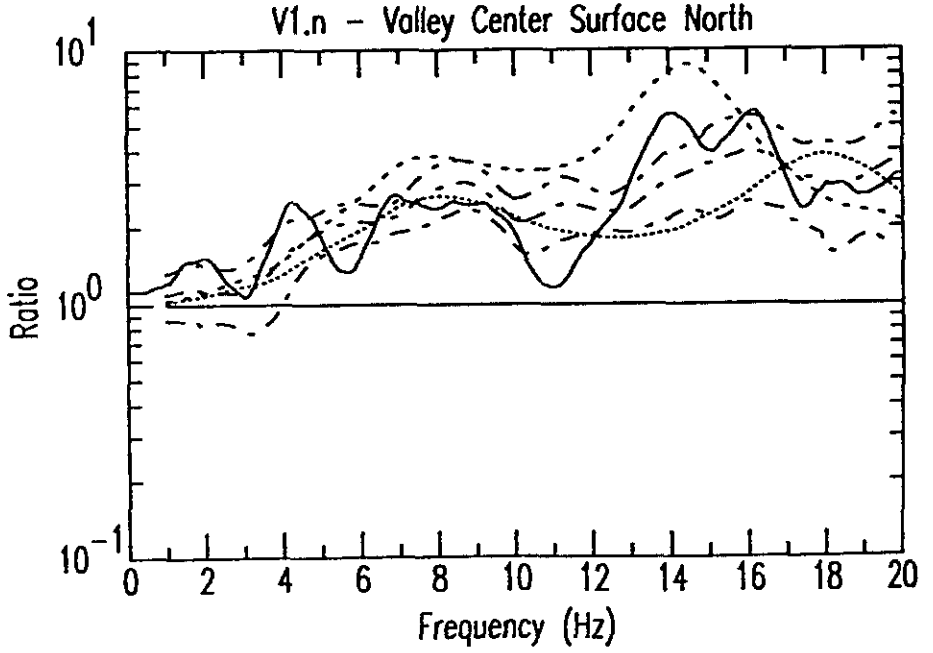

Figure G5b: R1 Preferred and Standard Spectral Ratio Predictions by #117 vs Observations

Spectral Ratio Predictions: Dashed – Standard Model; Dotted – Preferred Model

Observations: Solid – weak-motion test event; Dash-dotted – weak-motion mean and 1 std deviation

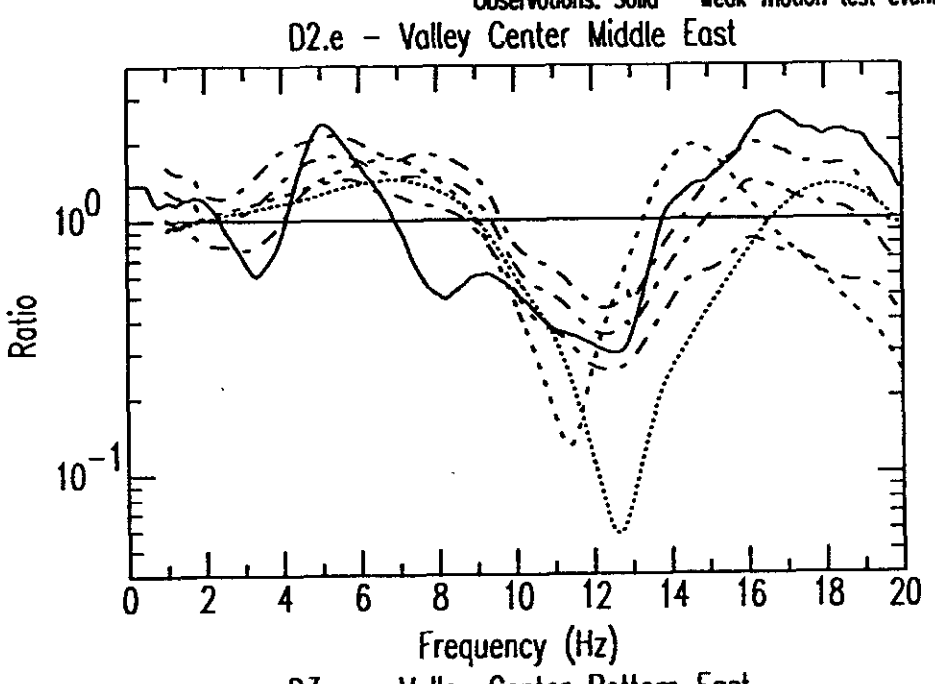

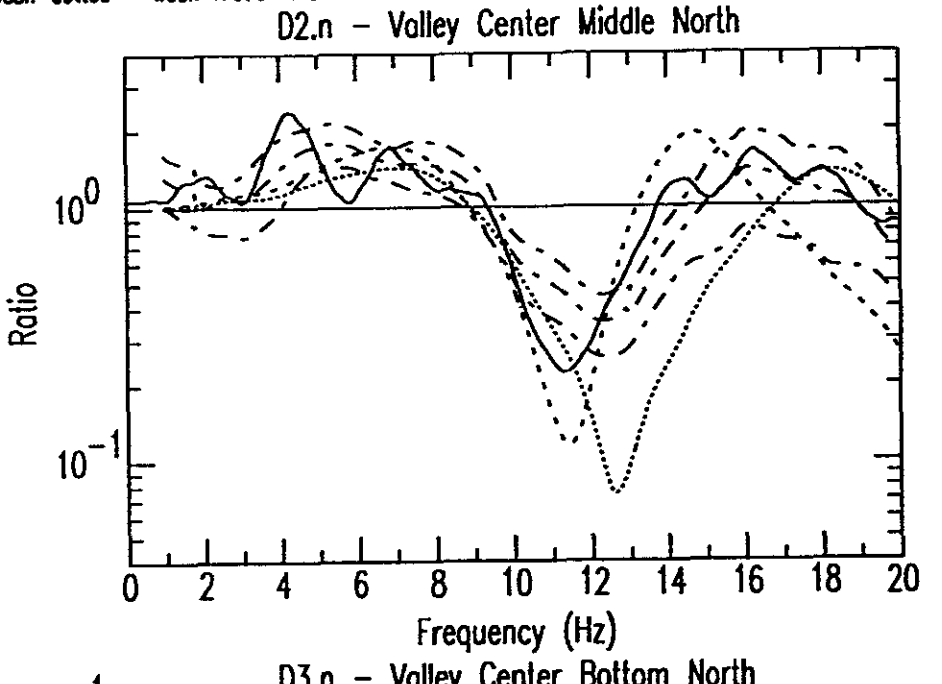

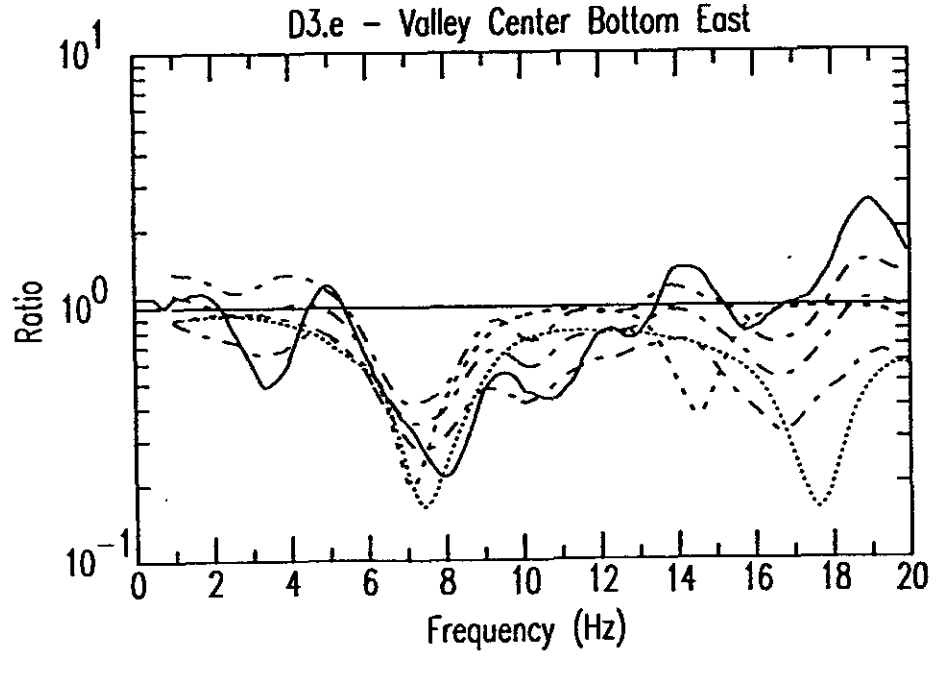

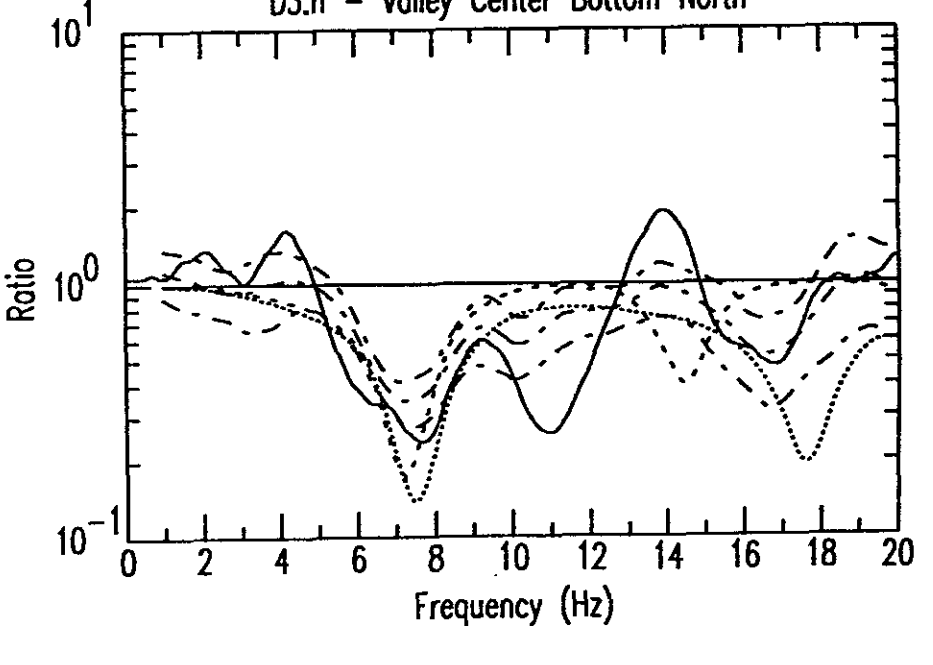

Figure G5d: R1 Preferred and Standard Response Spectra Predictions by #117 vs Observations

Response Spectra Predictions: Dashed - Standard Model; Dotted - Preferred Model

Observations: Solid - weak-motion test event

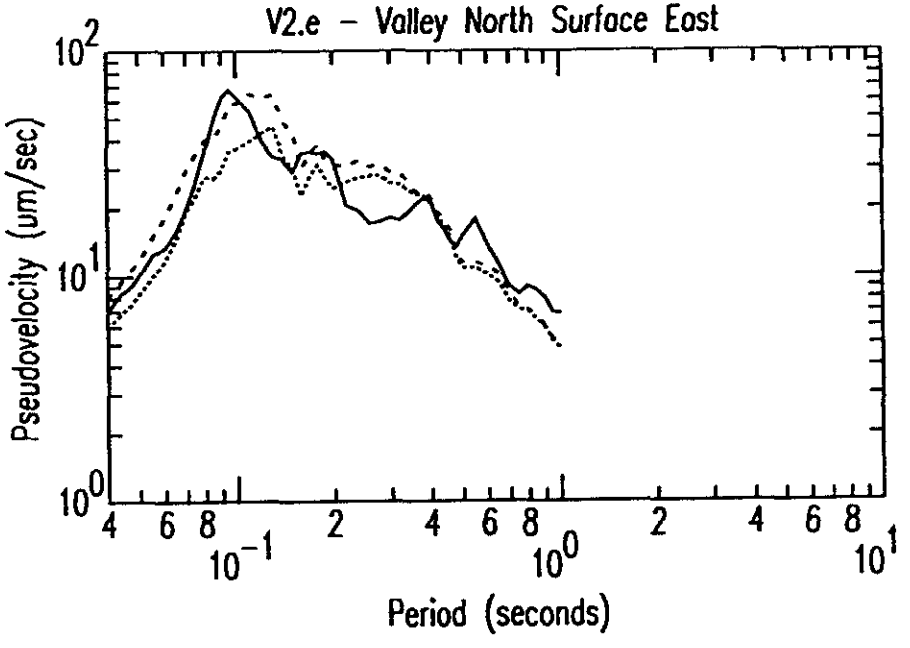

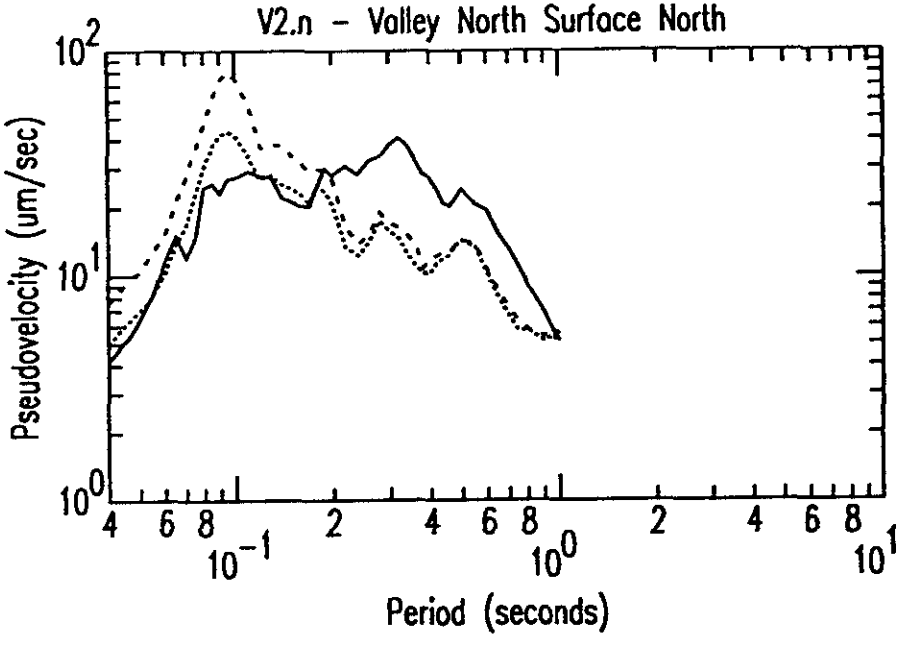

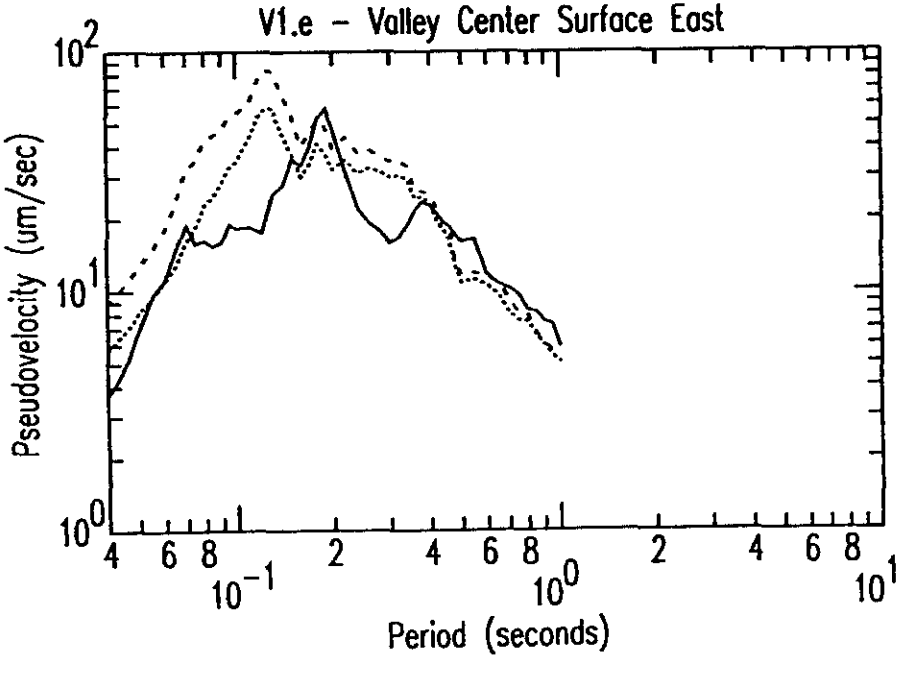

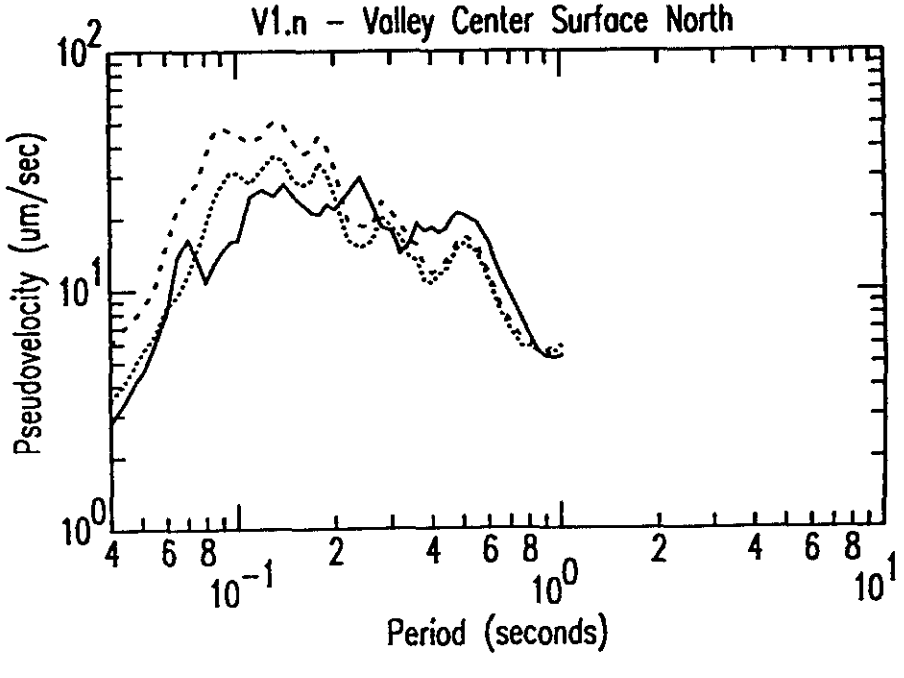

Figure G5c: R1 Preferred and Standard Spectral Ratio Predictions by #117 vs Observations

Spectral Ratio Predictions: Dashed – Standard Model; Dotted – Preferred Model

Observations: Solid – weak-motion test event; Dash-dotted – weak-motion mean and 1 std deviation

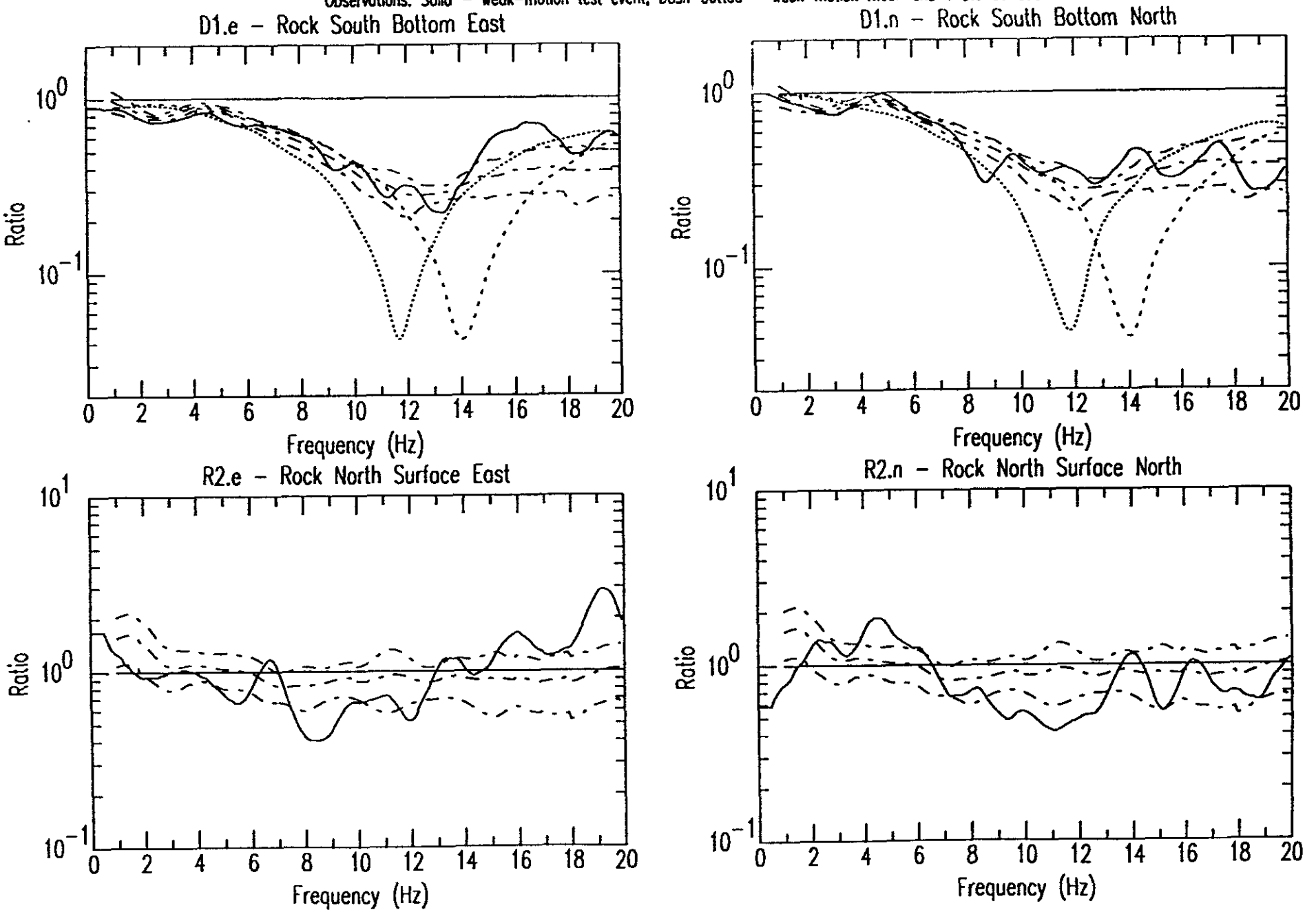

Figure G5f: R1 Preferred and Standard Response Spectra Predictions by #117 vs Observations

Response Spectra Predictions: Dashed - Standard Model; Dotted - Preferred Model

Observations: Solid - weak-motion test event

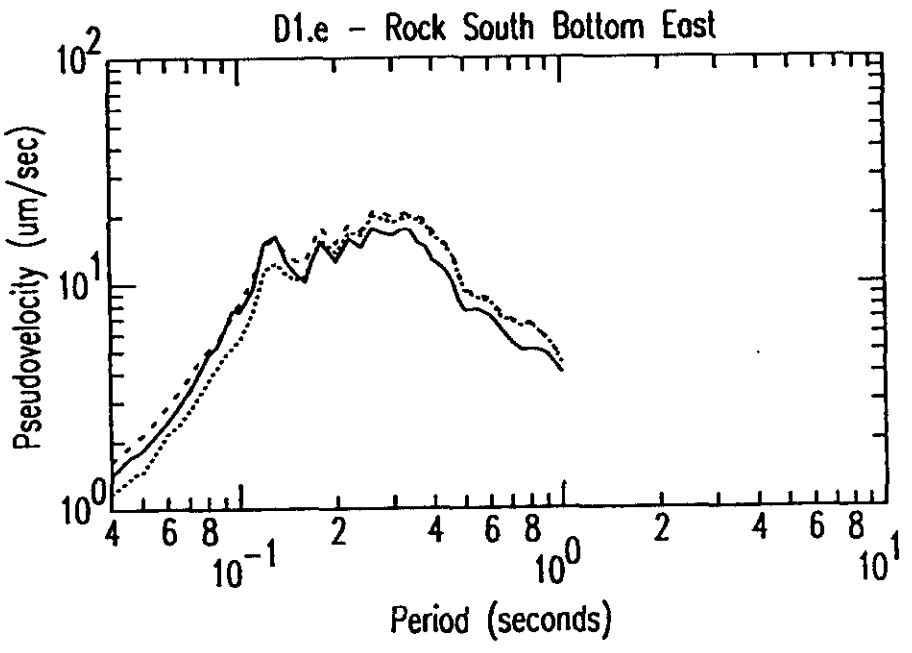

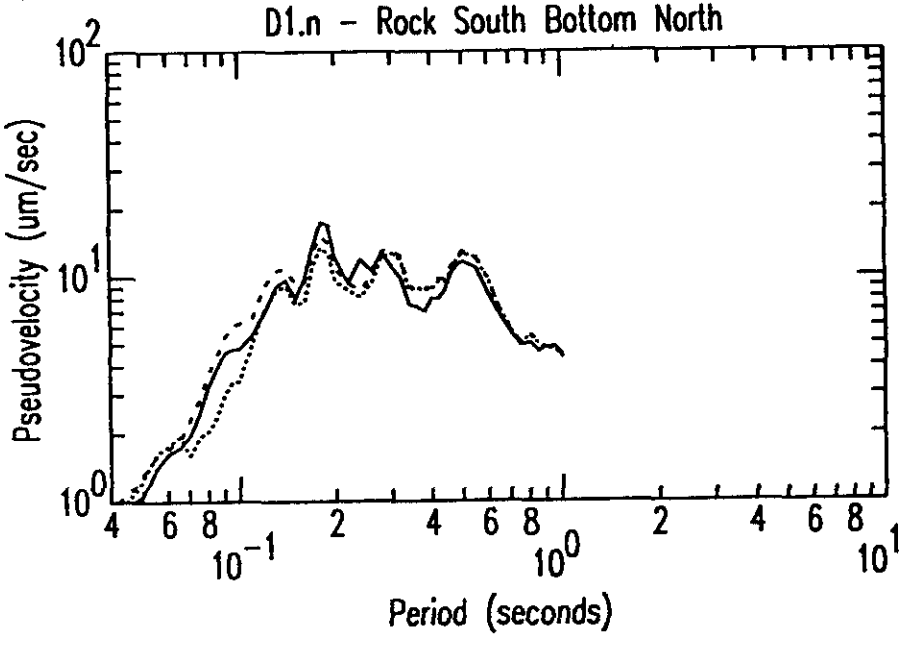

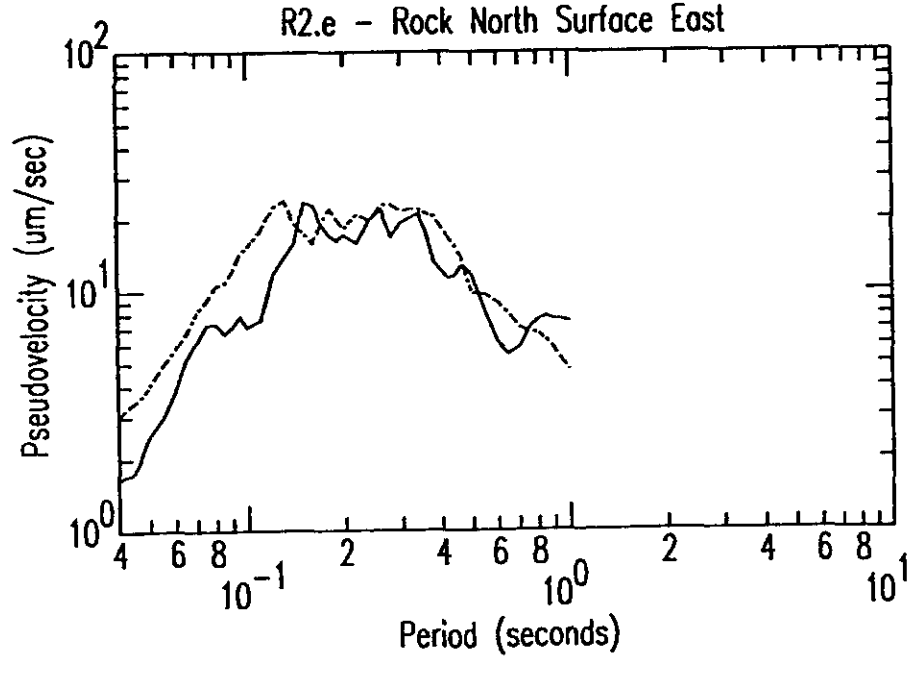

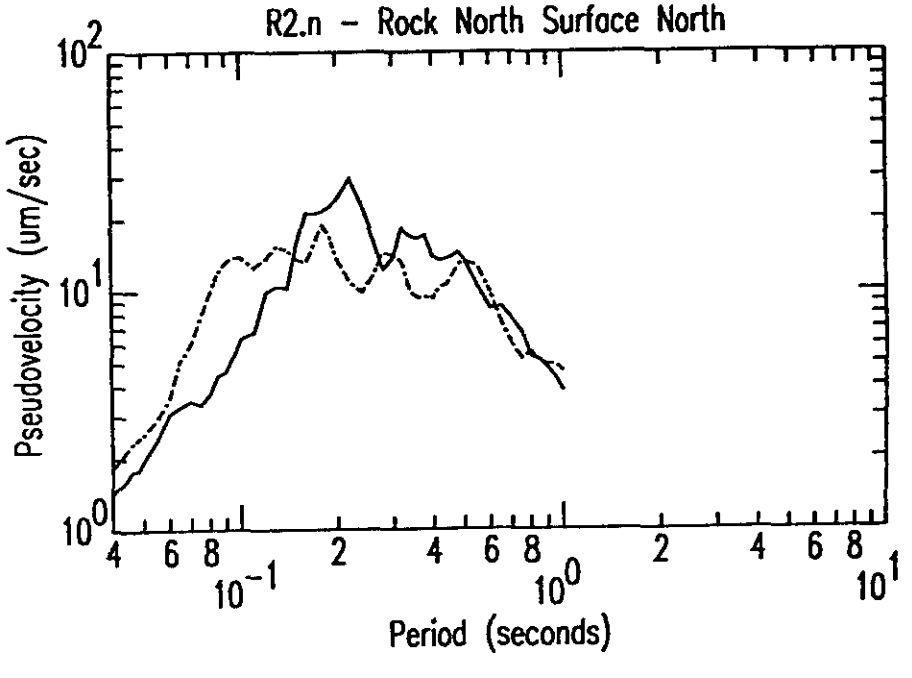

Figure G5e: R1 Preferred and Standard Response Spectra Predictions by #117 vs Observations

Response Spectra Predictions: Dashed – Standard Model; Dotted – Preferred Model

Observations: Solid – weak-motion test event

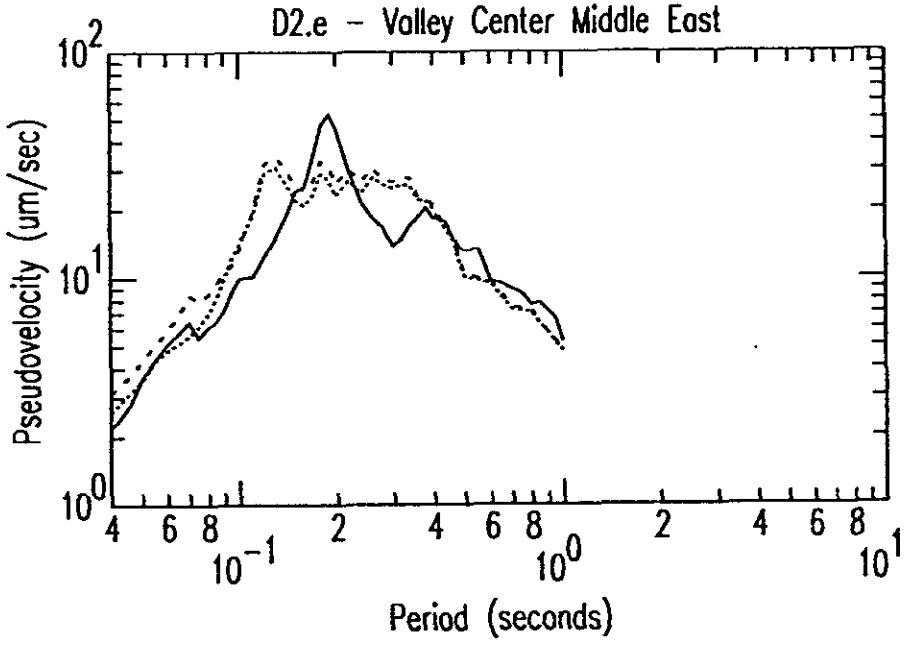

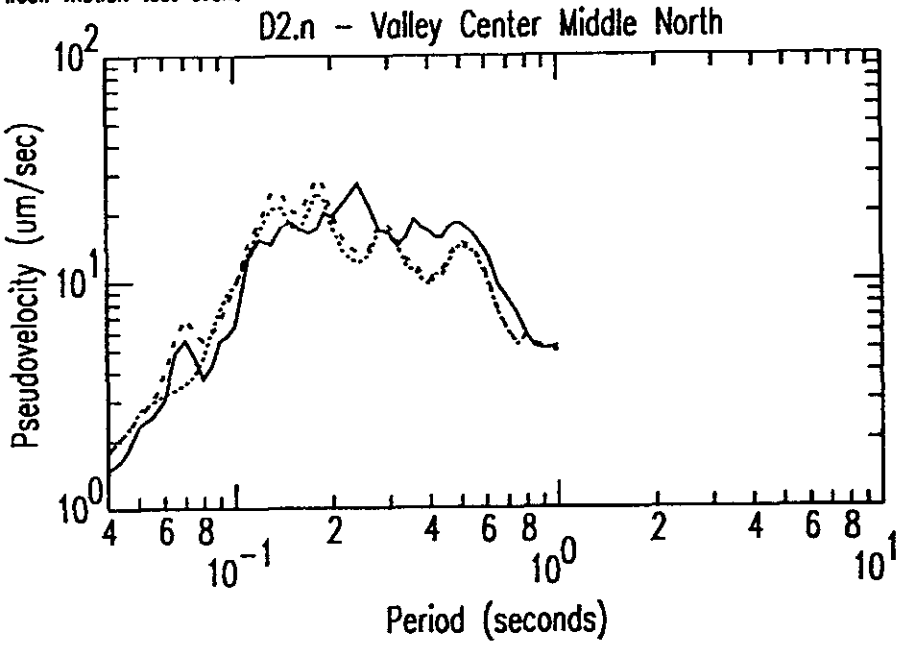

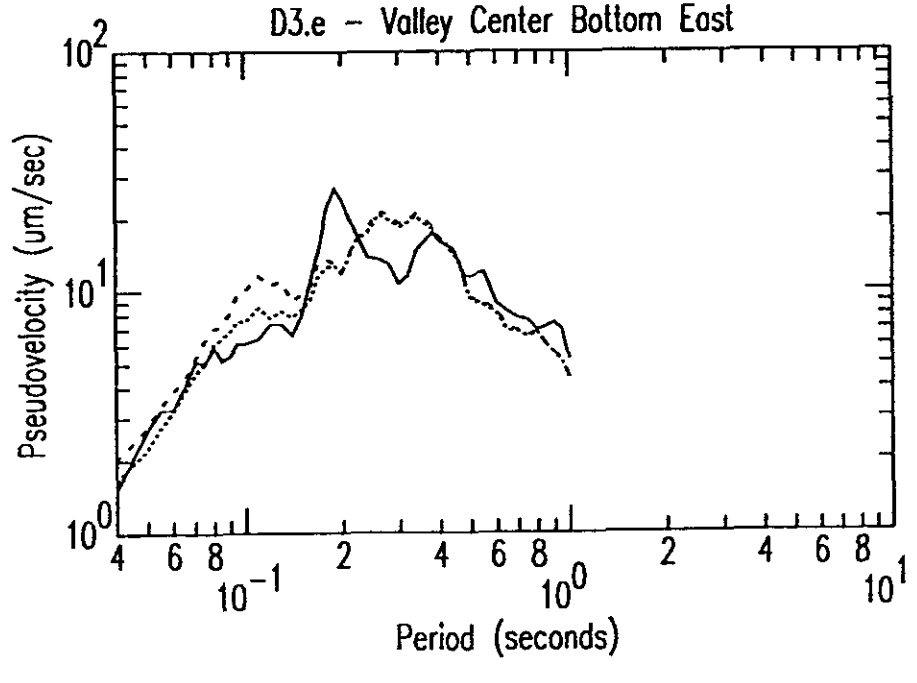

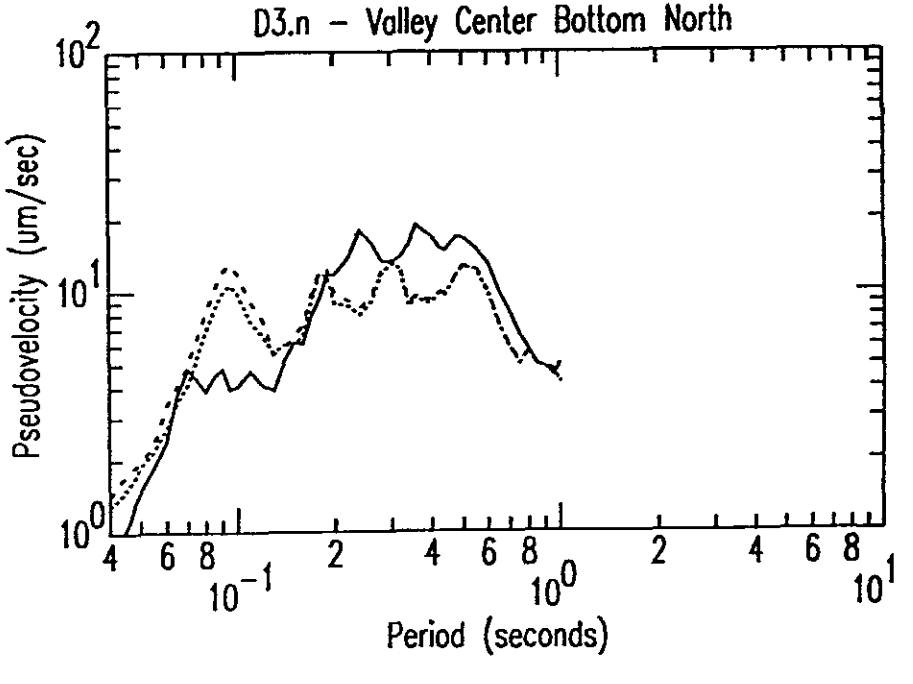

Figure G6b: R1 Preferred and Standard Spectral Ratio Predictions by #143 vs Observations

Spectral Ratio Predictions: Dashed – Standard Model; Dotted – Preferred Model

Observations: Solid – weak-motion test event; Dash-dotted – weak-motion mean and 1 std deviation

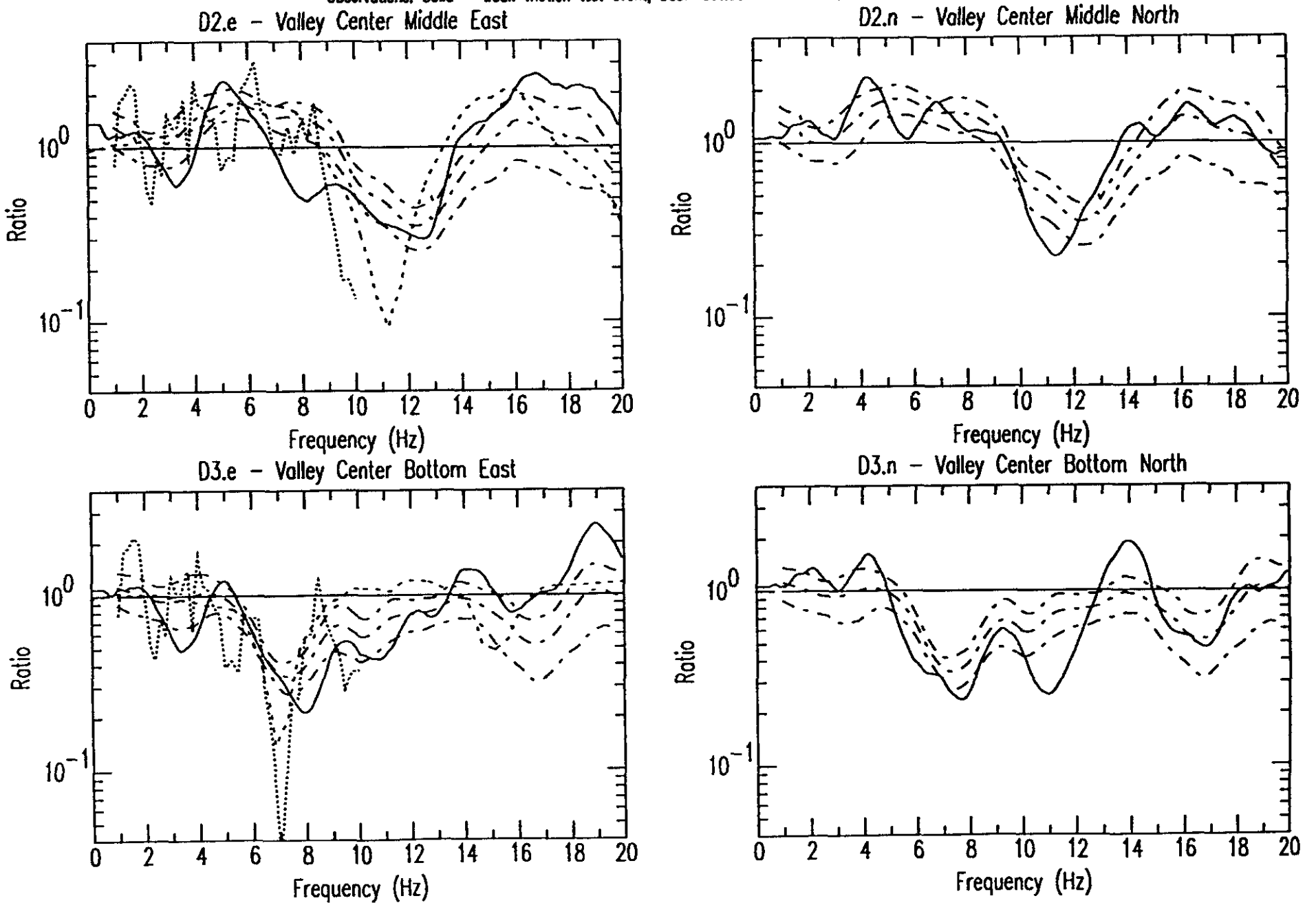

Figure G6a: R1 Preferred and Standard Spectral Ratio Predictions by #143 vs Observations

Spectral Ratio Predictions: Dashed – Standard Model; Dotted – Preferred Model

Observations: Solid – weak-motion test event; Dash-dotted – weak-motion mean and 1 std deviation

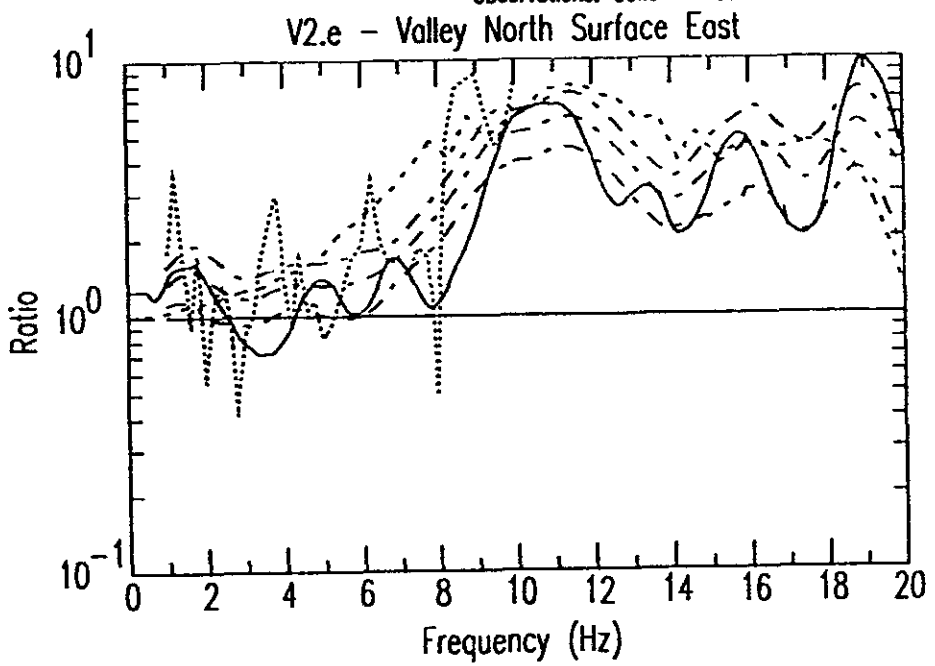

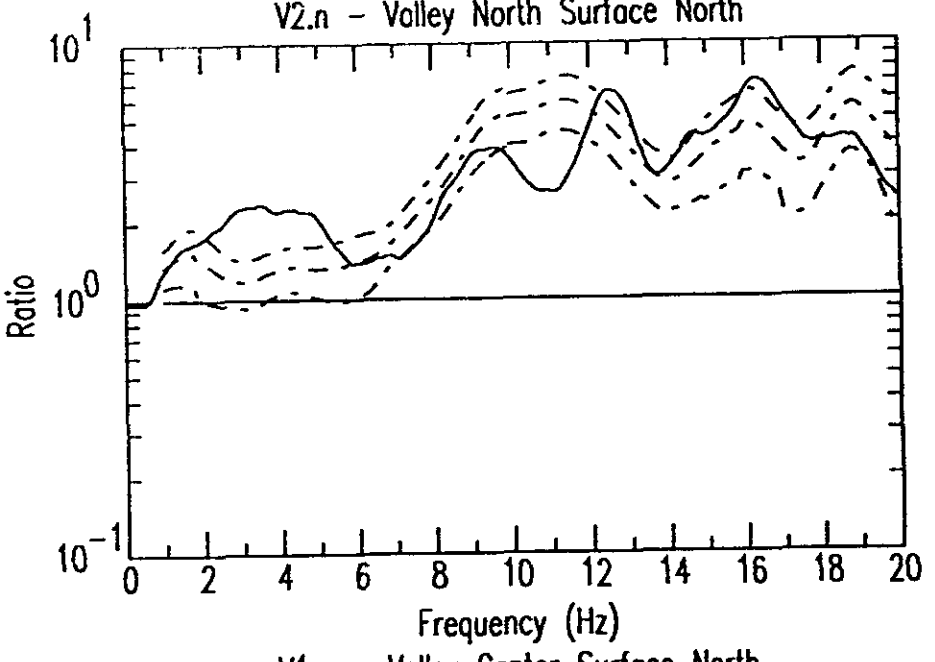

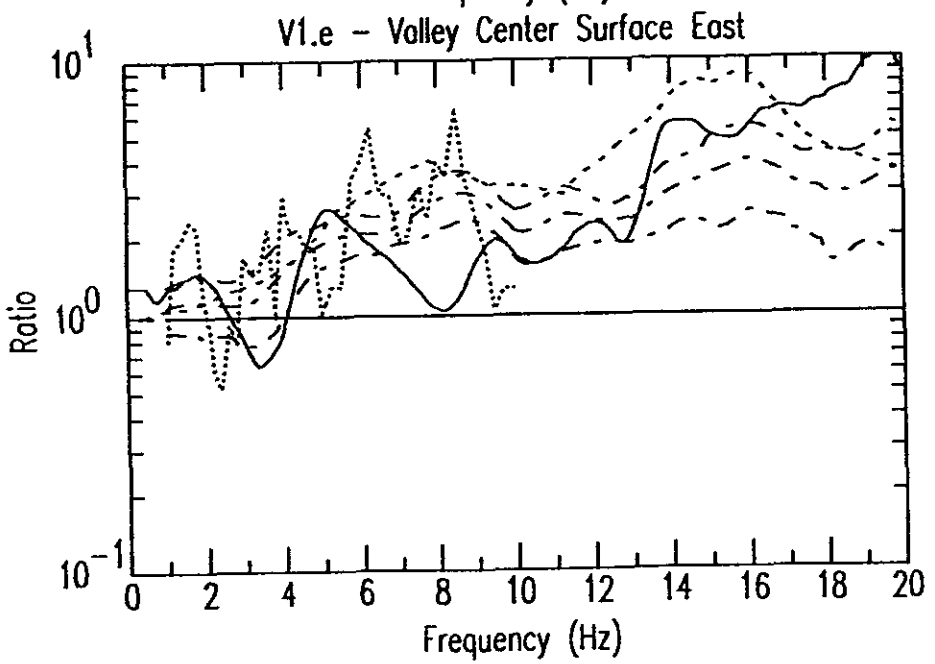

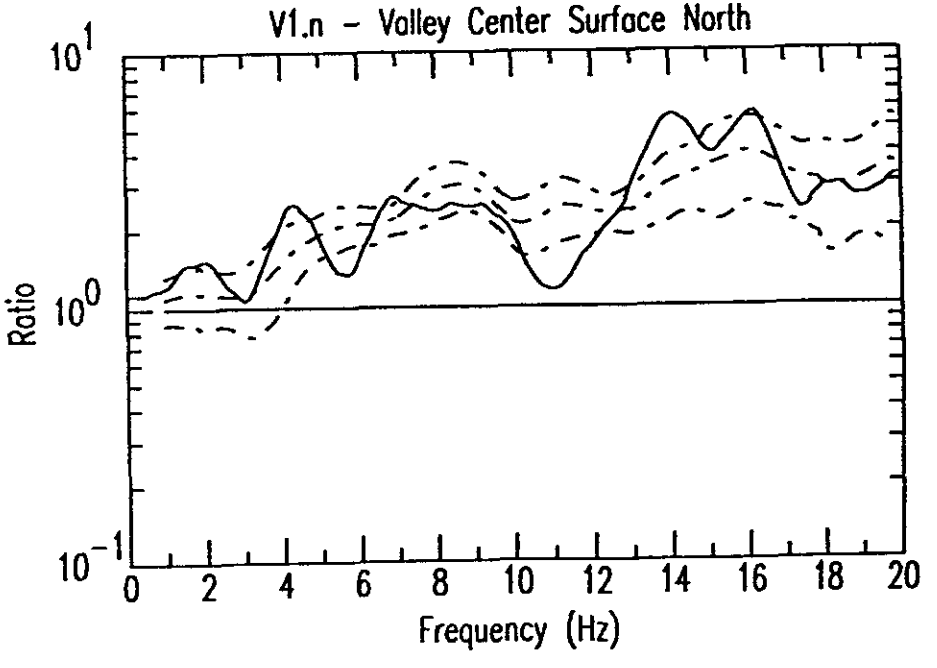

Figure G6d: R1 Preferred and Standard Response Spectra Predictions by #143 vs Observations

Response Spectra Predictions: Dashed - Standard Model; Dotted - Preferred Model

Observations: Solid - weak-motion test event

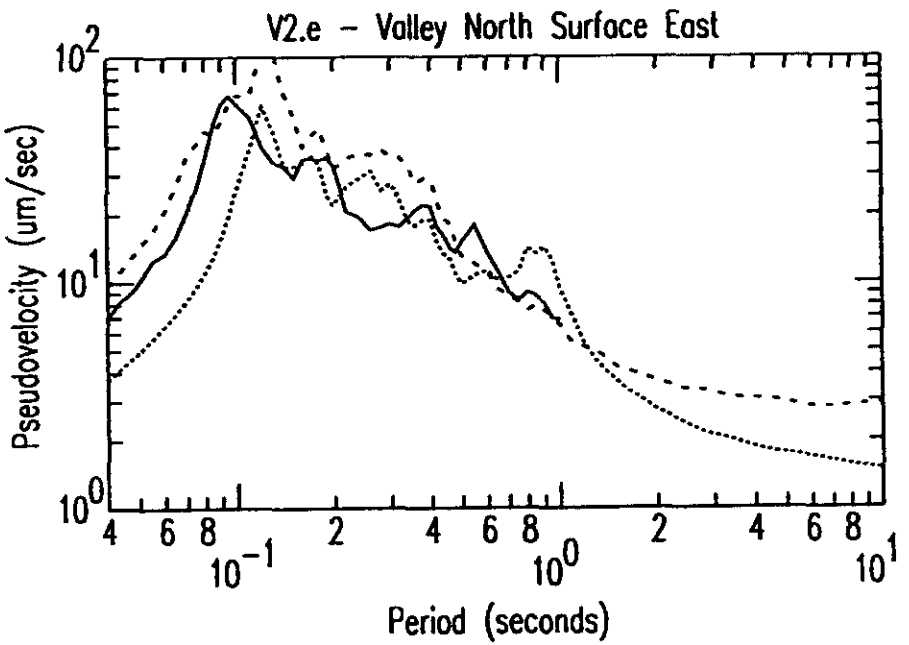

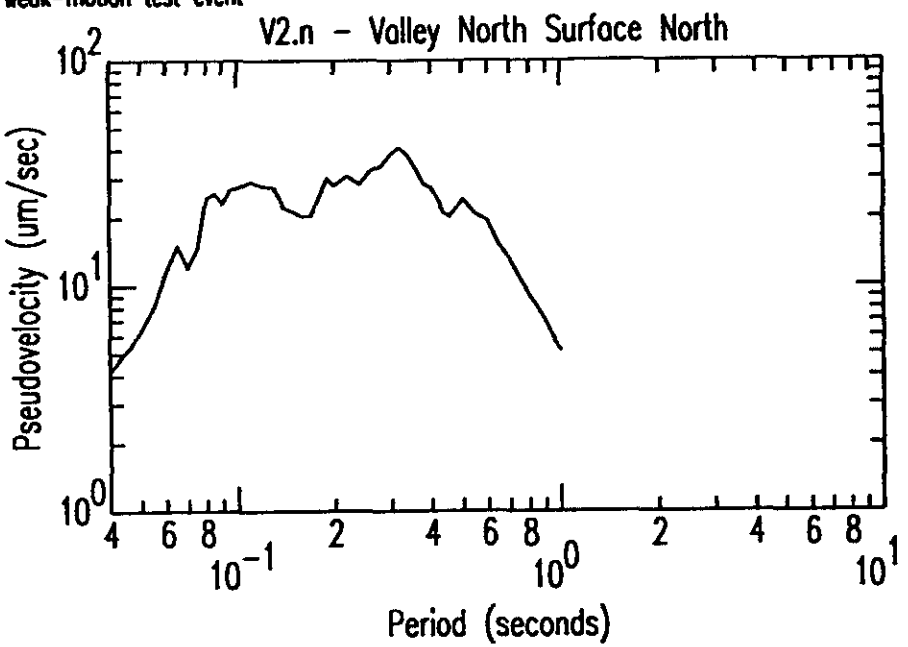

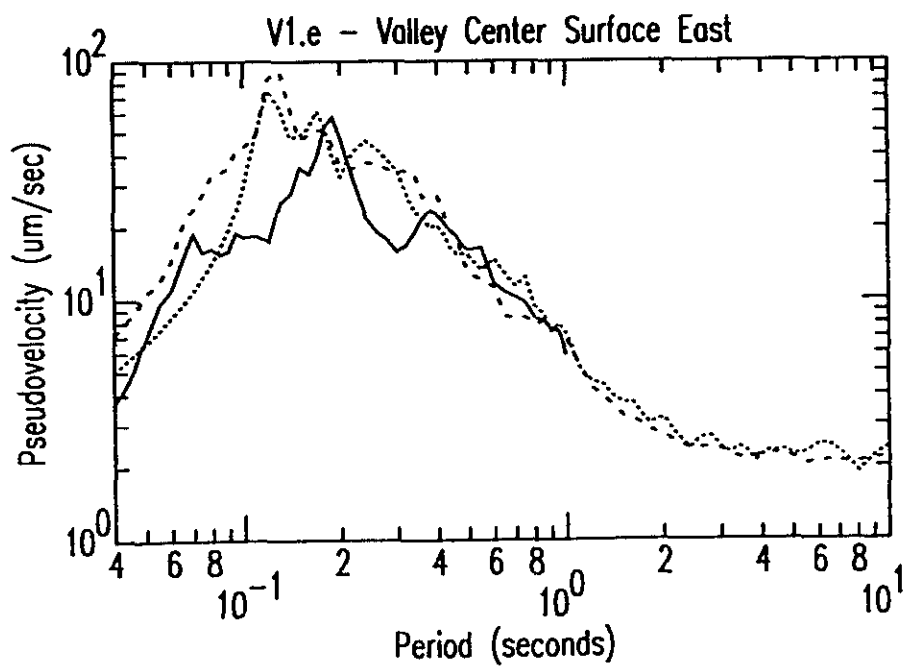

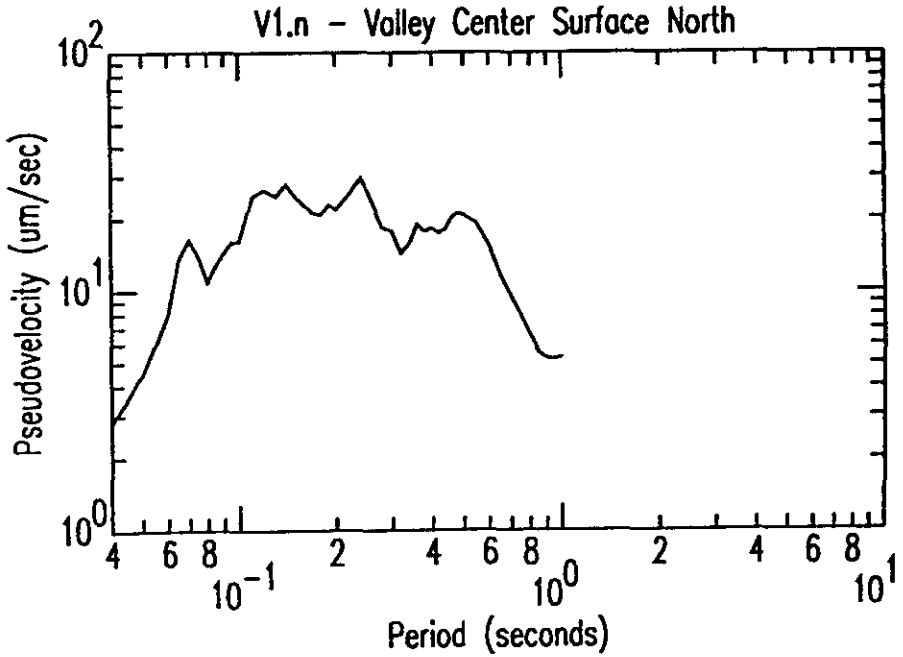

Figure G6c: R1 Preferred and Standard Spectral Ratio Predictions by #143 vs Observations

Spectral Ratio Predictions: Dashed - Standard Model; Dotted - Preferred Model

Observations: Solid - weak-motion test event; Dash-dotted - weak-motion mean and 1 std deviation

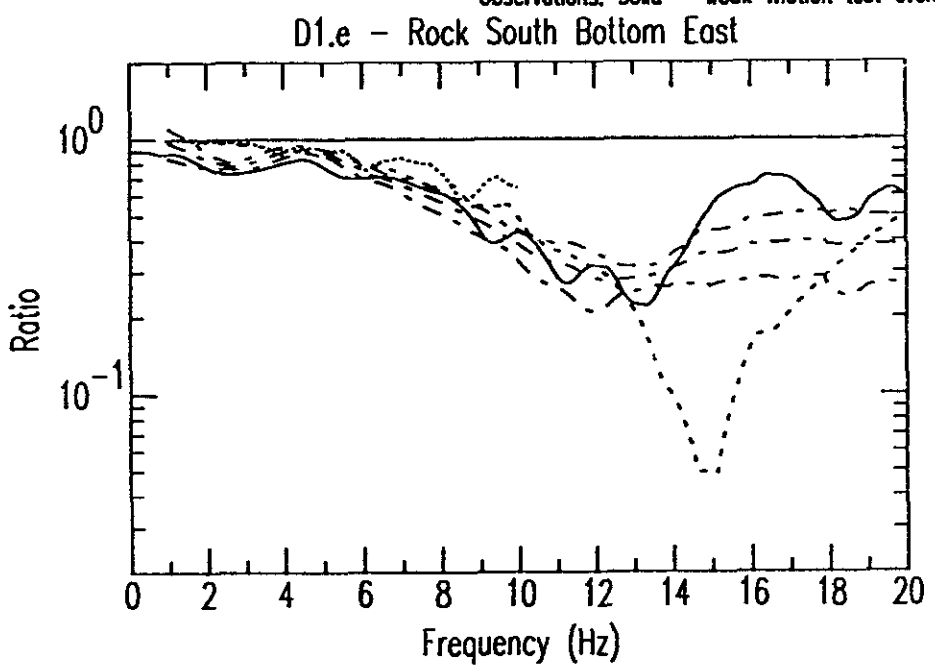

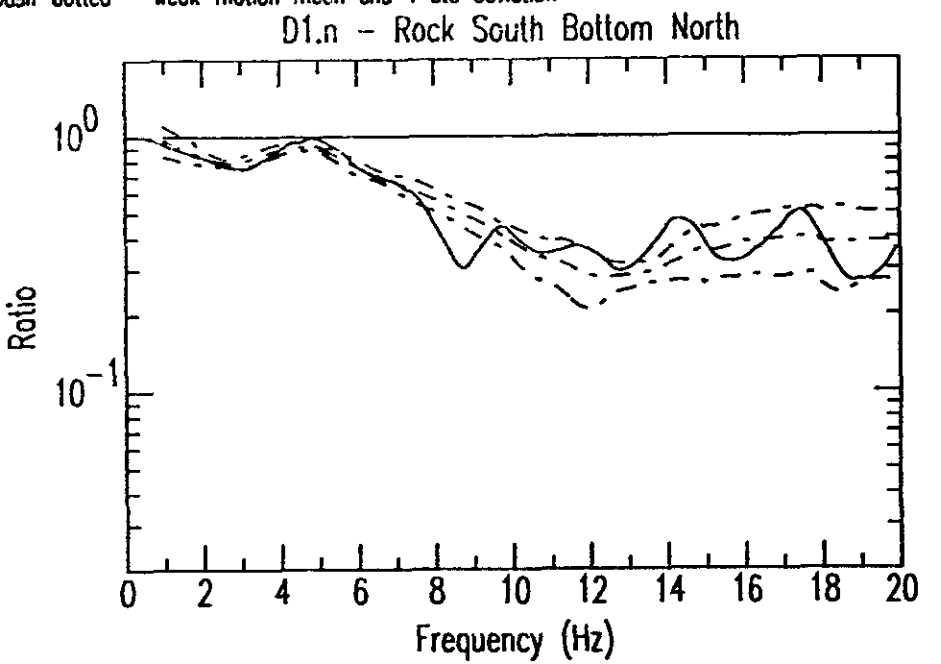

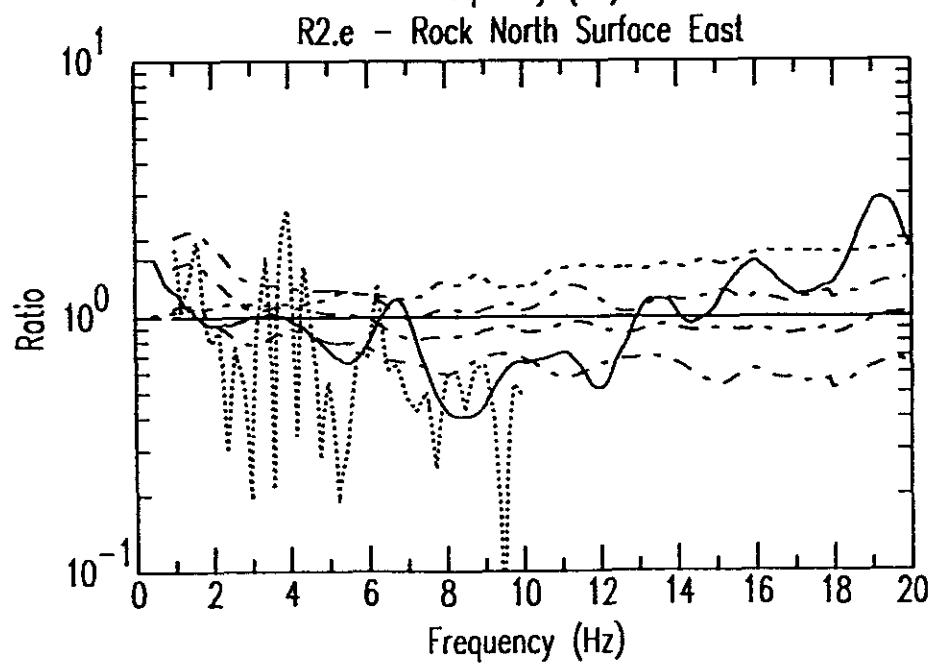

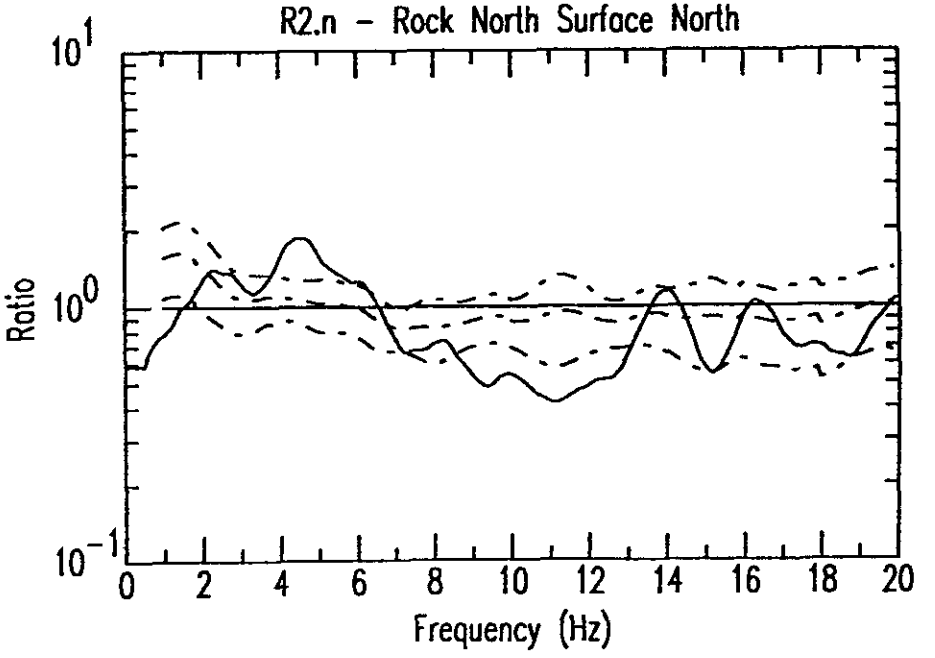

Figure G6f: R1 Preferred and Standard Response Spectra Predictions by #143 vs Observations

Response Spectra Predictions: Dashed - Standard Model; Dotted - Preferred Model

Observations: Solid - weak-motion test event

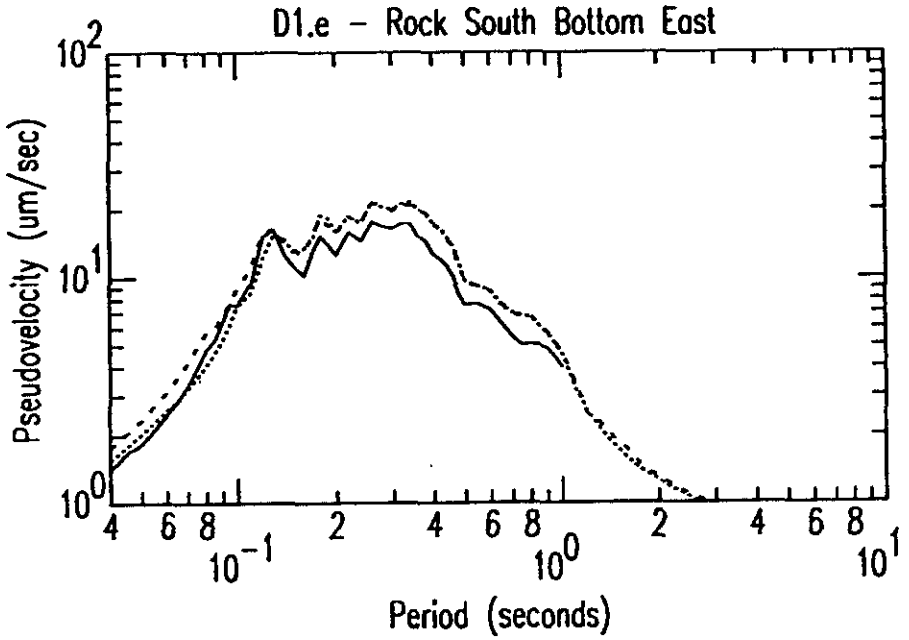

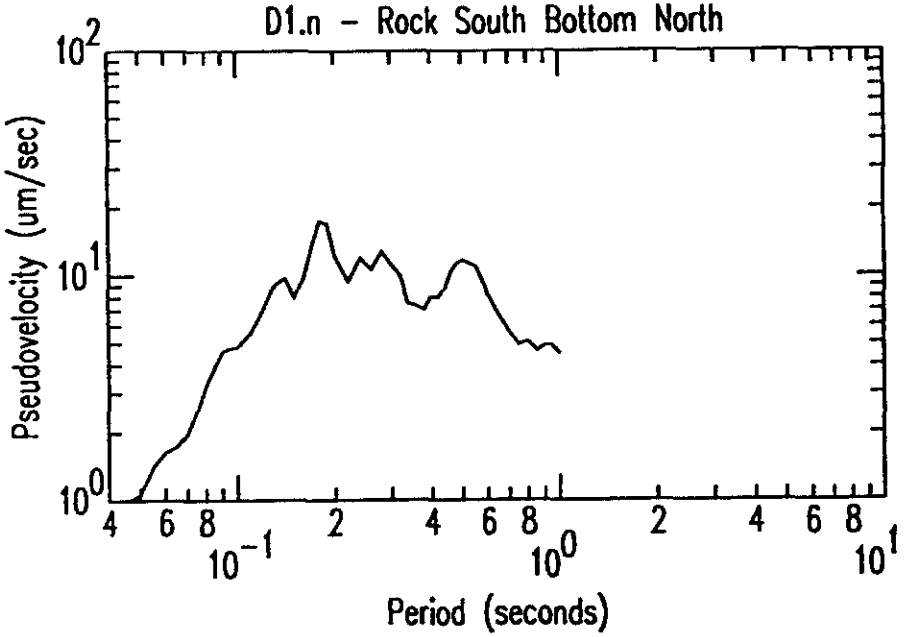

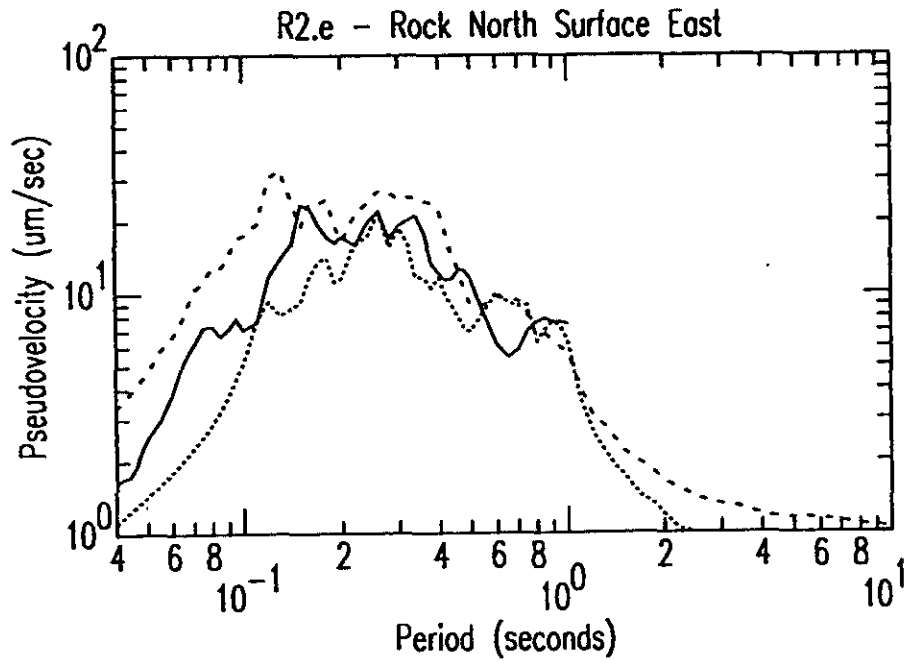

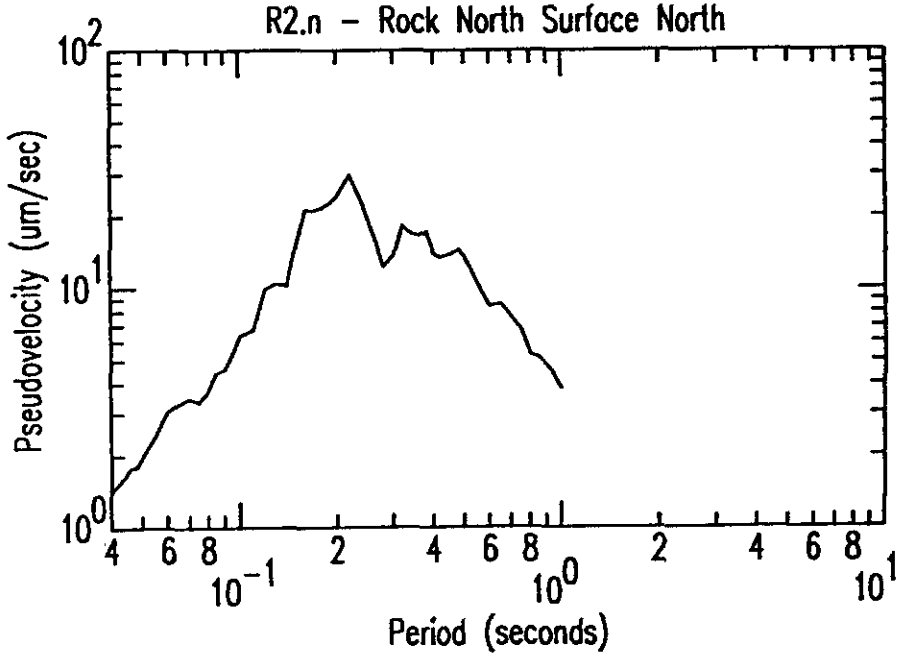

Figure G6e: R1 Preferred and Standard Response Spectra Predictions by #143 vs Observations

Response Spectra Predictions: Dashed – Standard Model; Dotted – Preferred Model

Observations: Solid – weak-motion test event

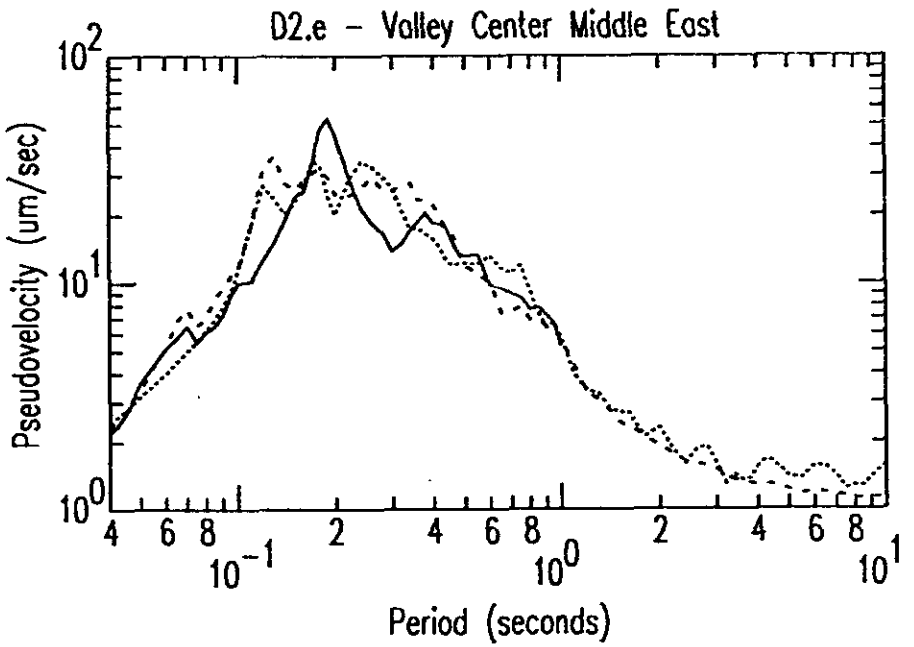

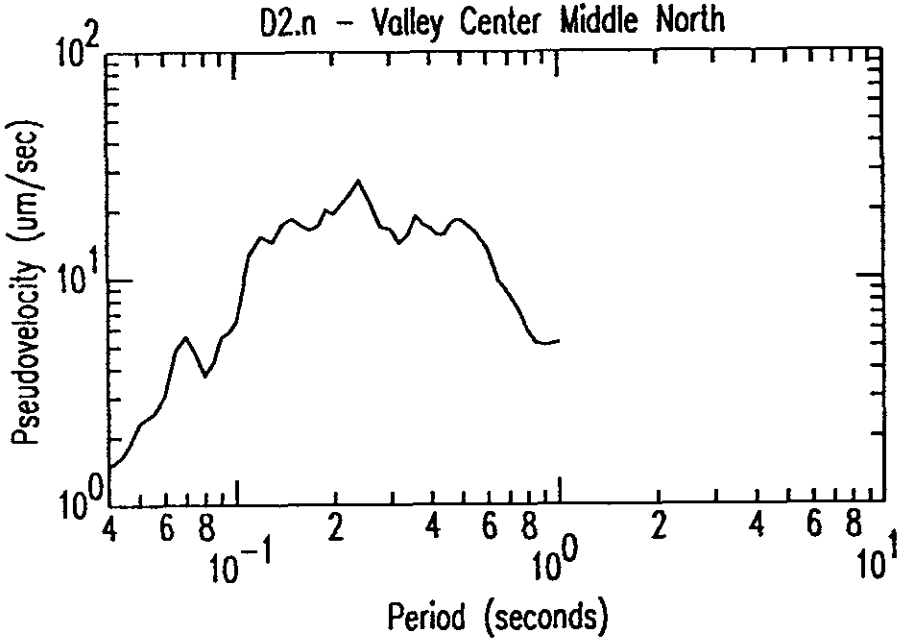

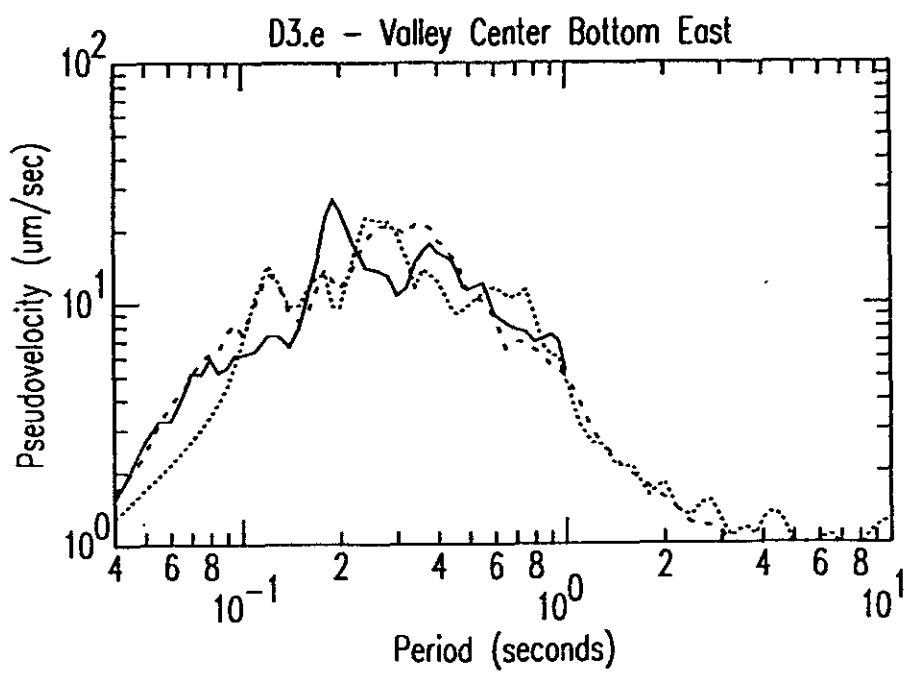

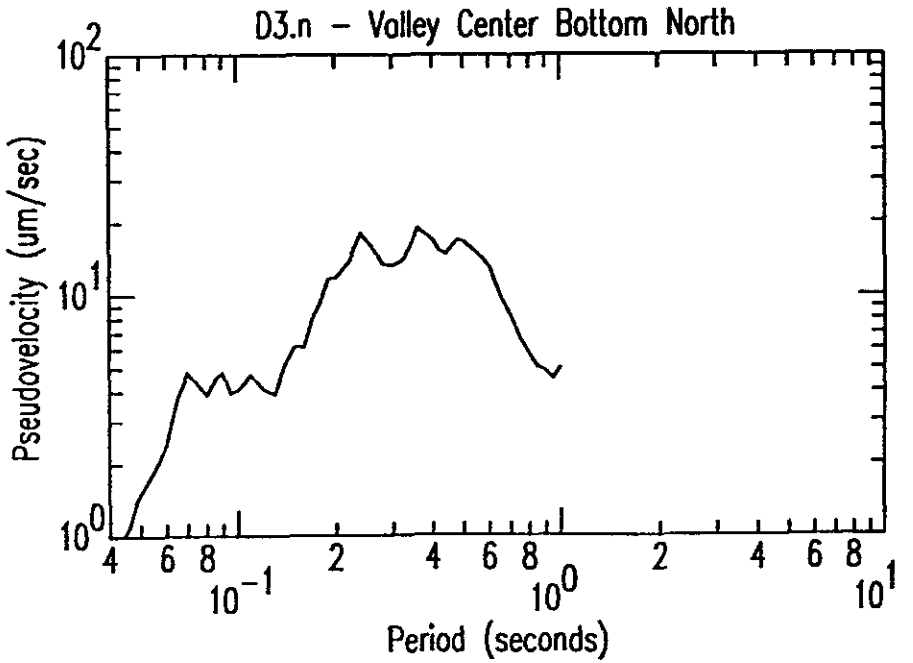

Figure G7b: D3 Preferred and Standard Response Spectra Predictions by #8 vs Observations

Response Spectra Predictions: Dashed - Standard Model; Dotted - Preferred Model

Observations: Solid - weak-motion test event

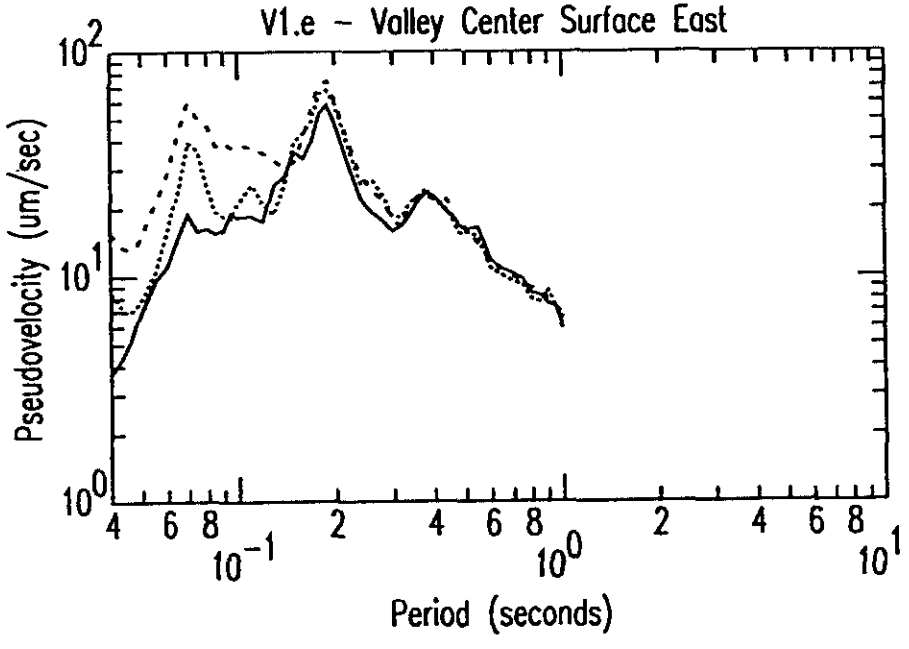

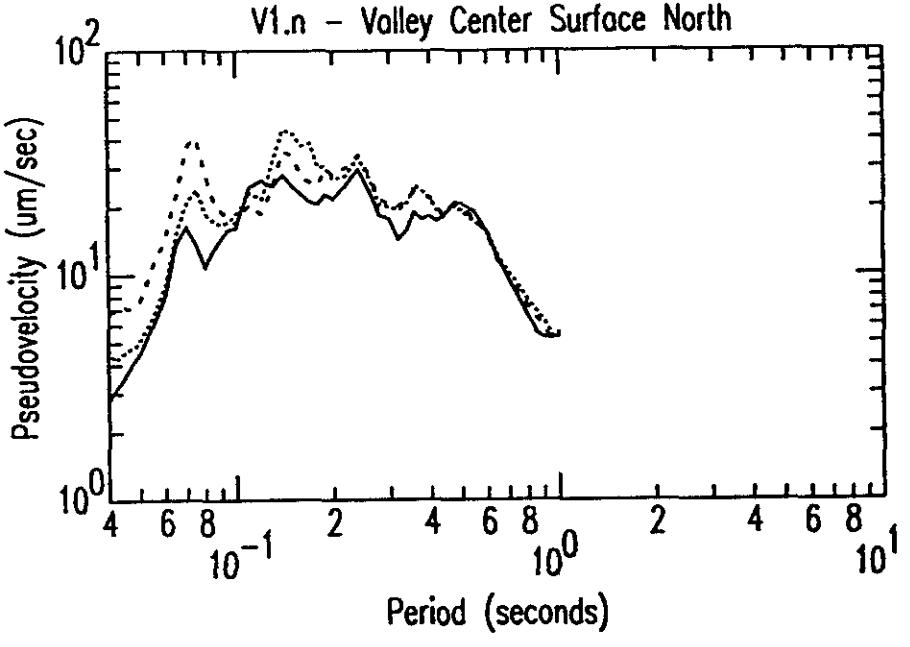

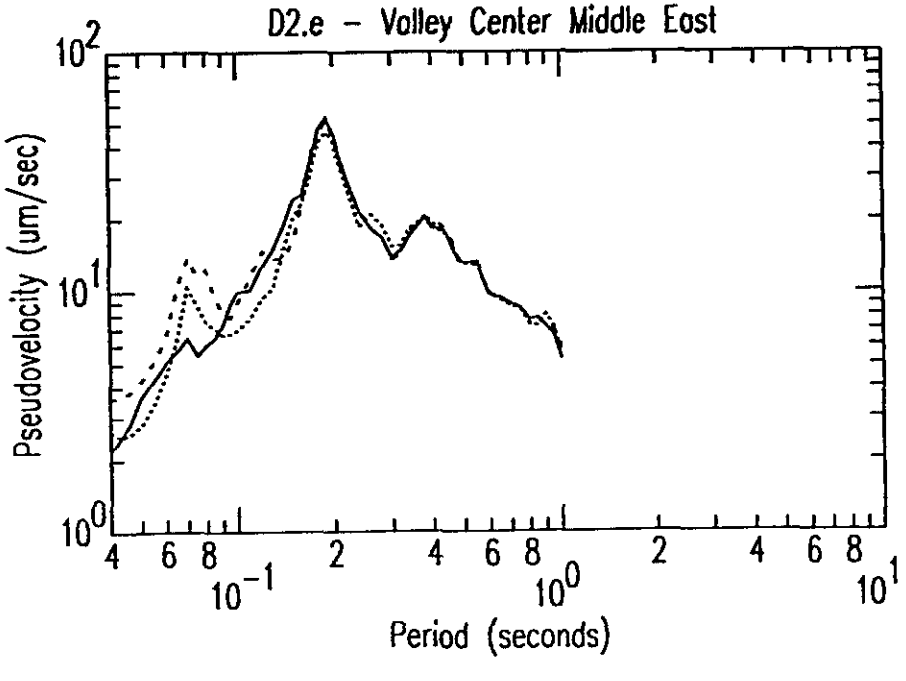

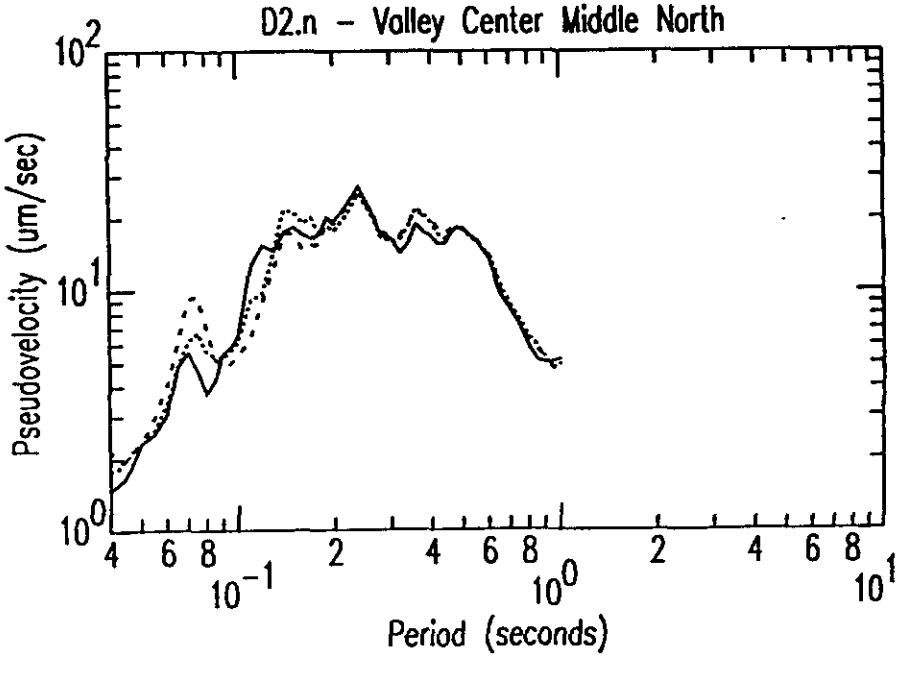

Figure G7a: D3 Preferred and Standard Spectral Ratio Predictions by #8 vs Observations

Spectral Ratio Predictions: Dashed – Standard Model; Dotted – Preferred Model

Observations: Solid – weak-motion test event; Dash-dotted – weak-motion mean and 1 std deviation

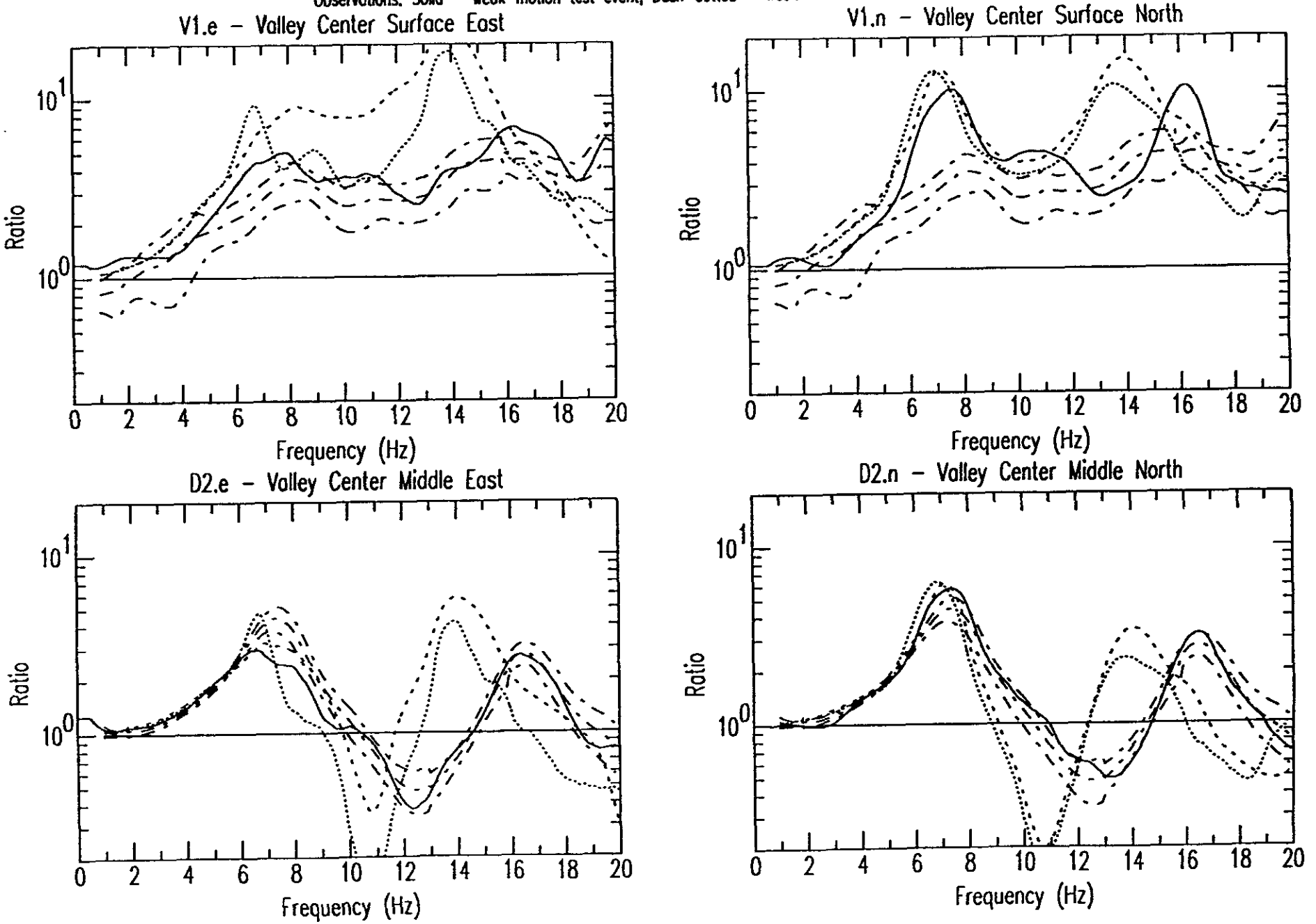

Figure G8b: D3 Preferred and Standard Response Spectra Predictions by #8sm vs Observation

Response Spectra Predictions: Dashed – Standard Model; Dotted – Preferred Model

Observations: Solid – weak-motion test event

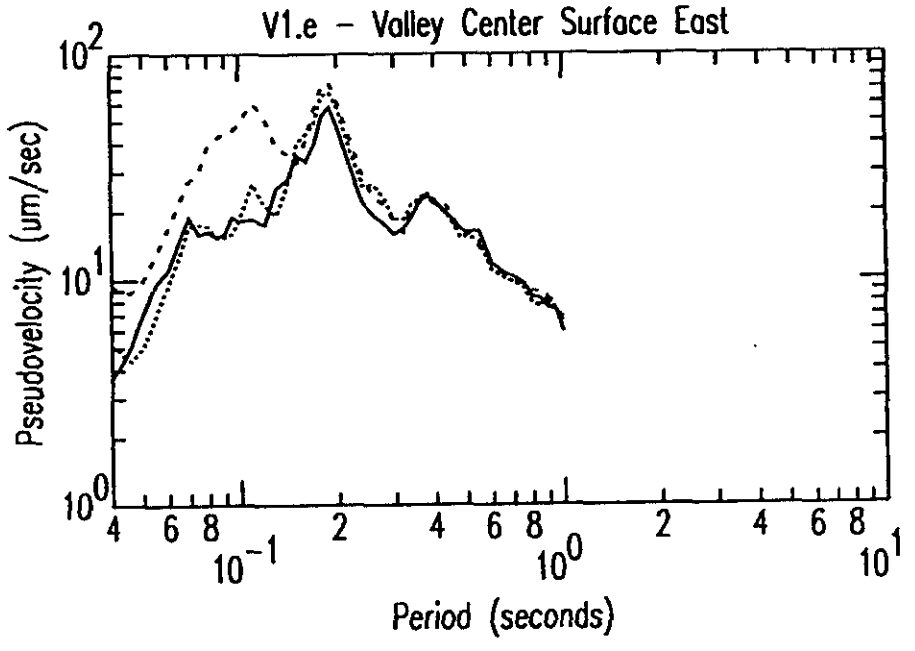

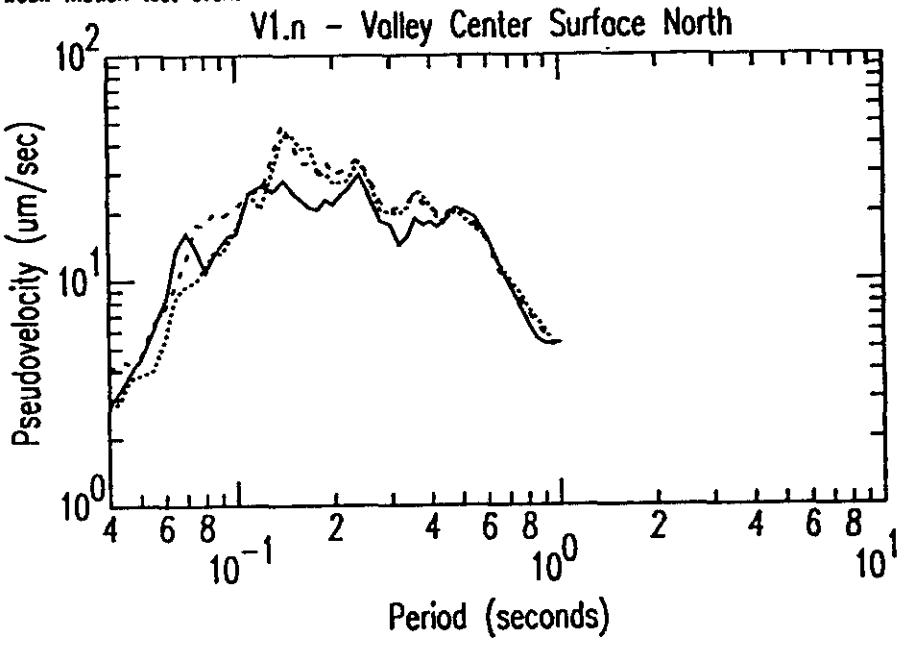

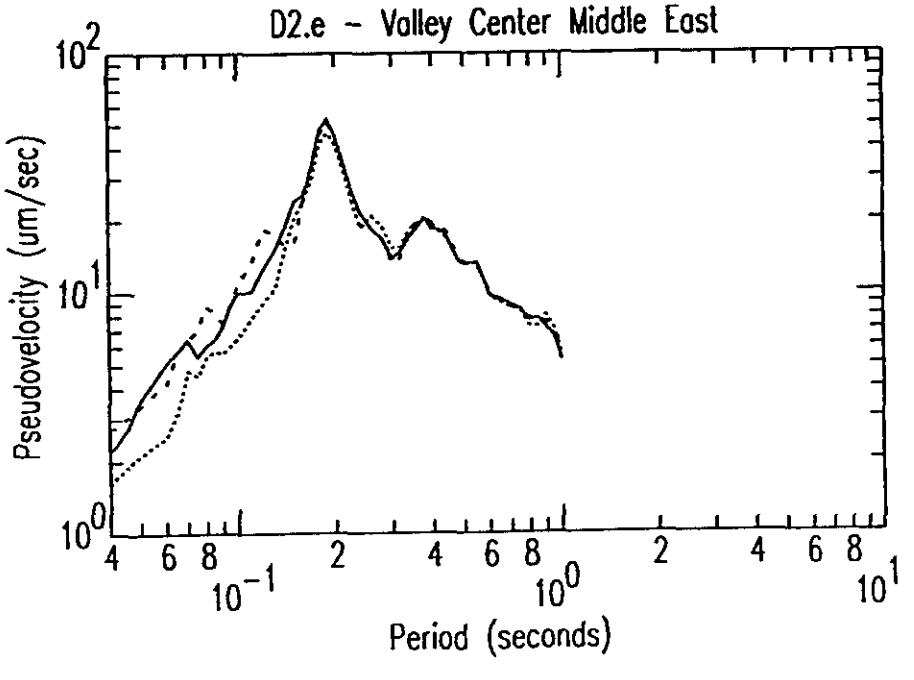

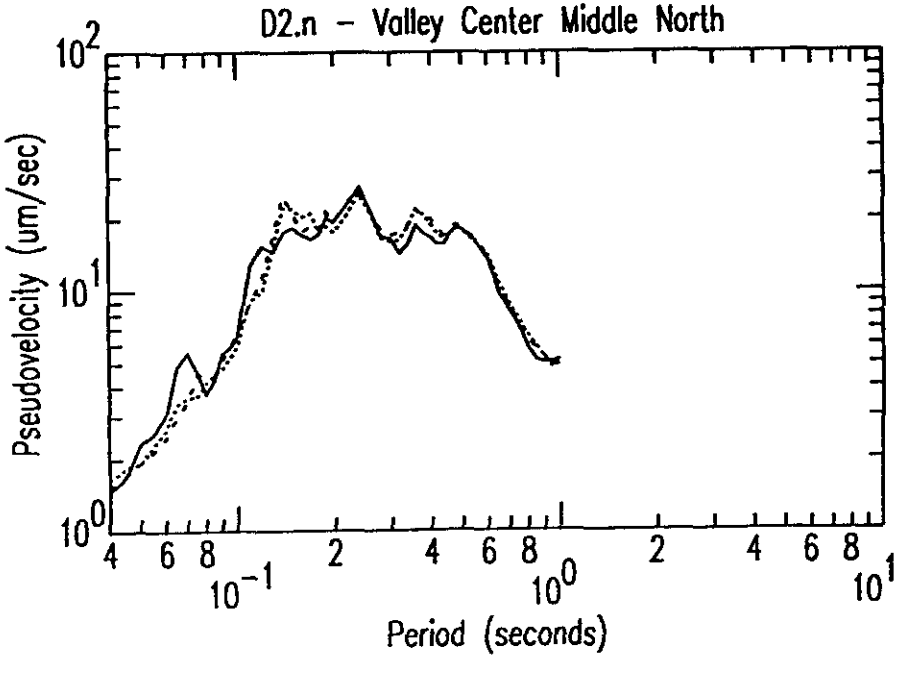

Figure G8a: D3 Preferred and Standard Spectral Ratio Predictions by #8sm vs Observations

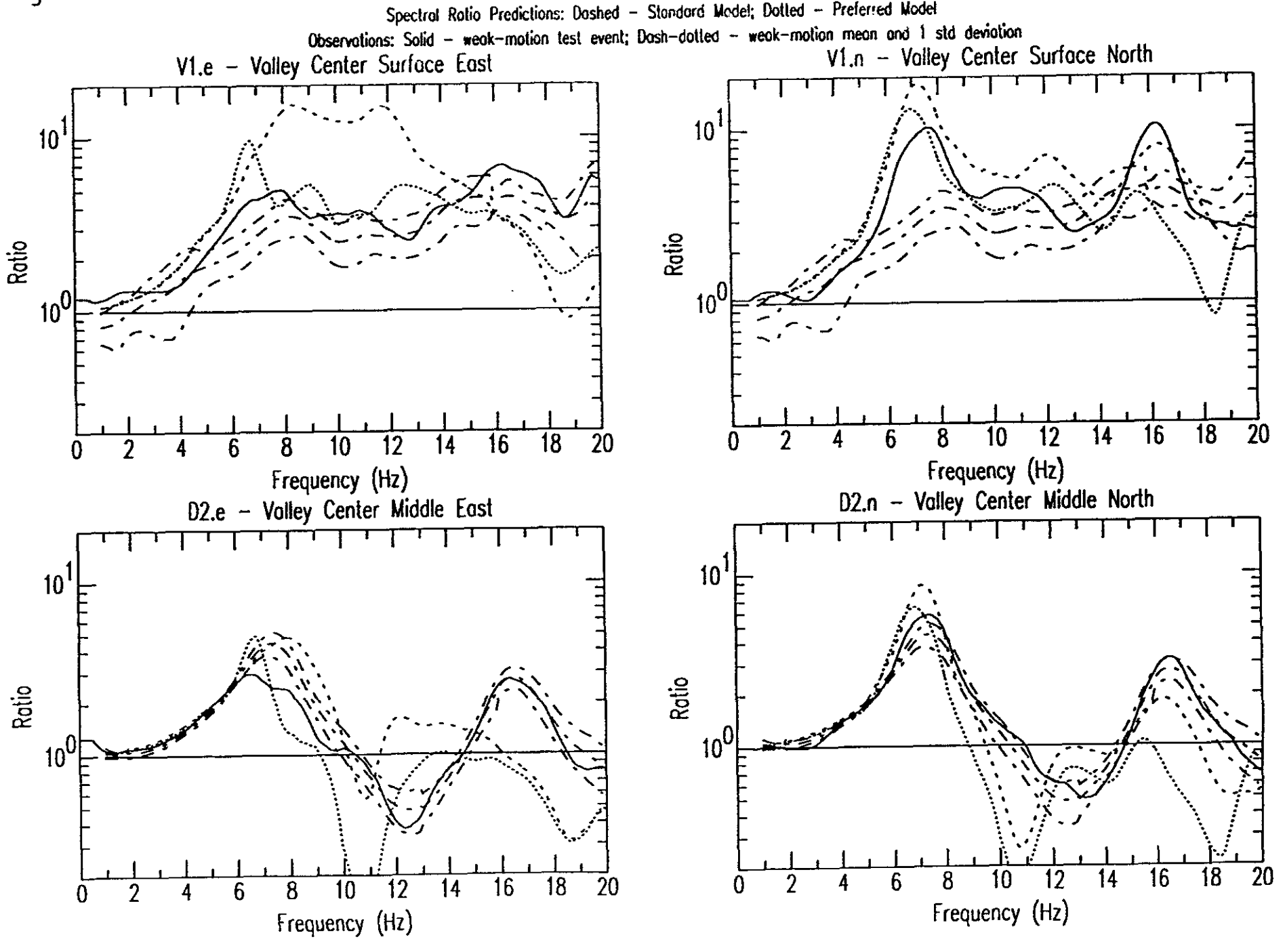

Figure G9b: D3 Preferred and Standard Response Spectra Predictions by #9 vs Observations

Response Spectra Predictions: Dashed – Standard Model; Dotted – Preferred Model

Observations: Solid – weak-motion test event

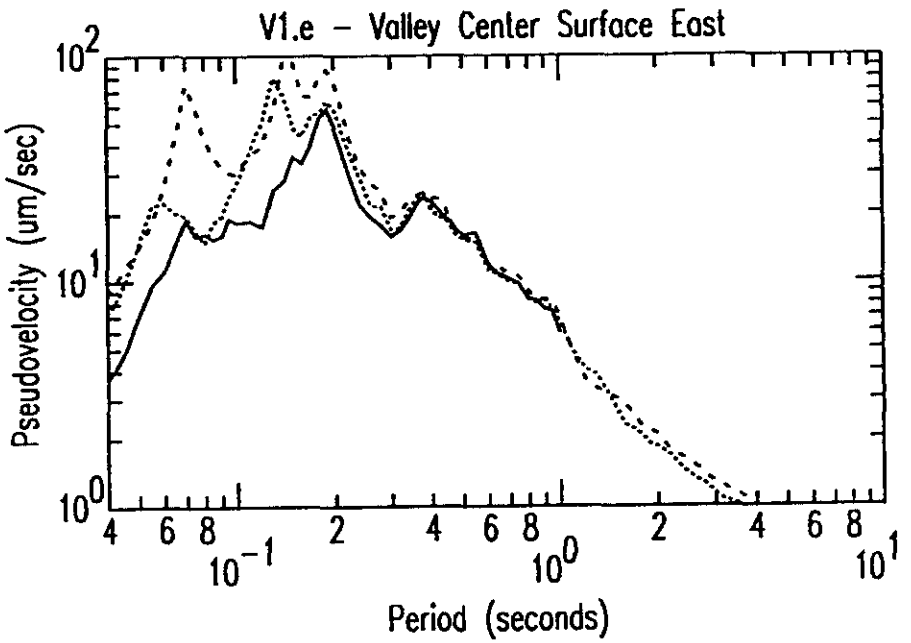

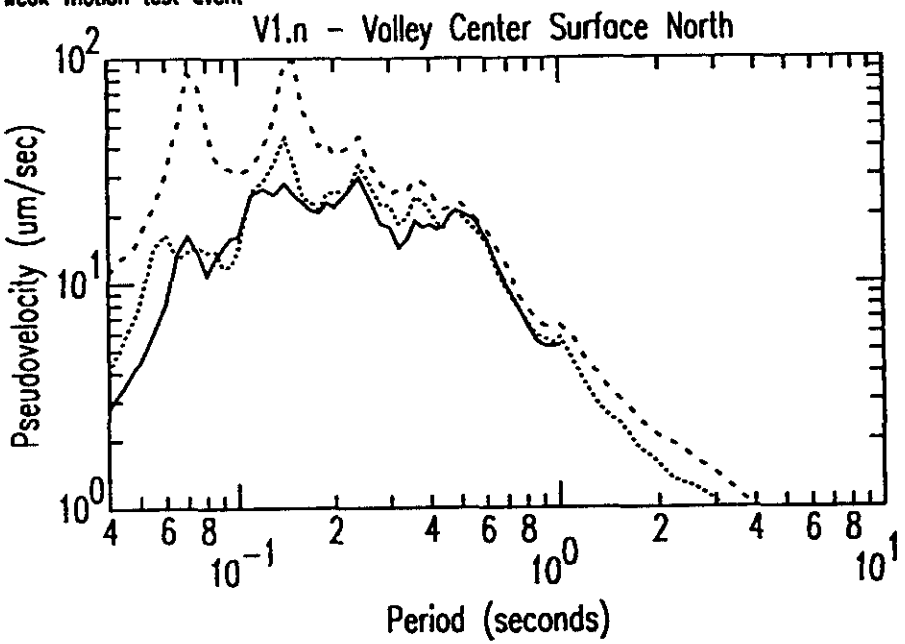

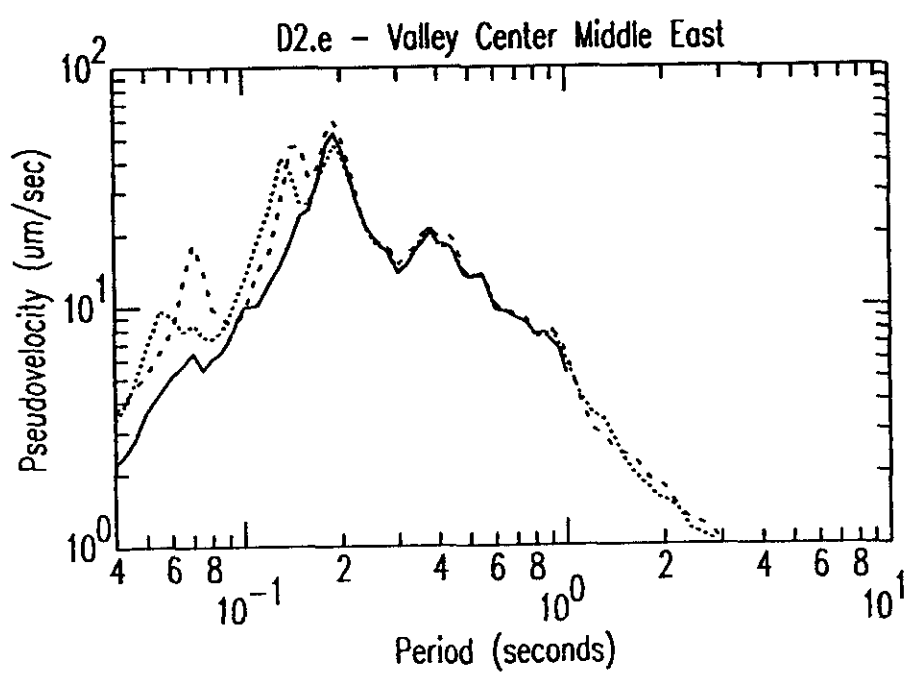

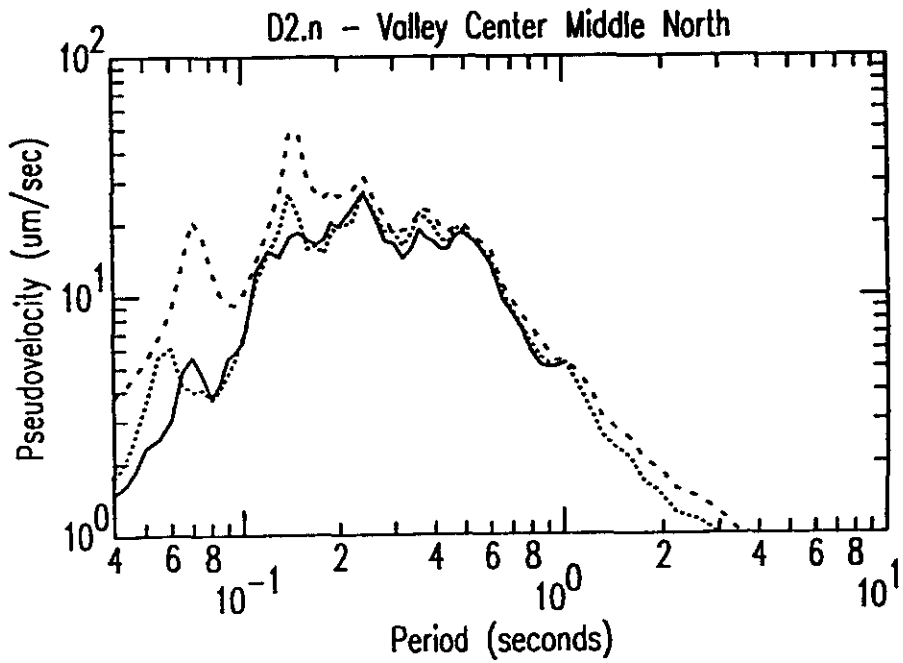

Figure G9a: D3 Preferred and Standard Spectral Ratio Predictions by #9 vs Observations

Spectral Ratio Predictions: Dashed – Standard Model; Dotted – Preferred Model

Observations: Solid – weak-motion test event; Dash-dotted – weak-motion mean and 1 std deviation

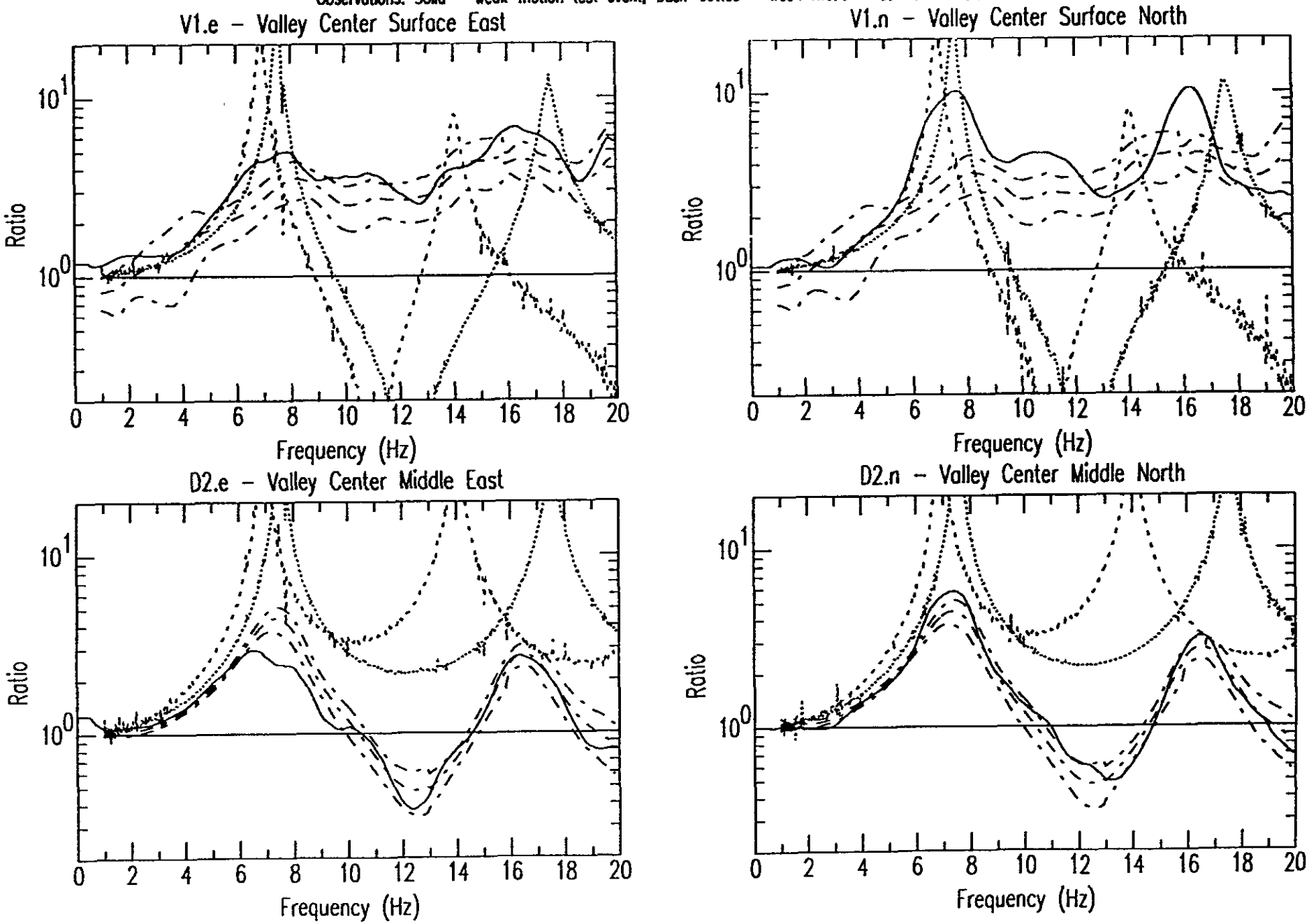

Figure G10b: D3 Preferred and Standard Response Spectra Predictions by #40 vs Observations

Response Spectra Predictions: Dashed - Standard Model; Dotted - Preferred Model

Observations: Solid - weak-motion test event

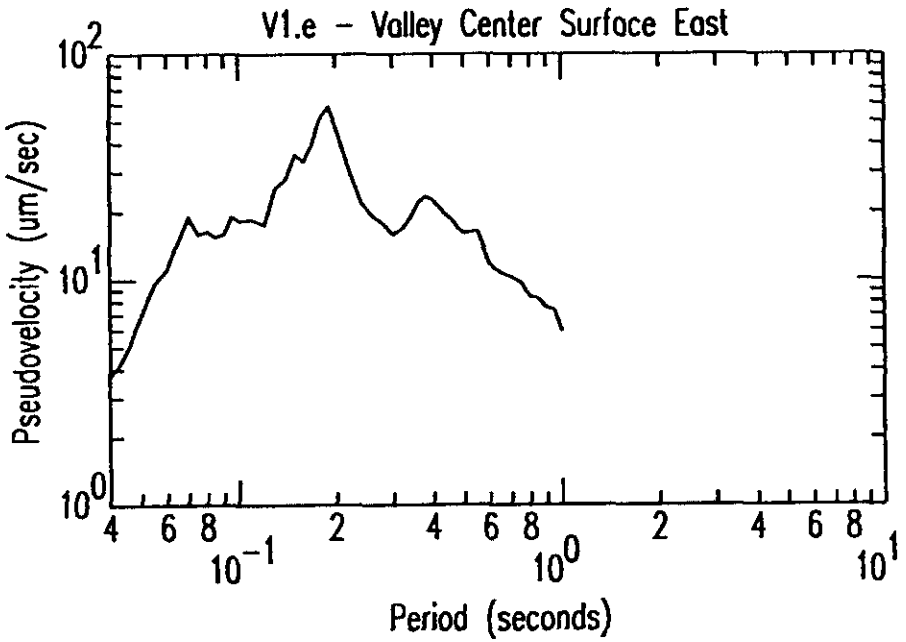

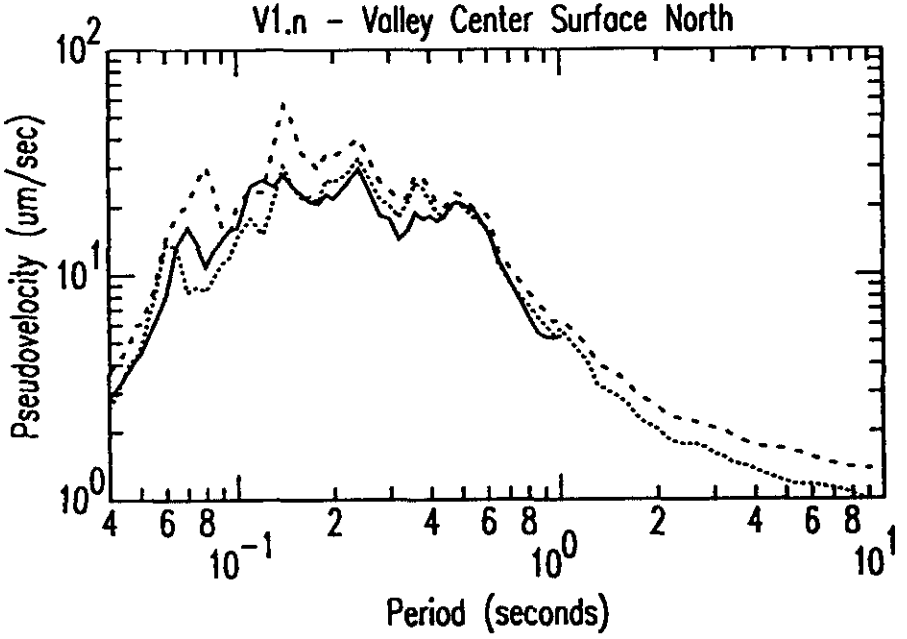

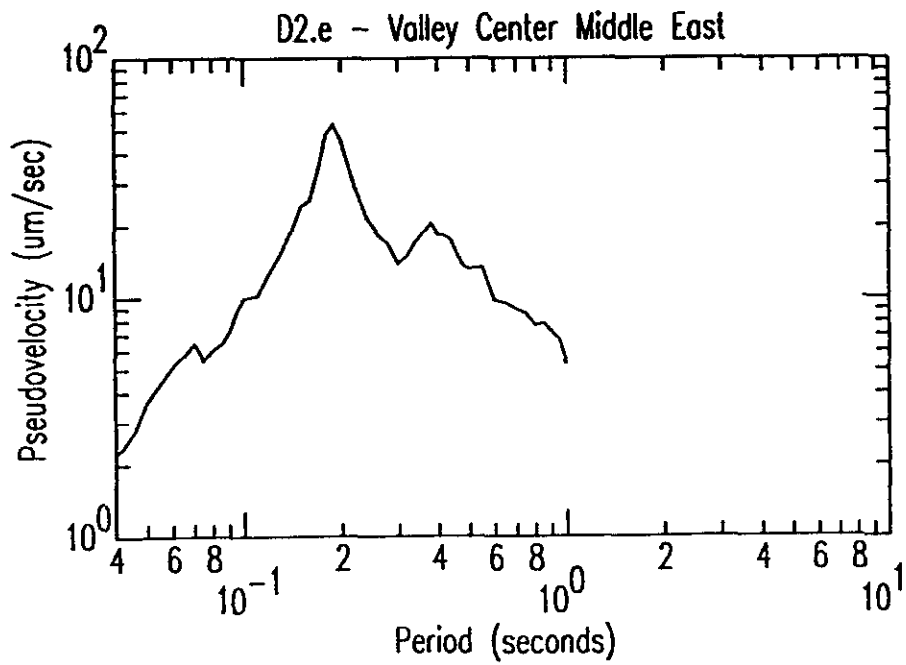

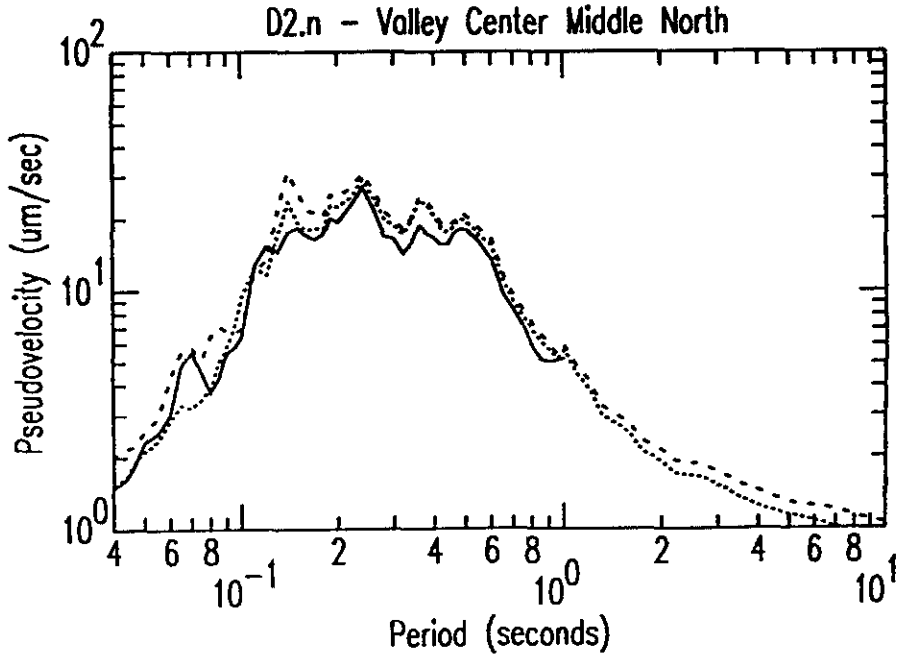

Figure G10a: D3 Preferred and Standard Spectral Ratio Predictions by #40 vs Observations

Spectral Ratio Predictions: Dashed – Standard Model; Dotted – Preferred Model

Observations: Solid – weak-motion test event; Dash-dotted – weak-motion mean and 1 std deviation

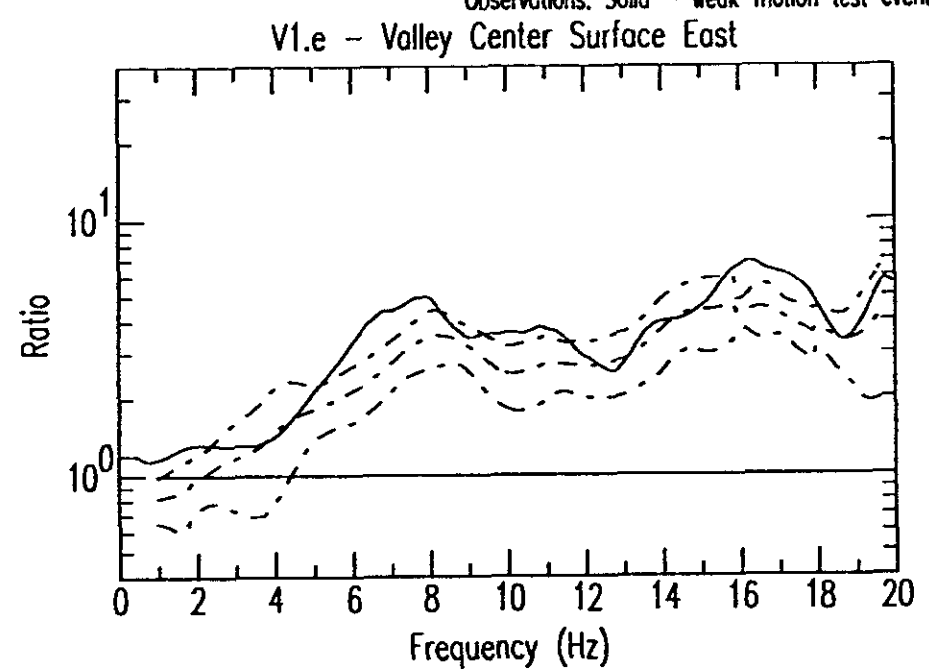

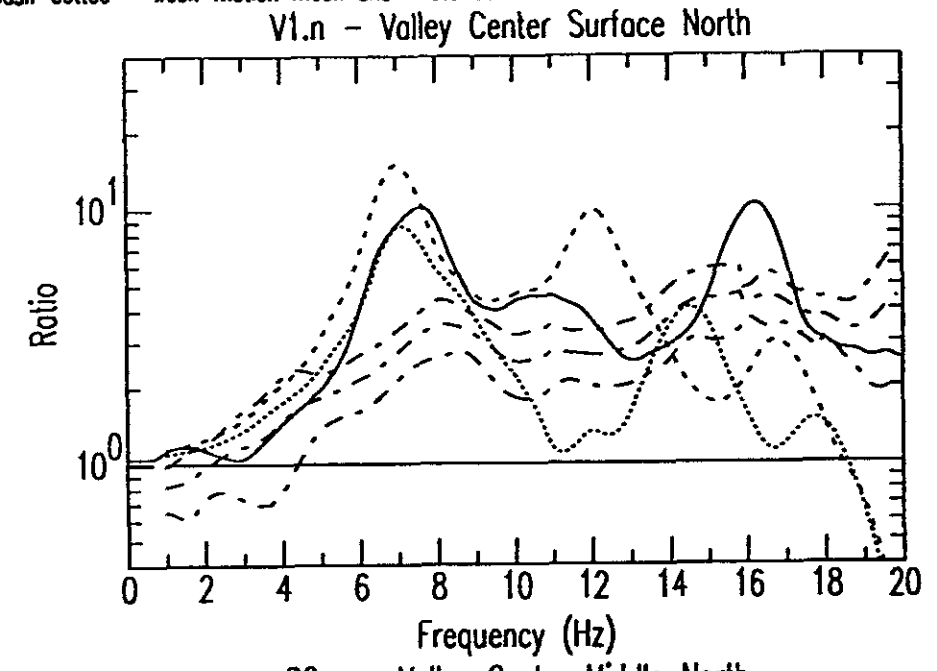

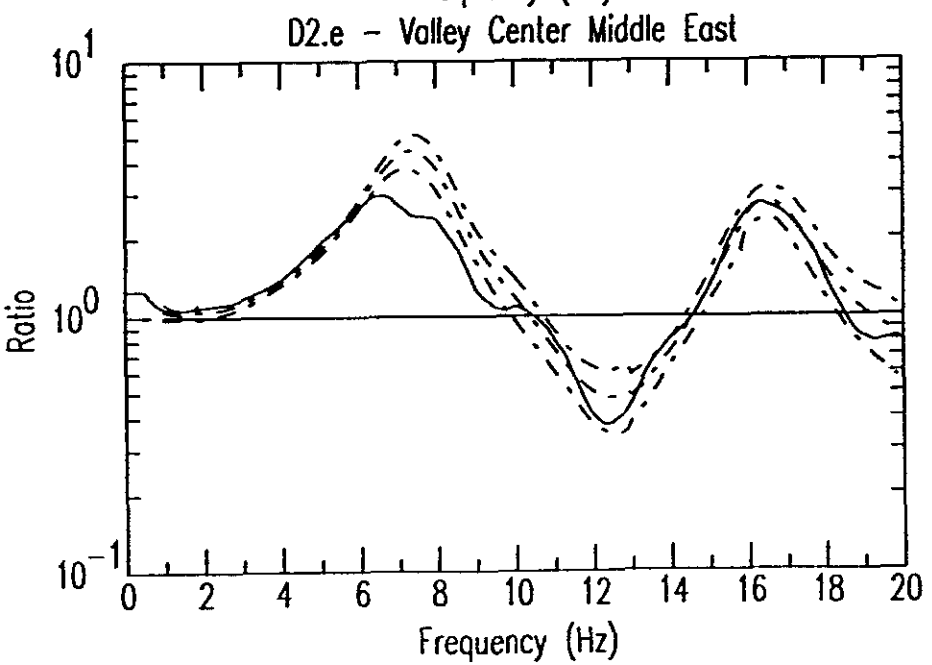

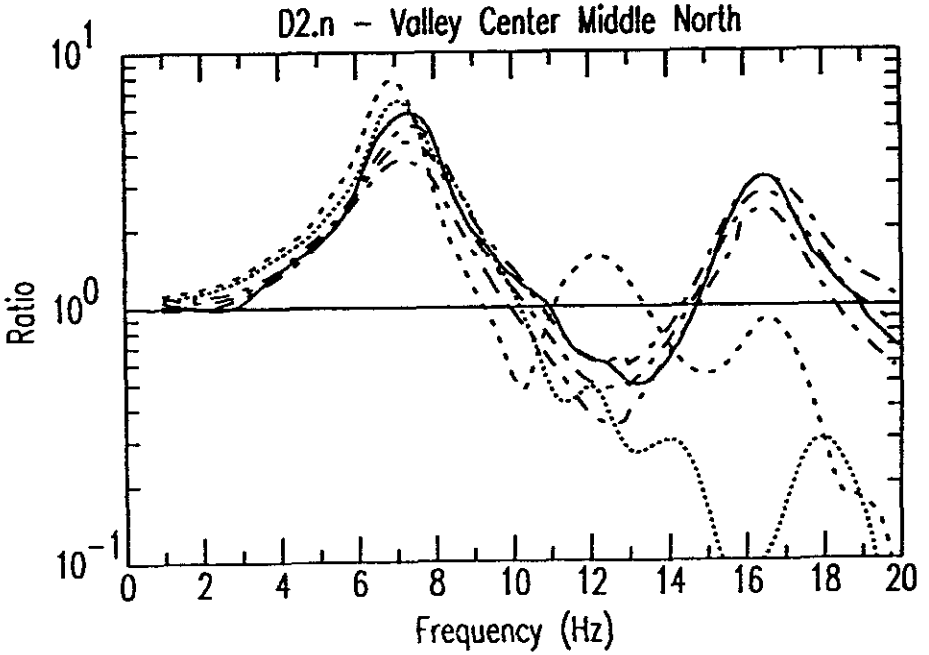

Figure G11b: D3 Preferred and Standard Response Spectra Predictions by #86 vs Observations

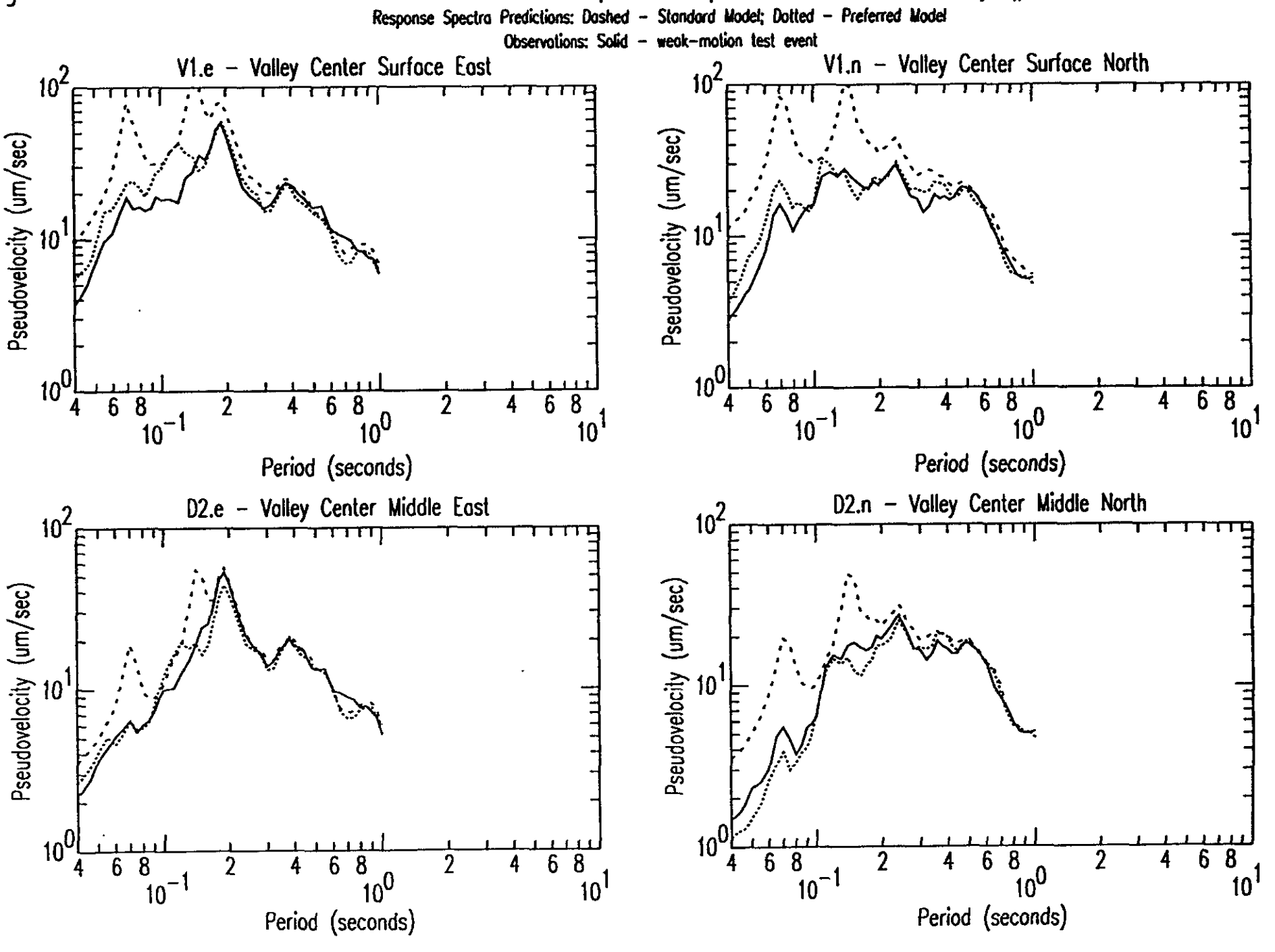

Figure G11a: D3 Preferred and Standard Spectral Ratio Predictions by #86 vs Observations

Spectral Ratio Predictions: Dashed – Standard Model; Dotted – Preferred Model

Observations: Solid – weak-motion test event; Dash-dotted – weak-motion mean and 1 std deviation

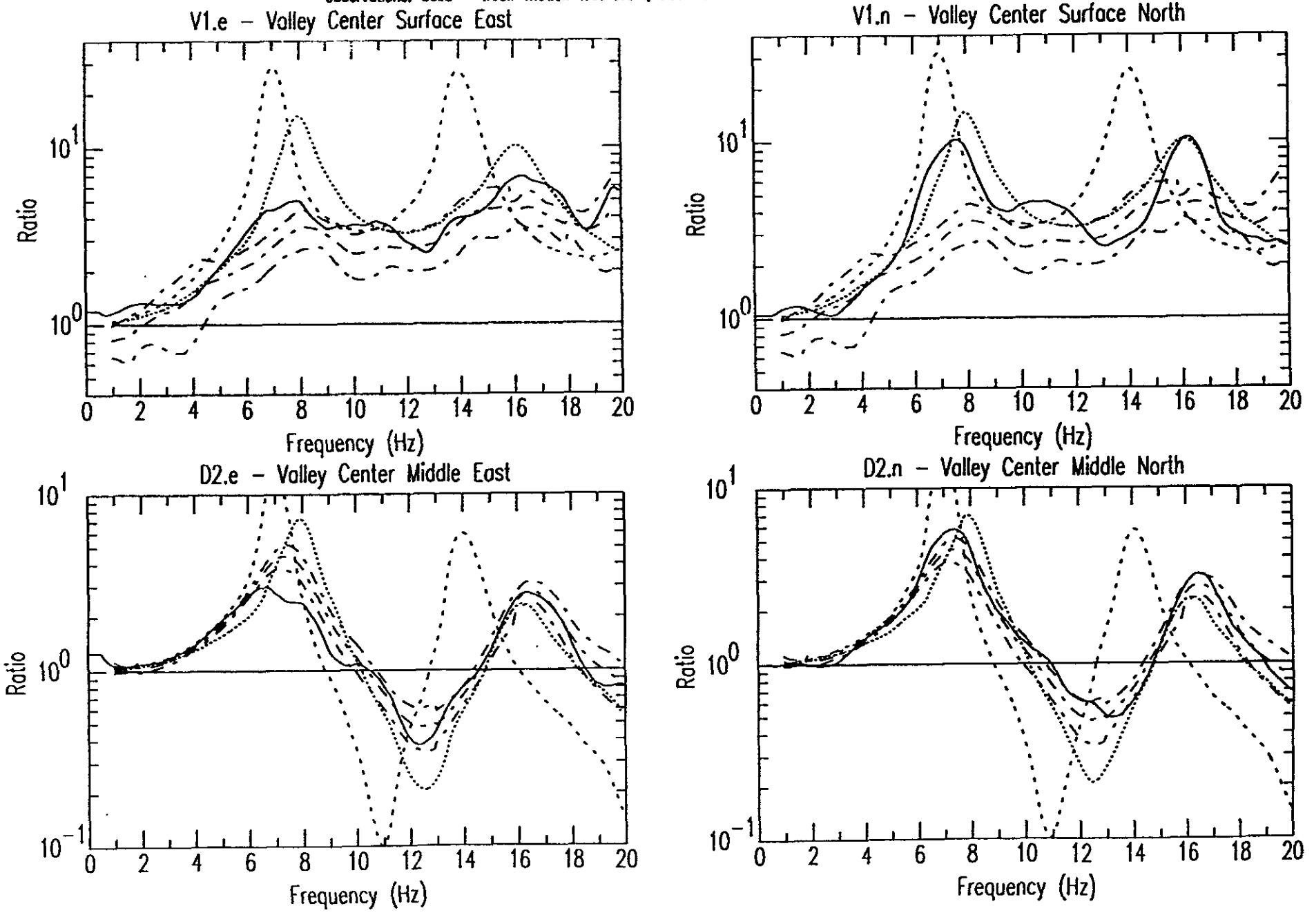

Figure G12b: D3 Preferred and Standard Response Spectra Predictions by #117 vs Observation

Response Spectra Predictions: Dashed - Standard Model; Dotted - Preferred Model

Observations: Solid - weak-motion test event

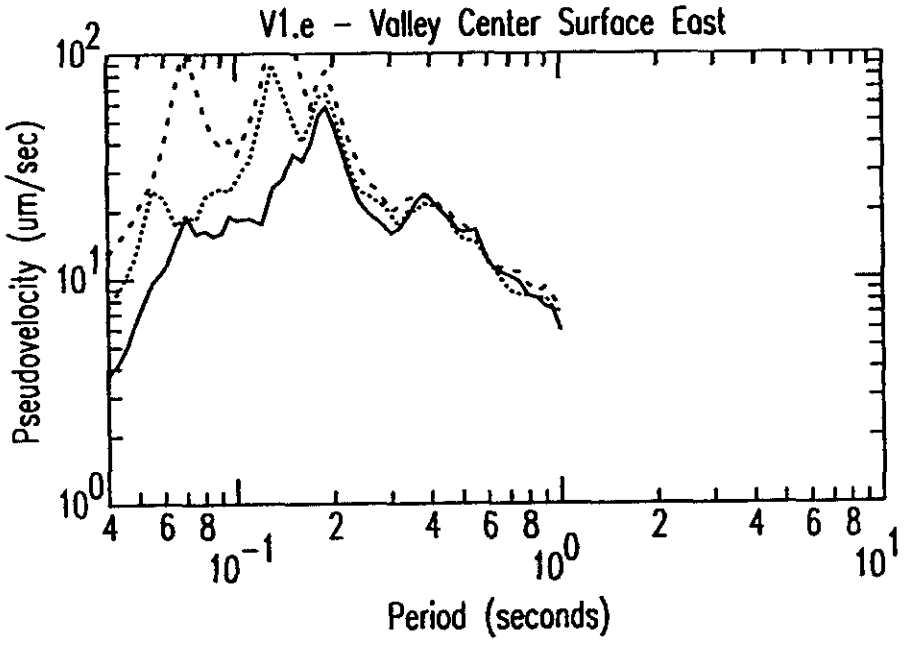

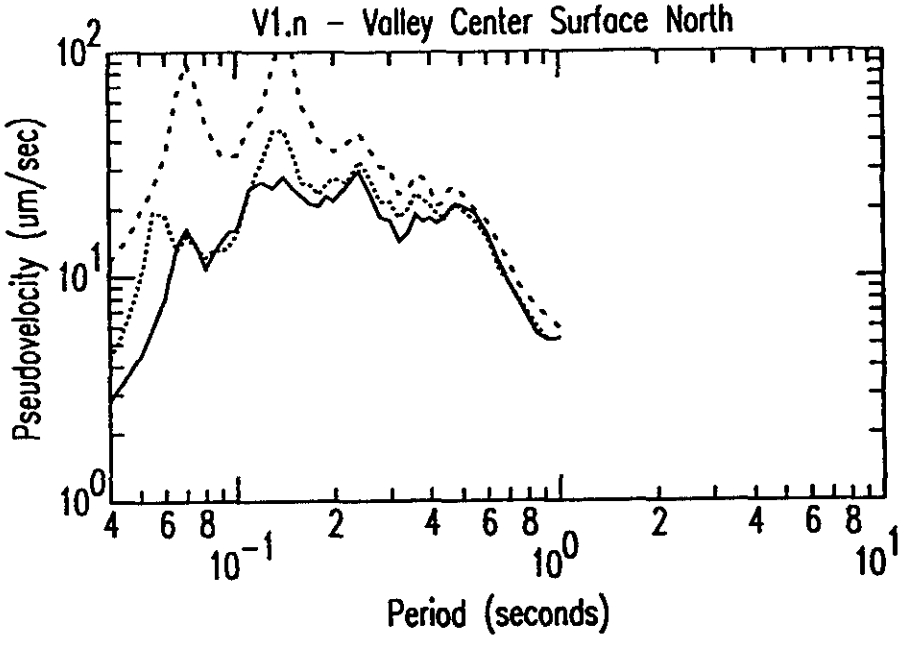

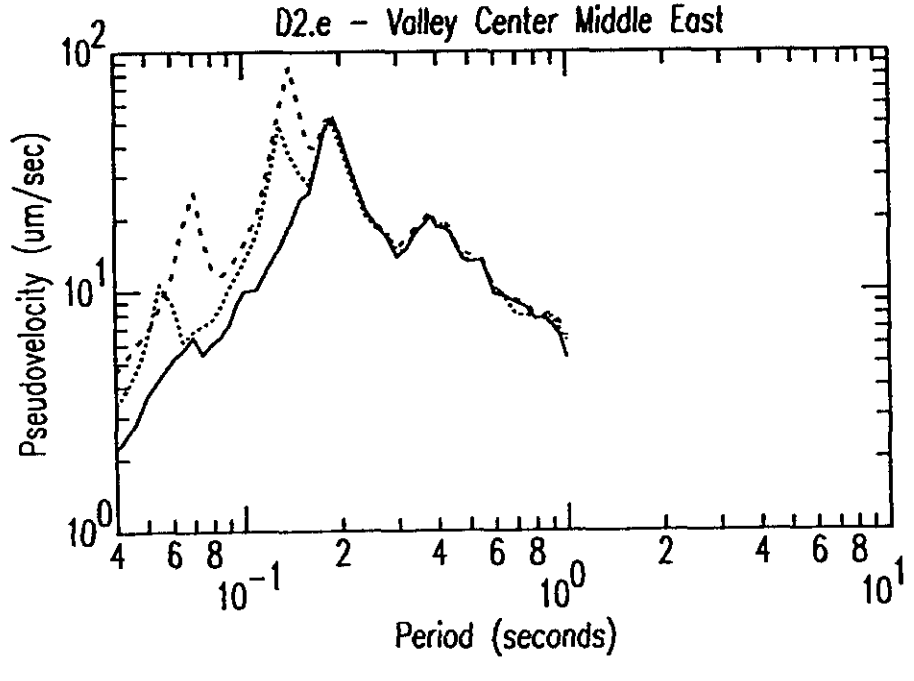

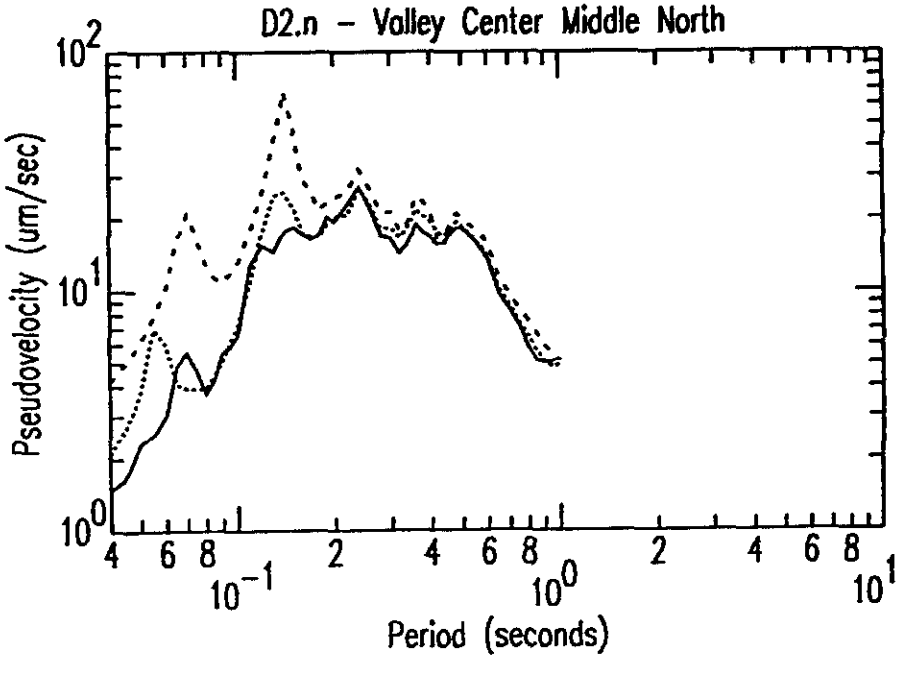

Figure G12a: D3 Preferred and Standard Spectral Ratio Predictions by #117 vs Observations

Spectral Ratio Predictions: Dashed - Standard Model; Dotted - Preferred Model

Observations: Solid - weak-motion test event; Dash-dotted - weak-motion mean and 1 std deviation